

Lecture Notes in Civil Engineering

Sergey Vasil'yevich Klyuev  
Alexander Vasil'yevich Klyuev  
Nikolay Ivanovich Vatin *Editors*

# Innovations and Technologies in Construction

Selected Papers of BUILDINTECH BIT  
2021

 Springer

# Lecture Notes in Civil Engineering

Volume 151

## Series Editors

Marco di Prisco, Politecnico di Milano, Milano, Italy

Sheng-Hong Chen, School of Water Resources and Hydropower Engineering,  
Wuhan University, Wuhan, China

Ioannis Vayas, Institute of Steel Structures, National Technical University of  
Athens, Athens, Greece

Sanjay Kumar Shukla, School of Engineering, Edith Cowan University, Joondalup,  
WA, Australia

Anuj Sharma, Iowa State University, Ames, IA, USA

Nagesh Kumar, Department of Civil Engineering, Indian Institute of Science  
Bangalore, Bengaluru, Karnataka, India

Chien Ming Wang, School of Civil Engineering, The University of Queensland,  
Brisbane, QLD, Australia

**Lecture Notes in Civil Engineering (LNCE)** publishes the latest developments in Civil Engineering - quickly, informally and in top quality. Though original research reported in proceedings and post-proceedings represents the core of LNCE, edited volumes of exceptionally high quality and interest may also be considered for publication. Volumes published in LNCE embrace all aspects and subfields of, as well as new challenges in, Civil Engineering. Topics in the series include:

- Construction and Structural Mechanics
- Building Materials
- Concrete, Steel and Timber Structures
- Geotechnical Engineering
- Earthquake Engineering
- Coastal Engineering
- Ocean and Offshore Engineering; Ships and Floating Structures
- Hydraulics, Hydrology and Water Resources Engineering
- Environmental Engineering and Sustainability
- Structural Health and Monitoring
- Surveying and Geographical Information Systems
- Indoor Environments
- Transportation and Traffic
- Risk Analysis
- Safety and Security

To submit a proposal or request further information, please contact the appropriate Springer Editor:

- Pierpaolo Riva at [pierpaolo.riva@springer.com](mailto:pierpaolo.riva@springer.com) (Europe and Americas);
- Swati Meherishi at [swati.meherishi@springer.com](mailto:swati.meherishi@springer.com) (Asia - except China, and Australia, New Zealand);
- Wayne Hu at [wayne.hu@springer.com](mailto:wayne.hu@springer.com) (China).

**All books in the series now indexed by Scopus and EI Compendex database!**

More information about this series at <http://www.springer.com/series/15087>

Sergey Vasil'yevich Klyuev ·  
Alexander Vasil'yevich Klyuev ·  
Nikolay Ivanovich Vatin  
Editors

# Innovations and Technologies in Construction

Selected Papers of BUILDINTECH BIT 2021

 Springer

*Editors*

Sergey Vasil'yevich Klyuev  
Belgorod State Technological University  
Belgorod, Russia

Alexander Vasil'yevich Klyuev  
Belgorod State Technological University  
Belgorod, Russia

Nikolay Ivanovich Vatin  
Peter the Great St. Petersburg  
Polytechnic University  
St. Petersburg, Russia

ISSN 2366-2557                      ISSN 2366-2565 (electronic)  
Lecture Notes in Civil Engineering  
ISBN 978-3-030-72909-7            ISBN 978-3-030-72910-3 (eBook)  
<https://doi.org/10.1007/978-3-030-72910-3>

© The Editor(s) (if applicable) and The Author(s), under exclusive license  
to Springer Nature Switzerland AG 2021

This work is subject to copyright. All rights are solely and exclusively licensed by the Publisher, whether the whole or part of the material is concerned, specifically the rights of translation, reprinting, reuse of illustrations, recitation, broadcasting, reproduction on microfilms or in any other physical way, and transmission or information storage and retrieval, electronic adaptation, computer software, or by similar or dissimilar methodology now known or hereafter developed.

The use of general descriptive names, registered names, trademarks, service marks, etc. in this publication does not imply, even in the absence of a specific statement, that such names are exempt from the relevant protective laws and regulations and therefore free for general use.

The publisher, the authors and the editors are safe to assume that the advice and information in this book are believed to be true and accurate at the date of publication. Neither the publisher nor the authors or the editors give a warranty, expressed or implied, with respect to the material contained herein or for any errors or omissions that may have been made. The publisher remains neutral with regard to jurisdictional claims in published maps and institutional affiliations.

This Springer imprint is published by the registered company Springer Nature Switzerland AG  
The registered company address is: Gewerbestrasse 11, 6330 Cham, Switzerland

# Preface

Proceedings contains reports of the Second International Scientific Conference “BUILDINTech BIT 2021. Innovations and Technologies in Construction” (March 9–10, 2021, Belgorod State Technological University named after V. G. Shukhov, Belgorod, Russia).

Proceedings includes reports of scientists, representatives of the construction industry, and postgraduate students from different technical universities not only from the Russian Federation (28 Russian institutes and universities). The conference was also attended by representatives of the near and far abroad from eight countries of the world (China, Azerbaijan, Kazakhstan, Uzbekistan, Belarus, the Ukraine, Georgia, and Abkhazia). Such wide geography of the conference participants, on the one hand, is very valuable from the point of view of the possibility of exchanging experience and knowledge on the issues of construction, building materials, as well as their application in various sectors of the construction industry. On the other hand, such a wide geography of the participants confirms the relevance of the thematic areas touched upon within the conference. Within the framework of the conference, three main directions are consecrated:

- Building materials, building constructions;
- Structural mechanics and theory of structures, industrial and civil construction;
- surveying, cartography and photogrammetry.

The reports of the conference touched upon the issues of synthesis and production of systems and materials for construction purposes and their application in various areas of the infrastructure of human life, as well as in industrial areas; construction and characteristics of structures and structures for various purposes; modern geodetic methods and approaches used in cartography, aimed at optimizing and efficient design and construction of facilities. The reports provide theoretical information in water patterns, models, author's concepts, etc., as well as practical data and experimental results in the form of dependencies that have the potential for real practical implementation. Thus, the choice of the declared directions of the conference is quite logical and justified, since the topics discussed touch upon the main problems in the construction industry.

A significant proportion of the research materials was prepared within the framework of implementation of state and national programs in the scientific field as a grant, federal targeted programs, decrees of the Government of the Russian Federation, and other programs.

All articles included in the collection have been reviewed by highly qualified scientists in the relevant scientific fields. The fifty best scientific manuscripts corresponding to the profile of the conference and reflecting the results of theoretical and experimental studies of the authors are recommended for publication.

Annual holding of such conferences is planned to be organized on the main topics of the construction industry.

Klyuev Sergey Vasil'yevich  
Alexander Vasil'yevich  
Vatin Nikolay Ivanovich

# Organization

## Organizing Conference Committee

Aksenov S. E.	Candidate of Technical Sciences, Associate Professor, Director of the Higher Engineering School of the Northern Arctic Federal University named after M. V. Lomonosov, Russia
Ayzenshtadt A. M.	Doctor of Chemical Sciences (Advanced Doctor), Professor, Northern (Arctic) Federal University named after M. V. Lomonosov, Arkhangelsk, Russia
Davydenko T. M.	Doctor of Pedagogical Sciences (Advanced Doctor), Professor, Belgorod State Technological University named after V.G. Shukhov, Russia
Eseev M. K.	Doctor of Physical and Mathematical Sciences (Advanced Doctor), Associate Professor, Northern (Arctic) Federal University named after M.V. Lomonosov, Russia
Evtushenko E. I.	Doctor of Engineering Sciences (Advanced Doctor), Professor, Belgorod State Technological University named after V. G. Shukhov, Russia
Fediuk R. S.	Candidate of Technical Sciences, Professor, Far Eastern Federal University, Russia
Klyuev S. V.	Candidate of Engineering Sciences (PhD), Associate Professor, Belgorod State Technological University named after V. G. Shukhov, Russia
Lesovik V. S.	Doctor of Engineering Sciences (Advanced Doctor), Professor, Corresponding Member of RAASN, Belgorod State Technological University named after V. G. Shukhov, Russia
Mestnikov A. E.	Doctor of Technical Sciences (Advanced Doctor), Professor, North-Eastern Federal University named after M. K. Ammosov, Russia



- Potapov V. V. Doctor of Engineering Sciences (Advanced Doctor),  
Professor, Research Geotechnological Center of the Far  
Eastern Branch of the Russian Academy of Sciences,  
Russia
- Uvarov V. A. Doctor of Engineering Sciences (Advanced Doctor),  
Professor, Belgorod State Technological University  
named after V. G. Shukhov, Russia
- Vatin N. I. Doctor of Engineering Sciences (Advanced Doctor),  
Professor, Peter the Great St. Petersburg Polytechnic  
University, Russia

### Scientific Conference Committee

- Amir Abdulrahman Iraq—Doctor of Engineering, Professor, Anbar University
- Ali Belloush Morocco—Ph.D., Professor, Rector, Funtius Institute
- Kovtun M. A. Australia—Ph.D.
- Kozhukhova M. I. the USA—Ph.D., University of Wisconsin-Milwaukee
- Loganina V. I. RF—Doctor of Engineering Sciences (Advanced Doctor),  
Professor, Penza State University of Architecture and  
Construction
- Lukutsova N. P. RF—Doctor of Engineering Sciences (Advanced Doctor),  
Professor, Bryansk State Engineering Technological  
University
- Nevzorov A. L. RF—Doctor of Engineering Sciences (Advanced Doctor),  
Professor, Northern (Arctic) Federal University named  
after M. V. Lomonosov
- Nenad Stoykovich Serbia—Ph.D., Nish Higher Technical School of  
Vocational Education
- Naumov A. E. RF—Candidate of Engineering Sciences (Ph.D.),  
Associate Professor, Belgorod State Technological  
University named after V. G. Shukhov
- Elyan Issa Jamal Issa Jordan—Ph.D., Amman University
- Salyamova K. D. Uzbekistan – Doctor of Engineering Sciences (Advanced  
Doctor), Professor, Institute of Mechanics and Seismic  
Stability of Structures of the Academy of Sciences  
of the Republic of Uzbekistan
- Sovann Chin Cambodia—Ph.D.
- Strokova V. V. RF—Doctor of Engineering Sciences (Advanced Doctor),  
Professor, Belgorod State Technological University  
named after V. G. Shukhov
- Suleymanova L. A. RF—Doctor of Engineering Sciences (Advanced Doctor),  
Professor, Belgorod State Technological University  
named after V. G. Shukhov
- Tabet Salem Yemen—Ph.D.  
Al-Azab

Fisher H. B.	Germany—Professor, Bauhaus-University of Weimar
Hisham Almama	Syria—Ph.D., Damascus University
Hussein Motawi	Egypt—Ph.D., Professor, Vice-Rector, Damanhour University
Eknik Jürgen	Switzerland—Ph.D., Professor, Executive Director of a Swiss Company, Performance Selling Academy Zurich Area GmbH
Shakarna Mahmoud Husni Ibrahim	Palestine – Ph.D.

All conference participants express deep gratitude to the science team.

# Contents

<b>Reuse of 3D Additive Manufacturing Concrete Scrap in Construction</b> . . . . .	1
V. S. Lesovik, N. M. Tolypina, E. S. Glagolev, and D. A. Tolypin	
<b>Study of Geological Setting of Naftalan-Northern Naftalan Area by Use of Attribute Analysis of 3D Seismic Data</b> . . . . .	7
M. A. Aghayeva	
<b>The Study of the Dynamics of Flotation Agent Decomposition in a Tailings Dump</b> . . . . .	15
A. I. Gorodov, N. A. Shapovalov, R. G. Shevtsova, and A. A. Krainiy	
<b>Method of Extrusion Granulation of Aggregates for the Preparation of Filling Mixtures</b> . . . . .	22
L. H. Zagorodnyuk, V. D. Ryzhikh, D. S. Makhortov, and D. A. Sumskey	
<b>Refinement of the Structure of the Eastern Govsan Area Using a New Method of Seismic Inversion and a Lithological Model of the Zyk Field of Azerbaijan Based on 3D and GRW Seismic Data</b> . . . . .	29
T. R. Ahmedov and K. A. Kurochkina	
<b>Determination of the Stress State of the Disk Using the Stress Function</b> . . . . .	36
V. N. Strel'nikov	
<b>Optimization of Technological Parameters of Foam Concrete Mix Preparation for Obtaining Foam Concrete with Improved Structure and Characteristics</b> . . . . .	43
S. A. Stel'makh, E. M. Shcherban', and K. E. Tkacheva	
<b>Energy Efficient Stone Cellular Concrete Masonry on Polyurethane Adhesive</b> . . . . .	50
L. A. Suleymanova, I. A. Pogorelova, and I. S. Ryabchevskiy	

<b>Experimental Studies of Deflections in Bending Reinforced Concrete Elements Taking into Account the Influence of the Shape of Their Cross-Section</b> . . . . .	56
D. V. Obernikhin and A. I. Nikulin	
<b>Predicting the Parameters of Construction Structures with Variable Action of Factors over Time and with Mutual Influence on Each Other</b> . . . . .	63
D. I. Korolkov, D. V. Nizhegorodtsev, V. I. Klevan, and S. G. Golovina	
<b>Experimental Studies of the Strength of Reinforced Concrete Flexible Elements Forced with Carbon Fiber</b> . . . . .	71
G. A. Smolyago and Y. L. Obernikhina	
<b>On the Issue on Dilatant Phenomena in Dispersed Systems</b> . . . . .	78
N. N. Onoprienko, O. N. Salnickowa, and Sh. M. Rahimbaev	
<b>The Use of Additional Conditions in Photogrammetric Constructions</b> . . . . .	85
V. Ya. Tsvetkov	
<b>Problems of Constructive Safety of Piled Foundations of Heighted Buildings at the Stages of Design and Construction</b> . . . . .	93
R. G. Abakumov	
<b>Construction Materials with Low Power Intensity Based on Cement</b> . . . . .	100
I. N. Borisov and A. A. Stronin	
<b>Determination of Material Properties of Composite Sleepers Taking into Account Operational Factors</b> . . . . .	107
V. I. Kondrashchenko and C. Wang	
<b>Comparative Studies of the Anticorrosive Activity of Oily Compositions, Containing Telaz-M, in Outdoor Conditions</b> . . . . .	116
R. G. Shevtsova, R. A. Lyubushkin, and I. V. Starostina	
<b>Rheotechnological Properties of Multicomponent Dispersed Suspensions of Glowing Architectural and Decorative Concrete</b> . . . . .	124
M. V. Maliukova, L. A. Suleymanova, and A. A. Koryakina	
<b>Influence of Inhomogeneity of the Foundation on the Stress-Strain State of a Free-Lying Beam</b> . . . . .	131
A. N. Leontiev, T. N. Gorbunova, K. V. Balandina, and A. A. Sitnikova	
<b>Clarification of the Structure of the East Hovsan Area by a New Method of Seismic Inversion</b> . . . . .	139
T. R. Ahmedov and K. A. Kurochkina	
<b>Determination of the Deflected Mode of the Disk</b> . . . . .	145
V. N. Strelnikov	

**Computer Simulation of Bent Reinforced Concrete Elements with External Composite Reinforcement** ..... 153  
 S. I. Merkulov, S. M. Esipov, and D. V. Esipova

**Compatibility of Plasticizing Mono-Admixtures for Modifying Concretes of Transitional Period** ..... 160  
 M. M. Kosukhin and A. M. Kosukhin

**Methodology for Assessing the Quality of Building Materials** ..... 167  
 V. I. Loganina, S. V. Klyuev, R. S. Fediuk, and I. A. Aksenov

**Evaluation of the Load-Bearing Capacity of the Combined Bolt-Welded Joint** ..... 174  
 N. V. Solodov and N. V. Vodyakhin

**The Structure of the Content and Cost of Materials in Bending Reinforced Concrete Element with Variable Section Height** ..... 181  
 V. S. Kuznetsov and Yu. A. Shaposhnikova

**Brief Overview of Complex Cadastral Works: Experience in Conducting** ..... 188  
 O. Yu. Kononova and N. M. Zatolokina

**Influence of Shear Deformations on the Buckling of Reinforced Concrete Elements** ..... 195  
 S. Yu. Savin

**Use of Unmanned Aerial Vehicles in the Creation of a Topographic Plan of a Chalk Pit** ..... 201  
 E. R. Shin, T. G. Kalachuk, N. V. Andreeva, and A. I. Polyakov

**The Effect of Moisture State on Kinetics of Damage Accumulation in the Structure of Epoxy Polymer Samples Under Tensile Stresses** ... 208  
 T. A. Nizina, N. S. Kanaeva, and D. R. Nizin

**Hydration Processes of Anhydrite-Containing Binders Using Volumetric Phase Composition** ..... 215  
 L. A. Anikanova, O. V. Volkova, A. I. Kudyakov, and V. A. Lotov

**Assessment of the Pile Foundations Reliability in the Cryolithozone for the Climate Changing Conditions** ..... 222  
 A. N. Yakubovich and I. A. Yakubovich

**Thermal Phase Transformations in Titanium Hydride - A Filler for Special-Purpose Construction Materials** ..... 228  
 R. N. Yastrebinsky, A. A. Karnauhov, A. V. Yastrebinskaya, and L. V. Denisova




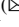

**Investigation of the Technical Condition of Buildings and Structures in the Conditions of Dangerous Geological Processes** ..... 234  
 N. Yu. Soyту, M. A. Aleynikova, and A. V. Novozhilova

<b>Use of UAV to Resolve Construction Disputes</b> .....	241
N. V. Shirina, T. G. Kalachuk, E. R. Shin, and E. A. Parfenyukova	
<b>Forecasting the Durability of Protective and Decorative Coatings of External Walls of Buildings</b> .....	247
V. I. Loganina, S. V. Klyuev, R. S. Fediuk, and I. A. Aksenov	
<b>Investigation of Physical and Chemical Properties of Architectural Glass Fibrous Concrete</b> .....	255
N. I. Bondarenko and D. O. Bondarenko	
<b>Impact of Polyurethane Foam Insulation on the Deformability of Three-Layer Frameless Cylindrical Vaults</b> .....	261
S. A. Makeev, A. A. Komlev, P. A. Korchagin, and S. V. Savelyev	
<b>Study of the Effect of Cryogenic Grinding on the Microstructure and Mechanical Properties of Polymer Composites</b> .....	268
V. V. Kashibadze, V. V. Sirota, A. I. Gorodov, and R. V. Sidelnikov	
<b>Investigation of the Effectiveness of the Method of Directional Horizontal Hydraulic Fracturing for Fixing Clay Bases</b> .....	274
S. A. Gubarev, A. S. Chernysh, and S. V. Gapon	
<b>Promising Technological Solutions for the Production of Compression-Molded Bricks in the Northern Ethiopia</b> .....	282
B. K. Gebru, V. D. Kotlyar, Yu. A. Bozhko, and S. N. Kurilova	
<b>Structural Analysis of Steel Membrane Roofing</b> .....	289
A. V. Dronov	
<b>Experimental Justification of Geometrical Model of Cut Chip Cross-Section during Asphalt Milling</b> .....	296
D. V. Furmanov, N. E. Lysakov, and L. M. Shamahov	
<b>Study of the Impact of the Composite “Rubber:Shungite” on the Properties of Bituminous Rubber Binder</b> .....	302
V. V. Yadykina, K. S. Vyrodova, and E. E. Potapov	
<b>Deterioration of Power Transmission Line Supports and Development of Proposals for Increasing their Durability</b> .....	309
V. A. Absimetov and E. V. Saltanova	
<b>Experimental Verification of the Isotropy Postulate on Orthogonal Curved Trajectories of Constant Curvature</b> .....	315
V. I. Gultyayev, A. A. Alekseev, I. A. Savrasov, and S. L. Subbotin	
<b>Design of Transformable Beam Systems</b> .....	322
L. A. Panchenko	

<b>Advanced Building Materials Based on Zeolite-Containing Raw Materials of Yakutia</b> .....	328
A. E. Mestnikov and A. L. Popov	
<b>Radiation-Protective Properties of a Structural Polyimide Composite</b> .....	336
R. N. Yastrebinsky, A. A. Karnauhov, E. O. Pilavidou, and A. V. Yastrebinskaya	
<b>Zoning the Urban Area on the Basis of the Principles and Methods of GIS-Mapping</b> .....	342
N. V. Shirina and E. A. Parfenyukova	
<b>Author Index</b> .....	349



# Reuse of 3D Additive Manufacturing Concrete Scrap in Construction

V. S. Lesovik , N. M. Tolypina , E. S. Glagolev , and D. A. Tolypin  

Belgorod State Technological University Named After V.G. Shukhov, Belgorod, Russia  
Tolypina.n@yandex.ru

**Abstract.** The paper studies the possibility of reusing fine concrete scrap of 3D additive production obtained by grinding fractions of various sizes. The ability to hydrate hardening depended on the size of the crushed fractions of concrete scrap. The greatest strength and ability to hydration hardening was shown by the pulverized fraction, which includes the largest number of fine particles of the cement matrix of concrete with the maximum content of non-hydrated particles of alite and belite. Then the strength is followed by samples of cement stone obtained by grinding the largest fractions (2.5–5 and 1.25–2.5 mm), in which the content of quartz increases and the content of alite and belite decreases. The minimum compressive strength was shown by samples of cement stone obtained by grinding fractions (0.16–0.315, 0.315–0.63 and 0.63–1.25 mm), in which quartz prevails and traces of alite and belite are observed. The strength of solidified samples is mainly due to coagulation bonds, which significantly weaken when wet. The water resistance of cement stone samples varies depending on the hydration capacity of the powdered material fractions. It is shown that the use of crushed concrete scrap as a binder requires additional measures to increase the strength and water resistance.

**Keywords:** Concrete scrap · Fine-grained concrete · Hydration · Clinker particles · Cement matrix · Strength

## 1 Introduction

Recently, 3D additive technologies have been playing an increasingly important role in the construction industry of the Russian Federation and industrially developed countries. This is due not only to the high speed of construction, but also to the possibility of 100% reuse of the material of buildings and structures of 3D-additive production. In the air-dry conditions of concrete hardening of 3D-additive technologies, the hydration of calcium silicates of Portland cement clinker gradually attenuates, so concrete scrap, as a rule, contains under-hydrated clinker particles with hydration activity, which makes it possible to reuse not only as filler, but also as a binder [1–4]. During the hardening of Portland cement, the hydration processes occur intensively for the first 7 days, then the rate of hydration slows down, by 28 days  $C_3S$  is hydrated approximately by 70–75%,  $C_2S$  by 45–50%, complete hydration is observed in the aluminates phases [5, 6].



These studies are devoted to the issue of obtaining binders based on concrete scrap, taking into account the composition and properties of fractions of various sizes obtained during crushing.

## 2 Methods and Materials

Concrete scrap was obtained by crushing samples of fine-grained concrete molded by 3D printing in the laboratory. Concrete solidified for 6–10 months in air-dry conditions, which is typical for the conditions of hardening of construction structures of 3D-additive production. The composition of fine-grained concrete C:S = 1: 4, very fine quartz sand of the fraction 0.16–0.63 mm was used as a fine aggregate, and CEM I, CEM II and CEM III (Table 1). Samples of fine-grained concrete were crushed on a laboratory jaw crusher, dispersed into fractions: 10–20 mm, 5–10 mm and 0–5 mm. For the fraction of 0–5 mm, the granulometric composition was determined in accordance with GOST 8735–88 “Sand for construction works. Test methods” (Table 2).

**Table 1.** Chemical composition of concrete scrap, %.

Fraction, mm	CaO	SiO <sub>2</sub>	Al <sub>2</sub> O <sub>3</sub>	Fe <sub>2</sub> O <sub>3</sub>	MgO
5–2.5	16.63	76.76	2.77	0.97	0.58
2.5–1.25	18.65	74.58	2.71	1.14	0.60
1.25–0.63	11.90	82.51	2.48	0.75	0.48
0.63–0.315	8.88	86.26	2.12	0.62	0.40
0.315–0.16	13.85	80.85	2.35	0.84	0.53
<0.16	57.21	29.28	4.59	3.42	1.18

**Table 2.** Particle size distribution of dropouts of the concrete scrap crushing process.

Indicators	Size of sieve holes, mm					
	2.5	1.25	0.63	0.315	0.16	Bottom
Weight of residues on the sieve, g	67	55	184	423	195	76
Specific residues, %	6.7	5.5	18.4	42.3	19.5	7.6
Full residues, %	6.7	12.2	30.6	72.9	92.4	100

The maximum number of particles has a size of 0.315–0.63 mm  $\approx 42\%$ , the share of particles of 0.16–0.315 mm and 0.63–1.25 mm accounts for  $\approx 19\%$ , large fractions of 1.25–2.5 mm and 2.5–5 mm are characterized by a small amount of 5.5 and 6.7%, respectively.

To study the hydration capacity, individual fractions of concrete scrap were crushed in a laboratory vibration mill to a specific surface area of ordinary Portland cement of 330–350 m<sup>2</sup>/kg. Samples of 3 × 3 × 3 cm were formed from a test of normal density obtained from fine powders. The normal density varied little depending on the size of the crushed fractions and corresponded to NG = 0.28–0.30, the samples hardened for 28 days under normal conditions. To identify the features of the secondary use of concrete scrap crushing products in order to obtain binders, a modern X-ray phase analysis was used. Data from ICSD-Inorganic Crystal Structure Database were used as structural models of mineral components for full-profile quantitative XFA.

### 3 Results and Discussions

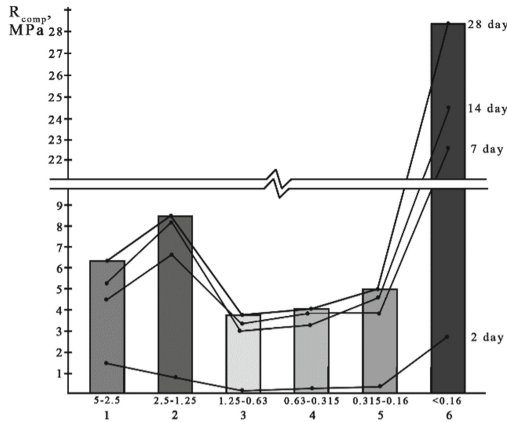
The kinetics of the strength gain of binders obtained by grinding various fractions of concrete scrap is shown in Table 3. The test results showed that the hydration activity of the powders depended on the size of the crushed fractions (Fig. 1).

**Table 3.** Kinetics of compressive strength gain of samples of 3 × 3 × 3 cm cement stone from concrete scrap.

№	Fraction, mm	Indicators					
		S <sub>sp</sub> m <sup>2</sup> /kg	W/T	Limit of compressive strength, MPa			
				2 day	7 day	14 day	28 day
1	2.5–5	360	0.29	1.65	4.45	5.16	6.42
2	1.25–2.5	355	0.28	0.91	6.63	8.15	8.49
3	0.63–1.25	360	0.28	0.06	3.30	3.17	3.64
4	0.315–0.63	410	0.28	0.22	3.83	3.44	3.98
5	0.16–0.315	330	0.30	0.30	3.83	4.20	4.87
6	0.00–0.16	500	0.30	2.75	22.57	24.82	28.54

The minimum strength of the fractions is 0.16–1.25 mm, which are mainly represented by quartz sand particles, with the inclusion of a small number of particles of the cement matrix of concrete. The strength is mainly due to the weak forces of coagulation interaction between fine particles acting through thin layers of water. According to chemical analysis (Table 1), these fractions contain the minimum amount of CaO (8.88–13.85%) and the largest SiO<sub>2</sub> (80.85–86.26%), and traces of reflections C<sub>3</sub>S (d = 2.776... Å) и C<sub>2</sub>S (d = 2.785... Å) are observed on radiographs (Table 4).

The strength is almost 1.5–2 times higher for large fractions of 1.25–5 mm. Despite the fact that the particles of these fractions differ in size, they differ slightly in composition, as they are fragments of 1.25–5 mm cement-sand mortar 1:4. The strength increases due to a larger number of hydrating alite and belite particles, the CaO content increases to 16.63–18.65%, and SiO<sub>2</sub> decreases to 74.58–76.76% (Table 1), radiographs show an increase in C<sub>3</sub>S and C<sub>2</sub>S reflections (Table 4).



**Fig. 1.** Dependence of the hydration activity of powders on the size of the crushed fractions.

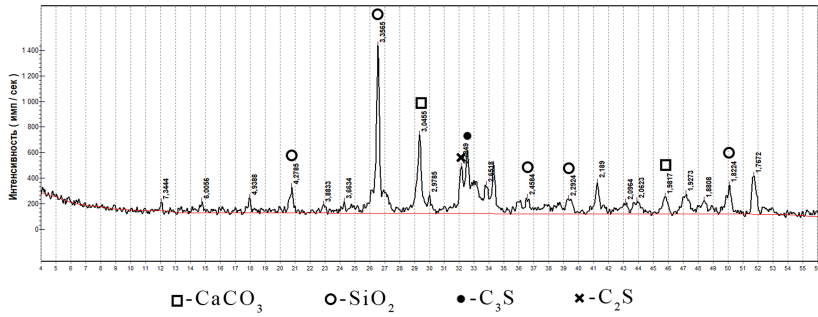
The pulverized fraction has maximum strength. The cement matrix of concrete during the crushing process breaks up into tiny particles, mainly in the form of dust-like fractions with a particle size less than 0.16 mm, which is practically no quartz sand, here there is the greatest amount of CaO (57.21%) and the lowest SiO<sub>2</sub> (29.28%) (Table 1). The destruction of cement stone, as a rule, occurs around non-hydrated clinker grains, along portlandite crystals, which have a tendency to split, and also passes through the pores [7, 8].

**Table 4.** Content of alite and belite by fractions.

2.5-5	1.25-2.5	0.63-1.25	0.315-0.63	0.16-0.315	<0.16

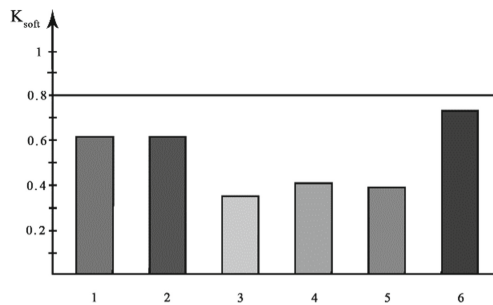
It is in the pulverized fraction that the maximum amount of non-hydrated clinker is found, as it can be seen from the intensity of reflections (Fig. 2) C<sub>3</sub>S (d = 2.776, 2.608, 2.606... Å) and C<sub>2</sub>S (d = 2.785, 2.748, 2.609... Å), which can reach 20–30% according to experts [9, 10]. But the amount of pulverized fraction is small, about 7%, the dust sticks to the particles of concrete scrap and is difficult to be filtered out, so the use of such dust in the future is not promising.

The hardening of the samples almost ends by 7 days due to the hydration of microdispersed non-hydrated alite and belite particles, and then by 14 and 28 days the strength increases slightly, mainly due to the continued slow hydration of belite particles.



**Fig. 2.** Radiograph of concrete scrap fraction <0.16 mm.

When water is saturated, the samples lose their strength sharply, as the coagulation bonds in the aqueous medium weaken quickly. Water resistance is provided by crystallization bonds between calcium hydrosilicates in the forming matrix, but their proportion is very small. Samples of cement stone from finely ground fractions of concrete scrap are characterized by a low softening coefficient – less than 0.8, which refers to the material as non-water resistant (Fig. 3). The water resistance of hardened samples varies according to their hydration activity. Minimum water resistance in samples of low-strength cement stone from small fractions ( $K_{\text{sof}} = 0.3\text{--}0.4$ ), in the structure of which there is a predominance of coagulation bonds. In stronger cement stone samples from crushed large fractions, the softening coefficient increases to  $K_{\text{sof}} = 0.5\text{--}0.6$ , as the proportion of chemical bonds that provide water resistance increases. The highest softening coefficient  $K_{\text{sof}} = 0.76$  is for the strongest cement stone from the pulverized fraction containing the largest amount of alite and belite, stability in the aqueous medium is provided by chemical bonds between the formed particles of calcium hydrosilicates.



**Fig. 3.** Water resistance of cement stone samples from fine fractions of concrete scrap.

Powdered materials obtained by grinding various fractions of 3D-printed concrete scrap have weak binding properties. With water saturation of the solidified material, the strength is significantly reduced, which indicates the predominance of coagulation bonds over crystallization ones. Coagulation bonds significantly weaken when wet, and the strength in the wet state is determined by more stable chemical bonds. Thus, the use

of crushed concrete scrap as a binder, without additional measures to increase hydraulic activity is impractical.

## 4 Conclusion

The composition and properties of various fractions obtained by crushing concrete scrap of 3D additive production, including 20% of the binder part and 80% of very fine quartz sand, are studied. All fractions crushed to the specific surface of ordinary cement have different ability to hydration hardening. It was found that the compressive strength of samples prepared from powders obtained by grinding the largest fractions (2.5–5 and 1.25–2.5 mm) is 1.5–2 times higher than that of samples from small fractions (0.16–0.315, 0.315–0.63 and 0.63–1.25 mm), which is due to the increased content of alite and belite in them. The best ability to hydration hardening was shown by the pulverized fraction consisting mainly of fine particles of the cement matrix of concrete with the maximum content of under-hydrated particles of alite and belite. The water resistance of cement stone samples varies depending on the hydration capacity of the powdered material fractions. Thus, the use of binders from crushed concrete scrap requires additional measures to increase strength and water resistance.


**Acknowledgements.** This work was realized in the framework of the Program of flagship university development on the base of the Belgorod State Technological University named after V.G. Shukhov, using equipment of High Technology Center at BSTU named after V.G. Shukhov.

## References

1. Lesovik, R.V., Tolypina, N.M., Alani, A.A., Jasim, A.S.J.: Composite binder on the basis of concrete scrap. In: *Lecture Notes in Civil Engineering*, vol. 95, pp. 307–312 (2020)
2. Ahmed, A.A.A.: Theoretical aspects of using fragments of destroyed buildings and structures of Iraq. In: *IOP Conference Series: Materials Science and Engineering*, vol. 945, p. 012039 (2020)
3. Klyuev, S.V., Klyuev, A.V., Shorstova, E.S.: Fiber concrete for 3-D additive technologies. *Mater. Sci. Forum* **974**, 367–372 (2019)
4. Lesovik, R.V., Klyuyev, S.V., Klyuyev, A.V., Ntrebenko, A.V., Kalashnikov, N.V.: Fiber concrete on composite knitting and industrial sand KMA for bent designs. *World Appl. Sci. J.* **30**(8), 964–969 (2014)
5. Bazhenov, Yu.M., Demyanova, B.C., Kalashnikov, V.I.: *Modified high-quality concrete*. Publishing House Of the Association of Construction Universities, Moscow (2006)
6. Kenai, S., Debieb, F.: Caraceterisation de la durability des betons recycles a base de gros et fins granulates de briques et de betoncjncasses. *Mater. And Struct.* **44**(4), 815–824 (2011)
7. Bochenek, A., Prokopski, G.: Badania Wplywu Stosunku Wodno-Cementowegona Mikromechanism Pecania Betonu Zwyklego. *Arch. Inz. Lad.* **2**, 261–270 (1988)
8. Struble, L.J., Stutzman, P.E., Fuller, E.R.: Microstructural aspects of the fracture of hardened cement paste. *J. Am. Ceram. Soc.* **12**, 2295–2299 (1989)
9. Rakhimbaev, Sh.M., Tolypina, N.M., Khakhaleva, E.N.: Resistance of hydration hardening materials on concrete scrap aggregate. *Bull. BSTU Named After V.G. Shukhov* **7**, 6–9 (2017)
10. Tolypina, N.M.: To the question about the interaction of cement matrix with placeholders. *Mod. High Technol.* **6**(1), 81–85 (2016)



# Study of Geological Setting of Naftalan-Northern Naftalan Area by Use of Attribute Analysis of 3D Seismic Data

M. A. Aghayeva<sup>(✉)</sup> 

Azerbaijan State Oil and Industry University, Baku AZ1010, Azerbaijan

**Abstract.** The paper is devoted to use of attribute analysis of 3D seismic data to more detailed study of geologic and tectonic setting of Naftalan-Northern Naftalan area of Ganja oil and gas region. For this, several attributes such as RMS amplitude, Acoustic relative impedance, Envelope have been calculated and analyzed. Aim of the study consists in selection of more effective attributes for identification and tracing of faults of various amplitude and disjunctive dislocations. In addition, the paper gives information about Naftalan field considered as the oldest brachianticline type field in Azerbaijan. The history of geological and geophysical studies covered the field is considered in brief. It has been noted in particular that two types of oil are extracted from the field: heavy oil with curative effect and light oil of commercial value. The aim of the study consisted in more detailed research on geological setting of the field in order to identify the intervals and zones of accumulation of light oil. The study resulted in compiling of a structural map for top of the I horizon of Maykop.

**Keywords:** 3D seismic survey · Attribute analysis · Disjunctive dislocation · I Horizon of Maykop · Vertical seismic sections (time and depth sections) · Naftalan-Northern Naftalan area

## 1 Introduction

For the last years, perspectives of the most oil and gas regions of Azerbaijan are tied to non-anticline traps of various genesis and morphology. Currently in the most oil and gas provinces the significant increase of share of non-anticline traps of origin related to faults presence and replacement of reservoirs by compacted rocks, etc. is observed [1].

Despite that seismic survey has a major role as a survey tool for exploration of both anticline and non-anticline traps, the decrease in geological efficiency of the tool is observed due to smaller sizes of the studied structure and poor lithological contrast. Limited application of seismic survey data for ultra deep drilling proceeds from resolution capability not high enough and due to this, the non-anticline traps, disjunctive dislocations, faults, faults of small amplitude in particular, are missed in most cases while exploration drilling [2, 3].

Naftalan-Northern Naftalan area of Ganja oil and gas region is under long-term production and its geological setting is sufficiently studied, however due to complex seismic

wave pattern the most portions of the field have not been studied enough. Today the interest to study this area is due to location here of one of the most ancient brachianticline type fields of Azerbaijan such as Naftalan field, the good infrastructure and ultra deep burial of major oil and gas targets [4].

The study area is located in foothill zone of the Small Caucasus, in Goranboy region to the south from Goran railway station. Terter water channel and Injichay river are in the south-east and Goranchay river is in the west, north-west. The area is under administration of Goranboy region and Naftalan city.

Geological setting of the area has been studied by use of geophysical tools, structural mapping, exploration and deep drilling data. The area has been covered by geological surveys at various time periods.

Natural oil shows in Naftalan area are observed from ancient times. In the XIII century the reknown Italian explorer Marco Polo wrote about curative effect for skin diseases of the oil named as “naphtha”. The area has been covered by geological studies since the end of XIX century [5]. 140 wells have been drilled in the field through the period of 1873–2003.

Oil and gas presence in the area is related in general to reservoirs of Maykop across the study area and nearby oil fields (Terter, Naftalan, Gazanbulag, Aghdere). Oil and gas perspectives in the area are attributed to Maykop, Eocene and Upper Cretaceous [6, 7] (Fig. 1).

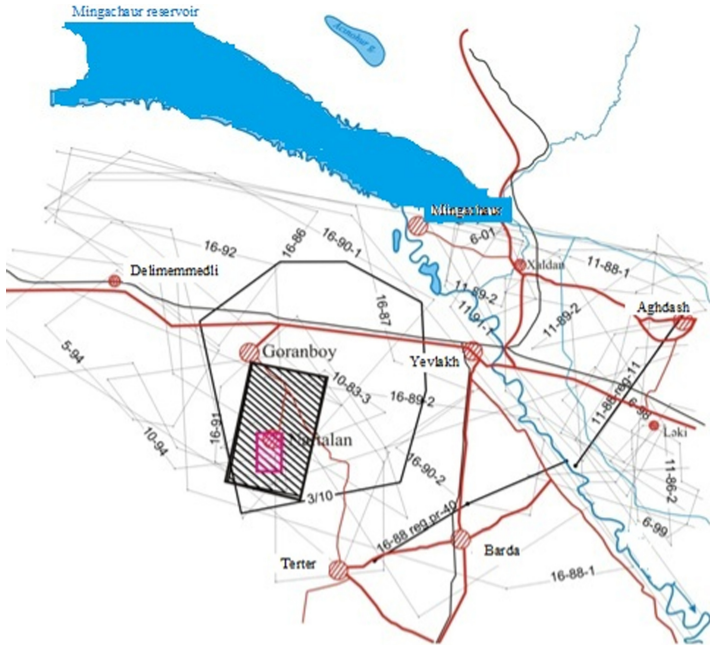


Fig. 1. General scheme of the study area.

The study area is located in the uplift zone in the front of Small Caucasus and embraces structures of Naftalan, Northern Naftalan and Godekboz.

**Naftalan structure** is the asymmetric brachianticline of submeridional direction buried over Maykop and characterized by steep (40–45°) western and relatively gentle (15–25°) eastern flanks.

**Northern Naftalan uplift** tectonically is the asymmetric brachianticline of submeridional direction. The northern pericline is separated from Godekboz structure by the narrow and shallow saddle.

**Godekboz structure** tectonically is brachianticline of submeridional direction with small redirection to the north-west.

## 2 Methods and Materials

Geological setting, the form and extensions of Naftalan structure have been studied partially in 2012 by use of 3D seismic data. Acquired data displayed that the structure is asymmetric anticlinal fold in the south-east trend. Geological setting of the area is featured by disjunctive dislocations, erosion surfaces, structural unconformities, etc. evidencing complicated deep seismogeological environment in the area.

It can be seen from sections that the study area has been complicated by a number of faults. Seismic records within the fault zone are chaotic and tracing is rather conditional.

To avoid this complication the several attributes – RMS amplitude, Acoustic Relative Impedance and Envelope attributes were calculated and sections of calculated attributes were analyzed. Seismic wavefield observed in these sections were analyzed in detail in order to research capability of 3D seismic survey, the attribute analysis in particular, used to study geological setting and tectonics of the area [8, 9].

It has been mentioned that geological setting, the form and extensions of Naftalan field were partially studied in 2012 by use of 3D seismic data. Some cross and longitudinal sections of 3D seismic cube derived for the area are considered as satisfactory and their analysis allows to infer the complex seismic wave pattern across the area.

In time and depth sections an interval featuring approximately the I horizon of Maykop is observed. Here the synphase reflected wave fronts are represented by more regular dynamic properties and correlation across the area. In the central and north-east portions of Naftalan structure the wave pattern is featured by poor seismic record.

In the central part of the area the desirable wave image is deteriorated and this is related to presence of settlements and attenuation of shotpoints in these areas. Tracing of desirable waves is deteriorated from the central portion of the area towards its south. This is due to complicated geological setting (sharp change of the angle, disjunctive dislocations, etc.) and the relief of the area.

It can be observed from the sections that in the western part of the area the fault zone of large amplitude elongated along north-south line divides the area in two portions. In the western part due to the impact of the fault the seismic horizons are traced in deeper layers. In the major – the eastern part of the area the horizons are traced across wide area at shallow depths.

Complicated seismic record areas which are areas difficult for interpretation are observed on lines crossing the fault zones.



Figures 2 and 3 display good quality seismic record within 0–4500 ms zone and this interval has been selected for further processing and interpretation (the attribute analysis, in particular). Analysis of calculated attribute sections displayed the presence of structural elements (or targets) of various type and extensions. Analysis results are described below.

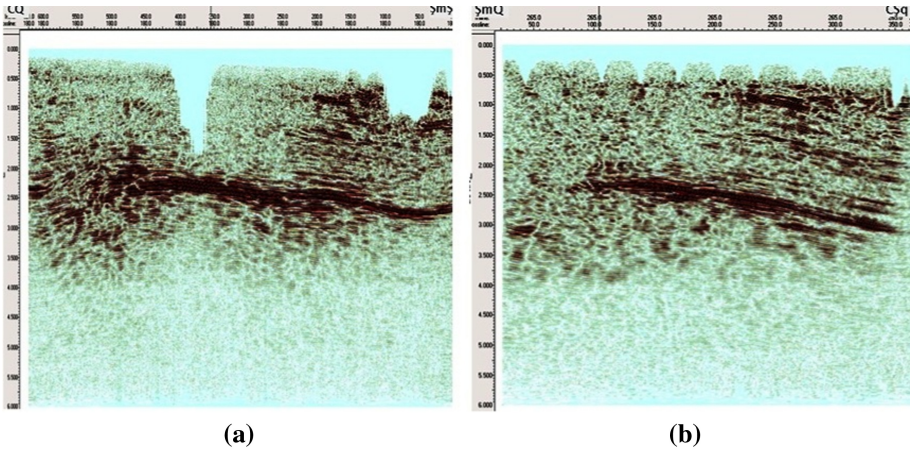


Fig. 2. a) Time section along longitudinal line. b) Time section along the cross line.

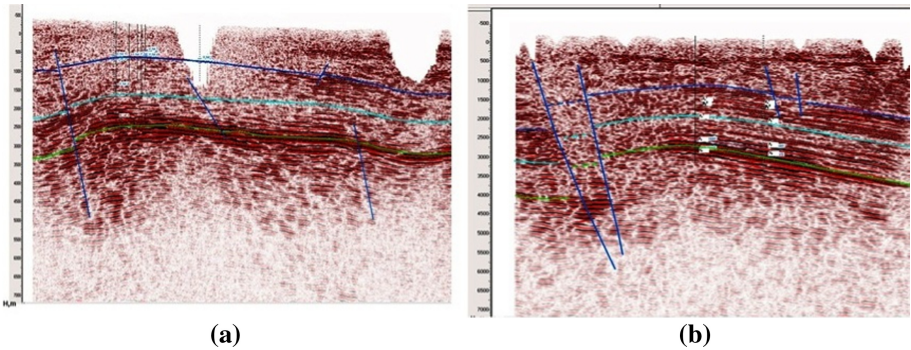
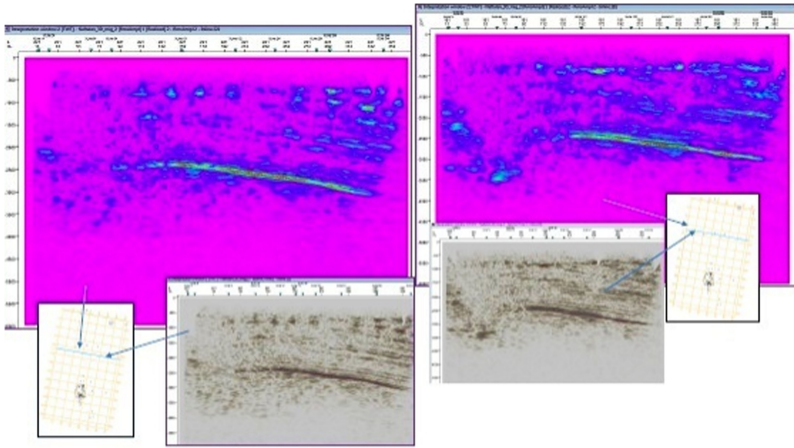


Fig. 3. a) Depth section along the longitudinal line b) Depth section along the cross line.

### 3 Results and Discussion

Analysis of **RMS** amplitude attribute for vertical (time and depth) sections of several lines crossing the portion of the area complicated by faults of various direction has been done. According to the results of attribute analysis it can be stated the interruptions in horizontal tracing of amplitudes in seismic records are due to the presence of faults. Several faults of large and small amplitude are clearly observed in various intervals

of derived section. For example, several large amplitude faults and small fractures are traced in **Maykop**.



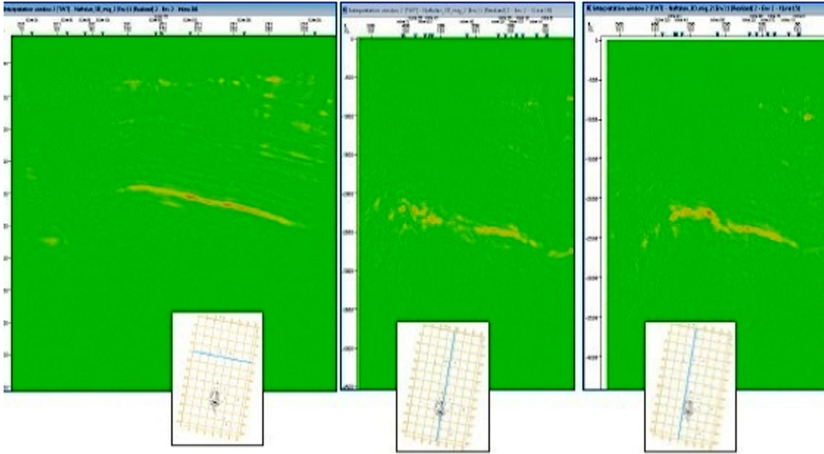
**Fig. 4.** Fragment of the attribute of RMS amplitude derived from 3D cube.

Derived sections confirm the complicated geological setting of the considered portion of the area. Faults are traced in sections of other lines as well (Fig. 4). As a result, it can be said that the structure is divided into the blocks by a large number of faults and the latter may play a sealing role while hydrocarbon migration.

Analysis results of attribute of **RMS amplitude** were further applied to interpretation of seismic horizon in the section, fault tracing and structural mapping. The attribute is also used as indicator of sand/clay ratio.

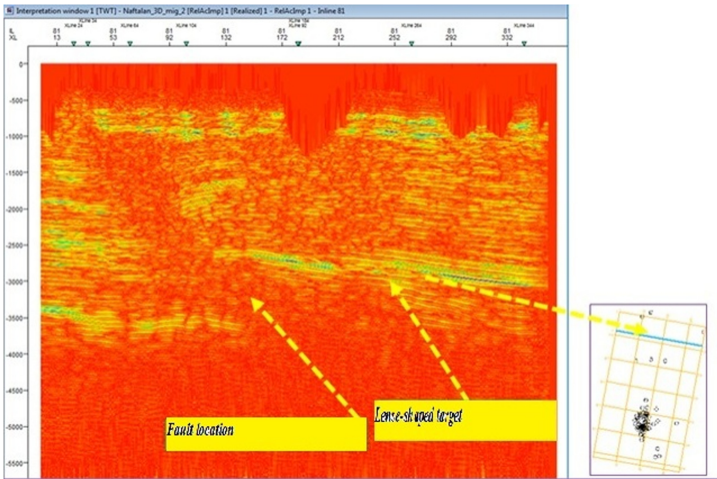
The **Envelope** attribute made it possible to trace poorly observed faults (faults of small amplitude, in particular) while continuous tracing of reflections for correlation of seismic horizons (Fig. 5). Analysis of sections of various directions in the study area allows to observe large amplitude faults in the west of the area and small amplitude faults in the east and south-east of the area.

Results of analysis of **RMS amplitude** v̄ **Envelope** attributes were applied while tracing of faults for geological studies.



**Fig. 5.** Fragment of Envelope attribute calculated by 3D cube.

Calculation of **Relative Acoustic impedance** attribute used to study various forms of rocks burial (cross layered, etc.), burial sequence of layers, unconformity surfaces and faults, enabled us to trace faults of higher amplitude in sections (at depths of approximately 2000 ms and below) (Fig. 6).



**Fig. 6.** Fragment of Relative Acoustic Impedance attribute calculated from 3D cube.

The attributes indicated above have been calculated separately and thoroughly analyzed. Finally, analysis of sections derived from attributes made it possible to clarify geological and tectonic setting for the top of horizon I of Maykop in the study area (Fig. 7).

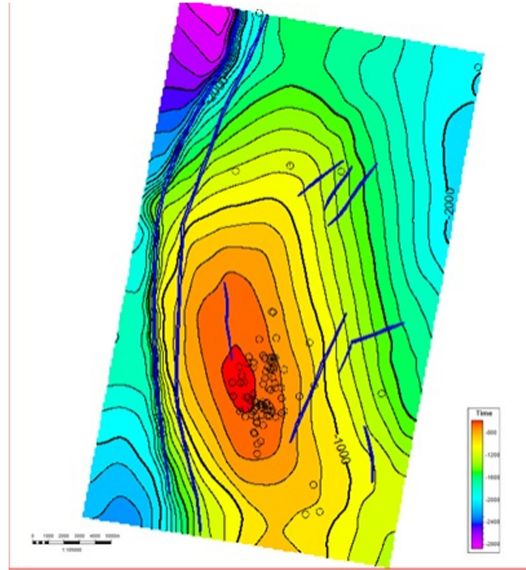


Fig. 7. Structural map for the top of horizon I of Maykop.

## 4 Conclusion

1. Based on 3D seismic data the seismic attributes - **RMS amplitude, Envelope and Relative Acoustic Impedance attributes** have been calculated for horizon I of Maykop.
2. As a result of analysis of various attribute sections it has been made clear that more universal and informative attributes such as **RMS amplitude, Envelope** can be used for identification and tracing of faults, while in some cases the **Relative Acoustic Impedance** attribute can be used for reliable interpretation of acquired data.
3. Applying attribute analysis the geological and tectonic setting of the study area has been studied in more detail and the structural map for top of horizon I of Maykop has been drawn.

## References

1. Ahmedov, T.R.: Geological efficiency of seismic survey while studies of various type non-anticline traps of Azerbaijan. *Newsl. Ural State Min. Univ.* **3**(43), 41–45 (2016)
2. Voskresenskiy, Yu.N.: *Field geophysics*. Nedra M. (2010)
3. Sheriff, R., Geldart, L.: *Seismic survey. Processing and interpretation of data*. Edition under supervision of A.V. Kalinin. M. Mir 400 (1987)
4. Ahmedov, T.R., Aghayeva, M.A.: Study of maykop deposits porosity across Naftalan field of Azerbaijan by integration of well log data and data of attribute analysis of seismic wave field. *Vect. Geosci.* **3**(1), 15–23 (2020)

5. Mamedov, Z.S., Miriyev, G.M.: Perspectives of Naftalan field development. *Azerbaijan Oil Ind.* **2**, 23–28 (2009)
6. Alizade, A.A., Ahmedov, G.A., Ahmedov, A.M., Zeynalov, M.M.: Geology of oil and gas fields of Azerbaijan. *M. Nedra*, p. 392 (1966)
7. Rakhmanov, R.R.: Regularities in evolution and distribution of oil and gas deposits in Mesozoic and Ceinzoic deposits of Yevlakh-Agjabadi trough, *Teknur. Baku*, p. 185 (2007)
8. Chopra, S., Marfurt, K.J.: Seismic attributes for prospect identification and reservoir characterization: *SEG. Geophys. Dev. Ser.* **11**, 464 (2007)
9. Kirilov, A.S., Zakrevskiy, K.Ye.: Practice of seismic interpretation by PETREL, Moscow, p. 284 (2014)



# The Study of the Dynamics of Flotation Agent Decomposition in a Tailings Dump

A. I. Gorodov<sup>(✉)</sup> , N. A. Shapovalov , R. G. Shevtsova , and A. A. Krainiy 

Department of Theoretical and Applied Chemistry, Belgorod State Technological University  
Named After V.G. Shukhov, Kostyukov Street, 46, Belgorod 308012, Russia

**Abstract.** Recently, waste from flotation enrichment of ferruginous quartzites has been widely used to produce building materials for various purposes. A special feature of using this type of waste is the modifying effect of the adsorbed flotation agent. As a rule, flotation reagents based on amino- and diaminoesters have insignificant desorption, which practically excludes their accumulation in the water of the tailings dump. However, with prolonged presence of aminoesters in water, not only the formation of organic bases, but also their hydrolytic cleavage is possible. This may lead to a weakening of the modifying effect of the flotation agent on the properties of the binding compositions. For 1.1-aminoesters, the hydrolysis process is very fast. Hydrolysis of 1.3-aminoesters, which include isodecyloxypropylamine (the main component of the flotation agent for additional enrichment of ferruginous quartzites) has not been studied. In this paper, changes in the chemical composition of the adsorption products of a flotation agent based on isodecyloxypropylamine (PA-14) on tailings during long-term storage in dumps are studied. To study the dynamics of decomposition of the flotation agent in the tailings dump, we used waste of flotation of ferruginous quartzites taken from the tailings dumps of the Mikhailovsky mining and processing plant. According to the results of research, it was found that the processes of chemical decomposition of isodecyloxypropylamine in industrial water are very slow. During long-term storage in a tailings dump, amino- and diaminoesters are partially hydrolyzed to form higher alcohols, amino alcohols, amines, and diamines.

**Keywords:** Flotation reagents · Flotation waste · Mining and processing plant · Flotation · Adsorption · The dynamics

## 1 Introduction

A significant reduction in the cost of construction is achieved through the use of local industrial waste in the production of construction materials [1–4].

Recently, studies of mining waste from the Kursk magnetic anomaly (KMA) deposits as filler for construction materials are very relevant [1–4]. Such research opens up the possibility of expanding the raw material base of various mineral additives and obtaining high-quality materials for construction on their basis. In particular, the possibility of using waste from flotation enrichment of ferruginous quartzites to produce low-water-demand binders (LWDB), fine-ground multicomponent cements (FGMC) and concretes

based on them is investigated; dry building mixes for various purposes (self-leveling floors, plaster solutions, repair compositions) and low-roasted loam-belite binder of hydrothermal hardening [5–11]. One of the important features of using waste from flotation enrichment of ferruginous quartzites is the modifying effect of the flotation agent adsorbed on their surface on the properties of binding compositions [12, 13]. However, the degradation of adsorbed flotation reagents is possible in the tailing dump, which depends on their structure [14–16]. This may lead to a weakening of the modifying effect of the flotation agent on the properties of the binding compositions.

In this paper, changes in the chemical composition of the adsorption products of a flotation agent based on isodecyloxypropylamine (PA-14) on tailings during long-term storage in a tailings storage facility are studied.

## 2 Materials and Methods

### 2.1 Materials

To study the dynamics of decomposition of the flotation agent in the tailings dump, we used waste flotation of ferruginous quartzites taken from the tailings dumps of the Mikhailovsky mining and processing plant (MMPP). Waste samples at MMPP were collected from beach areas of tailings dumps. Laboratory samples were taken from the average sample for research by quartering.

The bulk and true densities of flotation waste are  $1.46 \text{ g/cm}^3$  and  $2.53 \text{ g/cm}^3$ , respectively.

The chemical composition of ferrous quartzite flotation waste is shown in Table 1.

The object of research is the flotation agent PA-14 (TOMAH PRODUCTS ING, USA), which is currently used for flotation of hematite and magnetite concentrate. The chemical composition of the flotation agent consists of an aminoester (ethyramine), 3-(isodecyloxy)propylamine-1. Physical properties: light yellow liquid with a characteristic ammonia smell for amines, density  $\sim 0.851 \text{ g/cm}^3$ , insoluble in water. To increase the solubility, PA-14 was partially neutralized with acetic acid. The mass fraction of isodecyloxypropylamine acetate in the neutralized product is 25–30%.

### 2.2 Methods

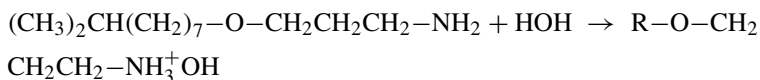
To study the hydrolysis of isodecyloxypropylamine in process water in the presence of tailings, the following was added to the test tube: 50 ml of process water, 1 g of waste from flotation re-enrichment of ferruginous quartzites, and 1.0 g of PA-14 flotation agent. The mixture was actively mixed for 5 h. We used the Fourier-IR method on a vertex 70 spectrometer manufactured by Bruker Optics. The survey was performed in the mid-infrared range from  $370$  to  $4000 \text{ cm}^{-1}$  using the OPUS software.

**Table 1.** Chemical composition of flotation waste.

Material ID	SiO <sub>2</sub>	Al <sub>2</sub> O <sub>3</sub>	Fe <sub>2</sub> O <sub>3</sub>	MgO	CaO	Na <sub>2</sub> O	K <sub>2</sub> O	SO <sub>3</sub>	CO <sub>2</sub>	ect
%	65–70	0.1–0.5	16–20	2.5–3.5	0.9–1.5	0.3–0.5	1–2.5	0.1–0.2	0.1–0.2	0.2

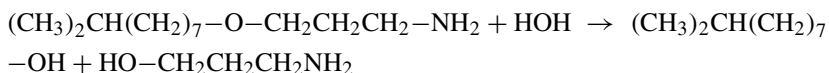
### 3 Results

According to the literature, it is known that water interacts with aliphatic amines, and consequently with amino- and diaminoesters to form organic bases. The interaction of aminoesters with water leads to the creation of an alkaline environment. The longer the hydrocarbon radical, the greater the electron density is forced on the nitrogen. As a result, the interaction of isodecyloxypropylamine creates a high alkalinity of the medium.



The reaction of aminoesters with water does not lead to degradation of the aminoester, as its structure is preserved.

If aminoesters are found in water for a long time, not only the formation of organic bases, but also their hydrolytic cleavage is possible. For 1.1-aminoesters, the hydrolysis process is very fast. Hydrolysis of 1.3-aminoesters, which include isodecyloxypropylamine, has not been studied. Theoretically hydrolysis should take place and be described by the reaction equation:



The reaction products are the highest limit alcohol (isodecyl) and the lowest amino alcohol (aminopropanol).

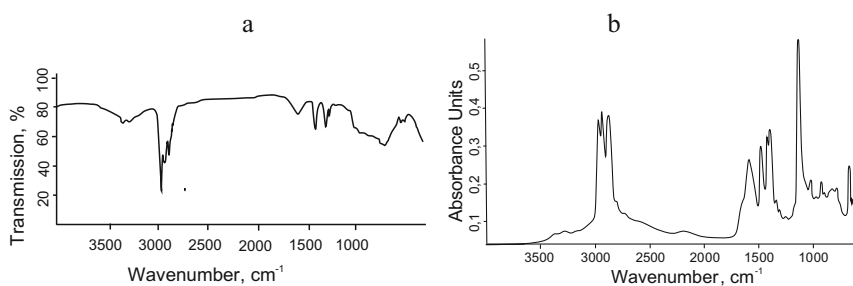
Visual changes in the flotation agent PA-14 as a result of long-term storage (for 3 years) in water at a temperature of 18–25 °C showed the following: the volume of the solution decreased, flotation waste was located at the bottom of the test tube, the liquid above the waste was divided into three layers: the upper orange-yellow color, the middle light yellow color, and the lower colorless (slight turbidity). On the basis of the coloring layers (the flotation reagent PA-14 in the beginning of the experiment had a bright yellow color) we made assumption that the upper layer is a solution of water in the flotation reagent, PA-14, the middle layer is the solution of a flotation reagent in water and the lower layer is also the solution of a flotation reagent in water, but with much lower concentrations. Isodecyloxypropylamine was partially oxidized, which explains the orange-yellow color of the upper layer.

A weak amine smell was preserved (less expressed than in the case of the initial flotation agent), the pH of the upper layer was 8.0, and the pH of the initial flotation agent was 10. The refractive index of the upper layer is 1.4510, the refractive index of



the initial flotation agent is 1.4644. The refractive index decreased, which indicates the possible presence of water, as water has a refractive index of 1.3330.

IR spectra of the initial flotation agent PA-14 (aliphatic aminoester) and all three layers were taken. For comparison, the spectrum of individual primary aliphatic amidautbutylamine (Fig. 1a) was removed, as it contains a branched radical, as well as the radical of the aminoester - the main component of the PA-14 flotation reagent. The spectrum of an individual primary amine should show strong, medium-strength, weak, narrow and wide bands of valence and strain vibrations. Valence vibrations **N-H**:  $3347\text{ cm}^{-1}$ , asymmetric **NH<sub>2</sub>**;  $3285\text{ cm}^{-1}$ , symmetrical **NH<sub>2</sub>** (overlap). Valence vibrations **C-H**:  $3000\text{--}2850\text{ cm}^{-1}$  **CH<sub>3</sub>**, **CH<sub>2</sub>**. Deformation vibrations **N-H**:  $1590\text{ cm}^{-1}$ , **NH<sub>2</sub>** (shear). Deformation vibrations **C-H**:  $1457\text{ cm}^{-1}$  **CH<sub>3</sub>** (shear);  $1375\text{--}1348\text{ cm}^{-1}$ , **CH<sub>3</sub>CH<sub>2</sub>**. **Nitrogen**:  $1200\text{--}800\text{ cm}^{-1}$ , valence **C-N** and rolling **N-H** (for a pure sample), mostly rolling **N-H**.



**Fig. 1.** IR-spectrum of a) Deut-butylamine and b) PA-14.

The formula of the aminoester is  $(\text{CH}_3)_2\text{CH}(\text{CH}_2)_7\text{O}(\text{CH}_2)_3\text{NH}_2$ . The deut-butylamine radical is smaller than the isodecyl radical, so some band shift is expected. In addition, the aminoester molecule has an oxygen bridge, which is typical for a simple ether bond. The presence of an ether bond should also be reflected by the appearance of bands in the infrared spectrum of the aminoester.

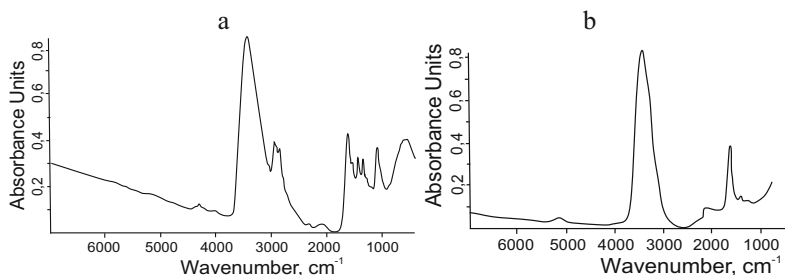
Shown in Fig. 1b, the range of flotation reagent PA-14 is largely the same spectrum of deut-butyl (should only note that in Fig. 1a the transmission spectrum of deut-butylamine is given, and in Fig. 1b the absorption spectrum of a flotation reagent PA-14). It is enough to compare the area of  $3500\text{--}3000\text{ cm}^{-1}$ , where two bands correspond to the valence vibrations of N-H, and the area of  $3000\text{--}2850\text{ cm}^{-1}$  (the bands correspond to the valence vibrations of C-H). Further, up to the frequencies of  $1590\text{ cm}^{-1}$ , there are no absorption (transmission) bands. Then the absorption bands of the PA-14 flotation agent are slightly shifted relative to the bands observed in the spectrum of deut-butylamine.

The infrared spectrum in the  $1200\text{--}800\text{ cm}^{-1}$  area of deut-butylamine differs significantly from the infrared spectrum of the PA-14 flotation reagent. A narrow very strong band  $1110.36\text{ cm}^{-1}$  appears - the characteristic frequency of  $\text{CH}_2\text{-O-CH}_2$ . This is how a simple ether bond can manifest itself, which is present in the aminoester of the flotation agent PA-14, but is naturally absent in deut-butylamine. The C-N valence vibrations and the N-H rolling vibrations are weak and are shielded by a very strong absorption band characteristic of simple ethers.

Thus, the aminoester of the flotation agent PA-14 has all the absorption bands characteristic of primary aliphatic amines and the absorption band characteristic of simple esters ( $1150\text{--}1060\text{ cm}^{-1}$ , p. s.).

Comparing the infrared spectrum of the upper layer of the emulsion (Fig. 2a) with the IR spectrum of PA-14, we can note the following: the nature of both spectra in the  $3000\text{--}1000\text{ cm}^{-1}$  area is identical. The spectra are characterized by the same set of absorption bands (transmittance) at equal frequencies (a slight shift in the absorption bands can be ignored). The bands corresponding to the valence vibrations C-H:  $3000\text{--}2850\text{ cm}^{-1}$   $\text{CH}_3$ ,  $\text{CH}_2$  and the deformation vibrations N-H:  $1590\text{ cm}^{-1}$ ,  $\text{NH}_2$  (shear) were preserved. There are bands of deformation vibrations C-H:  $1457\text{ cm}^{-1}$   $\text{CH}_3$  (shear);  $1375\text{--}1348\text{ cm}^{-1}$ ,  $\text{CH}_3$   $\text{CH}_2$ .

There are also major differences. Thus, the upper layer has a significant decrease in the height of the absorption band characteristic of  $\text{CH}_2\text{-O-CH}_2$  esters. This may indicate hydrolysis of the aminoester. Valence vibrations N-H:  $3347\text{ cm}^{-1}$ , asymmetric  $\text{NH}_2$ ;  $3285\text{ cm}^{-1}$ , symmetrical  $\text{NH}_2$  is absent from the upper layer spectrum.



**Fig. 2.** IR-spectrum of a) the top layer of the emulsion PA-14 and b) the middle layer of the emulsion PA-14.

But this can be explained not by the absence of an amino group, but by the valence vibrations of the OH group of water and the isodecyl alcohol  $(\text{CH}_3)_2\text{CH}(\text{CH}_2)_7\text{OH}$  formed as a result of hydrolysis of the aminoester. It should be noted that the process of hydrolysis of an aminoester at room temperature is a long process, so the initial aminoester is present simultaneously with the hydrolysis products, but its amount should decrease over time. The concentration of aminoester in the upper layer is quite understandable, as its density is less than that of water.

The aminoester is concentrated at the air-water interface. The hydrophobic radical is oriented to the air, while the  $\text{NH}_2$  polar group is directed to water and dissolved in it. As a result, the water surface is covered with a kind of “stockade” of aminoester molecules, forming a layer 0.1 nm or more thick. The surface tension of the water decreases. The number of aminoester molecules located at the air-water interface is determined by the size of the aminoester molecules and the area of the interface. Those aminoester molecules that could not concentrate at the air-water interface are freely distributed in the volume of water. Thus, the upper layer contains the maximum amount of aminoester that was not adsorbed on the tailings, water, and products of partial hydrolysis and

oxidation of the aminoester. This self-organization of aminoester molecules leads to less active evaporation of water over time than in the initial period.

The infrared spectra of the middle and lower layers are identical, so only the IR spectrum of the middle layer is shown (Fig. 2b). They differ significantly from the infrared spectrum of the upper layer. The bands corresponding to the valence vibrations **C-H**: 3000–2850  $\text{cm}^{-1}$  **CH<sub>3</sub>**, **CH<sub>2</sub>**, and the deformation vibrations **N-H**: 1590  $\text{cm}^{-1}$ , **NH<sub>2</sub>** (shear) disappeared. The relative intensity of the absorption band of deformation vibrations **C-H**: 1457  $\text{cm}^{-1}$  **CH<sub>3</sub>** (shear) can be characterized as weak; the absorption bands 1375–1348  $\text{cm}^{-1}$ , **CH<sub>3</sub>CH<sub>2</sub>** as very weak.

Stretching vibrations of **N-H**: 3347  $\text{cm}^{-1}$ , asymmetric **NH<sub>2</sub>**; 3285  $\text{cm}^{-1}$ , symmetric **NH<sub>2</sub>** on the spectrum of the middle and lower layers are absent. This can be explained either by the complete absence of aminoester in the middle and lower layers, or by its very low concentration. Therefore, these bands are shielded by bands of valence vibrations of the OH group of water and the isodecyl alcohol (**CH<sub>3</sub>)<sub>2</sub>CH(CH<sub>2</sub>)<sub>7</sub>OH** formed as a result of hydrolysis of the aminoester.

If the upper layer is characterized by a decrease in the intensity of the absorption band 1100  $\text{cm}^{-1}$ , then in the case of the middle and lower layers, the relative intensity of the absorption band 1100  $\text{cm}^{-1}$  can be characterized as very weak, which indicates an extremely low concentration of aminoester. The absorption band of 1600–1700  $\text{cm}^{-1}$  is due to the presence of water in the middle and lower layers in greater quantities than in the upper layer.

It should be noted that over time, the appearance of the test tubes practically did not change, which indicates a small influence of flotation enrichment tailings on the processes occurring in process water with the PA-14 flotation agent during long-term storage.

## 4 Conclusion

According to the conducted research, the processes of chemical decomposition of isodecyloxypropylamine in industrial water are very slow. During long-term storage in a tailings dump, amino and diaminoesters are partially hydrolyzed to form higher alcohols, amino alcohols, amines, and diamines. The higher alcohols formed because of hydrolysis (decyl, isodecyl, etc.) are safer than aminoesters. They have low volatility and, being surfactants, are concentrated at the water-air interface.

**Acknowledgments.** This work was realized under the support of the framework of the Program of flagship university development on the base of the Belgorod State Technological University named after V G Shukhov, using equipment of High Technology Center at BSTU named after V G Shukhov.

## References

1. Drozdyuk, T.A., Ayzenshtadt, A.M., Frolova, M.A., Rama, S.V.: Mineral wool composite with the use of saponite-containing mining industry waste. *Constr. Mater. Prod.* **3**(3), 21–27 (2020)

2. Ageeva, M.S.: On the use of industrial wastes in the production of binders. *Bull. BSTU Named After V. G. Shukhov* **9**, 58–62 (2016)
3. Zagorodnuk, L.H., Lesovik, V.S., Shkarin, A.V., Belikov, D.A., Kuprina, A.A.: Creating effective insulation solutions, taking into account the law of affinity structures in construction materials. *World Appl. Sci. J.* **24**(11), 1496–1502 (2013)
4. Lesovik, R.V.: The comprehensive use of tailings of wet magnetic separation of jaspellites. *Min. J.* **1**, 76–77 (2004)
5. Shapovalov, N.A., Tikunova, I.V., Zagorodnyuk, L.H., Bushuyeva, N.P., Shchekina, A.Yu., Panova, O.A.: Tailings from iron ore processing: a valuable feed for building material production: a monograph. *BSTU named after V.G. Shoukhov* (2014)
6. Shapovalov, N.A., Bushueva, N.P., Panova, O.A.: Low roasting cementitious matter of lime-belite components using flotation waste of residual dumps of wet magnetic separation at the mining and processing complex. *World Appl. Sci. J.* **25**(12), 1758–1762 (2013)
7. Varichev, A.V.: From ore recovery to metal production: the evolution of Mikhailovsky mining and processing plant from 2000 to 2010. *Min. J.* **7**, 6–9 (2006)
8. Shkarin, A.V., Zagorodnuk, L.H., Shchekina, A.J., Luginin, I.G.: Preparation of composite binders in different grinding units. *Bull. BSTU Named After Shukhov* **3**, 53–57 (2012)
9. Shapovalov, N.A., Zagorodnyuk, L.H., Tikunova, I.V., Shchekina, A.Y., Shirayev, O.I., Popov, D.Y., Gorodov, A.I.: Study of the use of waste iron ore flotation for blended cement. *Fundam. Res.* **10**, 1718–1723 (2013)
10. Shapovalov, N.A., Zagorodnyuk, L.H., Shchekina, A.J., Ageeva, M.S., Ivashova, O.V.: Microstructure of hydration product of cement with iron ore flotation tailings. *Bill. BSTU Named After V. G. Shoukhov* **5**, 57–63 (2013)
11. Shchekina, A.Yu., Mawuko, A.K., Cherkasov, R.A.: Research of colloid-chemical processes on the border of the phases section waste-floto reagent. *Vect. Geosci.* **2**(4), 5–8 (2019)
12. Shapovalov, N.A., Zagorodnyuk, L.H., Shchekina, A.Y., Gorodov, A.I.: Modified binders on the basis of flotation tailings. In: *IOP Conference Series: Materials Science and Engineering*, vol. 327, no. 3, p. 32050 (2018)
13. Shchekina, A.Y.: Influence of flotorea agent, in the composition of waste flotation, on the properties of bending compositions. *Bull. BSTU Named After V. G. Shukhov* **7**, 88–91 (2017)
14. Pogromsky, A.S., Anikanova, T.V.: The effect of long-term storage of electric steel smelting slags in dumps on their properties. *Constr. Mater. Prod.* **1**(1), 32–39 (2018)
15. Shachneva, E.Y.: Methods of sorption concentration of surface active substances. *Chem. Bull.* **1**(2), 24–30 (2018)
16. Ryzhakov, A.V.: Activation parameters of decomposition of nitrogen-containing organic compounds in natural water. *Environ. Chem.* **15**(4), 243–247 (2006)



# Method of Extrusion Granulation of Aggregates for the Preparation of Filling Mixtures

L. H. Zagorodnyuk<sup>(✉)</sup> , V. D. Ryzhikh , D. S. Makhortov , and D. A. Sumskey 

Belgorod State Technological University Named After V.G. Shukhov, Belgorod, Russia

**Abstract.** Underground mining technology is one of the most promising areas of mining. Optimization and cheapening of the production process of mining enterprises are important tasks for the scientific society. The use of technogenic waste, as well as unclaimed and substandard raw materials for the production of filling mixtures in all areas of the globe is an urgent problem of ecology and materials science. Research is being conducted in the direction of increasing energy efficiency and reducing the cost of technological production of filling mixtures for laying out the developed space. A number of works were carried out to obtain composite binders with different granulometric characteristics. As part of the research, extrusion granulation works were carried out on the basis of composite binders and quartz sands of different fractional compositions ( $\leq 0.16$  mm,  $\leq 0.315$  mm,  $\leq 0.63$  mm). 36 types of granulated aggregates with different component compositions were obtained. The partial replacement of fine quartz sands in the composition of the filling mixture with different types of granular aggregates was carried out. As a result, the most promising component compositions were identified and the economic and environmental efficiency of using certain granular aggregates as a large aggregate in filling complexes with a cement binder was proved.

**Keywords:** Filling mixtures · Portland cement · Composite binders · Granulation · Granulated aggregates · Quartz sand

## 1 Introduction

The underground mining industry is one of the most promising industries that needs active modernization and scientific and technical research in order to improve the technical and economic indicators of the production process. The technological growth and development of the mining industry, today, in the territory of the Russian Federation (RF) is at the stage of stagnation.

Currently, scientists are developing and optimizing the component compositions of filling mixtures that contribute to saving material, energy and financial resources [1–4]. In order to save financial resources, various mining enterprises using the underground mining system use local and technogenic raw materials in the production of filling mixtures. For the use of local cheap building materials and industrial waste, in most cases, individual development of composite compositions of filling mixtures and the arrangement or re-equipment of the production line is necessary, which requires significant financial investments.

A systematic urgent problem in the mines of the Russian Federation, using the technology of hardening laying, is the overspending of expensive Portland cement. Often, this overspend is due to the use of fine aggregates (fine quartz sands and industrial waste) in the component composition of filling mixtures, which reduce the physical and mechanical characteristics, and solidified filling masses.

Practice shows that the lack of large and small natural aggregates in different territorial areas slows down the development of the construction segment [5, 6].

Today, mining companies practically do not use inert fine aggregates in the composite compositions of filling mixtures. It should be noted that the use of quartz sand fractions less than 1 mm in concrete and filling mixtures is not regulated for the production of load-bearing building structures, as a result of which their storage reserves increase. Technological processes of agglomeration will help to get rid of substandard stocks of fine aggregates.

The use of technogenic waste in composite compositions of solutions and filling mixtures is an event aimed at creating a system of waste-free production with a consistent reduction of the negative impact of dumps of substandard raw materials on the ecological situation of the globe. Currently, there are a number of scientific studies [7–9] related to the granulation of technogenic waste and fine raw materials. It is noteworthy that to create cost-effective composite compositions of granular aggregates (GA), it is necessary to select the appropriate composite binders [10, 11].

The creation of effective composite filling mixtures with stable technological and physical-mechanical characteristics for the laying of the developed space is an important task for mining enterprises.

The problem of using unclaimed and substandard raw materials to create a hardening filling mass, with the possibility of implementation throughout the territory of the Russian Federation, while ensuring environmental protection measures is relevant.

## 2 Methods and Materials

The used raw materials are Portland cement (PC 500-D0-N), quartz sand (dispersion  $\leq 0.63$  mm  $\leq 0.315$  mm  $\leq 0.16$  mm).

Sifting of sand is carried out using standard laboratory sieves. Grinding of binders is carried out in a vortex jet mill VJM-01 [10]. Particle size distribution studies are being carried out on a laser analyzer FRITTSCH Analysette 22 NanoTec. Quartz sand granulation is carried out in a portable Gemlux screw unit with a power of 3 kW. Physical and mechanical tests of cube samples are carried out according to Russian National Standard 10180-2012 on a hydraulic press PGM-50MG4.

The method of obtaining filling mixtures includes several stages:

1. Preparation of raw materials (sieving of quartz sand, grinding of composite binders in VJM-01). Before grinding, 10, 20, 30% of quartz sand was added to the PC 500-D0-N to obtain three types of composite binders. The symbol and decoding of compositional binder formulas are presented in Table 1.

**Table 1.** Component composition of composite binders obtained in VJM-01.

Component composition of binder	Code (designation)
PC 500-D0-N	PC
PC 500-D0-N – 90% + quartz sand – 10%	Cb-1
PC 500-D0-N – 80% + quartz sand – 20%	Cb-2
PC 500-D0-N – 70% + quartz sand – 30%	Cb-3

2. Extrusion granulation of quartz sands of different dispersion in the Gemlux screw unit. GA formulas are presented in Table 2. In the mixed mixture, according to the required formula, water is added. At the same time, the water-binding ratio in component compositions with 5% of the composite binder is – 3; with 10% – 1.8; with 15% – 1.4. The technological process of granulation is carried out by extrusion molding with pre-pressing of the water-saturated material in the working chamber of the Gemlux screw unit. The resulting GA gain strength for 28 days in air-wet conditions.

**Table 2.** Granular aggregate formulas.

Quartz sand fraction, mm	Type of binder			
	Cb-1	Cb-2	Cb-3	PC
0.16	0.16 + 5% Cb-1	0.16 + 5% Cb-2	0.16 + 5% Cb-3	0.16 + 5% PC
	0.16 + 10% Cb-1	0.16 + 10% Cb-2	0.16 + 10% Cb-3	0.16 + 10% PC
	0.16 + 15% Cb-1	0.16 + 15% Cb-2	0.16 + 15% Cb-3	0.16 + 15% PC
0.315	0.315 + 5% Cb-1	0.315 + 5% Cb-2	0.315 + 5% Cb-3	0.315 + 5% PC
	0.315 + 10% Cb-1	0.315 + 10% Cb-2	0.315 + 10% Cb-3	0.315 + 10% PC
	0.315 + 15% Cb-1	0.315 + 15% Cb-2	0.315 + 15% Cb-3	0.315 + 15% PC
0.63	0.63 + 5% Cb-1	0.63 + 5% Cb-2	0.63 + 5% Cb-3	0.63 + 5% PC
	0.63 + 10% Cb-1	0.63 + 10% Cb-2	0.63 + 10% Cb-3	0.63 + 10% PC
	0.63 + 15% Cb-1	0.63 + 15% Cb-2	0.63 + 15% Cb-3	0.63 + 15% PC

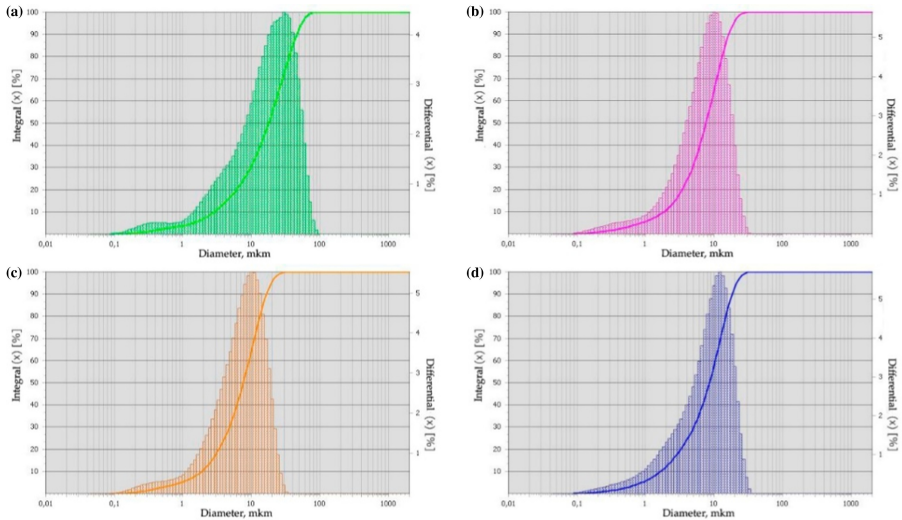
3. Mixing the components, forming the filling mixture and forming the sample cubes ( $3 \times 3 \times 3$  cm). The composite composition and the percentage of components in the compositions of the filling mixtures are presented in Table 3. After the strength set, physical and mechanical tests of the cube samples are performed on the PGM-50MG4 hydraulic press for 28 days.
4. Theoretical analysis of the results obtained and formulation of conclusions about the most effective form of GA for its use in the compositions of filling mixtures.

**Table 3.** Component composition of filling mixtures.

Type of filling mixture	Mass percent, %			
	PC	Quartz sand (fraction $\leq$ 0.315 mm)	Granular aggregate	Water
Without granular aggregates	30–35	30–35	–	30–40
With granular aggregates	20–25	10–20	40	20–25

### 3 Results and Discussion

As a result of grinding in VJM-01, 3 types of composite binders were obtained, the granulometric characteristics of which are shown in Fig. 1.

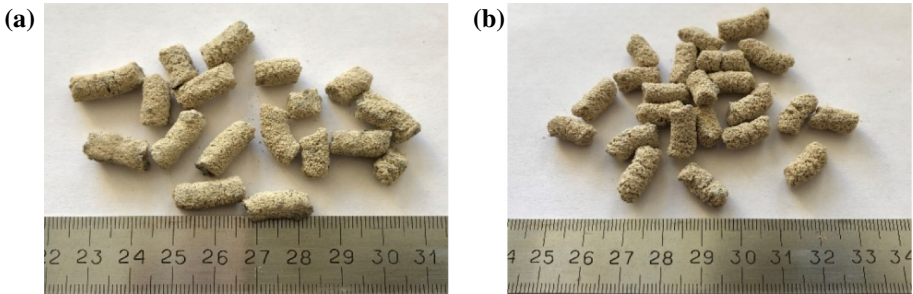


**Fig. 1.** Granulometric compositions of binders: PC (a), Cb-1 (b), Cb-2 (c), Cb-3 (d).

Analysis of granulometric curves of binders shows that after grinding in VJM-01 composite binders have increased dispersion characteristics than the original Portland cement PC 500-D0-N. According to the formula (Table 2), 36 types of GA of different density and porosity were produced by the extrusion method. The general view of the GA is shown in Fig. 2. Granulation is performed using three types of quartz sands of different dispersion. It is noted that with different dispersion of sand and the percentage of binder in the composition of GA, the physical and mechanical characteristics of the filling mixture will differ. Therefore, it is necessary and sufficient to identify the most rational composite compositions of granular aggregates for the purpose of their further refinement.



After the molding processes (according to the formulas specified in Table 3) and the strength of the samples-cubes  $3 \times 3 \times 3$  cm for 28 days, the proposed method provides for testing the compressive strength of the samples on a hydraulic press PGM-50MG4. As a result of testing the cube samples, the following values are obtained, presented in Table 4.



**Fig. 2.** Type of granular aggregates with linear dimensional units (millimeter) based on quartz sand fractions  $\leq 0.16$  mm (a),  $\leq 0.315$  mm (b).

The results of strength tests of cube samples indicate a positive effect of GA in the composition of the filling mixture. It is noted that the compressive strength of the samples-cubes with GA based on ground composite binders is higher than that of the samples-cubes with GA based on Portland cement. The interpretation of this fact is that the composite binder is characterized by high fineness of grinding, increased specific surface area and increased hydration activity. The rise of strength properties of samples-cubes with increasing the content of fractions of quartz sand in the GA from  $\leq 0.16$  mm to  $\leq 0.63$  mm and then adding a binder in GA from 5 to 15% is noted. It is noteworthy that the change in the strength characteristics of samples-cubes when replacing GA with different composite binders (from Cb-1 to Cb-3) in the composition of the filling mixture does not occur in a linear relationship. This phenomenon is explained by an increase in the percentage of quartz sand in the GA, as well as a decrease in the hydration activity of the binder Cb-3. The insertion of quartz sand more than 20% in composite binders for granulation of aggregates is impractical.

Based on the analysis of the results of strength tests of samples-cubes, it was found that GA with codes  $0.63 + 10\% \text{ Cb-2} - 6.26$  MPa and  $0.63 + 15\% \text{ Cb-2} - 6.75$  MPa are promising for use in the component composition of filling mixtures. Efficiency the use of GA in the component composition of the filling mixture is determined by the saving of expensive binders up to 10–15% with a parallel increase in strength indicators up to 6.82 MPa.

**Table 4.** Physical and mechanical characteristics of samples-cubes from the filling mixture under compression.

No. of composition	Code of sample-cube	Strength of samples-cubes, $R_{\text{compr}}$ , MPa		
		№ 1	№ 2	№ 3
	Without granular aggregates			
1	PC	5.54	6.1	6.2
	With granular aggregates			
2	0.16 + 5%Cb-1	2.84	2.65	3.01
3	0.16 + 10% Cb-1	3.54	3.32	3.63
4	0.16 + 15% Cb-1	4.76	4.32	4.88
5	0.315 + 5% Cb-1	3.92	4.21	4.32
6	0.315 + 10% Cb-1	4.64	5.21	5.04
7	0.315 + 15% Cb-1	4.36	4.53	4.55
8	0.63 + 5% Cb-1	3.92	3.86	3.69
9	0.63 + 10% Cb-1	5.32	4.92	5.41
10	0.63 + 15% Cb-1	4.89	4.98	5.05
11	0.16 + 5% Cb-2	3.18	3.01	2.94
12	0.16 + 10% Cb-2	3.43	3.84	3.32
13	0.16 + 15% Cb-2	4.32	4.18	4.25
14	0.315 + 5% Cb-2	3.43	3.51	3.39
15	0.315 + 10% Cb-2	3.85	3.79	3.94
16	0.315 + 15% Cb-2	4.21	4.23	4.65
17	0.63 + 5% Cb-2	4.35	4.62	4.44
18	0.63 + 10% Cb-2	5.96	6.43	6.39
19	0.63 + 15% Cb-2	6.72	6.71	6.82
20	0.16 + 5% Cb-3	3.29	3.11	3.51
21	0.16 + 10% Cb-3	3.45	3.08	3.39
22	0.16 + 15% Cb-3	4.23	4.25	3.96
23	0.315 + 5% Cb-3	4.03	4.08	3.15
24	0.315 + 10% Cb-3	3.76	3.43	3.84
25	0.315 + 15% Cb-3	5.16	5.37	5.10
26	0.63 + 5% Cb-3	3.97	3.43	3.86
27	0.63 + 10% Cb-3	4.99	5.11	5.09
28	0.63 + 15% Cb-3	5.72	5.90	5.88
29	0.16 + 5%PC	4.31	3.93	4.10
30	0.16 + 10%PC	4.43	4.57	4.32
31	0.16 + 15%PC	4.31	4.94	4.78
32	0.315 + 5%PC	3.21	3.50	3.42
33	0.315 + 10%PC	4.63	4.21	4.51
34	0.315 + 15%PC	4.55	3.91	4.72
35	0.63 + 5%PC	3.11	3.52	3.45
36	0.63 + 10%PC	4.25	4.31	4.33
37	0.63 + 15%PC	4.58	4.45	4.32

## 4 Conclusion

The technical, economic and environmental components in the innovative world will always be in the area of extreme interest of a prudent society. In this regard, analyzing the results of research, it can be argued that the resulting granular aggregates with codes 0.63 + 10% Cb-2; 0.63 + 15% Cb-2 are an effective replacement for substandard fine quartz sands. Production of granular aggregates with extrusion method allows to reduce the expensive energy-intensive Portland cement in the blend composition of filling mixtures, and authorizes the reduction of open dumps of substandard fine sands over large areas of the globe that have a positive impact on the ecological environment.

**Acknowledgements.** The work is realized in the framework of the RFBR support according to the research project № 18-29-24113; in the framework of the Program of flagship university development on the base of the Belgorod State Technological University named after V.G. Shukhov, using equipment of High Technology Center at BSTU named after V.G. Shukhov.

## References

1. Wu, J., Feng, M., Xu, J., Qiu, P., Wang, Y., Han, G.: Particle size distribution of cemented rockfill effects on strata stability in filling mining. *Minerals* **8**(9), 407 (2018). <https://doi.org/10.3390/min8090407>
2. Zhao, Y., Soltani, A., Taheri, A., Karakus, M., Deng, A.: Application of slag-cement and fly ash for strength development in cemented paste backfills. *Minerals* **9**(1), 22 (2018). <https://doi.org/10.3390/min9010022>
3. Ageeva, M., Sopin, M., Lesovik, R., Bogusevich, G.: The development of compositions of backfilling mixtures. *Bull. Belgorod State Technol. Univ. Named After V G Shukhov* **1**(12), 31–34 (2016)
4. Bur'yanov, A., Gal'ceva, N., Grunina, I.: The use of pyrometallurgical industry wastes in the production of materials for laying excavation. *Bull. BSTU Named After V.G. Shukhov* **4**, 21–26 (2019)
5. Cantero, B., Bravo, M., de Brito, J., del Bosque, I.F.S., Medina, C.: Thermal performance of concrete with recycled concrete powder as partial cement replacement and recycled CDW aggregate. *Appl. Sci.* **10**(13), 4540 (2020)
6. Thomas, C., Cimentada, A.I., Cantero, B., del Bosque, I.F.S., Polanco, J.A.: Industrial low-clinker precast elements using recycled aggregates. *Appl. Sci.* **10**(19), 6655 (2020). <https://doi.org/10.3390/app10196655>
7. Pichór, W., Kamiński, A., Szoldra, P., Frąc, M.: Lightweight cement mortars with granulated foam glass and waste perlite addition. *Adv. Civ. Eng.* **2019**, 1–9 (2019). <https://doi.org/10.1155/2019/1705490>
8. Korobanova, E., Onishchuk, V., Doroganov, V., Evtushenko, E.: The study of the process of granulation artificial ceramic binder based on alumina. *Bull. BSTU named after V.G. Shukhov* **2**, 141–146 (2017)
9. Montanari, D., Agostini, A., Bonini, M., Corti, G.: The use of empirical methods for testing granular materials in analogue modelling. *Materials* **10**(6), 635 (2017)
10. Zagorodnyuk, L.H., Lesovik, V.S., Sums koy, D.A., Elistratkin, M.Y., Makhortov, D.S.: Peculiarities of binding composition production in vortex jet mill. *IOP Conf. Ser.: Mater. Sci. Eng.* **327**, (2018). <https://doi.org/10.1088/1757-899X/327/4/042128>
11. Zagorodnyuk, L.H., Koryakina, A.A., Sevostyanova, K.I., Khaheleva, A.A.: Heat insulating composite mixtures with technogenic materials. *J. Phys: Conf. Ser.* **1066**, (2018). <https://doi.org/10.1088/1742-6596/1066/1/012011>



# Refinement of the Structure of the Eastern Govsan Area Using a New Method of Seismic Inversion and a Lithological Model of the Zyxh Field of Azerbaijan Based on 3D and GRW Seismic Data

T. R. Ahmedov<sup>1</sup>  and K. A. Kurochkina<sup>2</sup>  

<sup>1</sup> Azerbaijan State Oil and Industry University, Baku, Azerbaijan  
akhmedov.tofik@bk.ru

<sup>2</sup> Belgorod State Technological University Named After V.G. Shoukhov, Belgorod, Russia

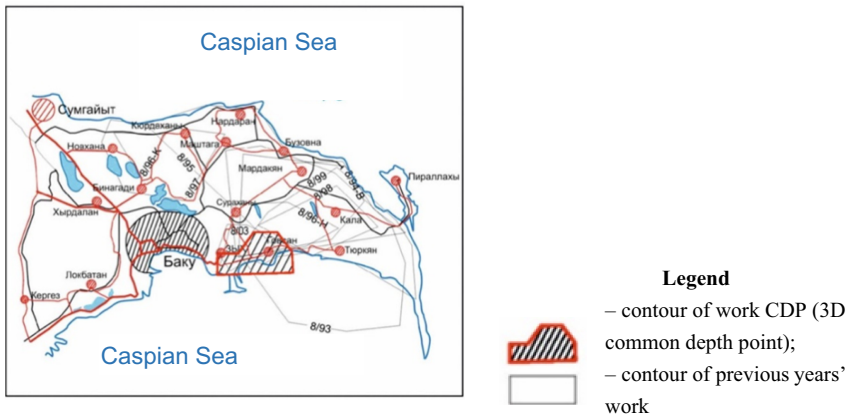
**Abstract.** This paper discusses current issues related to modeling the lithology of oil and gas-bearing rocks in the old field Zyxh using new technologies for processing and interpreting 3D seismic data and geophysical research of wells (GRW) to increase the resource base of the field. The purpose of this research is to identify the most promising lithological sections and intervals of the section that have higher reservoir properties according to the data of 3D and GRW seismic integration. The subjects of research are 3D seismic data and logging curves of geophysical research of wells (GRW), a priori geological and geophysical data accumulated during the period of exploration and operation of the field. The object of research is the Zyxh field. The paper presents a brief history of geological and geophysical study, stratigraphy and lithology of the deposition that make up the section of the Zyxh field. Research result: 1. Analysis of the obtained data shows that even within individual tectonic blocks (segments), the lithology of fields is variable and one or another fraction dominates during the transition from one block to another. The same is observed in sections A-B, which crosses the field from north to south. Modeling of deposition lithology was not carried out in all segments (tectonic blocks) of fields, but it should be noted that there are not very many of them.

**Conclusion:** The problem was solved successfully, the field was divided into separate tectonic blocks (segments) based on 3D seismic data, and a lithological model was built for each segment using 3D seismic data and GRW of wells. Examples of modeling of lithology on the example of one of the segments of the model of the lower part of the productive layer (layers PF and KaF) are shown in the form of maps and sections.

**Keywords:** Oil and gas field · Mud volcano · 3D seismic survey · Tectonic blocks · Lithological model · Seismic records · Processing and interpretation of seismic data · Time and depth sections

# 1 Introduction

The Zyxh oil and gas field is located in the South-Eastern part of the Absheron Peninsula, East of Baku [1]. The study of this field began in the XIX century by laying an exploration well within the Karachukhur field, located directly near it. In the 30 s of the XX century, geological and geophysical surveys were also conducted on the area under study, 2D seismic surveys were repeatedly conducted with single and multiple profiling, and 3D seismic surveys were conducted in 2012. Based on the results of geological and geophysical work and deep drilling within the study area, the Zyxh field was discovered and put into operation in 1935 [2]. Currently, the field is in the final stage of development. General information about the study of previous works by geophysical methods within and near the work area is shown in Fig. 1.



**Fig. 1.** Scheme of study of the area of work by seismic surveys.

The discoverer was well 12, which resulted in the production of industrial oil from the Balakhhan formation of the productive thickness.

Upper and middle Absheron deposits are exposed in the field. Wells opened a section of the entire Pliocene complex of deposits up to the Pontic stage. Neogene deposits within the work area are represented in the Miocene and Pliocene volumes [1, 3].

Oil-bearing capacity of Zyxh field is confined to the eight objects of the productive thickness: Kalinskaya (KaF), Podkirmanskaya (PF), Kirmakinskaya (KF), Nadkirman-skaya clay (NKC) and Balakhanskaya formations (layers VI, VII, VIII, IX). The Kalinskaya formation (KaF) is the lowest formation of deposition of the productive thickness, and is separated from the upper layer by a 4-meter clay interlayer. The total thickness of the KaF is 60 m with an average depth of 2600 m; the weighted average oil-saturated thickness is 7.5 m. Only the upper part of the Kalinskaya formation was opened by wells during drilling.

Podkirmanskaya formation (PF) on the field is the main operating entity. The size of the field is significant, the length of 4.2 km with a width of 1500 m, the height of the field is 250–490 m. The effective oil-saturated thickness as a whole for the PF of

the field reaches maximum values – 36.4 m, the total thickness of the reservoir – 123–132 m. It should be noted that the section of the Zykh field does not differ from the synchronous section of other areas of the Eastern Absheron. A distinctive feature of the PF section is an increase in its total capacity, mainly due to an increase in the capacity of the Surakhanskaya, Balakhanskaya, and Kalinskaya formations.

Tectonically, according to [4], the area under study is located within two major structural elements: the Kura (northern part) and the South Caspian (southern part) depressions. In the south of the section, the South Caspian depression is complicated by the Absheron-Kobystan trough. Zykh square is part of the East Absheron synclinorium and covers the Zykh section of the Karachukhur-Zykh anticline. The Karachukhur-Zykh anticline is the extreme southern elevation of the Sarygayabashy-Shah-Deniz anticline zone, which includes the largest oil and gas fields in Azerbaijan.

The main objective of these studies is to build a detailed three-dimensional lithological model of the Zykh field, taking into account its disjunctive structure, prepare for the determination of petrophysical properties and drawing up a detailed model of oil and gas prospective objects, in order to achieve an increase in the resources of Pliocene and Pleistocene reservoirs.

Construction of a detailed three-dimensional lithological model of the field to select optimal schemes for the development of oil deposits based on refined geological models, preparation of geological and geophysical justification before the exploration of hydrocarbon (HC) deposits.

The aim of this research is to refine the lithological model of the Zykh field and prepare the necessary data for constructing a more detailed lithological and petrophysical model of the studied field.

## 2 Methods and Materials

Loading the source data consisted of converting the necessary information to PETREL compatible formats [7–9]. The initial digital information for constructing a lithological model of the Zykh field was:

1. 196 wells for layers VIII and IX, 122 wells for the PF formation and 83 wells for the KaF formation (depth on the roof and bottom of the layers; inclinometry data: the coordinates of the wellheads and layers crossing, the trajectory of the wells).
2. 148 and 135 wells for formations VIII and IX, 81 wells for the PF formation and 52 wells for the KaF formation (parametric GRW curves: lithology, saturation, porosity, oil saturation).
3. structural surfaces on the roof and bottom of stratigraphic horizons [5].

Quality control of the source data after loading was performed visually in a software package developed by PETREL and Schlumberger [8–10].

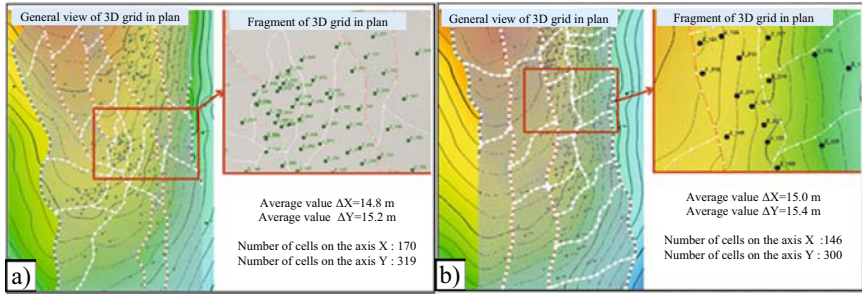
## 3 Results and Discussions

The prepared digital data sets were checked for systematic errors and matched to create a correct model. First, we started constructing a three-dimensional geological grid based

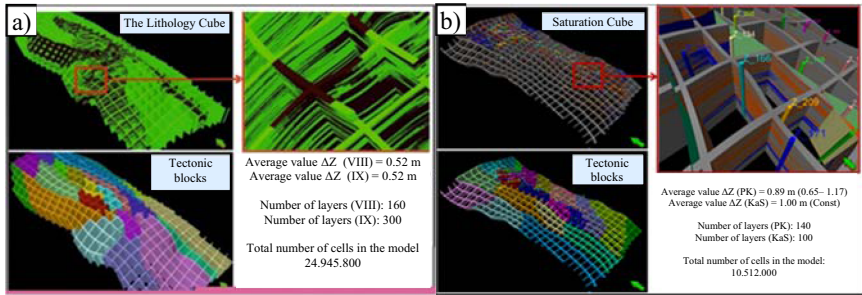
on the constructed 2D structural surfaces [11, 12]. Discrete three-dimensional grids were constructed based on stratigraphic marks on the roof and bottom of the layers, as well as constructed rift models. The grid type is Corner point, where the cell edges can form arbitrary corners. The Corner point type is currently the most common grid type, as it is more convenient for subsequent hydrodynamic modeling. The vertical structure grid type is proportional for all simulated layers. This type of grid describes best the geological model, corresponds to the concept of deposition of productive deposits, corresponds to the density of drilled wells and the seismic study of the area.

Figure 2 shows the geometric areal parameters of 3D grids for the layers of the upper and lower sections of the PT, respectively. Figure 3 shows fragments of saturation cubes with vertical and general parameters of 3D grids. The size of the 3D grid of layers VIII and IX of the Zykhn field along the XYZ coordinate axes was  $170 \times 319 \times 460$  cells. The size of the 3D grid of the PF and KaF layers of the Zykhn field along the XYZ coordinate axes was  $146 \times 300 \times 240$  cells. In space, the X-axis is directed to the east, the Y-axis to the north. The dimension of cells along the lateral of geological grids is on average  $15 \times 15$  m. The vertical dimension of the layers was determined by the total thickness of the formation, the degree of its heterogeneity, the minimum values of the thicknesses of permeable and impermeable layers, as well as the number of thin layers. Then we started averaging the well data: the well data contains the following parametric curve necessary for constructing a lithological model: a discrete lithology curve (reservoir – not reservoir) [13, 14]. The quantization step of continuous GRW curves in depth was 0.2 m. Averaging involves two stages: determining the grid cells through which the well passes and determining the weighted average value of the parameter in each such cell.

Building a lithological model (using the Simulation method). The construction of a lithology cube (LITO) is based either on modeling petrophysical properties, or on constructing a cube of the effective thickness coefficient (sandiness) for the reservoir-non-reservoir parameter and assigning a unit value to cells with the calculated parameter value higher than the boundary value. When constructing the lithology cube of the Zykhn field, the geological features of the simulated field are taken into account in the distribution of the reservoir saturation type vertically and in the plan. Taking into account the complex geological structure of the field, lithological modeling was performed in each tectonic block (segment of the model) separately. Thus, 13 models were built for the layers of the Balakhanskaya formation and 18 models for the layers of the Podkirmakinskaya and Kalinskaya formations. After that, the models were combined into a single cube of the lithology distribution. Figure 4 shows the model segment numbers for the upper (layers VIII and IX) and lower (PF and KaF) sections of the productive section, respectively. The yellow color shows the numbers of segments in which the simulation was performed, and the blue color shows that the simulation was not performed, as there are no productive wells in both layers.



**Fig. 2.** Geometrical parameters of the 3D grid of layers VIII and IX (a) and PF and KaF (b).



**Fig. 3.** Geometric parameters of the 3D grid of layers VIII and IX (a) and PF and KaF (b).

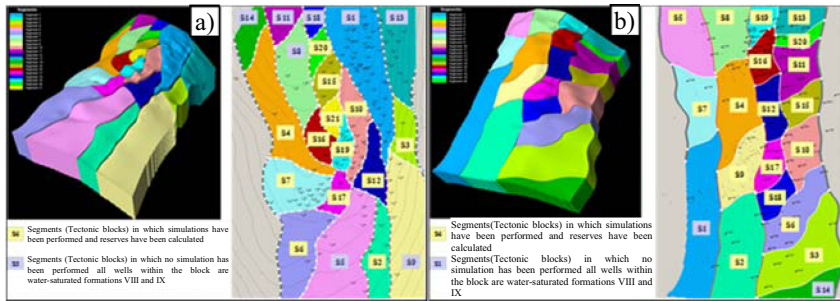
Below there is a method for constructing a “Lithology” cube for each of the segments: preparing a continuous SAT\_cont lithology curve for modeling the sandiness parameter (taking into account the nature of saturation). Reservoirs with a water-saturated reservoir are assigned an index  $[-1]$ . The current indexing allows separating water-saturated bodies from oil-saturated bodies based on the results of constructing the sandiness parameter, but if the body is two-phase in saturation and has a WSR, this approach introduces certain errors when determining the geometry of bodies in volume [15, 16]. In this connection, when modeling, the reservoirs of wells that open a water-saturated reservoir in bodies that have a WSR are also assigned an index [1]. The nature of saturation in such bodies was determined after the stage of constructing a cube of connected volumes.

The results of modeling lithology on the example of one of the segments of the model of the lower part of the productive strata (layers PF and KaF) are shown in Fig. 5.

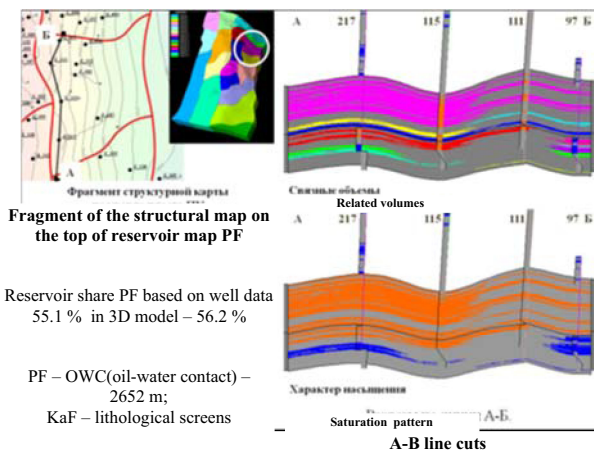
## 4 Conclusion

Analysis of the obtained data shows that even within individual tectonic blocks (segments), the lithology of deposits is variable and one or another fraction dominates during the transition from one block to another. The same is observed in sections A-B, which crosses the field from north to south. Modeling of lithology of the deposits was not in all segments (tectonic blocks) fields, it should be noted that there are not many such segments.





**Fig. 4.** Segment numbers for modeling layers VIII and IX (a) and layers PF and KaF (b).



**Fig. 5.** Modeling of lithology. A-B line cuts.

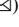

## References

1. Alizade, A.A., Akhmedov, G.A., Akhmedov, A.M.: *Geology of Oil and Gas Fields in Azerbaijan*. Nedra, Moscow (1966)
2. Ahmedov, T.R., Aliyeva, G.A., Abdurrahmanova, S.T.: Measurement Geological structure of the Hovsan-Zikh area in the light of 3D seismic survey data for Pontian and Miocene sediments and their oil and gas opportunities. *Vect. Geosci.* **1**(4), 15–27 (2018)
3. Alizade, A.A., et al.: *Productive Strata of Azerbaijan, vol. I and II*. Nedra, Moscow (2018)
4. Khain, V.E., Bogdanov, N.A., Abdulin, A.A., Ali-Zade, Ak.A., Akhmedbeyli, F.S., et al.: *International tectonic map of the Caspian Sea and its framing*. Scale, 1: 2,500,000. Moscow (2003)
5. Ahmedov, T.R.: Detailed study of Zyk field setting by use of attribute analysis of 3D seismic survey data. *Vect. Geosci.* **3**(3), 5–14 (2020)
6. Ampilov, Yu.P., Glogovskiy, V.M., Kolesov, V.V., Korostyshevskiy, M.B., Levyant, V.B., Ptetsov, S.N.: *Methodological recommendations on the use of seismic data (2D, 3D) for calculating oil and gas reserves*. Moscow (2006)
7. Muslimov, R.Kh.: Problems of modeling exploration and development of oil fields. *Georesources* **20**(3), 1, 134–138 (2018)

8. Putilov, I.S.: 3D Geological Modeling in the Development of Oil and Gas Fields. Publishing House of the Perm National Research Polytechnic University, Perm (2011)
9. Kirillov, A.S., Zakrevsky, K.E.: Workshop on Seismic Interpretation in Petrel. Publishing House MAI-Print, Moscow (2014)
10. Fozao, K.F., Fotso, L., Djieto-Lordon, A., Mbeleg, M.: Hydrocarbon inventory of the eastern part of the Rio Del Rey Basin using seismic attributes. *J. Petrol. Explor. Prod. Technol.* **8**(3), 655–665 (2017)
11. Yanevits, E.A.: Construction of seismic-geological models based on 2D seismic and well logging data (on the example of one of the areas of the Predatomy trough in eastern Siberia). *Geophys. J.* (2016)
12. Goodway, B., Varsek, J., Abaco, C.: Practical applications of P-wave AVO for unconventional gas resource plays. EnCana Corporation, Calgary, Alberta, Canada (2006)
13. Beep, N.S., Bogdanovich, N.N., Martynov, V.G.: Determination of the physical properties of oily rocks. LLC “Nedra-Business Center”, Moscow (2007)
14. Shimansky, V.V., Ronin, A.L., Rylkov, V.A., Karaev, N.A.: Geological interpretation of seismic data in regional and prospecting works in complex environments. *Geol. Oil Gas* **4** (2011)
15. Dyachuk, I.A.: On the issue of reforming oil fields and reservoirs. *Georesursy* **1**(60), 39–46 (2015)
16. Dyachuk, I.A., Knyazeva, E.V.: Features of the late stage of oil field development and measures to enhance oil recovery from depleted reservoirs. In: Materials of International scientific and practical Conference, Ikhlas, Kazan (2016)



# Determination of the Stress State of the Disk Using the Stress Function

V. N. Strelnikov  

Belgorod State Technological University Named After V.G. Shukhov, Belgorod, Russia

**Abstract.** The solution of the problem of the elasticity theory of a plane-stressed state of a wave generator disk with a through central hole is presented. An active load is applied on the outer cylindrical contour of the disk of radius  $R_2$ . The reactive load is applied along the inner contour – the central hole of the disk of radius  $R_1$ . The development and creation of high-performance transmission gears with minimal overall weight indicators and increased load capacity is an urgent problem of improving the quality and competitiveness of mechanical drives of road and construction equipment. The layout of the completed machines, technical and economic characteristics are largely determined by the overall dimensions, weight, load capacity and reliability of the built-in gearboxes. The most promising direction for optimizing the quality indicators of wave transmissions is the differentiation of the power flow by a number of parallel power flows that reduce the size, weight and noise effect. The relative weight and cost of wave reducers are 1.5–2 times lower than planetary ones, which contributes to the use of wave reducers in road and construction equipment. The most loaded nodes of a large wave gear train include a wave generator that integrates the reactive load of the gearing through disks mounted on a high-speed shaft with a given eccentricity. Minimizing the vibration of the disks is achieved by reducing their weight, precision manufacturing and assembly. The problem of the stressed state of the disks is relevant, and the results obtained are used to optimize the design and size of the bearing elements of the wave gear.

**Keywords:** Disk · Voltage · Wave transmission · Wave generator

## 1 Introduction

Construction and road vehicles operate under difficult conditions of overload, temperature fluctuations, abrasive wear, and other negative factors. These machines have a number of special requirements. This means high reliability, load capacity, service life, minimal overall weight characteristics and energy losses. The specified conditions correspond to wave transmissions embedded in the machine carrier nodes.

## 2 Materials and Methods

Commercially available wave reducers are designed to transmit small torques and are equipped with a cam wave generator with a flexible bearing [1–3]. Strength calculations

are mainly performed for a flexible wheel [4]. Studies of the wave generator are limited to force analysis and solving problems of rigidity [5–8]. The wave generator by means of disks compensates for the reactive load of the gearing, which in a large wave transmission can reach tens of tons [9, 10]. The disks have a significant mass, are installed with a given eccentricity on a high-speed shaft and largely determine the vibrational processes, vibration, and dynamic loads on the supports (Fig. 1). Minimizing the level of vibrational energy of rapidly rotating masses is primarily related to their size, regulated by the strength of the disks. With an increase in the size of the wave transmission, the influence of the mass of disks increases, and the problem of their stress state becomes particularly relevant. To optimize the design and refine the size of the wave generator, theoretical studies of the stress state of the disks are performed. The disks of the wave generator are in a plane-stressed state and have two contours: the outer radius  $R_2$  and the inner radius  $R_1$  (Fig. 1). The reactive component of the gearing load is transmitted to the outer contour through the flexible wheel within the angle of  $2\theta^*$ . The normal load on the external contour is approximated by the parabolic law

$$P_2 = \begin{cases} P_{2max} \left(1 - \frac{\theta^2}{\theta^{*2}}\right); & |\theta| \leq \theta^*; \\ 0; & |\theta| > \theta^*. \end{cases} \quad (1)$$

Tangential forces on the external and internal contours are not taken into account. The circumferential forces in engagement are approximated by the tangential load  $P_{2t}(\theta)$ , related to the unit of the disk surface, and we express the torque  $M_2$

$$M_2 = 2 \int_0^{\theta^*} P_{2t} R_2^2 \cdot b d\theta = \frac{4P_{2max} b R_2^2 \theta^*}{3tg\alpha} \quad (2)$$

where  $P_{2max} = \frac{3M_2 tg\alpha}{4\theta^* b R_2^2}$ ;  $\alpha$  – gearing angle.

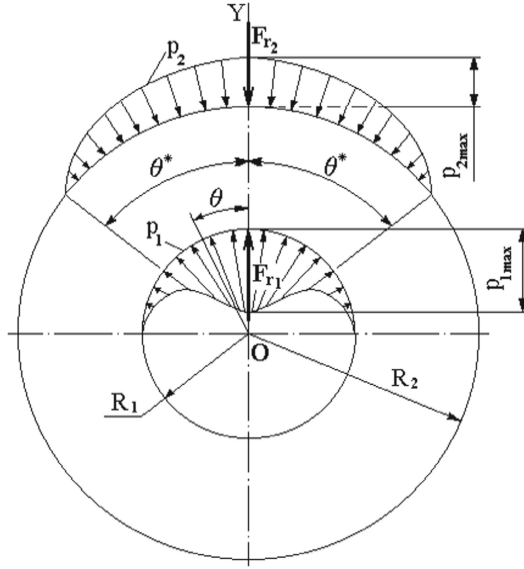
The disks are mounted on rolling bearings. The distribution of the normal load on the inner contour of the disk  $P_1$  in the interval  $0 \leq \theta \leq \frac{\pi}{2}$  according to the parabolic law, corresponds to the load distribution in the bearing.

$$P_1(\theta) = \begin{cases} P_{1max} \left(1 - \frac{4\theta^2}{\pi^2}\right) & 0 \leq |\theta| \leq \frac{\pi}{2} \\ 0 & \frac{\pi}{2} < |\theta| \leq \pi \end{cases} \quad (3)$$

We find the pressure  $P_{1max}$  from the condition of equality of the resultant forces for loads along the internal and external circuits, taking  $\beta = \frac{R_1}{R_2}$

$$2 \int_0^{\frac{\pi}{2}} P_{1max} b R_1 \left(1 - \frac{4\theta^2}{\pi^2}\right) \text{Cos } \theta d\theta = 2 \int_0^{\theta^*} P_{2max} b R_2 \left(1 - \frac{\theta^2}{\theta^{*2}}\right) \text{Cos } \theta d\theta, \quad (4)$$

$$P_{1max} = \frac{\pi^2 (\text{Sin}\theta^* - \theta^* \text{Cos}\theta^*)}{4\beta(\theta^*)^2} P_{2max}.$$



**Fig. 1.** Distribution of the normal load applied to the disk.

We represent the stress state in terms of the stress function  $\phi(r, \theta)$ , which satisfies the biharmonic equation:

$$\Delta \cdot \Delta \phi = \left( \frac{\partial^2}{\partial r^2} + \frac{1}{r} \frac{\partial}{\partial r} + \frac{1}{r^2} \frac{\partial^2}{\partial \theta^2} \right) \cdot \left( \frac{\partial^2 \phi}{\partial r^2} + \frac{1}{r} \frac{\partial \phi}{\partial r} + \frac{1}{r^2} \frac{\partial^2 \phi}{\partial \theta^2} \right) = 0 \quad (5)$$

Taking into account the parity of the external load, the solutions of Eq. (5) are found as a series of cosines

$$\phi(r, \theta) = \sum_{n=0}^{\infty} \varphi_n(r) \cos n\theta. \quad (6)$$

We substitute the values (6) in Eq. (5)

$$\begin{aligned} & \left( \frac{\partial^2}{\partial r^2} + \frac{1}{r} \frac{\partial}{\partial r} + \frac{1}{r^2} \frac{\partial^2}{\partial \theta^2} \right) \sum_{n=0}^{\infty} \left( \frac{d^2 \varphi_n}{dr^2} + \frac{1}{r} \frac{d \varphi_n}{dr} - \frac{n^2}{r^2} \varphi_n \right) \cos n\theta \\ & = \sum_{n=0}^{\infty} \left\{ \left( \frac{d^2}{dr^2} + \frac{1}{r} \frac{d}{dr} - \frac{n^2}{r^2} \right) \left( \frac{d^2 \varphi_n}{dr^2} + \frac{1}{r} \frac{d \varphi_n}{dr} - \frac{n^2}{r^2} \varphi_n \right) \right\} \cos n\theta = 0 \end{aligned} \quad (7)$$

The  $\cos n\theta$  functions are orthogonal in the interval  $(0; \pi)$ . Let us make an expression

$$\int_0^{\pi} \cos n\theta \cos k\theta d\theta = \begin{cases} 0 & n \neq k \\ \frac{\pi}{2} & n = k \end{cases}.$$

Multiplying Eq. (7) by  $\cos k\theta$ , we integrate within  $(0; \pi)$

$$\frac{\pi}{2} \cdot \left[ \left( \frac{d^2}{dr^2} + \frac{1}{r} \frac{d}{dr} - \frac{\kappa^2}{r^2} \right) \left( \frac{d^2 \varphi \kappa}{dr^2} + \frac{1}{r} \frac{d \varphi \kappa}{dr} - \frac{\kappa^2}{r^2} \varphi \kappa \right) \right] = 0.$$

The functions  $\varphi_n(r)$  satisfy the differential equations:

$$\left( \frac{d^2}{dr^2} + \frac{1}{r} \frac{d}{dr} - \frac{n^2}{r^2} \right) \left( \frac{d^2 \varphi_n}{dr^2} + \frac{1}{r} \frac{d \varphi_n}{dr} - \frac{n^2}{r^2} \varphi_n \right) = 0, \quad n = 0, 1, 2, \dots \quad (8)$$

The solution of Eqs. (8) is found in the form of power functions  $r^s$ . We find the values of  $s$  for each  $n$ :  $s_1 = n$ ;  $s_2 = -n$ ;  $s_3 = n + 2$ ;  $s_4 = -(n - 2)$ .

At  $n = 0$  and  $n = 1$  we get multiple roots.

For  $n = 0$ :  $S_1 = S_2 = 0$ ;  $S_3 = S_4 = 2$ .

For  $n = 1$ :  $S_1 = 1$ ;  $S_2 = -1$ ;  $S_3 = 3$ ;  $S_4 = 1$ .

At  $n = 0$  we get a special case of the Eqs. (8)

$$\left( \frac{d^2}{dr^2} + \frac{1}{r} \frac{d}{dr} \right) \left( \frac{d^2 \varphi_0}{dr^2} + \frac{1}{r} \frac{d \varphi_0}{dr} \right) = 0,$$

from which

$$\varphi_0 = \left( \frac{b_0}{4} - \frac{a_0}{4} \right) r^2 + (\ell_0 + a_0 d_0) \ell_n r + \frac{a_0}{4} r^2 \ell_n r + c_0,$$

where  $a_0, b_0, c_0, d_0, \ell_0$  – the constant of integration.

Introducing new arbitrary constants we present the solution in the form:

$$\varphi_0 = B_0 r^2 + C_0 \ell_n r + D_0 r^2 \ell_n r + E_0.$$

We consider the case  $\kappa = 1$ .

We think  $f_1 = \frac{d^2 \varphi_1}{dr^2} + \frac{1}{r} \frac{d \varphi_1}{dr} - \frac{\varphi_1}{r^2}$ , in this case,  $f_1$  satisfies the equation  $\frac{d^2 f_1}{dr^2} + \frac{1}{r} \frac{d f_1}{dr} - \frac{f_1}{r^2} = 0$ . We integrate this equation and find:  $f_1(r) = \frac{a'_0}{2} r + \frac{b'_0}{r}$ .

Replacing  $f_1$  with  $\varphi_1$ , after integration we get  $\varphi_1(r) = \frac{a'_0}{16} r^3 + \frac{b'_0}{2} r \ln r + \left( \frac{d'_0}{2} - \frac{b'_0}{4} \right) r + \frac{(b'_0 \ell'_0 + c'_0)}{r}$ .

By introducing new arbitrary constants, we get:

$$\varphi_1(r) = A_1 r^3 + B_1 \cdot \ln r + \frac{C_1}{r} + D_1 r$$

The solution of the biharmonic equation is represented in the Michell form

$$\begin{aligned} \phi(r, \theta) = & B_0 r^2 + C_0 \ln r + D_0 r^2 \ln r + E_0 + \left( A_1 r^3 + B_1 r \ln r + \frac{C_1}{r} + D_1 r \right) \cos \theta \\ & + \sum_{n=2}^{\infty} \left( C_{1n} r^n + C_{2n} r^{n+2} C_{3n} r^{-n} + C_{4n} r^{-(n-2)} \right) \cos n \theta. \end{aligned} \quad (9)$$

The components of the stress tensor are defined in terms of the stress function

$$\sigma_r = \frac{1}{r} \frac{\partial \phi}{\partial r} + \frac{1}{r^2} \frac{\partial^2 \phi}{\partial \theta^2}; \quad \sigma_\theta = \frac{\partial^2 \phi}{\partial r^2}; \quad \tau_{r\theta} = -\frac{\partial}{\partial r} \left( \frac{1}{r} \frac{\partial \phi}{\partial \theta} \right). \quad (10)$$

We substitute the value (9) in Eq. (10), differentiate and find expressions for the components of the stress tensor

$$\begin{aligned}
\sigma_r &= \left[ (2B_0 + D_0) \frac{C_0}{r^2} + 2D_0 \ln r \right] + \left( 2A_1 r + \frac{B_1}{r} + \frac{2C_1}{r^3} \right) \cos \theta - \sum_{n=2}^{\infty} \left[ n(n-1)C_{1n}r^{n-2} \right. \\
&\quad \left. + (n-2)(n+1)C_{2n}r^n + (n+1)nC_{3n}r^{-(n+2)} + (n+2)(n-1)C_{4n}r^{-n} \right] \cos n\theta; \\
\sigma_\theta &= \left( 2B_0 - \frac{C_0}{r^2} + 2D_0 \ln r + 3D_0 \right) + \left( 6A_1 r + \frac{B_1}{r} + \frac{2C_1}{r^3} \right) \cos \theta + \sum_{n=2}^{\infty} \left[ n(n-1)C_{1n}r^{n-2} \right. \\
&\quad \left. + (n+2)(n+1)C_{2n}r^n + n(n+1)C_{3n}r^{-(n+2)} + (n-2)(n-1)C_{4n}r^{-n} \right] \cos n\theta; \\
\tau_{r\theta} &= \left( 2A_1 r + \frac{B_1}{r} - \frac{2C_1}{r^3} \right) \sin \theta + \sum_{n=2}^{\infty} \left[ n(n-1)C_{1n}r^{n-2} + n(n+1)C_{2n}r^n \right. \\
&\quad \left. - n(n+1)C_{3n}r^{-(n+2)} - n(n-1)C_{4n}r^{-n} \right] \sin n\theta.
\end{aligned}$$

To avoid ambiguity when calculating the components of the displacement vector, for  $n = 1$ , we introduce an additional term in the expression of the stress function

$$\Phi_1^* = Br \cdot \theta \cdot \sin \theta \quad (11)$$

The function  $\Phi_1^*$  is even and satisfies the biharmonic equation

$$\Phi_1^* = \left( \frac{\partial^2}{\partial r^2} + \frac{1}{r} \frac{\partial}{\partial r} + \frac{1}{r^2} \frac{\partial^2}{\partial \theta^2} \right) (Br \cdot \theta \cdot \sin \theta) = \frac{2B}{r} \cdot \cos \theta.$$

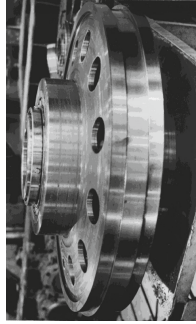
We find  $\Delta \cdot \Delta \Phi_1^* = \Delta \left( \frac{2B}{r} \cos \theta \right) \equiv 0$ .

We introduce the function  $\Phi_I^*$  and define the components of the stress tensor

$$\begin{aligned}
\sigma_{r1}^* &= \left( \frac{1}{r} \frac{\partial}{\partial r} + \frac{1}{r^2} \frac{\partial^2}{\partial \theta^2} \right) (Br \cdot \theta \cdot \sin \theta) = \frac{2B \cos \theta}{r}; \\
\sigma_{\theta 1}^* &= \frac{\partial^2}{\partial r^2} (Br \cdot \theta \cdot \sin \theta) = B \cdot \theta \cdot \sin \theta \frac{\partial^2}{\partial r^2} (r) \equiv 0; \\
\tau_{r\theta 1}^* &= -\frac{\partial}{\partial r} \left( \frac{1}{r} \frac{\partial}{\partial \theta} \right) (Br \cdot \theta \cdot \sin \theta) = -B \cdot \frac{\partial}{\partial r} (\sin \theta + \theta \cdot \cos \theta) \equiv 0. \quad (12)
\end{aligned}$$

Only the voltage  $\sigma_r$  will change. After differentiating expression (9) by formulas (10) and (12), we find the components of the stress tensor of the disk (Fig. 2).

$$\begin{aligned}
\sigma_r &= \left[ (2B_0 + D_0) \frac{C_0}{r^2} + 2D_0 \ln r + D_0 \right] + \left( 2A_1 r + \frac{B_1 + 2B}{r} - \frac{2C_1}{r^3} \right) \cdot \cos \theta - \sum_{n=2}^{\infty} \left[ n(n-1)C_{1n} \cdot \right. \\
&\quad \left. r^{n-2} + (n-2)(n+1)C_{2n}r^n + n(n+1)C_{3n}r^{-(n+2)} + (n+2)(n-1)C_{4n}r^{-n} \right] \cdot \cos n\theta; \\
\sigma_\theta &= \left( 2B_0 - \frac{C_0}{r^2} + 2D_0 \ln r + 3D_0 \right) + \left( 6A_1 r + \frac{B_1}{r} + \frac{2C_1}{r^3} \right) \cos \theta + \sum_{n=2}^{\infty} \left[ n(n-1)C_{1n}r^{n-2} \right. \\
&\quad \left. + (n+2)(n+1)C_{2n}r^n + n(n+1)C_{3n}r^{-(n+2)} + (n+2)(n-1)C_{4n}r^{-n} \right] \cdot \cos n\theta; \\
\tau_{r\theta} &= (2A_1 r + \frac{B_1}{r} - \frac{2C_1}{r^3}) \cdot \sin \theta + \sum_{n=2}^{\infty} \left[ n(n-1)C_{1n}r^{n-2} + n(n+1)C_{2n}r^n \right. \\
&\quad \left. - n(n+1)C_{3n}r^{-(n+2)} - n(n-1)C_{4n}r^{-n} \right] \cdot \sin n\theta \quad (13)
\end{aligned}$$



**Fig. 2.** Disk wave generator of the tilt drive reducer of the mobile mixer MP-600AS with a load capacity of 600 tons of molten metal.

### 3 Results

Gear building is one of the most complex and responsible areas of machine-building production and largely determines the technical and economic level of manufactured machines. The practice of modern production and operation of gearboxes in construction and transport engineering has identified a number of complex tasks of production and scientific and technical nature, related to increasing the load-bearing capacity, kinematic efficiency and reliability of gearboxes, reducing their overall dimensions and metal consumption, and excluding expensive structural materials. One of the most loaded nodes of a large wave gear is a wave generator that sums up the reactive load of the wave gear through disks mounted on a high-speed shaft with a given eccentricity. The components of the strain tensor are expressed by Hooke's law. Minimizing the level of vibrational energy of rapidly rotating masses is due to their mass capacity, regulated by the strength of the disks. The problem of the stressed state of disks is relevant, and the results of its solution have wide practical application in the design in order to optimize the parameters of the carrier elements of large wave transmissions. The aim of this work is a theoretical study of the stress state of a disk with a central hole to optimize the design parameters of the wave generator of large wave gearboxes. The problem under consideration is relevant, and the results of its solution have a wide practical application in the design in order to optimize the parameters of the bearing elements of large wave gears.

### 4 Conclusion

Analysis of the stress state of the wave generator disk in relation to the design features and load conditions of large wave transmissions used in the most critical, heavily loaded nodes of road and construction vehicles contributed to optimizing their design, reducing metal consumption, improving quality, technical characteristics, and load capacity.

**Acknowledgements.** This work was realized in the framework of the Program of flagship university development on the base of the Belgorod State Technological University named after V G Shukhov, using equipment of High Technology Center at BSTU named after V. G. Shukhov.






## References

1. Volkov, D. P., Krainev, A. F., Bondarenko, S.V.: Designing mechanisms with wave gears for construction and road vehicles. Cnitateoimas, Moscow (1975)
2. Volkov, D. P., Krainev, A. F., Yidyayev, A. I.: Wave transmissions and their use in construction and road cars. Cnitateoimash, Moscow (1970)
3. Volkov, D.P., Krainev, A.F., Guzenkov, V.P.: Study of the distribution of loads by elements of wave transmission of the crane turning mechanism. Constr. Road Mach. Excavat. Constr. Cranes **3**, 27–32 (1971)
4. Commissioners, A.F.: Methodology and some results of the experimental determination of load on the drives of the wave gear generator. Herald Mech. Eng. **3**, 52–54 (1973)
5. Shuvalov, S.A., Gorelov, V.N.: Study of the problems in a flexible jagged crown by the method of finite elements. Herald Mech. Eng. **1**, 10–12 (1983)
6. Shuvalov, S.A., Parshin, I.M.: Load on the generator of wave gear transmission. Izvestia Univ. Eng. **12**, 19–23 (1971)
7. Ivanov, M.N.: Wave gear. High school, Moscow (1981)
8. Poletuchii, A.I.: Theory and Design of High-Performance Wave Gears, p. 675. Natsional'nyi aviatsionnyi universitet publ., Kharkov (2005)
9. Strelnikov, V.N.: Increase the Load Capacity of Wave Gears: monograph. BGTU Publishing House, Belgorod (2015)
10. Hareesh, Y.S., Varghese, J.: Design and analysis of flex spline with involute teeth profile for harmonic drive mechanism. Int. J. Eng. Res. Technol. **4**(12), 613–618 (2015)



# Optimization of Technological Parameters of Foam Concrete Mix Preparation for Obtaining Foam Concrete with Improved Structure and Characteristics

S. A. Stel'makh , E. M. Shcherban'  <sup>(✉)</sup>, and K. E. Tkacheva 

Don State Technical University, Rostov-on-Don, Russia

**Abstract.** The paper investigated the influence of the tilt of the activator blades on the uniformity of the structure of the foam concrete mixture and the power consumed for mixing. In the experiments, a cylindrical mixer with a conical part was used. Blade activators with three flat blades were used. Analysis of the data investigating the effect of blade angle shows that the homogeneity of the concrete mix decreases with increase in blade angle. This is due to a decrease in the speed of rotation of the mixture, respectively, the intensity of mixing. With an increase in the tilt angle of the blades, the power consumed for mixing decreases. Studies showed that the degree of air entrainment, the nature of the pore structure and the physical and mechanical properties of foam concrete depend on the rotation speed of the activator of the turbulent mixer. The dependences of the quality of the prepared foam concrete mixture on the geometric parameters of the mixer, the type and speed of rotation of the activator, the presence and characteristics of reflective partitions are obtained. The shape and type of activator significantly affect the energy intensity of the process and the quality of the prepared foam concrete. The mixer with a vane perforated activator proved to be the most effective. The degree of influence of the tilt angle of the activator blades on the retention of binder and aggregate particles in the volume of the foam concrete mixture during mixing is determined.

**Keywords:** Mixer activator · Tilt of the activator blades · Uniformity of the foam concrete mixture · Power consumption · Air entrainment of the foam concrete mixture · Mixing speed

## 1 Introduction

An impeding factor in the formation of the mixer calculation method is the lack of research on the processes occurring during mixing:

- maximum developed interfacial surface for air entrainment due to turbulent diffusion;
- the most likely rate of interfacial surface change;
- resistance of gas phase bubbles to destruction;

- uniform distribution of bubbles and other components of the mixture throughout the volume;
- minimum energy costs for the process [1–7].

Today, various models of mixers are used in the construction industry. The volume of mixers varies from  $10 \text{ dm}^3$  to  $5 \text{ m}^3$ . There are known devices that make mixing possible in concrete structures with a volume of several hundred thousand cubic meters [3, 8].

The problem of determining the role of mixing is solved most easily when the designed mixer is assigned to produce a mixture with a certain degree of uniformity of composition. For example, the technological purpose of suspension devices, usually installed in conjunction with filters, is the suspension of sediment (maintaining the particles in a suspended state before feeding the pulp to the filters) by mixing them [3, 9].

Another example is the averaging of a synthetic rubber solution produced by several simultaneous polymerization cascades to reduce fluctuations in the concentration and molecular weight distribution of the polymer. The effectiveness of averaging at a given volume and productivity of the device is due only to the intensity of mixing. Intensification of mixing is a significant parameter, but not in all cases leads to optimization of production processes and is almost constantly characterized by an increase in energy consumption and equipment cost. That is why the choice of design and calculation of the mixing unit should be followed by an understanding of the role and requirements for the intensity of mixing in a particular technological process [3, 10–12].

Insufficient mixing intensity mainly contributes to the fact that even with the necessary average values of concentration and temperature in the mixer, their local values in various areas of the reaction volume will go beyond the permissible limits. Therefore, the task of mixing, along with the intensification of mass transfer, is to ensure the necessary degree of uniformity of the concentration and temperature fields in the device. The choice of mixing conditions in this case is carried out taking into account two requirements:

- ensuring the desired mass transfer coefficient from the mixed environment;
- obtaining a certain degree of uniformity in the distribution of reagent concentrations and temperature in the device [3, 4, 13].

After determining the purpose of mixing, the choice of the design type of the device and the mixer is made.

Early selection of production models allows estimating the possible limits of the speed of operations, the degree of uniformity of the concentration field and temperature. The task of pilot experiments with this approach is defined in checking the possibility of carrying out the process under study, in a pre-determined device and in clarifying the technological parameters of the process and the requirements for the mixed environment [3, 14].

## 2 Methods and Materials

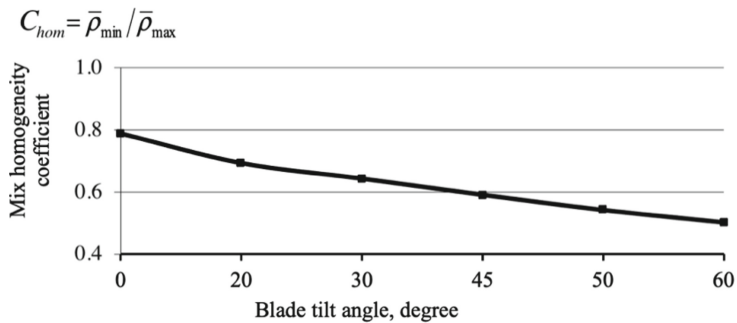
To assess the degree of influence of tilt of the blades of the activator, relative to the plane perpendicular to the axis of rotation of the activator to the homogeneity of the structure of foam concrete mix and the power required for mixing concrete mixture, there were experimental studies. In the experiment, a cylindrical mixer with a conical part  $V = 250$  l was used, the speed of rotation of the activator was 500 rpm, and blade activators with three flat blades were also used. On all devices, the blades were mounted radially and tilted at angles  $\alpha_{bl} = 20^\circ, 30^\circ, 45^\circ, 50^\circ$  and  $60^\circ$  relative to the plane perpendicular to the axis of rotation of the agitator (for straight blades  $\alpha_{bl} = 0^\circ$ ). Determination of density and power was carried out according to the method described in [15, 16].

## 3 Results and Discussion

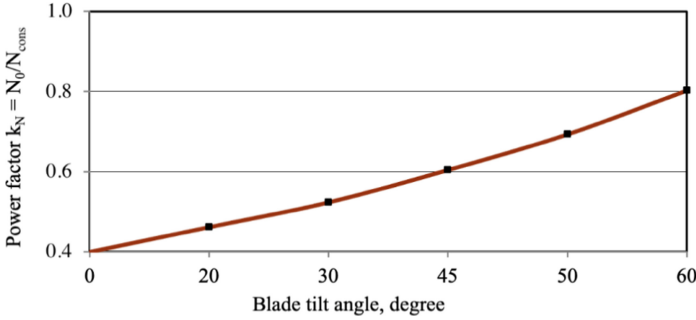
Analysis of the obtained data (Fig. 1) to study the effects of blade angle on degree of uniformity  $C_{hom}$  shows that the homogeneity of the concrete mix decreases with increase in blade angle. This is due to a decrease in the speed of rotation of the mixture, respectively, the intensity of mixing.

We consider the effect of blade angle and activator  $\alpha_{bl}$  on a mix homogeneity coefficient.

With an increase in the tilt angle of the blades, the power consumed for mixing decreases (Fig. 2).



**Fig. 1.** Effect of the tilt angle of the blades on the homogeneity coefficient of the foam concrete mixture.

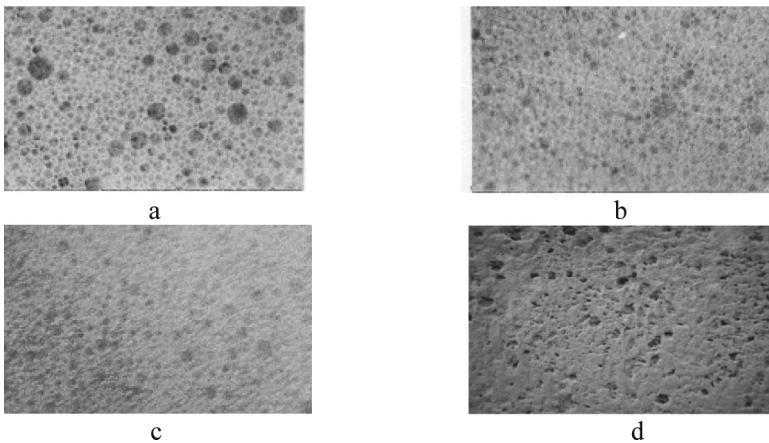


**Fig. 2.** Effect of the tilt angle  $\alpha_{bl}$  on the factor of power consumption spent on mixing the foam concrete mixture.

From the presented results (Fig. 2), it follows that in the case when the blades are tilted at an angle  $\alpha_{bl} = 45^\circ$  to the plane of rotation of the agitator, the power consumption factor is half as low in the area of turbulent flow compared to a similar agitator with blades with a tilt angle  $\alpha_{bl} = 0^\circ$ . At the same time, the effect on the uniformity of the structure of the foam concrete mixture is minimal, which is confirmed by the results presented in Fig. 1.

The obtained experimental data on the influence of the tilt angle of the activator blades on the quality of the foam concrete mixture and the mixing efficiency show that the rational tilt angle of the blades is in the range of 30... 45°.

It is known that the coefficient of structural quality ( $Aq$ ) of foam concrete largely depends on the quality of the pore structure of the material [17, 18, 19]. The value of the  $Aq$  coefficient is higher (all other things being equal), the smaller the pores of the material. Studies showed that the degree of air entrainment, the nature of the pore structure and the physical and mechanical properties of foam concrete depend on the rotation speed of the activator of the turbulent mixer (Fig. 3).



**Fig. 3.** Pore structure of foam concrete on the foaming agent “Penostrom”.

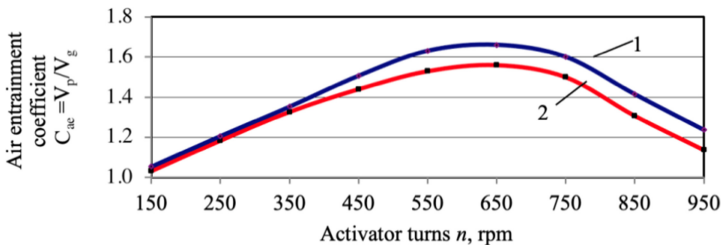
The mixtures are prepared in a mixer with a conical part and a three-bladed perforated activator: a) at a frequency equal to 250 rpm; b) at a frequency equal to 500 rpm; c) at a frequency equal to 650 rpm; d) at a frequency equal to 800 rpm, 900 rpm, 1000 rpm.

Mixers with perforated and conventional blades were considered (Fig. 4) as factors for studying the effect of the mixing rate of the mixture on the volume of air involved in mixing. In the case of use in the manufacture of mixers with perforated blades, with an increase in the mixing speed of the mixture in the range of 250–650 rpm, a continuous increase in the volume of air entrainment occurs.



**Fig. 4.** Perforation of the three-bladed activator.

After reaching the above value, the air entrainment decreases. Increasing the number of turns to a value of 950 rpm leads to a decrease in the volume of air involved in the mixture. The rational value of the mixing speed of the mixture for both types of considered mixers is from 500 to 700 rpm (Fig. 5).

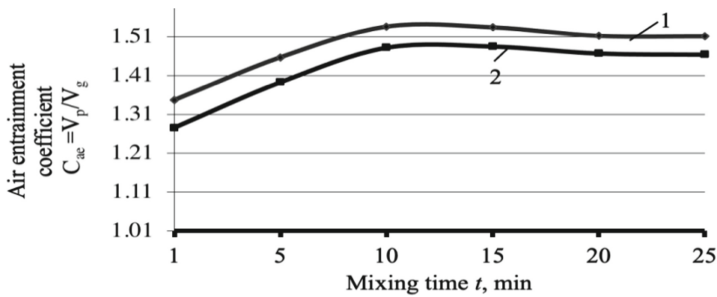


**Fig. 5.** Dependence of the volume of air involved in the foam concrete mixture on the number of the activator turns: 1 – activator with perforated blades; 2 – activator without perforation of the blades.

Let us consider the physical mechanism of the process of involving air in the mixture. Above the surface of the mixture there is some space from which air is drawn due to the appearance of cavities during mixing. The volume of air entrainment at low speeds has a small value. Exceeding the rational value of the mixing rate leads to the rupture of air bubbles and its penetration to the surface is more intense than the formation of new bubbles, as well as their crushing. Thus, with an unreasonable increase in the number of turns per minute in the mixing process, the volume of air entrainment decreases.

Figure 6 graphically shows the effect of the duration of mixing on the volume of air involved in the mixture. During the mixing process, the air saturation rate of the mixture reaches its maximum value. Subsequently, it becomes possible to reduce the volume of air involved after passing through this value.

In a mixer with perforated blades, the mixing area or the number of points of contact between the blade and the mixture increases. Due to this, the volume of air involved increases.



**Fig. 6.** Effect of mixing time on the volume of air involved in the foam concrete mixture: 1 – activator with perforated blades; 2 – with blades without perforation.

## 4 Conclusion

The conducted experimental and theoretical work indicates that:

- 1) the dependences of the quality of the prepared foam concrete mixture on the geometric parameters of the mixer, the type and speed of rotation of the activator, the presence and characteristics of reflective partitions are obtained;
- 2) an increase in the speed of rotation of the activator from 650 to 1000 rpm leads to a sharp decrease in the air entrainment of the foam concrete mixture. It is advisable to use the speed of rotation of the activator from 500 to 650 rpm;
- 3) the shape and type of activator affect significantly the energy intensity of the process and the quality of the prepared foam concrete. The mixer with a blade perforated activator proved to be the most effective;
- 4) the degree of influence of the tilt angle of the activator blades on the retention of binder and aggregate particles in the volume of the foam concrete mixture during mixing is determined. It is established that the appropriate tilt angle of the blades is  $45^\circ$ .

## References

1. Braginskii, L.N., Begachev, V.I., Barabash, V.M.: Mixing in liquid media: physical foundations and engineering calculation methods. Chemistry (1984)

2. Cai, R., Hou, Z., Zhao, Y.: Numerical study on particle mixing in a double-screw conical mixer. *Powder Technol.* **352**, 193–208 (2019). <https://doi.org/10.1016/j.powtec.2019.04.065>
3. Cazacliu, B.: In-mixer measurements for describing mixture evolution during concrete mixing. *Chem. Eng. Res. Design* **86**(12), 1423–1433 (2008). <https://doi.org/10.1016/j.cherd.2008.08.021>
4. Elgindi, T.M., Zlatoš, A.: Universal mixers in all dimensions. *Adv. Math.* **356**, (2019). <https://doi.org/10.1016/j.aim.2019.106807>
5. Haddadi, M.M., Hosseini, S.H., Rashtchian, D., Olazar, M.: Comparative analysis of different static mixers performance by CFD technique: an innovative mixer. *Chin. J. Chem. Eng.* **28**(3), 672–684 (2020). <https://doi.org/10.1016/j.cjche.2019.09.004>
6. Harish, V.V.N., Cho, M., Shim, J.: Effect of rotating cylinder on mixing performance in a cylindrical double-ribbon mixer. *Appl. Sci.* **9**(23), 5179 (2019). <https://doi.org/10.3390/app9235179>
7. Lerch, J.O., Bester, H.L., Van Rooyen, A.S., Combrinck, R., de Villiers, W.I., Boshoff, W.P.: The effect of mixing on the performance of macro synthetic fibre reinforced concrete. *Cem. Concr. Res.* **103**, 130–139 (2018). <https://doi.org/10.1016/j.cemconres.2017.10.010>
8. Liu, B., Xu, Z., Xiao, Q., Huang, B.: Numerical study on solid suspension characteristics of a coaxial mixer in viscous systems. *Chin. J. Chem. Eng.* **27**(10), 2325–2336 (2019). <https://doi.org/10.1016/j.cjche.2019.01.031>
9. Mobley, K.: Root cause failure analysis (1999). <https://doi.org/10.1016/B978-075067158-3/50010-7>
10. Pavlov, A.N., Gol'tsov, Yu.I., Mailyan, L.R., Shcherban', E.M., Stel'makh, S.A.: Relaxation processes during activation of cement mixing water. In: *IOP Conference Series: Materials Science and Engineering*, vol. 896, p. 012124 (2020). <https://doi.org/10.1051/mateconf/201712905011>
11. Sakharov, G.P.: New effective technology of non-autoclave porous concrete. **6**, 28–29 (2002)
12. Shuisky, A.I., Stelmakh, S.A., Shcherban, E.M., Torlina, E.A.: Recipe-technological aspects of improving the properties of nonautoclaved aerated concrete. **129**, 05011 (2017). <https://doi.org/10.1051/mateconf/201712905011>
13. Stel'makh, S.A., Shcherban', E.M., Shuiskii, A.I., Prokopov, A.Y., Madatyan, S.M., Parinov, I.A., Cherpakov, A.V.: Effects of the geometric parameters of mixer on the mixing process of foam concrete mixture and its energy efficiency. **10**, 8055 (2020). <https://doi.org/10.3390/app10228055>
14. Theron, F., Le Sauze, N.: Comparison between three static mixers for emulsification in turbulent flow. *Int. J. Multiphase Flow* **37**(5), 488–500 (2011). <https://doi.org/10.1016/j.ijmultiphaseflow.2011.01.004>
15. Valigi, M.C., Logozzo, S., Rinchi, M.: Wear resistance of blades in planetary concrete mixers. Part II: 3D validation of a new mixing blade design and efficiency evaluation. **103**, 37–44 (2016). <https://doi.org/10.1016/j.triboint.2016.06.040>
16. Valigi, M.C., Logozzo, S., Rinchi, M.: Wear resistance of blades in planetary concrete mixers. Design of a new improved blade shape and 2D validation. **96**, 191–201 (2016). <https://doi.org/10.1016/j.triboint.2015.12.020>
17. Wallevik, J.E., Wallevik, O.H.: Analysis of shear rate inside a concrete truck mixer. *Cem. Concr. Res.* **95**, 9–17 (2017). <https://doi.org/10.1016/j.cemconres.2017.02.007>





# Energy Efficient Stone Cellular Concrete Masonry on Polyurethane Adhesive

L. A. Suleymanova<sup>(✉)</sup> , I. A. Pogorelova , and I. S. Ryabchevskiy 

Belgorod State Technological University Named After V.G. Shukhov, Belgorod, Russia

**Abstract.** Ensuring the requirements of energy saving, environmental safety of residential and public buildings is one of the key areas of development of the construction industry. In particular, the use of cellular concrete blocks in enclosing structures is aimed at solving these problems. Cellular concrete blocks, due to their thermal and strength characteristics, perform simultaneously the functions of a wall-forming material and insulation. However, a factor that reduces the energy efficiency of cellular concrete masonry is the filling of masonry seams with adhesive or cement-sand mortar, which are temperature bridges, and the use of polyurethane adhesive, which has a lower thermal conductivity compared to adhesive mixtures, as filler for vertical and horizontal seams is unacceptable due to its low shear stiffness. The authors developed masonry walls made of cellular concrete blocks, which allow reducing the deformability of the enclosing structure on polyurethane adhesive due to the device of fixators in the form of glass composite rods in the vertical seams of the masonry and directly into the blocks. The paper also presents a study of the reduced resistance to heat transfer of the enclosing structure, taking into account heat-conducting inclusions, on the basis of which a conclusion is made about ensuring the energy efficiency of the developed wall fences due to the increased thermal uniformity of the masonry.

**Keywords:** Aerated concrete blocks · Masonry · Polyurethane adhesive · Enclosing structures · Shear stiffness

## 1 Introduction

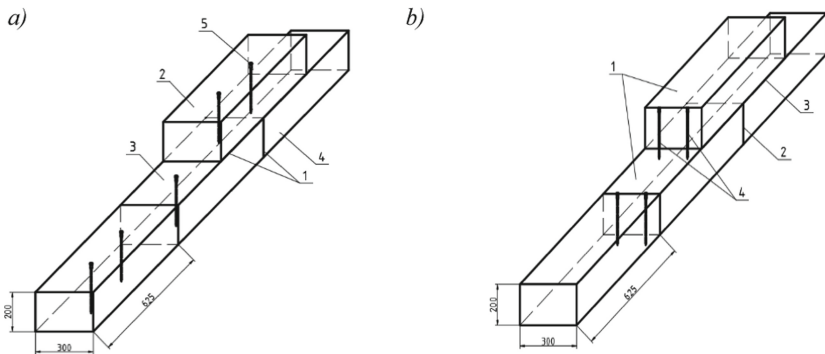
Masonry walls made of cellular concrete blocks is currently one of the most popular technologies for masonry exterior walls of residential and public buildings. The use of cellular concrete blocks is due to their thermal and strength characteristics. However, when assessing the energy efficiency of masonry, it is necessary to take into account the influence of heat-conducting inclusions on the parameters of thermal uniformity of external walls [1–4].

One of the options for improving the thermal insulation characteristics of masonry made of aerated concrete blocks is the use of one-component polyurethane adhesive as filler for vertical and horizontal seams. In comparison with the generally accepted technology of masonry on cement adhesive compositions or solutions, masonry on polyurethane adhesive eliminates wet processes on the construction site, provides the

required thermal performance due to high thermal uniformity of the structure, reduces material consumption and approximately doubles the speed of masonry construction [5–7].

However, this material has low shear stiffness, reducing the crack resistance of masonry, which limits the use of polyurethane adhesive, allowing it to be used only in the construction of partitions of buildings [8]. In this connection, the authors developed energy-efficient masonry walls made of cellular concrete blocks, which reduce the deformability of the enclosing structure on polyurethane adhesive by installing fixators in the form of glass-composite rods in the vertical seams of the masonry and directly into the blocks.

Energy-efficient masonry walls made of cellular concrete blocks with their fixation are shown in Fig. 1, *a*.



**Fig. 1.** Masonry walls made of cellular concrete blocks with their fixation: *a* – on the block; *b* – on the seam.

The developed enclosing structure consists of cellular concrete blocks connected to each other by a thin layer of polyurethane adhesive with a thickness of 1...3 mm (Fig. 1, *a*, pos. 1). The block of the overlying row (Fig. 1, *a*, pos. 2) of the masonry is attached to the blocks of the underlying row (Fig. 1, *a*, pos. 3 and 4) with two glass composite rods (Fig. 1, *a*, pos. 5) 50 mm longer than the block height. The rods are driven into the block at a distance of 1/3 of the length of the block from its poking sides. These rods, penetrating the block (Fig. 1, *a*, pos. 2) along its entire height, they are driven into the underlying blocks (Fig. 1, *a*, pos. 3 and 4) to a depth of 50 mm [9].

Energy-efficient masonry walls made of cellular concrete blocks with their fixation at the seam is shown in Fig. 1, *b*.

This wall fence consists of cellular concrete blocks (Fig. 1, *b*, pos. 1). Each vertical (Fig. 1, *b*, pos. 2) and horizontal (Fig. 1, *b*, pos. 3) masonry seam is made on polyurethane adhesive. To vertical (Fig. 1, *b*, pos. 2) seams two glass composite rods are driven (Fig. 1, *b*, pos. 4) 50 mm longer than the block height. The rods are driven at a distance of 1/4 from the spoon sides of the block. The device in the seams of masonry made of cellular concrete blocks on polyurethane adhesive of glass composite rods allows increasing the strength and cracking resistance of masonry by improving the flatness of masonry in the vertical and horizontal directions, while providing high thermal uniformity [10].

## 2 Methods and Materials

To justify the choice of the seam filler and the rod material that increases the deformative properties of the masonry, the reduced resistance to heat transfer of the enclosing structure was calculated taking into account heat-conducting inclusions. For the calculation, we consider a fragment of single-row aerated concrete masonry made on a thin-layer adhesive solution with a seam thickness of 5 mm (Fig. 2, *a*), a fragment of masonry made on polyurethane adhesive (Fig. 2, *b*), a fragment of energy-efficient masonry made on polyurethane adhesive, with fixing blocks with glass composite rods (Fig. 2, *c*) and a fragment of energy-efficient masonry made on polyurethane adhesive, with fixing blocks with glass composite rods along the seam (Fig. 2, *d*), with an area of 1 m<sup>2</sup> each. The masonry under consideration consists of aerated concrete blocks *D400* with a size of 200 × 400 × 600 mm.

The calculation of the reduced heat transfer resistance of energy-efficient masonry and aerated concrete masonry with transverse ligation through a row is made in accordance with [11].

## 3 Results and Discussion

The fragments under consideration are represented by two types of a homogeneous part of the structure:

- the site of bonding of horizontal rows of masonry in the form of a through seam (Fig. 2, pos. *I*);
- the site of bonding masonry blocks in the form of a through vertical seam with glass composite rods (Fig. 2, pos. *I*);

The reduced heat transfer resistance of the structure of the calculated fragment is determined by the formula (1) [11]:

$$R_o^r = \sum A_i / \sum A_i / R_{o,i} + \sum L_j \psi_j + \sum N_k K_k \quad (1)$$

where  $A_i$  – the area of the structure of the  $i$ -th type in the fragment under consideration, m<sup>2</sup>;

$L_j$  – the length of all seams of the  $j$ -th type in the fragment under consideration, m;

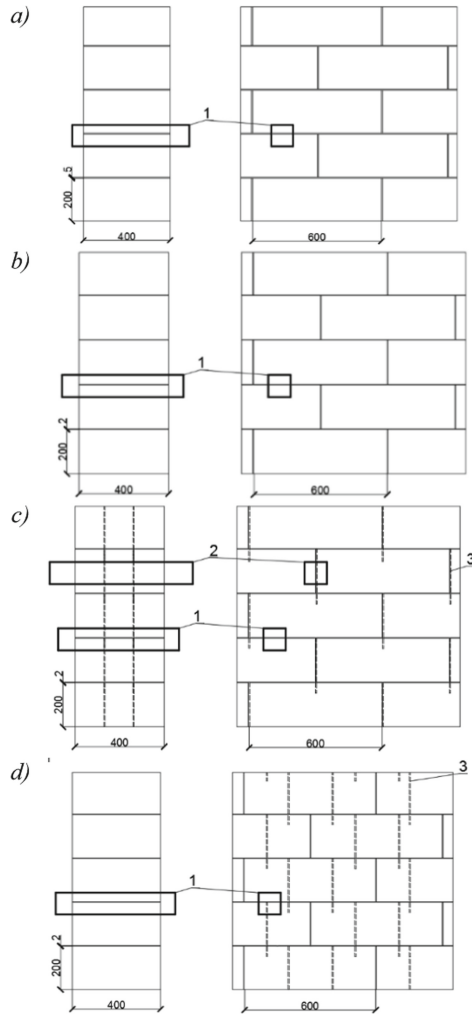
$N_k$  – the number of  $k$ -type point thermal inhomogeneities in the fragment under consideration, pcs;

$R_{o,i}$  – heat transfer resistance of a homogeneous part of the structure of the  $i$ -th type, (m<sup>2</sup> · °C)/W;

$\psi_j$  – additional specific linear heat losses through the joint of the  $j$ -th type, W/(m · °C);

$K_k$  – additional specific heat losses through a point heat engineering inhomogeneity of the  $k$ -th form, W/°C.

The reduced resistance to heat transfer of a fragment of single-row aerated concrete masonry made on a thin-layer adhesive solution, a fragment of masonry made on



**Fig. 2.** Cross-section and general view of fragments of single-row masonry made of aerated concrete blocks to determine the reduced resistance to heat transfer: *a* – aerated concrete masonry on cement adhesive composition; *b* – aerated concrete masonry on polyurethane adhesive; *c* – aerated concrete masonry on polyurethane adhesive with fixing blocks; *d* – aerated concrete masonry on polyurethane adhesive with fixing blocks at the seam; 1 – section of bonding of the masonry seams; 2 – section for bonding masonry blocks in the form of a through vertical seam with glass composite rods; 3 – glass composite rods.

polyurethane adhesive, a fragment of masonry with fixing blocks with glass composite rods is determined. The calculation data are presented in Table 1.

From the data presented in the table, it follows that the energy-efficient single-row masonry walls developed by the authors have the same reduced resistance to heat transfer as aerated concrete masonry on polyurethane seams. Glass composite rods, providing

**Table 1.** Thermal engineering indicators for determining the reduced resistance to heat transfer of masonry fragments.

Indicators	Masonry on a cement-adhesive mixture		Masonry on polyurethane adhesive		Masonry on polyurethane adhesive with fixing blocks		Masonry on polyurethane adhesive with fixing blocks at the seam	
	Block	Through seam	Block	Through seam	Block	Through seam	Block	Through seam
Masonry thickness, mm	400							
Area of the fragment section $A_f, m^2$	0.9702	0.0298	0.988	0.012	$\frac{0.9701^*}{0.0179}$	0.012	$\frac{0.9872^*}{0.0008}$	$\frac{0.008^*}{0.004}$
Heat transfer resistance of a homogeneous part of the structure $R_{0,i}, (m^2 \cdot ^\circ C)/W$	3.4917	1.0095	3.4917	11.2695	$\frac{3.4917^*}{3.4589}$	11.2695	$\frac{3.4917^*}{3.4589}$	$\frac{11.2695^*}{11.0096}$
Additional specific linear heat losses through the seam of the $j$ -th type $\psi_j, W/(m \cdot ^\circ C)$	0.00566		0.006		0.006		0.006	
The length of all seams of the $j$ -th type in the fragment under consideration $L_j, m$	11.92		11.968		11.968		$\frac{8^*}{3.968}$	
Reduced heat transfer resistance of the structure $R^*_o, (m^2 \cdot ^\circ C)/W$	2.55		2.8106		2.8105		2.8114	

\*Note: The upper value refers to the section of seams without heat-conducting inclusions, the lower value refers to the section of seams with glass composite rods.

thermal uniformity of the structure, contribute to the use of this masonry as a load-bearing enclosing structure.

## 4 Conclusion

Energy-efficient single-row masonry walls made of cellular concrete blocks have been developed, which allow reducing the deformability of the enclosing structure on polyurethane adhesive by installing fixators in the form of glass-composite rods in the vertical seams of the masonry and directly into the blocks. To determine the efficiency of masonry, the reduced heat transfer resistance of single-row masonry of a standard structural solution on a cement adhesive composition, single-row cellular concrete masonry on polyurethane adhesive, masonry on polyurethane adhesive with block fixation and masonry on polyurethane adhesive with block fixation along a vertical seam was calculated and conclusions were established. The use of developed masonry walls made of cellular concrete blocks allows:

- providing the required thermal performance due to the high thermal uniformity of the structure;
- erecting load-bearing wall fences with the use of polyurethane adhesive as filler for vertical and horizontal seams;

- reducing the material consumption of masonry by 10% due to the use of polyurethane adhesive;
- reducing the crack resistance and deformability of masonry due to the installation of glass composite rods.

The implementation of the developed energy-efficient solution for the construction of enclosing structures made of cellular concrete blocks in the construction of civil buildings will optimize the economic and technological factors of design solutions for modern capital construction projects.

**Acknowledgements.** The work is realized in the framework of the Program of flagship university development on the base of the Belgorod State Technological University named after V.G. Shukhov, using equipment of High Technology Center at BSTU named after V.G. Shukhov.

## References

1. Grinfeld, G.I.: Performance characteristics of autoclaved aerated concrete with density 400 kg/cub.m. *Constr. Unique Build. Struct.* **5**(10), 28–57 (2013)
2. Gushchin, S.V., Semenenko, A.S., Shen, C.: World trends in the development of energy-saving technologies. *Bull. BSTU Named After V.G. Shukhov* **5**, 31–43 (2020)
3. Karpov, D.F.: Application of active and passive thermal control in the flaw detection of building materials and products, protecting structures of buildings and structures. *Constr. Mater. Prod.* **4**, 39–44 (2019)
4. Stritih, U.: Heat transfer enhancement in latent heat thermal storage system for buildings. *Energy Build.* **35**(11), 1097–1104 (2003)
5. Pukhkal, V.A., Mottaeva, A.B.: FEM modeling of external walls made of autoclaved aerated concrete blocks. *Civ. Eng. J.* **5**, 202–211 (2018)
6. Ahmed, A.: Sustainable construction using autoclaved aerated concrete (aircrete) blocks. *Res. Dev. Mater. Sci.* **1**(4), 63–66 (2017)
7. Yang, F., Sun, L.Z., Xie, Z.L.: Theoretical study on optimal design of thermal performance of aerated concrete-based composite thermal insulation wall. *Adv. Mater. Res.* **450–451**, 663–666 (2012)
8. Gorshkov, A.S., Rymkevich, P.P., Vatin, N.I.: Properties of the wall structures made of autoclaved cellular concrete product on the polyurethane foam adhesive. *J. Civ. Eng.* **5**, 5–19 (2013)
9. Suleymanova, L.A., Ryabchevsky, I.S., Kolomatsky, A.S., Suleymanov, K.A., Monko, D., Kulakov, V.A.: Patent of the Russian Federation for utility model 2020126437, 05.08.2020. Masonry walls made of cellular concrete blocks with their fixation. Russian Patent No. 200967, Byul. No. 32 (2020)
10. Suleymanova, L.A., Ryabchevsky, I.S., Pogorelova, I.A., Suleymanov, K.A., Marushko, M.V., Amelin, P.A.: Patent of the Russian Federation for utility model No. 2020126438, 05.08.2020. Masonry walls made of cellular concrete blocks with their fixation at the seam. Russian Patent No. 200968, Byul. No. 32 (2020)
11. Suleymanova, L.A., Pogorelova, I.A., Marushko, M.V., Ryabchevsky, I.S.: Energy-efficient double-row masonry of the exterior walls in the buildings made of cellular concrete blocks. In: *IOP Conference Series: Materials Science and Engineering*, vol. 913, p. 022044 (2020).



# Experimental Studies of Deflections in Bending Reinforced Concrete Elements Taking into Account the Influence of the Shape of Their Cross-Section

D. V. Obernikhin<sup>(✉)</sup>  and A. I. Nikulin 

Belgorod State Technological University Named After V.G. Shukhov, Belgorod, Russia

**Abstract.** Experimental studies of the deformability of reinforced concrete beams of trapezoidal and reference rectangular sections have been carried out. Reinforced concrete structures of trapezoidal section are the object of research. The main subject of research is the deflections of the structures under study at all stages of loading up to failure. The investigated beams have the same overall dimensions with different concrete consumption. A methodology has been developed for the experimental study of the deflected mode, taking into account the features of the cross section of the samples under study. A universal model of a test setup is proposed that allows testing bending elements with control of the studied parameters. The features of the growth of deflections at different stages of loading are revealed. It was found that in the later stages of the load close to breaking, deflection value for the beams of trapezoidal cross-section with a wide upper edge becomes lower than the beams of rectangular cross section. It is shown that trapezoidal beams with a lower wide edge have the lowest deformative and strength characteristics.

**Keywords:** Bending reinforced concrete element · Deformability · Trapezoidal section · Reinforced concrete beam · Deflection

## 1 Introduction

In modern construction practice, there are structures with different cross-sectional shapes. The most widespread are the designs of rectangular, T-section, I-section and trapezoidal cross-sections.

Investigation of deflected mode consisting of bent reinforced concrete elements devoted to a fairly large number of works. Examples include works: Kodysh E.N., Trekin N.N., Trekin D.N [4], Tamrazyan A.G., Orlova M.A. [5], Popov V.M., Plyusnin V.M [6], M.S. Al-Ansari [7], P. Fantilli [8], W.Y. Lu, S.J. Hwang, I.J. Lin [9], J. Milton de Araújo [10], K.J.H. Zhou [11].

However, the experimental data on the work of reinforced concrete bending elements of trapezoidal cross-section are insufficient today.

It should be noted that earlier authors have developed the necessary techniques and algorithms [1, 2], by which have been carried out respective numerical studies [3], which

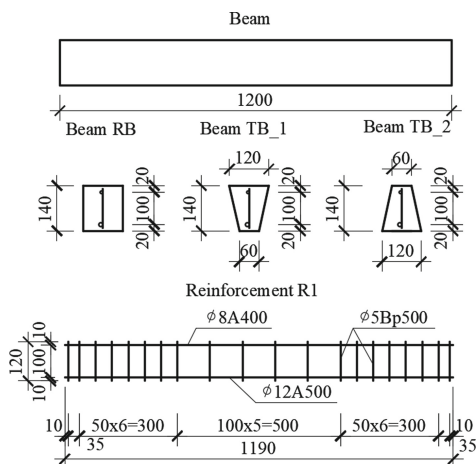
made it possible to give a preliminary assessment of the effect of the cross-sectional shape on the stress-strain state of bending reinforced concrete elements of a trapezoidal section. In order to further develop the above topic and test the developed methods, the authors conducted experiments on specially made reinforced concrete samples, partial results of which are given in this article.

Taking into account all of the above, the main tasks of experimental research were drawn up:

- develop a methodology of experimental research;
- to carry out experimental studies of the deformability of bending reinforced concrete elements of a trapezoidal section and compare with a rectangular one;
- to study the influence of the cross-sectional shape on the deformability of reinforced concrete elements;

To solve the set tasks, an experiment program was developed, in accordance with which the following samples were tested:

testing of standard samples to determine the physical and mechanical characteristics of materials (concrete and reinforcement);  
 testing of reference elements of rectangular section (RB);  
 test of the studied bending elements of a trapezoidal cross-section, with wide upper (TB\_1) and lower (TB\_2) faces (see Fig. 1).



**Fig. 1.** Geometrical dimensions and scheme of reinforcement of beams RB, TB\_1 and TB\_2.

## 2 Methods and Materials

For the study, 9 reinforced concrete beams were made, consisting of 3 series of 3 beams of each type of cross-section: rectangular beams (RB) and trapezoidal beams with wide



upper (TB\_1) and lower (TB\_2) edges (Fig. 1). The dimensions of the cross sections of the samples were taken such that the volume of concrete in the trapezoidal beams was 25% less than in conventional RB series beams.

Tests of control samples showed that concrete of class B20 corresponds to all beams (concrete characteristics are given in Table 1). The height of the concrete protective layer for the top and bottom reinforcement was 20 mm.

**Table 1.** Characteristics of concrete.

Characteristics of concrete samples	RB	TB_1	TB_2
Ultimate resistance to central compression $R_b$ MPa	20.35	20.70	20.01
Compression modulus of elasticity при сжатии $E_{bn}$	31500	31500	31500
Ultimate resistance to central tension $R_{bt}$ , MPa	1.53	1.68	1.50
Ultimate relative deformation under central compression $\varepsilon_{bR}$	0.0019450	0.0019561	0.0019383
Ultimate relative deformation at central tension $\varepsilon_{btR}$	0.0000886	0.0000945	0.0000885

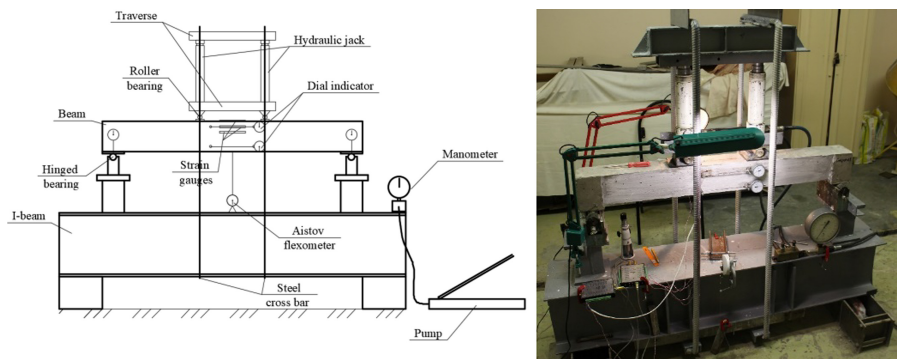
A diagram of the reinforcement of beams is shown in Fig. 1. Lower reinforcement  $\varnothing 12$  mm, upper reinforcement  $\varnothing 8$  mm, class A500, transverse bars -  $\varnothing 5$  mm Bp500. The characteristics of the longitudinal reinforcement are given in Table 2.

**Table 2.** Reinforcement characteristics.

Reinforcement class	$\sigma_{el}$ , MPa	$\sigma_y$ , MPa	$\sigma_u$ , MPa	$\varepsilon$ , %
$\varnothing 12$ A500c	575.86	591.75	668.56	13.87
$\varnothing 8$ A500	615.57	619.72	708.92	14.76

To conduct experimental research, the authors have developed a universal test rig (see Fig. 2). Hydraulic 15-ton jacks with manual pumping of oil into the system were used as power elements. The measurement of deformations in the compression and tension zones of concrete was carried out on the basis of 200 mm using dial indicators with a graduation of 0.001 mm. In the middle of the beam span, an Aistov deflection meter was installed to determine deflections. In order to control the compliance of the supporting sections of the beams, dial indicators with a division value of 0.01 mm were installed above the supports.

The transfer of forces from the jacks to the beam took place through steel traverses. To control the uniformity of load application, strain gauges were installed on the rods.



**Fig. 2.** Universal test rig with installed reinforced concrete beam and measuring instruments.

The reinforced concrete beams were thoroughly cleaned prior to testing. Measurements were made of the actual geometric dimensions. All irregularities on the edges were eliminated with sandpaper, after which the places for the installation of measuring instruments were marked. Then the beam was installed on the supports of the rig, after which it was painted with lime whitewash 2 times. This was done in order to more accurately determine the moment when the first crack appeared in the tensile zone of concrete. After installing all the distribution traverses, dial indicators were attached to the beam with the help of special accessories. The complete universal rig is shown in Fig. 2.

The load was applied to each beam in steps with a step of not more than 10% of the expected breaking load. At each stage, the load was held for 10 min. At the beginning and at the end of each stage, all readings of the measuring instruments were recorded and a thorough examination of the beam from both sides was carried out for the appearance of new cracks. To assess the deformability, the values of the deflections were recorded at each stage up to destruction. It should be noted that the deflections were recorded at the beginning and at the end of each step, thereby taking into account the creep of concrete. The values of the deflections at the stage of destruction of the experimental samples were obtained using video equipment.

### 3 Results and Discussion

To compare the deflections, as well as the crack resistance of the investigated beams, Table 3 was compiled containing the values of the deflections at control loads of 9 kN, 16 kN, 24 kN, 32 kN and at destruction.

**Table 3.** Test results.

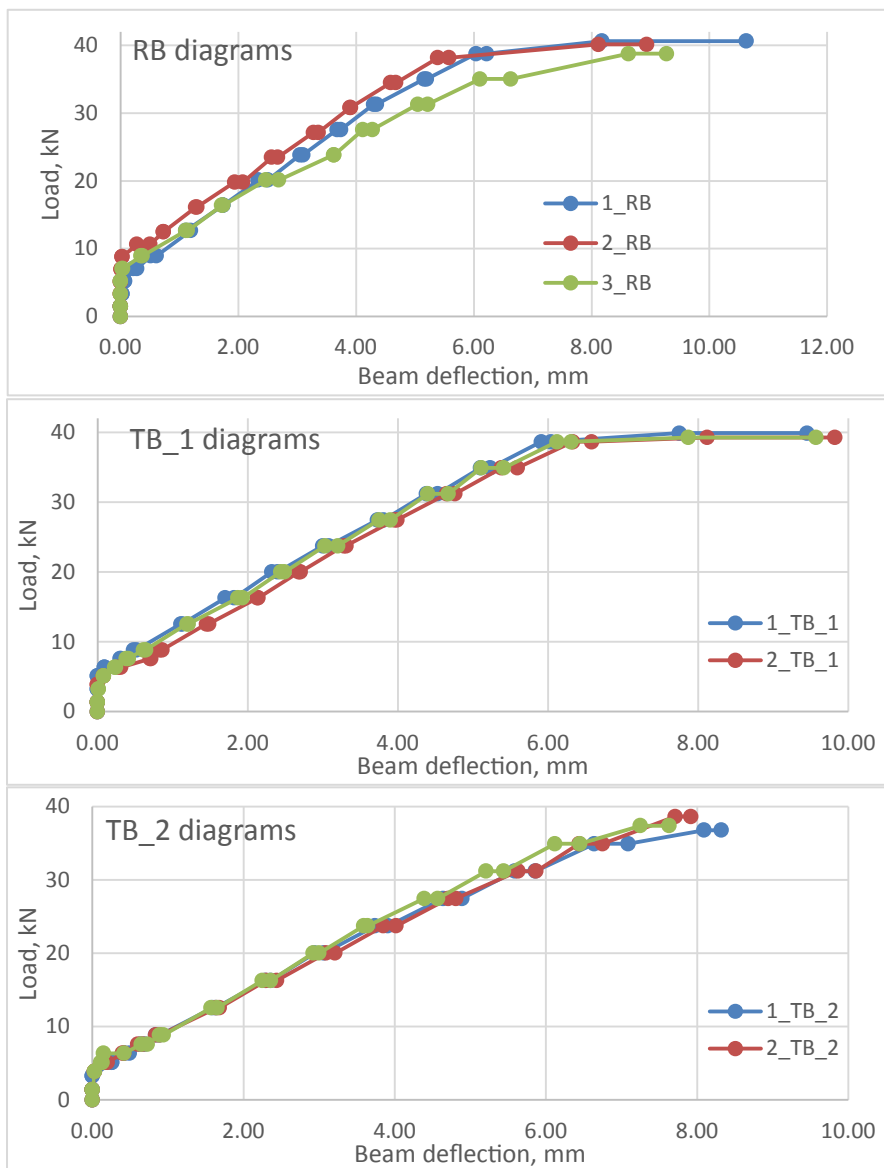
Beam type	№	Beam deflection (mm) under load (kN)				Beam deflection (mm) at destruction	Breaking load
		9	16	24	32		
RB	1	0.61	1.76	3.17	4.58	10.63	40.62
	2	0.28	1.77	2.78	4.59	8.94	40.12
	3	0.37	1.76	3.73	5.55	9.28	38.75
TB_1	1	0.52	1.83	3.20	4.60	9.45	39.90
	2	0.86	2.15	3.40	4.96	9.82	39.28
	3	0.64	1.88	3.24	4.83	9.57	39.30
TB_2	1	0.89	2.38	4.07	6.25	8.3	36.79
	2	0.89	2.46	4.16	6.15	7.92	38.65
	3	0.94	2.38	3.80	5.76	7.63	37.41

Based on the data given in the table, the following conclusions can be drawn:

- at fixed loads of 9 kN, 16.0 kN, 24.0 kN, the average deflections of trapezoidal beams of the TB\_1 series in comparison with specimens of rectangular cross-section turned out to be higher, respectively, by 59.52%, 10.78%, 1.64%, and already at a load of 32 kN were less by 2.24%. Deflections of beams of the TB\_2 series under the same fixed loads increased, respectively, by 115.95%, 36.53%, 24.26% and 23.35% in relation to the reference specimens of rectangular cross-section, which is explained by the earlier onset of the crack formation process in tensile zone of concrete of trapezoidal beams with a lower wide edge;
- the average value of the breaking load for trapezoidal beams with the upper and lower wide edges is less, respectively, by 0.85% and 5.56% compared to the reference specimens of rectangular cross-section;

Based on these data, we were constructed diagrams Load-deflection (see Fig. 3).

Based on the obtained experimental diagrams, it can be seen that at the initial stages of loading the beams, before the first crack appears, the “Load-deflection” diagrams are linear. As the breaking load is approached, the deflection value begins to increase practically without increasing the load.



**Fig. 3.** Experimental “load-deflection” diagrams for specimen types RB, TB\_1 and TB\_2.

## 4 Conclusion

Analysis of the data obtained shows that trapezoidal beams with a wide upper face are not much inferior to rectangular beams in terms of their bearing capacity, and at later stages of loading they even have smaller deflections than rectangular beams. At the same time, their production requires 25% less concrete. Trapezoidal beams with a wide

bottom edge have proven to be the most ineffective. The results of this study allow us to conclude about the relevance of further research on the strength and crack formation process of trapezoidal beams.

**Acknowledgements.** This work was realized in the framework of the Program of flagship university development on the base of the Belgorod State Technological University named after V. G. Shukhov, using equipment of High Technology Center at BSTU named after V. G. Shukhov.

## References

1. Nikulin, A.I., Obernikhin, D.V.: Deformability of bent reinforced concrete elements of trapezoidal section with cracks in the tension zone. *Bull. BSTU Named After V.G. Shukhov* **5**, 88–93 (2016)
2. Obernikhin, D.V., Nikulin, A.I.: Strength and crack resistance of bent reinforced concrete elements of trapezoidal cross-section with a lower wide face. *Bull. BSTU Named After V. G. Shukhov* **4**, 66–72 (2016)
3. Obernikhin, D.V.: Numerical studies of strength, crack resistance and deformability of bending reinforced concrete elements of trapezoidal section of the model. *Bull. BSTU Named After V.G. Shukhov* **5**, 24–29 (2017)
4. Kodysh, E.N., Trekin, N.N., Trekin, D.N.: Analysis of the deformability of bent reinforced concrete elements. *Ind. Civ. Eng.* **6**, 59–61 (2013)
5. Tamrazyan, A.G., Orlova, M.A.: Experimental studies of the stress-strain state of reinforced concrete bending elements with cracks. *Bull. Tomsk State Univ. Archit. Civ. Eng.* **6**(53), 98–105 (2015)
6. Popov, V.M., Plyusnin, V.M.: Influence of the deformation characteristics of concrete on the bearing capacity of bent reinforced concrete elements. *Ind. Civ. Eng.* **8**, 5–10 (2015)
7. Al-Ansari, M.S.: Flexural safety cost of optimized reinforced concrete beams. *International J. Civ. Eng. Technol.* **4**(2), 15–35 (2013)
8. Fantilli, A.P., Ferretti, D., Iori, I., Vallini, P.: Flexural deformability of reinforced concrete beams. *J. Struct. Eng.* **124**(9), 1041–1049 (1998)
9. Lu, W.Y., Hwang, S.J., Lin, I.J.: Deflection prediction for reinforced concrete deep beams. *Comput. Concr.* **7**(1), 1–16 (2010)
10. de Araújo, J.M.: Improvement of the ACI method for calculation of deflections of reinforced concrete beams. *Teoria Prática Engenharia Civ.* **7**, 49–60 (2005)
11. Zhhou, K.J.H., Ho, J.C.M., Su, R.K.L.: Flexural strength and deformability design of reinforced concrete beams. *Proc. Eng.* **14**, 793–796 (2011)



# Predicting the Parameters of Construction Structures with Variable Action of Factors over Time and with Mutual Influence on Each Other

D. I. Korolkov , D. V. Nizhegorodtsev  <sup>(✉)</sup>, V. I. Klevan , and S. G. Golovina 

Saint Petersburg State University of Architecture and Civil Engineering, Saint-Petersburg, Russia

**Abstract.** This paper presents a method for predicting the parameters of building structures and calculating the residual life using regression equations. It is proposed to apply one-factor regression equations, in which the variable is time, and the dependent value is the parameter of the building structure, the changes of which the researcher needs to determine. The authors also proposed the use of the “reduced” interval for constructing a system of regression equations. A step-by-step algorithm for constructing these systems of equations is developed. For ease of use by other researchers, the presented method is summarized in a block diagram.

The developed forecasting technique was tested by processing the results of experimental studies of small samples of glued wood under prolonged loading. The tests were carried out according to GOST 34349–2017 and are aimed at assessing the long-term strength of the adhesive seam in samples of glued wooden structures. For the application of long-term load, a lever-type test device was developed and assembled, which allows adjusting the shoulder of the load application depending on the strength of the control samples.

In the process of testing, the error in predicting the theoretical value of long-term strength was no more than 5%. This fact suggests that the developed forecasting technique allows performing a theoretical assessment of the parameters of building structures with high convergence with experimental results.

According to the results of the conducted research, the advantages and disadvantages of the developed methodology are revealed. The scope of application of the forecasting technique is determined, which makes it possible to level these shortcomings.

The tasks of further improving the forecasting methodology, including taking into account the multicollinearity of factors, as well as developing a convenient method for determining numerical criteria that allow identifying the adequacy of regression equations in specific conditions, are set.

**Keywords:** Residual life · Construction structures · Regression equations · Long-term strength · Forecasting

## 1 Introduction

Assessment of the service life of construction structures of buildings and structures is an important technical and economic task. The calculation of this indicator allows determining the time for repair, reconstruction or replacement of certain structures and makes it possible to avoid accidents.

Existing methods of inspection of construction structures allow assessing the technical condition of buildings and structures only at the time of the study. They do not give an idea of how much the object can still be operated in these conditions.

For this reason, the development of methods for predicting changes in the parameters of construction structures over time is relevant. Having the ability to predict the properties of construction structures, they can estimate their residual life, load-bearing capacity, characteristics of the used materials, operating conditions, etc. at a certain point in time.

## 2 Methods and Materials

Predicting the parameters of structures should be made taking into account the variability and interdependence of factors acting on the structure.

As the number of possible combinations of parameter changes can be infinitely large, and changes can be caused spontaneously, a mathematical description is excluded. Therefore, it is advisable to divide the time interval under consideration into sections where the value of the analyzed parameters will be constant.

$$R = \begin{cases} \text{regression equation 1 } 0 \leq \Delta t_1 \leq t_1 \\ \text{regression equation 2 } t_1 \leq \Delta t_2 \leq t_2 \\ \dots & \dots \\ \text{regression equation } n \ t_{n-1} \leq \Delta t_n \leq t_n \end{cases} \quad (1)$$

$t_1, t_2, \dots, t_n$  – the boundary values of the time intervals in which parameter values are constant.

$\Delta t_1, \Delta t_2, \dots, \Delta t_n$  – the time intervals at which parameter values are constant.

As with the growth of the number of input parameters, the time interval at which their value will be constant tends to zero  $\Delta t_i \rightarrow 0$ , then it is impossible to directly apply such equations in practice.

The way out of the situation can be the use of a “reduced” interval, i.e. such an interval in which it is possible to construct a regression equation with a coefficient of determination higher than 0.85:

$$R = \begin{cases} \text{regression equation 1 } 0 \leq \Delta t_{\text{red.1}} \leq t_{\text{red.1}} \\ \text{regression equation 2 } t_{\text{red.1}} \leq \Delta t_{\text{red.2}} \leq t_{\text{red.2}} \\ \dots & \dots \\ \text{regression equation } n \ t_{\text{red.}n-1} \leq \Delta t_{\text{red.}n} \leq t_{\text{red.}n} \end{cases} \quad (2)$$

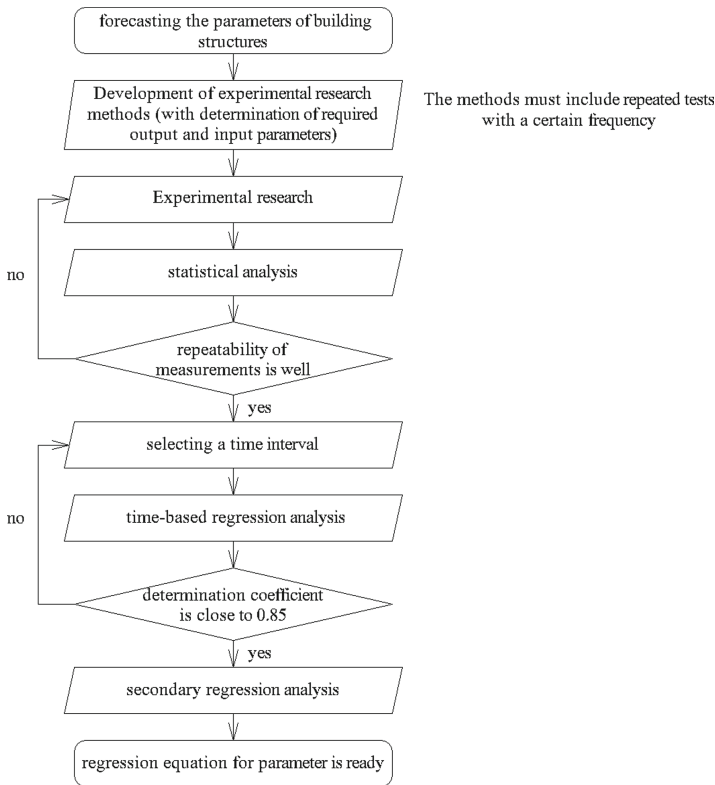
$t_{\text{red.1}}, t_{\text{red.2}}, \dots, t_{\text{red.}n}$  – boundary values of time “reduced” intervals, within which regression equations are constructed.

$\Delta t_{red.1}, \Delta t_{red.2}, \dots, \Delta t_{red.n}$  – time “reduced” intervals within which regression equations are constructed.

As these intervals are unknown to us in advance, their construction is carried out by selecting boundary values.

For the preliminary calculation, a section of the time interval is taken. Then the regression equation is constructed and the determination coefficient is calculated. If necessary, the calculation is repeated with a decrease or increase in the interval. Iterations are repeated until the determination coefficient is at least 0.85.

Ideally, it is necessary to ensure that the constructed regression equation has a value of the determination coefficient equal to 0.85 or close to it. This allows obtaining the minimum number of “reduced” intervals and, at the same time, obtaining for each given interval a regression equation with acceptable accuracy.



**Fig. 1.** Block diagram of the proposed methodology for predicting the parameters of construction structures.

As in reality the factors affecting the construction structures have a mutual influence on each other, it is necessary to take this into account in the regression equations.

On the basis of all the above, the authors propose a method for predicting the parameters of construction structures, presented in the form of a block diagram in Fig. 1.



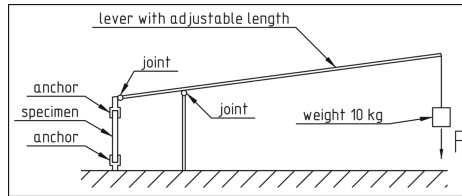
The presented method was tested by testing small samples of glued wooden structures for long-term strength.

For testing the long-term strength of glued wooden structures, four series of samples of wooden glued structures for testing for chipping under tension (made of beech) are made.

Samples from № 1 series are subjected to control tests in order to determine the short-term strength (breaking load).

Samples of № 2, 3, and 4 series are subjected to prolonged static loading with a load equal to 0.9, 0.8, and 0.7 of the average destructive load of the control samples, respectively.

For carrying out long-term tests, an experimental device was designed and constructed, the principle of operation of which is based on a system of levers. The general scheme of the experimental device is shown in Fig. 2.



**Fig. 2.** Scheme of an experimental device for conducting long-term tests of adhesive seams of wooden glued structures.

The duration of long-term tests, i.e. the time from the beginning of loading of samples to their destruction, was recorded using special video recording devices with a timer. The time was controlled with an accuracy of 1 min.

### 3 Results and Discussion

The results of testing samples of glued wooden structures for long-term strength are presented in Table 1.

For each series, a different regression equation of the form was constructed.

$$y = a \cdot \ln t + b \tag{3}$$

where  $t$  – time to destruction of the sample;

$y$  – value of the glue strength fraction.

$a$  and  $b$  – the regression equation coefficients.

9 regression equations were constructed. Fig. 3 shows examples of graphs for test series 2, 3, and 4.

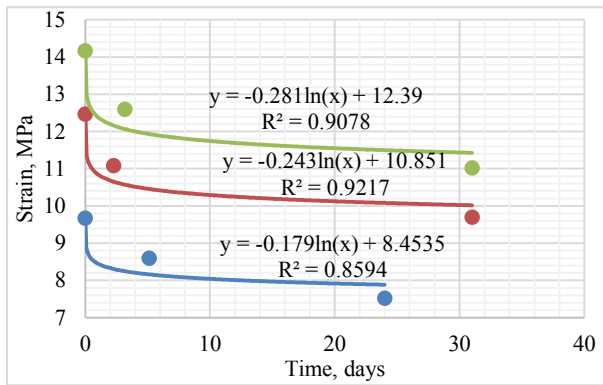
As a result, secondary regression equations were obtained.

$$a = -0.0177 \cdot \sigma_H + 0.0059 \tag{4}$$

$$b = 0.7907 \cdot \sigma_H - 0.0374 \tag{5}$$

**Table 1.** Test results of samples of glued wooden structures.

Strength of control samples, MPa	Strain during long-term testing, MPa			Time, s		
	Long-term strength coefficients					
	0.9	0.8	0.7	0.9	0.8	0.7
11.55	10.395	9.24	8.085	87	180000	4406400
13.85	12.465	11.08	9.695	72	198000	2678400
10.74	9.666	8.592	7.518	69	442800	2073600
15.74	14.166	12.592	11.018	101	273600	2678400
11.11	9.999	8.888	7.777	82	266400	3974400
16.05	14.445	12.84	11.235	78	190800	2764800
11.4	10.26	9.12	7.98	105	342000	3024000
16.57	14.913	13.256	11.599	102	453600	4924800
14.45	13.005	11.56	10.115	86	342000	3974400



**Fig. 3.** Regression equations for test series 2, 3, 4.

After substituting into the main equation, instead of the regression equations coefficients of the secondary equations, it was obtained:

$$y = (-0.0177 \cdot \sigma_H + 0.0059) \cdot \ln t + 0.7907 \cdot \sigma_H - 0.0374 \quad (6)$$

The convergence of the data obtained using this equation was verified by comparing the theoretical values of long-term strength with the experimental values for another series of tests. The results of the comparison are shown in Table 2.

We find the time to destruction by expressing it from the resulting equation:

$$t = e^{\frac{y-b}{a}} = e^{\frac{y-(0.7907 \cdot \sigma_{H\text{нп}} - 0.0374)}{(-0.0177 \cdot \sigma_{H\text{нп}} + 0.0059)}} \quad (7)$$

**Table 2.** Results of estimation of convergence of theoretical and experimental data.

	Long-term strength experimental			Long-term strength theoretical			Difference between theoretical and practical values		
	Long-term strength coefficients			Long-term strength coefficients					
	0.9	0.9	0.8	0.9	0.8	0.7	0.9	0.8	0.7
15.88	14.292	12.704	11.116	14.49	12.02	11.48	1.36%	5.66%	3.2%

The value of the correction to the  $y$  parameter will be equal to the difference between the theoretical and practical values.

$$t = e^{\frac{11.116 \cdot 1.032 - (0.7907 \cdot \sigma_{\text{нап}} - 0.0374)}{(-0.0177 \cdot \sigma_{\text{нап}} + 0.0059)}} = e^{3.8056} = 44.95 = 45 \text{ days} \tag{8}$$

The difference between the theoretical and practical value of the time to destruction does not exceed 5%.

We note the advantages and disadvantages of this method of predicting the parameters of construction structures in Table 3.

**Table 3.** The method of construction structures parameters predicting: advantages and disadvantages.

Advantages	Disadvantages
<ol style="list-style-type: none"> <li>1. Universality. These equations can be applied to any design and operating conditions</li> <li>2. The ability to take into account an unlimited number of parameters</li> <li>3. Each variable of the equation can be represented as a separate function</li> <li>4. Easy to calculate. Regression analysis has long been “computerized”, i.e. these equations are calculated in programs almost instantly</li> </ol>	<ol style="list-style-type: none"> <li>1. The limitations of practical implementation. Despite the simplicity of the method, its implementation is optimal for cases where no more than three values are used as input parameters. To obtain a sufficient amount of data with a large number of variations in these parameters, testing is required</li> <li>2. The problem of physical interpretation. The dimension of the coefficients does not always coincide with the existing physical quantities</li> </ol>

Further, an example of a situation where there is a discrepancy between the obtained coefficients and the physical meaning of the process is given. Based on the test results, after processing the obtained results, it obtained a second-order polynomial regression equation.

$$R = a_2 \cdot t^2 + a_1 \cdot t + a_0 \tag{9}$$

Let us substitute the units of strength and time [MPa] and [s] into this equation. The coefficient  $a_0$  in this equation is the initial strength value. As a result, we get:

$$\text{MPa} = a_2 \cdot s^2 + a_1 \cdot s + \text{MPa} \quad (10)$$

As both parts of the equation should end up with the same units of measurement, the coefficients  $a_1$  and  $a_2$  will take the form:

$$\text{MPa} = \left[ \frac{\text{MPa}}{s^2} \right] \cdot s^2 + \left[ \frac{\text{MPa}}{s} \right] \cdot s + \text{MPa} \quad (11)$$

Thus, the physical meaning of the coefficient  $a_1$  is that it is the rate of change in strength, and the coefficient  $a_2$  is the acceleration of the process of changing strength. Therefore, it is impossible to correlate these coefficients with any physical quantities.

## 4 Conclusion

There are a number of questions that inevitably arise when considering this method of predicting the parameters of construction structures.

The first problem arises when evaluating the coincidence of the type of the secondary and the main equation. As the number of input parameters increases, the equation type may change. The question arises as to how well the previous equation can be used. In this case, it is necessary to establish criteria by which it will be permissible to use those regression equations that did not pass the determination coefficient.

When constructing a multiple regression equation, the problem of multicollinearity of factors may arise – a linear relationship of two or more explanatory variables, which can manifest itself in a functional or stochastic form. There is a need to modernize the proposed methodology taking into account this factor.

The use of this method for predicting the parameters of construction structures can significantly help in describing those processes or phenomena that have not received proper justification yet, and those who are engaged in the design and operation of construction objects.

## References

1. Aven, T.: Interpretations of alternative uncertainty representations in a reliability and risk analysis context. *Reliabil. Eng. Syst. Saf.* **96**(3), 353–360 (2011)
2. Aven, T., Zio, E.: Some considerations on the treatment of uncertainties in risk assessment for practical decision making. *Reliabil. Eng. Syst. Saf.* **96**, 64–74 (2011)
3. Jiang, C., Zhang, Z., Han, X., Liu, J.: A novel evidence-theory-based reliability analysis method for structures with epistemic uncertainty. *Comput. Struct.* **129**, 1–2 (2013)
4. Li, H., Nie, X.: Structural reliability analysis with fuzzy random variables using error principle. *Eng. Appl. Artif. Intell.* **67**, 91–99 (2018)
5. Wang, Y.: Imprecise probabilities based on generalized intervals for system reliability assessment. *Int. J. Reliabil. Saf.* **4**(4), 319–342 (2010)

6. Korolkov, D.I., Chernykh, A.G., Kazakevich, T.N., Mamedov, S.M., Gravit, M.V.: Use of two-parameter distributions for a joint assessment of the residual resource of building structures and engineering systems of buildings and structures. In: IOP Conference Series: Materials Science and Engineering. International Conference on Civil, Architectural and Environmental Sciences and Technologies, pp. 138–142 (2019)
7. Köhler, J.: Reliability of timber structures Doctoral thesis, Technische Wissenschaften, Eidgenössische Technische Hochschule ETH Zürich 16378 (2006)
8. Faydi, Y., Brancheriau, L., Pot, G., Collet, R.: Prediction of oak wood mechanical properties based on the statistical exploitation of vibrational response. *Bioresour. North Carolina State Univ.* **12**(3), 5913–5927 (2017)
9. Chernykh, A., Korolkov, D., Nizhegorodtsev, D., Kazakevich, T., Mamedov, S.: Estimating the residual operating life of wooden structures in high humidity conditions. *Archit. Eng. Saint-Petersburg* **5**(1), 10–19 (2020)



# Experimental Studies of the Strength of Reinforced Concrete Flexible Elements Forced with Carbon Fiber

G. A. Smolyago  and Y. L. Obernikhina  

Belgorod State Technological University, Belgorod, Russia

**Abstract.** Reinforcement of reinforced concrete flexible elements with polymer composite materials has found wide application in modern construction, so the accumulation of experimental studies of the strength of such structures is relevant. This paper presents the results of experimental studies of the stress-strain state of flexible reinforced concrete elements forced with carbon fiber. Namely, six beams of three types. The first type of beams - reference samples without reinforcement. The second type of beams – beams loaded at the stage corresponding to the standard load, in the presence of cracks and deflections, reinforced with carbon fiber, by gluing it to a stretched zone with a U-shaped anchorage on the supporting areas after unloading. The third type of beams includes samples reinforced, similar to the second type of beams but before the application of loads. In addition, during the experimental study, control images of concrete, rebar and carbon fiber were tested to establish their basic physical and mechanical characteristics. The limit values of experimental bending moments in the middle of the span of samples of all series are obtained. It was found that all samples externally reinforced with carbon fiber were destroyed as a result of increasing the width and height of normal cracks located in the zone of pure bending and increasing deflections, which led to the separation of the composite material from the concrete and the indent of the concrete of the compressed zone.

**Keywords:** Reinforced concrete beam · Load-bearing capacity · Reinforcement · Polymer composite materials · Carbon fiber · Anchoring

## 1 Introduction

Strengthening of load-bearing structures is one of the main directions of the construction industry. In modern construction practice, external reinforcement technologies with high specific strength and resistance to electrochemical corrosion are widely used [1, 2]. Due to its high physical and mechanical properties, the use of an external carbon fiber reinforcement system for strengthening load-bearing structures is recognized as an effective method [3].

In [4], experimental studies of reinforced concrete samples of rectangular cross-section with a width of 120 mm and a height of 220 mm were carried out. Design class of concrete for compressive strength B20 and B35. The samples were divided

into series: “a” – non-reinforced, “b” – reinforced with one layer of carbon fiber, “c” – reinforced with two layers of carbon fiber. In the course of the study, the authors found that strengthening the beams with one and two layers of carbon fiber allowed increasing their load-bearing capacity by 52 and 120%, respectively.

To study the operation of the normal cross-section of beams reinforced at a stage close to the exhaustion of the bearing capacity (with large deformations, deflections and cracks), the author [5] conducted experimental studies - 20 samples with a height of 120 mm and a width of 190 mm were tested (reinforced with three rods with a diameter of 8 mm A400 located on the neutral axis), having the same characteristics, loading method.

According to the experimental program, the samples were preloaded to a stage close to the exhaustion of the load-bearing capacity (the first stage).

At the second stage, the beam samples were reinforced along the lower face by external carbon fiber reinforcement with varying its cross-sectional area and then brought to destruction. Of the 20 tested samples, 4 reference samples were tested without reinforcement, 4 samples of each subsequent series were reinforced with external carbon fiber reinforcement in 1–4 layers, respectively. The reinforcement system consisted of strips of unidirectional carbon fiber.

Based on the experimental data obtained, the author [5] concluded that the effectiveness of this reinforcement method is expressed in an increase in strength - with an increase in the area of carbon fiber by 4 times - by 2.3 times;

In [6], experiments are described to study the behavior of two groups of reinforced concrete beams with different reinforcement schemes, and concrete of compressive strength class B30 and reinforcement of classes A400 and A240 were used for the manufacture of beams.

The samples were reinforced using the MBrace external reinforcement system (manufactured by BASF) and the FibARM system (manufactured by CJSC HK Composite). 16 series of samples of type “A” and 9 series of samples of type “B”, with different amplification schemes, were subjected to the bending test.

The increase in the load-bearing capacity of the beams, depending on the reinforcement scheme, was from 64% to 140% in relation to the non-reinforced beam.

The paper [7] presents the results of bending tests of two types of T-beams with a length of 12 and 18 m. Tests were carried out on three groups of beams. The first A group consisted of beams without reinforcement, the second B group – beams, reinforced with canvas FibARM Tape 530/300, and the third group beams reinforced with slats FibARM Lamel 14/100. Beams with a length of 12 m, belonging to the group B, amplified by the label on the bottom face of the edge of the canvas with a length of 11.6 m and a width of 300 mm in the form of U – shaped clips, and beams of B group – strip lamellas with a length of 11.6 m and a width of 100 mm.

The beam 18 m long, belonging to the group B, amplified by the label on the bottom face of the edge of the canvas with a length of 17.6 m and a width of 300 mm in the form of U – shaped clips, and beams of B group – strip lamellas with a length of 17.6 m and a width of 100 mm. Moreover, in the support zones of the beams, two clamps with a width of 300 mm were glued. Gluing of canvases and lamellas was performed with FibARM Resin glue.

The author [7] found that the reinforcement of reinforced concrete beams 12 and 18 m long with FibARM Tape 530/300 canvases and FibARM Lamel 14/100 based on carbon fibers led to an increase in their load-bearing capacity from 53% to 62%.

The accumulated world experience of using composite materials to strengthen building structures is positive, that is, in all cases, reinforced structures are in operational condition, and the failure of external reinforcement made of composite materials was not observed. As a result, in modern construction practice, more and more often they try to use composite materials for the repair and strengthening of building structures of industrial and civil buildings.

## 2 Methods and Materials

To study the stress-strain state of flexible reinforced concrete elements forced with carbon fiber, experimental studies of test samples – 6 beams of three types were carried out. The first type of beams - reference samples without reinforcement. The second type of beams – beams loaded to the stage corresponding to the loading of the standard load, in the presence of cracks and deflections, reinforced with carbon fiber after unloading, by gluing it to a stretched zone with a U-shaped anchorage on the supporting areas. The third type of beams includes samples reinforced with carbon fiber before the load is applied, similar to the second type of beams.

The design of the test samples and the scheme of their reinforcement are shown in Fig. 1.

Flat welded frames were used to reinforce the beams. As the working and structural reinforcement of the frames, hot-rolled steel reinforcement of class A400 with a diameter of 10 and 6 mm, respectively, is adopted. Cold-drawn wire made of low-carbon steel of class Bp500 with a diameter of 5 mm is used as a transverse reinforcement.

The beams were made of concrete of the B35 compressive strength class. As a binding component of the concrete mix, cement (C) of the M500 brand (GOST 31108) is provided. As a fine and coarse aggregate washed quarry sand (S) fractions from 0.16 – 0.66 mm (GOST 8736) and granite rubble (R) with a size of 5-20 mm (GOST 8267) respectively are used. The volume ratio of the components of the concrete mixture C/S/R for concrete of the compressive strength class B35 is 1/1.2/2.5. After forming, the samples were kept for 28 days under normal temperature and humidity conditions of hardening.

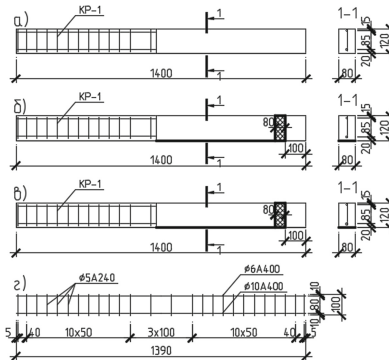
As the reinforcement material, a unidirectional carbon canvas based on high-strength carbon fiber with a glass weft fabric of the FibARM 530/300 brand with a tensile strength of 4200 MPa and an elastic modulus of 240,000 MPa was used. The adhesive is based on FibARM Resin 530 + epoxy resin, with the following characteristics:

- adhesion strength of at least 2.0 MPa (concrete failure);
- shear strength of adhesive samples, when held for 7 days at a temperature of 23 °C, not less than 10 MPa.

The experimental study consisted of several stages [8].

The first stage was to prepare experimental samples for testing. To do this, all samples of the same batch were examined for irregularities, chips. Then the test beam was installed





**Fig. 1.** Design and reinforcement scheme of test samples: a) beams of the “A” series; b) beams of the “B” series; c) beams of the “C” series; d) frame KR-1.

on a test bench [9], where marking and subsequent installation of measuring devices was performed.

The second stage included the preparation and examination of control samples. Control tests of the compressive strength of concrete samples were performed in accordance with GOST 10180.

At the third stage of the experimental study, the beams were tested directly (Fig. 2).

Beams of the “A” series were loaded in stages until destruction.

Beams of the “B” series, loaded up to 70% of the destructive load, were unloaded and reinforced with carbon fiber according to the previously described scheme and technology [10]. Then re-loaded until destruction.

Beams of the “C” series were reinforced with carbon fiber and loaded in stages until destruction.



**Fig. 2.** General view of the test before and after carbon fiber reinforcement.

### 3 Results and Discussion

All test samples were brought to destruction. According to the results of the experimental study, the average limit bending moment of the reference beams without reinforcement (beams A1 and A2) was 5.07 kNm. All samples of this batch were destroyed as a result of

an increase in the width and height of normal cracks located in the zone of pure bending and increasing deflections, which led to the indent of the concrete of the compressed zone at the final stage of the experiment.

The average value of the maximum bending moment obtained during the test for beams reinforced with carbon fiber at the stage close to the exhaustion of the load-bearing capacity (beams B1 and B2) was 8.1 kNm, and for beams reinforced without loading (beams B1 and B2) – 6.6 kNm.

All samples externally reinforced with carbon fiber were destroyed as a result of increasing the width and height of normal cracks located in the zone of pure bending and increasing deflections, which led to the separation of the composite material from the concrete and the indent of the concrete of the compressed zone (Fig. 3).



**Fig. 3.** General character of destruction of samples externally reinforced with carbon fiber.

The composite material itself was not destroyed. The exfoliation of the carbon fiber occurred, as expected, as a result of the destruction of concrete directly at the bonded surface (Fig. 4).



**Fig. 4.** Fracture surface of reinforced samples.

The strength characteristics of the beams obtained in the course of experimental studies are shown in Table 1.

**Table 1.** Strength parameters of experimental samples.

Beam grade	Breaking load of $P_{break}$ , kN	Average breaking load $P_{av}$ , kN	Destructive moment of $M_{ult}$ kNm	Average breaking moment $M_{medium/ult}$ kNm
A1	21.41	22.625	5.36	5.07
A2	23.84		4.82	
B1	37.84	36.02	8.51	8.1
B2	34.19		7.69	
C1	29.32	29.32	6.6	6.6
C2	29.32		6.6	

## 4 Conclusion

In the course of an experimental study of flexible reinforced concrete elements, the following was established:

- The destruction of the reference non-reinforced samples occurred due to the achievement of deformations in the compressed zone of concrete limit values.
- All samples, externally reinforced with carbon fiber, were destroyed along the normal cross-section with the extraction of the concrete of the compressed zone and the separation of the composite material from the concrete. While, the composite material itself was not destroyed.

Based on the obtained values of bending moments, it can be argued that reinforcement with external carbon fiber reinforcement increases the strength over the normal cross-section by 59% - for samples reinforced with carbon fiber after unloading, and by 30% - for samples reinforced with carbon fiber without preloading, compared to reference samples without reinforcement.

**Acknowledgements.** This work was realized in the framework of the Program of flagship university development on the base of the Belgorod State Technological University named after V.G. Shukhov, using equipment of High Technology Center at BSTU named after V.G. Shukhov.




## References

1. Ovchinnikov, I.I., Ovchinnikov, I.G., Chesnokov, G.V., Mikhaldykin, E.S.: Analysis of experimental studies strengthening of reinforced concrete structures by polymer composite materials. Part 1. Native experiments under static load. *Naukovedenie* **8**(3), 1–29 (2016)
2. Ovchinnikov, I.I., Ovchinnikov, I.G., Chesnokov, G.V., Mikhaldykin, E.S.: Analysis of experimental studies strengthening of reinforced concrete structures by polymer composite materials. Part 2. Study of the effect of temperature. *Naukovedenie*. **8**(4), 1–27 (2016)

3. Shilin, A.A.: External bonding of concrete structures with composite materials. Part 1. Stroizdat (2007)
4. Bykov, A.A., Rummyantsev, S.D., Birin, A.S.: Experimental study of the strength and deformation characteristics of reinforced concrete beams reinforced with carbon fiber. PNRPU Bull. 2(22), 112–126 (2016)
5. Grigorieva Y.E.: The strength and deformability of reinforced concrete beams reinforced with carbon fiber at a stage close to the exhaustion of the bearing capacity. Author's abstract. Ph.D. MGSU, Moscow (2013)
6. Nerovnykh, A.A.: Improvement of the methodology for assessing the carrying capacity of reinforced concrete spans of railway bridges, reinforced with composite materials. Author's abstract. Ph.D. SibGUPS, Novosibirsk (2013)
7. Smerdov, M.N., Smerdov, D.N., Klementyev, A.O.: Experimental studies of the strength and deformability of bent reinforced concrete elements reinforced in the compressed and stretched zone with non-metallic composite reinforcement. Transp. Urals 4, 49–54 (2014)
8. Ishchuk, Y.L.: Program for studying the strength, rigidity and cracking resistance of reinforced concrete bending elements, reinforced with polymeric composition materials. In: Conference on International Student Construction Forum – 2016, pp. 349–353. BSTU, Belgorod (2016)
9. Obernikhin, D.V., Nikulin, A.I.: Experimental studies of the deformability of bending reinforced concrete elements of various cross sections. Bull. BSTU Named After V.G. Shukhov 4, 56–59 (2017)
10. Smolyago, G.A., Ishchuk, Y.L.: Technology of using polymer-composite materials in the reconstruction of civil buildings. In: Nikulina, O.M. (ed.) Conference on Actual Problems of Renovation of the City's Housing Stock: The Relationship of Economic, Technical and Legal Aspects, pp. 366–370 (2016)



# On the Issue on Dilatant Phenomena in Dispersed Systems

N. N. Onoprienko<sup>(✉)</sup> , O. N. Salnickowa , and Sh. M. Rahimbaev 

Belgorod State Technological University Named After V.G. Shukhov, Belgorod, Russia

**Abstract.** The special role of rheological phenomena - thixotropy and dilatation - in various natural and technogenic processes is shown. Practical examples of the phenomenon of dilatancy in various dispersed systems are given: ceramic suspensions, highly concentrated binder systems of quartz sand, two-phase foams, cement-polymer suspensions, soils. The manifestation of dilatancy in sandy and clay soils is analyzed, taking into account the forecast of changes in the strength and deformation characteristics of soils under the influence of various influences. Rheological properties of cement suspensions with additives of water-soluble polymers are investigated. The peculiarity of the phenomenon of dilatancy, which consists in the manifestation in inorganic dispersions, as well as in organic ones, is established. It is shown that cement systems with additives of polymers containing carboxylate functional groups exhibit latent dilatant properties at low shear rates. It is established that the thixotropic properties of cement systems are more clearly manifested under the influence of additives of polymers of various compositions. The effectiveness of water-soluble polymers as modifiers of cement systems in the compounds of cement-polymer compositions is shown. Dilatancy is caused by the breakdown of solvate layers of molecules, including surfactants of complex composition, adsorbed on the surface of solid particles. It is established that the breakdown of hydrate shells at a moderate shear rate is possible only in suspensions of materials with relatively low hydrophilicity; more dispersed suspensions exhibit dilatant properties at increased shear rates.

**Keywords:** Dilatancy · Thixotropy · Shear rate · Dispersed systems · Soils · Cement-polymer systems

## 1 Introduction

A special role in the course of various natural and technical processes belongs to such rheological phenomena as thixotropy and dilatation. Thixotropy facilitates the flow of such processes as mixing, introduction into the medium, laying [1]. Studies of the properties and structure of thixotropy have shown that there is an inverse phenomenon, which is called dilatancy [1–3].

Dilatancy as a process consists in thickening as a result of mechanical action and is observed, for example, in suspensions of quartz grains in water or in concentrated solutions of potassium metasilicate with an excess of silicic acid. One of the manifestations

of dilatancy is an increase in the viscosity of quartz sand suspensions, as well as other dispersions, with an increase in the rate of their deformation during plastic flow [1–3].

As a rule, very concentrated, aggregative stable suspensions that do not have constant contact between particles have dilatancy. In some cases, the phenomenon of dilatancy can be traced in casting clay masses, in the processes of chemical technologies of ceramic and other non-metallic materials [2]. Dilatancy is an important component in construction in areas of quartz sand and other weakly hydrophilic rocks [4–10].

When choosing soil models, methods for calculating foundations, to assess the load-bearing capacity of foundations, the stability of slopes, embankments, retaining walls, the parameters of soil strength and soil deformability are used. Studying the behavior of dispersed soils in various conditions, it is necessary to pay attention to the influence of dynamic impacts [4, 8]. This kind of impact on the soil leads to the manifestation of the properties of dilatancy. They are expressed in changes in the stability of structural bonds under the influence of external impacts, which, due to the peculiarities of the natural structure of soils, changes their deformation and strength properties [5–9]. The effect of dilatancy on the concentration of deformations of various types of soils is noted [3, 9, 10].

Dynamic impacts during pile driving cause certain vertical deformations of the base of buildings [4, 8], which can cause loss of strength and stability of soils in slopes, earth embankments. The irreversible changes in the strength properties of soils after dynamic loads are evidenced by a number of works on this issue [4, 6, 7].

In sandy soils, plastic deformations are associated with dilatancy and its development in the shear band; in clay soils, discontinuities occur more often in the zone of local deformations [9, 10]. For sandy soils, the manifestation of dilatancy at large deformations is characteristic, which leads to softening of the soil and a decrease in strength parameters during deformation.

Thus, for accurate calculations, it is important to predict changes in the strength and deformation characteristics of soils, which can change under the influence of various influences, including dilatancy. Underestimation of the manifestation of dilatant properties of soils leads to a distortion of the calculated strength and deformation indicators, to a discrepancy between the calculation and the experiment, to an erroneous choice of the type and design of the foundation [6, 7].

Dilatancy manifests itself not only in soils, but also in other dispersed systems. This phenomenon is of particular importance in the processes of chemical technologies of ceramic and other non-metallic materials [1, 2, 11].

Dilatancy is a known disadvantage of ceramic suspensions and worsens the technology of forming products and their strength after heat treatment, and therefore the regulation of the rheological and technological characteristics of these systems is an important task [11].

Analysis of the data on the dependence of the effective viscosity of the systems of highly concentrated binding systems (HCBS) of quartz sand without additives and with additives on the shear rate, given in Table 1, shows that the HCBS of quartz sand exhibit dilatant properties [11]. The insertion of a plasticizing clay additive contributes to the stabilization of the effective viscosity of HCBS systems, and a complex modifying additive [11] reduces the viscosity of the system (Table 1).

**Table 1.** Dependence of the effective viscosity of the HCBS systems on the shear rate.

The gradient of shear rate, $s^{-1}$	0	50	100	150	200	250
Composition of HCBS:	Effective viscosity, Pa·s					
HCBS of quartz sand	0.20	0.23	0.27	0.35	0.44	0.59
HCBS of quartz sand with the addition of 5% Latna clay	0.20	0.16	0,17	0,18	0,18	0.19
HCBS quartz sand with a complex modifying additive	0.19	0.18	0.16	0.15	0.14	0.13

In many cases, water-soluble polymers act as stabilizers of dispersed systems based on various binders. These additives are most widely used to regulate the rheological properties of grouting solutions in drilling wells [13], as well as in the construction materials industry in the production of finishing, masonry, and facing compositions [13–15]. Due to its high environmental performance, the prospect of using water-soluble polymers in other technologies of construction production is not excluded. It is obvious that different requirements are imposed on cement-polymer compositions, depending on their purpose [13], so the rheological and technological properties of such systems can take different optimal values [13, 16].

Taking into account the importance of the dilatancy phenomenon, experimental rheological studies of cement systems with polymer additives were carried out and the data obtained were analyzed.

## 2 Methods and Materials

In this paper, systems based on cement suspensions without additives and with additives of polymers with different compounds of functional groups used in the production of cement-polymer compositions are studied.

To study the rheological properties of cement-polymer systems, a rotary viscometer “REOTEST-2.1” was used. The device is suitable for both Newtonian fluids and non-Newtonian systems, and detects anomalies such as dilatancy. In the studies, the rotor speed gradient was in the range of  $0.33 \dots 145.8 \text{ s}^{-1}$ . Based on the measurements and calculations carried out, rheograms of variances were constructed.

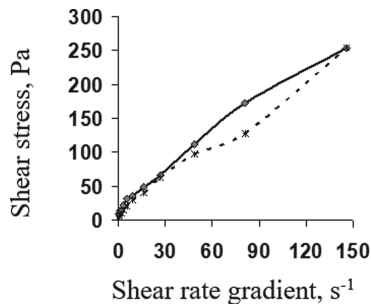
Belgorod Portland cement was used as a binder; polymer additives had different compound of functional groups (Table 2).

**Table 2.** Polymer additives.

Name of polymer additive	Shorthand notation	Functional group of polymer	Functional group formula
Methylcellulose	(MC)	Methoxyl	(-OCH <sub>3</sub> )
Oxyethyl cellulose	(OEC-1)	Ethoxyl	(-OCH <sub>2</sub> CH <sub>2</sub> OH)
Carboxymethylcellulose	(CMC)	Carboxylate	(-COO <sup>-</sup> )
Polyvinyl acetate	(PVA)	Ether	(-CO-O-)

### 3 Results and Discussion

Figures 1, 2 and 3 show rheograms of cement suspensions without additives and with polymer additives.



**Fig. 1.** Rheogram of cement suspension without additives at  $W/C = 0.35$ .

Comparison of rheograms of cement paste without additives with cement-polymer suspensions shows that thixotropic properties are more clearly manifested under the influence of additives of polymers of different composition. This phenomenon is favorable in their practical use in various types of construction work.

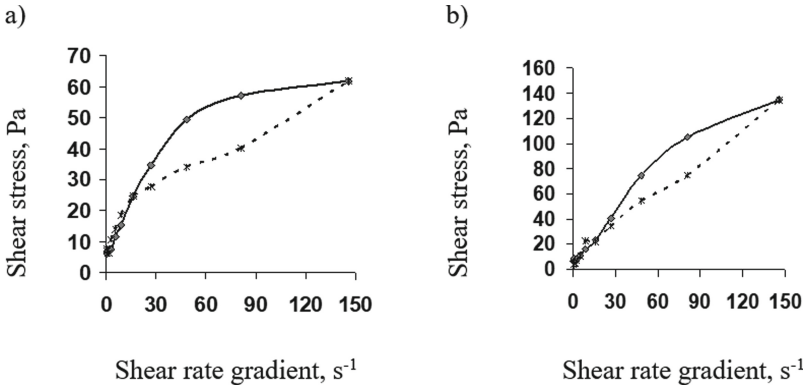
However, cement suspensions with additives of 0.5% PVA at  $W/C = 0.5$  and 0.5% CMC at  $W/C = 0.35$  in the area of small shear rate gradients ( $20 \text{ s}^{-1}$  and less) exhibit hidden properties of dilatant systems (Fig. 2). This can cause certain difficulties in the technology of construction work.

From previous studies [13], it follows that the additives MC and OEC, which do not contain carboxylate groups, are of interest as stabilizers of cement-polymer systems. Suspensions with these additives do not exhibit dilatant properties (Fig. 3).

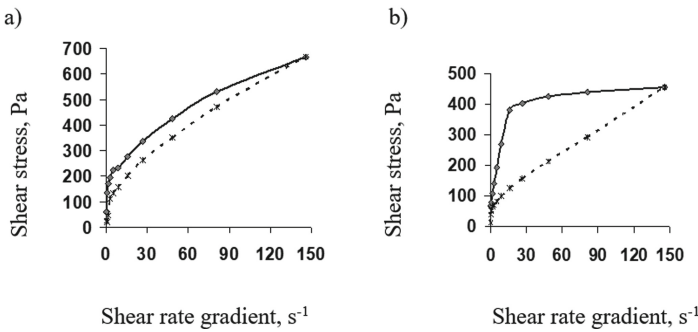
Insertion to the studied model systems (Fig. 1, 2 and 3) fillers and additives-regulators of properties can significantly change the nature of rheological curves due to the different nature and compatibility of the components.

Based on a detailed consideration of the phenomenon of dilatancy, the authors of the paper put forward a working hypothesis on the mechanism of dilatant phenomena. It is reduced to the condition of dilatancy by the breakdown of hydrate (in a more general





**Fig. 2.** Rheograms of cement suspensions with polymer additives PVA 0.5% at W/C = 0.5 (a) and CMC 0.5% at W/C = 0.35 (b).



**Fig. 3.** Rheograms of cement suspensions with polymer additives MC 0.5% at W/C = 0.35 (a) and OEC 0.5% at W/C = 0.35 (b).

form – solvate) layers of molecules adsorbed on the surface of solid particles. During the process, the friction of particles in the region of small gradients and shear stresses is carried out along these hydrate (solvate) shells and dilatant phenomena are not observed. An increase in the shear rate leads first to partial, and then to complete desorption, the breakdown of solvate shells around solid particles.

The analysis of the hypothesis allows establishing the following provisions:

- the breakdown of hydrate shells at a moderate shear rate is possible only in suspensions of materials with relatively low hydrophilicity. These include the quartz sand already mentioned, etc.;
- increasing the dispersion of the solid phase increases the hydrophilicity of the particles, so more dispersed suspensions exhibit dilatant properties at increased shear rates.

Validation of the hypothesis put forward by the authors leads to the conclusion: dilatant phenomena can be observed not only as a result of the breakdown of hydrate layers on the surface of solid phase particles, but also molecules of surfactants of a more

complex composition adsorbed on them. This forecast is confirmed by the experimental data presented in the paper [12].

## 4 Conclusion

A consequence of the proposed hypothesis is that any dispersions can have dilatant properties, even on the basis of hydrophilic particles, but at a high shear rate: the more hydrophilic the surface of the solid phase and the more strongly water and surfactant molecules are adsorbed on it, the more dilatancy will be observed at high shear rates.

Analyzing the above data, we can distinguish such a feature of the phenomenon of dilatancy as the manifestation not only in inorganic dispersions, but also in organic ones. A similar relationship is observed here: an increase in the affinity of solid and liquid phase particles leads to an increase in the rate at which dilatancy is observed.

As it can be seen from the experimental data and other examples given above, the dilatancy effect has scientific and applied significance. At the same time, its nature continues to be insufficiently studied, and to some extent completely undiscovered. In this regard, a comprehensive, systematic coverage of this phenomenon in the chosen direction is required.

**Acknowledgements.** This work was realized in the framework of the Program of flagship university development on the base of the Belgorod State Technological University named after V G Shukhov, using equipment of High Technology Center at BSTU named after V.G. Shukhov.


## References

1. Rayner, M.: Deformation and Flow. Gostekhizdat, Moscow (1963)
2. Uryev, N. B.: Physical and chemical bases of the technology of disperse systems and materials. Chemistry, Moscow (1988)
3. Vyalov, S.S.: Rheological Foundations of Soil Mechanics: Textbook for Construction Universities. Higher School, Moscow (1978)
4. Chernysh, A.S.: Effect of dynamic load on strength characteristics of clay soil and stability subgrade. *Bull. BSTU Named After V.G. Shukhov* **6**, 64–67 (2016)
5. Chernysh, A.S., Gubarev, S.A.: Given the rheological characteristics of the soil. *Vect. Geosci.* **1**(1), 5–7 (2018)
6. Kalachuk, T.G., Chernysh, A.S.: Strength parameters of sagged loess soils during the soaking. In: *IOP Conference Series: Earth and Environmental Science*, p. 042007 (2018)
7. Chernysh, A.S., Kalachuk, T.G.: Determination of compacting parameters of dispersed rocks. In: *IOP Conference Series: Earth and Environmental Science*, p. 062008 (2018)
8. Kalachuk, T.G., Onoprienko, N.N.: To the question of piles calculations which are dipped into leading peeps and auger rigs. In: *Proceedings of Universities, Investment, Construction, Real Estate*, vol. 3, pp. 77–81 (2017)
9. Mirny, A. Yu: Studies of dilatancy in dispersed soils and methods of its quantitative assessment. *Eng. Geol.* **14**(2), 34–43 (2019)
10. Chen, X., Yu, Y., Xuebao, G.: Study of dilatancy effect of redstone coarse grained soil by large scale triaxial tests. **29**(1), 3145–3149 (2010)

11. Cherevatova, A.V.: Construction composites based on highly concentrated binding systems: abstract dissert. Doctor of Engineering Sciences, 05.23.05. BSTU named after V.G. Shukhov, Belgorod, p. 44 (2007)
12. Tverdokhlebov, D.V.: Influence of component composition on rheological and other technological properties of foam cement mixtures: diss. ... Candidate of Eng. Sciences. BSTU named after V.G. Shukhov, Belgorod (2006)
13. Onoprienko, N.N., Rakhimbaev, Sh.M.: Building solutions and dry mixtures with additives of water-soluble polymers of domestic production. Belgorod BSTU named after V.G. Shukhov, p. 155 (2016)
14. Onoprienko, N.N., Rahimbaev, Sh.M.: Influence of composition of functional additives and deformation modes on flow behavior of polymer composite materials. In: IOP Conference Series: Materials Science and Engineering, vol. 327, p. 032043 (2018)
15. Onoprienko, N.N., Salnikova, O.N.: Interconnection of intrinsic deformations and adhesive phenomena in modified disperse systems. Mater. Sci. Forum **974**, 440–445 (2019)
16. Elistratkin, M.Yu., Minakov, S.V., Shatalova, S.V.: The effect of mineral additives in the composition of a composite binder on the efficiency of the plasticizer. Constr. Mater. Prod. **2**(2), 10–16 (2019)



# The Use of Additional Conditions in Photogrammetric Constructions

V. Ya. Tsvetkov<sup>(✉)</sup> 

Center for Strategic Analysis and Development, Moscow, Russia

**Abstract.** The article explores the spatial relationships and spatial patterns that appear when shooting flat rectangular objects in oblique and perspective images. The article explores a new type of spatial relationship between a feature and a spatial model. The study of relations allows us to reveal the patterns of photogrammetric constructions. These regularities can be used when transforming photographs as additional conditions. The article analyzes the spatial relationships between the lines of the object and their images in the photograph, giving vanishing points. The article shows. That the calculation of vanishing point coordinates on the image allows solving the transformation problem in a new way and reduces the requirements for the number of control points for transformation. The article analyzes the spatial relationships between the lines of the object and the lines of their images in the image. Using the duality theorem allows new formulas to transform images of rectangular objects. The applicability and limitations of this method are described.

**Keywords:** Photogrammetry · Analytical geometry · Photogrammetric constructions · Image transformation · Spatial patterns · Vanishing points · Duality theorem · Spatial relations

## 1 Introduction

Photogrammetric constructions are based on geometry, affine transformations, and more rarely on projective transformations. Photogrammetric constructions use spatial relations of a special type. Most spatial relations describe relationships between spatial features, for example in the cadaster [1] or in environmental studies [2]. Other spatial relations describe relationships between spatial models. The spatial relations under study describe the relationship between projection models and objects. The spatial relations under study describe the relationship between projection models and objects. When performing any spatial constructions, including photogrammetric ones, it is necessary to use the cognitive principles of spatial analysis [3]: visibility, perceptibility, interpretability. If a feature is not visible, it cannot be processed and modeled. If the spatial model is not perceptible, then it is impossible to analyze and apply it. If a spatial model cannot be interpreted, it is useless for use and analysis. These principles limit the application of photogrammetric constructions to any models and objects. The result of the photogrammetric construction should be visible, perceived and interpreted. Modern photogrammetry [4, 5] uses

all existing types of images obtained with the help of various equipment: analog cameras, digital cameras, television cameras, scanner shooting systems, radar cameras, laser shooting systems, etc. In photogrammetry, there are three main directions. The first direction is related to the creation of maps and plans based on images. This direction is often called phototopography. Photogrammetry is an integral part of geoinformatics [6]. All its areas are integrated into geoinformatics. The second direction of photogrammetry is associated with the solution of applied problems in various fields of science and technology: in architecture, construction, land cadaster, land monitoring, monitoring of precipitation and deformations of structures, medicine, criminology, automotive industry, robotics, military affairs, geology, etc. This direction is referred to as applied photogrammetry. The third direction of photogrammetry is related to space studies of both the Earth from space and photography in outer space. This direction is called space photogrammetry [7] and it is included in space geoinformatics [8]. Images of the Earth taken from space are used to study its natural resources and to monitor environmental protection. Images of other celestial bodies are used in astronomy and comparative planetology.

## 2 Methods and Materials

Photogrammetric constructions serve as a theoretical basis for constructing photographs in ground, air and space photogrammetry. Photogrammetric constructions serve as the basis for constructing spatial models and forming spatial images. Spatial models allow analyzing and obtaining knowledge, spatial knowledge and geological knowledge.

## 3 Results and Discussions

In many cases of photography, a situation occurs when the subject is flat or contains flat surfaces [9]. For example, the facades of houses or the water surface on lakes and rivers are flat. For these cases of photogrammetric constructions, it is permissible to introduce the terms real object plane and photograph plane. Depending on the location of the image plane relative to the plane of the object being photographed, different types of photography are distinguished. Simplistically, the image can be considered as the central projection of the object on the plane. The projection of the object obtained in the intersection of a plane with the projecting rays intersect at a single point, called the central, and the point of intersection of these rays - center of projection. We consider a flat object or an object containing a plane. Let us consider the case of normal shooting of such an object (Fig. 1).

On Fig. 1, the main optical axis  $Oo$  is parallel to the distance axis  $SY$  of the external coordinate system. In normal photography, the distance to the object plane  $H$  and the focal length  $f$  of the image lie on the same straight line. Section of the object plane (Ob)  $AB$  converts the picture of the image to the image plane (Ph) in the section  $ab$ . For such shooting, the shape of the object lying in the Ob plane is similar to the shape of the picture (Fig. 2). The plane of the object is called frontal. For normal shooting, it is parallel to the image plane. For simplicity, we consider a rectangle in the plane of the object.

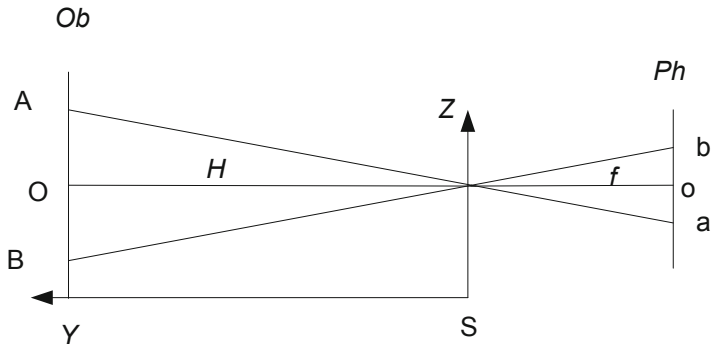


Fig. 1. Normal shooting profile.

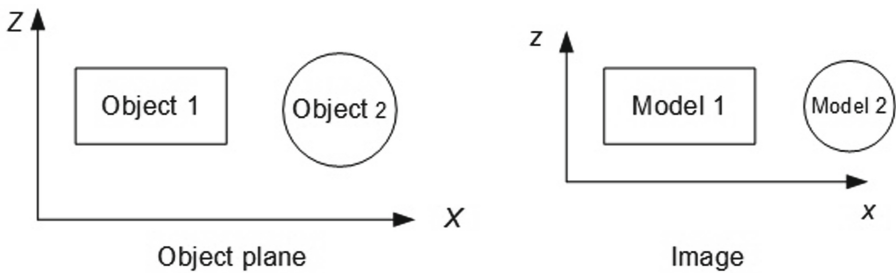


Fig. 2. Spatial relations between the object and its model in the image during normal shooting.

The drawing and shooting conditions in Fig. 2 are characterized by the similarity between a flat object and its model (picture) in the image. The similarity coefficient is determined by the scale ( $f/H$ ). When the angle of the optical axis changes with respect to the external coordinate system, the projecting rays of the camera will lead to a new construction of the object model in the image. This spatial situation is shown in Fig. 3.

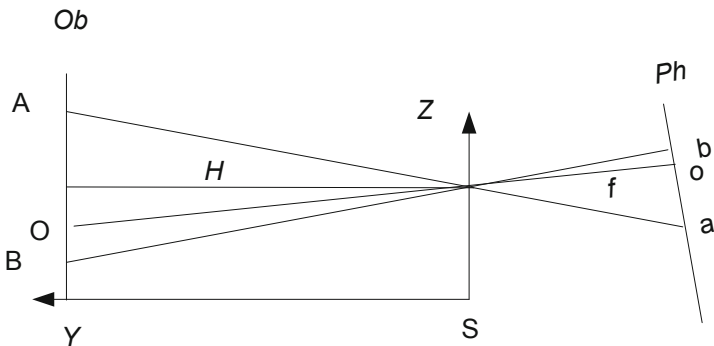


Fig. 3. Spatial relations between an object and its model in a tilted shooting.

On Fig. 3, the coordinate system of the image is not aligned with the coordinate system of the object. For the situation in Fig. 3, the main optical axis of the  $O_o$  is not parallel to the SY axis. For this shooting, the front plane of the subject is not parallel to the image plane. The plane of the object AB is not parallel to the image plane (Ph) ab. If you tilt only one angle in the vertical ZSY plane, you will get the image shown in Fig. 4.

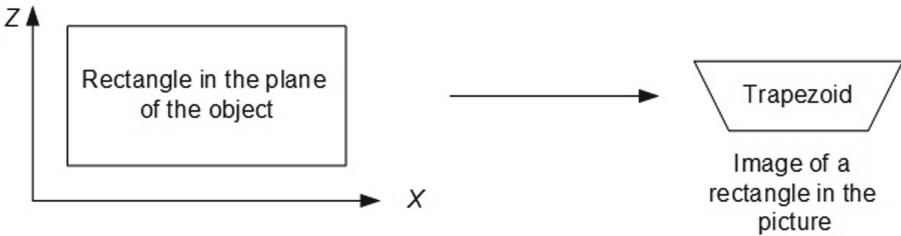


Fig. 4. Image of a rectangle at a tilted shooting.

With this transformation, the rectangle is transformed into a trapezoid. If there are parallel lines (vertical lines) on the object, they are all converted to non-parallel lines in the image. Regardless of the slope of the image and its focal length, there are analytical dependencies (1) and (2) between the coordinates of the points of the object plane for ground shooting (X, Z) and the coordinates of the points of the image plane (x, z) [10].

$$x = \frac{A_1X + A_2Z + A_3}{A_7X + A_8Z + 1} \tag{1}$$

$$z = \frac{A_4X + A_5Z + A_6}{A_7X + A_8Z + 1} \tag{2}$$

Expressions (1) (2) include 8  $A_i$  coefficients, which are called transformation coefficients. They define a one-to-one relation between the coordinates of the object plane and the coordinates of the image plane. The  $A_i$  coefficients are determined if there are at least 4 reference points, the coordinates of which are defined in the plane of the object and the image. It is less known that for the images in Fig. 4, the vertical lines of the object in the image will converge at a common point, which is called the vanishing point T1 (Fig. 5).

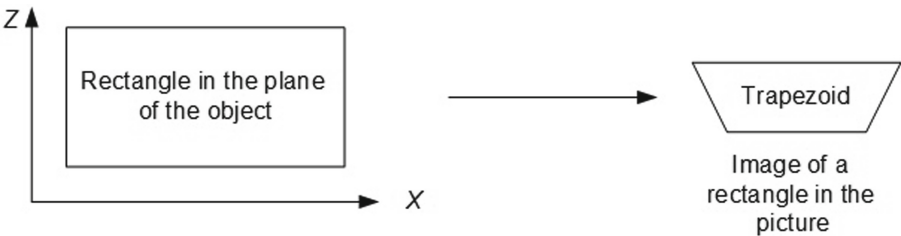
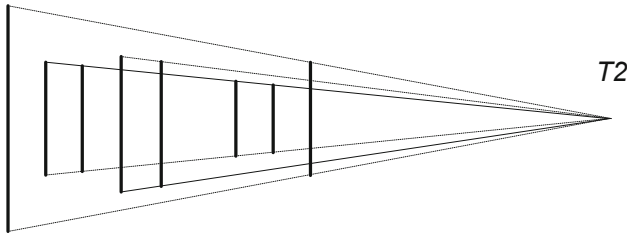


Fig. 5. Trapezoid models when the image is tilted only in the vertical plane.

For the image in Fig. 5, it is characteristic that the vanishing point appears in the image, at which all the vertical lines of the frontal plane on the object converge. In this case, the vertical lines may even lie in different frontal planes, but converge at a common vanishing point in the image.

In another case, if you rotate the image plane only in the horizontal plane, the object shown in Fig. 5 on the left will have a different image (Fig. 6).



**Fig. 6.** Image of the object from Fig. 5 when the image is tilted only in the horizontal plane.

With this shooting, another vanishing point  $T_2$  is formed, shown in Fig. 6.

The regularity of photogrammetric constructions in this case is that when the image is rotated only in the horizontal plane, a vanishing point appears on the picture of the image, at which all horizontal lines on the object converge. In this case, the horizontal lines may even lie in different frontal planes, but converge at a common vanishing point. If you rotate the projecting plane of the image by two angles in the vertical and horizontal plane, this will cause the original regular rectangle on the projecting plane to transform into a model of an irregular quadrilateral (Fig. 7).

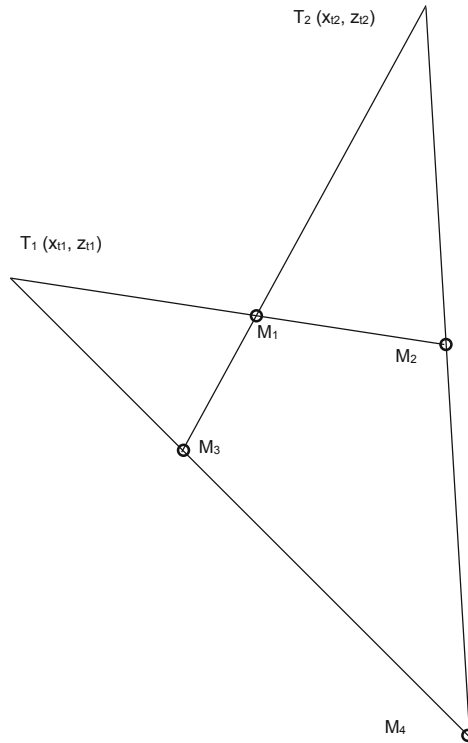
On Fig. 7, the four points  $M_1$ ,  $M_2$ ,  $M_3$ , and  $M_4$  define the vertices of an irregular quadrilateral obtained from the rectangle of the frontal plane of the object. In this case, it can be stated that when the image is tilted by two angles in the horizontal and vertical planes, two vanishing points appear in the image, at which all horizontal and vertical lines converge. Such a picture is called promising. These patterns are used by restorers when restoring lost elements of architectural monuments from archival photographs. The model in Fig. 7 provides a new solution to the transformation problem with a smaller number of reference points [20]. If it is possible to calculate the coordinates of the vanishing points in the image (Fig. 7)  $T_1(x_1, z_1)$  and  $T_2(x_2, z_2)$ , the expressions for analytical transformation are simplified and take the form:

$$x = \frac{A_7X x_2 + A_8Z x_1 + A_3}{A_7X + A_8Z + 1} \quad (3)$$

$$z = \frac{A_7X z_2 + A_8Z z_1 + A_6}{A_7X + A_8Z + 1} \quad (4)$$

Expressions (3), (4) include not eight, but four unknown coefficients. They require determining the transformation parameters at least two reference points located on the perspective image, for which the rectangle is transformed into an irregular rectangle of the type in Fig. 7  $M_1, M_2, M_3, M_4$ . This is a case of perspective shooting, which allows





**Fig. 7.** Model of a quadrilateral in the image with two vanishing points.

determining the coordinates of the vanishing points  $T_1$ ,  $T_2$  from the image. For cases where there is only one vanishing point in the image (Fig. 5 and Fig. 6), three reference points are required.

Another pattern that is not described in photogrammetry textbooks is that the transformation of a picture from the image plane to the object plane can be carried out in the presence of a perspective image not only by reference points, but also by the slopes of straight lines in the image. From the point of view of analytical geometry, this is nothing new. This is the result of the so-called duality theorem [11]. The duality theorem says that the family of two parameters that characterize lines in bundles of intersecting lines, pairs of coordinates of points that intersect lines, are mutually invertible. You can use lines to determine the coordinates of intersection points. You can use the intersection points to determine the parameters of the lines.

In the process of transforming images, the points of the lines of the image are converted to the points of the lines of the object. Each line is characterized by two parameters. A point, as a result of the intersection of such lines, is characterized by two coordinates. This duality gives reason to look for parameters of the relation not only between the coordinates of the points of the image and the object plane, but also the relation between the parameters of the straight lines of the object plane and the parameters of the projections of these lines in the image.

The analysis of this issue allowed creating a new solution to the transformation problem. The ideas of this approach are laid down in the transition from the coordinate space to the parameter space. We will denote the coordinates of the image and the parameters of the lines in the image with small letters, and on the object with large ones. The equation of a line in the plane of an object has the form  $Z = KX + H$ .

The equation of the image of the same line in the picture (ground shooting) has the form  $z = kx + h$ .

It is established that there is a one-to-one correspondence between the parameters of the lines on the image ( $k, h$ ) and on the object ( $K, H$ ).

$$K = \frac{B_1 \times k + B_2 \times h + B_3}{B_7 \times k + B_8 \times h + 1} \quad (5)$$

$$H = \frac{B_4 \times k + B_5 \times h + B_6}{B_7 \times k + B_8 \times h + 1} \quad (6)$$

In expressions (5), (6),  $B_i$  are constant transformation coefficients, analogs of the coefficients  $A_i$  in expressions (1), (2). This approach allows solving the problem of transforming a rectangular object into an image in a snapshot or vice versa in a new way. The  $B_i$  coefficients are determined if there are at least 4 straight lines (a rectangle) in the object plane and their corresponding straight lines (Fig. 7) in the image of the picture. The advantage of this approach is the ability to transform without reference points. Engineering structures and residential objects often have strictly vertical and horizontal lines in the facade plane. The angular coefficients ( $k$ ) and line parameters ( $h$ ) in the image can be defined in the coordinate system of the image. This makes it possible to find the  $B_i$  transformation coefficients without making measurements on the object. This approach is very important in the restoration and reconstruction of destroyed objects, photos of which have been preserved.

However, this approach makes it possible to obtain an out-of-scale model of the object. To bring the model to real dimensions, it is necessary to measure the linear basis on the object. That is, you need to measure a pair of points in the preserved base of the object. This approach can be used when monitoring high-rise structures, the practical measurement of which at high altitude is difficult.

## 4 Conclusion

A limitation of the application of the methods is the condition for the presence of rectangular objects in the frontal plane and parallel planes. For a tilted plane, additional constructions are needed. For a non-planar surface, the method is also not applicable. Photogrammetric constructions used in classical photogrammetry are quite generalized. They do not use configuration information that occurs for some type of object with a characteristic line arrangement or with a characteristic shape of objects. Additional conditions appear when considering the form or shape of an object. These additional conditions cause the appearance of regularities of photogrammetric constructions. In particular, in a perspective image, images of rectangles lying in the plane of the object give the appearance of vanishing points in the image. This additional information can


be used in modeling and transformation. In most textbooks on photogrammetry, this pattern is not used. This additional information allows reducing the requirements for the number of points required for transformation. It is shown in [12] that the use of three vanishing points makes it possible to solve the resection problem in a new way with a smaller number of reference points. Using the parameters of straight lines on images of rectangular objects is also a new method. This method allows performing transformation to eliminate perspective distortions in the image without the presence of reference points, but under certain conditions of the location of straight lines on the object.

## References

1. Bahareva, N.A.: Spatial relationships as a factor in land valuation. *ITNOU: Inf. Technol. Sci. Educ. Manage. Upravlenii* **6**(10), 61–69 (2018)
2. Bahareva, N.A.: Spatial relations in environmental research. *Prospect. Sci. Educ.* **3**, 16–19 (2016)
3. Tsvetkov, V.Ya.: Spatial Information Models. *Eur. Res.* **10-1**(60), 2386–2392 (2013)
4. Ullah, S.: Potential of modern photogrammetry versus airborne laser scanning for estimating forest variables in a mountain environment. *Remote Sens.* **11**(6), 661–669 (2019)
5. Deane, E., Macciotta, R., Hendry, M.T., Gräpel, C., Skirrow, R.: Leveraging historical aerial photographs and digital photogrammetry techniques for landslide investigation –a practical perspective. *Landslides* **17**, 1989–1996 (2020)
6. Majorov, A.A., Tsvetkov V.Ya.: Geoinformatics as the most important approach of Informatics development. *Inf. Technol.* **11**, 2–7 (2013)
7. Urmaev, M.S. *Space photogrammetry*. Nedra, Moscow (1989)
8. Bondur, V.G., Tsvetkov, V.Ya.: New scientific direction of space geoinformatics. *Eur. J. Technol. Design* **4**(10), 118–126 (2015)
9. Miroshnichenko, N.O.: Determination of the accuracy of the specified photogrammetric shooting performed by a non-metric camera. In: *Actual Problems in Science and Engineering*, pp. 333–334. DSTU, Rostov-on-Don (2018)
10. Ivannikov, A.D., Kulagin, V.P., Tihonov, A.N., Tsvetkov, V.Ya.: *Applied Geoinformatics*. MAKS Press, Moscow (2005)
11. Modenov, P.S.: *Analytical geometry*. MSU, Moscow (1969)
12. Tsvetkov, V.Ya.: Solution of the photogrammetric resection under additional conditions. *News of higher educational institutions. Geodesy Aerial Photogr.* **2**, 94–98 (1998)



# Problems of Constructive Safety of Piled Foundations of Heighted Buildings at the Stages of Design and Construction

R. G. Abakumov<sup>(✉)</sup> 

Belgorod State Technological University Named After V.G. Shukhov, Belgorod, Russia

**Abstract.** The article is devoted to the analysis of problems of ensuring the structural safety of pile foundations of high-rise buildings at the design and construction stages. The relevance of this study is determined by the increasing requirements for the structural safety of buildings and structures, the need to use modern construction technologies and tests of pile Foundation in determining the possibility of resuming work on the object of unfinished construction. The content of the article is based on the platform of the theoretical basis for designing structures of pile foundations of high-rise buildings and is predetermined by the subsequent synthesis of innovative solutions in the construction of pile foundations on objects of unfinished construction. The characteristics that affect the design of foundations are analyzed. The factors that influence the choice of the Foundation type (location and type of construction, the size and distribution of loads, soil conditions, access to construction equipment, durability requirements, the impact of installation on adjacent foundations, relative costs, local construction practices), the advantages and disadvantages of slab, pile, and pile-slab Foundation structures are considered. A critical review of the methods of pile Foundation construction (pressing into the ground, driving, sinking the pile into the pipe, vibration driving) is presented. The technology of testing the integrity of the pile using the ultrasonic method is described. The use of the proposed methods and technology for testing piles will allow detecting possible critical defects at the early stages of construction and ensuring the structural safety of the future building.

**Keywords:** Pile foundation · Slab foundation · Pile testing · Static load · Dynamic load · Type of foundation · High-rise buildings · Geotechnical characteristics · Structural safety

## 1 Introduction

Due to the rapid development of the construction industry and the growing number of high-rise buildings, the quality requirements for construction projects are constantly increasing. To improve the quality of construction, it is necessary that construction departments and designers, builders pay attention to scientific research and efficiently apply construction technologies. Therefore, the design and construction processes of the pile Foundation must be of the highest quality to ensure compliance with the requirements of construction loads, as well as to ensure the safety and stability of building structures.

In recent years, the number of collapses of buildings and structures has been increasing. Statistics indicate that most accidents occur due to critical defects in the manufacture and installation of the main structures. At the same time, the severity of the consequences of an accident depends on the degree of danger of defects made during the construction of load-bearing structures and the device of bases and foundations. The high degree of collapse of load-bearing structures in the increased number of construction accidents proves that the current problem of modern construction is to ensure the structural safety of the object under construction.

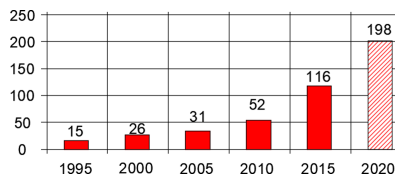
## 2 Methods and Materials

To solve the problems of designing and building pile foundations of high-rise buildings, innovative technologies are used in construction activities. Innovative technologies are a synthesis of the theoretical base, advanced technologies in the field of programming and design, advanced methods and technologies of construction and construction expertise. Consideration of the problems faced by designers and builders will reflect the state of innovative directions in the development of construction, design and expertise of pile foundations.

Innovative trends in the design of pile foundations are associated with the use of information modeling in construction, which offers cost-effective design solutions that meet the necessary requirements for load-bearing capacity and safety. The development of innovations in construction is associated with technologies in the field of improving the performance of construction and installation works and the use of new technological methods for the production of building materials. Trends in the development and improvement of design, construction and construction expertise technologies can be traced in scientific publications of domestic and foreign literature.

## 3 Results and Discussions

Over the past two decades, the rate of construction of “ultra-high” buildings, whose height exceeds 300 m, has increased significantly. A large number of these buildings are located in the middle East or China. Dubai is now home to the world’s tallest building, the Burj Khalifa, which is 828 m high, while in Jeddah, Saudi Arabia, the Kingdom’s Tower is under construction, and will eventually exceed 1,000 m in height. Figure 1 shows a significant increase in the number of such buildings.



**Fig. 1.** The total number of buildings over 300 m high.

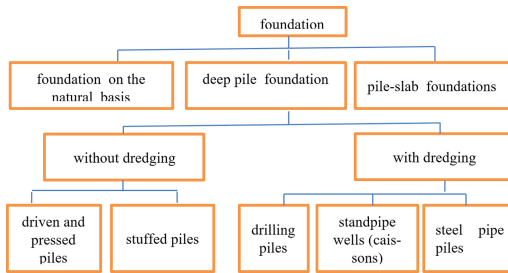
Ultra-high buildings with a height of more than 300 m pose new challenges for engineers, especially in terms of structural and geotechnical design. Many of the traditional design methods cannot be applied because they require extrapolation that goes far beyond previous experience, so designers and geotechnical designers are forced to use more complex analysis and design methods. In particular, geotechnical engineers who design foundations for high-rise buildings are leaving behind empirical methods and are increasingly applying modern methods.

*There are a number of characteristics of high-rise buildings that can have a significant impact on Foundation design, including the following [1]:*

1. the weight of the building, i.e. the vertical load supported by the Foundation, can be significant. In addition, the construction weight increases non-linearly with height, so it is necessary to carefully consider both the maximum load-bearing capacity and the draft.
2. high-Rise buildings are often surrounded by low-rise podium structures that are subjected to much less stress. Thus, differential calculations between high-rise and low-rise sections must be controlled.
3. the Lateral forces generated by the wind load and subsequent moments in the Foundation system can be very high. These moments can create increased vertical loads on the Foundation, especially on external piles inside the Foundation system. The design of the piles must take into account these increased loads, which act in combination with lateral forces and moments.
4. Side loads and moments caused by wind are cyclical. Therefore, it is necessary to consider the impact of cyclical vertical and lateral loads on the Foundation system, since cyclical loads can lead to a decrease in Foundation performance and cause an increase in subsidence.
5. the Seismic impact will cause additional lateral forces in the structure, as well as side movements in the base supporting the structure. Thus, additional lateral forces and moments can be induced in the Foundation system by two mechanisms:
  - \* Inertial forces and moments that occur during lateral excitation of the structure;
  - \* Kinematic forces and moments that occur in the Foundation piles under the action of ground movements acting on the piles.
6. Wind and seismic loads are dynamic in nature, and therefore it is necessary to evaluate their ability to cause resonance within the structure. The risk of dynamic resonance depends on a number of factors, including the prevailing dynamic loading period, the natural period of the structure, and the stiffness and damping of the Foundation system.
7. Dynamic response of high rise buildings creates some problems of the structure and Foundation. In particular, the main vibration period of a very high structure can be very long (10 s or more), and conventional dynamic load sources such as wind and earthquakes have a much shorter prevailing period and will generally not excite the structure through the fundamental vibration mode. However, some of the higher vibrations will have significantly shorter natural periods and may be well excited by wind or seismic action. These higher periods will depend primarily on

structural characteristics, but may also depend on the response characteristics of the Foundation.

The ultimate strength of each pile must comply with structural and geotechnical constraints to provide a reliable Foundation for operation in accordance with the requirements. The pile load test is a direct method for determining the maximum load-bearing capacity of a pile. Dynamic load testing is a fast and reliable way to evaluate the load-bearing capacity of a pile. This testing can help you choose the right type of pile that can withstand the loads on the road while driving, and warns you if the pile draught reaches the required amount, avoiding over-design sediments. It also provides information about structural integrity and stresses [2]. If a dynamic load test cannot be performed, a static load test can be performed. General options for foundations for high-rise buildings are shown in Fig. 2.



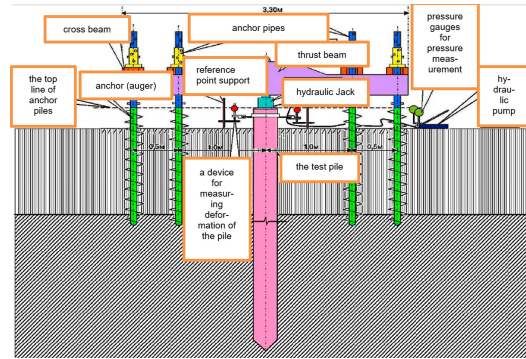
**Fig. 2.** Classification of foundations for high-rise buildings.

In a static load test, the load will be applied by a hydraulic Jack to the Kent ledge (concrete blocks) with the load measured by calibrated and certified pressure gauges (Fig. 3).

The value of the loading stages for static indentation load is taken from the calculation of no more than 1/10 of the specified maximum vertical load on the pile.

At each stage of loading, readings should be taken for all devices in accordance with clause 8.2.2 of GOST 5686–2012 in the following sequence: zero count - immediately before applying the load, the first - immediately after applying the load, then three reports sequentially with an interval of 30 min and then every hour until the conditional stabilization of deformation (damping of displacement). After the next stage of loading is smoothly reached, the specified load must be maintained with an accuracy of at least 5%.

The criterion for conditional stabilization of the pile sediment from the next loading stage is the precipitation rate of no more than 0.1 mm for the last 60 min of observations (clause 8.2.3 of GOST 5686–2012). The holding time at the last stage of loading after reaching the required value of the conditional stabilization of the precipitation is taken for 120 min. Unloading of the pile should be performed after reaching the maximum load on the pile in steps equal to twice the values of the loading stages, with each step holding for at least 15 min. Readings for strain measurement devices are taken immediately after each stage of unloading and after 15 min of observation. After full unloading (to zero),



**Fig. 3.** Hydraulic Jack Device when testing the pile for static load.

observations of the elastic movement of the pile should be carried out for 60 min, with the removal of samples every 15 min of observations (1.8.2.6 GOST 5686–2012).

The result of the pile test will be recorded using dial sensors registered by the control beam. [6] the optical level can be used to confirm the indicators. The piles will be checked by incrementing the load according to the required standard, taking into account time, load and calculation. Interpretation of the pile load test will be presented for estimating the pile capacity. *The criteria for determining the load on piles are as follows:*

1. Load, where the draft continues to increase without further increase in load.
2. Load, beyond which there is an increase in precipitation, disproportionate to the increase in load.

For verification, the minimum load applied during the test will be equal to 1.5 times the pile's working load. It is therefore important to determine the working load of the pile prior to testing.

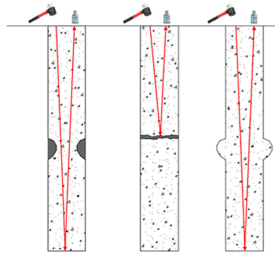
Integrity testing is an important part of quality control for both monolithic and precast concrete. This is due to the fact that this method can detect possible structural defects in the construction of the pile, such as cracks, changes in the cross section, and the like. This method can evaluate the uniformity and consistency of the pile material, length, and cross-sectional area.

The integrity of monolithic and precast concrete is checked by ultrasound. The main shock wave that runs along the length of the pile is reflected from the bottom of the pile. However, any inhomogeneities and defects that occur within its length will be reflected and added to the reverse signal. The hammer is used to impact the pile head and must be applied vertically with the piles. Multiple impacts are applied to the top of the pile, and then echoes are recorded for each individual impact using a motion sensor. This device will provide signal conversion and integrate acceleration to get the speed.

*Since integrity testing uses echoes or sounds to measure inhomogeneities, accelerations, and pile speeds, this technique does not provide any information about the load-bearing capacity of the pile that dynamic and static load tests are capable of. It*



*restricts the estimation of the cross-section of piles located below the cracks that intersect the entire cross-section of the pile (Fig. 4).*



**Fig. 4.** Study of pile integrity.

It is recommended to refer to this test method when performing the installation of Packed piles.

## 4 Conclusion

Currently, the number of high-rise buildings in cities is growing, their number of storeys is growing, which increases the pressure on the pile Foundation. Designing foundations for high-rise buildings involves a number of tasks from a geotechnical point of view. The Foundation system is subject to high vertical, lateral, and torque loads, which can degrade the rigidity and load-bearing capacity of the piles inside the Foundation. The geological structure of the construction site may cause additional potential problems for the load-bearing capacity of the piles. Geotechnical uncertainty is the biggest risk in any Foundation design and construction process. It is necessary to have accurate data on the geological structure of the site in order to select an appropriate Foundation system.

Requirements for the quality of construction work are increasing. Statistics indicate an increased number of collapses of buildings and structures. Most accidents occur due to critical defects in the manufacture and installation of the main structures. At the same time, the severity of the consequences of an accident depends on the degree of danger of defects made during the construction of load-bearing structures and the device of bases and foundations.

To improve the quality of construction, it is necessary that construction departments and designers, builders pay attention to scientific research and efficiently apply construction technologies. Therefore, the design and construction processes of the pile Foundation must be of the highest quality to ensure compliance with the requirements of construction loads, as well as to ensure the structural safety of building structures. Pile load testing, combined with advanced analysis and design techniques, helps to develop efficient and cost-effective design solutions and ensure the structural safety of the future building or structure.

**Acknowledgments.** This work was realized in the framework of the Program of flagship university development on the base of the Belgorod State Technological University named after V. G. Shukhov, using equipment of High Technology Center at BSTU named after V. G. Shukhov.

## References

1. Abakumov, R.G., Avilova, I.P., Ursu, I.V., Kapustina, E.O.: Methodical toolkit of managing reproduction of the fixed assets of an organization. *J. Soc. Sci.* **10**, 1449 (2015)
2. Abakumov, R.G., Naumov, A.E., Zobova, A.G.: Advantages, tools and efficiency of implementation of information modeling technologies in construction. *Bull. BSTU Named After V.G. Shukhov* **5**, 171–181 (2017)
3. Abakumov, R.G., Naumov, A.E.: Building information model: advantages, tools and adoption efficiency. In: *IOP Conference Series: Materials Science and Engineering*, vol. 11, no. 6, p. 22001 (2017)
4. Dolzhenko, A.V., Naumov, A.E., Shevchenko, A.E.: Bearing capacity and rigidity of short plastic-concrete-tubal vertical columns under transverse load. In: *IOP Conference Series: Materials Science and Engineering*, vol. 327, p. 042024 (2018)
5. Abdrazakov, F.K., Pomorova, A.V., Shchenyatskaya, M.A., Litvishko, O.V.: Organizational partnership for building, reconstruction and capital overhaul of hydrotechnical structures. *Int. Bus. Manage.* **9**, 1163–1168 (2015)
6. Kara, K.A., Dolzhenko, A.V., Zharikov, I.S.: Influence of processing factors over concrete strength. In: *IOP Conference Series: Materials Science and Engineering*, vol. 327, p. 032027 (2018)
7. Klyuev, S.V., Klyuev, A.V., Abakarov, A.J., Danilov, V.F., Chubenko, E.Ph.: Optimization of building constructions on the basis of genetic algorithm. *J. Comput. Theor. Nanosci.* **16**(7), 2950–2953 (2019)
8. Klyuev, S.V., Shlychkov, D.I., Muravyov, K.A., Ksenofontova, T.K.: Optimal design of building structures. *Int. J. Adv. Sci. Technol.* **29**(5), 2577–2583 (2020)
9. Naumov, A.E., Koshlich, Yu., Oberemok, M.I., Belousov, A.: Comparative analyzes for increasing the energy efficiency of civil constructions. In: *19th International Multidisciplinary Scientific GeoConference SGEM 2019 Conference Proceedings*, Sofia, pp. 277–284 (2019)
10. Obolenskaya, Y.V., Abakumov, R.G., Naumov, A.E.: Global market of 3D technologies as the basis for innovative economic development. *Innov. Econ. Prospect. Dev. Improve.* **7**, 2(33), 90–95 (2019)



# Construction Materials with Low Power Intensity Based on Cement

I. N. Borisov  and A. A. Stronin<sup>(✉)</sup> 

Belgorod State Technological University Named After V.G. Shukhov, Belgorod, Russia

**Abstract.** The ball mill has an energy efficiency of no more than 3.5% (taking into account the measures taken to intensify the process of grinding the material). This is due to the imperfection of the design of the grinding unit, which consists in the fact that it is impossible to convert completely the mechanical energy accumulated by the grinding load into grinding energy (i.e., energy directly spent on the destruction of material particles). Most of the stored energy is converted into heat, noise, and vibration. The existing directions of intensification of the grinding process are as follows: improving the design and internal equipment of the cement mill; changing the physical and chemical properties of the grinding environment; improving the grinding scheme. The authors of this paper work in the direction of improving the internal equipment, which is reflected in the scientifically based selection of the range of grinding bodies for the fine grinding chamber, as the rational composition of the grinding load can significantly reduce the energy consumption of the grinding process. The authors continue to study the possibility of using a two-ball grinding load in the fine grinding chamber, as well as the possibility of reducing significantly the power intensity of the grinding process. This paper provides a brief overview of such grinding loads, which differ from each other only in the range of grinding bodies.

**Keywords:** Clinker · Grinding Index · Two-ball grinding load · Ball mill · Clinker dispersion characteristics

## 1 Introduction

Cement production is associated with high energy costs, which amount to about 110 kW·h/t of cement, while from 40 to 50% (depending on the method and culture of production) falls on the cement grinding shop, i.e. on average  $40 \pm 5$  kW·h/t is spent on clinker grinding [1, 2]. These figures show the need to improve the process of fine grinding of clinker. The high value of the specific energy consumption associated with fine grinding of cement is primarily due to the insufficient perfection of the design of the grinding units themselves, as in most cases, tube ball mills are used, having a very low energy efficiency of no more than 3.5%. The following positive characteristics contribute to the wide spread of ball mills: simplicity of design, high reliability of operation, low metal consumption, high productivity, the ability to grind material of various hardness and humidity (for material with high humidity, a dryer is installed in front of the mill) [3–7].

The authors of this paper continue their research on the creation of an energy-efficient range of two-ball grinding loading for the fine grinding chamber [8, 9]. The fundamental difference of which, from traditional factory grinding loads, is the simultaneous combined use of a large and small ball, which together make up a single two-ball grinding load.

In this work, we studied 6 ranges of such loads, which have the following designations: GL I; GL II; GL III; GL IV; GL V and GL VI, where GL stands for grinding load, and Latin numbers indicate the serial number. Each loading range differs from the other only in the mass ratio between large and small balls.

In order to avoid repetitions, the clinker was given synonymous designations-clinker №, sample №, where the number sign is followed by a number corresponding to the number of the assortment of the two-ball grinding load. For example, if at the second stage of the clinker grinding, a grinding load designated GL I was used, then the synonymous designation of the clinker in this case is clinker № 1 or sample № 1.

## 2 Methods and Materials

As part of this work, the material was crushed in a laboratory ball mill GIPROTSEM  $0.5 \times 0.56$  m, operating in an open cycle without a separator. Grinding balls were used as grinding bodies. In all experiments, the filling factor of the grinding chamber with grinding environment was constant and amounted to 20%, and the mass of the grinding load was 55 kg.

A study of the influence of the range double-ball download on dispersion characteristics of grinding material and energy intensity of the entire grinding process was studied on the example of clinker CJSC “Oskolcement” fraction  $-10 + 1.25$  mm, which were ground without added gypsum. In order to eliminate the influence of the first grinding chamber on the results of the research, it was necessary to use a grinding load that is characterized by high energy efficiency. As a similar loading, it was decided to use a dense ball package (DBP) [10]. Range of DBP grinding bodies (for the first chamber) in all tests was constant:  $\text{Ø}74/\text{Ø}54 = 2:1$ . The material was first ground for 10 min in the first chamber, then the grinding bodies were removed from it, and the test load was loaded, after which the grinding continued for another 25 min in the second chamber.

Every 5 min, the mill was stopped, and samples were taken from the crushed material in order to determine the degree of its dispersion. The fineness of the clinker grinding was determined by such indicators as the specific surface area and the total residue on the sieve № 008. The determination of the specific surface area was determined by the air permeability method, and the value of the total residue on the sieve № 008 was determined by mechanical sieving on standard sieves.

The results obtained during the experiments were subjected to mathematical analysis using the least squares method. These data are presented in Tables 1 and 2, on the basis of tabular data, the grinding kinetics were constructed (Figs. 1 and 2).

## 3 Results

As it can be seen from Figs. 1 and 2, clinkers № 1 and 2 after grinding at the first stage have the same specific surface area of  $151 \text{ m}^2/\text{kg}$ , while samples № 3 and 6 have a  $S_{sp}$

= 123 m<sup>2</sup>/kg, and clinkers № 4 and 5–114 m<sup>2</sup>/kg. The observed differences between the pairs of clinkers with the same specific surface area are probably caused, on the one hand, by the statistical distribution of the values of the dispersion indicators during grinding, and on the other hand, by the fact that between these pairs there is a fluctuation of the fractional composition within the fraction – 10 + 1.25 mm. The latter fact is confirmed by the results presented in Fig. 2, which clearly shows that clinkers № 1 and 2 have the same total residue on the sieve № 008 equal to 52%. Clinker № 4 and № 5, which make up the other pair, also have the same value of this indicator, which in this case is 56%. But the samples numbered 3 and 6 in terms of specific surface area, which made up the other pair, here differ significantly in the total residue on the sieve № 008, and the difference was 21%. Such a combination of clinkers, characterized by the same value of one of the 2 dispersion indicators, and forming a group on this basis, will be repeatedly observed in the future throughout the entire process of clinker grinding, which is clearly seen in Tables 1 and 2.

Thus, all six clinkers were equally prepared (as far as possible) for grinding in the second stage. When considering Figs. 1 and 2 together, it follows that the grinding of clinker on a double-ball grinding load of GL VI is accompanied by a significant increase in the specific surface area in 25 min from 123 to 410 m<sup>2</sup>/kg, i.e. by 70%. At the same time, there is a significant decrease of about 89% in the total residue on the sieve № 008 (Fig. 2 GL VI). The replacement of the range of grinding loadings located in the series GL I – GL II – GL III – GL IV – GL V led to an increase in the specific surface area by approximately 54.6%; 61.5%; 67.0%; 68.6% and 68.6%, respectively.

**Table 1.** Impact of the assortment of double-ball grinding loading on the value of the specific surface of the crushed clinker, m<sup>2</sup>/kg.

	Total time of grinding, min						
	I stage of grinding		I stage of grinding				
	5	10	15	20	25	30	35
GL I	75	150	193	238	282	307	333
GL II	76	152	212	276	338	365	392
GL III	61	123	199	276	306	336	372
GL IV	57	115	174	233	278	324	363
GL V	56	112	177	242	280	318	363
GL VI	61	123	196	270	316	362	409

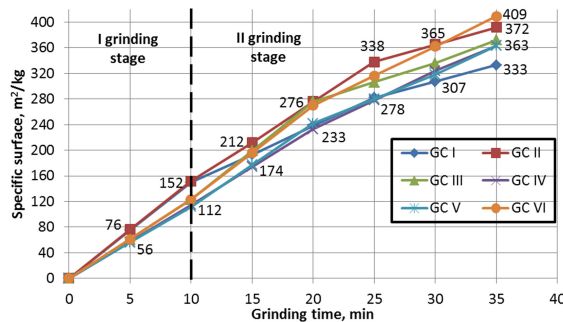
The successive replacement of the range of grinding loadings located in the series GL I – GL II – GL III – GL IV – GL V led to an increase in the specific surface area by approximately 54.6%; 61.5%; 67.0%; 68.6% and 68.6%, respectively.

**Table 2.** Impact of the assortment of the double-ball grinding load on the value of the total residue on the sieve № 008 of the crushed clinker, %.

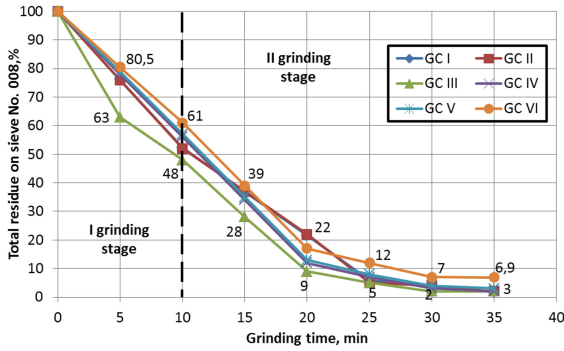
	Total time of grinding, min						
	I stage of grinding		I stage of grinding				
	5	10	15	20	25	30	35
GL I	76.0	52.0	36.8	21.5	6.0	3.8	1.6
GL II	76.0	52.0	36.8	22.0	5.3	3.8	2.2
GL III	62.7	48.0	28.4	8.8	5.3	2.0	1.6
GL IV	78.3	56.0	34.6	12.5	7.4	2.6	2.2
GL V	78.3	56.0	34.6	12.5	8.3	3.8	3.5
GL VI	80.5	61.0	39.0	17.0	12.0	7.0	6.9

In this case, for the above samples, the residue on the sieve changes in a different way, different from the nature of the change in the specific surface area. Before grinding at the second stage, the samples numbered 1, 2, 3, 4, 5 had a total residue on the sieve № 008 presented in Table 2, which clearly shows that after grinding at this stage, the value of this indicator decreased by about 90%; 95.7%; 96.7%; 96.1% and 93.7%, respectively.

Based on the data obtained, it is difficult to draw an unambiguous conclusion about the range of grinding loads that allows getting a finished product with a high degree of dispersion in the shortest possible period of grinding time. On the example of GL VI, we can see an ambiguous relationship between the value of the specific surface area and the total residue on the sieve № 008.



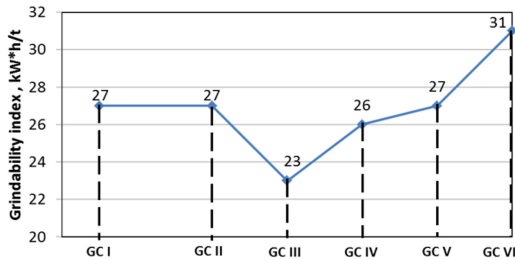
**Fig. 1.** Dependence of the specific surface of the clinker on the range of double-ball grinding charge used at the II stage of milling.



**Fig. 2.** Dependence of the total clinker residue on sieve No. 008 on the range of double-ball grinding charge used at the II stage of milling.

From the above, it follows that it is impossible to choose the most energy-efficient double-ball grinding load based on a simple analytical comparison of the experimental data obtained (Tables 1, 2), which characterize the dispersion of the crushed clinker. For this reason, for each range of double-ball grinding loading, the grinding index was determined, which is a technical and energy indicator that characterizes the energy intensity of the clinker grinding process in a ball mill.

According to the GIPROTSEM method [1] calculations of the grinding index ( $E_{ind}$ ) for all samples was carried out. The obtained results are, for clarity, presented in the form of graphic dependences between  $E_{ind}$  and range used in the second stage grinding of double-ball mill loading (Fig. 3). A value of 28 kW·h/t of clinker is taken as the average value of the grindability index of clinker in a ball mill.



**Fig. 3.** Dependence of the grindability index on the assortment of the double-ball grinding charge for fine grinding.

Figure 3 shows that GL III provides a significant reduction in the clinker grinding index by about 18% compared to the average value. While the use of grinding loadings for fine grinding of GL I, GL II and GL V slightly affects the value of this indicator, as in this case the grinding index does not reach values less than 27 kW·h/t of clinker. On the contrary, the use of the GL VI load resulted in an increase of approximately 12.5% in the value of this indicator compared to its average value.

## 4 Conclusion

Based on the experimental data obtained, the following main conclusions can be formulated:

- The investigated assortment of grinding loadings for fine grinding has an ambiguous effect on such disperse characteristics as the specific surface area and the total residue on the sieve № 008 throughout the grinding process (Fig. 1 and 2);
- The double-ball grinding load of the GL III has the most optimal range of grinding bodies in terms of composition, as it causes a decrease in the clinker grinding index by about 17.8% (the lowest indicator of all the studied GL), compared with the grinding of the clinker of average grinding capacity on the general accepted traditional grinding load (Fig. 3);
- The use of double-ball loads of the GL I, GL II and GL V ranges was not accompanied by a noticeable decrease in the energy component of the grinding process;
- The use of the GL VI grinding load, on the contrary, led to a significant increase in the energy consumption of the clinker fine grinding process, as in this case, the value of the grinding index increased by about 12.5% compared to the average selected value of 28 kW·h/t.

Thus, only the double-ball grinding load GL III has an optimal range of grinding bodies, the use of which can significantly reduce the energy consumption of the process of fine grinding of clinker.

The results obtained in the course of this research work allow judging the practical feasibility of using a double-ball grinding load in the fine grinding chamber, which at this stage of development already allows reducing significantly the energy consumption of the clinker grinding process. In addition to all of the above, there is a need for further research on the creation of energy-efficient double-ball loads.

**Acknowledgements.** This work was realized in the framework of the Program of flagship university development on the base of the Belgorod State Technological University named after V.G. Shukhov, using equipment of High Technology Center at BSTU named after V.G. Shukhov.

## References

1. Pirotsky, V.Z.: Cement mills: technological optimization. Informatization of education, St. Petersburg (1999)
2. Goysis, M.: Introduction to the technology of grinding. *Cem. Appl.* **3**, 36–41 (2014)
3. Bogdanov, V.S.: Ball drum mills: textbook BelSTU, Belgorod (2002)
4. Krykhtin, G.S., Kuznetsov, L.N.: Intensification of the Work of Mills. Science, Novosibirsk (1993)
5. Sharapov, R.R.: Ball mills of the closed cycle: monograph. BSTU named after V.G. Shukhov, Belgorod (2008)
6. Buyanova, A.S., Devyataeva, N.V.: Application of energy-efficient and energy-saving technologies in the cement industry of Russia. *Curr. Probl. Hum. Nat. Sci.* **3-1**, 161–164 (2014)



7. Barbanyagre, V.D., Matveev, A.F., Smal, D.V., Moskvichev, D.S.: Physical and technical bases of grinding materials in pipe mills. Bull. BSTU Named After V.G. Shukhov **4**, 182–185 (2016)
8. Stronin, A.A., Barbanyagre, V.D.: Increasing the productivity of an open-cycle ball mill using a double-ball loading. In: Proceedings of the X International Forum with International participation, pp. 1615–1619. BSTU named after V. G. Shukhov, Belgorod (2018)
9. Borisov, I.N., Stronin, A.A., Klassen, V.K.: Comparison of the efficiency of using a double-ball grinding load in an open cycle mill compared to traditional loading ranges. Bull. BSTU Named After V.G. Shukhov **12**, 121–129 (2019)
10. Barbanyagre, V.D.: Pat 2477659. Ball loading of the drum mill. Belgorod State Technological University named after V.G. Shukhov, Belgorod (2013)



# Determination of Material Properties of Composite Sleepers Taking into Account Operational Factors

V. I. Kondrashchenko  and C. Wang  

Russian University of Transport (MIIT), Moscow, Russia

**Abstract.** The physical and technical properties of the material of composite sleepers can be varied in a wide range, which formulates the problem of determining their rational values that provide the most favorable conditions for the operation of the railway track and rolling stock. The solution of this problem lies on the way of assessing the influence of technological factors on the material properties of composite sleepers, which was solved by method of planning of active experiments, in which the variable factors were the parameters characterizing the properties of sleepers, seasonality of their operation, as well as the rails and fastening system used, and the response functions describing the characteristics of the stress-strain state of the “roadbed – ballast bed – sleeper – rail – rolling stock” system. The relations between the material properties of composite sleepers and the operational conditions of the railway track were studied during constant parameters characterizing the type of rolling stock (locomotive VL-80) moving at a speed of 80 km/h in a curve with a radius of 350 m.

**Keywords:** Composite properties · Variable factors · Response functions · Composite sleeper · Railway track

## 1 Introduction

The material characteristics of composite sleepers can be varied in a wide range of physical and technical properties, which is based on the difference in the properties of raw materials that constitute the composite – polymer matrix, micro-, macro-fillers and reinforcing elements [1–4]. In this regard, rational physical and technical properties of the material of composite sleepers should achieve a compromise between rigid (on reinforced concrete sleepers) and elastic (on wooden sleepers) modes of operation of rolling stock. This can be achieved by regulating, for example, important indicators such as the bending coefficient of sleepers which integrates the material properties of the sleepers and its structure features, and its mass, which determines the track stability against track bulking that is higher than tracks on wood sleepers and lower than on concrete sleepers; other properties of the polymer composite material that differ significantly from the properties of traditional materials – wood, concrete and steel [5–10]. Other important factors affecting the condition of the track and rolling stock are the characteristics of

the ballast bed and the roadbed, which change in the long term in the process of operation and in the short term – from season to season (winter, summer and off-season) of operation. These indicators can be taken into account integrally by varying the value of the elastic modulus of the “roadbed – ballast bed” system in the vertical and horizontal planes.

To study the complex multifactor system “roadbed – ballast bed – sleeper – rail – rolling stock”, it is advisable to use experimental planning methods that implement the idea of a “black box” with inputted variable factors  $X$ , characterizing the parameters of railway track elements, and outputted response functions  $Y$ , determining the state of the railway track. This approach makes it possible to obtain reliable mathematical models of response functions  $Y$  from variable factors  $X$  without considering the complex physical laws of the system [11].

## 2 Materials and Methods

To obtain mathematical models  $Y = Y(X)$  of the system “roadbed – ballast bed – sleeper – rail – rolling stock” (RBSRR), methods of planning of active experiments were used. The variable factors were the bending coefficient of the sleeper  $X_1$ , its mass  $X_2$ , the elastic modulus of the railway track in the horizontal  $X_3$  and vertical  $X_4$  planes. For four variable factors, the Box-Wilson experiment plan  $B_4$  was used [12].

We used indicators  $Y$  as response functions which characterize the stress-strain state of the RBSRR system, namely:  $Y_1$  – axial stress in the rail base, MPa;  $Y_2$  – vertical deflection of the rail, cm;  $Y_3$  – vertical deflection of the sleeper, cm;  $Y_4$  – vertical acceleration of the sleeper in fractions of  $g$ , rel. units.

The values of the response functions in the experimental plan are obtained from the results of a computational experiment performed in experiments of points in the experimental plan with constant parameters characterizing the type of rolling stock (locomotive VL-80) moving at a speed of 80 km/h in a curve with a radius of 350 m. Calculations for determining the response functions  $Y$  in the experimental plan were performed using the program “Interaction of the crew and the track under spatial vibrations of rolling stock” (ICT), developed by the All-Russian Scientific Research Institute of Railway Transport [13].

The material properties of composite sleepers were considered by complex indicators including bending coefficient  $X_1$  and the mass  $X_2$ , and variable factors  $X_3$  and  $X_4$  are used considering the influence of seasonal conditions (winter, summer, off-season) of railway track. Meanwhile, the operating condition of composite sleepers in winter corresponds to the values of variables  $X_3$  and  $X_4$  at the upper level (in the coded scale  $x_3 = 1$  and  $x_4 = 1$ ), which are the highest values due to ice formation in the roadbed and ballast bed, and in summer – at the lower level (in the coded scale  $x_3 = -1$  and  $x_4 = -1$ ), which they take at positive temperatures; and in the off-season (during “winter – spring” and “autumn – winter” transitions) – at the basic level (in the coded scale  $x_3 = 0$  and  $x_4 = 0$ ), when the variable factors take intermediate values. The levels of variable factors in the experimental plan  $B_4$  in natural  $X$  and coded  $x$  values are shown in Table 1.

As a result of processing the data obtained by using the ICT program for computational experiment at the points of the Box-Wilson plan  $B_4$ , the coefficients of

**Table 1.** The values of the variable factors  $X$  at the points of the experiment plan B4.

Variable factor	Values of $X$ at the levels of variation of $x$			Interval of variation $h = X_{max} - X_o$
	Lower ( $X_{min}$ ) $x = -1$	Basic ( $X_o$ ) $x = 0$	Upper ( $X_{max}$ ) $x = +1$	
$X_1$ , rel. Units	0.700	0.775	0.850	0.075
$X_2$ , kg	71	168	265	97
$X_3$ , mN/cm <sup>2</sup>	2.2	3.9	5.6	1.7
$X_4$ , mN/cm <sup>2</sup>	3.4	5.7	8.0	2.3

mathematical models describing the response functions  $Y$  by polynomial models were determined:

$$Y = b_0 + \sum_{i=1}^4 b_i x_i + \sum_{1 \leq i < j \leq 4} b_{ij} x_i x_j + \sum_{i=1}^4 b_{ii} x_i^2, \tag{1}$$

where  $x$  – variable factors in coded values, varying from  $-1$  to  $+1$ ,  $b$  – coefficients of the polynomial models.

In this case, the transition from the natural value of the  $i$ -th variable factor  $X_i$  to its coded value  $x_i$  is performed by the formula

$$x_i = \frac{X_i - X_0}{h}, \tag{2}$$

where  $X_i$  – the basic level of the  $i$ -th variable factor in natural quantities;  $h_i$  – interval of variation of the  $i$ -th variable factor (see Table 1).

### 3 Results and Discussion

By processing the data of the computational experiment obtained by using the ICT program at the points of the plan B<sub>4</sub>, mathematical models that accurately (the error does not exceed 1.26%, which characterizes their high predictive ability) describe the studied  $Y$  response functions were established. The significant values of the coefficients  $b$  (with a probability of 0.95) of the obtained polynomial models are shown in Table 2.

Using the obtained mathematical models, the analysis of the influence of variable factors on the values of the response functions  $Y$  characterizing the state of the railway track was performed in the coded scale  $x$ .

The influence of variable factors  $x_i$  ( $i = 1, \dots, 4$ ) was studied by constructing isolines of the analyzed function  $Y_i$  on a square with vertex coordinates  $(-1, -1)$ ,  $(-1, +1)$ ,  $(+1, -1)$ ,  $(+1, +1)$ , the sides of which were two variable factors on a coded scale – the sleeper bending coefficient ( $x_1$ ) and its mass ( $x_2$ ), varying in the range from the lower

**Table 2.** Values of coefficients  $b$  of polynomial models  $Y$ .

Function	$b_0$	$b_1$	$b_2$	$b_3$	$b_4$	$b_{11}$	$b_{12}$	
$Y_1$	111.91	-0.037	-0.037	-0.037	2.452	-0.17	0.011	
$Y_2$	0.229	0	0	0	-0.054	0	0	
$Y_3$	0.197	0	0.001	0	-0.046	-0.001	0	
$Y_4$	3.220	-0.002	0.133	-0.002	0.284	-0.007	0	
Function	$b_{13}$	$b_{14}$	$b_{22}$	$b_{23}$	$b_{24}$	$b_{33}$	$b_{34}$	$b_{44}$
$Y_1$	0.011	0.012	-0.17	0.011	0.012	-0.17	0.012	1.97
$Y_2$	0	0	0	0	0	0	0	0.018
$Y_3$	0	0	0	0	0	0	0	0.0168
$Y_4$	0.002	0.001	-0.003	0	0.004	-0.007	0.001	0.008

(-1) to the upper (+1) levels, and under specific fixed values of the other two factors – the elastic modulus of the railway track in the horizontal ( $x_3$ ) and vertical ( $x_4$ ) plane.

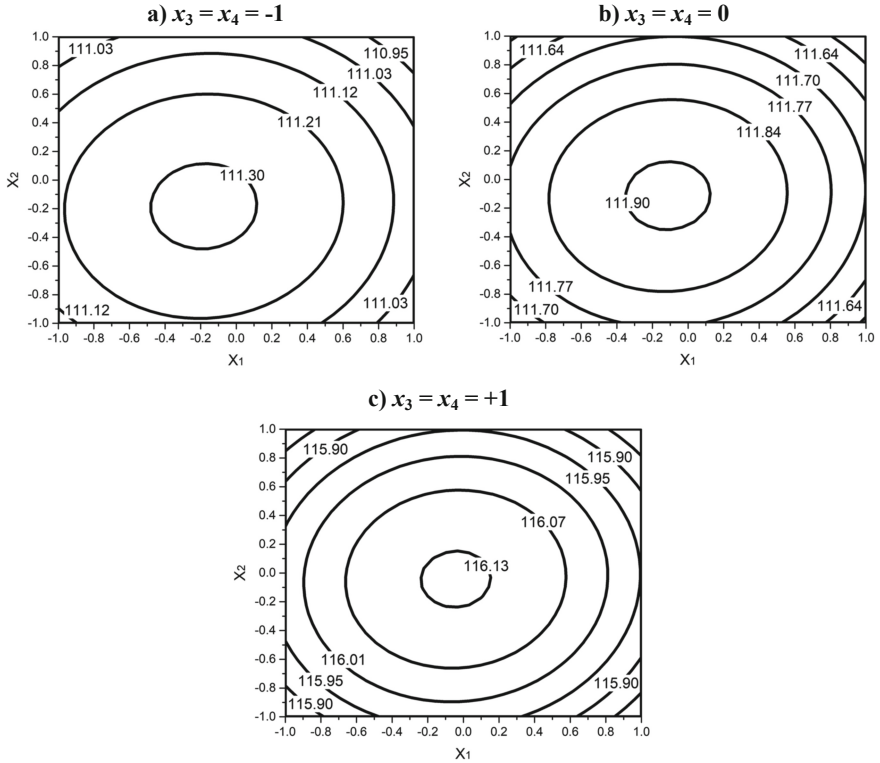
The isolines of the analyzed response functions  $Y (Y_j, j = 1, \dots, 4)$  on the square depending on the values of the variable factors  $x$  were constructed by program “Origin”, are shown in Figs. 1, 2, 3 and 4.

Evaluation of the influence of the composite sleeper parameters on the stresses in rail base  $Y_1$  is important from the viewpoint of reducing the risk of its brittle destruction during train operation.

According to dependences shown in Fig. 1, it follows that the rate of change of the bending coefficient  $x_1$  and mass  $x_2$  of the sleepers have a roughly equivalent effect on the stresses in the rail base  $Y_1$ , a maximum value is achieved when the values of  $x_1$  and  $x_2$  are on a basic level, i.e., when  $x_1 \approx 0$  and  $x_2 \approx 0$ . While by the impact degree a stronger influence on the value of  $Y_1$  does not imposed by the bending coefficient  $x_1$  and the sleeper mass  $x_2$  (in this case changing amplitude of  $Y_1$  is 0.1–0.3 MPa), but by seasonal factors associated with the transition from summer mode of the railway operation (when  $x_3 = x_4 = -1$ ) to off-season mode (when  $x_3 = x_4 = 0$ ) and from off-season mode to winter mode (when  $x_3 = x_4 = +1$ ) and oppositely, in which there is a significant change of the modulus of elasticity of under rail basement in the horizontal  $x_3$  and vertical  $x_4$  plane especially in winter, when the change in the value of  $Y_1$  reaches 5.5 MPa. At the same time, as it follows from the similarity of the isolines in Fig. 1, the impact of material properties of composite sleepers on the value of stresses in the rail base do not depend on seasonality of operation of the railway track.

The study of the influence of composite sleeper parameters on the vertical deflections of the rail  $Y_2$  is important for reducing the risk of its destruction during cyclic loading induced by rolling stock.

From the dependences shown in Fig. 2, it follows that, as in the case of the analysis of influence of the composite sleeper parameters on the stresses in the rail base  $Y_1$  (see Fig. 1), the changes of bending coefficient  $x_1$  and sleeper mass  $x_2$  have almost the same influence on the vertical rail deflection  $Y_2$ , and the minimum value which, in contrast

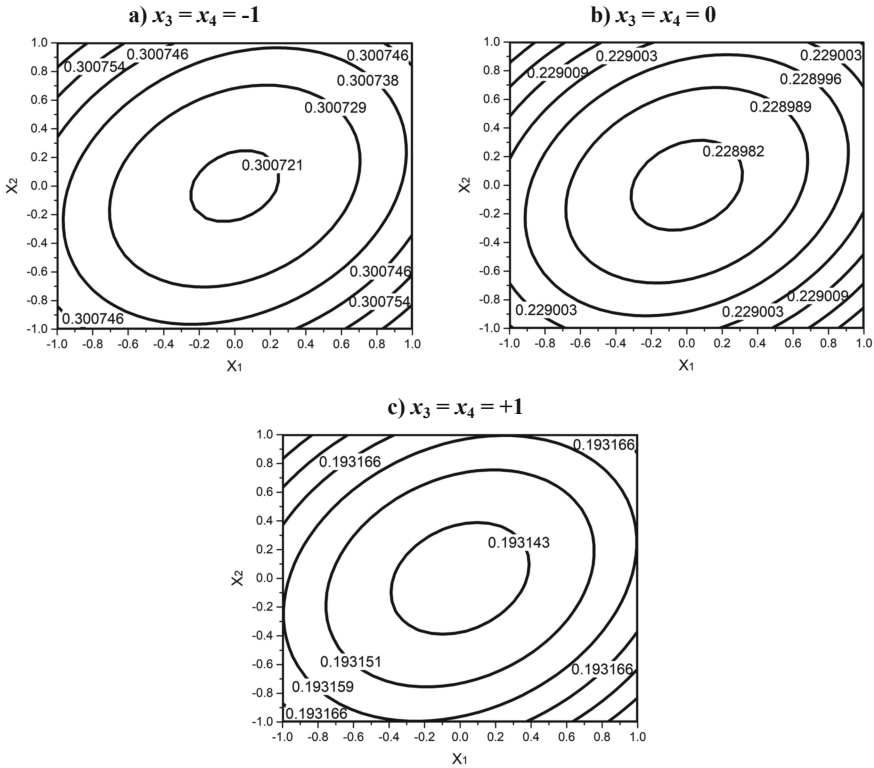


**Fig. 1.** Stress isolines in the rail base  $Y_1$ , MPa, in the coordinates of the variable factors  $x$  in the coded scale  $x_i$  ( $i = 1-4$ ).

to the stresses in the rail base  $Y_1$ , achieved during the values of  $x_1$  and  $x_2$  on their basic level, i.e. when  $x_1 \approx 0$  and  $x_2 \approx 0$ . At the same time, as in the previous case, a stronger influence on the value of  $Y_2$  is exerted not by the changes of bending coefficient  $x_1$  and sleeper mass  $x_2$  (the changing amplitude in  $Y_2$  was 0.001 cm), but by seasonal factors characterized by the elastic modules of the roadbed and the ballast bed in the horizontal  $x_3$  and vertical  $x_4$  planes. Moreover, the transition from the summer to the off-season (Fig. 2a and 2b) has a more significant effect on the change in the deflection of the rail  $Y_2$  than from the off-season to the winter (Fig. 2b and 2c). As in the previous case, as it follows from the similarity of the isolines in Fig. 2, the seasonality of the track operation does not affect the feature of the change in the vertical deflections of the rail when the material properties of the composite sleeper change.

Evaluation of the influence of composite sleeper parameters on the value of its vertical deflections  $Y_3$  is important to reduce the risk of its fatigue failure under cyclic impacts from rolling stock.

From the dependences shown in Fig. 3, it follows that in the range of change of  $x_2$  from  $-1$  to  $0$ , the value of the vertical deflection of the sleeper  $Y_3$  is mainly affected by an increase in the sleeper mass, and when the value of  $x_2$  change from  $0$  to  $1$ , the bending coefficient of sleeper  $x_1$ , which characterizes its rigidity, also begins to affect the



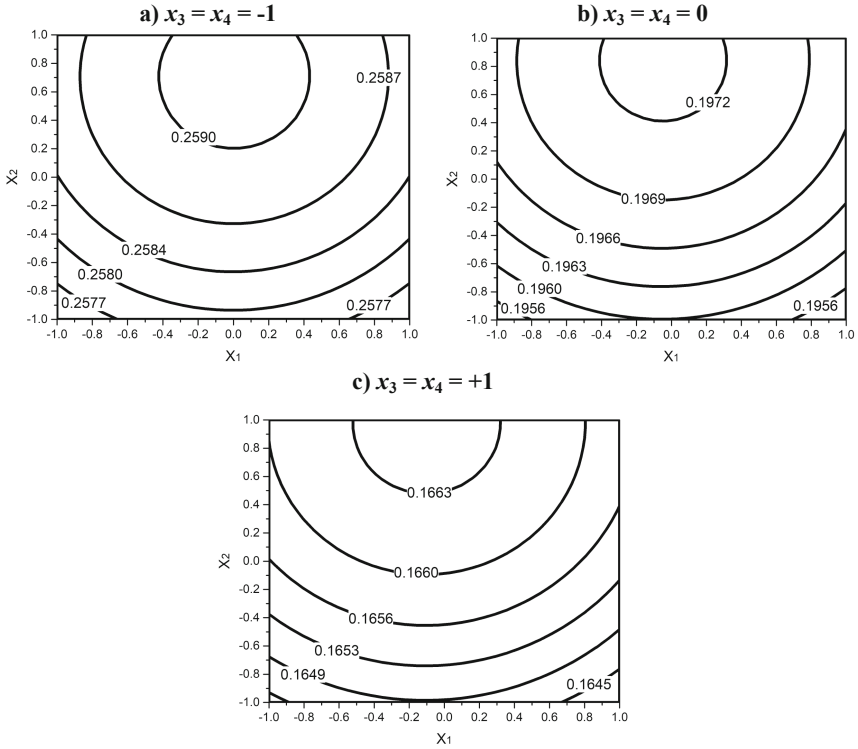
**Fig. 2.** Isolines of vertical deflections of the rail  $Y_2$ , cm, in coordinates of variable factors  $x$  in the coded scale  $x_i$  ( $i = 1-4$ ).

value of  $Y_3$ . At the same time, a stronger influence on the value of the vertical deflection of the composite sleeper  $Y_3$  is not exerted by the change in the bending coefficient  $x_1$  and mass  $x_2$  of the sleeper (the changing amplitude in this case  $Y_3$  is 0.002 cm), but, as noted earlier, by seasonality of operation of railway track characterized by variable factors  $x_3$  and  $x_4$  – during the transition from summer to winter ( $x_3, x_4$  vary from  $-1$  to  $+1$ ), the decrease in the value of  $Y_3$  reaches 0.09 cm (see Fig. 3a and 3c). The feature of the dependence of vertical deflections of sleeper  $Y_3$  practically does not depend on the seasonality of operation of the railway track.

At the same time, the possibility of controlling the value of  $Y_3$  by changing the material properties of composite sleepers is not so unambiguous and during low sleeper mass ( $x_2 \rightarrow -1$ ) the vertical deflection depends less on its stiffness, which exert more influence on  $Y_3$  when sleeper mass increases, i.e.,  $x_2 \rightarrow 1$ .

Evaluation of the influence of the parameters of composite sleepers on the value of its vertical acceleration  $Y_4$  is important to reduce the risk of its destruction under the dynamic influence of rolling stock.

According to dependences shown in Fig. 4, it follows that under other constant conditions the variation range of the bending coefficient  $x_1$  predominant influence on the value of the vertical acceleration  $Y_4$  is imposed by the mass of sleeper  $x_2$ , with its



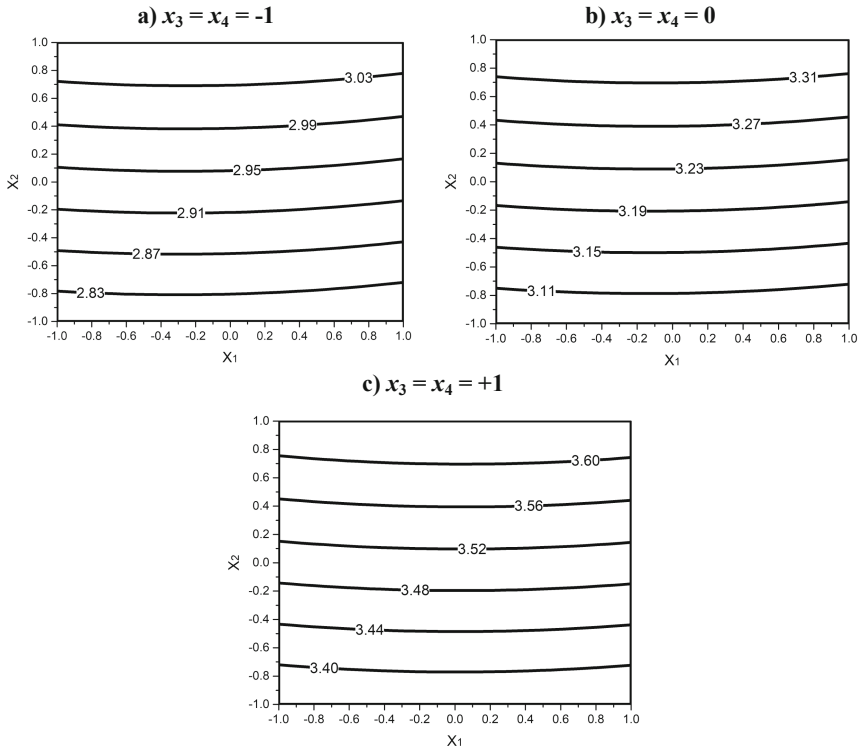
**Fig. 3.** Isolines of vertical deflections of the sleeper  $Y_3$ , cm, in coordinates of variable factors  $x_i$  ( $i = 1-4$ ).

growth the vertical acceleration of the sleeper also increases. In this case, as previous for the studied response function  $Y$  greater impact on the value of  $Y_4$  does not exerted by the bending coefficient  $x_1$  and the sleeper mass  $x_2$  (the changing amplitude of  $Y_4$  is 0.22 in fractions g, rel. Units), but by the seasonality which estimated magnitude of the elastic modulus of the roadbed and the ballast bed in the horizontal  $x_3$  and vertical  $x_4$  plane – from summer to winter ( $x_3, x_4$  range from  $-1$  to  $1$ ) the changing amplitude of  $Y_4$  reaches 0.83 (see Fig. 4a and Fig. 4c).

Moreover, the highest values of vertical acceleration of the sleeper are observed in winter ( $x_3, x_4 \rightarrow +1$ ), and the seasonality of railway track operation does not affect the feature of isolines of  $Y_4$  depending on changes of the properties of composite sleeper material.

At the same time, it is possible to control the value  $Y_4$ , the minimum value of which is achieved at the minimum value of the sleeper mass, i.e.,  $x_2 \rightarrow -1$ ; the bending coefficient of the sleeper does not significantly affect its vertical acceleration.





**Fig. 4.** Isolines of the vertical acceleration of the sleeper Y4 (in fractions of  $g$ , rel. Units) in the coordinates of the variable factors  $x$  in the coded scale  $x_i$  ( $i = 1-4$ ).

## 4 Conclusion

The problem of finding rational properties of the material of composite sleepers was solved by the method of experimental and statistical modeling (ESM-method) by conducting a computational experiment on mathematical models of the studied properties (response functions)  $Y$  in the system “roadbed – ballast bed – sleeper – rail – rolling stock” from varying factors  $X$ . On the basis of the constructed isolines, the dependences between the properties of composite sleepers  $X$  and the operational state  $Y$  of the railway track were established, which is essential for optimizing the material properties of composite sleepers, which provides the lowest stress-strain state of the “roadbed – ballast bed – sleeper – rail – rolling stock” system and rational conditions for its operation.

**Acknowledgements.** The reported study was funded by RFBR, project number 19-38-90179.





## References

1. Kondrashchenko, V.I., Wang, Ch.: Composite underrail basements. *Materials. Constr. Mater.* **1-2**, 95–111 (2020)

2. Senthilkumar, K., Saba, N., Chandrasekar, M.: Evaluation of mechanical and free vibration properties of the pineapple leaf fibre reinforced polyester composites. *Constr. Build. Mater.* **195**, 423–431 (2019)
3. Shah, A.U.M., Sultan, M.T.H., Jawaid, M.: A review on the tensile properties of bamboo fiber reinforced polymer composites. *BioResources* **11**(4), 10654–10676 (2016)
4. Khalil, A.A.: Mechanical testing of innovated composite polymer material for using in manufacture of railway sleepers. *J. Polym. Environ.* **26**(1), 263–274 (2018)
5. Kaewunruen, S., You, R., Ishida, M.: Composites for timber-replacement bearers in railway switches and crossings. *Infrastructures* **2**(4), 13 (2017)
6. AXION ECOTRAX(R), Composite Railroad Ties. <https://axionsi.com/products/ecotrax-railroad/>. Accessed 08 Dec 2020
7. Fraunhofer ICT. Mixed Plastic Waste (MPW) Sleeper. <https://nachhaltigwirtschaften.at/en/fdz/projects/susprise/railwaste-production-of-railway-sleepers-by-mixed-plastic-waste.php>. Accessed 08 Dec 2020
8. SEKISUI. FFU® synthetic wood railway sleepers. [https://www.sekisui-rail.com/en/ffu\\_en.html](https://www.sekisui-rail.com/en/ffu_en.html). Accessed 08 Dec 2020
9. KLP. Hybrid Polymer Sleepers. <https://www.lankhorstrail.com/en/recycled-plastic-sleepers>. Accessed 08 Dec 2020
10. Manalo, A., Aravinthan, T.: Behavior of full-scale railway turnout sleepers from glue-laminated fiber composite sandwich structures. *J. Compos. Constr.* **16**(6), 724–736 (2012)
11. Lyashenko, T.V., Voznesensky, V.A.: Methodology of compounding and technological fields in computer construction materials science. Astroprint, Odessa 168 (2017)
12. Finney, D.: Introduction to the theory of planning experiments. M.: Home edition of physical and mathematical literature publishing house “Science” 300 (2019)
13. Standard test procedure for the impact on the path. TM-14-01-02-Moscow: ARRIRT 39 (2002)



# Comparative Studies of the Anticorrosive Activity of Oily Compositions, Containing Telaz-M, in Outdoor Conditions

R. G. Shevtsova , R. A. Lyubushkin , and I. V. Starostina  

Belgorod State Technological University named after V.G. Shukhov, Belgorod, Russia

**Abstract.** To protect metal surfaces from the atmospheric corrosion the film-forming inhibitors are applied. This work presents the comparative analysis findings of the protective abilities of such corrosion inhibitors as preserving oil M-8V2 and composition on the basis of an oil-soluble inhibitor Telaz-M and M-8V2 oil. It is demonstrated that the oil composition, containing 20% of Telaz-M inhibitor, has high protective action against atmospheric corrosion for steel of grade St20 and alloy steel St12X18H10T. The protective action of the composition is explained by the formation on a steel plate's surface of a film, which is an inverted emulsion (water in oil). This means that the drops of water, present on the metal surface, are encapsulated in the inhibitor's oily solution, forming an emulsion. As a result, the metal contacts not with water, but with the oily solution of the inhibitor. The adding of Telaz-M increases the composition's viscosity, which forms a thicker protective film on the surface of a steel plate.

**Keywords:** Atmospheric corrosion · Grades of steel · Corrosion inhibitor · Preserving oil

## 1 Introduction

Steel structures have found wide application in various branches of industry – in transport, construction, aerospace engineering, oil-producing and oil-refining industry etc. This is explained by their high corrosive resistance. But during their use, steel structures inevitably contact with the atmosphere, containing water, gaseous and dust-like pollutants, which can cause metal corrosion. Besides, before the metal structures are put into service, they are often stored in unheated premises or outdoors.

What is corrosion? This is the process of the gradual degradation of materials' and metals' properties, which is initiated by their chemical or electrochemical reactions with the atmospheric components [1, 2]. Metal corrosion can be designated as belonging to «costly» problems of material science and construction materials engineering. This is due to the fact that corrosion can result in failures of boilers and high-pressure storage tanks, breakdowns of turbine blades or engines, damage of containers with deleterious or toxic substances, deterioration of bridge structures, pipelines etc. Losses of steel due to corrosive processes make up about 30% of its annual production. The atmosphere

corrosion accounts for 60–80% of total financial losses from metal corrosion. In industrialized countries the losses from metal corrosion make up from 4 to 10% of the national income, and the costs of repair and replacement of equipment and communication lines exceed the cost of construction materials by many times [2].

In the work [3] it is demonstrated that in warehousing conditions steel articles are prone to the intensive atmospheric corrosion, which causes their discoloration. The resistance of stainless steel products to the atmospheric corrosion is influenced by the following factors [4]: atmospheric composition; character of metal products' surface - wettability and roughness; chemical composition of steel, presence of sulfide inclusions etc.

Being in the atmosphere, metals contact with water and water solutions of acids, salts, alkalis, as well as with aggressive media, containing organic compounds or gaseous components. Thus, chlorides can destroy passive film on the surface of stainless steel, especially in the damp marine environment. This results in the intensive corrosion and deterioration of not only aesthetic characteristics of structures, but also can reduce the critical structures' operation life or cause equipment failures [5]. Dust particles, settling onto the surface of metal products, made of commercial-quality steel and stainless steel, accelerate the pitting corrosion. This is especially relevant when the surface is somehow rough, as the dust particles are more likely to stay on the rough surface, than on the smooth surface. Besides, the microcracks on the rough surface can become pitting corrosion centers [6].

In the work [4] it is demonstrated that the occurrence of corrosion stains and pits on the surface of stainless steel in conditions of the simulated marine atmosphere is associated with the dissolution of MnS inclusions. The pits depth is increased linearly with the increase of the corrosion time.

In case when metal surfaces have coatings of non-metallic materials – plastic, wood, natural stone or artificial stone on the basis of cement binders, the deterioration of metal would directly depend on these materials' resistance. Thus, plastic or wood can crack, expand or undergo biochemical deterioration, limestones or cement composite materials are prone to dealcalization with the formation of pores, cavities, cracks etc. This provides the access for atmospheric components to the surface of metal structures, and, consequently, increases the probability of atmospheric corrosion.

In order to reduce the corrosion attack on metal products in the modern industry corrosion inhibitors are widely used. Corrosion inhibitors are chemical compounds or their compositions, the small amounts of which in aggressive media inhibit or prevent the development of metal surfaces corrosion [2].

Corrosion inhibitors can be classified by various features – by character and mechanism of their action, by the chemical nature and type of the medium and by the degree of metal surface insulation [2]. By the character of protective action inhibitors can be anodic, cathodic or mixed.

In their mechanism of action they can be passivating and adsorptive; in their chemical nature – inorganic, organic and volatile. By the type of medium, in which the inhibitors are most efficient, they can be: for acid corrosion media, for hydrosulfuric medium, for petroliferous media, for neutral corrosion media and for atmospheric corrosion.

The action of corrosion inhibitors can be conveniently divided into two stages – the transfer of inhibitor molecules onto the metal surface and the subsequent interaction of the inhibitor's functional groups with the metal surface.

As for the atmospheric corrosion of structural materials in neutral media, according to the research [3], in this case the material damage occurs due to the contact of corrosible surfaces with water. That is why the most widely used reagents for protecting metal surfaces and equipment from atmospheric corrosion are the substances, which can form a dense and durable protective film on the surface of metal products, inhibiting electrochemical reactions. Such substances include the film-forming corrosion inhibitors [7, 8]. This group of inhibitors includes surface-active agents (SAA) and organic compounds. Adsorption of an organic substance on the surface of metal products is considered an essential condition of the first stage of its protective action [9].

In the work [10] the research findings of new corrosion inhibitors on the basis of carboxylic acids, extracted from vegetable oils, are presented. It is demonstrated that the anticorrosion properties of new non-toxic inhibitors are conditioned by the formation on the metal surface of a protective iron-carboxylate layer, which results from the interaction of carboxylic acids and metal.

Among the film-forming substances polymeric materials are paid great attention. This is explained by their low cost, availability, environmental friendliness and many adsorption centers for binding to the metal surface.

To increase their inhibition efficiency, polymeric materials are subjected to various methods of modification. Thus, the authors of work [11] have determined that chitosan, modified with thiosemicarbazide and thiocarbohydrazide, has the high inhibiting ability on steel in the 2% acetic acid solution. It is demonstrated that the modified polymer can be efficiently used as an anticorrosion agent in the researched acid medium.

The adding of halogenid ions as modifying agents to polymers' formulas produces a synergetic effect in increasing the polymers inhibition property [12].

In the work [8] the authors studied the protective efficiency of hydroxyethyl cellulose against soft steel corrosion in aerated 0.5 M  $H_2SO_4$  solution. It has been determined that the polymer inhibits both cathodic and anodic partial reactions of soft steel corrosion processes.

Nicotinic acid (NA) and its derivatives – nicotinamide (NAA) and 4-methoxypyridine (MP) – are known to be used as inhibitors of soft steels corrosion in hydrochloric acid solution [13]. It is shown that the considerable anticorrosive action of NAA inhibitor is conditioned by its high adsorption capacity to metal surface.

The work [14] reports about studying the efficiency of using crude ethanolic extracts of leaves and seeds of date palm as inhibitors of X60 carbon steel corrosion in the 15% HCl solution at 25–60 °C. It has been determined that the crude extracts of both leaves and seeds of date palm contain saponins, flavonoids, cardiac glycosides and reducing sugars. The obtained extracts act as mixed-type inhibitors, their anticorrosive action is conditioned by the adsorption of extract components on steel surface.

In general, metal corrosion inhibitors increase the operating life of products, equipment and instruments. They have made it possible to draw a clear line between an element and the environment and to postpone the corrosion development for a long time. Now they are widely available protective agents, having a large range of types and

prices. In spite of the wide range of corrosion inhibitors, nowadays research is continued in designing new efficient and safe inhibiting substances on the basis of natural raw materials.

The purpose of this research is comparing the protective abilities of corrosion inhibitors – preserving oil M-8V2 and composition on the basis of an oil-soluble inhibitor Telaz-M and M-8V2 oil. The parameters researched: the thickness of protective film on the metal surface, corrosion rate and protection degree of various grades of steel in the outdoor conditions of moderate climate in central Russia.

## 2 Methods and Materials

In the experimental research the mineral oil M-8V2, which is a mixture of distillate and residual components of sour and sweet crude oils, and the corrosion inhibitor Telaz-M were used. The characteristics of mineral oil are presented in Table 1.

**Table 1.** Characteristics of mineral oil M-8V2.

Parameter name	Values	Parameter name	Values
Viscosity grade by SAE	20	Open-cup flash-point	255 °C
Density at 20 °C	885.6 kg/m <sup>3</sup>	Chill point	–31 °C
Kinematic viscosity at 100 °C	8.3 mm <sup>2</sup> /s	Base number	4.7 mg/g
Kinematic viscosity at 40 °C	62.9 mm <sup>2</sup> /s	Sulfated ash content	0.8%
Viscosity index	99		

Telaz-M is a product of oleic acid condensation with diethanolamine over a catalyst - boric acid.

As metal products the plates, made of various grades of steel - St10, St20 and St12X18H10T of austenite class.

The prepared steel plates in the shape of rectangles of required sizes had the pronounced metallic luster and the same roughness grade. For surface activation the samples were kept in the 10% hydrochloric acid solution, washed with running water, and then with distilled water, dried with filter paper and placed into a dessicator.

The plates were divided into 3 parties. Samples of parties number I and II were used for studying the protective effect of the 5% and 20% solutions of Telaz-M in the oil M-8V2, respectively. Samples of party III – control samples – were preserved only with oil M-8V2. The corrosion monitoring of samples, made of various grades of steel, was conducted in harsh atmospheric environment of autumn-winter period in central Russia.

The research was carried out in the following way: the previously prepared metal plates were weighed with analytic balance, then put into the oily solutions of the inhibitor (with concentration 5% and 20%) and into the oil M-8V2. They were kept there for 5 min and then taken out of the preservation tank. After the dropping stopped, the samples with the protective film, formed on their surface, were weighed with analytic balance

and suspended outdoors on special holders. The exposure time was 70 days. Then the plates were taken from the holders, and corrosion products were thoroughly removed with a cloth, soaked in ethanol. The plates were dried and weighed. The thickness of oil composition film was calculated by the Formula 1:

$$H = \frac{m_1 - m_0}{\rho \cdot s}, \quad (1)$$

where  $m_1$  – the plate weight after the experiment (with the protective film), g;  $m_0$  – the plate weight before the experiment, g;  $\rho$  – composition density,  $\text{g}/\text{m}^3$ ;  $s$  – sample surface area,  $\text{m}^2$ .

The corrosion rate was calculated by Formula 2:

$$K = \frac{(m_0 - m_2)}{s \cdot \tau}, \quad (2)$$

where  $m_0$  – the plate weight before the experiment, g;  $m_2$  – the plate weight after the experiment, g;  $s$  – sample surface area,  $\text{m}^2$ ;  $\tau$  – exposure time of samples in the atmosphere, h.

The inhibitor protection degree was calculated by Formula 3:

$$Z = \frac{K_1 - K_2}{K_1} \cdot 100, \quad (3)$$

where  $K_1$  – rate of corrosion (resolution) of metal without the inhibitor,  $\text{g}/\text{m}^2 \cdot \text{h}$ ;  $K_2$  – corrosion rate of metal with the inhibitor,  $\text{g}/\text{m}^2 \cdot \text{h}$ .

### 3 Results and Discussion

The average values of the formed protective film thickness on the samples under study and on the control samples, weight loss of samples after the experiment completion are presented in Table 2. The thickness of preserving film on the surface of plates, treated

**Table 2.** Some characteristics of steel samples during the experiment.

No party	Telaz-M inhibitor content in the oil solution, %	Steel grade	Film thickness, H, $\mu\text{m}$	Weight loss of samples, %
I	5	St10	51.7	0.0231
		St20	53.3	0.0043
		St12X18H10T	64.2	0.0005
II	20	St10	662.1	0.0037
		St20	701.4	0.0013
		St12X18H10T	883.2	0.0003
III	0	St10	32.0	0.1170
		St20	34.1	0.0319
		St12X18H10T	35.8	0.0053

with the M-8V2 oil, is small. In the 5% oil solution of Telaz-M inhibitor the film thickness is increased by about 20  $\mu\text{m}$ . In the 20% oil solution of Telaz-M the film thickness is increased by over 10 times. The thickest film is observed on the surface of plates, made of steel St12X18H10T.

The corrosion rate and the protection degree of steel samples in the 5% and 20% solutions of Telaz-M in the oil M-8V2 are presented in Table 3.

**Table 3.** Corrosion rate and protection degree of steel samples in Telaz-M solutions in the oil M-8V2.

№ party	Steel grade	Weight content of Telaz-M, %	Corrosion rate, $\text{g}/(\text{m}^2 \cdot \text{h})$		Protection degree, Z, %
			in oil only, $K \times 10^{-3}$	in oil solution of the inhibitor, $K_{\text{in}} \times 10^{-3}$	
I	St10	13.230	13.230	4.28–4.86	63–67
	St20	6.369	6.369	1.55–1.91	70–75
	St12X18H10T	0.879	0.879	0.10–0.21	76–86
II	St10	13.230	13.230	0.44–1.29	90–97
	St20	6.369	6.369	0.09–0.50	92–98
	St12X18H10T	0.879	0.879	0.01–0.03	98–99

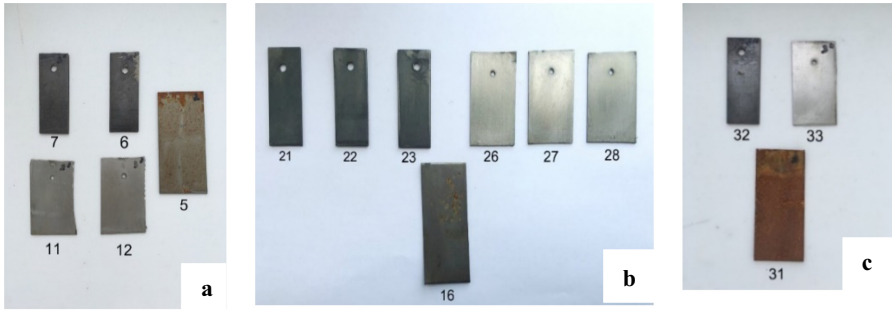
Comparison results of the inhibition efficiency of two preserving compositions of Telaz-M in oil M-8V2 with concentrations 5% and 20% have demonstrated that the highest protection degree for steel samples St10, St20 and St12X18H10T against the atmospheric corrosion is shown by the 20% solution. The preserving composition, containing 5% of Telaz-M, has demonstrated the low protective effect.

The visual assessment of the plates' appearance was carried out throughout the whole exposure time. In Fig. 1 the photos of plates after the 70-days exposure time are presented. The visual assessment of the plates, treated with oil M-8V2 (control samples), has demonstrated that after 70 days all the plates were corroded to a different extent.

In Fig. 1 the photos of party III samples, treated with the oil, are presented. The steel sample of St10 grade has undergone uniform corrosion (№ 31). In steel sample St20 (№ 32) the pitting corrosion all over the surface is observed, as well as a pronounced corrosion stain. The alloy steel sample of St12X18H10T grade (№ 33) has the pitting corrosion in several places, and has lost metallic luster – the plate has turned yellow. The plates of party I, i.e. treated with the composition, containing 5% of Telaz-M, were corroded to a lesser degree. The steel plate St10 (№ 5) is covered with pitting corrosion. For steel plates St20 (№ 6 and № 7) the pitting corrosion is observed not on the whole surface. The alloy steel samples St12X18H9T (№ 11 and № 12) have turned yellow and lost metallic luster.

Increase of the Telaz-M inhibitor weight content up to 20% results in the considerable improvement of the plates' appearance (party II). On steel samples St10 the rare pitting corrosion is registered, the steel samples St20 (№ 21, 22 and 23) – have only lost





**Fig. 1.** Photos of sample parties: a – I, b – II, c – III.

metallic luster, and the steel samples St12X18H10T (№ 26, 27 and 28) have proved more resistant – have not even lost metallic luster. The visual assessment of the plates has demonstrated that the increase of the Telaz-M weight content in the composition up to 20% considerably reduces the corrosion damage of plates, made of steel St20 and St12X18H10T.

## 4 Conclusion

Composition on the basis of Telaz-M inhibitor with weight content 20% and oil M-8V2 has the high protective action against atmospheric corrosion for steel samples of grade St20 and for alloy steel St12X18H10T. The protective action of the composition is explained formation of an inverted emulsion (water in oil) and the thickness of oily film on the steel plate surface. The drops of water, present on the metal surface, are encapsulated in the inhibitor's oily solution and, as a result, the metal contacts not with water, but with the oily solution of the inhibitor. The adding of Telaz-M increases the composition's viscosity, which increases the oily film's thickness on the surface of a steel plate. Composition on the basis of Telaz-M inhibitor and oil M-8V2 has low cost and high protective ability for commonly used steel grades.

**Acknowledgements.** The work is realized in the framework of the Program of flagship university development on the base of the Belgorod State Technological University named after V.G. Shoukhov, using equipment of High Technology Center at BSTU named after V.G. Shoukhov.




## References

1. Klyuchnikova, V.V., Denisova, L.V.: *Fundamentals of Electrochemistry and Chemical Properties of Construction Metals*. Belgorod state Technological University Press, Belgorod (2008)
2. Kozlova, L.S., Sibileva, S.V., Chesnokov, D.V., Kutryev, A.E.: Corrosion inhibitors (review). *Aircr. Mater. Technol.* **2**, 67–75 (2015)
3. Malaibari, Z., Kahraman, R., Saricimen, H., Quddus, A.: Investigation of atmospheric corrosion of mild steel after treatment by several inhibitor solutions. *Corros. Eng. Sci. Technol.* **42**(2), 112–118 (2007)

4. Lu, W., Pan, C., Su, W., Wang, Z., Liu, S., Wang, C.: Atmospheric corrosion mechanism of 316 stainless steel in simulated marine atmosphere. *Corros. Eng. Sci. Technol.* **51**(3), 155–162 (2006)
5. Cook, B., et al.: Assessing the risk of under-deposit chloride-induced stress corrosion cracking in austenitic stainless steel nuclear waste containers. *Corros. Eng. Sci. Technol.* **49**, 529–534 (2014)
6. Wallinder, D., Wallinder, I.O., Leygraf, C.: Influence of surface treatment of type 304L stainless steel on atmospheric corrosion resistance in urban and marine environments. *Corrosion* **59**, 220–227 (2003)
7. Knyazeva, L.G., Kuznetsova, E.G., Prokhorenkov, V.D., et al.: Rapid assessment of protective properties of «Geron» water-wax compositions. *Bull. Tambov Univ. Ser. Nat. Eng. Sci.* **18**(5), 2299–2303 (2013)
8. Arukalam, I.O., Madufor, I.C., Ogbobe, O., Oguzie, E.E.: Inhibition of mild steel corrosion in sulfuric acid medium by hydroxyethyl cellulose. *Chem. Eng. Commun.* **202**, 112–122 (2015)
9. Galyamov, I.I., Galimov, M.R., Andriyanov, O.P.: Modeling of the corrosion inhibitor protective layer formation initial stage by molecular dynamics method. *Autom. Teleautom. Commun. Pet. Ind.* **9**, 44–45 (2011)
10. Hollner, S., Mirambet, F., Rocca, E., Reguer, S.: Evaluation of new non-toxic corrosion inhibitors for conservation of iron artefacts. *Corros. Eng. Sci. Technol.* **45**(5), 362–366 (2010)
11. Li, M., et al.: Simple preparation of aminothiourea-modified chitosan as corrosion inhibitor and heavy metal ion adsorbent. *J. Colloid Interface Sci.* **417**, 131–136 (2014)
12. Solomon, M., Umoren, S.: Performance evaluation of poly (methacrylic acid) as corrosion inhibitor in the presence of iodide ions for mild steel in H<sub>2</sub>SO<sub>4</sub> solution. *J. Adhes. Sci. Technol.* **29**(11), 1060–1080 (2015). <https://doi.org/10.1080/01694243.2015.1017436>
13. Liu, X., Pan, X., Lu, M., Sun, Y., Wang, Z., Zheng, Y.: Nicotinic acid derivatives as corrosion inhibitors for mild steel in hydrochloric acid solutions: an experimental and computational chemistry study. *J. Adhes. Sci. Technol.* (2020). <https://doi.org/10.1080/01694243.2020.1787934>
14. Umoren, S.A., Solomon, M.M., Obot, I.B., Suleiman, R.K.: Comparative studies on the corrosion inhibition efficacy of ethanolic extracts of date palm leaves and seeds on carbon steel corrosion in 15% HCl solution. *J. Adhes. Sci. Technol.* **32**(17), 1934–1951 (2018)



# Rheotechnological Properties of Multicomponent Dispersed Suspensions of Glowing Architectural and Decorative Concrete

M. V. Maliukova<sup>(✉)</sup> , L. A. Suleymanova , and A. A. Koryakina 

Belgorod State Technological University named after V.G. Shukhov, Belgorod, Russia

**Abstract.** Architectural concretes are subject to high requirements for decorative-ness, which implies obtaining products of various shapes with a relief structure and different textures. The basis for obtaining high-strength luminous architectural and decorative concretes is to provide the required rheotechnological characteristics of the concrete mix. The technological properties of mineral suspensions in combination with various fine fillers were studied, the results showed the possibility of using technological waste to produce stone flour as a rheologically-active component for glowing architectural and decorative concrete. As a result of the experiments, the dependence of the change in the water-reducing effect of the plasticized cement-mineral suspension of the “white Portland cement – stone flour” system on the ratio of the components was determined. Optimal ratios of Portland cement and stone flour were determined, and the recommended dosage of photoluminescent pigment in the rheological matrix of architectural and decorative concrete was determined. The obtained data of rheotechnological properties and water-reducing effects of multicomponent suspensions became the basis for the development of compositions of self-compacting high-strength architectural and decorative glowing concretes.

**Keywords:** Rheotechnological properties · Architectural and decorative concrete · Stone flour · Glowing concrete · Multicomponent dispersed suspensions

## 1 Introduction

Architectural and decorative concretes are a new generation of concretes: HPC and UHPC, which are multi-component compositions with the inclusion of powder dispersed filler. Therefore, the basis for ensuring their high rheotechnological and qualitative characteristics is optimally selected Portland cement and modifier, highly dispersed pigments, organic and mineral components that allow you to control the rheological properties of concrete mixes and change the structure of architectural and decorative concrete at the micro level, ensuring maintenance durability and expanding the architectural possibilities of using such concrete [1–5].

The relevance of this research is due to the possibility and reasonableness of the use of rheologically-active components in the form of dispersed fillers in the compositions of architectural and decorative concretes. At the same time, waste from rock crushing is used as fine fillers, the recycling of which is one of the most actual problem for solving environmental problems.

## 2 Materials and Methods

Materials Used for the Research: Egyptian White Portland Cement Aalborg CEM I 52.5 N, Admixture MC-Power Flow 6955, MC-Power Flow 7951, MC-Power Flow 3100, Polyplast PC Type S, Photoluminescent Pigment Waterproof LLA-2 Brand a (Luminophore of Long Afterglow). Marble Stone Crushing Waste and Limestone Stone Crushing Waste Are Used for the Preparation of Fine Filler. The Physical and Mechanical Properties of the Components and the Rheological Characteristics of the Suspensions Were Evaluated in Accordance with Normative Documents. The Overall Dispersion of Fillers Was Estimated by the Specific Surface Area.

## 3 Results and Discussion

The rheotechnological properties of cement suspensions, mineral dispersed fillers and pigments, binary and triple systems, as well as the possibility of obtaining architectural and decorative concretes of a new generation on their basis were studied. Rheotechnological properties are rheological engineering properties of concrete mixes – consistency, workability, self-leveling and flow of mixes, important to produce concrete products, the main of which were evaluated during testing [6].

Photoluminescent pigment is used to glow architectural and decorative concrete. The introduction of photoluminescent pigment into cement suspensions, and subsequently into the mix, can affect the rheotechnological properties of the concrete mix. Therefore, it is important to take into account the effect of luminous pigments on the water-reducing effect ( $W_{EF}$ ), plasticity and persistence of the suspension.

The conducted studies [7, 8] revealed that the maximum water-reducing effect of cement suspensions was noted when using a polycarboxylate-type modifier in an amount of 0.4%. In this regard, there is an obvious need to study the rheotechnological properties of pure and modified suspensions of pigments. Presents the results of investigating the rheotechnological properties of suspensions of photoluminescent pigments.

Analysis of the received data shows high values of  $W_{EF}$  for each of the types of photoluminescent pigment, therefore, the particle size in the range of 40–100 microns has a minimal impact on rheotechnological properties. Meanwhile, the greatest rheotechnological effect is obtained in a suspension modified by MC-Power Flow 7951.

Taking into account that photoluminescent pigments are introduced into the composition in a dosage of up to 20%, it is important to understand the effect of the amount of pigment on the rheotechnological parameters of the binary system “Portland cement – photoluminescent pigment”. The correct dosage of the photoluminescent pigment ensures its uniform distribution and glow throughout the entire volume of the product. Cement suspensions with the use of Portland cement have the highest rates of water reduction [9, 10], so subsequent studies were conducted on plasticized systems “Portland cement – photoluminescent pigment” with the introduction of photoluminescent pigments in the dosage 5%, 7%, 10%, 15% from the weight of Portland cement.

Analysis of the received data showed that for water-cement suspensions consisting of white Portland cement, with the introduction of the modifier MC-Power Flow 7951, the  $W_{EF}$  was 3–3.4, which is more than the value of the  $W_{EF}$  of pure cement suspension (the  $W_{EF}$  of pure cement suspension is 1.73). This effect remains with the introduction of photoluminescent pigment up to 10%. With a further increase in the amount of pigment, there is a decrease in W/S and a decrease in the value of the water-reducing effect, which confirms the inexpediency of increasing the percentage of pigment introduction into the mix.

The characteristics of concrete depend on the structure of the dispersed systems on the basis of which they are obtained. The rate of destruction and restoration of the structure of the dispersed concrete system, workability and liquefaction are closely interrelated [11–13].

The next stage of research was the study of rheotechnological properties of mixed cement-mineral suspensions. Glowing architectural and decorative concretes should be highly decorative and, in the daytime, the use of white Portland cement is rational in combination with light dispersed fillers. Therefore, the combinations “white Portland cement – marble flour” and “white Portland cement – limestone flour” were chosen for the research.

Portland cement was mixed with a dispersed filler in a ratio of 1:1 with a total amount of solid components of 400 kg/m<sup>3</sup>. The ratio was chosen to assess the effect of fillers on the rheotechnological properties of suspensions.

The data in Table 1 show that the introduction of a dispersed filler into a suspension with white Portland cement reduces the value of W/S relative to pure cement suspension. This is typical for all types of modifiers used. In turn, the  $W_{EF}$  of the suspension in a combination of white Portland cement and marble flour with all plasticizers is higher than that of pure cement and mineral suspensions. Thus, in the system: “white Portland cement – marble flour” when modifying one of the components enhances the effect of the other.

**Table 1.** Changes in the values of W/S of plasticized suspensions “white Portland cement – dispersed filler”.

Type of Portland cement and dispersed filler	Type of polycarboxylate modifier, content of 0.4% by weight of dry components	W/S	The diameter of the flowability, D, mm	W <sub>EF</sub>
White Portland cement 100%	Without modifier	0.45	235	-
	MC-Power Flow 6955	0.30	237	1.61
	MC-Power Flow 7951	0.26	239	1.73
	MC-Power Flow 3100	0.31	237	1.59
	Polyplast PC type S	0.35	236	1.48
White Portland cement 50% Marble flour 50%	Without modifier	0.50	235	-
	MC-Power Flow 6955	0.29	235	1.72
	MC-Power Flow 7951	0.26	234	1.89
	MC-Power Flow 3100	0.31	239	1.57
	Polyplast PC type S	0.30	235	1.66
White Portland cement 50% Limestone flour 50%	Without modifier	0.45	239	-
	MC-Power Flow 6955	0.26	233	1.69
	MC-Power Flow 7951	0.25	235	1.80
	MC-Power Flow 3100	0.28	238	1.59
	Polyplast PC type S	0.28	213	1.57

In the conducted research, the effect of stone flour in modified suspensions was studied at a ratio of Portland cement and filler 50%:50%. For architectural and decorative concretes, it is important that the ratio of Portland cement and mineral filler is in the range from 50%: 50% to 80%: 20% [14]. An experiment was conducted to determine the rheotechnological properties of modified suspensions “white Portland cement – limestone flour” and “white Portland cement – marble flour” with different component ratios (total number of solid components 400 kg/m<sup>3</sup>), modified with an additive of polycarboxylate type MC-PowerFlow 7951 with a content of 0.4% by weight of dry components.

Analysis of the data in Table 2 showed that for water suspensions consisting of 70–80% Portland cement and 30–20% marble flour, with the introduction of the MC-Power Flow 7951 modifier, the W<sub>EF</sub> was 3.11 and 3.26, which is more than the W<sub>EF</sub> value of pure cement suspension. With a further increase in the amount of marble flour, a decrease in the W/S and an increase in the value of the water-reducing effect are observed. The water reduction value on pure marble flour is 3.12, which is also higher than on pure cement suspension.

Analysis of the results received in the research of the influence of the dosage of limestone flour on the water-reducing effect showed that marble and limestone filler in

**Table 2.** Rheotechnological properties of modified suspensions “white Portland cement – marble flour” depending on the ratio of components.

Type of Portland cement and dispersed filler	Type of polycarboxylate modifier, content of 0.4% by weight of dry components	W/S	The diameter of the flowability, D, mm	W <sub>EF</sub>
White Portland cement 100%	Without modifier	0.53	235	-
	MC-Power Flow 7951	0.188	232	2.76
White Portland cement 80% Marble flour 20%	Without modifier	0.52	234	-
	MC-Power Flow 7951	0.167	239	3.11
White Portland cement 70% Marble flour 30%	Without modifier	0.51	235	-
	MC-Power Flow 7951	0.156	236	3.26
White Portland cement 40% Marble flour 60%	Without modifier	0.50	233	-
	MC-Power Flow 7951	0.140	235	3.51
Marble flour 100%	Without modifier	0.53	232	-
	MC-Power Flow 7951	0.17	233	3.12

combination with white Portland cement and the modifier MC-Power Flow 7951 show similar values of the W<sub>EF</sub>. An increase in water reduction indicators was found at all ratios, except for pure limestone flour. Suspensions consisting of 70% Portland cement and 30% limestone and marble flour have the best characteristics. With a further increase in the mineral part of the binary system “white Portland cement – limestone flour” and “white Portland cement – marble flour”, there is a decrease in W/S and an increase in the value of W<sub>EF</sub>. Further research was carried out for the triple system “white Portland cement – marble flour – photoluminescent pigment” taking into account the results received and presented above (Table 3).

As a result of research, it was determined that at a dosage of photoluminescent pigment of 5–10% of the weight of Portland cement, the rheotechnological properties of the fine matrix of the modified suspension of the triple system “white Portland cement – stone flour – photoluminescent pigment” are preserved. This is due to the fact that the photoluminescent pigment, having a high particle dispersion, has a specific surface for adsorption of polycarboxylate-type modifier molecules. When adding a photoluminescent pigment to the system, the water reduction values remain almost the same as in the “white Portland cement – mineral filler” system. With the introduction of a mineral component-marble flour at a ratio of 30%:70% in the system, there is a slight increase in the value of W<sub>EF</sub>, which is the maximum value for the system under consideration in a preset ratio of components. The use of white Portland cement and marble flour, MC-Power Flow 7951 modifier with a content of 0.4% by weight of dry components,

**Table 3.** Rheotechnological properties of modified suspensions “white Portland cement – marble flour – photoluminescent pigment” depending on the ratio of components.

Type of Portland cement, dispersed filler and pigment	Type of polycarboxylate modifier, content of 0.4% by weight of dry components	W/S	The diameter of the flowability, D, mm	W <sub>EF</sub>
White Portland cement 70% Marble flour 30% Photoluminescent pigment waterproof LLA-2 brand A (40) 5%	Without modifier	0.45	235	-
	MC-Power Flow 6955	0.164	237	2.74
	MC-Power Flow 7951	0.150	233	3.0
	MC-Power Flow 3100	0.195	235	2.3
	Polyplast PC type S	0.217	234	2.0
White Portland cement 70% Marble flour 30% Photoluminescent pigment waterproof LLA-2 brand A (40) 7%	Without modifier	0.52	235	-
	MC-Power Flow 6955	0.179	239	2.9
	MC-Power Flow 7951	0.150	231	3.4
	MC-Power Flow 3100	0.199	233	2.6
	Polyplast PC type S	0.214	235	2.42
White Portland cement 70% Marble flour 30% Photoluminescent pigment waterproof LLA-2 brand A (40) 10%	Without modifier	0.51	239	-
	MC-Power Flow 6955	0.169	237	3.0
	MC-Power Flow 7951	0.152	232	3.3
	MC-Power Flow 3100	0.190	238	2.68
	Polyplast PC type S	0.217	233	2.3

photoluminescent pigment in a dosage of up to 10% are technologically effective from the point of view of rheology and savings of Portland cement.

## 4 Conclusions

The optimal ratio of the components of the mineral suspension of the three-component system “Portland cement-stone flour-photoluminescent pigment” modified with a polycarboxylate type additive MC-Power Flow 7951 was determined. The obtained data of rheotechnological properties and water-reducing effects of triple suspensions became the basis for the development of compositions of self-compacting high-strength architectural and decorative glowing concrete. In addition, the expediency of using stone crushing waste of various rocks to produce stone flour as a rheologically active component in architectural and decorative concrete was confirmed.

**Acknowledgements.** This work was realized in the framework of the Program of flagship university development on the base of the Belgorod State Technological University named after V. G. Shukhov, using equipment of High Technology Center at BSTU named after V. G. Shukhov.



## References

1. Ranade, R., Stults, M.D., Li, V.C., Rushing, T.S., Roth, J.: Development of high strength high ductility concrete. In: 2nd International RILEM Conference on Strain Hardening Cementitious Composites, pp. 1–8 (2011)
2. Wałach, D., Dybeł, P., Sagan, J., Gicala, M.: Environmental performance of ordinary and new generation concrete structures – a comparative analysis. *Environ. Sci. Pollution Res.* **26**(4), 3980–3990 (2019)
3. Thomas, C., Setién, J., Polanco, J.A., Alaejos, P., Sánchez, D.J.M.: Durability of recycled aggregate concrete. *Constr. Build. Mater.* **40**, 1054–1065 (2013)
4. Xincheng, P., Jixin, D., Milestone, N.: Super-high-strength high performance concrete. In: IOP Conference Series: Materials Science and Engineering, vol. 890, pp. 1–243. CRC Press (2012)
5. Suleymanova, L., Maliukova, M., Ryabchevskiy, I.S., Koryakina, A.A., Levshina, D.E.: Effects of waterproofing materials with different basis on asphalt concrete. *World Appl. Sci. J.* **25**(2), 347–353 (2019)
6. Marchon, D., Flatt, R.J.: Impact of chemical admixtures on cement hydration. In: Science and Technology of Concrete Admixtures, pp. 279–304. Elsevier Inc. (2016)
7. Nizina, T.A., Balykov, A.S., Korovkin, D.I., Volodin, V.V.: Modified fine-grained concretes based on highly filled self-compacting mixtures. *IOP Conf. Ser.: Mater. Sci. Eng.* **481**, 012048 (2019)
8. Suleymanova, L., Maliukova, M., Koryakina, A.: Architectural and decorative concrete with photoluminescent pigment. *IOP Conf. Ser.: Mater. Sci. Eng.* **896**, 41–49 (2020)
9. Houst, Y.F., Bowen, P., Perche, F., Kauppi, A., Borget, P., Galmiche, L., Reknes, K.: Design and function of novel superplasticizers for more durable high performance concrete (superplast project). *Cement Concrete Res.* **38**(10), 1197–1209 (2008)
10. Suzdaltsev, O.: Dis. Cand. Techn. science, PGUAS, Penza (2015)
11. Gołaszewski, J., Szwabowski, J.: Influence of superplasticizers on rheological behaviour of fresh cement mortars. *Cement Concrete Res.* **34**(2), 235–248 (2004)
12. Zega, C.J., Di Maio, Á.A.: Use of recycled fine aggregate in concretes with durable requirements. *Waste Manag.* **31**(11), 2336–2340 (2011)
13. Ćosić, K., Korat, L., Ducman, V., Netinger, I.: Influence of aggregate type and size on properties of pervious concrete. *Constr. Build. Mater.* **78**, 69–76 (2015)
14. Alyousef, R., Khadimallah, M.A., Soussi, C., Benjeddou, O., Jedidi, M.: Experimental and theoretical study of a new technique for mixing self-compacting concrete with marble sludge grout. *Adv. Civil Eng.* **5**, 1–1 (2018)



# Influence of Inhomogeneity of the Foundation on the Stress-Strain State of a Free-Lying Beam

A. N. Leontiev<sup>(✉)</sup> , T. N. Gorbunova , K. V. Balandina , and A. A. Sitnikova 

National Research Moscow State University of Civil Engineering, Moscow, Russia

**Abstract.** The stress-strain state of beams freely lying on an inhomogeneous elastic Winkler foundation is investigated. It is accepted that the value of the base bed coefficient has a symmetrical character of change relative to the middle of the beam, and within its limits is described by a quadratic law. Single-span beams under the influence of a uniformly distributed load are considered. To determine the stress-strain state, the Ritz-Timoshenko variational method and the Lira software package were used. In the first case, the calculation was carried out in the Excel environment, while trigonometric functions were taken as approximating functions. It is shown that satisfactory results can be obtained with 6 terms of the series approximating the required function. Beams with different relative lengths are considered: short, medium and long. The influence of the degree of inhomogeneity of the base on deflections and bending moments is shown. It was found that in short beams with an increase in the degree of inhomogeneity of the base, the bending moments significantly increase. For long beams, the deflection values increase significantly. Calculations in the Lira software package, taking into account the symmetry of the problem, were performed for a half of the beam with a breakdown of the region into 20 elements. Within each element, the value of the bed coefficient was assumed constant. The results obtained in two ways are in complete agreement.

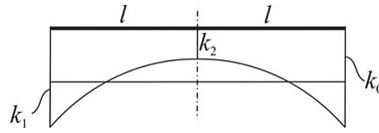
**Keywords:** Beam · Elastic foundation · Winkler model · Ritz-Timoshenko method · Lira software package · Calculation examples

## 1 Introduction

The development of the theory of calculating beams and slabs located on an elastic foundation can contribute to a more efficient and economical method of building various kinds of structures. In most works, the base is assumed to be homogeneous, but in practice it is often possible to observe a change in the value of the bed coefficient along the length of the structure, which undoubtedly affects its stress-strain state. The most common model describing the properties of an elastic foundation is Winkler's model [1], according to which it is assumed that between the load  $q_0(x)$ , acting on the foundation and its settlement  $v(x)$  there is a directly proportional relationship of the form:  $q_0(x) = k_0 v(x)$ , where  $k_0$  – coefficient of proportionality, called the coefficient of bed.

It is known that under the action of a uniformly distributed load, beams freely lying on a homogeneous elastic foundation, in accordance with Winkler's model, behave like

a stamp, i.e. they have no inner efforts. It is obvious that even a slight inhomogeneity of the base will cause bending moments and shear forces. In this work, it is assumed that the value of the bed coefficient of the elastic foundation has a symmetrical character of change relative to the middle of the beam, and within the beam is described by a quadratic law (Fig. 1).



**Fig. 1.** Character of change of coefficient of the bed under a beam.

In this case, if the origin is taken in the center of the beam, the dependence of the bed coefficient on the x coordinate is written as:

$$k(x) = \frac{\alpha}{10} \frac{12k_0}{L^2} x^2 + \frac{10 - \alpha}{10} k_0. \tag{1}$$

Here:  $\alpha$  is the degree of inhomogeneity of the base,  $L = 2l$  is the length of the beam,

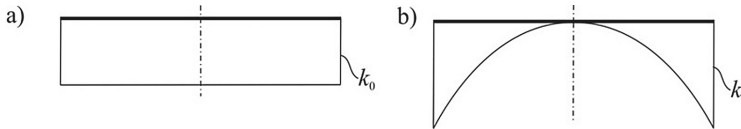
$k_0$  – is the average value of the bed coefficient, determined from the condition of equality of the areas of the graphs describing the rebound of the base in the case of a heterogeneous and homogeneous base,

$k_1$  – the value of the bed coefficient at the left end of the beam:  $k_1 = k_0 \alpha/5 + k_0$ ,

$k_2$  – the value of the bed coefficient under the center of the beam:  $k_2 = (10 - \alpha) k_0/10$ .

Here, the parameter  $\alpha$  is introduced for the possibility of varying the degree of base heterogeneity from its absence to the maximum value.

In our case, it is assumed that the value of the parameter  $\alpha$  can vary from 0 (no inhomogeneity) to 10 (the largest value) (Fig. 2).



**Fig. 2.** Character of change of coefficient of the bed under a beam a) when  $\alpha = 0$ , b) when  $\alpha = 10$ .

After performing the integration, one can see that expression (1) does not depend on the nonlinearity parameter and is equal to  $k_0L$ .

## 2 Methods and Materials

Free-lying single-span beams under the influence of a uniformly distributed load are considered (Fig. 3).

To solve this problem, the Ritz-Timoshenko variational method was used [2].

For the general case of transverse bending of a bar lying on an elastic foundation, the total energy is determined by the formula:

$$U = \int_0^L \left[ \frac{1}{2} \frac{M^2}{EJ} + bk(x) \frac{v^2}{2} \right] dx - \int_0^L qv dx = \int_0^L \left[ \frac{1}{2} \frac{(EJv'')^2}{EJ} + bk(x) \frac{v^2}{2} \right] dx - \int_0^L qv dx. \quad (2)$$

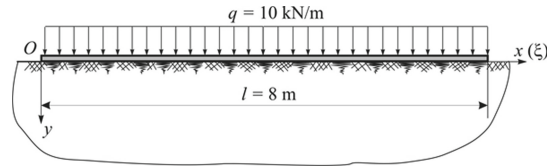


Fig. 3. Design diagram of a beam.

Here  $E$  is the modulus of elasticity of the material of the beam,  $b$  is the width of the cross-section of the beam,  $J$  is its moment of inertia and  $q$  is the external load.

Let's represent the required deflection as a series:

$$v(x) = c_0 \varphi_0(x) + c_1 \varphi_1(x) + c_2 \varphi_2(x) + \dots \quad (3)$$

substitute series (3) into the expression for the total energy (2) and write down the condition for its minimum (Lagrange condition):

$$\frac{\partial U}{\partial c_i} = \int_0^l \{ EJ [c_0(\varphi_0)'' + c_1(\varphi_1)'' + \dots](\varphi_i)'' + bk(x)(c_0 \varphi_0 + c_1 \varphi_1 + \dots) \varphi_i \} dx - \int_0^l q \varphi_i dx = 0. \quad (4)$$

As a result, to determine the coefficients of series (3), we obtain a system of linear algebraic equations, which in matrix-vector form can be represented as

$$A\bar{c} = \bar{b} \quad (5)$$

The coefficients of system (5) are determined by the expression:

$$a_{ij} = \int_0^l \{ EJ [(\varphi_j)''](\varphi_i)'' + bk(x)(\varphi_j \varphi_i) \} dx. \quad (6)$$

Elements of the right side of the system can be found by integrating

$$b_i = \int_0^l q \varphi_i dx. \quad (7)$$

Substitute expression (1) for  $k(x)$  into formula (6) and introduce the notation

$$\lambda^4 = \frac{bk_0}{4EJ} \quad (8)$$

we obtain the expression:

$$a_{ij} = EJ \int_0^l \left\{ [(\varphi_j)'''](\varphi_i)'' + \frac{4}{10}\lambda^4 \left( \frac{3\alpha}{l^2}x^2 + 10 - \alpha \right) (\varphi_j \varphi_i) \right\} dx. \quad (9)$$

Let us take the following functions as approximating ones

$$\varphi_n(x) = \cos \frac{n\pi x}{2l}, \quad \text{where } n = 0, 1, 2, \dots \quad (10)$$

Substituting functions (10) into (3) and then into the expression (9) and multiply both sides of all equations of system (5) by  $l^4/EJ$  the coefficients of the system of equations (5) can be represented as:

$$a_{ij} = d_{ij} \int_0^l \cos \frac{j\pi x}{2l} \cos \frac{i\pi x}{2l} dx + e_{ij} \int_0^l x^2 \cos \frac{j\pi x}{2l} \cos \frac{i\pi x}{2l} dx, \quad (11)$$

$$\text{where, } d_{ij} = \left[ \frac{j^2 i^2 \pi^4}{16} + \frac{4}{10}(\lambda l)^4 (10 - \alpha) \right], \quad e_{ij} = \frac{12\alpha}{10l^2}(\lambda l)^4.$$

The elements of the right side will take the form:

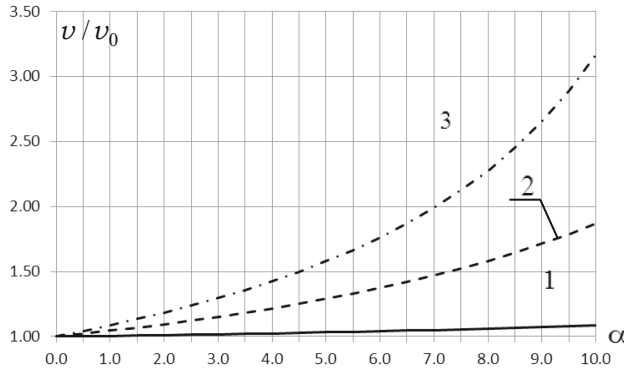
$$b_i = \frac{l^4}{EJ} \int_0^l q \varphi_i dx = \frac{l^4}{EJ} \int_0^l q \cos \frac{i\pi x}{2l} dx = \frac{ql^4}{EJ} \frac{2l}{i\pi} \sin \frac{i\pi}{2}.$$

### 3 Results and Discussion

The influence of the degree of base inhomogeneity on deflections and bending moments under the action of a uniformly distributed load is analyzed.

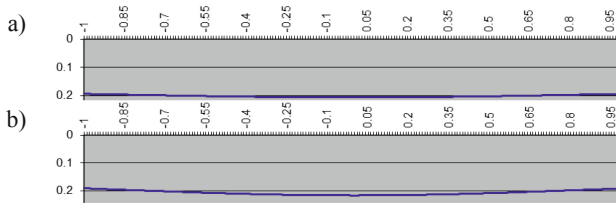
As you know, the assignment of a particular beam to a particular category (short, long) depends not on its actual length  $L$ , but on the product  $\lambda L$ , where the parameter  $\lambda$ , as follows from formula (8), depends on both the stiffness of the beam and from the bedding ratio of the base. For  $\lambda L < 1.2$  the beam belongs to the category of absolutely rigid (stamp), for  $1.2 < \lambda L < 2.2$  it can be considered short, for  $2.2 < \lambda L < 4.5$  – a beam of medium length, for  $4.5 < \lambda L$  – long.

Figure 4 shows the effect of the degree of base heterogeneity on the deflections of short beams, beams of medium length and long beams under the action of a uniformly distributed load. Here are the relative deflections at the center of the beam, depending on the parameter,  $v_0$  – deflection of a beam located on a homogeneous base.

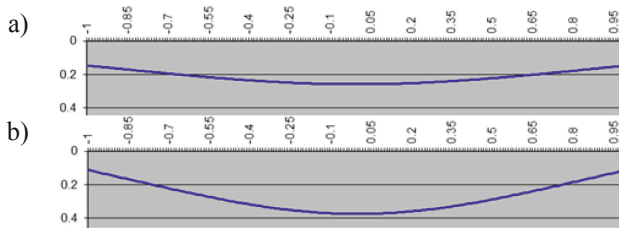


**Fig. 4.** The influence of the degree of heterogeneity of the base on the deflections 1. – short beam ( $\lambda L = 1.5$ ), 2. – beam of medium length ( $\lambda L = 3.0$ ), 3. – long beam ( $\lambda L = 4.5$ ).

Below, for three types of beams, deflection diagrams are given for two values of the base inhomogeneity parameter  $\alpha$  (Figs. 5, 6 and 7).



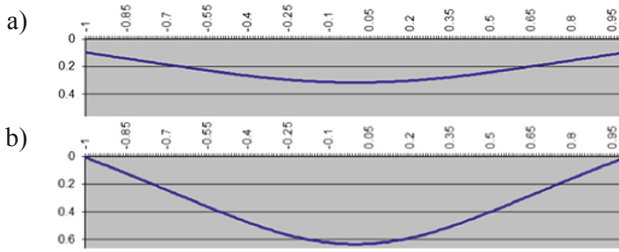
**Fig. 5.** Deflection plots for short beam ( $\lambda L = 1.5$ ) a) for  $\alpha = 5$ , b) for  $\alpha = 10$ .



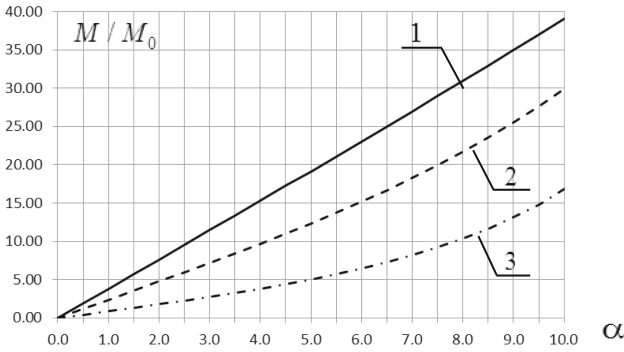
**Fig. 6.** Deflection plots for beam of medium length ( $\lambda L = 3.0$ ) a) for  $\alpha = 5$ , b) for  $\alpha = 10$ .

Figure 8 shows the effect of the degree of inhomogeneity of the base on the bending moment at the center of the beam for short beams, beams of medium length and long beams under the action of a uniformly distributed load.

To verify the results obtained by the Ritz-Timoshenko method, beams of various lengths were calculated using the Lira software package. Some of the results of this calculation are shown in Figs. 9, 10 and 11. Here, taking into account the symmetry of the problem, the diagrams of bending moments for the right half of the beam are shown.

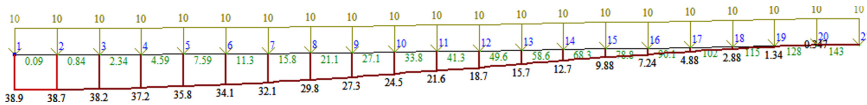


**Fig. 7.** Deflection plots for long beam ( $\lambda L = 4.5$ ) a) for  $\alpha = 5$ , b) for  $\alpha = 10$ .

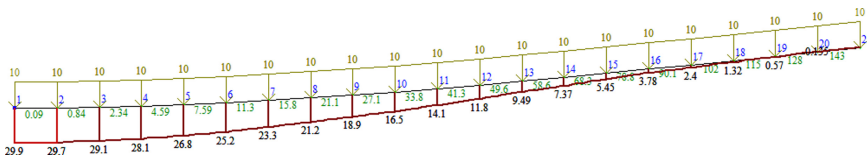


**Fig. 8.** The influence of the degree of heterogeneity of the base on the magnitude of the bending moment in the center of the beam. 1. -  $\lambda L = 1.5$ , 2. -  $\lambda L = 3.0$ , 3. -  $\lambda L = 4.5$ .

Lira calculations, taking into account the symmetry of the problem, were performed for a half of the beam with a breakdown of the region into 20 elements. Within each element, the value of the bed coefficient was assumed constant.

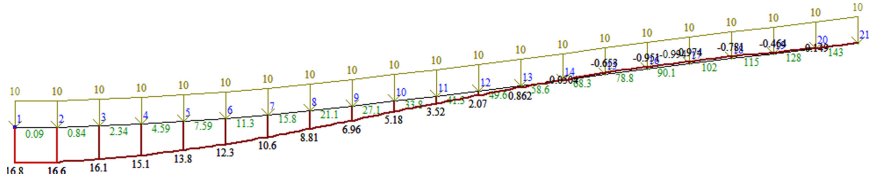


**Fig. 9.** Bending moment plots for short beam ( $\lambda L = 1.5$ ) for  $\alpha = 10$ .



**Fig. 10.** Bending moment plots for beam of medium length ( $\lambda L = 3.0$ ) for  $\alpha = 10$ .

Let us give a table comparing the results obtained in two ways for long beams (Table 1).



**Fig. 11.** Bending moment plots for long beam ( $\lambda L = 4.5$ ) for  $\alpha = 10$ .

**Table 1.** Calculation results.

The degree of heterogeneity of the base	$v(0)$ , cm		$M(0)$ , kNm	
	Lira	Ritz method	Lira	Ritz method
2	0.237	0.237	1.79	1.79
5	0.315	0.316	5.05	5.06
8	0.455	0.455	10.33	10.34
10	0.633	0.634	16.85	16.86

Can see that the results are almost the same.

#### 4 Conclusion

The technique presented in the article allows one to take into account the influence of the inhomogeneity of the base on the stress-strain state of the beam located on it. It is shown that satisfactory results can be obtained with 6 terms of the series approximating the required function.

In contrast to a homogeneous base, on which, under the action of a uniformly distributed load, at any relative stiffness, the beam behaves like a stamp, i.e. moves without bending, heterogeneity leads to bending of the beam. At the same time, this is most noticeable for long beams, in which the deflection at the central point can increase more than 3 times. For beams of medium length, the increase in deflection can be 1.5–2 times, and for short beams only by 8–10%.

The inhomogeneity of the base also results in bending moments. This is most noticeable for short beams, in which the value of the bending moment in the central section can be very significant. For beams of medium length, the value of the bending moment is 1.5 times less, and for long beams, 2.5 times, but at the same time, there are regions in the long beam in which the upper fibers are stretched.

It should be noted the problems of calculating structures on an elastic foundation do not lose their relevance. The development of new models makes it possible to find engineering solutions that allow for analysis at the pre-design stage and for a simpler analysis of the stress-strain state of structures and soil foundations [3–7].



## References

1. Leontiev, N.N.: Fundamentals of the theory of beams and slabs on a deformable foundation. MISI (1982)
2. Leontiev, N.N., Sobolev, D.N.: Variational principles of structural mechanics and basic theorems on elastic systems. MISI (1980)
3. Andreev, V.I., Barmenkova, E.V., Matveeva, A.V.: On the nonlinear effect of joint work of the basis, foundation slab and the structure. *Adv. Mater. Res.* **250–253**, 3591–3594 (2011)
4. Andreev, V.I., Barmenkova, E.V.: The modeling of the real building objects by using the model of a two-layer beam of variable rigidity on an elastic basis. *Appl. Mech. Mater.* **204–208**, 3596–3599 (2012)
5. Andreev, V.I., Matveeva, A.V., Barmenkova, E.V.: The calculation of the two-layer beam model on an elastic basis with variable modulus of subgrade reaction. *Appl. Mech. Mater.* **351–352**, 566–569 (2013)
6. Mkrtychev, O.V., Mondrus, V.L., Mkrtychev, A.E.: Reliability evaluation of a long-span structure with due regard for interaction with foundation bed soil. *Ind. Civil Eng.* **9**, 14–16 (2012)
7. Filatov, V.V.: About calculation of composite plates on a Winnkler elastic foundation. *Ind. Civil Eng.* **11**, 48–49 (2010)
8. Gabbasov, R.F., Uvarova, N.B., Filatov, V.V.: On calculation of beam resting on two-parameter elastic foundations. *Vestnik MGSU* **2**, 25–29 (2012)



# Clarification of the Structure of the East Hovsan Area by a New Method of Seismic Inversion

T. R. Ahmedov<sup>1</sup>  and K. A. Kurochkina<sup>2</sup>  

<sup>1</sup> Azerbaijan State Oil and Industry University, Baku, Azerbaijan

akhmedov.tofik@bk.ru

<sup>2</sup> Belgorod State Technological University named after V.G. Shoukhov, Belgorod, Russia

**Abstract.** The article provides a critical analysis of existing methods for forecasting hydrocarbon accumulations. It is noted that the main disadvantages of the existing methods are that it is a priori assumed that a very high signal-to-noise ratio was obtained, as well as a high resolution of seismic data, while in reality this is not the case. The proposed forecasting technique differs in that here the well log data (WGD) are used in an intermediate stage of processing to improve the signal-to-noise ratio of seismic data and their resolution. The forecasting technique is described, in the development of which the author also participated. The developed technique was tested in the Hovsan area of the Absheron oil and gas region of Azerbaijan, its brief geological and geophysical characteristics were reflected in the article. In the main part, the results of the application of this method are presented, with a recommendation of the location of the new planned well and the wells currently in operation. The reliability of the results is closely related to the seismic-geological conditions of the study area, as well as the depth and level of seismic data processing and the degree of similarity of the two seismic traces taken near the reference and projected wells, as well as the accuracy of the log interpretation data.

**Keywords:** Seismic exploration · Well geophysical surveys (WGS) · Geological section predicting (GSP) · Seismic inversion · Signal-to-noise ratio · Resolution · Correlation

## 1 Introduction

There are various approaches to studying the heterogeneity of the section in the interwell space according to seismic data [5]. It is well known that in dynamic analysis, if possible, complete information about the seismic wave field is used, then, in combination with the data of geophysical studies of wells, correlations are established between the predicted seismic parameters of productive deposits and their capacitive properties.

It is assumed that the processing of seismic materials was performed at a very high level and that the best signal-to-noise ratio and high resolution of the seismic records were achieved. The developed software package has been applied at several fields in Azerbaijan. As an example, we give here the results of a study carried out at the Hovsan

field of the Absheron oil and gas region of Azerbaijan. The Hovsan field is located on a coastal plain covered with ancient Caspian sediments, located in the southern part of the Absheron Peninsula of Azerbaijan (Fig. 1) [7].

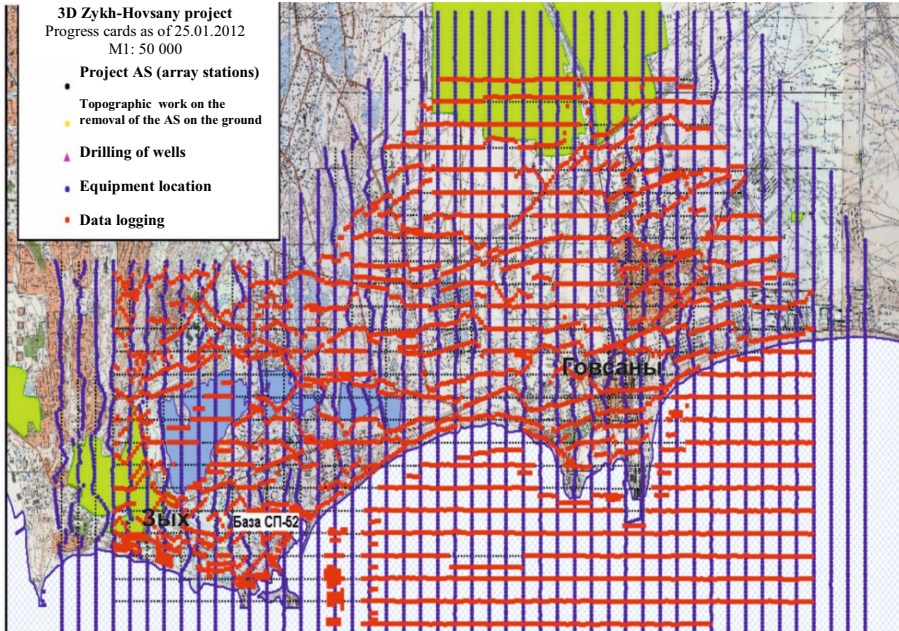


Fig. 1. ZykH-Hovsany area with 3D excitation and registration lines.

## 2 Methods and Materials

Here we are considering a completely different approach to seismic inversion and forecasting oil and gas content at the recommended location of a new deep drilling well based on seismic and logging data, the essence of which is as follows:

Here we are considering a completely different approach to seismic inversion and forecasting oil and gas content at the recommended location of a new deep drilling well based on seismic and logging data, the essence of which is as follows:

1. First, we select a reference well and use the WGS of this well to improve the signal-to-noise ratio of the seismic record and its resolution;
2. The resulting higher quality and higher resolution seismic record is used to improve the quality and resolution of the seismic record in a new section of the work area, ie. at the proposed location of the new well;
3. Seismic inversion is applied [3] and synthetic logs are obtained, which are used for further interpretation using one of the software packages “GEOGRAPHIX” and “PRISMA” and quantitative estimates of the exploitation objects are obtained.

This software package, compiled by us, is called “AZERI”. The package includes the following programs: loading of WGS and its visualization; determination and optionally changing the parameters of the seismic profile output to the display screen; it is possible to simultaneously display a complete or fragmentary seismic profile on the display screen; changing the dynamic expressiveness of seismic traces; demonstration of individual fragments of the time section on a full screen at different scales; selection and tracking, i.e. correlation of seismic horizons; input of logging data of a reference well; selection of the target track; inclusion in the work of the main calculation algorithms; saving the obtained results in the computer memory and printing them.

The main algorithm for calculating the program includes the following procedures:

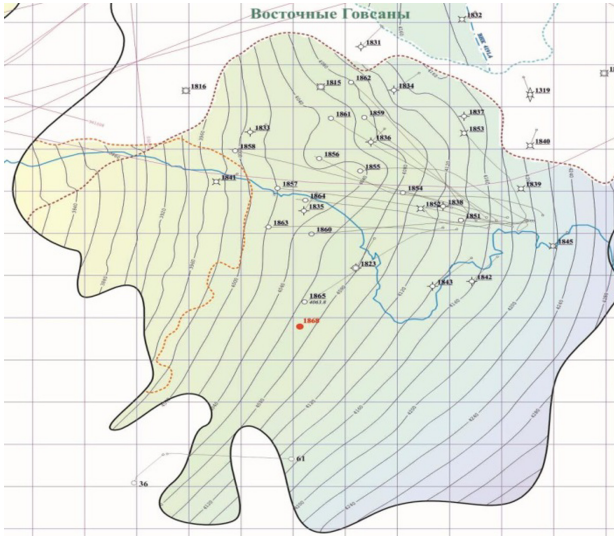
- the seismic trace selected near the reference well, the logging data of the same well, as well as the target seismic trace at the proposed location of the production well are brought to the same sampling step and the same level;
- WGS is applied to the seismic profile and the seismic trace having the same coordinate as the well is transferred to the LAS file and stored in the computer memory;
- the seismic trace recorded near the proposed location of the future well is also transferred to the LAS file and stored in the computer memory;
- the similarity factor [7] is calculated between these two seismic traces and if the calculated similarity factor is greater than or equal to 0.5, the research continues;
- WGS of the reference well, the first and second seismic traces are used to invert the target seismic trace into the synthetic log of the recommended well and this process continues until a set of logs is obtained to build a section of the section with predicted data, and all the information obtained is stored in the LAS file;
- using the GEOGRAPHIX or PRISMA programs, we interpret synthetic log curves, obtain all the necessary geological and geophysical information at the location of the projected well.

### 3 Results and Discussion

The geological structure of this field has been repeatedly studied by various geological and geophysical methods [1, 2, 4]. The last 2D CDPP seismic survey was conducted here in 2004. In 2010, the VSP (Vertical seismic profiling) was held here [1, 2], and in 2011–12. This area has been studied by 3D seismic survey. The oil field in the Kalinskaya suite in the Hovsan area was discovered in 1948. According to seismic data on the bottom of the productive strata, including the Kalinskaya Formation, the Govsan area is located on the southwestern edge of the Govsaninskaya syncline and is characterized by a monoclinical bedding. The available deep drilling data and seismic material do not allow us to determine an accurate geological model of oil traps in the Kalinskaya suite of the Hovsan area [4]. Oil accumulations here can presumably be associated with lithofacies alteration and low-amplitude faults.

The oil-bearing capacity of the geological section of the Govsany area is associated with the KaS1, KaS2, KaS3 horizons of the Kalinskaya suite. Their relatively powerful parts are more productive, and in some areas they are filled with gas. In recent years, the fourth horizon has been exposed, which presumably also belongs to the Kalinskaya Formation. Currently, this deposit is intensively used [4].

The main task of our research was to check the developed algorithm and the compiled program at the wells currently in operation. The studies were carried out for pairs of wells, one of which played the role of a reference, and the other was designed. Wells # 1865 and # 1868 constituted the first pair through which the 3D CDPM seismic profile passed (Fig. 2).



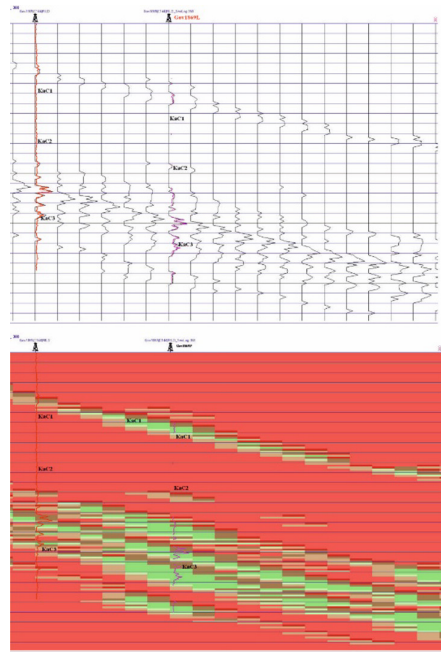
**Fig. 2.** Eastern Hovsans: structural map of the Kalinskaya suite with deep drilling wells.

In the case under consideration, well No. 1865 played the role of a reference well, the WGS (AP - ILD) of this well are plotted on a seismic profile on the scale of a seismic deep section. Another task facing this research was to determine the best oil and gas bearing location for a new production well in the eastern part of the Hovsan field using 3D seismic data, as well as logging data from wells No. 1865 and 1868. As noted, the studies were carried out in the following sequence: first, a number of orthogonal profiles (or sections) were selected and synthetic traces [6] were calculated along the selected profiles using data from wells No. 1865 and the coefficients of similarity of the traces with real ones (Fig. 3) and the resulting traces were plotted on a time section, where the section intervals characterized by high (>10) values are shown in green (Fig. 4).

Naturally, the intervals of the cut with high values of apparent resistivity (AR) are of great practical interest. The best indicators were obtained at station 368 of profile No. 132, where the trace similarity coefficient is 0.9318 at the point of the planned well No. 1869, i.e. with a confidence threshold above 90%. Synthetic logs were processed and interpreted using the PRIZMA software package. Recommended location of wells No. 1869 at the intersection of profiles 132 and 368 ( $X = 420612$ ,  $Y = 4468978$ ).

360	, 420412 ; 4468978	, 0.9604
361	, 420437 ; 4468978	, 0.9737
362	, 420462 ; 4468978	, 1
363	, 420487 ; 4468978	, 0.9413
364	, 420512 ; 4468978	, 0.9464
365	, 420537 ; 4468978	, 0.948
366	, 420562 ; 4468978	, 0.9354
367	, 420587 ; 4468978	, 0.9321
368	, 420612 ; 4468978	, 0.9318
369	, 420637 ; 4468978	, 0.928
370	, 420662 ; 4468978	, 0.9335
371	, 420687 ; 4468978	, 0.9287
372	, 420712 ; 4468978	, 0.9351
373	, 420737 ; 4468978	, 0.9387
374	, 420762 ; 4468978	, 0.9328
375	, 420787 ; 4468978	, 0.9246
376	, 420812 ; 4468978	, 0.9041
377	, 420837 ; 4468978	, 0.8791
378	, 420862 ; 4468978	, 0.8534
379	, 420887 ; 4468978	, 0.8391
380	, 420912 ; 4468978	, 0.856

**Fig. 3.** The coefficients of similarity of seismic traces.



**Fig. 4.** Synthetic deep section with a forecast of prospective intervals, selected from synthetic AP curves and indicating the recommended location of the well 1869.

## 4 Conclusion

The obtained results are in good agreement with the data of the studies carried out here by PANGEYA from Moscow. Naturally, the reliability of the results is closely related to the seismic-geological conditions of the study area, as well as the depth and level of seismic data processing and the degree of similarity of two seismic traces taken near the reference and projected wells, as well as the accuracy of the log interpretation WGS.

## References

1. Alizade, A.A., Akhmedov, G.A., Akhmedov, A.M.: Geology of oil and gas fields in Azerbaijan. Nedra, Moscow (1966)
2. Akhmedov, T.R., Akhundlu, A.A., Giyasov, N.: On some results of surface and borehole seismic surveys at the Hovsaninskoye field. Karotazhnik. Sci. Tech. Bull. **6**(216), 3–16 (2012)
3. Ahmadov, T.R., Axundlu, A.A., Giyasov, N.Sh.: Complex interpretation of land & borehole seismics (VSP) data in the Hovsan area. In: International conference “Integrated approach for unlocking hydrocarbon resources”. Baku (2012)
4. Boganik, G.N., Gurvich, I.I.: Seismic survey. AIS, Tver (2006)

5. Mamedov, P.Z.: On the reasons for the rapid subsidence of the earth's crust in the SCB. Azerbaijan Oil Industry 1 (2008)
6. Kopilevich, E.A., Mushin, I.A., Davydova, E.A., Afanasyev, M.L.: Complex spectral-velocity prediction of the types of geological section and filtration-capacity properties of reservoirs. Izhevsk Institute of Computer Research, Research Center "Regular and Chaotic Dynamics", M.-Izhevsk (2010)
7. Crawford, M., Medwedeff, D.: U.S. Patent Number 5,987,388 Automated extraction of fault surfaces from 3-D seismic prospecting data (1999)
8. Mamedov, P.Z.: Productive Strata of Azerbaijan. Nedra, Moscow (2018)
9. Mushin, I.A., Korolkov, Yu.S., Chernov, A.A.: Revealing and mapping of disjunctive dislocations by methods of exploration geophysics. Scientific World, Moscow (2001)
10. Salaev, S.G., Kastrulin, N.S.: The role of tectonic ruptures in the formation of oil and gas deposits in Kobystan. Elm, Baku (1977)
11. Shimansky, V.V., Ronin, A.L., Rylkov, V.A., Karaev, N.A., Shimansky, S.V.: Geological interpretation of seismic data during regional and prospecting works in complex environments. Geol. Oil Gas **4**, 68–73 (2011)
12. Satinder, C.: Interpreting fractures through 3D seismic discontinuity attributes and their visualization. Arcis Corp. **34**(08), 1–3 (2009)
13. Sheriff, R., Geldart, L.: Seismic Survey, vol. II. Mir Publishing House, Moscow (1987)
14. Ahmedov, T.R., Aliyeva, G.A., Abdurrahmanova, S.T.: Measurement geological structure of the Hovsan-Zikh area in the light of 3D seismic survey data for Pontian and Miocene sediments and their oil and gas opportunities. Vect. Geosci. **1**(4), 15–27 (2018)



# Determination of the Deflected Mode of the Disk

V. N. Strelnikov<sup>(✉)</sup> 

Belgorod State Technological University named after V.G. Shukhov, Belgorod, Russia

**Abstract.** An effective direction for improving drive technology is the rational use of flexible links, elastic deformations of which provide multi-threaded power transmission in the engagement of higher kinematic pairs. The distribution of the force flow in the field of long-distance gearing reduces the specific loads on the teeth, eliminates restrictions on the bearing capacity of wave gears according to the criteria of jamming, bending and contact stresses of the teeth, and ensures the transmission of the highest torques with reduced dimensions and metal consumption. Commercially available small wave gears with a cam wave generator have been used commercially. Their force analysis and strength calculations differ significantly from the formulation and solution of similar problems of large wave transmissions with a disk wave generator. Strength calculations of mass-produced wave gears are performed without taking into account the features of the deflected mode of the wave generator disks. Therefore, studies of the load capacity of large wave transmissions, in particular the disk wave generator, have not found an objective solution yet. In the heavy and transport industry, in the production of road and construction machinery, the tasks of improving the quality, reliability, durability, service life, efficiency of machines and technological equipment, and reducing their metal consumption are of particular importance. The specified set of scientific and technical tasks is largely due to the requirements of a significant increase in labor productivity while reducing the operating costs of the consumer.

**Keywords:** Disk · Voltage · Wave transmission · Wave generator

## 1 Introduction

Technical characteristics of road and construction vehicles are associated with multi-factor studies, strength calculations of loaded units [1–3], the reliability of which is determined by a reasonable consideration of load modes during operation, technological parameters. The wave generator is the first stage of the wave transmission that converts the rotational motion of the drive shaft into the wave motion of the flexible wheel. For an objective assessment of the strength of the loaded elements of the wave transmission, it is necessary to know the load distribution in the area of contact of the flexible wheel with the disks of the wave generator. The relevance of research is to optimize the technical characteristics of large wave gearboxes at the design stage [4–7].



## 2 Materials and Methods

Gear building is one of the most complex and responsible areas of machine-building production and largely determines the technical and economic level of manufactured machines. The practice of modern production and operation of gearboxes in construction and transport engineering has identified a number of complex tasks of production and scientific and technical nature, related to increasing the load-bearing capacity, kinematic efficiency and reliability of gearboxes, reducing their overall dimensions and metal consumption, and excluding expensive structural materials. One of the most loaded nodes of a large wave transmission is a wave generator that sums up the reactive load of the wave gear through disks mounted on a high-speed shaft with a given eccentricity. Minimizing the level of vibrational energy of rapidly rotating masses is determined by their value, regulated by the strength of the disks. The problem of the deflected mode of disks is relevant; the results of its solution have wide practical application in the design in order to optimize the parameters of the carrier elements of large wave transmissions. The aim of this work is a theoretical study of the deflected mode of the disk to optimize the design parameters of the wave generator of large wave gearboxes.

## 3 Results

The problem under consideration is relevant, the results of its solution have a wide practical application in the design in order to optimize the parameters of the carrier elements of large wave transmissions.

The components of the strain tensor are expressed by Hooke's law:

$$\left. \begin{aligned} \varepsilon_r &= \frac{1}{E} \left[ 2(1-\nu)B_0 + (1+\nu)\frac{C_0}{r^2} + 2(1-\nu)D_0 \ln r + (1-3\nu)D_0 \right] + \frac{1}{E} \left[ 2(1-3\nu)A_1 r + (1-\nu) \cdot \right. \\ &\cdot B_1 \frac{1}{r} - 2(1+\nu)C_1 \frac{1}{r^3} + \frac{2B}{r} \left. \right] \cos\theta - \frac{1}{E} \sum_{n=2}^{\infty} \left[ (1+\nu)n(n-1)C_{1n}r^{n-2} + (n+1)((1+\nu)n-2) \cdot \right. \\ &\cdot (1-\nu)C_{2n}r^n + (1+\nu)n(n+1)C_{3n}r^{-(n+2)} + (n-1)((1+\nu)n+2(1-\nu))C_{4n}r^{-n} \left. \right] \cos n\theta; \\ \varepsilon_\theta &= \frac{1}{E} \left[ 2(1-\nu)B_0 - (1+\nu)\frac{C_0}{r^2} + 2(1-\nu)D_0 \ln r + (3-\nu)D_0 \right] + \frac{1}{E} \left[ 2(3-\nu)A_1 r + (1-\nu)\frac{B_1}{r} + \right. \\ &+ 2(1+\nu)\frac{C_1}{r^3} - 2\nu\frac{B}{r} \left. \right] \cos\theta + \frac{1}{E} \sum_{n=2}^{\infty} \left[ (1+\nu)n(n-1)C_{n1}r^{n-2} + (n+1)((1+\nu)n+2(1-\nu)) \cdot \right. \\ &C_{2n}r^n + (1+\nu)n(n+1)C_{3n}r^{-(n+2)} + (n-1)((1+\nu)n-2(1-\nu)) + C_{4n}r^{-n} \left. \right] \cos n\theta. \end{aligned} \right\} \quad (1)$$

The components of the strain tensor are expressed in terms of the components of the displacement vector:

$$\varepsilon_r = \frac{\partial U_r}{\partial r}; \varepsilon_\theta = \frac{1}{r} \frac{\partial U_\theta}{\partial \theta} + \frac{U_r}{r}; \varepsilon_{r\theta} = \frac{1}{2} \left( \frac{1}{r} \frac{\partial U_r}{\partial \theta} + \frac{\partial U_\theta}{\partial r} - \frac{U_\theta}{r} \right). \quad (2)$$

Integrating the expressions (4.15) taking into account (4.14), we find the components of the displacement vector U. We consider separately the cases  $n = 0$ ;  $n = 1$  and  $n \geq 2$ .

At  $n = 0$ .  $U_{r0} = \frac{1}{E} \left[ 2(1 - \nu) B_0 r - (1 + \nu) \frac{C_0}{r} + 2(1 - \nu) D_0 r \ln r - (1 + \nu) D_0 r \right];$

$$U_{\theta 0} = \frac{2(1 - \nu)}{E} D_0 r \times \theta.$$

At  $D_0 \neq 0$  value of  $U_{\theta 0}$  leads to ambiguity.

At  $\theta = \pi$  and  $\theta = -\pi$  the same cross section and two different values  $U_{\theta 0}$ .

At  $\theta = \pi$   $U_{\theta 0}(\pi) = \frac{2(1-\nu)\pi}{E} \cdot r$ . At  $\theta = -\pi$   $U_{\theta 0}(-\pi) = -\frac{2(1-\nu)\pi}{E} \cdot r$ .

We suppose  $D_0 = 0$ . Then  $U_{r0} = \frac{1}{E} \left( 2(1 - \nu) B_0 r - (1 + \nu) \frac{C_0}{r} \right); U_{\theta 0} = 0$ .

At  $n = 1$

$$U_{r1} = \frac{1}{E} \left[ (1 - 3\nu) A_1 r^2 + (1 - \nu) \cdot B_1 \cdot \ln r + (1 + \nu) \frac{C_1}{r^2} + 2B \ln r - K_1 \right] \cos \theta; \quad (3)$$

$$U_{\theta 1} = \frac{1}{E} \left[ (5 + \nu) A_1 r^2 + ((1 - \nu) B_1 - 2\nu B) + (1 + \nu) \frac{C_1}{r^2} - (2B + (1 - \nu) B_1) \ln r + K_1 \right] \sin \theta. \quad (4)$$

Substituting expressions (4.14), (4.16), (4.17), in the third Eq. (4.15), we obtain the condition of compatibility of deformations.

$$(1 - \nu) B + 2B_1 = 0 \quad (5)$$

The value of  $B_1$  from equality (5) is substituted into Eqs. (3) and (4)

$$U_{r1} = \left[ (1 - 3\nu) A_1 r^2 + (1 + \nu) \frac{C_1}{r^2} + \frac{1}{2} (1 + \nu) (3 - \nu) B \ln r - K_1 \right] \frac{\cos \theta}{E} \quad (6)$$

$$U_{\theta 1} = \left[ (5 + \nu) A_1 r^2 + (1 + \nu) \frac{C_1}{r^2} - \frac{1}{2} (1 + \nu)^2 B - \frac{1}{2} (1 + \nu) (3 - \nu) B \ln r + K_1 \right] \frac{\sin \theta}{E}. \quad (7)$$

For  $n = 1$  we define the components of the stress tensor by the formula (5)

$$\left. \begin{aligned} \sigma_{r1} &= \left[ 2A_1 r - \frac{2C_1}{r^3} + \frac{1}{2} (3 + \nu) \frac{B}{r} \right] \cos \theta; \\ \sigma_{\theta 1} &= \left[ 6A_1 r - \frac{2C_1}{r^3} - \frac{1}{2} (1 - \nu) \frac{B}{r} \right] \cos \theta; \\ \tau_{r\theta 1} &= \left[ 2A_1 r - \frac{2C_1}{r^3} - \frac{1}{2} (1 - \nu) \frac{B}{r} \right] \sin \theta. \end{aligned} \right\} \quad (8)$$

The terms  $-K_I \cos \theta$  and  $K_I \sin \theta$ , in the formulas for displacements  $U_{rI}, U_{\theta I}$  appear when integrating equations (2). Integrating the first Eq. (6) with  $r$ , we introduce, as an arbitrary constant function

$$U_{r1*} = \alpha_1(\theta).$$

From the second equation of system (2) we obtain

$$\frac{1}{r} \frac{\partial U_{\theta 1}^*}{\partial \theta} + \frac{1}{r} \alpha_1(\theta) = 0; \quad U_{\theta 1}^* = - \int \alpha_1(\theta) d\theta.$$

From the third equation of the system (2) we have

$$\frac{1}{r} \frac{\partial U_{r1}^*}{\partial \theta} + \frac{1}{r} \int \alpha_1(\theta) d\theta = 0, \quad \alpha_1'(\theta) + \alpha_1(\theta) = 0.$$

Here the solution is the function  $\alpha_1 = -K_I \cos \theta$ . Additional terms in expressions for  $U_{rI}$  and  $U_{\theta I}$ :  $U_{r1}^* = -K_I \cos \theta$ ;  $U_{\theta 1}^* = K_I \sin \theta$ .

$$\Sigma \varepsilon_{rm} = \frac{\partial U_m}{\partial r} = -\frac{1}{E} [(1 + \nu)n(n - 1)C_{1n}r^{n-2} + (n + 1)((1 + \nu)n - 2(1 - \nu))C_{2n}r^n + (1 + \nu)n(n + 1)C_{3n}r^{-(n+2)} + (n - 1)((1 + \nu)n + 2(1 - \nu))C_{4n}r^{-n}] \cos n\theta.$$

Integrating by  $r$

$$U_m = -\frac{1}{E} \left[ (1 + \nu)nC_{1n}r^{n-1} + ((1 + \nu)n - 2(1 - \nu))C_{2n}r^{n+1} - (1 + \nu)nC_{3n}r^{-(n+1)} - ((1 + \nu)n + 2(1 - \nu))C_{4n}r^{-(n-1)} \right] \cos n\theta.$$

From the second Eq. (2) we find:

$$\frac{\partial U_{\theta n}}{\partial \theta} = rE_{\theta n} - U_{rm} = \frac{1}{E} [(1 + \nu)n^2C_{1n}r^{n-1} + ((1 - \nu)n + 4) \cdot nC_{2n}r^{n+1} + (1 + \nu)n^2C_{3n}r^{-(n+1)} + ((1 + \nu)n - 4)nC_{4n}r^{-(n-1)}] \cos n\theta$$

Integrating by  $\theta$  we get:

$$U_{\theta n} = \frac{1}{E} \left[ (1 + \nu)nC_{1n}r^{n-1} + ((1 - \nu)n + 4)C_{2n}r^{n+1} + (1 + \nu)C_{3n}r^{-(n+1)} + ((1 + \nu)n - 4)C_{4n}r^{-(n-1)} \right] \sin n\theta.$$

Let us make expressions for the components of the displacement vector

$$U_r = U_{r0} + U_{r1} + \sum_{n=2}^{\infty} U_m = \frac{1}{E} \left( 2(1 - \nu)B_0 \cdot r - (1 + \nu) \frac{C_0}{r} \right) + \frac{1}{E} \left[ (1 - 3\nu)A_1 r^2 + (1 + \nu) \cdot \right]$$

$$\left[ \frac{C_1}{r^2} + \frac{1}{2}(1 + \nu)(3 - \nu)Blr - K_1 \right] \cos\theta + \frac{1}{E} \sum_{n=2}^{\infty} [(1 + \nu)nC_{1n}r^{n-1} + ((1 + \nu)n - 2(1 - \nu)) \cdot C_{2n}r^{n+1} - (1 + \nu)nC_{3n}r^{-(n+1)} - ((1 + \nu)n + 2(1 - \nu))C_{4n}r^{-(n-1)}] \cos n\theta; \quad (9)$$

$$U_\theta = U_{\theta 1} + \sum U_{\theta n} = \frac{1}{E} \left[ (5 + \nu)A_1r^2 + (1 + \nu)\frac{C_1}{r^2} - \frac{1}{2}(1 + \nu)^2B - \frac{1}{2}(1 + \nu)(3 - \nu)Blr + K_1 \right] \sin\theta + \frac{1}{E} \sum_{n=2}^{\infty} \left[ (1 + \nu)nC_{1n}r^{n-1} + ((1 - \nu)n + 4)C_{2n}r^{n+1} + (1 + \nu)nC_{3n}r^{-(n+1)} + ((1 + \nu)n - 4)C_{4n}r^{-(n-1)} \right] \sin n\theta. \quad (10)$$

For setting boundary value problems, we present the external load in the form of trigonometric series with cosines in the interval  $-\pi \leq \theta \leq \pi$ .

For an External Contour

$$P_2(\theta) = a_0 + \sum_{n=1}^{\infty} a_n \cos n\theta \quad (11)$$

Integrating Eq. (11) within  $[0; \pi]$ , we obtain

$$a_0 = P_{2max} \cdot \frac{2\theta^*}{3\pi}; \quad a_n = \frac{4P_{2max}}{\pi\theta^*2n^2} \cdot \left( \frac{1}{n} \sin n\theta^* * -\theta * \cos n\theta^* \right).$$

Substituting  $a_0, a_n$  in Eq. (11) we obtain the Fourier expansion

$$P_2(\theta) = \frac{2\theta^*}{3\pi} P_{2max} - \frac{4P_{2max}}{\pi\theta^*2} \sum_{n=1}^{\infty} \frac{1}{n^2} \left( \theta^* \cos n\theta^* - \frac{1}{n} \sin n\theta^* \right) \cos n\theta \quad (12)$$

From expression (12), we obtain the expansion of the external load for the internal contour, if  $P_{2max}$  and put  $\theta^* = \pi/2$ :

$$P_1(\theta) = \frac{1}{3} P_{1max} - \frac{16P_{1max}}{\pi^3} \sum_{n=1}^{\infty} \frac{1}{n^2} \left( \frac{\pi}{2} \cos \frac{\pi n}{2} - \frac{1}{n} \sin \frac{\pi n}{2} \right) \cos n\theta \quad (13)$$

The expansion coefficients of the stress tensor are determined from the boundary conditions:

$$\Sigma_r(r = R_2) = -P_2; \quad \Sigma_r(r = R_1) = -P_1; \quad \tau_{rQ}(r = R_2) = 0; \quad \tau_{rQ}(r = R_1) = 0. \quad (14)$$

We substitute the expressions in the boundary condition formulas  $\sigma_r$  and  $\tau_{r\theta}$  at  $r = R_1$  and  $r = R_2$ ; taking into account  $D_0 = 0$ , as well as the relation (5), we obtain:

$$\left( 2B_0 + \frac{C_0}{R_2^2} \right) + \left( 2A_1R_2 - \frac{2C_1}{R_2^3} + \frac{1}{2}(3 + \nu)\frac{B}{R_2} \right) \cos\theta - \sum_{n=2}^{\infty} \left[ n(n-1)C_{1n}R_2^{n-2} + (n-2) \cdot (n+1)C_{2n}R_2^n + n(n+1)C_{3n}R_2^{-(n+2)} + (n+2)(n-1)C_{4n}R_2^{-n} \right] \cos n\theta = -\frac{2\theta^*}{3\pi} P_{2max}$$

$$\begin{aligned}
 & + \frac{4P_{2max}}{\pi\theta^*2}(\theta * \text{Cos}\theta * -\text{Sin}\theta*) \text{Cos}\theta + \frac{4P_{2max}}{\pi\theta^*2} \sum_{n=2}^{\infty} \frac{1}{n^2}(\theta * \text{Cos}n\theta * -\frac{1}{2}\text{Sinn}\theta*) \text{Cos}n\theta; \\
 & \left(2B_0 + \frac{C_0}{R_1^2}\right) + \left(2A_1R_1 - \frac{2C_1}{R_1^3} + \frac{1}{2}(3 + \nu)\frac{B}{R_1}\right) \text{Cos}\theta - \sum_{n=2}^{\infty} \left[n(n-1)C_{1n}R_2^{n-2} + (n-2) \cdot \right. \\
 & \cdot (n+1) \cdot C_{1n}R_1^n + n(n+1)C_{3n}R_1^{-(n+2)} + (n+2)(n-1)C_{4n}R_1^{-n}\left. \right] \text{Cos}n\theta = -\frac{1}{3}P_{1max} - \\
 & - \frac{16}{\pi^3}P_{1max}\text{Cos}\theta + \frac{16}{\pi^3}P_{1max} \sum_{n=2}^{\infty} \frac{1}{n^2} \left(\frac{\pi}{2}\text{Cos}\frac{\pi n}{2} - \frac{1}{n}\text{Sin}\frac{\pi n}{2}\right) \text{Cos}n\theta; \quad (15) \\
 & \left(2A_1R_2 - \frac{2C_1}{R_2^3} - \frac{1}{2}(1-\nu)\frac{B}{R_2}\right) \text{Sin}\theta + \sum_{n=2}^{\infty} \left[n(n-1)C_{1n}R_2^{n-2} + n(n+1)C_{2n}R_2^n - \right. \\
 & \left. - n(n+1)C_{3n}R_2^{-(n+2)} - n(n-1)C_{4n}R_2^{-n}\right] \text{Sinn}\theta = 0; \\
 & \left(2A_1R_1 - \frac{2C_1}{R_1^3} - \frac{1}{2}(1-\nu)\frac{B}{R_1}\right) \text{Sin}\theta + \sum_{n=2}^{\infty} \left[n(n-1)C_{1n}R_1^{n-2} + n(n+1)C_{2n}R_1^n - \right. \\
 & \left. - n(n+1)C_{3n}R_1^{-(n+2)} - n(n-1)C_{4n}R_1^{-n}\right] \text{Sinn}\theta = 0.
 \end{aligned}$$

From Eqs. (15) a system of equations follows, from which we find the coefficients of expansion into series of components of the stress tensor. At  $n = 0$

$$\begin{aligned}
 B_0 &= \frac{P_{2max}}{6(1-\beta^2)} \left[ (\text{Sin}\theta * -\theta * \text{Cos}\theta*) \left(\frac{\pi}{2\theta*}\right)^2 \cdot \beta - \frac{2\theta*}{\pi} \right]; \\
 C_0 &= \frac{P_{2max}R_2^2 \cdot \beta}{3(1-\beta^2)} \left[ \frac{2\theta * \beta}{\pi} - \left(\frac{\pi}{2\theta*}\right)^2 (\text{Sin}\theta * -\theta * \text{Cos}\theta*) \right]; \\
 B &= \frac{2P_{2max}R_2(\theta * \text{Cos}\theta * -\text{Sin}\theta*)}{\pi\theta^*2} = \frac{8P_{1max}R_1}{\pi^3} \quad (16) \\
 A_1 &= \frac{(1-\nu)(\theta * \text{Cos}\theta * -\text{Sin}\theta*)P_{2max}}{2\pi\theta^*2(1+\beta^2)R_2}; \\
 C_1 &= \frac{(1-\nu)(\theta * \text{Cos}\theta * -\text{Sin}\theta*)\beta^2P_{2max}R_2^3}{2\pi\theta^*2(1+\beta^2)}.
 \end{aligned}$$

At  $n \geq 2$  from Eqs. (15) we obtain a new system of equations:

$$\left. \begin{aligned}
 &n(n-1)C_{1n}R_2^{n-2} + (n-2)(n+1)C_{2n}R_2^n + n(n+1)C_{3n}R_2^{-(n+2)} + \\
 &+(n+2)(n-1)C_{4n}R_2^{-n} = -\frac{4P_{2max}}{\pi\theta^*2} \left( \theta^* \text{Cos}n\theta^* - \frac{1}{n} \text{Sinn}\theta^* \right) \cdot \frac{1}{n^2}; \\
 &n(n-1)C_{1n}R_2^{n-2} + n(n+1)C_{2n}R_2^n - n(n+1)C_{3n}R_2^{-(n+2)} - n(n-1)C_{4n}R_2^{-n} = 0; \\
 &n(n-1)C_{1n}R_1^{n-2} + (n-2)(n+1)C_{2n}R_1^n + n(n+1)C_{3n}R_1^{-(n+2)} + (n+2)(n-1)C_{4n}R_1^{-n} = \\
 &= -\frac{16}{\pi^3} \left( \frac{\pi}{2} \text{Cos} \frac{\pi n}{2} - \frac{1}{n} \text{Sin} \frac{\pi n}{2} \right) \frac{1}{n^2} P_{1max} = -\frac{4}{\pi n^2 \beta \theta^* 2} (\theta^* \text{Cos}\theta^* - \text{Sin}\theta^*) \left( \frac{\pi}{2} \text{Cos} \frac{\pi n}{2} - \frac{1}{n} \text{Sin} \frac{\pi n}{2} \right); \\
 &n(n-1)C_{1n}R_1^{n-2} + n(n+1)C_{2n}R_1^n - n(n+1)C_{3n}R_1^{-(n+2)} - n(n-1)C_{4n}R_1^{-n} = 0.
 \end{aligned} \right\} \tag{17}$$

In the system of Eqs. (17), we introduce new constants:

$$\left. \begin{aligned}
 C_{1n} &= \frac{2P_{2max}}{\pi\theta^*2R_2^{n-2}} \cdot \frac{b_{1n}}{n^2(n-1)}; & C_{2n} &= -\frac{2P_{2max}}{\pi\theta^*2R_2^n} \cdot \frac{b_{2n}}{n^2(n+1)} \\
 C_{3n} &= \frac{2P_{2max}R_1^{n+2}}{\pi\theta^*2} \cdot \frac{b_{3n}}{n^2(n+1)}; & C_{4n} &= -\frac{2P_{2max}R_1^{-n}}{\pi\theta^*2} \cdot \frac{b_{4n}}{n^2(n-1)}.
 \end{aligned} \right\} \tag{18}$$

We substitute the values (18) in the Eqs. (17):

$$\begin{aligned}
 &b_{1n} - \left(1 - \frac{2}{n}\right)b_{2n} + \beta^{n+2}b_{3n} - \left(1 + \frac{2}{n}\right)\beta^n b_{4n} = \frac{2}{n} \left( \frac{1}{n} \text{Sinn}\theta^* - \theta^* \text{Cos}n\theta^* \right) = g_{1n}; \\
 &b_{1n} - b_{2n} - \beta^{n+2}b_{3n} + \beta^n b_{4n} = 0; \\
 &\beta^{n-2}b_{1n} - \left(1 - \frac{2}{n}\right)\beta^n b_{2n} + b_{3n} - \left(1 + \frac{2}{n}\right)b_{4n} = -\frac{2}{n} (\theta^* \text{Cos}\theta^* - \text{Sin}\theta^*) \left( \frac{1}{n} \text{Sin} \frac{\pi n}{2} - \frac{\pi}{2} \text{Cos} \frac{\pi n}{2} \right) = g_{3n}; \\
 &\beta^{n-2}b_{1n} - \beta^n b_{2n} - b_{3n} + b_{4n} = 0.
 \end{aligned} \tag{19}$$

The solution of the system (19) is found in the Kramer’s form

$$b_{1n} = \frac{\Delta_{1n}}{\Delta_n}; \quad b_{2n} = \frac{\Delta_{2n}}{\Delta_n}; \quad b_{3n} = \frac{\Delta_{3n}}{\Delta_n}; \quad b_{4n} = \frac{\Delta_{4n}}{\Delta_n}; \tag{20}$$

We find the values of the determinants  $\Delta_n, \Delta_{1n}, \Delta_{2n}, \Delta_{3n}, \Delta_{4n}$ :

$$\begin{aligned}
 \Delta_{3n} &= 2g_{1n} \cdot \beta^{n-2} \left[ (1 - \beta^2) + \frac{1}{n}(1 - \beta^{2n}) \right] - 2g_{3n} \left[ (1 - \beta^2) \cdot \beta^{2n-2} + \frac{1}{n}(1 - \beta^{2n}) \right]; \\
 \Delta_n &= \frac{4}{n^2} \left[ (1 - \beta^{2n})^2 - n^2 \beta^{2n-2} (1 - \beta^2)^2 \right]; \\
 \Delta_{1n} &= 2g_{1n} \left[ (1 - \beta^2) \cdot \beta^{2n} + \frac{1}{n}(1 - \beta^{2n}) \right] - 2g_{3n} \beta^n \left[ (1 - \beta^2) + \frac{1}{n}(1 - \beta^{2n}) \cdot \beta^2 \right]; \\
 \Delta_{2n} &= 2g_{1n} \left\{ -(1 - \beta^2) \cdot \beta^{2n-2} + \frac{1}{n}(1 - \beta^{2n}) \right\} - 2g_{3n} \cdot \beta^n \left\{ (1 - \beta^2) + \frac{1}{n}(1 - \beta^{2n}) \right\}; \\
 \Delta_{4n} &= 2g_{1n} \cdot \beta^{n-2} \left[ (1 - \beta^2) + \frac{1}{n}\beta^2(1 - \beta^{2n}) \right] - 2g_{3n} \left[ (1 - \beta^2) \cdot \beta^{2n} + \frac{1}{n}(1 - \beta^{2n}) \right].
 \end{aligned} \tag{21}$$

Replacing  $g_{1n}$  and  $g_{3n}$  from formula (19) we find  $\Delta_{1n}, \Delta_{2n}, \Delta_{3n}, \Delta_{4n}$ :

The deflected mode of the wave generator disks is studied depending on the size and nature of the load distribution along the external and internal contours. Disk deformation has a wave character with a cyclic load from 0 to  $F_{max}$ . Normal  $r$  stresses are maximal on the outer contour of the disk, in the area of the generator major axis ( $\theta = 0$ ). Normal  $r$  (compression) stresses have a maximum equal to the maximum external load on the disk, i.e.  $\sigma_{r1max\theta=0^\circ} = -|p_{2max}|$ . On the internal contour, the maximum stresses (compressions) are  $\sigma_{r2max\theta=0^\circ} = -|0.77 \cdot p_{2max}|$ .

## 4 Conclusion

The results of studies of large wave gears with torques on a low-speed shaft up to  $M_{2\max} = 5 \times 10^5$  N·m installed on mining, metallurgical equipment, construction and road machines are presented. The main relationships between the parameters of the most loaded components and parts of wave gears are established, in which the scale factor takes on an independent value.

**Acknowledgements.** This work was realized in the framework of the Program of flagship university development on the base of the Belgorod State Technological University named after V G Shukhov, using equipment of High Technology Center at BSTU named after V. G. Shukhov.

## References

1. Rudenko, V.N.: Planetary and Wave Transmissions. Mechanical Engineering, Moscow (1980)
2. Ginsburg, E.G.: Wave gears. Mechanical engineering, Moscow (1969)
3. Hareesh, Y.S., Varghese, J.: Design and analysis of flex spline with involute teeth profile for harmonic drive mechanism. *Int. J. Eng. Res. Technol.* **4**(12), 613–618 (2015)
4. Patel, D.M., Jivani, R.G., Pandya, V.A.: Harmonic drive design & application: A review. *Global Res. Dev. J. Eng.* **1**(1), 34–37 (2015)
5. Demidov, S.P.: Theory of Elasticity. High school, Moscow (1979)
6. Ivanov, M.N.: Wave Gear. High School, Moscow (1981)
7. Poletuchii, A.I.: Theory and Design of High-Performance Wave Gears. *Natsional'nyi aviatsionnyi universitet publ, Kharkov* (2005)
8. Strelnikov, V.N.: Increase the Load Capacity of Wave Gears: Monograph. BGTU Publishing House, Belgorod (2015)
9. Strelnikov, V.N., Sukov, M.G.: Experimental investigation on interaction of wave disk generator with flexible gear. *IOP Conf. Ser.: Earth Environ. Sci.* **194**, 032028 (2018)
10. Strelnikov, V.N., Sukov, M.G.: Analysis of axial forces in harmonic drives of mining machines and heavy industrial equipment. *J. Phys.: Conf. Ser.* **1353**, 012042 (2019)



# Computer Simulation of Bent Reinforced Concrete Elements with External Composite Reinforcement

S. I. Merkulov<sup>1</sup> , S. M. Esipov<sup>2</sup> , and D. V. Esipova<sup>2</sup>(✉) 

<sup>1</sup> Kursk State University, Kursk, Russia

<sup>2</sup> Belgorod State Technological University V. G. Shukhov, Belgorod, Russia

**Abstract.** The article discusses the issues and features of modeling the external reinforcement of reinforced concrete structures during bending using the ANSYS software. A method for modeling flexible reinforced concrete elements reinforced in a stretched zone with external reinforcement made of composite materials based on carbon fibers, tested during field experiments, is presented. This was used as clarifying factors to develop a methodology with different approaches to the reinforcement of reconstructed reinforced concrete. Qualitative and quantitative relationships between experimental and numerical studies are established, confirming the prerequisites of the study. The limit values of deformations of concrete, steel reinforcement, composite reinforcement during destruction are determined. A comparative characteristic of variational approaches to modeling the joint work of external reinforcement and damaged concrete is given. Comparative analyses of the dependence of the increase in load-bearing capacity on the degree of damage and load of the element were also performed. Theoretical and actual values of the opening width and height of cracks in the zone of pure bending, including before and after reinforcement, are determined.

**Keywords:** External reinforcement · Carbon fiber · Composite material · Simulation · Models

## 1 Introduction

The most dynamically developing method of strengthening reinforced concrete structures in the world and domestic construction market is the method of external reinforcement with high-strength non-metallic materials. The highest efficiency of the method is achieved by using high-modulus materials in those areas of structures where the greatest tensile forces are present. However, many parameters of reinforcing elements are required for calculation and design, such as design resistance, cross-sectional area, effective length, and others. At the stage of operation of a reinforced structure under load, a flexible mathematical apparatus is required that can simultaneously take into account the transformation of the design scheme from definable to statically indeterminate, differences in the mechanical characteristics of materials, and criteria for uniformity of deformations of the reinforced structure and reinforcement elements.



To date, experimental and numerical studies of reinforced concrete elements reinforced with external composite reinforcement have been carried out, the results of which have been published in leading scientific publications. In [1], a computer simulation of a two-span pivotally supported beam, a control beam without reinforcement and reinforced with composite clamps in the zone of the Central support, is considered. Reinforcement was performed to increase the load-bearing capacity in the area of formation of inclined cracks. The simulation was performed in the ANSYS 18 software package. Concrete was modeled using solid volume elements of the SOLID65 type, longitudinal and transverse working steel reinforcement-LINK180 rod elements. External reinforcement was defined as the shell end element SHELL181, and the connection between the concrete surface and the shell was determined using the end elements conta173 and TARGE170. The classical two-line diagram was adopted as a generalized form of the deformation law. The computer experiment made it possible to obtain the formation zone and the trajectory of the opening of a critical inclined crack, the values of extreme values of the main stresses in the stretched region, and the values of stresses in the external elements. When comparing the results obtained in the software package and the results obtained when calculating according to the current sets of rules [2–4], it was found that the use of the developed author's modeling technique allows increasing the load-bearing capacity for the perception of the transverse force of non-reinforced beams by 6–10% compared to [2] and by 12% compared to [3, 4] in the case of reinforcement. The critical stresses in the external armature obtained by the author are 73–167% higher than those obtained in the calculation according to [1, 2], and are close to the actual experimental laboratory values. In [5, 6], characteristic methods for modeling the reinforcement of normal cross-sections of bridge span beams by carbon composite materials in a stretched zone were considered. Used modeling method in ANSYS 18, which is almost completely similar to that described in [1], with the exception of the method of defining the interaction between concrete and composites: is the contact and target surfaces using a conditional Fe thin layer of glue consisting of solid elements, which has the passport parameters. The calculation using this method showed a decrease in the actual load-bearing capacity for the perception of bending moment by 2–14% compared to experimental laboratory tests.

Thus, a comparative analysis of the results of experimental and numerical studies conducted by various authors has shown that there are several equally applicable approaches to modeling reinforced concrete elements with external reinforcement in the form of composite fabrics, lamellas or strips. The greatest interest in this situation is the question of specific methods for setting the correct interaction of heterogeneous layers of a multi-layer structure in the program [7–9].

## 2 Methods and Materials

For comparison and analysis, before the numerical experiment, full-scale laboratory tests were performed on 4 series of reinforced concrete beams, 2 beams in each, in accordance with the author's methodology described in articles [10–12]. During the experiment recorded the current values of bending moment, shear force, deflection at the middle of the span and the opening width of the critical crack in the area of pure

bending. The ANSYS 18 finite element complex was used as a platform for the numerical experiment. it allows modeling and calculating structures of any shape and structure, performing cross-section selection, and performing necessary checks at any stage of operation. The beam model was created from three-dimensional finite elements with specified mechanical parameters of materials (see Fig. 1), boundary conditions, and external load specified as a function of time.

The calculations used an implicit differential equation solver. Solving a nonlinear problem using an iterative tangent method with automatic step-by-step optimization if the number of iterations exceeds 10,000 units. The iterative solver in ANSYS 18 is implemented by the method of conditionally conjugate gradients. The load convergence control was set in the range of 2–5%.

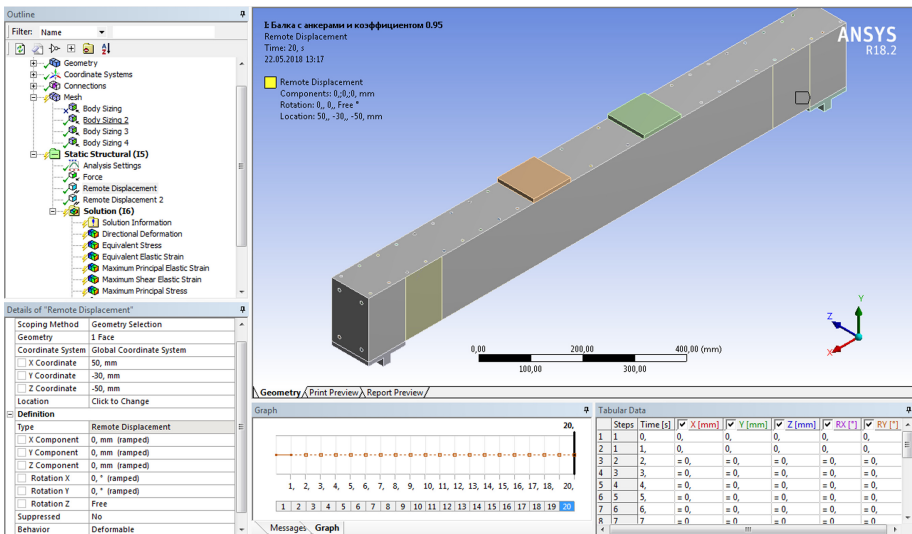


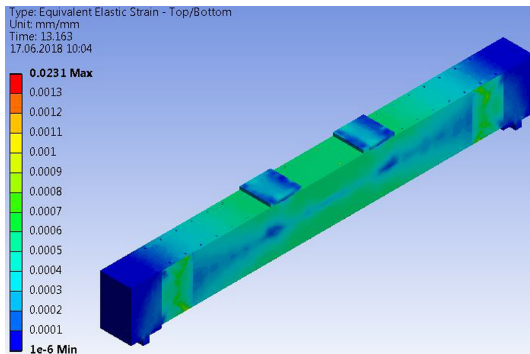
Fig. 1. General view of the finite element beam model.

Concrete was defined as final elements of the SOLID65 type. The stress-strain state of concrete was described by the William-Warнке model. 2 mechanisms of destruction were considered: from the loss of compressive strength of concrete and from the loss of tensile strength of concrete. The deformation model is a classic five-line state diagram. Longitudinal and transverse working steel reinforcement-rod end elements of the LINK180 type. The two-line Prandtl diagram was used as the deformation law. The composite material was modeled by shell end elements of the SHELL181 type. To match the actual design, the external load was applied to the beam through distribution plates - end elements of the SOLID65 type. The dimensions of the final elements in the structural groups are differentiated: for concrete - 20 mm, for steel - 4 mm, for distribution plates and external reinforcement - 10 mm.

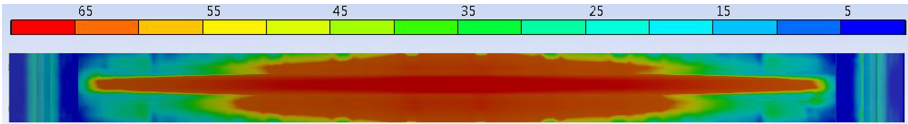
For the most complete analysis of the model, were used 3 variants of interaction of the composite shell elements with the concrete surface:

1. Rigid connection - that is, a complete union of deformations;
2. End elements of types CONTA173 and TARGE170. The diagram obtained during deep statistical processing of the results of field tests described in [11, 14, 15] is used as a deformation model.
3. a Friction joint with a variable coefficient of friction (friction). The range of 0.80–1.00 was chosen for the experiment.
4. Contact zone in the form of three-dimensional elements that imitate glue. It should be noted that this method of modeling with the specified parameters determined in the course of experimental studies [12] simulating the adhesive composition [14] gave high errors (more than 50%) in comparison with experimental data. Along with the analysis of the applicability and feasibility of a specific method for creating a model of a reinforced concrete element with external reinforcement, the authors also had a difficult task to develop a method for clarifying the initial data on the presence of stresses and deformations in the reinforced element at the reinforcement stage. The problem was solved by programming in the APDL environment and the SVAR operator. For series 3, the preload applied before amplification was set by recording plastic deformations and state variables during the pre-calculation of the non-violent element (with the composite element disabled) in a temporary file. After turning on the composite element, the grid nodes were moved to the deformed position, information about the state of the material was read from the file, and the load was applied again. The calculation for series 4 was performed similarly, except for additional registration of elastic deformations.

### 3 Results and Discussion



**Fig. 2.** Isofields of equivalent deformations of the B-3-2 beam under destructive load.



**Fig. 3.** Isofields of shear stresses in the adhesive joint of the B-3-2 beam.

As a result of the numerical experiment, the isofields of the main stresses, deformations, and displacements were obtained. As an example, Fig. 2 and Fig. 3 shows the deformation isofield of the B-3-2 sample. Data obtained from the program for various approaches to the problem of compatibility of concrete and composite material were compared with the results of field tests of samples. The difference between theoretical and experimental data is shown in Table 1. The results of numerical studies show high convergence with the results of a full-scale experiment. The most accurate data were obtained when modeling the contact zone “composite-concrete” using finite elements of target surfaces with the specification of the interaction law developed in [11–13, 15]: the deviation of the bending moment strength was 0.5% for the b-2 series, 4.47% for the B-3 Series, and 2.91% for the B-4 Series. The stiffness deviation was 2.2% for the B-2 Series, 6.35% for the B-3 Series, and 18.18% for the B-4 Series. The crack opening width of crack formation did not exceed the experimentally obtained one.

The use of the rigid coupling technique gives higher values of the strength and stiffness of the elements [14]: the value of the strength deviation under the action of the bending moment was 11.47% for the b-2 series, 19.54% for the B-3 Series, and 20.66% for the B-4 Series. The stiffness deviation was 27.87% for the B-2 Series, 21.46% for the B-3 Series, and 18.18% for the B-4 Series. The crack opening width at all stages of crack formation is less than that obtained experimentally.

The application of the technique is pliable friction compounds underestimates the experimentally obtained data: the deviation of the strength from the action of bending moment made up 11.85% for series 2, 3.8% for Series 3 and 5.99% for series 4 and hard – of 11.27% for series 2, of 13.32% for Series 3 and 1.86% for Series 4. The crack opening width at all stages of crack formation is greater than that obtained experimentally.

The results of series 2 have a high convergence with the results of the authors’ studies [5, 6, 12, 15] in terms of the limiting bending moment and the width of the normal crack opening. Comparison of beam stiffness parameters was not performed due to the lack of these data for the listed authors. In addition, during the numerical study using the multi-line diagram method, graphic images of the post-stage destruction of the contact zone “composite-concrete” were obtained, the distribution of relative deformations of the side and lower faces of the beam is shown when a load is applied in the range of 25–100% of the breaking one with a step of 15%. The figure clearly shows the accumulation of deformation in the zone of junction of the external reinforcement with the anchor, moving the point of maximum deformation (red flag) from the beam to the support, and area the beginning of the peeling of the composite element. Analysis of the color indication of deformations allows us to conclude that the “pliable” model shows a picture closer to reality, which is indirectly confirmed by the conclusions [13–15]. The nature of the destruction and the areas of exfoliation from concrete in the software package coincide with those obtained during field tests. Linking the model to a scale ruler allows

**Table 1.** Changes in the results using different methods compared with the experiment.

Marking	Design methodology		
	Rigid	Multiline clutch	Frictional
Ultimate bending moment			
B-2-1	+19.76%	<b>0%</b>	-6.2%
B-2-2	+3.18%	<b>-1%</b>	-16.3%
B-3-1	+17.5%	<b>+1.05%</b>	-6.6%
B-3-2	+21.58%	+7.9%	<b>-1%</b>
B-4-1	+19.56%	<b>+1.19%</b>	-7.12%
B-4-2	+21.76%	<b>+4.63%</b>	-4.86%
Vertical deflection in the middle of the span			
B-2-1	-30.75%	<b>-1.8%</b>	-1.8%
B-2-2	-25%	<b>-2.67%</b>	-4.4%
B-3-1	-26.58%	<b>+5.35%</b>	+12.3%
B-3-2	-16.34%	<b>+5.34%</b>	+14.34%
B-4-1	-18.35%	-5.06%	<b>+2.2%</b>
B-4-2	-18%	<b>-7.7%</b>	<b>+1.53%</b>
Normal crack opening width			
B-2-1	-24.93%	<b>-3.08%</b>	+1.8%
B-2-2	-16.32%	<b>+1.5%</b>	+5.3%
B-3-1	-6.27%	<b>+4.6%</b>	+10%
B-3-2	-11.38%	<b>+4.3%</b>	+7.2%
B-4-1	-20%	-3.6%	<b>-1.46%</b>
B-4-2	-17.2%	<b>+1.1%</b>	-1.33%

«+» means an increase in the index compared to the experiment

«-» means a decrease in the index compared to the experiment

The results closest to the experimental ones are highlighted in bold

you to determine the effective length of the attachment, as well as the most vulnerable points that require additional fasteners.

## 4 Conclusion

- A numerical experiment has shown that external reinforcement has a positive effect on the performance of reinforced concrete bending elements and increases their load-bearing capacity and rigidity, as well as reduces cracking at the extreme stages.
- One of the decisive factors in the calculation of composite multilayer structures is the method of modeling the joint operation of adjacent layers of the structure with different deformation characteristics [12–14].

- The use of three-dimensional elements in modeling thin shell structures that are part of multilayer structures is irrational and leads to high distortions.

## References

1. Yushin, A.V., Morozov, V.I.: Experimental studies of two-span reinforced concrete beams reinforced with composite materials on an inclined section. *Bull. Civ. Eng.* **5**(46), 50–57 (2014)
2. SR 164.1325800.2014 Strengthening of reinforced concrete structures with composite materials, p. 50. Ministry of Construction, Moscow (2015)
3. ACI 440.2R-08. Guide for the Design and Construction of Externally Bonded FRP Systems for Strengthening Concrete Structures. Michigan/American concrete Institute, ACI Committee 440, p. 80 (2008)
4. *Fib Bulletin 14. Externally Bonded FRP reinforcement for RC structures*, p. 138 (2001)
5. Bokarev, S.A., Smerdov, D.N.: Experimental studies of bent reinforced concrete elements reinforced with composite materials. *Construction* **2**(614), 112–124 (2010). Proceedings of higher educational institutions
6. Nevolin, D.G., Smerdov, D.N., Smerdov, M.N.: Experimental studies of the bearing capacity of reinforced concrete structures of mining buildings and structures. *Min. J.* **8**, 138–142 (2015). Proceedings of higher educational institutions
7. Dai, J., Ueda, T., Sato, Y.: Development of the nonlinear bond stress–slip model of fiber reinforced plastics sheet–concrete interfaces with a simple method. *J. Compos. Constr.* **9**, 52–62 (2005)
8. Lu, X.Z., Teng, J.G., Ye, L.P., Jiang, J.J.: Bond–slip models for FRP sheets/plates bonded to concrete. *Eng. Struct.* **27**, 920–937 (2005)
9. Rimshin, V.I., Merkulov, S.I., Esipov, S.M.: Concrete structures reinforced with composite material. *Bull. Eng. Sch. Far Eastern Fed. Univ.* **2**(35), 93–100 (2018)
10. Merkulov, S.I., Esipov, S.M.: Experimental studies of coupling of external composite non-metallic reinforcement with concrete. *Probl. Solut.* **1**, 93–97 (2017). Safety of the construction fund of Russia
11. Merkulov, S.I., Esipov, S.M.: Increase in the bearing capacity of reinforced concrete structures by strengthening the external reinforcement composite material. *BST Bull. Constr. Equip.* **2**(1002), 56–57 (2018)
12. Esipov, S.M., Merkulov, S.I.: Aspects of modeling and calculation of bent concrete elements in the PC ANSYS 18.2. In: *The collection: Science and Innovation in Construction Collection of Reports of the International Scientific and Practical cConference (to the 165 Anniversary of the Birth of V. G. Shukhov)*, pp. 49–55 (2018)
13. Dai, J., Ueda, T., Sato, Y.: Development of the nonlinear bond stress–slip model of fiber reinforced plastics sheet–concrete interfaces with a simple method. *J. Compos. Constr.* **1**(9), 52–62 (2005)
14. Lu, X.Z., Teng, J.G., Ye, L.P., Jiang, J.J.: Bond–slip models for FRP sheets/plates bonded to concrete. *Eng. Struct.* **6**(27), 920–937 (2005)
15. Smerdov, D.N., Selivanova, E.A.: The study of the creep properties in the elements of the system of external reinforcement during prolonged exposure to load. In: *Polytransport System Materials IX International Scientific-Technical Conference. Siberian State University of Railway Engineering*, pp. 53–56 (2017)



# Compatibility of Plasticizing Mono-Admixtures for Modifying Concretes of Transitional Period

M. M. Kosukhin<sup>(✉)</sup> and A. M. Kosukhin

Belgorod State Technological University named after V. G. Shukhov, Belgorod, Russia

**Abstract.** The scientific achievements in the theory and practice of concrete production and application have been summarized. It has been demonstrated that the present-day level of scientific developments allows obtaining up-to-date modified concretes with high technological and service properties. Nevertheless, such concretes have not yet found wide application in the industry, and the existing raw-materials, production and regulatory-technical base are not ready for such concretes production. This, in its turn, results in the considerable cost increase of the existing general-purpose concretes and the unreasonable overconsumption of costly chemical admixtures. At the same time, there is a real opportunity of obtaining low-cost and efficient modifiers on the basis of chemical production waste, the implementation of which would expand the range of modifying the widely used general-purpose concretes without increasing their cost. The research findings of new highly-efficient plasticizing admixtures on the basis of chemical production waste have been presented. Their influence on the properties of concretes and concrete mixes has been studied. The experimental data demonstrate that at a certain ratio of superplasticizer with sulfo-groups and hydroxyl groups in a poly-functional modifier (PFM) a synergistic effect is observed, caused by attractive interactions of molecules on the dispersed phase particles' surface. This would allow considerably reducing not only the consumption of the expensive admixtures, but also the final cost of concrete. At present the leading role in construction and in housing and utilities infrastructure belongs to the application of up-to-date domestic materials and technologies. This is especially relevant nowadays, within the framework of import phaseout of materials and technologies.

**Keywords:** Polyfunctional modifiers · Concretes of transitional period · PlastiCizing Mono-Admixtures · Synergistic effect · Adsorption-active groups · Rheological properties · Yield point · Plastic viscosity

## 1 Introduction

The global strategy of the industrial development in advanced countries in the foreseeable future is based on using concrete as the main construction material. The centuries-old history of the origin and development of the main structural material of humanity is now breaking the new qualitative and quantitative grounds of scientific and technological progress. The evolutionary character of concrete science development by the end of the 20<sup>th</sup> century experienced a revolutionary breakthrough. From a relatively simple, mostly

descriptive branch of knowledge, the concrete science has become an interdisciplinary science [1]. This is evidenced by the numerous findings of fundamental and applied theoretical and experimental research, carried out in recent decades by various scientific schools all over the world. The elementary opportunities of conventional concrete technologies of the old and transitional periods are being replaced with knowledge-intensive technologies, giving the opportunity of the targeted regulation of hydration and structure formation processes in cement systems, thus obtaining new-generation concretes with required service properties. Due to the modern scientific achievements the concrete science and the practice of its production start being based on the application of nanotechnological approaches – the implementation of structure formation processes of modern concretes, which imply their assembly or self-assembly by sol-gel technologies «bottom-up» at crystal synthesis or «top-down» at mechanochemical activation of components. All this is nothing but the controllable and adjustable influence on structure formation processes, beginning from the nano-scale level [2].

The crucial role in this matter is assigned to chemization of concrete, i.e., designing and applying chemical admixtures-modifiers of various nature, structure and mechanism of action. It has been established that the main trends in modifying cement systems with surface-active agents are determined with the character of the latter's structure and are the basis of modifying concrete mixes and obtaining concretes with the preset construction and technological parameters [3]. In fact, this means designing modifiers at the stage of their production. The most complete view on the theory and practice of concrete modification is presented in the work [4].

All the above said allow us making a conclusion that the scientific development level of the modern concrete science is impressive. Nevertheless, all these findings have not yet found any wide application in practice, but still only have a «promising outlook». The existing raw-materials, production and regulatory-technical base are not ready for producing such concretes. This means that concretes of grade B 12,5-B 40 in the total amount of the concrete, produced today, make up 95–97% [5], and the other concretes of grades B 40-B 90 are produced at test and experimental-industrial units, firstly. Secondly, the concrete should keep all its advantages, which have made it the main structural material in construction industry, i.e. be prepared mostly of local resources, in close vicinity to construction sites and with small labor costs, both at preparing mixes, and at concrete laying. This is especially relevant nowadays, with the universal development of cast-in-situ concreting. Moreover, the properties of concretes should be determined with account of their specific purpose and service conditions. Thus, for example, in the context of regulating rupture resistance of concrete, the authors [6] suggest a generalized principles system of designing and synthesizing concretes with the predetermined rupture resistance degree, which completely embraces the necessary and sufficient conditions of obtaining concretes of various quality levels.

As the objective reality, existing nowadays at the market of concrete and chemical admixtures, shows, the scientific progress in concrete technologies, on one hand, has determined development prospects of high-strength concretes of the future. And on



the other hand, it has resulted in the considerable costs increase and quality deterioration of general-purpose and high-strength concretes, widely used in modern construction. For concretes with strength up to 80 MPa, the quality can be achieved by various modifications of conventional fine-aggregate and crushed-stone concretes.

The application of admixtures, apart from achieving the operational benefits, should be also, first of all, economically feasible, i.e. should eventually allow obtaining the cheaper concrete, and not increase its cost. The complicated and resource-consuming technologies of obtaining most of the efficient chemical admixtures predetermine their high prime costs and even higher market price.

In this regard, the purpose of this work was carrying out the research in synthesizing low-cost and efficient mono-admixtures on the basis of chemical production waste, studying their colloid-chemical properties and obtaining on their basis, with applying synergetics principles, the available highly-efficient polyfunctional modifiers (PFM) for widely used concretes of the so-called transitional period.

## 2 Methods and Materials

The study of polyfunctional modifiers' and mono-admixtures' efficiency was carried out by means of performing standard research in determining the colloid-chemical properties of admixtures and physico-mechanical and technological properties of the modified concretes and concrete mixes.

To exclude the influence of hydration processes on the instability of cement-water system with admixtures, a model chalk suspension was used. For the experiment the mono-admixtures, varying in their nature and structure, were used, which contained various adsorption-active groups: fluidizing agent S-3, LST – hydrophilic sulfo-groups –  $\text{SO}_3^-$ , SP SB-3 – hydroxyl groups and their mixes.

To determine the composition and structure of oligomeric molecules such methods as the gas-liquid and liquid chromatography, ultraviolet and infrared spectroscopy, NMR-spectroscopy, conductometry and potentiometry were used. The molecular weight of the synthesized oligomers was determined by cryoscopy method.

To identify the modifiers' mechanism of action the physico-chemical research methods were used. The water solutions of modifiers were studied, as well as the cement paste hardening kinetics, alterations in the phase composition of cement stone samples with admixtures, sporadic transformations in model systems and in clinker minerals at hydration and hardening.

The rheological properties of cement paste and mortars were studied and the cement concrete's composition was proportioned in accordance with the methodology, developed in CRCRI, concerning the application of various types of admixtures in the precast and cast-in-situ concrete technologies [7].

The fluidity of the modified cement suspensions was determined by means of mini-cone method, according with the methodology of CRCRI (Concrete and Reinforced Concrete Research Institute) of Gosstroy [8], which consists in determining the diameter of the cement suspension flow under the action of gravity.

The rheological parameters of suspensions were studied by means of a rotary viscosimeter «Reotest-2.1». The concentration of polyfunctional modifier ( $C_m$ ) was calculated in dry wt. % of the dispersed phase amount. In the course of the research the dependence between the values of shearing stress and shear rate were determined. According to the obtained data, the rheological curves were plotted, from which the yield point  $\tau_0$  and the plastic viscosity  $\eta_{пл}$  were found.

### 3 Results and Discussions

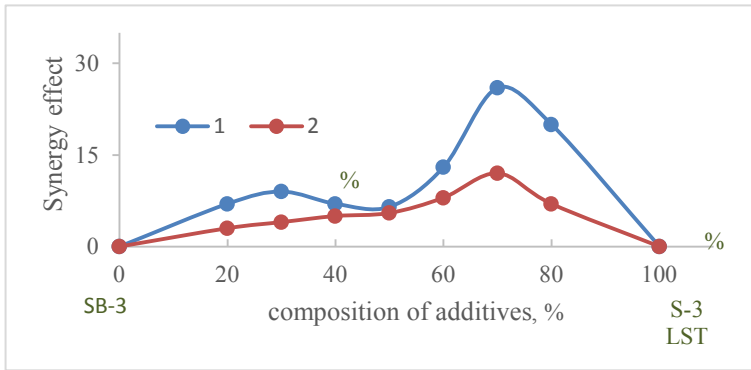
In the course of the experiment, as source raw materials for obtaining mono-admixtures, the waste of various branches of chemical production industry was used: resorcin, pyrocatechin, hydrocarbon pyrolysis products and a number of others. From analyzing the chemical technologies of these substances production it has been determined that in their production waste oligomeric compounds of various nature, composition and structure can be formed, due to polymerizing processes with an acid catalyst. Besides, the residual resorcin and pyrocatechin, contained in the waste, are typical fungicides by their chemical nature, which can be the basis for providing the future concretes with resistance to biologically aggressive media. As a result of simple chemical synthesis the water-soluble products of various composition and structure were obtained, which had both plasticizing and fungicidal activity. The colloid-chemical properties of the obtained admixtures were studied, as well as the properties of concretes and concrete mixes on their basis; the findings of these studies were reflected in a number of works [9–12].

Taking into account a well-known fact that at using complex admixtures, containing components of various natures, with various mechanism of action, a synergetic effect is implemented, i.e. the effect of mutual strengthening of each admixture's plasticizing activity, the properties of a polyfunctional modifier, made of the synthesized resorcinol-formaldehyde superplasticizer (SP) SB-3 and the known SP fluidizing agent S-3, were studied [13].

In the course of the research complex admixtures with various hydrophilic groups of SP SB-3 +S-3 and SB-3+LST were prepared in the entire range of concentrations, and their combined effect on cement mixes' properties was studied. The synergetic efficiency was assessed by the plasticizing activity value, which was determined by a well-known method of mini-cone flow diameter. The findings of the research have demonstrated that in a certain range of concentrations in complex admixtures a synergistic effect is observed – the increase of plasticizing activity in comparison with the additive action of admixtures. In Fig. 1 the dependence of the synergetic effect on the ratio of individual components at dosage 0.2% of cement weight, is presented.

The relative synergetic effect was calculated by the difference between the experimental value of mini-cone flow and the value, calculated by the rule of additivity and referring to the latter value.

As we can see in the picture, synergistic effect is observed in a certain range of individual components' concentrations. For the complex admixture SB-3+S-3 two maximums are registered: one at the SB-3 concentration, equal to 30%, and another, a stronger one, at the SB-3 concentration 70%. For the complex admixture SB-3+LST there is only one feebly-marked maximum at the SB-3 concentration, equal to 70%. This is most likely



**Fig. 1.** The influence of complex admixtures' composition on the synergistic effect: 1 – SB-3 + S-3; 2 – SB+LST.

due to the fact that LST already contains hydrophilic groups of various natures, so the synergistic effect manifests itself only marginally. The fact that the synergistic effect in either case is the mostly pronounced at the same concentration of SB-3 is obviously no accident, as well.

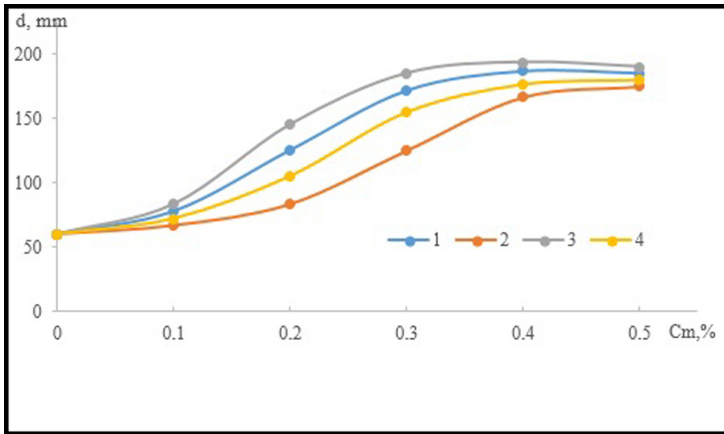
Replacement of a sulfo-group with molecular weight 80 with a hydroxyl group with molecular weight 16 results, *ceteris paribus*, in the decrease of the plasticizer's molecular weight by 30–35%. This corresponds to about the same alteration of the plasticizing activity of SB-3 in comparison with S-3. LST, the molecule of which contains various hydrophilic groups ( $\text{SO}_3^-$ ,  $\text{O}^-$ ,  $\text{COO}^-$ ), falls in between SB-3 and S-3 in its plasticizing activity.

It should be also noted that for complex admixtures at their optimum ratio the mini-cone flow's attainment of saturation occurs at lower concentrations of admixtures, i.e. their plasticizing activity is increased. As an example, in Fig. 2 the dependencies of mini-cone flow on the dosage of SB-3, S-3 admixtures and compositions on their basis, are shown. As we can see in the picture, the experimental curve for the complex admixture is higher, than that calculated by the rule of additivity, and besides, the attainment of saturation is observed at a slightly lower dosage.

The mini-cone method doesn't allow evaluating some of rheological parameters, though the mini-cone flow is determined by the value of these parameters. Therefore, the rheological properties of cement pastes were also studied by means of rheoviscosimeter with coaxial cylinders «Reotest-2.1». According to the obtained data, the rheological curves were plotted, from which the yield point and the plastic viscosity were found.

All the admixtures under study reduce the yield point to zero. With that, of the individual admixtures the highest plasticizing activity is shown by SB-3, as  $\tau_0$  goes to zero at a lower dosage. The synergistic effect for complex admixtures makes itself evident in the fact that the experimental values for  $\tau_0$  are lower, than the values, calculated by the rule of additivity, and  $\tau_0$  goes to zero at lower dosages.

The comparison of the data, obtained from the rheological research and from the mini-cone method, shows that the dosage of admixtures, at which the highest value of mini-cone flow is achieved, correlates with the admixtures' dosages, at which the yield



**Fig. 2.** The influence of admixtures' dosage on the mini-cone flow: 1 – SB-3; 2 – S-3; 3 – (70% SB-3 + 30% S-3); 4 – calculated curve.

point equals to zero. This is understandable, if we take into account that the cone spreads under the action of gravity, and the flow of cement paste would proceed until the gravity force, acting on the cement paste lower layer, would exceed the shearing stress of the cement paste.

## 4 Conclusion

So, the carried-out research of the admixtures' plasticizing ability and activity by means of mini-cone method and rheoviscosimetry have demonstrated, that, firstly, the nature of hydrophilic groups influences the plasticizing properties of an admixture, while the highest plasticizing activity is shown by the admixture with hydroxyl groups. Secondly, at obtaining complex admixtures from individual ones, which contain either sulfo-groups, or hydroxyl hydrophilic groups, a significant synergistic effect is observed at certain ratios of admixtures. This fact can be successfully used as a basis for reducing the PFM components consumption and the considerable cost-cutting for concretes of transitional period.

**Acknowledgements.** The work is realized in the framework of the Program of flagship university development on the base of the Belgorod State Technological University named after V. G. Shukhov, using equipment of High Technology Center at BSTU named after V. G. Shukhov.



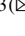


## References

1. Ushero-Marshak, A.V.: Future outlook of concrete. *Build. Mater.* **3**, 4–5 (2014)
2. Stepanova, M.P., Potamoshneva, N.D., Chernyshov, E.M., Bazhenov, Y.: Nanostructured portlandite-aluminosilicate contact-condensational hardening systems and composites on their basis. *Bull. MSUCE* **2**, 114–122 (2013)

3. Batrakov, V.G.: Concrete modifiers: new opportunities and prospects. *Build. Mater.* **10**, 4–7 (2006)
4. Batrakov, V.G., Kalashnikov, V.I., Tarakanov, O.V., Volodin, V.M., Erofeeva, I.V., Abramov, D.A.: *Modified concretes. Theory and Practice.* Tekhnoprojekt, Moscow (1998)
5. Kalashnikov, V.I., Tarakanov, O.V., Volodin, V.M., Erofeeva, I.V., Abramov, D.A.: Concretes of the transitional and new generations: current state and trends. *Curr. Issues Sci. Educ.* **2**, 151–160 (2015)
6. Bazhenov, Y., Chernyshov, E.M., Korotkikh, D.N.: Designing of modern concretes' structures: defining principles and technological platforms. *Build. Mater.* **3**, 6–14 (2014)
7. Recommendations on evaluating the efficiency of concrete admixtures application. CRCRI, Moscow (2020)
8. Recommendations on physical-chemical control of the composition and quality of superplasticizer S-3. CRCRI, Moscow (2020)
9. Kosukhin, M.M., Kosukhin, A.M.: The role of surface phenomena in modified cement dispersions at studying polyfunctional modifiers' mechanism of action. *Solid State Phenom.* **299**, 1038–1043 (2020)
10. Kosukhin, M.M.: Regulating the properties of concretes and concrete mixes with complex admixtures, having various hydrophilic groups: diss.... cand. of engineering. VGASU, Voronezh (1995)
11. Kosukhin, M.M., Shapovalov, N.A., Kosukhin, A.M.: Colloid-chemical bases on creation of multifunctional modifiers of concrete mix and concrete. *Solid State Phenom.* **265**, 331–336 (2017)
12. Shapovalov, N.A., Latypova, M.M., Slyusar, O.A., Lomachenko, V.A.: Receiving of plasticisers from waste of chemical production. *Ecologiya i promyshlennost Russii* **1**, 15–17 (2000)
13. Slyusar, A.A., Poluektova V.A., Mukhacheva, V.D.: Colloid-chemical aspects of the plasticizing mineral suspensions of oxy-phenol-furfural oligomers. *Bulletin of BSTU named after V.G. Shukhov* **2**, 66–69 (2008).



# Methodology for Assessing the Quality of Building Materials

V. I. Loganina<sup>1</sup> , S. V. Klyuev<sup>2</sup> , R. S. Fediuk<sup>3</sup>  , and I. A. Aksenov<sup>4</sup> 

<sup>1</sup> Penza State University of Architecture and Construction, Penza, Russia

<sup>2</sup> Belgorod State Technological University named after V.G. Shukhov, Belgorod, Russia

<sup>3</sup> Far Eastern Federal University, Vladivostok, Russia

<sup>4</sup> Vladimir State University named after Alexander and Nikolay Stoletovs, Vladimir, Russia

**Abstract.** Assessment of the quality of building materials is an important step in obtaining commercial products. The information on the assessment of the representativeness of the sample in determining the quality of building materials is provided. In the work, we used a technique for assessing the quality of ceramic bricks in accordance with the Russian standard GOST 530-2012, as well as plaster mixtures in accordance with the Russian standard GOST 33083-2014. The number of samples in the sample was calculated taking into account the risk of the supplier and the consumer. The discrepancy between the number of samples specified in the regulatory documents and the calculated data was revealed. The values of standard confidence probabilities, supplier's and consumer's risk are revealed. It is proposed to indicate, when determining the sample size in the methods for assessing the quality of building materials, the value of the confidence level, the maximum error, which will make it possible to more objectively judge the entire batch of products.

**Keywords:** Representativeness of the Sample · Sample size · Construction materials · Reliability of control · Test methods

## 1 Introduction

To assess the quality of products, sampling is carried out, while the minimum sample size is of great importance, since the sample must be representative [1–5]. This requires the following requirements [6–9]:

- a sample must have the characteristics of the batch of products;
- a sample must be of sufficient size, i.e. by the number of observations.

There are several approaches to determining a sample size, according to which the sample should be 5% of the total general population, or the sample size is determined on the basis of statistical analysis taking into account the requirements for the reliability of the results [10–14].

## 2 Methods and Materials

If the size of the general population is known, then the size of the required sample is determined by the formula.

$$n = \frac{N\sigma^2 t^2}{N\Delta^2 + \sigma^2 t^2} \quad (1)$$

where  $n$  is a sample size;  $t$  - coefficient (calculated according to special tables depending on the confidence level);  $\sigma$  - sample variance;  $\Delta$  - limiting (set) sampling error;  $N$  is the size of the batch of products.

When the size of the population is not known, the minimum sample size can be given by:

$$n = \frac{t^2 \sigma^2}{\Delta^2} \quad (2)$$

where  $n$  is the minimum sample size;  $\sigma$  - sample standard deviation.

The mean and limiting sampling errors are related by the following relationship:

$$\Delta = t\mu \quad (3)$$

An average error is determined by the formula:

$$\mu = \frac{\sigma^2}{\sqrt{n}} \text{ or } \mu = \sqrt{\frac{\sigma^2}{n} \left(1 - \frac{n}{N}\right)} \quad (4)$$

When carrying out statistical acceptance control according to the Russian standard GOST R 50779.30-95, the sample size is determined by the following formula:

$$n = N \left[ 1 - \left( \frac{\beta}{100} \right)^{\frac{100}{qN}} \right] \quad (5)$$

where  $\beta$  is an average percentage of accepted batch of products;  $q$  is a share of defective products, %.

There is also a formula for determining a number of samples required for testing, which has the form:

$$n = \left( \frac{z_{1-\alpha} + z_{1-\beta}}{R_o - R_1} \right)^2 \sigma^2 \quad (6)$$

where  $z_{1-\alpha}$  and  $z_{1-\beta}$  - quantiles of the standard normal distribution of levels  $(1 - \alpha)$  and  $(1 - \beta)$ , respectively.

The values  $\alpha$  and  $\beta$  will characterize, respectively, the risks of the “supplier” and “consumer”.

In accordance with the Russian standard GOST 530-2012, the number of samples required for testing the quality indicators of bricks ranges from 3 to 35. The determination of the compressive strength is carried out on 10 samples, the ultimate bending strength - on 5 samples.

In accordance with EN 1052-1-1998, a number of samples when testing a mortar should be at least 3. However, the regulatory documents do not indicate the degree of reliability with which the representativeness of the sample is ensured.

Taking into account the above, the representativeness of the sample was analyzed when assessing the quality of some building materials, in particularly bricks and dry building mixtures [15–21].

The work used a technique for assessing the quality of ceramic bricks in accordance with the Russian standard GOST 530-2012, as well as dry building mixtures according to the Russian standard GOST 33083-2014.

### 3 Results and Discussion

Calculations using the formula (2) showed that the required number of samples for testing bricks of grade 125 for compression is from 3 to 156 pieces (Table 1). The calculations were carried out with the following data: standard deviation - 4.16, confidence probability 95% ( $t = 2$ ) and 99.7% ( $t = 3$ ), deviation of the sample mean from the true value of the average result by no more than 1–5 kg/cm<sup>2</sup>.

**Table 1.** Estimated sample size.

Marginal sampling error $\Delta$ , kg/cm <sup>2</sup>	Estimated sample size $n$	
	Confidence probability 95%	Confidence probability 99.7%
1	70	156
3	8	18
5	3	7

The calculation results show that the minimum sample size differs sharply from the data given in Russian Standard GOST 530-2012.

The number of samples required for testing bricks was also calculated, depending on the level of defectiveness  $NQL$  and the supplier's risk  $\beta$  according to formula (6). The calculation results are shown in Table 2.

Thus, the number of samples for assessing the strength of bricks, taking into account the risk of the supplier and the consumer, also differs from the sample size values specified in the Russian standard GOST 530-2012.

We also compared the calculated sample volume according to formulas (2) and (6) of dry building mixtures with the data given in the Russian standard GOST 33083-2014. As an example, a light plaster mortar with a density of less than 1300 kg/m<sup>3</sup> was taken. In accordance with the Russian standard GOST 31356-2013, for quality control of dry mixtures packed in bags or packages, one sample is taken from each package unit included in the sample. Then, according to a specific test method, a certain number of samples are made. So, when determining the water-holding capacity, the mobility of the mortar mixture, the number of samples is 2. When determining the water absorption with capillary suction, the compressive strength, the number of samples should be at least



**Table 2.** Number of samples for testing bricks when determining the compressive strength.

Defectiveness level $NQL, \%$	Supplier's risk $\alpha = 0.05$ at consumer's risk $\beta$		
	0.1	0.25	0.5
1	19	12	6
2	9	6	3
3	7	5	3
4	6	4	2
6.5	4	3	2

three, and the number of samples. Samples when determining the adhesion strength should be at least five.

The assessment of the minimum volume of samples when controlling the quality of mortar and plaster was carried out according to the following indicators:

- flowability;
- compressive strength;
- water absorption at capillary suction.

The results of calculating the minimum volume of samples by formula (2) are presented in Table 3.

**Table 3.** Estimated number of samples when controlling the quality indicators of mortars.

Quality indicator of mortars	Mean quality indicator	Standard deviation	Marginal sampling error	Number of test pieces at confidence level	
				95%	99.7%
Flowability, cm	10	0.666	0.5 cm	8	16
			1 cm	2	4
Compressive strength, MPa	3.75	0.416	1 MPa	1	2
			0.5 MPa	3	7
Water absorption at capillary suction, $\text{kg} / (\text{m}^2 \text{hour}^{0.5})$	0.2	0.0666	0.1 $\text{kg}/(\text{m}^2 \text{hour}^{0.5})$	2	4
			0.05 $\text{kg}/(\text{m}^2 \text{hour}^{0.5})$	8	16

Table 4 shows the values of the number of samples required for testing of mortars, calculated according to the formula (6), depending on the level of defectiveness  $NQL$  and the consumer's risk  $\beta$ .

**Table 4.** The number of samples for testing mortars.

Defectiveness level $NQL, \%$	Supplier's risk $\alpha = 0.05$ at consumer's risk $\beta$		
	0.1	0.25	0.5
1	2	3	4
Determination of compressive strength			
1	19	12	6
2	10	6	3
3	7	5	2
Determination of bond strength			
1	42	27	14
2	17	10	5
3	10	7	3
Determination of average density			
1	19	12	6
2	10	6	3
3	7	5	2
Determination of flowability			
1	19	12	6
2	10	6	3
3	17	5	2
Determination of water retention capacity			
1	42	27	14
2	16	10	5
3	10	7	3
Determination of capillary water absorption			
1	19	12	6
2	10	6	3
3	7	5	2

Thus, the calculation according to formulas (2) and (6) also showed a discrepancy between the number of samples specified in the Russian standards GOST 31356-2013, GOST 33083-2014, and the data in Table 4.

## 4 Conclusion

Thus, when determining the sample size in the methods for assessing the quality of building materials, the value of the confidence level, the marginal error should be indicated, which will make it possible to more objectively judge the entire batch of products.



## References

1. Klyuev, S.V., Khezhev, T.A., Pukharenko, Y.V., Klyuev, A.V.: Fiber concrete on the basis of composite binder and technogenic raw materials. *Mater. Sci. Forum* (2018). <https://doi.org/10.4028/www.scientific.net/MSF.931.603>
2. Fediuk, R.S., Lesovik, V.S., Liseitsev, Y.L., Timokhin, R.A., Bituyev, A. V., Zaiakhanov, M.Y., Mochalov, A.V.: Composite binders for concretes with improved shock resistance. *Mag. Civ. Eng.* (2019). <https://doi.org/10.18720/MCE.85.3>
3. Usanova, K., Barabanshchikov, Y.G.: Cold-bonded fly ash aggregate concrete. *Mag. Civ. Eng.* (2020). <https://doi.org/10.18720/MCE.95.10>
4. Tolstoy, A.D., Lesovik, V.S., Glagolev, E.S., Krymova, A.I.: Synergetics of hardening construction systems. In: IOP Conference Series: Materials Science and Engineering (2018). <https://doi.org/10.1088/1757-899X/327/3/032056>
5. Amran, M., Fediuk, R., Vatin, N., Mosaberpanah, M.A., Danish, A., El-Zeadani, M., Klyuev, S.V., Vatin, N.: Fibre-reinforced foamed concretes: a review. *Materials* **13**(19), 4323 (2020)
6. de Azevedo, A.R.G., Klyuev, S., Marvila, M.T., Vatin, N., Alfimova, N., de Lima, T.E.S., Fediuk, R., Olisov, A.: Investigation of the potential use of curauá fiber for reinforcing mortars. *Fibers* **8**, 0069 (2020)
7. Klyuev, S.V., Khezhev, T.A., Pukharenko, Y.V., Klyuev, A.V.: Fiber concrete for industrial and civil construction. *Mater. Sci. Forum* **945**, 120–124 (2018)
8. Klyuyev, S.V., Guryanov, Y.V.: External reinforcing of fiber concrete constructions by carbon fiber tapes. *Mag. Civ. Eng.* (2013). <https://doi.org/10.5862/MCE.36.3>
9. Fediuk, R., Pak, A., Kuzmin, D.: Fine-grained concrete of composite binder. In: IOP Conference Series: Materials Science and Engineering (2017). <https://doi.org/10.1088/1757-899X/262/1/012025>
10. Korsun, V., Vatin, N., Korsun, A., Nemova, D.: Physical-mechanical properties of the modified fine-grained concrete subjected to thermal effects up to 200 °C. In: *Applied Mechanics and Materials* (2014). <https://doi.org/10.4028/www.scientific.net/AMM.633-634.1013>
11. Fediuk, R.S.: Mechanical activation of construction binder materials by various mills. In: IOP Conference Series: Materials Science and Engineering (2016). <https://doi.org/10.1088/1757-899X/125/1/012019>
12. Klyuev, S.V., Klyuev, A.V., Khezhev, T.A., Pukharenko, Y.V.: High-strength fine-grained fiber concrete with combined reinforcement by fiber. *J. Eng. Appl. Sci.* **13**, 6407–6412 (2018)
13. Jabir, H.A., Abid, S.R., Murali, G., Ali, S.H., Klyuev, S., Fediuk, R., Vatin, N., Promakhov, V., Vasilev, Y.: Experimental tests and reliability analysis of the cracking impact resistance of UHPFRC. *Fibers* **8**, 0074 (2020)
14. Fediuk, R., Yushin, A.: Composite binders for concrete with reduced permeability. In: IOP Conference Series: Materials Science and Engineering (2016). <https://doi.org/10.1088/1757-899X/116/1/012021>
15. Fediuk, R.: Reducing permeability of fiber concrete using composite binders. *Spec. Top. Rev. Porous Media* **9**, 79–89 (2018)
16. Kharun, M., Klyuev, S., Koroteev, D., Chiadighikaobi, P.C., Fediuk, R., Olisov, A., Vatin, N., Alfimova, N.: Heat treatment of basalt fiber reinforced expanded clay concrete with increased strength for cast-in-situ construction. *Fibers* **8**, 0067 (2020)
17. Begich, Y.E., Klyuev, S.V., Jos, V.A., Cherkashin, A.V.: Fine-grained concrete with various types of fibers. *Mag. Civ. Eng.* (2020). <https://doi.org/10.18720/MCE.97.2>
18. Ibragimov, R., Fediuk, R.: Improving the early strength of concrete: effect of mechanochemical activation of the cementitious suspension and using of various superplasticizers. *Constr. Build. Mater.* (2019). <https://doi.org/10.1016/j.conbuildmat.2019.07.313>

19. Fediuk, R.S., Yevdokimova, Y.G., Smoliakov, A.K., Stoyushko, N.Y., Lesovik, V.S.: Use of geonics scientific positions for designing of building composites for protective (fortification) structures. In: IOP Conference Series: Materials Science and Engineering (2017). <https://doi.org/10.1088/1755-1315/221/1/012011>
20. Loganina, V.I., Simonov, E.E., Jezierski, W., Małaszkiwicz, D.: Application of activated diatomite for dry lime mixes. *Constr. Build. Mater.* (2014). <https://doi.org/10.1016/j.conbuildmat.2014.04.098>
21. Jing, Z., Benin, D., Snezhko, V., Vorona-Slivinskaya, L., Aksenov, I.: Mechanical stresses in building structures and dry friction-ways to improve the durability of architectural structures. *J. Adv. Res. Dyn. Control Syst.* **12**(2 Special Issue) 578–585 (2020)



# Evaluation of the Load-Bearing Capacity of the Combined Bolt-Welded Joint

N. V. Solodov  and N. V. Vodyakhin <sup>(✉)</sup> 

Belgorod State Technological University named after V.G. Shukhov, Belgorod, Russia  
partietz5000@bk.ru

**Abstract.** Combined bolt-welded joints on links of different deformability have already been used in the practice of metal construction. One of these applications is newly designed structures. Another possible area is to restore or increase the load-bearing capacity of bolted joints by welding in operational structures. The efficiency potential of bolt-welded joints makes it possible to use the advantages of both types of connections and neutralize their disadvantages. However, this also creates a well-known problem: the rationale for working together in a single interface node of such different-formative monoconnected joints as bolted and welded. In the case of welding in combination with prestressed high-strength bolts, the problem of different deformability has already been solved in tests of physical samples of nodes and in the study of their computer models. However, when a bolted joint perceives the shear force when the joint is made on ordinary non-stressed bolts, the problem of different deformability of bolts and welding is more acute when ensuring their joint operation in one combined joint. The paper attempts to investigate experimentally the operation of a bolted joint reinforced by welding, in which at the previous stage of operation, some of the deformations of the bolted joint crumpling have already occurred.

**Keywords:** Bolted joints · Welded joints · Combined joints · Reinforcement · Multiformative connections · Load-bearing capacity

## 1 Introduction

Steel frame elements can be connected by various types of fasteners, such as bolts, rivets, welds. Bolted connections are very common. When carrying out reconstruction, repair or reinforcement, it is often necessary to increase or restore the load-bearing capacity of bolted joints. The classic options used in practice are replacing existing bolts with high-strength ones, increasing the number of bolts, as well as their diameter. However, often, these options are not always possible to be applied, due to the limited dimensions of the unit or cross-section, as well as due to corrosion damage to the parts of the bolted joint and (or) the bolts themselves. In this case, the reinforcement can be made by applying welds. As a result, we get a combined bolt-welded joint, the load-bearing capacity of which must be determined. Due to the different deformability, the load-bearing capacity of the connection of such a joint is not the arithmetic sum of the individual components.

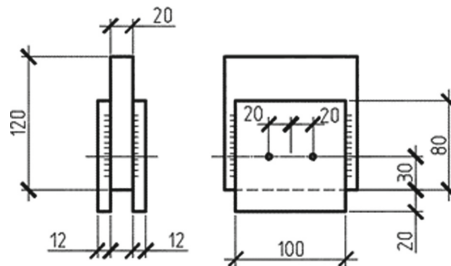
In national practice, the use of combined bolt-welded joints has long been prohibited. In the latest version of SP 13.16330.2017, paragraph 14.1.13 states: “Combined joints, in which part of the shear force is perceived by the friction joint, and part – by the welds, are used provided that the welding is performed after tightening the bolts to the calculated force and then tightening them when necessary. The distribution of force between the friction and welded joints should be taken in proportion to their load-bearing capacity. The use of bolts without controlled tension in combined joints, as well as the use of shear joints, is not allowed”.

Recently, a fairly large number of paper have been published, which present the results of studies of combined bolt-welded joints. In this direction, it is worth noting the works of Zhang D. X., Hou Z. X., and Sun L. [1], T.J. Manuel, G.L. Kulak [2], G.L. Kulak, G.Y. Grondin [3], M. S. Liu, C. A. Li, J. R. Huang, and J. S. Ju [4], Y. J. Shi, L. Wang, Y. Q. Wang [5], J. J. Wang, Y. J. Shi, Y. Q. Wang [6], Q. Chen, F. X. Li, J. Q. Lei [7].

## 2 Characteristics of Test Samples

This paper presents the results of an experimental evaluation of the load-bearing capacity of combined bolt-welded joints based on the test results of test samples. The sample is an overlapping joint of three sheet parts connected by two bolts and welds. The outer plates have dimensions of  $100 \times 100$  mm, 12 mm thick, the middle plate -  $120 \times 120$  mm, 20 mm thick. A general view of the design of the sample is shown in Fig. 1.

The sample is made of C345 steel. As bolts, bolts of ordinary strength of strength class 5.8 were used, the diameter of the bolts was 14 mm, and the diameter of the holes was 16 mm. The welds had a 6 mm weld leg, 60 mm weld length, semi-automatic welding method, Sv-08A wire  $\varnothing 1.5$  mm. To determine the actual bearing capacity of the combined bolt-welded sample and accounting collaboration of bolts and weld a value of the bearing capacity of samples with connections to the bolt and welding separately was pre-determined. For this purpose, the designed samples were divided into three groups, each of which had 2 samples. The samples of the first group were a bolted joint of accuracy class B. The samples of the second group were a welded joint with angular flank seams. The third group includes combined bolt-welded samples.



**Fig. 1.** General view of the design of combined samples.

The parameters of the samples and bolts were selected in such a way that the calculated maximum load on the sample with bolts is the value of the bearing capacity of the bolts according to the cut-off criterion.

Tests of bolted and welded samples were carried out in a universal hydraulic machine WEW-600D, with a load capacity of 60 tons, combined bolt-welded - in a press PMM-125, with a load capacity of 125 tons. Loading of samples of each group was carried out in stages, with an exposure time at each stage for three minutes. A general view of the design of bolted and welded samples is shown in Fig. 2.

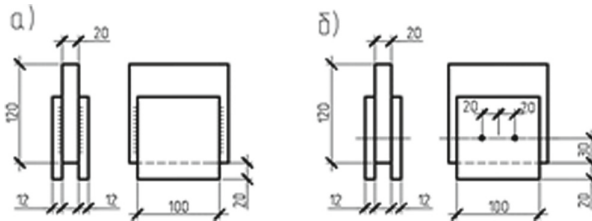


Fig. 2. General view of the design of the samples: a) welded sample; b) bolt sample.

### 3 Test Results

The value of the actual load-bearing capacity of the samples of the first group according to the test results was 171.04 kN and 183.72 kN. The estimated load-bearing capacity of bolted joint samples in accordance with SP 16.13330.2017 is 117.8 kN. Figure 3 shows a photo of the sample in the test unit and a diagram of the loading of the samples of the first group in the axes load (kN) - traverse stroke (mm). Figure 4 shows a photo of the bolted joint sample after testing. The estimated load-bearing capacity of samples of welded joints, in accordance with SP 16.13330.2017, is 218.9 kN. A general view of the test diagram of the samples of the second group is shown in Fig. 5.

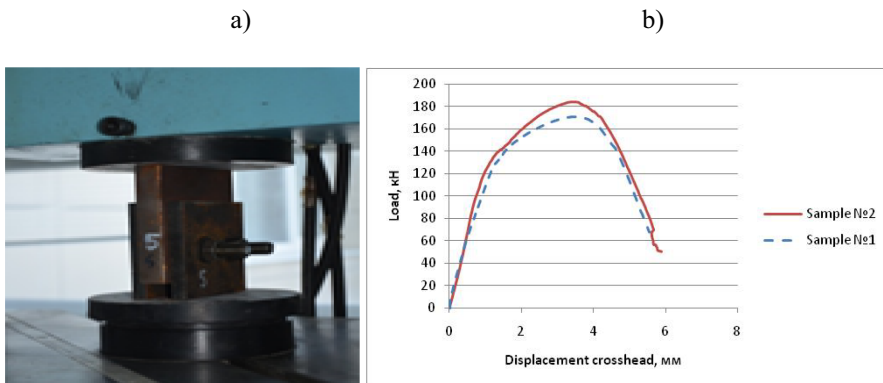


Fig. 3. Testing of samples of the first group a) sample photo in the installation; b) loading diagram.

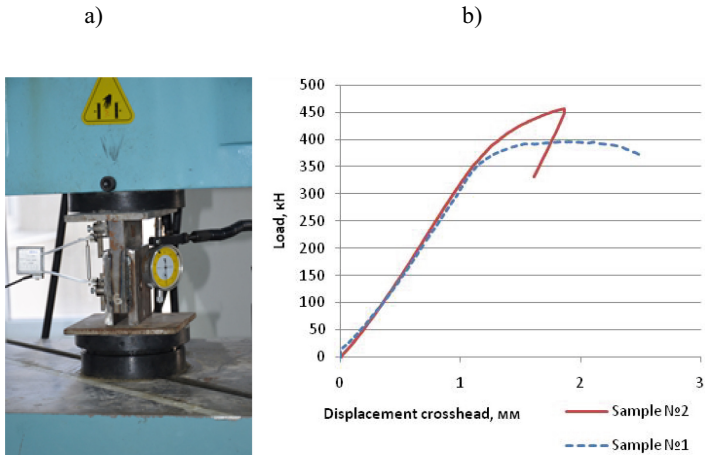
The actual load-bearing capacity of the welded joint samples is 456.5 kN and 395.8 kN. Such a significant difference in the load-bearing capacity of the two welded samples is explained by the deviations of the actual dimensions of the joint legs from the design values and, accordingly, the difference in the actual cross-section area of the welds. The destruction of the samples occurred on the seam metal.

In the tested samples, the actual cross-section areas of the joints were 13.31 cm<sup>2</sup> and 10.83 cm<sup>2</sup> with a design value of 10.2 cm<sup>2</sup>. The actual bearing capacity of 1 cm<sup>2</sup> of the weld of the samples is 34.29 kN/cm<sup>2</sup> and 36.54 kN/cm<sup>2</sup>, the average value is 35.41 kN/cm<sup>2</sup>.



**Fig. 4.** Photo of the sample of the first group after testing.

The design and testing of the samples of the third group was carried out as follows. First, a sample of the bolted joint was assembled, a load equal to 85% of the calculated bearing capacity (100 kN) was applied to it according to the bolt cut criterion, the sample was unloaded, then flank seams were applied.



**Fig. 5.** Testing of samples of the second group a) sample photo in the installation; b) loading diagram.



It is assumed that this test method corresponds to the bolted joint reinforcement scheme under load, when most of the deformations of the bolted joint have already been worked out before the welding seams are applied [8]. Thus, conditions were created for the joint work of different-formative connections, which closely corresponds to their real work after strengthening under load. After that, the combined sample was tested in a hydraulic press with an exposure time at each loading stage.

The destruction of the combined compound samples was brittle. The actual load capacity was 425 kN and 625 kN. Figure 6 shows a test diagram of the combined compound samples, as well as a photo of the sample during the tests.

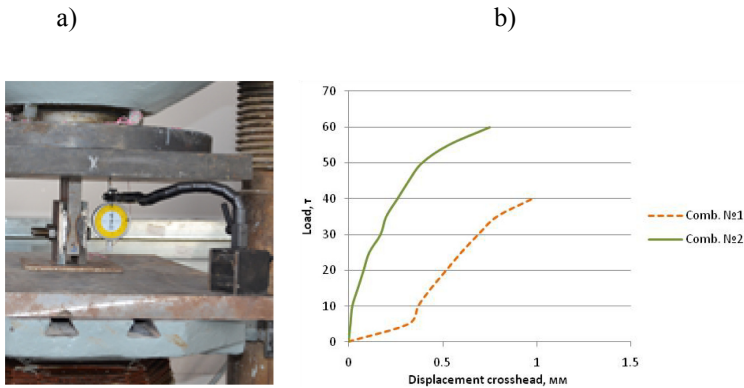


Fig. 6. Testing of samples of the third group a) sample photo in the installation; b) loading diagram.

## 4 Results Discussion

To determine the experimental value of the load-bearing capacity of each type of bond in the combined samples, the actual cross-section area of the welds in each of them was determined.

The actual cross-section areas of the welds in the samples of the third group were  $9.7 \text{ cm}^2$  and  $13.3 \text{ cm}^2$ . Taking into account the bearing capacity of  $1 \text{ cm}^2$  of the cross-section area on the seam metal, calculated on the basis of the test results of the welded samples (second group), equal to  $35.41 \text{ kN/cm}^2$ , the actual bearing capacity of the welds in the combined samples can be estimated at 343.12 kN and 472 kN.

Based on the analysis of the area of the slice weld samples as well as taking into account the size of the actual bearing capacity of the bolts, it can be stated that in the samples of the third group (mixed joints) was implemented conditions for joint work different-deformative connections. The actual load-bearing capacity of the combined joint samples exceeds the load-bearing capacity of the actual weld area in these samples by 81.9 kN and 153.0 kN, respectively. This difference can be considered as the “contribution” of the bolts to the load-bearing capacity of the combined joint.

The analysis of the test results of the samples gives the main calculated dependence for assessing the load-bearing capacity can be a formula of the form: there are reasons

to believe that in the design methodology of combined bolt-welded joints (when bolted joints are reinforced with welded seams)

$$[N]_{comb} = N_{reinf} + \alpha_{def} (N_{b,min} n_b - N_{reinf}) + [N]_{w,min} \quad (1)$$

where:  $N_{reinf}$  - the force perceived by the bolted joint before reinforcement;  $N_{b,min}$  - maximum design force for 1 bolt, the smaller of the two according to the cut-off or crumple criterion;  $n_b$  - number of bolts in the joint;  $\alpha_{def} \leq 1$  - a coefficient that takes into account the effect of increased deformability of the bolted joint in comparison with the welded joints on the joint operation of the bolts and welding in the combined joint.

## 5 Conclusion

The performed experimental studies give grounds to believe that the main components determined by the load-bearing capacity of combined bolt-welded joints in the method of their calculation three terms will be:

- the force perceived by the bolts in the joint at the time of the reinforcement by applying the welds, taking into account the actual loads on the structure;
- estimated load-bearing capacity of reinforcement welds (the lower of the cut-off conditions for the weld metal and the metal of the fusion boundary) [10];
- the difference between the calculated load-bearing capacity of the bolts (the lesser of the cut and crumple conditions in the bolted joint) [9], adjusted by a lowering factor to account for the greater compliance of the bolted joint, compared to the welds.

For a more complete analysis of the joint work of bolt-welded joints and a detailed method for calculating their load-bearing capacity, it is necessary to conduct a larger series of tests.

**Acknowledgements.** This work was realized in the framework of the Program of flagship university development on the base of the Belgorod State Technological University named after V G Shukhov, using equipment of High Technology Center at BSTU named after V.G. Shukhov.


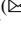

## References

1. Zhang, D.X., Hou, Z.X., Sun, L.: Nonlinear finite element analysis of shear bearing capacity of joint with combined bolts and welds. *Steel Constr.* **8**, 9–13 (2011)
2. Manuel, T.J., Kulak, G.L.: Strength of joints that combine bolts and welds. *J. Struct. Eng.* **3**, 279–287 (2000)
3. Kulak, G.L., Grondin, G.Y.: Strength of joints that combine bolts and welds. *Eng. Second Q. J.* **40**(2), 89–98 (2003)
4. Liu, M.S., Huang, C.A., Li, J.R., Ju, J.S.: Numerical modeling and mechanical analysis of combined connection with bolts and welds. *Strength Mater.* **48**(6), 862–869 (2017)
5. Shi, Y.J., Wang, L., Wang, Y.Q., et al.: Finite element analysis of the combined connection with bolts and welds. *Build. Sci. Res. Sichuan* **2**, 100–104 (2013)

6. Wang, J.J., Shi, Y.J., Wang, Y.Q.: Finite element analysis on the bearing capacity for connection of sharing on a shear load by friction-type high-strength bolts and side welds. *Build. Sci. Res. Sichuan* **1**, 15–19 (2013)
7. Chen, Q., Li, F.X., Le, J.Q., et al.: Tensile capacity and design method of combined connections with bolts and welds. *Eng. Mech.* **33**(1), 112–121 (2015)
8. Solodov, N.V., Vodyakhin, N.V.: On the features of application, design and calculation of combined bolt-welded joints . In: *Science and Innovations in Construction. Collection of Reports of the IV*, pp. 80–85. International Scientific and Practical Conference, Belgorod (2020)
9. Solodov, N.V.: Strength and deformability when collapsing in a bolted connection. *Bull. BSTU Named After V.G. Shukhov* **1**, 82–87 (2017)
10. Solodov, N.V., Vodyakhin, N.V.: Results of tests of a welded joint sample. In: *Science-Intensive Technologies and Innovations Jubilee International Scientific and Practical Conference Dedicated to the 60th Anniversary of BSTU Named After V. G. Shukhov, XXI Scientific Readings*, pp. 116–119. Belgorod State Technological University named after V. G. Shukhov, Belgorod (2014)



# The Structure of the Content and Cost of Materials in Bending Reinforced Concrete Element with Variable Section Height

V. S. Kuznetsov  and Yu. A. Shaposhnikova  

Moscow State University of Civil Engineering, Yaroslavskoe shosse, 26, Moscow 129337, Russia

**Abstract.** A new approach to optimization of linear reinforced concrete elements of variable height without prestressing reinforcement is proposed. It is based on the design situation, which is determined by the strength requirements of normal and inclined sections. At the same time, the design and design requirements for sections of various heights are fully met without the need to set the design compressed reinforcement. The study was carried out on the basis of taking into account the regularities of the resistance of reinforced concrete and the main provisions of the regulatory documents governing design and construction activities in the Russian Federation. Also used are the actual works of domestic and foreign scientists, corresponding to the research in this area. During the study, the results of strength calculations of normal and inclined sections were used, as well as the cost indicators of materials used for the manufacture of structures. The method of structural and analytical analysis was used using the correlation dependences of the factors under study. Analytical dependencies and graphic materials are presented that establish the optimal parameters of an element with a minimum cost of materials in order to use them in design practice. The proposed method for determining the efficiency of a structure, taking into account the cost indicators of materials, can be applied in design practice. Recommendations for design are given to ensure the construction of the minimum cost and meet the requirements of strength and durability.

**Keywords:** Inclined sections · Normal sections · Reinforcement · Reinforced concrete elements · Strength

## 1 Introduction

The cost of any prefabricated element includes the cost of the materials themselves: concrete, reinforcement, embedded parts and the cost of manufacturing the element. Works aimed at studying the content of components in a product in order to reduce its cost are always relevant both from a theoretical and practical point of view.

In the present study, the structure was considered with the required theoretical amount of reinforcement, ensuring the strength of the product and design requirements at various heights of the element cross-section. The volume of concrete of the product was calculated by geometric dimensions without taking into account its reduction due to the volume of reinforcement.

## 2 Literature Review

Many Russian and foreign scientists dealt with the problems of optimal design of reinforced concrete beams, for example, Karpenko N.I., Baikov V.N., Skladnev I.O., Alekseev A.V., Jensen C., Garstecki A. and many others.

The development of methods for calculating reinforced concrete structures was carried out by V.N. Baykov. And Karpenko N.I. In the works of Karpenko N.I. the general theory of deformation and destruction of reinforced concrete under various types of loading was formulated [1]. Baikov V.N. paid great attention to the development of calculation methods for precast concrete structures [2]. Skladnev N.N. was engaged in the problems of optimal design of reinforced concrete structures, taking into account reliability and efficiency. [3]. Tamrazyan A.G. and Alekseytsev A.V. studied the problems of optimization of structures taking into account the ratio of production costs and risks of material losses in emergency situations [4, 5].

Chakrabarty B.K. studied the relationship between beam cost and unit cost of materials and beam sizes [6]. Jensen C. and Lapko A. investigated the design of shear reinforcement in reinforced concrete beams [7]. Carlos Coello Coello, Filiberto Santos Hernández and Francisco Alonso Farrera, as well as Lee C. and Ahn J., used genetic algorithms for optimal design beams [8, 9]. Jiin-Po Yeh, Guerra A., Hare W. and others have studied the design optimization of reinforced concrete structures, including beams [10–12]. Also Garstecki A., Glema A. and Scigallo J. developed a software package for the optimal design of reinforced concrete beams and columns [13]. Demby Michal addressed the problem of the optimal and safe design of reinforcement structures in reinforced concrete elements [14]. Nemirovsky Ju. V. considers critical characteristics of concrete failure, such as shrinkage, temperature sensitivity, and the influence of production technology [15].

Currently, reinforced concrete structures in the Russian Federation are calculated in accordance with [16, 17]. In Europe, a regulatory document is used [18, 19], as well as various literature, for example, [20–22].

## 3 Methods and Materials

The cost of a precast concrete element  $C$  consists of the cost of concrete  $C_b$ , the cost of reinforcement  $C_a$  and the cost of manufacturing  $C_u$ . In this work, the cost of manufacturing  $C$  was not taken into account.

$$C = C_b + C_a \quad (1)$$

The cost of concrete is determined by the volume of the product  $V_b$  and the price of a cubic meter of concrete  $K_b$

$$C_b = K_b V_b \quad (2)$$

In the general case, the cost of reinforcement  $C_a$  is equal to the total cost of the lower longitudinal reinforcement  $C_s$ , the cost of the upper longitudinal  $C'_s$  of the transverse reinforcement  $C_{sw}$ , structural reinforcement  $C_{sk}$  and the cost of embedded parts  $C_{sd}$ .

$$C_a = \Sigma C_i = C_s + C'_s + C_{sw} + C_{sk} + C_{sd} \quad (3)$$

The cost of each component is determined by the amount of reinforcement, expressed by its weight or molding, and the price of the reinforcement of the applicable class.

As an object of research, we considered girders of rectangular cross-section without prestressing the reinforcement. The load is evenly distributed. Full design load  $q = 50.0$  kN/m. Structural length  $l = 5.68$  m, design span  $l_0 = 5.54$  m, section width  $b$ , height  $h$ . Concrete class B25,  $R_b = 14.5$  MPa, longitudinal reinforcement of class A400,  $R_s = 350$  MPa, transverse reinforcement of class A240. The variable parameter was the section height: 40 cm (1/13.85); 50 cm (1/11.08); 60 cm (1/9.23); 70 cm (1/7.91); 80 cm (1/6.93).

The price of concrete and reinforcement of various classes was established on the basis of a study of the reinforcement sales market in the central region of Russia. Accounting for the difference in prices was carried out by applying price correction coefficients. The price of reinforcement A400  $k_1 = 1.0$  was taken as the base price, then for A500C  $k_2 = 1.1$ , for A240  $k_3 = 0.80$ , for B500  $k_4 = 0.80$ . Clarification of prices for beam reinforcement leaves the possibility of obtaining more reliable results.

The cost of the lower longitudinal reinforcement is determined by its price  $K_s$  and quantity in terms of weight

$$C_s = K_s \gamma V_s = k_1 K_s G_s \quad (4)$$

The cost of the upper longitudinal reinforcement.

$$C'_s = K'_s \gamma V'_s = k_1 K'_s G'_s \quad (5)$$

The cost of additional longitudinal reinforcement with a section height  $h > 700$  mm, an additional longitudinal bar with a cross-sectional area is installed at the lateral edges of the element  $A'_{s1} \geq 0,001 \cdot 0,5b(h_0 - a')/2$ .

$$C'_{s1} = K'_{s1} \gamma V'_{s1} = k_1 K'_{s1} G'_{s1} \quad (6)$$

Here the  $\gamma$  - density of steel (7850 kg/m<sup>3</sup>). The number of longitudinal reinforcement  $V_s$  and  $V'_s$  is determined by the design cross-sectional area of the reinforcement  $A_s$  and  $A'_s$ , multiplied by the structural length of the element  $l$  minus the end cover, taken equal to 1 cm from each end. The required amount of longitudinal tensile reinforcement was determined under the condition,  $\xi \leq \xi_R$  in accordance with the requirements of [16, 17] from expression (7).

$$A_s = R_b b h_0 \left( 1 - \left( 1 - q l^2 / (4 R_b b h_0^2) \right)^{1/2} \right) / R_s \quad (7)$$

The amount of upper longitudinal reinforcement was taken as 20% of the design tensile reinforcement.

The cost of transverse reinforcement is

$$C_{sw} = K_{sw}\gamma V_{sw} = k_3 K_{sw} G_{sw} \quad (8)$$

The number of transverse reinforcement  $V_{sw}$  is determined by the design area of the transverse bars  $A_{sw}$ , their number and length equal to the section height minus 20 mm. The calculated area of transverse rods  $A_{sw}$  was determined in accordance with [16, 17] without considering inclined sections from the condition

$$Q \leq Q_{b1} + Q_{sw,1} \quad (9)$$

Here

$$Q_{b1} = 0, 5R_{bt}bh_0 \quad (10)$$

$$Q_{sw,1} = Q - Q_{b1} \quad (11)$$

$$Q_{sw,1} = q_{sw}h_0 \quad (12)$$

$$q_{sw} = R_{sw}A_{sw}/s_w \quad (13)$$

The spacing of the cross bars is determined from the design requirements. Knowing the intensity of the linear load  $q_{sw}$ , the calculated amount of reinforcement  $A_{sw}$  was determined.

$$A_{sw} = Q_{sw}s / h_0R_{sw} \quad (14)$$

The cost of structural reinforcement was determined as

$$C_{sk} = K_{sk}\gamma V_{sk} = k_3 K_s G_{sk} \quad (15)$$

Consumption of connecting structural reinforcement  $V_{sk}$  is determined by the calculated area of connecting rods  $A_{sk}$ , their number and length equal to the section width minus 20 mm.

## 4 Results and Discussion

The calculation results in weight and price terms are presented in the form of graphs (see Figs. 1, 2 and 3).

Figure 1 shows that quantitatively, the content of longitudinal reinforcement  $\Sigma A_s$  is 80–90% of the total amount of reinforcement, which significantly exceeds the content of transverse and structural reinforcement. An increase in structural reinforcement  $\Sigma A_{sk}$  with a height value of  $0.144l_0$  (800 mm) is associated with the need to install additional longitudinal bars at the lateral faces of the element. In price terms, the difference will be more significant, since for longitudinal reinforcement, as a rule, higher quality and, therefore, more expensive steels are used.

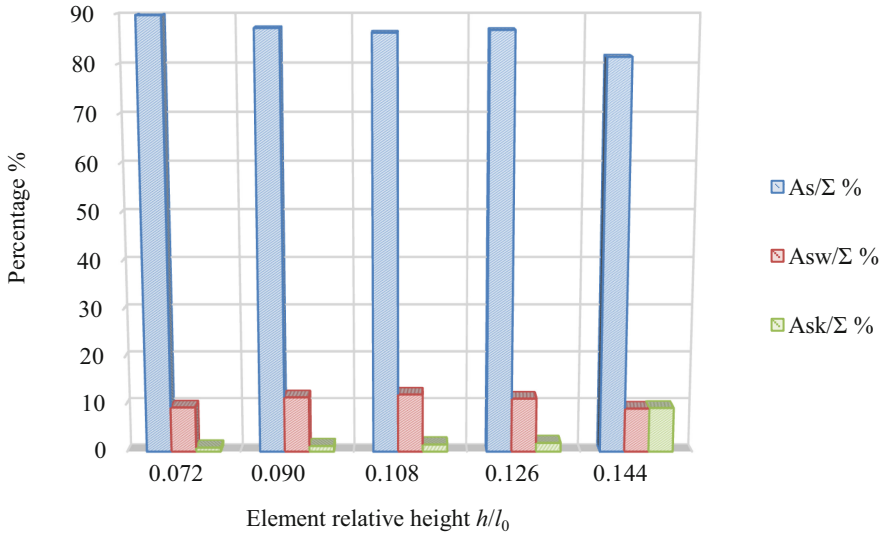


Fig. 1. Percentage of various fittings in the beam.

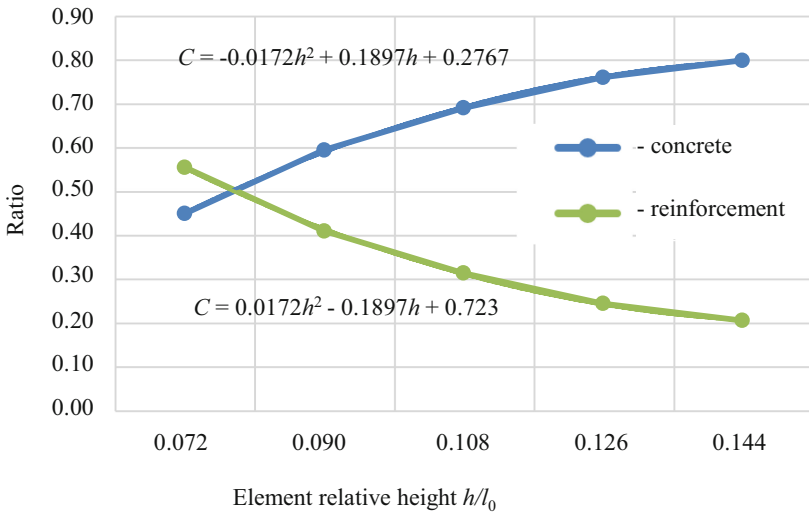


Fig. 2. Relative cost of concrete and reinforcement in a beam.

The relative cost of concrete and reinforcement in the total cost of the beam is presented in the graphs in Fig. 2. Obviously, with an increase in the height of the element, the cost of concrete increases, while the total cost of reinforcement decreases. Analytical dependencies that determine the cost of materials in an element are presented as a polynomial of the second degree.



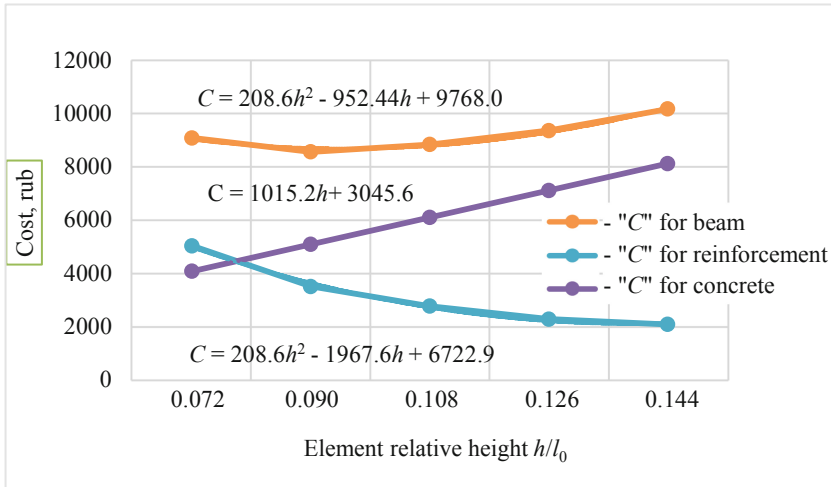


Fig. 3. Components of the cost of the beam.

Figure 3 shows graphs characterizing the change in the cost of the element as a whole, as well as of concrete and reinforcement, depending on the change in the height of the element. Obviously, the beams with the minimum cost of materials are in the range of heights  $(0.08\text{--}0.11)l_0$ .

## 5 Conclusion

The presented materials make it possible to envisage such ratios of concrete classes and reinforcement classes that, for given height ranges, lead to the creation of structures of minimum cost at the design stage of linear bending elements without prestressing.

## References

1. Karpenko, N.: General models of reinforced concrete mechanics. Stroyizdat, Moscow (1996)
2. Baykov, V., Sigalov, A.: Reinforced concrete structures. General course. Stroyizdat, Moscow (2009)
3. Skladnev, N.: Optimal design of reinforced concrete structures taking into account the requirements of profitability, manufacturability, reliability, durability, dissertation, Doctor of technical sciences, 05.23.01, Moscow (1979)
4. Alekseytsev, A., Tamrazyan, A.: Optimal design of load-bearing structures of buildings taking into account the relative risk of accidents. *Vestnik MGSU* **14**(7), 819–830 (2019)
5. Tamrazyan, A., Alekseytsev, A.: Modern methods for optimizing structural solutions for the bearing systems of buildings and structures. *Vestnik MGSU* **15**(1), 12–30 (2020)
6. Chakrabarty, B.K.: Models for optimal design of reinforced concrete beams. *Comput. Struct.* **42**(3), 447–451 (1992)
7. Jensen, B., Lapko, A.: On shear reinforcement design of structural concrete beams on the basis of theory of plasticity. *J. Civ. Eng. Manag.* **15**(4), 395–403 (2009)

8. Coello, C., Hernandez, F., Farrera, F.: Optimal design of reinforced concrete beams using genetic algorithms. *Expert Syst. Appl.* **12**(1), 101–108 (1997)
9. Lee, C., Ahn, J.: Flexural design of reinforced concrete frames by genetic algorithm. *J. Struct. Eng.* **129**(6), 762–774 (2003)
10. Yeh, J.-P., Yang, R.-P.: Optimal design of continuous reinforced concrete beams using neural networks. *Trans. Mach. Learn. Artif. Intell.* **3**(4) (2015)
11. Guerra, A., Kioussis, P.: Design optimization of reinforced concrete structures. *Comput. Concr.* **3**(5), 313–334 (2006)
12. Hare, W., Nutini, J., Tesfamariam, S.: A survey of non-gradient optimization methods in structural engineering. *Adv. Eng. Softw.* **59**, 19–28 (2013)
13. Garstecki, A., Glema, A., Ściagałło, J.: Optimal design of reinforced concrete beams and frames. *Comput. Assist. Mech. Eng. Sci.* **3**(3), 223–231 (1996)
14. Demby, M., Scigallo, J.: Design aspects of the safe structuring of reinforcement in reinforced concrete bending beams. *Procedia Eng.* **172**, 211–217 (2017)
15. Nemirovsky, Ju.: Problems and Methods of Structural Design of Reinforced Concrete Constructions. *Izvestiya of Altai State University* (2014)
16. SR 63.13330.2012 Concrete and reinforced concrete structures. The main provisions. Updated edition of SNiP 52–01–2003. Moscow (2015)
17. SR 52–103–2007. Monolithic reinforced concrete structures of buildings. M, 2007. A guide for the design of concrete and reinforced concrete structures made of heavy concrete without prestressing reinforcement (to SR 52–101–2003). Moscow (2005)
18. EN 1992 Eurocode 2: Design of concrete structures (2004)
19. BS8110 British Standart. Structural use of concrete (2010)
20. Seinturiere, P.: Service Limit State, IUT, Civil Engineering of Grenoble (2006)
21. Paille, G.: Calculation of reinforced concrete structures. AFNOR, Paris (2013)
22. Kuznetsov, V., Shaposhnikova, Yu., Yandiev, A.: Selection of the optimal parameters of a reinforced concrete rectangular beam with single reinforcement. In: *IOP Conference Series: Materials Science and Engineering (MSE)*, vol. 962 (2020)



# Brief Overview of Complex Cadastral Works: Experience in Conducting

O. Yu. Kononova  and N. M. Zatolokina  

Belgorod State Technological University named after V.G. Shukhov, Belgorod, Russia

**Abstract.** Currently, the state is trying to create a full-fledged database that would contain information about absolutely all real estate objects, including storage facilities located on the territory of the Russian Federation, in particular about their borders. The unified state register of real estate – (USRRE) is the only state reliable source of information about real estate objects, rights and encumbrances on real estate objects on the territory of the Russian Federation. URRE information is required for transactions, property valuation, and other real estate transactions. However, the information of the USRRE is currently not always accurate and reliable, and therefore, the task of filling the USRRE database is very acute for the state. Thus, since mid-2015, with the introduction of changes to the land legislation, it became possible to conduct complex cadastral works (CCW). In accordance with the legislation, complex cadastral works became possible from June 1, 2015. This article describes the current procedure for organizing and conducting complex cadastral works, provides practical experience in conducting complex cadastral works.

**Keywords:** Cadaster · Complex cadastral works · Registration of rights · Results of complex cadastral works · Land category · Land plots · Unified state register of real estate

## 1 Introduction

An integral part of the tasks of ensuring the socio-economic development of the country, solving social, economic and environmental problems, improving the quality of life of the population and promoting regional development is the introduction and development of a unified state system of registration of rights and cadastral registration of real estate. Federal target program “Development of the unified state system of registration of rights and cadastral registration of real estate (2014–2020)” [3], which was approved by resolution of the RF Government dated 10.10.2013 No. 903, is the basis for the development of all the constituent entities of the Russian Federation, the unified registration system.

Within the framework of this program, event No. 25 “Carrying out complex cadastral works” is provided. The main purpose of complex cadastral works (hereinafter referred to as CCW) is determined by the state policy to increase the investment attractiveness and efficiency of taxation at the regional level. According to the evaluation criteria of this program, one of the key indicators is the percentage of land plots (hereinafter - LP) with

borders registered in the Unified State Register of Real Estate (hereinafter – USRRE), in the total number of all LP registered in the USRRE [1].

These characteristics are primarily economic characteristics, because they directly affect the cadastral value of the object (which affects both the rent and the purchase price in the administration, etc.) and the calculated tax.

Currently, the state is striving to create a full-fledged database that would contain information about absolutely all immovable objects, including storage facilities, located on the territory of the Russian Federation, in particular about their borders. According to the results of the first quarter of 2020, in the territory of the Russian Federation, the number of storage units, information about which is included in the USRRE, is 60.5% (36,739,254 units), with a total of 60,719,141. This means that only 60.5% of the land tax is calculated based on the actual occupied area [8].

A slight increase in the separated land plots is due to the fact that at present this procedure is carried out by an independent decision of the owners of real estate, who, in turn, do not seek to bear the time and financial costs of processing all the necessary documents [13].

Thus, in the country there was a need to organize such events that will allow updating the information of the USRRE quickly and accurately. The way to solve the above problem is CCW.

## 2 Methods and Materials

CCW refers to cadastral works that are performed simultaneously in respect of all real estate objects located on the territory of one cadastral quarter or on the territories of several adjacent cadastral quarters.

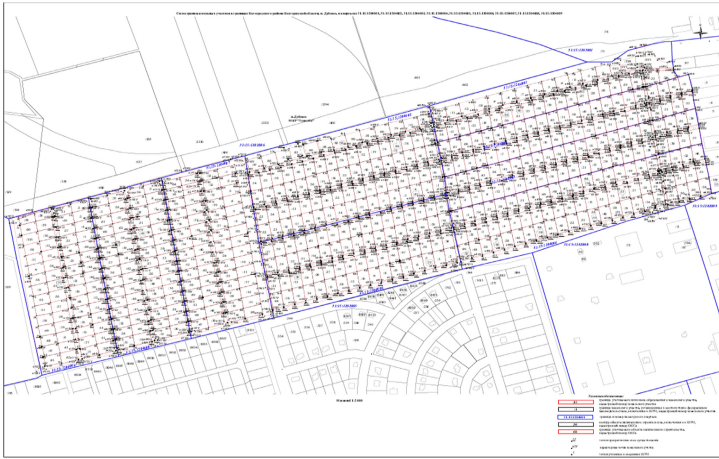
Thus, CCW will be carried out in relation not only to the storage facilities, but also to capital construction objects (CCO) within the boundaries of a specific territory [11, 12].

Law No. 221 establishes a list of objects in respect of which CCW can be performed. Among them are, for example: LP, USRRE information about which does not meet the established requirements for describing the location of the borders of the LP; buildings, structures (with the exception of linear objects), as well as objects of unfinished construction, information about which is contained in the URRE [2].

An important factor is that the repeated implementation of the CCW on the territory of a certain cadastral quarter is not allowed.

The procedure for performing CCW is established and regulated by the chapter 4.1. “Complex cadastral works” of the Federal Law “On Cadastral Activities” of 24.07.2007 No. 221-FZ.

In order to ensure consultation of interested parties established by the location of boundaries of the LP the customer of CCW must place on its website the draft map-plan of the territory simultaneously with notification of the meeting of the conciliation commission on the issue of coordination of the location of the borders the LP with the simultaneous direction to: the executive body of state power of a subject of the Russian Federation on the territory of which are CCW, for posting on its official site; the body of



**Fig. 1.** Fragment of the map-plan of the territory “Map of the borders of the LP within the borders of the Topolek microdistrict of the Belgorod district”.

the registration of rights to be placed on its official website; the conciliation commission [9].

The result of CCW is ensured by the following: clarification of the location of boundaries of LP by establishing or updating the location in the LP of buildings, structures, objects of unfinished construction; education is provided by the memory, on which the buildings, including apartment buildings, structures, except the structures are linear objects; provides LP formation for general use, busy squares, streets, roads, embankments, squares, boulevards, water bodies, beaches and other objects; correction of registry errors in the information about the location of the boundaries of real estate objects is provided (Fig. 1).

In 2017 and in 2019, CCW were conducted on the territory of the Belgorod district of the Belgorod region.

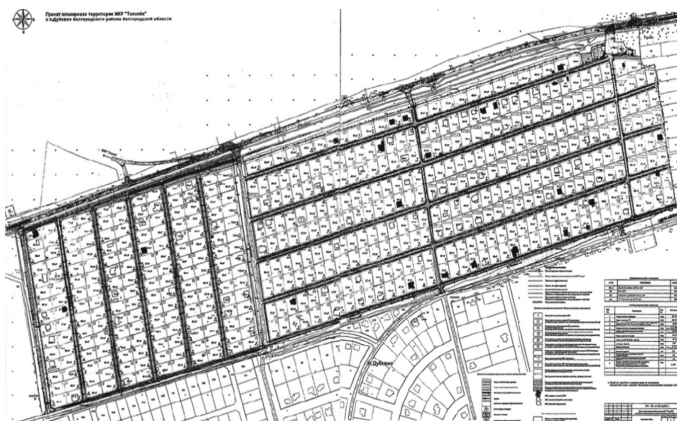
The Government of the Belgorod district adopted Order No. 613 of December 19, 2016 “On the arrangement of CCW on the territory of the Belgorod district”, within the framework of which the Department of Property and Land Relations of the Belgorod district developed a project: “Implementation of CCW on the territory of settlements of the Belgorod district (in pilot municipalities)” [4].

The analysis of the implementation of the CCW showed that it is a complex and multifunctional form of state land use management. These works cover several areas of activity in the field of land relations: from obtaining the coordinates of the borders of LP and other real estate objects to entering them into the URRE, from resolving land disputes to directly regulating the tax base [10].

In the budget of Belgorod district in 2017 was provided funds in the amount of 3 215 000, 00 rubles for the conclusion of a contract for the CCW, to conduct CCW in the amount of 7 603 961.16 rubles including subsidies [4, 5].

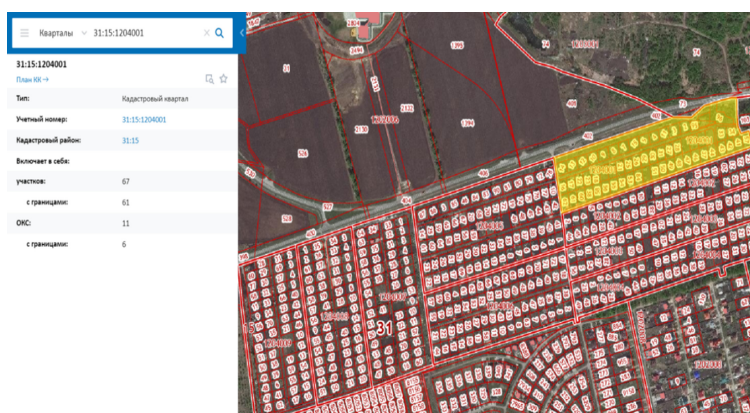
CCW in the Belgorod district of the Belgorod region were conducted on the territories of horticultural associations. Selection criteria of the territory to perform the CCW is

the presence of a surveying project (or project of arrangement and development of the territory for the horticultural and vegetable associations of citizens) (Fig. 2), and the share of the LP that are not on the cadastral account in the “coordinate” or reported errors in the corresponding quarter of not less than 30% [6, 7].



**Fig. 2.** Project of territory planning within the boundaries of the Topolek microdistrict of the Belgorod district.

As a result, the CCW was carried out on the territory of 15 cadastral blocks – this is 176.07 hectares, information about 1707 real estate objects was entered into the URRE database. Thus, in relation to 1707 objects, information on the boundaries and area of objects was updated in the URRE database, which will ensure the correct establishment of the cadastral value of objects, and as a result, a fair amount of tax and other values (Fig. 3).



**Fig. 3.** The result of the CCW - all land plots on the territory of the cadastral quarter with established borders.

### 3 Results and Discussions

Also, one important and positive experience of the CCW is the following. As practice showed, the implementation of CCW in the territory involved in urban planning activities simplifies and accelerates the task of changing the type of permitted use and boundaries of land plots. In this connection, the project of planning (the project of land surveying) was approved, which provides for an increase in public land by reducing the gardening plots of citizens for communications and the organization of driveways. As a result of the implementation of the CCW, information was entered about the boundaries of all the LP in full accordance with the approved draft layout. Citizens did not have to prepare their own land management documents, apply to the state registration authorities for changes and bear the associated costs.

On the other hand, when implementing the measures provided for by the current legislation in the field of CCW, local government employees and cadastral engineers encountered a number of problems that made it difficult to carry out these works.

For example, here are some of them:

1. Two blocks of the territory of one horticultural association, which were included in the objects of the CCW due to the presence of a large number of registry errors in the information of the URRE regarding the location of the LP (their coordinates are incorrectly determined), are located in different rural settlements. Despite the fact that the project of arranging the land of the horticultural association is a single document, in accordance with the current legislation, it was necessary to create two conciliation commissions on the territory of each rural settlement. To resolve this issue, at the legislative level, it is necessary to provide for the possibility of forming a conciliation commission by the local self-government body of the municipal district not only in relation to the inter-settlement territory, but also taking into account the location of objects on the territory of two or more settlements.
2. The cadastral division has conditional borders on the area. In some cases, the boundaries of the cadastral quarter include territories that are not connected by a single planning space, a planning project, or a project for arranging the territory of the HCA, which makes it difficult to include these cadastral quarters in the list for conducting the CCW.
3. The mass allotment of land for the organization of horticultural associations took place in the Belgorod region mainly in the period from 1990–1996. During the same period, projects for the organization and development of horticultural associations were approved. For a long time, the procedure of land use in some cases, significantly changed, the parcel gardening associations differed from the project, the land area increased, and then decreased by more than 10%, which also complicated the task assigned to cadastral engineers.
4. Irrelevant data in the URRE statements about the addresses of copyright holders, which leads to the impossibility of notifying all interested parties in full.
5. Parallel registration of the state cadastral registration of the LP by the owners of the LP during the CCW.
6. Obstruction by the owners of the LP and CCO to the implementation of the CCW.

In 2019, only two cadastral quarters on the territory of the Belgorod district were selected for the CCW, according to the results, information on 274 real estate objects was entered into the URRE database.

As a result of the CCW both in 2017 and in 2019, the following result can be noted:

- the location and area of all previously recorded LP located on the territory of cadastral quarters selected for the CCW was clarified
- on the territory of the cadastral districts the LP under lands of the public (the roads) were formed.

## 4 Conclusion

Summing up, it can be noted that the CCW can significantly improve the quality of the data contained in the URRE due to the mass entry of information about the boundaries of all the LP in the cadastral quarter, the cadastral registration of which is carried out. This ensures both the protection of property rights of citizens and legal entities, as well as the formation of the tax base, the improvement of land and property relations, and in the future-increasing the investment attractiveness of the region. It is also worth noting that the results of the CCW allow to simplify and speed up the registration of rights to the land, correct registry errors in the location of the boundaries of real estate objects without financial and time costs for the owners of the land, and reduce the number of land disputes.

**Acknowledgements.** This work was realized in the framework of the Program of flagship university development on the base of the Belgorod State Technological University named after V G Shukhov, using equipment of High Technology Center at BSTU named after V G Shukhov.

## References

1. Zatolokina, E.I., Chernikova, A.M.: Cadastral work in relation to land plots. *Vector Geosci.* **3**(1), 46–50 (2020). <https://doi.org/10.24411/2619-0761-2020-10005>
2. Kononova, O.Y., Zatolokina, N.M.: Cadastral challenges of forest resource surveying in Belgorod oblast. In: *IOP Conference Series: Earth and Environmental Science*, vol. 459, no 4, p. 042041 (2020)
3. Khabarova, I.A., Khabarov, D.A., Popova, O.O., Kozhevnikov, V.A.: Digitalization of the cadastral registration process. *Vector Geosci.* **2**(3), 55–61 (2019)
4. Federal Law No. 221-FZ of 24.07.2007 “On cadastral activity” [Electronic resource]. [https://www.consultant.ru/document/cons\\_doc\\_LAW\\_70088/](https://www.consultant.ru/document/cons_doc_LAW_70088/)
5. Khabarova, I.A., Khabarov, D.A., Valiev, D.S., Chugunov, V.A.: Cadastral works in the case of refining the boundaries of the land plot. *Vector Geosci.* **3**(1), 51–61 (2020). <https://doi.org/10.24411/2619-0761-2020-10006>
6. Decree of the Government of the Russian Federation of October 10, 2013 No. 903 “On the Federal target program” Development of the unified state system of registration of rights and cadastral registration of real estate (2014–2020) [Electronic resource]. <https://base.garant.ru/70474300/>



7. Kara, K.A.: Determining the cadastral value of real estate properties with account of the current legislation. *Vector Geosci.* **1**(1), 51–58 (2018)
8. Order of the government of the Belgorod district dated December 19, 2016 No. 613-RP “on the organization of complex cadastral works on the territory of the Belgorod region” [Electronic resource]. <https://docs.cntd.ru/document/444922819>
9. Atamanov, S.A., Grigorév, S.A.: The use of voice assistants in cadastral activities. *Vector Geosci.* **1**(2), 65–69 (2018)
10. Order of the administration of the Belgorod district from 3.02.2017 No. 109 “on carrying out complex cadastral works on the territory of the Belgorod district” [Electronic resource]. <https://belrn.ru/2017/03/20/rasporyazhenie-administracii-belgorodskogo-rajiona-ot-3-02-2017-g-109/>
11. Zatulokina, N.M., Gubarev, S.A.: The use of unmanned aerial vehicles for carrying out cadastral works. *Vector Geosci.* **3**(3), 51–54 (2020). <https://doi.org/10.24411/2619-0761-2020-10031>
12. Action Plan (road map) for the implementation of complex cadastral works on the territory of the Belgorod district in the framework of the Federal target program “Development of the unified state system for registration of rights and cadastral registration of real estate (2014–2020)”
13. Zatulokina, N.M., Kurochkina, K.A., Lukashova, N.V.: Geological geomorphological analysis of the town of Belgorod. In: *IOP Conference Series: Earth and Environmental Science*, vol. 459, no. 4, p. 042041 (2020)



# Influence of Shear Deformations on the Buckling of Reinforced Concrete Elements

S. Yu. Savin  

National Research Moscow State University of Civil Engineering, Moscow, Russia  
savinsyu@mgsu.ru

**Abstract.** When constructing design diagrams of reinforced concrete bearing systems of buildings and structures using a bar or plate analogy between structural elements and their models, as a rule, absolutely rigid adhesion of reinforcement to concrete is implied, which does not fully reflect the nature of their actual joint work in areas with a high gradient stresses, for example, at the joints of the column with the girder. In this regard, the paper proposes a deformation model of eccentrically compressed reinforced concrete bar elements, taking into account shear deformations in the contact zone of reinforcement and concrete in areas with a high stress gradient. The obtained analytical dependences can be used to analyze the stability of the deformed states of eccentrically compressed reinforced concrete elements of the frames of buildings and structures.

**Keywords:** Reinforced concrete · Composite bar · Buckling · Cohesion · Shear deformation · Stability analysis

## 1 Introduction

Analysis of emergencies with capital construction objects [1–3] that occurred in recent decades, such as the collapse of the Hotel New World (1986, Singapore), the Sam-pun shopping center (1995, Seoul, Republic of Korea), the collapse of the Basmany market (2006, Moscow, Russia), the eight-story Rana Plaza building (2013, Savar, Bangladesh), Maxima Shopping Center (2013, Zolitude, Latvia), the Synagogue Church Of All Nations (2014, Lagos State, Nigeria), Xinjia Express Hotel (2020, Quanzhou, Fujian Province, China), etc., shows that the destruction of reinforced concrete structures of load-bearing systems of buildings and structures in many cases occurs after some time has elapsed since the completion of their construction and commissioning. This scenario of collapse is the most dangerous because it leads to catastrophic consequences: a large number of human casualties and significant material damage. With regard to reinforced concrete frames of buildings and structures of normal and increased levels of responsibility according to [4], in order to reduce the risk of developing such a scenario of progressive collapse after the sudden removal of one of the elements of the bearing system, at the stage of calculation justification of the adopted design decisions, it is necessary to take into account not only the physical nonlinearity of materials and the geometric nonlinearity of elements during their short-term loading, but also the growth

of deformations developing in time due to creep, as well as the accumulation of environmental [5, 6] or mechanical damage [7]. All this leads to a change in the stiffness and, as a consequence, to a redistribution of efforts in the elements of the bearing system, i.e., changes in the design scheme of the structure in time.

You should also pay attention to the fact that when constructing design schemes, as a rule, bar or plate analogies are used to model the work of load-bearing elements of the frames of buildings and structures. Within the framework of such modeling, as a rule, absolutely rigid adhesion of reinforcement to concrete is implied, which does not fully reflect the nature of their actual joint work in areas with a high stress gradient, for example, at the junctions of a column with a girder [8, 9].

Experimental, numerical and theoretical studies of the adhesion of reinforcement to concrete [8–11] have shown that adhesion is influenced by a number of factors: the resistance of concrete to axial tension, the type of reinforcement surface and its diameter, the presence or absence of pre-stress, etc. In studies [12] under dynamic loading of a reinforced concrete element, an increase in the adhesion resistance of reinforcement to concrete by more than 1.3 times was observed at a loading rate of  $1 \text{ N}/(\text{mm}^2 \cdot \text{ms})$ . At the same time, in reinforced concrete elements subject to long-term action of force and environmental factors, the adhesion parameters can decrease with time due to changes in the stress-strain state of the elements, strength and deformation characteristics of the concrete matrix [5, 6].

In this regard, the purpose of this work is to construct design dependencies and methods for analyzing the stability of the deformed state of rod elements of reinforced concrete frames of buildings and structures, taking into account shear deformations along the contact surface of reinforcement and concrete.

## 2 Methods and Materials

Consideration of the effect of shear deformations along the contact surface of reinforcement and concrete on the bending stiffness of a composite section of a reinforced concrete bar element (Fig. 1, a) under eccentric compression will be performed using the theory of composite bars and plates with shear and transverse links distributed over the surface, proposed by A.R. Rzhanitsyn [13], following which the equilibrium condition for a composite rod (Fig. 1, b) can be written as:

$$\begin{cases} M = M^0 + M_i^T, \\ N_i = N_i^0 - T_i, \end{cases} \quad (1)$$

where  $M^0 = M_i^0 + M_{i+1}^0 + M_{i-1}^0$ ;  $M_i^T = -T_i c_i$ ;  $T_i = \int_0^x \tau_i dx$ .

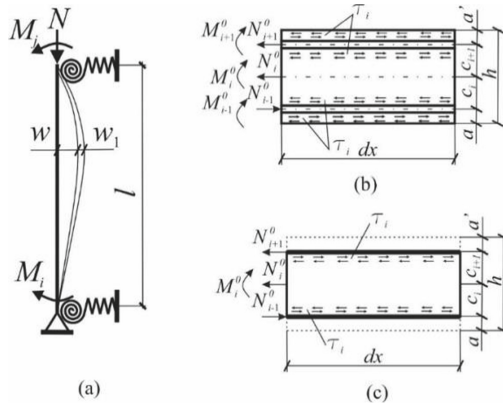
Here  $M_i^0$ ,  $M_{i+1}^0$ ,  $M_{i-1}^0$  are the moments in the rods of the composite element obtained under the assumption that there are no adhesion forces between them. Since the dimensions of the cross-sections of the reinforcing bars are small compared to the dimensions of the cross-section of the entire reinforced concrete element, in what follows we will assume that the moments in the reinforcing bars are equal to zero, and the tangential forces acting on the surface of the reinforcing bar, we will refer to the axis passing

through the center of gravity of its cross-section (Fig. 1, c). The assumptions made are in good agreement with the generally accepted model used to calculate bending and eccentrically compressed members.

$N_i^0$  is the resultant of normal forces in the bar from an external load, provided that there are no adhesion forces between the bars of the composite element (in this case, between the reinforcement and the concrete matrix);

$\tau_i$  - conditional shear stresses acting on the contact surface of reinforcement and concrete. They are called conditional because the actual nature of the stress distribution in a concrete cylinder adjacent to a reinforcing bar is a rather complex scheme.

In this case, we assume that the stiffness of the cross-links is large enough to consider them infinitely stiff within the framework of the developed model. This assumption allows us to reduce the number of unknowns in the resolving equations.



**Fig. 1.** Design scheme: an eccentrically compressed rod element (a), an elementary section of an eccentrically compressed reinforced concrete element (b), a modified design scheme of an elementary section of an eccentrically compressed reinforced concrete element (c).

### 3 Results and Discussion

Taking into account expression (1), shear deformations of reinforcing bars can be written as:

$$\begin{aligned} \Gamma'_1 &= \frac{T''_1}{\xi_1} = \Delta_{11}T_1 + \Delta_{12}T_2 + \frac{\sum N_0}{\sum B_{M,red}}c_1w + \Delta_{10}; \\ \Gamma'_2 &= \frac{T''_2}{\xi_2} = \Delta_{12}T_1 + \Delta_{22}T_2 + \frac{\sum N_0}{\sum B_{M,red}}c_2w + \Delta_{20}, \end{aligned} \quad (2)$$

where

$$\begin{aligned} \Delta_{10} &= \frac{N_1^0}{B_{N,red,1}} - \frac{N_0^0}{B_{N,red,0}} - \frac{M^0c_1}{\sum B_{M,red}}; & \Delta_{20} &= \frac{N_2^0}{B_{N,red,2}} - \frac{N_1^0}{B_{N,red,1}} - \frac{M^0c_2}{\sum B_{M,red}}; \\ \Delta_{11} &= \frac{1}{B_{N,red,1}} + \frac{1}{B_{N,red,0}} + \frac{c_1^2}{\sum B_{M,red}}; & \Delta_{22} &= \frac{1}{B_{N,red,2}} + \frac{1}{B_{N,red,1}} + \frac{c_2^2}{\sum B_{M,red}}; \end{aligned}$$

$$\Delta_{12} = \Delta_{21} = \frac{c_1 c_2}{\sum B_{M,red}}.$$

In these expressions, the following designations are accepted:  $\Gamma'_1, \Gamma'_2$  are shear deformations;  $T_1, T_2$  are total shear forces acting on the contact surface of the reinforcing bar and concrete;  $\xi_1, \xi_2$  are shear stiffness coefficients of the contact surface of reinforcing bars and concrete, determined from the diagrams  $\tau - \Gamma'$ ;  $B_{N,red,1}$  is the compressive (tensile) stiffness of the cross-section of the concrete matrix taking into account the deformed state  $B_{N,red,0}, B_{N,red,2}$  are respectively, the stiffness of the cross-sections of the reinforcing bars tension (compression) taking into account the deformed state;  $\sum B_{M,red}$  is the bending stiffness of the cross-section of the concrete matrix under the assumption that there are no adhesion forces along the contact surface of the reinforcement and concrete, taking into account the deformed state;  $c_1, c_2$  are the distances between the centers of gravity of the reinforcing bars and the concrete matrix, taking into account the deformed state;  $\sum N^0$  is the sum of longitudinal forces acting in reinforcement and concrete, obtained under the assumption of the absence of cohesion forces;  $w$  - displacement of the elastic axis of the eccentrically compressed reinforced concrete element.

The equilibrium equation of the deformed state of an eccentrically compressed composite bar element (Fig. 1, a), following the approach proposed in [14] for a reinforced concrete bar element without regard to shear, can be written in increments as follows:

$$\sum B_{M,red} w_1'' + N w_1 = - \sum N_i \left( e_0 + e_i \frac{x}{l} + e_j \left( 1 - \frac{x}{l} \right) \right) + \sum T_i c_i, \quad (3)$$

where  $w_1$  is the increment in the deflection of the elastic line of the composite bar;

$N$  - external longitudinal force acting on a composite bar element;

$e_0 = e_0(x)$  is initial deflection of the elastic line of the composite bar element;

$e_i, e_j$  are calculated eccentricities at the ends of a composite bar element, defined as the ratio of bending moments applied to the end sections to the longitudinal force.

To determine the deformed state of a rod eccentrically compressed reinforced concrete element, taking into account shear deformations along the contact surface of reinforcement and concrete, Eq. (3) must be solved together with system (2). In this case, the increments of the deflection  $w_1$  should be replaced by its absolute value  $w$ .

In the first approximation, let us set the functions of the shear forces  $T_i$  and the deflection  $w$  in the form of a half-wave of a sinusoid:

$$T_i = \alpha_i \sin \chi x; \quad w = \alpha_w \sin \chi x, \quad (4)$$

where  $\alpha_i, \alpha_w, \chi$  are some parameters corresponding to the boundary conditions of the problem.

Taking into account the substitution of expression (4), the system of Eqs. (2), (3) can be written in matrix form:

$$[\alpha_k] \times [\Delta_{kj}] \times \sin \chi x = [\Delta_{k0}]. \quad (5)$$

where  $[\alpha_k]^T = [\alpha_1 \ \alpha_2 \ \alpha_w]$  is the matrix of unknown parameters from expression (4);

$$[\Delta_{kj}] = \begin{bmatrix} \left(\Delta_{11} + \frac{\chi^2}{\xi_1}\right) & \Delta_{12} & \frac{\sum N_i}{\sum B_{M,red}} c_1 \\ \Delta_{21} & \left(\Delta_{22} + \frac{\chi^2}{\xi_2}\right) & \frac{\sum N_i}{\sum B_{M,red}} c_2 \\ \frac{\sum N_i}{\sum B_{M,red}} c_1 & \frac{\sum N_i}{\sum B_{M,red}} c_2 & \left(\frac{(\sum N_i)^2}{\sum B_{M,red}} + \chi^2 \sum N_i\right) \end{bmatrix},$$

$$[\Delta_{k0}]^T = [\Delta_{10} \ \Delta_{20} \ \Delta_{w0}], \Delta_{w0} = -\frac{\sum N_i}{\sum B_{M,red}} \sum N_i \left(e_0 + e_i \frac{x}{l} + e_j \left(1 - \frac{x}{l}\right)\right).$$

The solution of the matrix Eq. (5) by the step-iterative method under the assumption of a nonlinear elastic law of concrete deformation makes it possible to find the deformed state of an eccentrically compressed element for given parameters of the impact.

When assessing the stability of this deformed state, we will assume that a small perturbation causing the deviation of the elastic axis of the composite bar element from its equilibrium deformed state is caused only by the increment in deformation. Then the right-hand side of matrix Eq. (5), which is the increment of the moment external to the rod, can be equated to zero  $[\Delta_{k0}] = 0$ , and in the expressions for the stiffness of the cross-sections it is necessary to replace  $2\hat{e}_{bt}$  and  $2\hat{e}_b$  by  $\hat{e}_{bt}$  and  $\hat{e}_b$ , respectively, in order to go from the stiffness of the sections to their resilience that is the ability to balance infinitely small increments of external forces.

## 4 Conclusion

Analysis of the results of studies on the adhesion of reinforcement and concrete presented in the scientific literature shows that shear deformations in the contact zone of reinforcement and concrete can have a significant effect on deformation and destruction in areas with a high stress gradient. Such areas in the reinforced concrete frames of buildings include nodal connections, which, in the scenario of removing a column, are overloaded.

The paper proposes a model to take into account the effect of shear deformations in the contact zone of longitudinal reinforcing bars and concrete on the buckling of eccentrically compressed reinforced concrete elements.

Prospects for further research in this direction can be associated with solving the problem with fuzzy boundary conditions with respect to shear forces. It seems that such a solution can be found on the basis of a combined approach, including preliminary modeling using 3D models of characteristic nodal joints or elements, as well as the proposed model for accounting for shear deformations.





## References

1. Adam, J.M.: Research and practice on progressive collapse and robustness of building structures in the 21st century. *Eng. Struct.* **173**, 122–149 (2018)
2. Abdelwahed, B.: A review on building progressive collapse, survey and discussion. *Case Stud. Constr. Mater.* **11**, e00264 (2019)

3. Kiakojouri, F., De Biagi, V., Chiaia, B., Reza Sheidaii, M.: Progressive collapse of framed building structures: current knowledge and future prospects. *Eng. Struct.* **206**, 110061 (2020)
4. Standard of RF GOST 27751-2014 [Reliability of building structures and foundations. Basic provisions. Moscow: JSC “Research Center” Construction (2019)
5. Bondarenko, V.M.: Exposition of the stability of reinforced concrete columns operated in an aggressive environment. *Stroitel'naya mekhanika i raschet sooruzheniy* **3**(254), 27–34 (2014)
6. Kolchunov, V.I., Kolchunov, V.I., Fedorova, N.V.: Deformation models of reinforced concrete under special influences. *Promyshlennoye i grazhdanskoye stroitel'stvo* **8**, 54–60 (2018)
7. Fan, W., Liu, B., Consolazio, G.R.: Residual capacity of axially loaded circular RC columns after lateral low-velocity impact. *J. Struct. Eng.* **145**(6), 04019039 (2019)
8. Park, R.: A summary of results of simulated seismic load tests on reinforced concrete beam-column joints, beams and columns with substandard reinforcing details. *J. Earthq. Eng.* **6**, 147–174 (2002)
9. Mazzarolo, E., Scotta, R., Berto, L., Saetta, A.: Long anchorage bond–slip formulation for modeling of RC elements and joints. *Eng. Struct.* **34**, 330–341 (2012)
10. Engström, B., Magnusson, J., Huang, A.: Pull-out behavior of ribbed bars in normal and high-strength concrete with various confinements. In: Leon, R. (ed.) *Bond and Development of Reinforcement: A Tribute to Dr. Peter Gergely*. ACI Special Publication: ACI International, vol. 180, pp. 215–242 (1998)
11. Tamrazyan, A.G., Popov, D.S., Ubysz, A.: To the dynamically loaded reinforced-concrete elements' calculation in the absence of adhesion between concrete and reinforcement. In: *IOP Conference Series: Materials Science and Engineering*, vol. 913, p. 022012 (2020)
12. Eric, J., Murat, S.: High strain rate bond characteristics of reinforced concrete beam-ends. *Int. J. Impact Eng.* **130**, 192–202 (2019)
13. Rzhantsyn, A.R.: *Composite Rods and Plates*. Stroyizdat, Moscow (1986)
14. Fedorova, N.V., Savin, S.Y., Kolchunov, V.I.: Affecting of the long-term deformation to the stability of RC frame-bracing structural systems under special accidental impacts. In: *IOP Conference Series: Materials Science and Engineering*, vol. 753, p. 032005 (2020)



# Use of Unmanned Aerial Vehicles in the Creation of a Topographic Plan of a Chalk Pit

E. R. Shin<sup>(✉)</sup> , T. G. Kalachuk , N. V. Andreeva , and A. I. Polyakov 

Belgorod State Technological University named after V.G. Shukhov, Belgorod, Russia

**Abstract.** Creating topographic plans of terrain sections in the classical way takes a lot of time. It is proposed to use modern equipment and software products to solve the task, which should lead to a reduction in time during the production of work, as well as reduce the cost of the final product. This paper describes the process of drawing up a topographic plan of the chalk pit area for the purposes of landscaping with the use of an unmanned aerial vehicle, followed by processing the data obtained in a specialized software product. The basic preparations for the shooting of unmanned aircraft, also the process of shooting and processing photos in a specialized software product “Agisoft Metashape” for receiving and decoding of the orthophotomap were analyzed.

An approach to laying a network of identification marks on the ground with the use of GPS receivers and determining their spatial coordinates is considered in detail. Also, due to the large volume of work and some technical limitations of the work of the unmanned aerial vehicle, it became necessary to divide the terrain into survey areas, followed by combining the broken sections into a single orthophotomap. The principle of dividing the terrain into separate flight zones is also described in the paper.

**Keyword:** Aerial photography of the terrain · Chalk quarry · Unmanned aerial vehicles · Digital terrain model · Orthophotomap · Topographic plan · Geodetic survey base

## 1 Introduction

The subject of the survey is the working area of the chalk pit of CJSC “Belgorod Cement” (Fig. 1). Since 2011, the object has been included in the list of specially protected natural areas, as an area with a unique geological section. The total area of the survey was 227.3 ha.

The object of research is located in the western district of the city of Belgorod. The geological structure of the survey area is expressed by the foundation of Precambrian crystalline rocks at a depth of 300–500 m below sea level, as well as by the thickness of sedimentary rocks. Above the crystalline basement, limestone and sand-clay deposits occur at elevations of 250–400 and 140–180 m. The upper layer is represented by a layer of Upper Cretaceous sediments.

The shooting area is characterized by large elevation differences within short distances. Also, not a small part of the site is covered by a reservoir formed in the process





**Fig. 1.** The territory of the chalk pit.

of opening the extracted rocks. Part of the area is covered with dense vegetation. These factors had the most negative impact on the aerial photography process.

## 2 Methods and Equipment

### 2.1 Preparing for Shooting

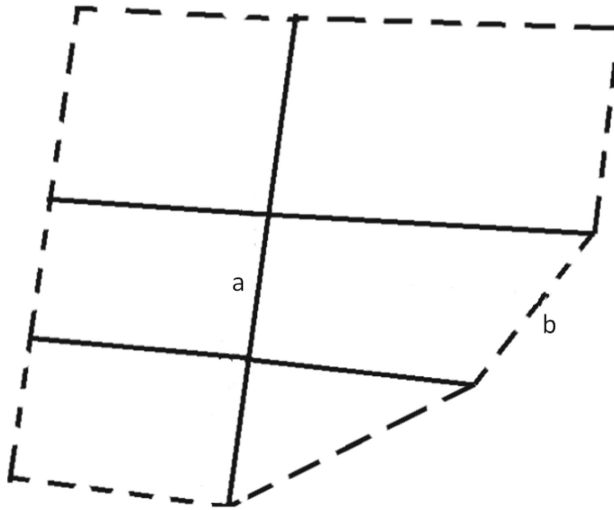
The process of preparing for shooting can be divided into 2 stages: drawing up a route assignment and creating a planned altitude justification.

The process of designing the route assignment for aerial photography was built on the basis of the requirements of accuracy and technical capabilities of the aircraft. The existing regulatory documentation for aerial photography regulates the height of photography and the degree of longitudinal and transverse overlap of adjacent images to ensure the required accuracy for the selected scale.

According to the characteristics stated by the manufacturer of the UAV, the flight time on a single battery charge is up to 30 min. However, this result is possible only under ideal climatic conditions. In practice, as a rule, the maximum time is about 25 min. Based on this value, the length of the routes was selected.

In addition to technical limitations, the methodological conditions of the shooting play an important role. When calculating the horizontal distance between the lines of the route they must take into account the requirements to the longitudinal and transverse beams shooting (Fig. 1). A detailed algorithm for calculating the characteristics of the flight task is given in the work of E. R. Shin, A. Yu. Schekina, R. A. Cherkasov: Technology of creating topographic plan of scale 1:500 according to the shooting quadcopter PHANTOM 4; A. S. Semenov, K. A. Slonich: Survey of buildings and structures with the use of unmanned aerial vehicles [1–4].

After performing all the calculations and produce the desired characteristics of the route, namely the height of the photography, the transverse basis and interval photography the route over the area taking into account the technical characteristics of the UAV is designed. In addition to the calculated characteristics, it is also necessary to provide an overlap directly between the routes so that the edges of adjacent routes are on the same straight line (Fig. 2).



**Fig. 2.** The layout of the routes in the flight task: a – adjacent sides of routes, b – single sides of routes.

The creation of a planned high-altitude justification consists in laying identification marks on the territory to be removed. The identification marks are clearly visible against the ground red circles with a diameter of 35 cm. To coordinate them more precisely, a crosshair was plotted in the center of the circle, the coordinates of which were later determined using GNSS equipment, taking into account the corrections received from the base station.

The identification marks were placed in such a way that at least 3 pieces were present at each shooting area. Together, a closed geodesic network was formed along all the routes, built on the “envelope” principle.

## 2.2 Shooting Process

When shooting during field work, special attention should be paid to pre-flight training, described in the instructions for the aircraft. A responsible approach to this stage will allow avoiding a number of problems during the shooting process.

Weather conditions have a strong influence on the shooting process. Do not shoot under unfavorable conditions, such as strong wind gusts of more than 10 m/s, snow, rain, and fog. In this case, the electronic components of the aircraft may fail. It is also

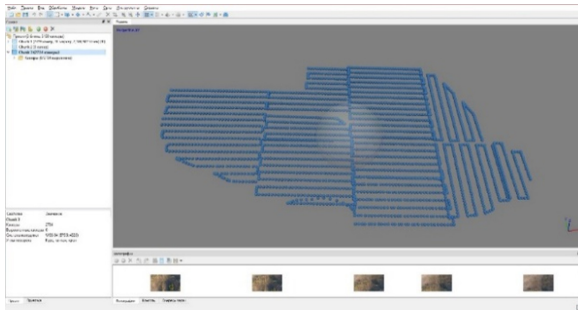
mandatory to comply with the local regulatory requirements of the air space regulatory authorities, which includes compliance with no-fly zones, altitude and distance restrictions [5].

### 3 Results

As a result of the field work, the resulting images can be downloaded from the recording device of the aircraft in the format .JPEG images and be processed in software products [6].

Agisoft Metashape tools were used to build an orthophotomap and a three-dimensional digital terrain model [7]. After loading all the images into the working project, the images are externally oriented by aligning the images according to their position at the time of shooting by the aircraft (Fig. 3). Then, the search for connecting points between the images is performed. In the course of the described processing, a sparse cloud of terrain points is obtained, which combine at least 2 images. If the alignment is not performed for some photos, then the alignment is performed separately for these images. At the alignment stage, it is advisable to use high processing accuracy, as the further processing process will rely on data from a sparse cloud. To reduce the processing time, if the coordinates of the photographing points are present in the metadata of the images, it is possible to select one more time pairs of images by reference [7, 8].

After the images are aligned and the connecting points on them are found, data on the positions of the identification marks is loaded into the project. It is worth noting that the coordinates of the identification marks must be obtained in the same coordinate system as the working project, otherwise it is necessary to recalculate the coordinates.

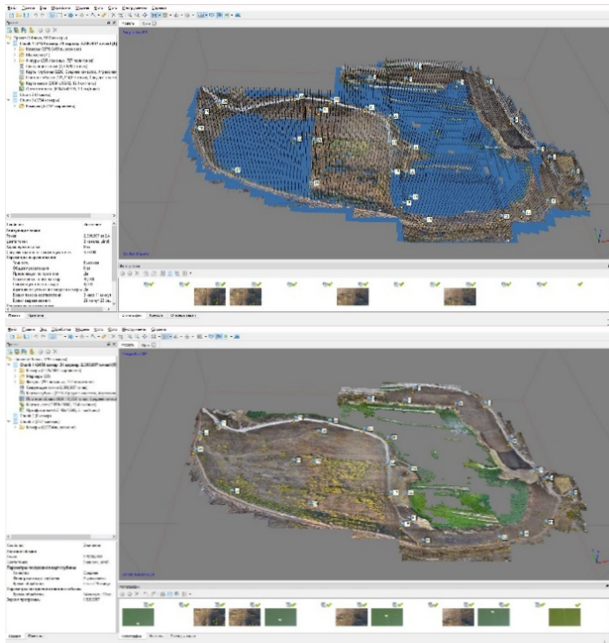


**Fig. 3.** The location of the cameras at the time of photographing, obtained after uploading the images to Agisoft Metashape.

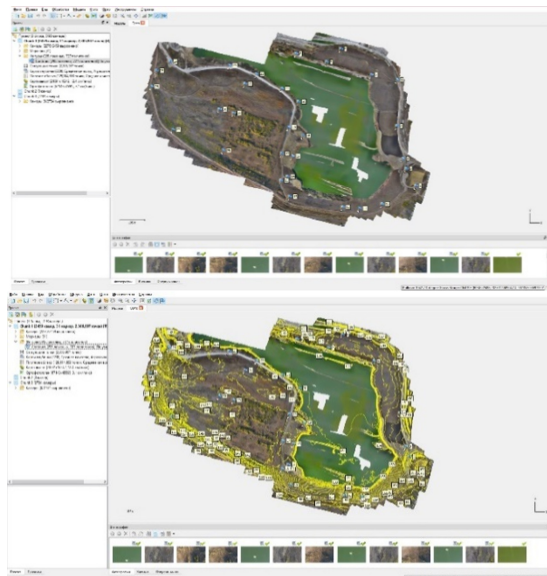
After loading, the appeared markers are placed on the control points on the terrain. After placing the identification markers, a dense point cloud is constructed (Fig. 4).

Based on the resulting dense cloud, an orthophotomap and a digital terrain model are constructed. This data is used to build a map of heights, and then horizontals that reflect the terrain (Fig. 5).

Further processing is aimed at obtaining a topographic plan and is performed in any CAD that supports working with geodata. For example, we used AutoCAD with

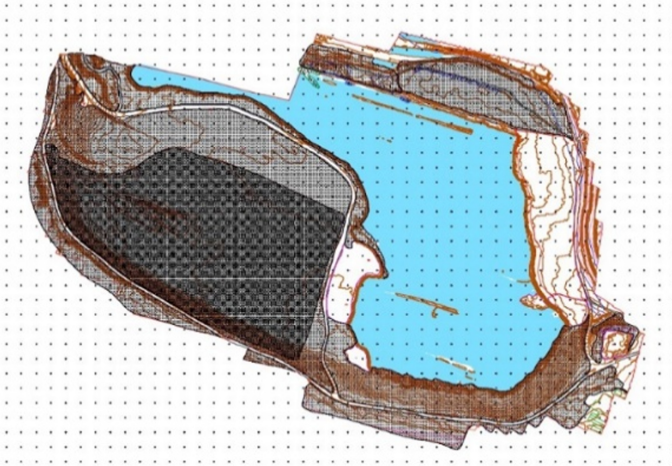


**Fig. 4.** Image processing in Agisoft Metashape: a – building connecting points and adding reference points, b – building a dense point cloud.



**Fig. 5.** Work with a dense cloud points: a – orthophotomap building, b – building horizontals.

the Geinics add-in [9]. The unloaded orthophotomap and horizontals were imported as a substrate. To load the horizontals, it was necessary to convert them to a two-dimensional view first, as Agisoft Metashpe exports them as 3D polylines. After drawing the orthophotomap, a topographic plan was obtained at a scale of 1:1000 (Fig. 6) [10].



**Fig. 6.** Topographic plan, which is the result of processing images of a chalk pit in Belgorod.

## 4 Conclusion

The method described in the paper proved to be the best in the course of the work performed. When shooting this object, the method of drawing up an orthogonal photo plan made it possible to speed up significantly the work of surveyors by automating the process. In addition, the cost of work has been significantly reduced. The data obtained after image processing is more visual and informative. The advantages of the considered method include the fact that the shooting can be carried out in places where the surveyor cannot reach without additional equipment.

However, it is worth considering a number of drawbacks that affect the process of shooting and the accuracy of the results. To date, the procedure for mandatory registration of UAVs has been introduced, with which certain difficulties may arise. The shooting process is also significantly affected by meteorological conditions such as rain and strong wind gusts, which can make it difficult to fly around the territory. The accuracy of the results may be affected by the presence of dense vegetation, which introduces errors in the process of determining the elevation of the earth surface.

**Acknowledgments.** This work was realized under the support of the President Scholarship; in the framework of the Program of flagship university development on the base of the Belgorod State Technological University named after V G Shukhov, using equipment of High Technology Center at BSTU named after V G Shukhov.

## References

1. Shin, E.R., Schekina, A.Yu., Cherkasov, R.A.: Technology for creating topographic plans at a scale of 1:500 based on survey data from the Phantom 4 quadcopter. *Vector Geosci.* **2**(1), 54–59 (2019)
2. Kostyuk, A.S.: Features of aerial photography from ultralight unmanned aerial vehicles. *Omsk Sci. Bull.* **1**, 236–240 (2011)
3. Semenov, A.S., Slonich, K.A.: Survey of buildings and structures with the use of unmanned aerial vehicles. *Bull. BSTU named after V.G. Shukhov* **9**, 160–163 (2017)
4. Instructions for aerial photography (AFS) using UAV DJI Phantom 4 Geobox RTK/PPK. <https://geospb.ru/blog/articles/instrukciya-po-aerofotosemochnym-rabotam-afs-s-pomosshyu-bpla-dji-phantom-4-geobox-rtkppk>. Accessed 11 Oct 2019
5. Gubarev, S.A., Shin, E.R.: Changes in the functionality and structures of unmanned aerial vehicles for civil purposes. *Bull. Geosci.* **3**(2), 64–68 (2020)
6. Phantom 4 Characteristics. <https://www.dji.com/ru/phantom-4/info>. Accessed 18 Oct 2017
7. Tikhonov, A.A., Akmatov, D.Zh.: Review of programs for processing aerial photography data. *Mining Inf. Anal. Bull. (Sci. Tech. J.)* **12**, 192–198 (2018)
8. Schreiner, K.A.: Using the capabilities of unmanned aerial vehicles for remote sensing on the example of open-pit mining. *Bull. Siberian State Geodetic Acad.* **2**(18), 47–50 (2012)
9. Verzilov, N.E., Pakhomov, A.S., Sukharev, V.G., Belyavskaya, O.Sh.: Application of the GeoniCS software package for reconnaissance in military affairs. In: *Information and Graphic Technologies in Professional and Scientific Activities*, pp. 113–116 (2019)
10. Essin, A.S., Essin, S.S.: Technology of photogrammetric processing of aerial photographs obtained from UAV in order to create orthophotomaps. *Geo-Siberia* **4**(1), 72–75 (2009)



# The Effect of Moisture State on Kinetics of Damage Accumulation in the Structure of Epoxy Polymer Samples Under Tensile Stresses

T. A. Nizina<sup>(✉)</sup> , N. S. Kanaeva , and D. R. Nizin 

National Research Mordovia State University, Saransk, Russia

**Abstract.** The paper studies the influence of the moisture state on the elastic-strength parameters and kinetics of damage accumulation in the structure of epoxy polymer samples based on Etal-247 resin and Etal-45TZ2 hardener. Damage accumulation process is quantitatively described based on the author's technique determining the position of critical points on deformation curves of polymer materials using fractal analysis methods. To assess critical fraction of cumulative failures of the polymer matrix structural elements, we used the parameter defined as the ratio of the number of points with a fractality index less than 0.5 to the total number of points on deformation curves (until reaching the "critical" level of tensile stresses). It has been established that an increase in the moisture content of a polymer material makes it possible to achieve, under tensile loads, formation of a pronounced stage of forced highly elastic deformations. We have revealed a decrease in the ultimate tensile strength and an increase in the relative elongation at break for moisture-saturated specimens compared to the polymer in the equilibrium-moisture state, by 6.0 and 6.7 times, respectively. It was found that at the ultimate moisture saturation, the rate of failure accumulation accelerates with an increase in the level of applied stress at strain compared to the samples in the equilibrium-moisture state, by 4.3–5.5 times.

**Keywords:** Epoxy polymers · Deformation curves · Moisture content · Fractal analysis · Fractality index · Failure accumulation

## 1 Introduction

At present, the objective of ensuring reliable operation of building materials, products and structures exposed to natural climatic effects is becoming more and more urgent. Along with the temperature and intensity of actinometric factors, the most significant climatic factors influencing the properties of polymeric building composites during operation are humidity and precipitation [1–3]. Moisture absorbed by polymer composites activates the processes of structural relaxation, has a partially reversible plasticizing effect, and also participates in hydrolysis and afterhardening reactions [4].

Studies [5–7] have shown that moisture absorption of polymeric materials and the associated loss of strength are determined by structure and type of polymer matrix,

binder composition, hardening degree, thickness and porosity of samples, as well as the state of the interfacial layer at the matrix/filler interface. Chemical interaction of moisture with polymer composites causes the hydrolysis of macromolecules and subsequent material destruction reactions [7]. However, the effect of moisture manifests itself not only in chemical interaction. Water fills in various microdefects, causing matrix microcracking in residual stress concentration zones. In addition, moisture absorbed by the polymer matrix can act as a plasticizer, weakening the absorption interactions between macromolecules (or their links) of the polymer and the strength of adsorption interaction at the interface [8, 9]. Penetrating between the polymer matrix molecules, water causes relaxation of internal stresses, increases mobility of macromolecules, decreases the cross-linking level.

Under natural climatic operation conditions, maximum moisture saturation of the polymer material is virtually not achieved due to relatively low moisture sorption rate and the competing desorption process due to surface heating and cooling, changes in the environmental humidity, and atmospheric pressure, etc. However, the need to take into account the polymer moisture content effect, including in ultimate equilibrium-moisture states (dry and moisture-saturated), is extremely important for understanding the operation of polymers under natural climatic conditions. Quantitative assessment of kinetics of damage accumulation in polymer sample structure under mechanical loads is of additional interest.

## 2 Methods and Materials

The objects of the study were epoxy polymer samples based on Etal-247 resin and Etal-45TZ2 hardener by ENPTs EPITAL JSC. Etal-247 epoxy resin (TU 2257-247-18826195-07) is a low-viscosity modified resin with Brookfield viscosity of  $650 \div 750$  cP at 25 °C. Mass fraction of epoxy groups for Etal-247 and is at least  $21.4 \div 22.8\%$ .

Mechanical tensile testing of the samples of compositions under study was made using an AGS-X series tensile testing machine with TRAPEZIUM X software. Test temperature was  $23 \pm 2$  °C and relative air humidity was  $50 \pm 5\%$ . The tensile testing machine clamp movement speed was 2 mm/min. The readings were registered at 0.01 s. At least 10 samples were tested for each composition in parallel (type 2 according to GOST 11262-2017). Strength and deformation characteristics of the test polymer samples were determined in three different moisture states - equilibrium-moisture, dry, and moisture-saturated. Samples were dried at a temperature of 60 °C, and moistened in desiccators over water until reaching constant weight values according to GOST R 56762-2015 Polymer Composites. Method for Determining Moisture Absorption and Equilibrium State.

This work assesses the effect of epoxy polymer moisture state on the change in its strength and deformation characteristics, as well as kinetics of failure accumulation in the sample structure under tensile loads. Quantitative values of accumulated failures are determined on the basis of the author's technique, which allows determining the coordinates of critical points of deformation curves built by methods of fractal analysis [10–13]. The proposed technique involves determining the coordinates of “critical” points of the deformation curves for which the fractality index values calculated over

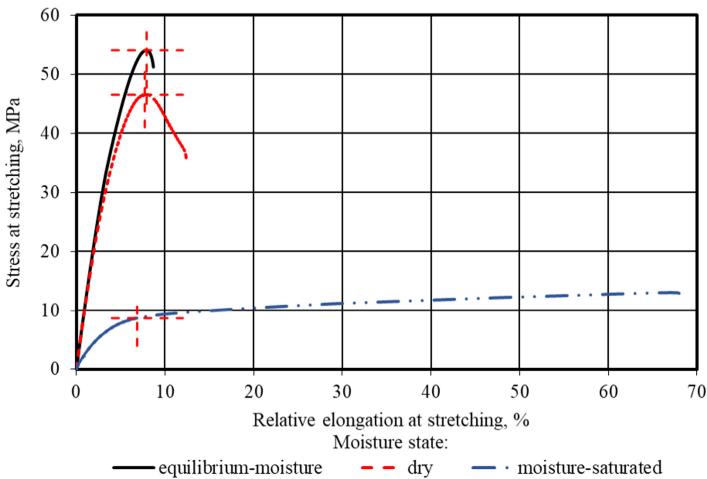


the previous short time intervals using the least coverage method, are less than 0.5. Time intervals of 0.16 s were studied with analyzed area shifted with a step of 0.01 s.

To estimate the level of accumulated failures leading to the destruction of samples under tensile loads, we used a parameter defined as the ratio of the number of points with a fractality index less than 0.5 to the total number of points on deformation curves (until reaching the level of “critical” tensile stresses). An algorithm for assessing failure accumulation is described in [12]. At the same time, to assess the behavior of polymer composites in different moisture conditions under mechanical loads, the data of all samples of the studied series was processed.

### 3 Results and Discussion

Analysis of the results showed that sample deformation curves (in equilibrium-moisture and dry states) have both ascending and descending branches, which makes it possible to determine strength and deformation characteristics of the epoxy polymer under tension and at break (Fig. 1). The arithmetic mean values of the tensile strength and elongation at the maximum load of a series of samples in an equilibrium-moisture state, respectively, are equal to 53.5 MPa and 7.98%, in a dry state – 48.18 MPa and 7.79%; ultimate strength and elongation at break in the equilibrium-moisture state – 47.06 MPa and 8.74%, in dry state – 36.67 MPa and 12.54%.

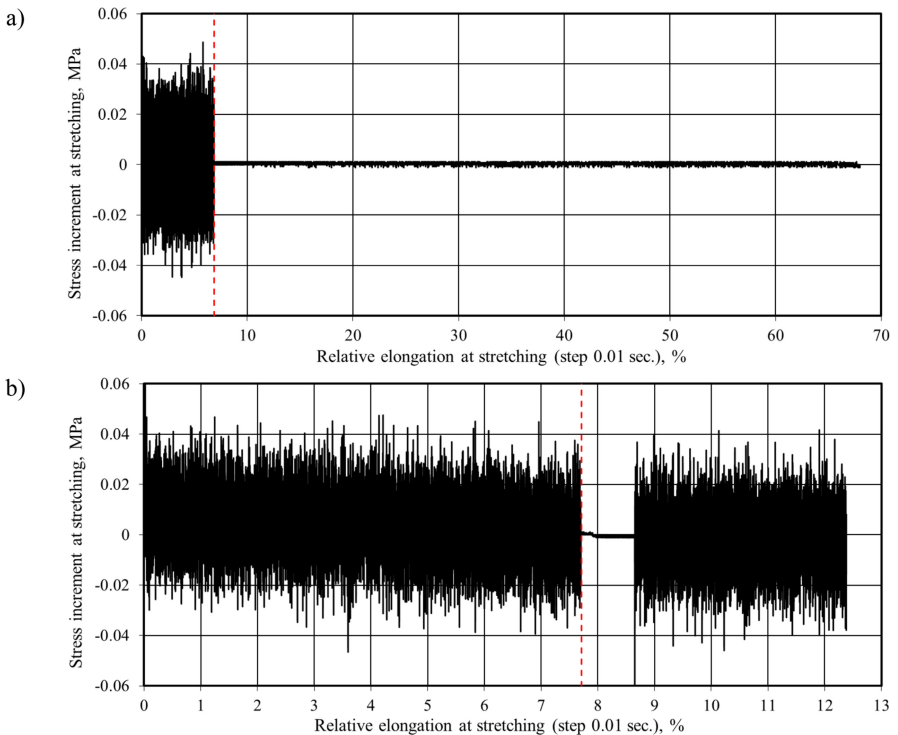


**Fig. 1.** Deformation curves of epoxy polymer samples under tension in different moisture conditions: equilibrium-moisture, dry and moisture-saturated (red dashed lines show the levels of ultimate tensile strength and the corresponding elongations).

Moisture saturation of samples of control compositions before equilibrium state sets in them leads to a significant decrease in strength and an increase in elongation at break (Fig. 1). Deformation curves of moisture-saturated samples are ascending with two different slope sections which causes certain difficulties in identifying the ultimate

tensile strength. To determine it, we have assessed the change in the increase in tensile stresses registered with a frequency of readings 0.01 s depending on relative elongation (Fig. 2). It was found that at a certain level of tensile deformations, the increase in stresses tends to zero, which manifests itself both for samples in moisture-saturated (Fig. 2a), and in dry (Fig. 2b) and equilibrium-moisture states. It is this level of relative deformations highlighted in Fig. 2 with a red vertical line, was taken in further analysis as the one where the samples achieve “critical” stresses identified as ultimate tensile stress.

In Fig. 1, these “critical” levels of tensile stresses in polymer samples and the corresponding relative elongations are shown by intersecting red dashed lines. The average values of the studied characteristics after statistical processing of a series of samples in different moisture conditions are given in Table 1. The average moisture content of samples in the equilibrium-moisture state was 1.41%, and 4.92% wt. in the moisture-saturated state.



**Fig. 2.** The change in stress increment (step of readings registration is 0.01 s.) depending on relative elongation during tension of epoxy polymer samples in the moisture-saturated (a) and dry (b) states (red dashed vertical line shows the level of relative elongation corresponding to the “critical” stress at stretching).

According to the results of the studies, it was found (Table 1) that a change in the moisture content of samples from 1.41 to 4.92% leads to a decrease in the tensile strength from 53.30 to 8.95 MPa, which corresponds to a residual strength of only 16.7% from

control values. In this case, deformation characteristics of moisture-saturated samples at break increase 6.7 times, reaching a relative elongation of 67.5%. Such significant changes in elastic-strength parameters are associated with a change in the behavior of moisture-saturated samples under load from glassy to highly elastic.

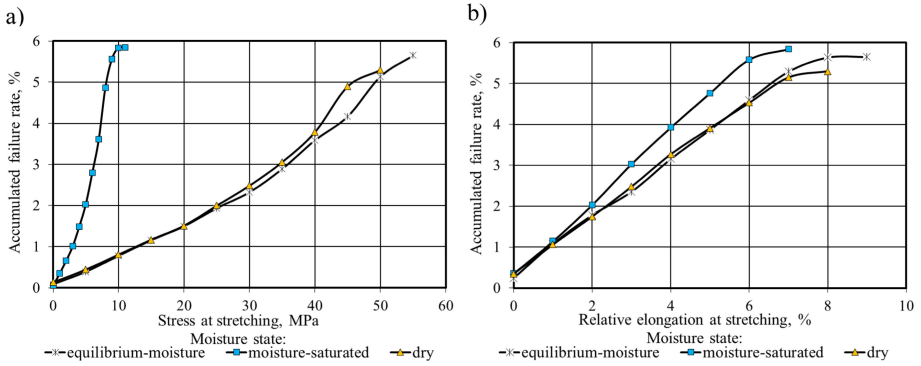
Removal of free moisture leads to a decrease in the strength characteristics of Etal-247 + Etal-45TZ2 epoxy polymer by 9.9% with virtually unchanged deformation characteristics at stretching (-2.4%). At the same time, it is obvious to assume that diffusion of moisture into the polymer in this case is accompanied by a decrease in the intermolecular interaction forces, which, up to a certain level, may turn out to be “useful” in terms of strength characteristics. However, a further increase in moisture content can have a negative effect on the strength of polymer materials [14], which was clearly manifested for the studied compound.

The next analysis stage included assessing the influence of the moisture state of epoxy polymer samples on kinetics of damage accumulation in their structure under tensile stresses (Fig. 3). This analysis was done for deformation curves until the samples reached the “critical” stress levels. The algorithm for determining the latter was described above. Limit levels of the number of failures for equilibrium-moisture, moisture-saturated and dry states were 5.65, 5.84 and 5.30%, respectively.

**Table 1.** Elastic-strength and sorption characteristics of Etal-247 + Etal-45TZ2 epoxy polymer in various moisture states.

Moisture state of samples during testing	Average values of the studied characteristics for a series of samples				
	Moisture content of samples, % wt	Tensile strength at stretching, MPa	Relative elongation at stretching, %	Tensile strength at break, MPa	Relative elongation at break, %
Equilibrium-moisture	1.41	53.50	7.98	47.06	8.74
Moisture-saturated	4.92	8.95 (-83.3%)	7.05 (-11.7%)	12.40 (-73.7%)	67.48 (+672%)
Dry	0	48.18 (-9.9%)	7.79 (-2.4%)	36.67 (-22.1%)	12.54 (+43.5%)

The analysis results show (Fig. 3a) that curves of failure rate accumulation depending on the level of applied stress for samples in equilibrium-moisture or dry states are similar. A similar nature of failure accumulation curves was registered for the given series of samples and depending on relative elongation at stretching (Fig. 3a). At the same time, if the failure accumulation rate for moisture-saturated samples just slightly accelerates with an increase in relative elongation at stretching (Fig. 3a), then, depending on the level of tensile stresses, failure accumulation rates accelerate in comparison with samples in equilibrium-moisture state from 4.3 to 5.5 times (Fig. 3a). In particular, 50% of the total number of failures, where achieving this number causes sample destruction, is achieved for moisture-saturated samples already at stresses of about 6.2 MPa. A similar value



**Fig. 3.** Failure accumulation curves for a series of samples in different moisture states depending on the level of applied stresses (a) and relative elongations at stretching (b).

for equilibrium-moisture and dry samples is achieved at tensile stress levels of 34.0 and 31.4 MPa, respectively.

#### 4 Conclusion

In the course of the study, a significant effect of the moisture state of samples on the elastic-strength parameters of Etal-247 epoxy resin- and Etal-45TZ2 hardener-based polymer was found. It was found that an increase in the moisture content of a polymer material up to 4.92% is accompanied by formation of a pronounced stage of forced highly elastic deformations with an increase in relative elongation at break and a decrease in tensile strength at stretching, by 6.7 and 6.0 times, respectively. It was found that at the ultimate moisture saturation, failure accumulation rate accelerates with an increase in the level of applied stress at stretching compared to the samples in equilibrium-moisture state, by 4.3–5.5 times.

**Acknowledgement.** The reported study was funded by RFBR according to the research project № 20-31-70001.

#### References

1. Kirillov, V.N., Efimov, V.A.: Problems of studying the climatic resistance of aviation non-metallic materials. In: Aviation Materials. 75 Years Old. Selected Works of “VIAM”: Jubilee Scientific and Technical Collection, pp. 379–388 (2007)
2. Pavlov, N.N.: The aging of plastics under natural and artificial conditions. Chemistry, Moscow (1982)
3. Kuchinov, V.F., Kireev, V.A., Startsev, O.V., Shevaldin, V.N.: The influence of climatic ageing on the characteristics of elasticity and strength of polymeric composite materials. Sci. Notes TSAGI **4**, 54–64 (2006)
4. Startsev, V.O., Plotnikov, V.I., Antipov, Y.: Reversible effects of moisture in determining the mechanical properties of PCM under climatic influences. Proc. VIAM **5**(65), 110–118 (2018)

5. Kirillov, V.N., Efimov, V.A., Shvedkova, A.K., Nikolaev, E.V.: Investigation of the influence of climatic factors and mechanical loading on the structure and mechanical properties of PCM. *Aviat. Mater. Technol.* **4**(21), 41–45 (2011)
6. Maxwell, A.S., Broughton, W.R., Dean, G., Sims, G.D.: Review of accelerated ageing methods and lifetime prediction techniques for polymeric materials. NPL Report DEPC MPR 016 (2005)
7. Valevin, E.O.: Influence of heat and humidity influence on the properties of heat-resistant polymer composite materials based on phthalonitrile matrix. Diss. Cand. Techn. Sc. MAI, Moscow (2018)
8. Kablov, E.N., Startsev, O.V., Krotov, A.S., Kirillov, V.N.: Climatic aging of composite materials for aviation purposes. I. Mechanisms of aging. *Deform. Destr. Mater.* **11**, 19–27 (2011)
9. Kirillov, V.N., Efimov, V.A., Vapirov, Yu.M.: To the question of the possibility of predicting the atmospheric resistance of PCM. In: Collection of reports of the VII International Scientific Conference on Hydroaviation “Hydrosalon-2008”, pp. 307–313 (2008)
10. Nizina, T.A., Nizin, D.R., Kanaeva, N.S., Kuznetsov, N.M., Artamonov, D.A.: Applying the fractal analysis methods for the study of the mechanisms of deformation and destruction of polymeric material samples affected by tensile stresses. *Key Eng. Mater.* **799**, 217–223 (2019)
11. Nizina, T.A., Selyaev, V.P., Nizin, D.R., Artamonov, D.A., Kanaeva, N.S.: Fractal analysis of deformation curves of epoxy polymers under tension. *Polym. Constr.* **1**, 48–57 (2019)
12. Nizina, T.A., Nizin, D.R., Kanaeva, N.S.: Statistical analysis of the frequency of damage accumulation in the structure of epoxy composites under tensile loads. *Lect. Notes Civ. Eng.* **95**, 1–8 (2020)
13. Nizina, T.A., Selyaev, V.P., Nizin, D.R., Kanaeva, N.S.: Quantitative analysis of the kinetics of damage accumulation in the structure of polymer materials under tension. *Constr. Reconstr.* **2**, 77–89 (2020)
14. Kryzhanovsky, V.K., Burlov, V.V., Primachenko, A.D., Kryzhanovskaya, Yu.V.: Technical properties of polymer materials. Manual under the general editorship of prof. V. K. Kryzhanovsky. Profession, Saint Petersburg (2005)



# Hydration Processes of Anhydrite-Containing Binders Using Volumetric Phase Composition

L. A. Anikanova , O. V. Volkova  , A. I. Kudyakov , and V. A. Lotov 

Tomsk State University of Architecture and Building, 2 Solyanaya Sq., 634003 Tomsk, Russia

**Abstract.** The paper presents the results of studies of the use of bulk phase characteristics or their combinations in the quantitative assessment of the restructuring of the structure in the process of hydration and hardening of anhydrite-containing binder. The main advantage of using volumetric phase characteristics is the possibility to evaluate qualitative and quantitative composition of a disperse system, with true equality, which is a mathematical expression of the law of constancy of volume of the dispersed phase structure. The quantitative composition of dispersed systems was estimated by the volume content of phases ( $K_s$ ,  $K_l$ ,  $K_g$ ), taking into account their presence equally. It is shown that the use of volumetric phase characteristics of this system makes it possible to quantify effectively the changes in the structure during the interaction of anhydrite binder with water, and the construction of a phase diagram of this process opens up new approaches to elucidate the mechanisms of hydration and hardening of binders.

**Keywords:** Fluorine-anhydrite · Phase composition · Solid phase · Liquid phase · Gas phase · Volumetric concentration · Hydration process · Phase diagram

## 1 Introduction

Dispersed systems containing the solid phase are widely used in various industries. The technology of their production is inextricably linked with the use of natural and technogenic materials with high dispersion of the solid phase, which is a necessary condition for the effective flow of chemical reactions and physical and chemical processes associated with the synthesis of new chemical compounds [1–4].

Technological process of obtaining materials based on dispersed systems (S+L+G) consists of four main stages: preparation of the initial dispersed system, giving it the necessary shape, transfer of the coagulation structure of products to condensation and further, to a structure of a higher order and strength – crystallization. Despite the relatively high level of knowledge achieved in the study of the processes of preparation of dispersed systems, product formation and condensation-crystallization structure formation, the lack of a systematic approach and unified criteria for evaluating the properties of the dispersed system at all stages of the technological process does not allow using the existing knowledge with sufficient efficiency in managing the process of transformation of structures, as a single and continuous process of forming the structure of products based on dispersed systems [5].

The technological process associated with the use of dispersed systems is accompanied by a change in the structural characteristics and quantitative ratio between the individual phases of the system at each technological stage. The method that takes into account the mass content of liquid and solid phases is the most widely used method for estimating the quantitative ratio between phases. The use of mass and specific characteristics does not give a clear idea of the quantitative content of the gas phase, which is an equal component in two-phase (S+G) or three-phase (S+L+G) systems. Therefore, it is advisable to estimate the quantitative composition of dispersed systems by the volume content of phases, which takes into account their presence equally.

The main advantage of using volumetric phase characteristics is the possibility to evaluate qualitative and quantitative composition of a disperse system, with true equality, is the mathematical expression of the law of the constancy of the volumetric phase composition of the disperse structure or system under which, regardless of the type of system and type of energy or technological impact on it, at any time, the sum of volumetric concentrations of solid, liquid and gaseous phases of the system is constant:

$$K_{s1} + K_{l1} + K_{g1} = K_{s2} + K_{l2} + K_{g2} = K_{sn} + K_{ln} + K_{gn} = 1, \quad (1)$$

where  $K_s$ ,  $K_l$ ,  $K_g$  – volume content of solid, liquid and gaseous phases in the system at the corresponding technological stage.

In addition, the current state of technology of materials based on dispersed systems requires new approaches involving structural characteristics that display the most common features of the system, regardless of the technological stage. These properties are characterized by volume phase characteristics and, first of all, the content of the solid phase ( $K_s$ ), which is constantly present in the system regardless of the content of the liquid and gas phases. This property, as well as the normalized variation in the range (0–1) or (0–100%), allow using the volume concentration of the solid phase of  $K_s$  as a criterion for optimizing the formation of structures at all stages of the technological process. In this case, the  $K_s$  acts as a generalized and simplest characteristic of the structure, regardless of its type and physical and mechanical properties.

## 2 Methods and Materials

The gypsum-water system is a heterogeneous system consisting of three phases: solid, liquid, and gaseous, which makes it difficult to control the development of hydration and hardening processes. Studying the processes of hydration, the authors minimized the number of factors by excluding non-essential ones and using the main ones: volume concentrations (VC) of solid ( $K_s$ ), liquid ( $K_l$ ), and gaseous ( $K_g$ ) phases. The aim of this study is to identify the benefits of using volume phase characteristics and their combinations in the quantitative assessment of restructuring in the process of hydration and hardening of anhydrite-containing binder – fluorine-anhydrite (FLA) neutralized in the factory conditions, the chemical composition of which is represented mostly by insoluble anhydrite [6, 7]. This technique is used to study the process of cement hydration by extrusion; for the presented system the method was applied for the first time.

Samples with a size of  $2 \times 2 \times 2$  cm were made by injection molding from anhydrite paste with a water-solid ratio (W/S: 0.5; 0.45; 0.4). After extraction of samples out of

forms their mass, volume and density in the wet state ( $\rho_w$ ) was determined. The average density of FLA samples ( $\rho_m$ ) is calculated by the formula:

$$\rho_m = \frac{\rho_w}{1 + W}, \text{ kg/m}^3 \tag{2}$$

where W – W/S ratio in the sample.

The volume content of phases in the initial samples was determined by the formulas:  $K_{s1} = \rho_m / \rho_{tr}$ , rel. units;  $K_{l1} = \text{where } \frac{W \rho_m}{\rho_l}$ , rel. units;  $K_{g1} = 1 - (K_{s1} + K_{l1})$ , rel. units.

where  $\rho_{tr}$  – the true density of FLA,  $\rho_{tr} = 2900 \text{ kg/m}^3$ ;

$\rho_l$  – water density,  $\rho_l = 1000 \text{ kg/m}^3$ .

The phase composition of the samples in the initial state is shown in Table 1.

**Table 1.** Phase composition of samples in the initial state.

W/S,	$\rho_{tr}$ , kg/m <sup>3</sup>	$K_{s1}$	$K_{l1}$	$K_{g1}$
0.50	2900	0.439	0.587	0.024
0.45	2900	0.398	0.530	0.080
0.40	2900	0.360	0.440	0.200

After the specified periods of hardening of the samples at the age of 3, 7, 14 and 28 days in air-dry conditions, the average density of the hardened samples, the density in the dried state at  $t = 80 \text{ }^\circ\text{C}$  and the compressive strength were determined.

The pieces of the sample obtained after destruction were crushed in a porcelain mortar (without grinding) to a particle size of less than <100 microns, then the powder was treated with an absolute standard to remove free water residues and again dried in a vacuum desiccator at  $t = 22\text{--}24^\circ\text{C}$ . The resulting moisture correction was used to determine the density of hydrated samples that did not contain free water, and dry powder was used to determine the true density of hydrated FLA (pycnometer method, ethanol). Based on the obtained data, the phase composition of the samples ( $K_{s2}$ ,  $K_{l2}$ ) and some other parameters are calculated. The intensity of the ongoing processes of restructuring the structure can be estimated by the value of the structural-energy parameter n, which is determined by the formula:

$$n = \frac{K_{s2}}{1 - K_{s2}} / \frac{K_{s1}}{1 - K_{s1}}, \tag{3}$$

where  $(1 - K_{s1})$  and  $(1 - K_{s2})$  – the volume fraction of the pore space in the original and cured samples;

$K_{s2}$  – volume fraction of the solid phase in hydrated samples.

The values of this parameter at  $n > 1$  characterize the compaction, and at  $n < 1$  the expansion of the system (porization).



The degree of restructuring of the structure  $\alpha$  in the interaction of cement with water is determined by:

$$\alpha_n = \frac{n-1}{n}, \text{ rel. units, or } n = \frac{1}{1-\alpha_n} \quad (4)$$

The degree of hydration FLA  $a_{hs}$  on the solid phase:

$$\alpha_{hs} = \frac{K_{s2} - K_{s1}}{K_{s1}}, \text{ rel. units;} \quad (5)$$

The degree of hydration FLA  $a_{hl}$  in the liquid phase:

$$\alpha_{hl} = \frac{K_{l1} - K_{l2}}{K_{l1}}, \text{ rel. units, where} \quad (6)$$

$$K_{l2} = (1 - K_{s2})(1 - \Delta K_s), \text{ rel. units} \quad (7)$$

Degree of filling (N) of the initial pore space  $(1 - K_{s1})$  with hydration products are determined by the formula:

$$N = \frac{K_{s2} - K_{s1}}{1 - K_{s1}}, \text{ rel. units or cm}^3/\text{cm}^3; \quad (8)$$

All parameters proposed for the assessment of structure formation during hydration and hardening of FLA are closely related, which is based on the values of  $K_{s1}$  and  $K_{s2}$ .

### 3 Experimental Results and Discussion

The processes of hydration and hardening of FLA, accompanied by a change in the phase composition, develop over a long time, and therefore the parameters that reflect the process of restructuring the structure, are advisable to use to describe the kinetics of the processes [8, 9].

Table 2 shows the values that characterize the change in the phase composition and the main characteristics of the system structure: FLA – water over time of hydration.

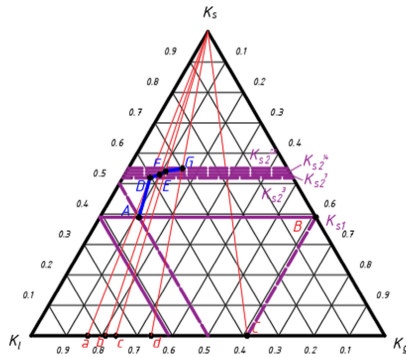
It is shown that the maximum degree of hydration  $\alpha_{hs} = 0.29$ . Increase in the content of the solid phase in the initial layer of FLA ( $K_{s1}$ ) fluorine-anhydrite binder is 29% at the age of 28 days and depends on the W/S. In the initial period of hardening, the degree of hydration is minimal. On the results of the calculations the phase diagram of the processes of hydration and hardening of binder is made, it is shown that the intensity of the processes of hydration of the binder without the use of additives is minimal, especially in the first three days, but later the intensity of these processes has slightly increased, as evidenced by the values of the rate constants of hydration and the value of the degree of hydration ( $\alpha_{hs}$ ). The latter is explained by the limited size of the initial free pore space  $(1 - K_{s1})$ , in which the formed hydration products harden during recrystallization and form a sufficiently strong FLA structure [10–13].

The graphical representation of changes in the phase composition during hydration and hardening allows to quantify these measurements at different W/S ratios, pressure,

**Table 2.** Changes in the phase composition of samples and the main characteristics of their structure.

$K_{S1}$	$K_{S2}$	N	$n$	$\alpha_n$	$\alpha_{hs}$	$R_{com}$ , MPa
After 3 days of hardening						
0.40	0.40	0.01	1.01	0.01	0.01	1.0
0.39	0.41	0.04	1.10	0.09	0.06	1.5
0.36	0.39	0.04	1.13	0.11	0.08	0.8
After 7 days of hardening						
0.40	0.41	0.41	1.05	0.05	0.03	2.1
0.39	0.42	0.42	1.14	0.12	0.08	2.7
0.36	0.40	0.40	1.18	0.15	0.19	5.0
After 14 days of hardening						
0.40	0.43	0.43	1.11	0.10	0.06	3.0
0.39	0.45	0.45	1.28	0.22	0.15	4.0
0.36	0.43	0.43	1.33	0.25	0.19	5.0
After 28 days of hardening						
0.40	0.46	0.46	1.26	0.20	0.14	4.4
0.39	0.49	0.49	1.48	0.32	0.25	5.4
0.36	0.46	0.46	1.53	0.35	0.29	5.8

temperature, changes in dispersion and various chemical additives. When using the phase characteristics of the initial and final parameters of the system, expressed in the proposed formulas and presented on the phase diagram, it is simplified to calculate the degree of hydration for the solid and liquid phases, the degree of filling of the pore space with hydration products, the degree of restructuring of the structure and the intensity of the flow of hydration processes (Fig. 1).



**Fig. 1.** Phase diagram of hydration and hardening processes.

The law of constancy of the volumetric phase composition of dispersed systems allows representing all changes in the FLA-water system graphically in the triple coordinate system  $K_s - K_l - K_g$ . An example of constructing a phase diagram of hydration and hardening processes (Fig. 1) is shown for samples with  $K_{s1} = 0.39$ , (Table 2).

The initial phase composition is represented by the point (1). We draw auxiliary horizontal lines AB and BC. During hydration of FLA, water binds and hydration products with a lower true density are formed, as a result, the volume fraction of the solid phase increases, so the diagram contains auxiliary lines  $K_{s2} = \text{const}$  for anhydrite stone at the age of 3, 7, 14, 28 days.  $K_{s2} = 0.41$ , at  $\tau = 3$  days,  $K_{s2} = 0.42$ , at  $\tau = 7$  days,  $K_{s2} = 0.45$ , at  $\tau = 14$  days,  $K_{s2} = 0.49$ , at  $\tau = 28$  days. For further construction, we use the triangle  $K_l, K_s, K_g$  whose side  $K_l, K_g$  characterizes the value of the initial free pore space  $(K_{l1} + K_{g1}) = 1 - K_{s1}$ .

Using the data of Table 2, a phase diagram of the hydration processes of anhydrite binder is constructed.

## 4 Conclusion

The authors propose a method for calculating the main structural characteristics of an anhydrite-containing binder with a change in its phase composition and construct a phase diagram of the fluorine-anhydrite-water system. It is shown that the use of volumetric phase characteristics of this system makes it possible to quantify effectively changes in the structure occurring during the interaction of the binder with water, and the construction of a phase diagram of this process opens up new approaches to elucidating the mechanisms of hydration and hardening of binders.

## References

1. Loganina, V.I., Pyshkina, I.S., Martiashin, G.V.: Effect of supplement based on calcium hydrosilicates on the resistance of lime coatings. *Mag. Civ. Eng.* **4**(72), 20–27 (2017)
2. Anikanova, L.A., Kudyakov, A.I., Volkova, O.V.: Wall and finishing materials with fluorogypsum. In: *Proceedings of Bratsk State University*, pp. 230–234 (2015)
3. Petropavlovskaya, V.B.: Use of mineral ultrafine modifiers based on industrial waste in gypsum composites. *Build. Mater.* **8**, 18–24 (2018)
4. Kurmangalieva, A.I., Anikanova, L.A., Volkova, O.V., Kudyakov, A.I., Sarkisov, Yu.S., Abzaev, Yu.A.: Activation of hardening processes of fluorogypsum compositions by chemical additives of sodium salts. *Izv. Vyssh. Uchebn. Zaved. Khim. Khim. Tekhnol* **8**, 73–80 (2020)
5. Lotov, V.A.: On interaction of cement particles with water or a mechanism of the cement hydration and hardening processes. *News Tomsk Polytech. Univ. Eng. Geosour.* **1**, 99–110 (2018)
6. Kudyakov, A.I., Anikanova, L.A., Redlikh, V.V.: Composite binding acid fluoride materials for fencing structures. *Vestnik TSUAB* **1**, 106–111 (2012)
7. Anikanova, L.A., Volkova, O.V., Kudyakov, A.I., Kurmangalieva, A.I.: Activated composite fluorogypsum binder. *Constr. Mater.* **1–2**, 36–42 (2019)
8. Anikanova, L.A., Volkova, O.V., Kudyakov, A.I., Sarkisov, Yu.S., Tolstov, D.A.: Influence of solidification accelerators on structure formation of anhydrite-containing binders. In: *IOP Conference Proceedings*, vol. 1, p. 070002 (2016)

9. Adewumi, A.A., Ismail, M., Ariffin, M.A.M., Yusuf, M.O., Maslehuddin, M., Mohamed, H.D.: Strength and microstructure of alkali-activated natural pozzolan and limestone powder mortar. *Mag. Civ. Eng.* **92**(8), 36–47 (2019)
10. Kudyakov, A.I., Anikanova, L.A., Kopanitsa, N.O., Gerasimov, A.A.: Influence of grain composition and type of fillers on properties of building solutions. *Build. Mater.* **11**, 28–29 (2001)
11. Muhsin, J., Nihad, A.Q., Ali, A.N.: Effect of adding industrial wastes on the mechanical properties of gypsum. *Int. J. Sci. Res. (IJSR)* **8**, 2123–2125 (2019)
12. Ushero-Marshak, A., Sopov, V.: Isometric calorimetry: a standard method for studying cement hydration kinetics. *Cem. Appl.* **5**, 106–107 (2009)
13. Moser, B.: Progress in building materials analysis. *ZKG Zement Kalk Gips Int.* **2**, 63–72 (2010)



# Assessment of the Pile Foundations Reliability in the Cryolithozone for the Climate Changing Conditions

A. N. Yakubovich<sup>(✉)</sup> and I. A. Yakubovich

Moscow Automobile and Road Construction State Technical University (MADI), Moscow, Russia

**Abstract.** Predictive estimates of the reliability of pile foundations located on permafrost soils were obtained under scenario assumptions of air warming by 2 °C. An indicator of reduced reliability is climate risk, which can range from 0 to 1000. The dependences of the risk value on the length of the pile are obtained for 4 types of soil in which the piles are located, and for 5 territorial points with different annual temperature conditions of atmospheric air. A strong dependence of the risk on the climatic characteristics of the territory was revealed. It is shown that for all types of soil, the climatic risk decreases with increasing pile length. The maximum risk of 810 points is predicted for short piles with a length of 3 m, located in low-moisture sandy soil and operated in the climatic conditions of Urengoy. Piles with a length of 6 m are characterized by a risk of 158 to 453 points, 9 m long – from 92 to 386 points. In general, the climate risks for piles with a length of less than 6 m are estimated as high, requiring reduction through engineering and technical measures. With a pile length of 6 m or more, the risks are average.

**Keywords:** Climate risks · Pile foundations · Permafrost soils · Simulation modeling

## 1 Introduction

Global climate change has a significant impact on all aspects of human life. According to forecasts, the average increase in air temperature in 2030 will average 1.41 °C, and by 2100 it will reach 3.17 °C [1]. At the same time, it is expected that the rate of warming in the Arctic will exceed the global average by about three times. Satellite observations for 1984–2004 showed that the average annual surface temperature in the Arctic regions increases at a rate of 0.34° per decade [2]. The paper [3] systematizes the main hazards caused by global climate change. Among them, it is necessary to highlight the acceleration of slow natural processes, which include an increase in the rate of degradation of permafrost soils.

The impact of climate change on the operational condition of buildings and structures, their reliability and durability, has a multidimensional nature and is considered in a significant number of works. The study of the durability of enclosing materials and

building elements, taking into account the expected climate changes, was carried out in [4]. It is shown in [5] that the effect of climate change leads to a reduction in the service life of reinforced concrete structures by an amount from 1.4 to 2.3%, with an increase of up to 7% for structures subject to cyclic loading. The impact of climate change on the operational condition and durability of buildings and structures depends significantly on the characteristics of the territory on which these objects are located. The projected frost resistance of the stone facades of Montreal will decrease by 2050, and will increase by 2080 relative to the current state of the climate [6]. An increase in the frost resistance of concrete facades in southern Finland is projected by 2030 [7]. The sensitivity of the forecast characteristics of buildings to the values of climatic parameters was studied in [8]. To increase the reliability of forecasting the future state of the climate in [9] an information system is proposed for collecting data on the current values of climate parameters and automated forecasting of the future state of the climate based on constantly updated data. Another method for obtaining geographically-linked climate forecasts is a weather generator [10].

The probabilistic nature of climate change causes uncertainties in the magnitude of future loads affecting buildings and structures and determining their reliability and durability. The spread of forecast values for the intensity of rain with strong winds within a 30-year interval can be up to 13% [11]. The error in predicting the air temperature using a neural network, carried out on the basis of data for the previous 65-year period, is estimated at 0.9 °C [12]. In some cases, large uncertainties in the magnitude of future impacts on engineering structures can lead to ambiguous results when assessing their safety [13].

Within the cryolithozone, the main factor that causes a decrease in the reliability and durability of buildings and structures under the influence of climate change is the accelerated thawing of permafrost. This leads to a decrease in the load-bearing capacity of the bases of engineering objects. The influence of global warming on the operational state of cryolithozone infrastructure facilities is considered in [14, 15]. In this paper, we predict the decrease in the reliability of buildings and structures on pile foundations under the influence of climate change and quantify the climate risks for certain territories of the cryolithozone of Russia.

## 2 Methods and Models

When quantifying the climate risk  $R$ , first, depending on the type of object, the criterion indicator  $k$  is selected, the change of which indicates an increase or decrease in the risk of a violation of the functionality of the object. Next, two climate states are recorded, described by the same set of parameters, the values of which change over the course of one average year. The first of these states is called the base climate  $\mathbf{B}$ , it corresponds to the climatic conditions adopted when designing the object and characterizes the specific territory on which the object is located. The second state (future climate  $\mathbf{C}$ ) is formed on the basis of accepted scenario assumptions about upcoming climate changes. For each climate state, a simulation of heat transfer in the soil mass is performed, as a result of which the temperature dynamics of the soil over the average year for the base and future climate ( $\mathbf{D}_B$  and  $\mathbf{D}_C$ , respectively) are determined. The worst value of the criterion indicator for the base climate  $k_B$  (determined on the basis of  $\mathbf{D}_B$ ) corresponds to the design climatic conditions of operation, and, consequently, the absence of climate risk

( $R = 0$ ). The difference between  $k_B$  and  $k_C$  (calculated for the future climate based on  $D_C$ ) determines the magnitude of the climate risk. The risk prediction procedure can be represented as:

$$R(\mathbf{B}, \mathbf{C}, \mathbf{G}) = F\{M[Q(\mathbf{B}, \mathbf{G})], M[Q(\mathbf{C}, \mathbf{G})]\}, \quad (1)$$

where  $\mathbf{G}$  – a set of physical-mechanical and geometric parameters describing the soil mass;  $Q$  – algorithm for modeling heat transfer in the ground and the formation of temperature dynamics  $\mathbf{D}$ ;  $M$  – algorithm for identifying the worst value of the criterion indicator during the year;  $F$  – an algorithm for determining the climate risk by comparing the  $k$  values for the baseline and future climate. The climate risk assessment procedure is discussed in more detail in [16, 17].

For the pile foundation under consideration, the criterion indicator was the load-bearing capacity of the base of a vertically loaded pile, determined in accordance with SP 25.13330.2012. An enlarged description of the base climate for the points where the climate risk assessment was carried out is given in Table 1; long-term data from instrumental climate observations were used in the simulation. The future climate was characterized by a uniform, throughout the average year, increase in air temperature by 2 °C compared to the base climate.

**Table 1.** Enlarged characteristics of the atmospheric air temperature regime for the base climate.

№	Locality	Period of positive temperatures, days	Average air temperature, degrees Celsius		Average wind speed, m/s
			For the period of negative temperatures	For the period of positive temperatures	
1	Yakutsk	153	−26.0	+11.9	2.1
2	Urengoy	131	−17.3	+9.5	4.2
3	Susuman	131	−25.3	+9.0	2.1
4	Saskylakh	110	−23.1	+7.7	3.3
5	Srednekan	139	−24.4	+10.4	1.8

The characteristics of the base soils are given in Table 2. The geometric dimensions of the simulated soil mass were equal to 10 × 10 × 10 m, the soil temperature was determined at points located in increments of 10 cm.

**Table 2.** The parameters of the soil at the base of the pile foundation used in the modeling.

№	Name of the indicator	Type of soil			
		1	2	3	4
1	Type of soil	Sand	Sand	Clay	Clay
2	The total moisture content of frozen soil, %	20	35	30	50
3	Humidity of the frozen ground located between the ice inclusions, %	10	17.5	15	25
4	Total ice content of frozen ground, %	2	3.5	3	5
5	Soil density, kg/m <sup>3</sup>	1800	1800	2000	2000

The value of the climate risk was normalized to the range [0; 1000]. Thus, it was possible to compare risks for different types of objects characterized by different criteria indicators.

### 3 Results and Discussion

The predicted climatic risks are shown in Fig. 1. One can see an expressed reduction in risk with an increase in the length of the pile, which is explained by the almost complete preservation of the bearing capacity of the soil in the new climatic conditions at a depth of 6 m or more. At the same time, a noticeable increase in temperature in the upper layers of the soil, accompanied by an increase in the thickness of the seasonal melt layer, is very sensitive for short piles (less than 6 m long), the risk value for which in most cases exceeds 500 points, with a maximum value of 810 points.

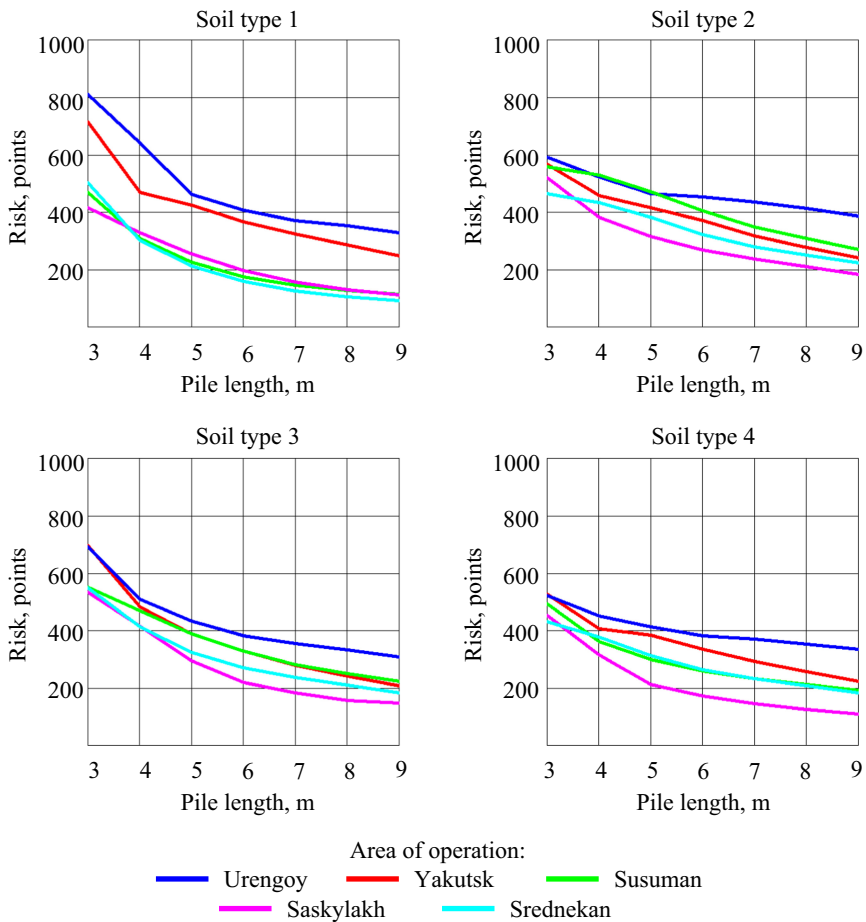


Fig. 1. Predicted risks of climate warming by +2 °C.



With the exception of the length of the pile, the influence of other factors (the type of soil, its humidity, climatic features in the territory) on the climate risk does not follow a certain pattern, and the risk value is determined by a combination of all these factors. In most cases, warming by 2° is most dangerous for the pile foundations of Urengoy, and the greatest resistance to these climate changes is predicted for the foundations in Saskylakh (with the exception of sandy low-moisture soil, where the lowest risk values are obtained for Susuman and Srednekan).

It should be noted that the maximum risk of 1000 points does not mean an immediate failure of the foundation. In this case, there is a decrease in the bearing capacity of the foundation by the amount determined by the reserve coefficients used in the design, but the physical destruction of the foundation is likely not to occur. At the same time, the operation of such a facility should be stopped immediately.

## 4 Conclusion

Climate risks in relation to pile foundations on permafrost soils, predicted as a result of a fairly conservative scenario of warming by +2 °C, are significant and should be taken into account in the operation of the relevant facilities in the cryolithozone.

A strong dependence of the magnitude of the climate risk on the climatic and ground conditions was revealed. Accordingly, the risk assessment according to the methodology considered in this paper should be carried out individually for each object.

In the framework of the accepted climate change scenario, the predicted risks for short piles (less than 6 m) are high and require mandatory implementation of engineering and technical measures to preserve the temperature regime of the soil in the new climatic conditions. Piles with a length of 6 m or more are characterized by an average level of risk, in which it is necessary to control the amount of observed warming of the atmospheric air. If the scenario limit of warming is exceeded, the risk value needs to be clarified.





## References

1. Wang, F., Tokarska, K.B., Zhang, J., Ge, Q., Hao, Z., Zhang, X., Wu, M.: Climate warming in response to emission reductions consistent with the Paris agreement. *Adv. Meteorol.* 2487962 (2018). <https://doi.org/10.1155/2018/2487962>.
2. Wang, X., Key, J., Liu, Y., Fowler, C., Maslanik, J., Tschudi, M.: Arctic climate variability and trends from satellite observations. *Adv. Meteorol.* 505613 (2012). <https://doi.org/10.1155/2012/505613>.
3. Glasser, R.: The climate change imperative to transform disaster risk management. *Int. J. Disaster Risk Sci.* **11**(2), 152–154 (2020). <https://doi.org/10.1007/s13753-020-00248-z>
4. Lacasse, M.A., Gaur, A., Moore, T.V.: Durability and climate change – implications for service life prediction and the maintainability of buildings. *Buildings* **10**(3), 53 (2020). <https://doi.org/10.3390/buildings10030053>
5. Bastidas-Arteaga, E.: Reliability of reinforced concrete structures subjected to corrosion-fatigue and climate change. *Int. J. Concr. Struct. Mater.* **12**, 10 (2018). <https://doi.org/10.1186/s40069-018-0235-x>
6. Sehizadeh, A., Ge, H.: Impact of future climates on the durability of typical residential wall assemblies retrofitted to the PassiveHaus for the Eastern Canada region. *Build. Environ.* **97**, 111–125 (2016). <https://doi.org/10.1016/j.buildenv.2015.11.032>

7. Pakkala, T.A., Köliö, A., Lahdensivu, J., Kiviste, M.: Durability demands related to frost attack for Finnish concrete buildings in changing climate. *Build. Environ.* **82**, 27–41 (2014). <https://doi.org/10.1016/j.buildenv.2014.07.028>
8. Tian, W., Wilde, P.: Uncertainty and sensitivity analysis of building performance using probabilistic climate projections: A UK case study. *Autom. Constr.* **20**(8), 1096–1109 (2011). <https://doi.org/10.1016/j.autcon.2011.04.011>
9. Yakubovich, A.N., Yakubovich, I.A., Trofimenko, Yu.V., Shashina, E.V.: Intelligent management system of the automobile road's technical and operational condition in the Cryolithozone. In: *Proceedings Systems of Signals Generating and Processing in the Field of on Board Communications, SOSG 2019'03* (2019). <https://doi.org/10.1109/SOSG.2019.8706742>
10. Kershaw, T., Eames, M., Coley, D.: Assessing the risk of climate change for buildings: a comparison between multi-year and probabilistic reference year simulations. *Build. Environ.* **46**(6), 1303–1308 (2011). <https://doi.org/10.1016/j.buildenv.2010.12.018>
11. Nik, V.M., Mundt-Petersen, S.O., Kalagasidis, A.S., Wilde, P.D.: Future moisture loads for building facades in Sweden: climate change and wind-driven rain. *Build. Environ.* **93**(2), 362–375 (2015). <https://doi.org/10.1016/j.buildenv.2015.07.012>
12. Zhang, Z., Dong, Y.: Temperature forecasting via convolutional recurrent neural networks based on time-series data. *Math. Prob. Eng.* 3536572 (2020). <https://doi.org/10.1155/2020/3536572>
13. Wang, Y., Gong, J., Liu, Y., Sh, C., Zheng, J.: Effect of climate change on flexural reliability of highway continuous girder bridge under wind load. *Bridge Struct.* **15**(3), 103–110 (2019). <https://doi.org/10.3233/BRS-190155>
14. Yakubovich, A., Yakubovich, I.: Using the response surface to assess the reliability of the Russian Cryolithozone road network in a warming climate. *Adv. Intell. Syst. Comput.* **1258**, 486–495 (2021). [https://doi.org/10.1007/978-3-030-57450-5\\_42](https://doi.org/10.1007/978-3-030-57450-5_42)
15. Kronik, Y.A.: Reliability and safety of the foundations of buildings and structures on permafrost. *Soil Mech. Found. Eng.* **54**(3), 198–201 (2017). <https://doi.org/10.1007/s11204-017-9458-0>
16. Yakubovich, A., Mayorov, S., Pyatkin, D., Yakubovich, I.: Monitoring and predicting the state of the road network in Russia's cryolitic zone. *Adv. Intell. Syst. Comput.* **1116**, 924–933 (2020). [https://doi.org/10.1007/978-3-030-37919-3\\_91](https://doi.org/10.1007/978-3-030-37919-3_91)
17. Trofimenko, Y., Yakubovich, A.N., Yakubovich, I.A., Shashina, E.V.: Modeling of influence of climate change character on the territory of the cryolithozone on the value of risks for the road network. *Int. J. Online Biomed. Eng.* **16**(07), 65–74 (2020). <https://doi.org/10.3991/ijoe.v16i07.14557>



# Thermal Phase Transformations in Titanium Hydride - A Filler for Special-Purpose Construction Materials

R. N. Yastrebinsky<sup>(✉)</sup> , A. A. Karnauhov , A. V. Yastrebinskaya ,  
and L. V. Denisova 

Belgorod State Technological University named after V.G. Shukhov, Belgorod, Russia

**Abstract.** Thermal phase transformations in titanium hydride, used as a filler for special-purpose construction materials, operated in the temperature range 100–700 °C, are considered. It has been established that the phase composition of the titanium hydride fraction is represented by the main reflection  $T_iH_{1.924}$  of the cubic crystal system with crystallographic indices  $hkl \{111\}$ . Heat treatment of titanium hydride in the temperature range from 300 to 400 °C, with a constant phase composition and interplanar distances, changes the intensity and broadening of the diffraction lines of the main reflection, which indicates the defective structure of the crystal. In the temperature range from 100 to 400 °C, the density of dislocations in the structure of the titanium hydride crystal increases. At 700 °C, the phase composition of titanium hydride changes with the formation of titanium oxide TiO of the hexagonal crystal structure and the rutile TiO<sub>2</sub> phase of the tetragonal system. There is a sharp increase in the density of dislocations and the degree of defectiveness of the crystal. At titanium atoms, tetrahedral voids arise due to the dissociation of titanium hydride.

**Keywords:** Titanium Hydride · Crystal system · Heat treatment · Phase Composition · Dislocation Density

## 1 Introduction

Metal hydrides have recently been used to create special-purpose structural materials. Their use as fillers of both polymer and silicate matrices determines the properties of composites and the possibility of their use as protective structures against neutron radiation [1, 2]. These materials can be widely used at nuclear power facilities to protect stationary and transport nuclear power reactors. The study of the properties of these materials in various conditions of their operation will allow, with a sufficient degree of probability, to predict the reliability of building structures and structures based on them [3–5].

Titanium hydride is one of the promising materials used in this direction for nuclear power [5, 6]. Due to the increased hydrogen content, it is effectively used as a neutron protection layer in the structures of the radiation and biological protection of the reactor

under radiation exposure, due to the energy of interaction of neutron and gamma radiation with the substance, thermal heating of the shielding material occurs. The thermal heating process, starting from a certain temperature, is accompanied by the dissociation of titanium hydride and the evolution of hydrogen. This significantly reduces the radiation-protective properties of the material and causes the possibility of fire hazardous situations, especially at the facilities of operation of transport nuclear power plants.

The thermal stability of a metal hydride is understood as its ability to maintain the atomic ratio of hydrogen to metal when exposed to elevated temperatures. The loss of hydrogen from a metal hydride depends on the atomic ratio of hydrogen to metal, temperature, composition and pressure of the environment.

In this regard, this article discusses the issues of thermal stability and structural-phase transformations in titanium hydride subjected to treatment in air in the temperature range 100–900 °C.

## 2 Methods and Materials

For research used titanium hydride obtained by dispersing granular titanium hydride with a hydrogen content of 3.5 wt. %, obtained, in turn, according to TU 162 - 2010.

X-ray phase (XPA) and X-ray diffraction analysis was performed on a “Dron-2.0” X-ray diffractometer with  $\text{Cu}_{\text{K}\alpha}$  radiation ( $\lambda_{\text{K}\alpha} = 1.542 \text{ \AA}$ ) and a nickel filter according to the method [7] using the ASTM file (USA). The spectra were recorded with an MSTR-4 ionization counter at angles from 4 to 112°. The diffraction patterns were measured with a RK-3A comparator. The X-ray diffraction patterns of the sample under study were processed separately for each shooting interval using the PDWin program. At the end of the processing, a general output file of spectral characteristics of the sample was created: angle  $2\theta$  and intensity at the peak maximum, or angle  $2\theta$  of the center of gravity and integral intensity. The determination of the initial and newly formed phases was carried out by analyzing the interplanar distance  $d$  and the intensity of spectral reference lines.

## 3 Results and Discussion

Analysis of the diffraction patterns of titanium hydride heat-treated in the temperature range 100–700 °C showed the constancy of the phase composition up to 500 °C. In the samples of titanium hydride dried at 100 °C, the interplanar distances are  $d = 2.5537$ ;  $2.2220$ ;  $1.5691$  correspond to titanium hydride with nonstoichiometric hydrogen content  $\text{TiH}_{1.924}$  cubic crystal structure and crystallographic indices  $hkl \{111\}$ .

Heat treatment of titanium hydride at temperatures from 300 to 500 °C did not lead to a change in the phase composition. In this case, there was a change in the intensity and broadening of the diffraction lines of the main reflection (Tables 1, 2, 3, 4 and 5). These changes indicate the defectiveness of the crystal structure.

At a temperature of 700 °C, the diffraction pattern of shot samples changes with the formation of basic reflections with an interplanar distance  $d = 3.2608$ ;  $1.8715 \text{ \AA}$ , corresponding to titanium oxide  $\text{TiO}$  of the hexagonal crystal system, and reflections with  $d = 2.2675$ ;  $1.7554 \text{ \AA}$ ;  $4.8087 \text{ \AA}$ , corresponding to the rutile  $\text{TiO}_2$  phase of the

**Table 1.** Diffraction characteristics of the main phases of titanium hydride heat-treated at a temperature of 100 °C.

Angle $2\theta$ , °	Area	Intensity, imp./sec	Half-width, Å	d, Å	% max.
35.140	860.832	5299	0.5100	2.5537	100.00
40.600	397.137	1040	1.0050	2.2220	19.63
58.850	376.692	1075	0.7050	1.5691	20.29

**Table 2.** Diffraction characteristics of the main phases of titanium hydride heat-treated at a temperature of 300 °C.

Angle $2\theta$ , °	Area	Intensity, imp./sec	Half-width, Å	d, Å	% max.
35.140	961.192	5803	0.5200	2.5537	100.00
40.600	344.912	984	0.8500	2.2220	16.96
58.950	266.384	1083	0.6700	1.5667	18.66

**Table 3.** Diffraction characteristics of the main phases of titanium hydride heat-treated at a temperature of 400 °C.

Angle $2\theta$ , °	Area	Intensity, imp./sec	Half-width, Å	d, Å	% max.
35.140	822.503	4872	0.5300	2.5537	100.00
40.550	404.390	979	0.9500	2.2246	20.09
58.950	231.827	984	0.7000	1.5667	20.20

**Table 4.** Diffraction characteristics of the main phases of titanium hydride heat-treated at a temperature of 500 °C.

Angle $2\theta$ , °	Area	Intensity, imp./sec	Half-width, Å	d, Å	% max.
35.140	893.112	5680	0.4800	2.5537	100.00
40.650	315.316	1021	0.9000	2.2194	17.98
58.950	251.738	1045	0.7100	1.5667	18.40

tetragonal system. At the same time, the titanium hydride phase with the interplanar distance  $d = 2.5516$  is retained;  $1.5643$  Å.

Using the approximation method to determine the size of the coherent scattering regions, based on the diffraction characteristics of the main phase of titanium hydride of maximum intensity, an assessment of the defectiveness of its crystals in the temperature range 100–700 °C is given (Table 6).

**Table 5.** Diffraction characteristics of the main phases of titanium hydride heat-treated at a temperature of 700 °C.

Angle 2θ, °	Area	Intensity, imp./sec	Half-width, Å	d, Å	% max.
27.350	19.930	152	0.2900	3.2608	11.40
48.650	14.801	176	0.1350	1.8715	13.20
39.750	669.345	1333	1.0250	2.2675	100.00
52.100	112.830	232	0.6550	1.7554	17.40
18.450	80.275	152	0.8150	4.8087	11.40
35.170	377.137	1040	0.7500	2.5516	78.02
59.050	122.386	205	0.8200	1.5643	15.38

It is known that titanium hydride of stoichiometric composition TiH<sub>2</sub> is characterized by a face-centered cubic lattice [8]. In this case, the compositions with a lower hydrogen content also have a cubic system, but with the presence of tetrahedral voids at titanium atoms [9].

**Table 6.** Diffraction characteristic of the maximum reflection of titanium hydride at different temperatures.

T, °C	Angle 2θ, °	Area	Intensity, imp./sec	Half-width, Å	d, Å	% max.
100	35.140	860.832	5299	0.5100	2.5537	100.00
300	35.140	961.192	5803	0.5200	2.5537	100.00
400	35.140	822.503	4872	0.5300	2.5537	100.00
500	35.140	893.112	5680	0.4800	2.5537	100.00
700	35.170	377.137	1040	0.7500	2.5516	78.02

Analysis shows that in the temperature range 100–400 °C, the diffraction line broadens  $d = 2.5537 \text{ \AA}$  from 0.5100 to 0.5300 Å. An analysis of the broadening showed that at 400 °C there is a noticeable fragmentation of the coherent scattering regions. In this case, the value of the interplanar distances remains constant, which indicates the invariability of the period of the crystal unit cell ( $a$ ). According to the data [10–13], the broadening (smearing) of diffraction lines is due to the presence of microdeformations of the crystal lattice and indicates an increase in the density of dislocations ( $\rho$ ), and their growth is proportional to the square of the broadening ( $\beta$ ) by the formula:

$$\rho = \frac{\pi\beta^2 ctg^2\theta}{16b^2}, M^{-2} \quad (1)$$

where  $\theta$  - is the angle corresponding to the maximum of the X-ray line;  $b$  - Burgers vector.

Thus, in the temperature range from 100 to 400 °C, the dislocation density in the structure of the titanium hydride crystal increases. An increase in temperature to 500 °C decreases the dislocation density, which, according to [14], is due to the annealing regime without changing the structural elements. A further increase in temperature to 700 °C leads to a sharp increase in the density of dislocations and the degree of defectiveness of the crystal. In this case, the interplanar distance decreases to  $d = 2.5516 \text{ \AA}$ , which indicates the presence of microstresses in the crystal lattice of titanium hydride and a less dense filling of the atomic plane by structural elements. At titanium atoms, tetrahedral voids arise due to the dissociation of titanium hydride. This is consistent with the data [15], where it was shown that a decrease in the hydrogen content in titanium hydride leads to a defective structure and the presence of voids in the FCC sublattice between titanium atoms.

A change in the interplanar distance leads to a change in the period of the crystal unit cell, which for the cubic system of titanium hydride is determined by the formula [16]:

$$a = dhkl\sqrt{h^2 + k^2 + l^2} \quad (2)$$

For the temperature range of 100–500 °C, the cell period is  $a = 4.4231 \text{ \AA}$ , and for 700 °C  $a = 4.4195 \text{ \AA}$ . In this case, the period of the unit cell of the reference crystal is  $a = 4.4200 \text{ \AA}$  (according to the ASTM card index for the  $\text{TiH}_2$  crystal). Thus, an increase in temperature to 700 °C brings the parameters of the unit cell closer to the parameters of the reference crystal. This may be due to the fact that for XRD we used crushed titanium hydride shot after its heat treatment. It can be assumed that an increase in temperature and the processes of thermal diffusion of hydrogen from the bulk of the shot to the surface lead to additional hydrogenation of metallic titanium in the surface layer and the formation of crystals with a structure close to  $\text{TiH}_2$ .

In this case, there is a general significant decrease in the intensity of hydride phases and the formation of a rutile phase, which indicates intense oxidation and dissociation of titanium hydride.

## 4 Conclusion

1. The thermal stability and phase composition of titanium hydride were investigated in the temperature range 100–700 °C. The sizes of the regions of coherent scattering and microdistortions of the crystal lattice of hydride phases at different annealing temperatures are determined.
2. It was found that the phase composition of the titanium hydride fraction is represented by the main reflection  $\text{TiH}_{1.924}$  of the cubic crystal system with crystallographic indices  $hkl \{111\}$ .
3. It was found that in the temperature range from 100 to 400 °C the density of dislocations in the structure of the titanium hydride crystal increases. At 400 °C, a noticeable fragmentation of the coherent scattering regions occurs.

**Acknowledgements.** The work is realized using equipment of High Technology Center at BSTU named after V.G. Shukhov the framework of the State Assignment of the Ministry of Education and Science of the Russian Federation, project No. FZWN-2020-0011.




## References

1. Sickafus, K.E.: Radiation-induced amorphization resistance and radiation tolerance in structurally related oxides. *Nat. Mater.* **6**(3), 217–223 (2007)
2. Fukai, Y.: *The Metal-Hydrogen System. Basic Bulk Properties.* Springer Series in Materials Science, vol. 21, p. 1237 (1993)
3. Cherkashina, N.I., Pavlenko, A.V.: Influence of SiO<sub>2</sub> crystal structure on the thermal cycle of polymer composites. *Constr. Mater. Prod.* **1**(4), 21–29 (2018)
4. Pavlenko, V.I., Cherkashina, N.I., Yastrebinsky, R.N.: Synthesis and radiation shielding properties of polyimide/Bi<sub>2</sub>O<sub>3</sub> composites. *Heliyon* **5**, E01703 (2019)
5. Nasser, M.M.: Comparison of HfB<sub>2</sub> and ZrB<sub>2</sub> behaviors for using in nuclear industry. *Ann. Nucl. Energy* **114**, 603–606 (2018)
6. Sorokin, V.V., Sharapov, O.N., Shunkin, N.M., Kiryushina, N.Yu.: New polymeric composites based on epoxy resin with techogenic wastes. *Bull. BSTU named after V.G. Shukhov* **6**, 8–13 (2019)
7. Pavlenko, A.V., Cherkashina, N.I., Yastrebinskii, R.N.: Nanodisperse metalloorganosiloxane fillers of polymers. *Nanotechnol. Constr. Sci. Internet-J.* **8**(4), 113–130 (2016)
8. Pavlenko, A.V., Cherkashina, N.I., Noskov, A.V.: Calculation of the frequency electronic transmission factors at the passage through the polymeric polyimide composite material filled by bismuth silicate. *Prob. Atomic Sci. Technol.* **5**, 21–26 (2017)
9. Cherkashina, N.I., Pavlenko, V.I., Yastrebinskii, R.N.: Phase transitions and electrophysical properties of tungsten(VI) oxide in a 83–673 K temperature range. *Russ. Phys. J.* **62**(5), 870–875 (2019)
10. Pavlenko, V.I., Edamenko, O.D., Cherkashina, N.I., Kuprieva, O.V., Noskov, A.V.: Study of the attenuation coefficients of photon and neutron beams passing through titanium hydride. *J. Surf. Invest-X-ray.* **9**, 546–549 (2015)
11. Pavlenko, A.V., Cherkashina, N.I., Yastrebinski, R.N.: Nanodisperse metalloorganosiloxane fillers of polymers. *Nanotechnol. Constr. Sci. Internet-J.* **8**(4), 113–130 (2016)
12. Yastrebinsky, R.N., Karnauhov, A.A., Yastrebinskaya, A.V.: Improving the radiation-thermal stability of titanium hydride. *J. Phys.: Conf. Ser.* 1–6 (2020)
13. Guseynov, R.M., Radzhabov, R.A., Magomedova, U.M.: The element with constant phase shift in galvanodynamic mode. *Chem. Bull.* **2**(2), 4–8 (2019)
14. Slyusar, O.A., Cherkashina, N.I., Yastrebinskaya, A.V.: Effect of additives on dispersed system structure formation. *Refract. Ind. Ceram.* **55**(6), 562–564 (2015)
15. Shestakov, I.Ya., Veretnova, T.A., Strekalova, T.A.: Investigation of water electrical activator with coaxial arrangement of electrodes. *Chem. Bull.* **4**(1), 12–18 (2018)
16. Arbuzova, A.A., Votyakov, M.A.: Estimation of the influence of the state of the reinforcing polymer in the structure of polymeric fiber material using mathematical prediction methods. *Chem. Bull.* **1**(1), 12–17 (2018)





# Investigation of the Technical Condition of Buildings and Structures in the Conditions of Dangerous Geological Processes

N. Yu. Soytu<sup>(✉)</sup> , M. A. Aleynikova , and A. V. Novozhilova 

St. Petersburg State University of Architecture and Civil Engineering, St. Petersburg, Russia

**Abstract.** The paper is devoted to the study of topical issues related to the assessment of the technical condition of buildings and structures in the conditions of dangerous geological processes. The analysis of the existing scientific heritage and the methods used revealed the need to develop new refined calculation methods and software tools for conducting research of construction objects in geologically hazardous areas. Based on the results obtained, the paper proposes a set of interrelated measures to determine the parameters of the technical condition of structures in the conditions of hazardous geological processes. The developed set of actions is based on the creation of a spatial-coordinate model, which involves the use of geodetic measurements and spatial-coordinate survey of the monitoring object, as well as the construction of a soil model. The ground model makes it possible to represent visually the isofields of the building subsidence, and the spatial-coordinate model determines the geometric parameters, deflections, displacements, strength and rigidity of individual elements of buildings in the conditions of geological disturbances. The recommendations formulated in the paper allow determining with a high degree of confidence the maximum permissible values of shifts of the controlled components of the building and the corresponding parameters of spatial movements by modeling possible variants of deformation actions, as well as to establish the values of the maximum permissible deformations of the bases.

**Keywords:** Technical condition · Assessment · Deformations · Geological processes · Model · Soil · Stress · Survey · Space

## 1 Introduction

The economic efficiency of the modern management system depends crucially on the quality of the technical operation of fixed assets, which include buildings and structures. At the same time, dangerous geological processes pose a significant threat to industrial and residential development [1]. The problem of safety of construction facilities in areas of development of dangerous exogenous geological processes is one of the main technical, scientific and socio-environmental problems of our time due to the losses caused by these changes. The main types of exogenous geological transformations that entail the most negative consequences are landslides, mudslides and karst [2, 3]. In addition, the significance of the issues is also due to the deeper development of soils,

which includes: increasing depth of mining coal seams and the changing nature of distribution and magnitude of deformations in the mold displacement; depreservation of stocks of minerals from pillars protected under densely populated areas; increasing the proportion of undermined areas with difficult geological conditions, increasing the height of the urban development and related problem of protection of buildings from rolls etc.

In this context, the study of the influence of hazardous geological processes on the stability of buildings and structures becomes very relevant, which in turn determines the need for a comprehensive review of the actual parameters of the reliability of buildings and their stress-strain state.

At the same time, it should be noted that in the process of evaluating the technical characteristics of buildings and structures, it is usually assumed that the construction object is affected as a system in which, at any time interval and at the same level, all points of the plan are located in the same phase in terms of acceleration, displacement, speed and at their same amplitude. In reality, due to the fact that dangerous geological processes do not occur instantly, but have a certain final speed, which depends on the characteristics of the building itself, the density of the soil, various elements of the building fluctuate nonsynchronously, while demonstrating different values of acceleration, which in turn leads to additional longitudinal forces of compression-stretching and horizontal displacement [4].

In addition, the evaluation of the technical state of the construction object according to the analysis of stress-strain state can be made only if that solved the contact problem, that is not considered a separate building and the calculation of system “base-building” taking into account the spatial stiffness and deformation characteristics of the subgrade. Methods for calculating deformations of the ground surface, which have not been independently analyzed for a long time and have well-established false assumptions, also need to be improved.

Thus, taking into account the above, it seems that the important scientific and practical task today is to develop such a research system of technical condition of buildings and constructions in hazardous geological processes which took into account the main parameters of operation of the construction object, the deformation modulus of each soil layer and was optimized by the criterion of minimum total cost. At the same time, we believe that such a system should be based on the accumulation of a posteriori data, be comparable at different levels of surveys, and have the properties of accumulating experimental values for analyzing the technical condition of buildings and structures, as well as predicting it.

The issues of determining and improving the stability of construction objects in the conditions of dangerous geological processes are covered in the works of well-known foreign authors, that include Coïsson Eva; Segalini Andrea; Bonetto Sabrina, Maria Rita, Cevik S. Y., Ulusay, R.

Russia is also actively working to improve methods and approaches for calculating the stability and reliability of structures under the influence of geological changes. The works of I. S. Kazakova, N. A. Kuznetsova, S. A. Aliev, A. M. Beybulatov, R. S. Murtazaeva and others are devoted to this problem.

At the same time, theoretical and applied research is characterized by its incompleteness, the optimization of organizational and technological solutions in this scientific segment is not done enough. This applies to comprehensive studies to determine the parameters of buildings, structures and site development throughout the design, construction and operation as an integrated system in terms of unstable geological changes; development and justification of scientific classifications of systems for measuring of parameters of objects for different conditions of construction and operation.

## **2 Aim of the Research**

Development and improvement of the methodological basis for the study of the technical condition of buildings and structures in the conditions of hazardous geological processes.

## **3 Materials and Methods**

In the course of the study, a large number of available reports were processed, which contain information about the technical condition of about 700 buildings constructed from various types of materials and structures - stone structures, buildings with stone load-bearing walls in areas with varying degrees of danger of geological shifts. Foundations, external and internal walls, ceilings and roofs were considered as load-bearing and capital structures of the buildings under study.

The methodological basis of the research is the following set of methods:

- parametric method, which provides for the establishment of parameters that determine the safety, functionality and quality of buildings and structures;
- methods of inspection of building structures for determining the controlled parameters using modern approaches and devices;
- mathematical modeling of the stress-strain state of structures of buildings and structures;
- methods of construction mechanics in the process of calculating the structures of buildings and structures under various influences;
- assessment of the technical condition based on the conducted surveys and calculations.

## **4 Results and Discussion**

The technical condition of a building is a set of properties of its structures that change during operation and repair, and are characterized at a certain point in time by the values of indicators (technical parameters), as well as by the quality characteristics established in the operational and repair documentation [5].

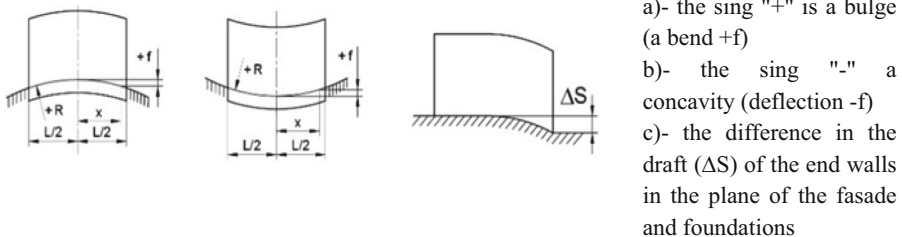
To date, in addition to the visual and normative assessment of the state of building structures located in geologically dangerous areas, a numerical analysis of their SSS is carried out on the basis of verification calculations based on the updated data obtained during the survey [6]. The design and calculation of building structures, as a rule, is carried out by numerical methods on a computer using specialized computer systems,

the algorithms of which are overwhelmingly based on the finite element method [7]. This technology is currently the main engineering tool for automated mathematical analysis of the technical condition of building structures that are under the influence of any type of external influences, including uneven deformations of the bases.

However, in order to increase the accuracy and maximize the consideration of soil deformations, geological and tectonic processes, it seems appropriate to supplement the finite element method with automated creation of a soil model and calculation of elastic base parameters.

In addition, if, according to Building norms and rules it is recommended to use approaches to calculations of foundations as systems “base-foundation” or “base-foundation-building” on the foundation deformation, then for geologically hazardous areas, it seems appropriate instead of “deformation of the ground surface” to use the expression “deformation of foundation” as a more local activity distribution and redistribution of stresses between the foundations of the building and the ground.

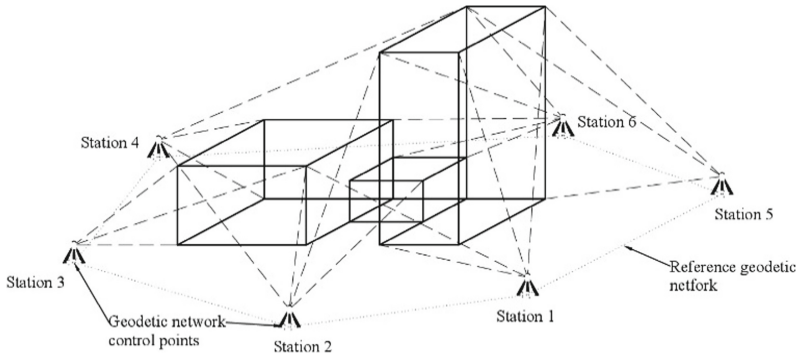
Also in the process of assessing the technical condition of buildings and grounds they should take into account the actual “deformation of foundations”, which are divided into the following types (Fig. 1): S precipitation, mm; a difference residue  $\Delta S$ , mm; the deflection  $f$  mm; the inclination  $i$ , mm/m; the curvature (convexity, concavity)  $p$ ., 1/km; the radius of curvature  $R = 1/r$ , km vertical offset between the individual houses or their parts usually in areas with abrupt changes in vertical stiffness.



**Fig. 1.** Diagrams of vertical movements of the base under the foundations at formation of the corresponding radii of curvature  $\pm R$ .

It is advisable to identify the spatial movement of the complex of main points of a construction object located in mobile geological conditions, which are marked with deformation marks at various levels along the perimeter and height of the structure, using spatial coordinate (SC) surveys based on data obtained from electronic tacheometers (Fig. 2).

Based on the differences in the spatial coordinates ( $x_i$ ,  $y_i$ ,  $c_i$ ), which correspond to the actual planned-altitude position of the control points of the structure at different monitoring periods, its horizontal and vertical movements are calculated (Fig. 3). To systematize the entire data array, a spatial-coordinate model (SC-model) is developed, which allows monitoring the technical condition of the building (Fig. 3). The main points



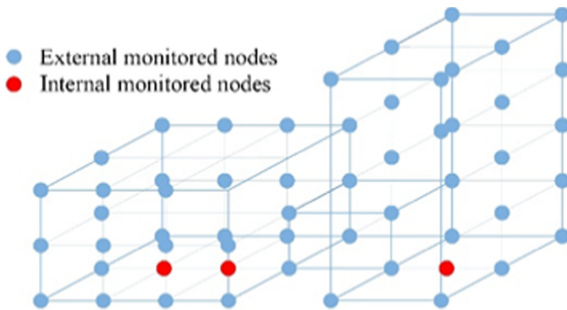
**Fig. 2.** Spatial-coordinate shooting of the monitoring object.

of the construction object are controlled nodes of the SC-model.

$$\Delta X_i^j = x_i^0 - x_i^j, \Delta Y_i^j = y_i^0 - y_i^j, \Delta Z_i^j = z_i^0 - z_i^j, \Delta XY_i^j = \sqrt{(\Delta X_i^j)^2 + (Y_i^j)^2}$$

$$\varphi_i^j = \arctg \frac{\Delta X_i^j}{\Delta Y_i^j}; \gamma_{i \rightarrow i-1}^j = \arctg \frac{\Delta XY_i^j}{z_i^j - z_{i-1}^j}$$

Taking into account the design scheme and the size of the structure, the intensity of geological disturbances, the SC model can cover only the external contour of the object, i.e. it is based on external controlled nodes that are fixed on the facades [8, 9]. If the building has significant dimensions or is characterized by a complex structure, in order to increase the accuracy of the assessment of the technical condition and the possibility of additional control of deformations, the PC model should also include controlled nodes inside the construction object (Fig. 3).



**Fig. 3.** SC-model for monitoring the technical condition of a building.

For integrated use in the process of technical assessment of the building of the SC model and the soil model, it seems appropriate to use the SOIL system. This will make it possible to determine the stress in the soil mass from the circular load area by numerical

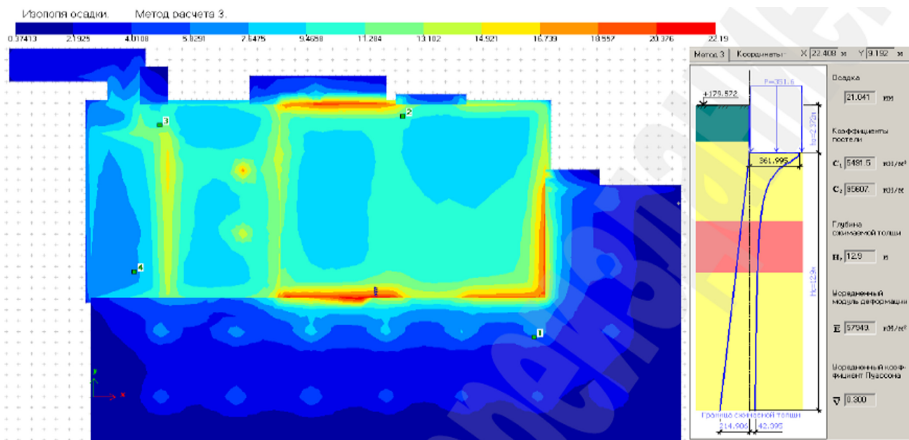
integration for the entire array of elementary layers of all foundation slabs, taking into account the mutual influence.

The soil model contains information about the geology in each monitored building node. Each composite IGE (engineering-geological element) is described by the following characteristics of the soil: modulus of deformation  $E$ ; Poisson's ratio  $\nu$ ; specific gravity of the soil  $\gamma$ .

The calculation is the iterative way in which in the first stage are going to load in the form of reactions at the level of the base of the foundation, taking into account the rigidity of the construction object by a constant value of the stiffness of the foundation [10, 11]. Then the obtained data of the base reactions are transmitted as the values of the pressure loads to the calculated model of the base, followed by its calculation by deformations (precipitation), on the basis of which new (redistributed) stiffness coefficients of the base are determined.

To calculate the base sediment at each calculated point at the contact with the foundations, the method of summing the deformations of the elementary layers along this vertical without taking into account the lateral expansion should be used. In this case, the stress from the ground's own weight can be calculated by the generally accepted method, and the distributed stresses can be calculated on the basis of closed solutions for the model of a half-space that is linearly deformed [12]. In the process of calculating distributed stresses, it is necessary to take into account the mutual influence of the sections of this foundation. After that, the obtained values of stiffness of foundation considering soil work in the linear stage is added to the source data for the model calculation. Based on the final results, a conclusion is made about the technical condition of the evaluated building and its stress-strain state.

Figure 4 shows an example of an isofield model of the building.



**Fig. 4.** Isofield precipitation of a building in a geologically hazardous area, mm.

The proposed approach to assessing the technical condition of a building structure in hazardous geological conditions allows determining the forces and movements of all its controlled nodes.

## 5 Conclusion

According to the results of the analysis carried out in the work, the lack of elaboration of existing methods for studying the technical condition of buildings and structures in the conditions of dangerous geological processes was revealed.






Taking into account modern achievements of information and communication technologies the proposed revised assessment methodology that includes procedures of engineering survey of technical state of constructions, monitoring of movement in space set of control points in the building using the spatial-coordinate surveying and analysis of changes in the stress-strain state of structures at the base was in the course of monitoring movements. In addition, in order to improve the accuracy of the results, the necessity and expediency of constructing a soil model is justified, which makes it possible to predict changes in the technical condition of the building over time with a high degree of reliability and to prevent the occurrence of accidents. The use of the proposed approach in practice will enable more efficient use of funds for execution of current and capital repairs and regulate the technical state of the construction object in such a way as to achieve maximum efficiency of use of fixed assets.

## References

1. Construction of buildings on expansive soils E. A. Sorochan. CRC Press, Boca Raton, vol. 365 (2020)
2. Belash, V.V.: Features of engineering and geological surveys in the conditions of dense city building. In: IOP Conference Series. Materials Science and Engineering, vol. 913, pp. 15–28 (2020)
3. Biryukov, Y.: Methodology for monitoring the technical condition of buildings and structures in limited operational and emergency conditions. Rationing Remuneration Labor Constr. **2**, 43–51 (2019)
4. Barbagallo, F.: A database for assisted assessment of torsional response of in-plan irregular buildings. Geotech. Geol. Earthq. Eng. **48**, 69–82 (2020)
5. Dobryshkin, E.O.: Planning of capital repairs of buildings on the basis of the results of monitoring the technical condition. Rationing Remuneration Labor Constr. **2**, 70–74 (2019)
6. Fontara, I.-K.: Behaviour of 3D R/C irregular buildings considering complex site conditions. Geotech. Geol. Earthq. Eng. **48**, 279–290 (2020)
7. Biryukov, Yu.: Technique for examining the technical condition of damaged buildings and structures. Rationing Wages Constr. **1**, 25–38 (2019)
8. Wu, K.: Identifying the cause of abnormal building damage in mining subsidence areas using InSAR technology. IEEE Access: Pract. Innov. Open Solutions **7**, 172296–172304 (2019)
9. Bolotov, T.T., Bekbolotov, T.B.: Survey of the technical condition of a non-residential building. Bull. Kyrgyz State Univ. Constr. Transp. Archit. named after N. Isanov **4(66)**, 628–633 (2019)
10. Ciampalini, A.: Evaluation of subsidence induced by long-lasting buildings load using InSAR technique and geotechnical data: the case study of a freight terminal (Tuscany, Italy). ITC J. **82**, 34–39 (2019)
11. Grebennikova, N.S., Kuprienko, P.S., Nikolenko, S.D., Sazonova, S.A.: Modeling of complex stress-strain state and technical diagnostics of brick buildings. Model. Syst. Processes **2**, 4–11 (2020)
12. Fedorov, A.V., Shapovalenko, V.A.: Existing assessment of the technical condition of buildings and structures. Educ. Sci. Russia Abroad **4**, 365–368 (2019)



# Use of UAV to Resolve Construction Disputes

N. V. Shirina  , T. G. Kalachuk , E. R. Shin , and E. A. Parfenyukova 

Belgorod State Technological University named after V.G. Shukhov, Belgorod, Russia

**Abstract.** Monitoring and inspection of buildings and structures using the classical method is the most labor-intensive. It is proposed to use modern and effective methods for measuring the work performed on an object under construction, which has a non-standard complex geometric shape. The topic of relevance of the use of unmanned aerial vehicles in construction has been developed. To solve this problem, we used modern technologies for building an orthophotomap, a 3D model of the object, and an unmanned aerial vehicle (UAV). The unmanned aerial vehicle made it possible to fulfill the production tasks set by the construction industry enterprise with a minimum number of labor resources. The need to perform this task arose in a dispute between the customer and the contractor about the volume of construction and installation work performed and the amount of their payment. The results of photo processing in the Agisoft Metashape software product are presented: an orthophotomap and a 3D model of the object are obtained. The resulting model was used to calculate the roof area of the water park to resolve a construction dispute between the customer and the contractor. The results obtained made it possible to assert that the considered option is a promising technology for survey and monitoring, including for resolving disputes in the construction industry and, in particular, conducting expert examinations.

**Keywords:** UAV · Orthophotomap · 3D model · Aerial photo · Building disputes · Monitoring · Evaluation

## 1 Introduction

Every year, the construction industry is increasingly using new tools and technologies, and unmanned aerial vehicles (UAV) are proof of this. Quadcopters in construction make it possible not to disrupt the technological processes on the construction site during monitoring, they are controlled remotely and change the viewing points, allowing getting objective evidence in real time without interrupting the progress of work. Monitoring large-scale objects such as gas pipelines, bridges, and unique buildings with complex geometries in traditional form from the ground is time-consuming and endangers human life and health. The use of UAV in such cases is more justified. Detection of possible violations during construction, control of the accuracy of installation of structures, compliance with project documentation, detection of defects – all this can be done remotely using quadcopters, really saving time and financial costs. Thus, today there are many options for using UAV in construction and every year the scope of their activities is expanding [1, 2].



In the construction industry, there is a very high probability of all sorts of risks that lead to contradictions between contractors. The most common cases are the resolution of disputes in the performance of contractual obligations. Parties who are involved in conflicting relationships rarely come to a solution on their own [3].

In such cases, control checks are one of the main ways to detect violations in the system of execution of contracts for construction and reconstruction, current and heavy repairs of capital construction objects and to ensure the principle of efficient use of the customer's funds [4]. The purpose of such a control check is to assess and establish the reliability of the volume and cost of work performed on capital construction projects, as well as to identify the compliance of the quantity and parameters of materials actually used and installed equipment.

The paper provides recommendations on the use of UAV and provides the results of measuring the work performed on an object that has a non-standard complex geometric shape. The need for such an assessment arose during a dispute between the customer and the contractor about the volume of construction and installation works performed and the amount of their payment [6].

## 2 Methods and Materials

Examination of large or hard-to-reach buildings and structures, which include the object under investigation – the roof of an indoor water park – requires specialized equipment and highly qualified personnel. Specially trained personnel, such as mountain climbers, can access hard-to-reach structures, but they cannot evaluate the site based on the nature and scope of the work performed.

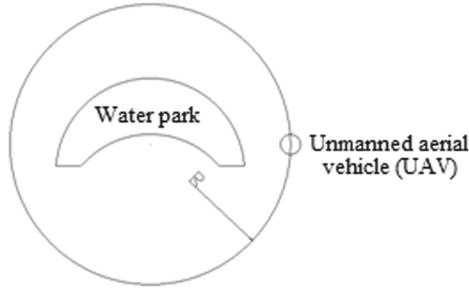
Theoretically, this problem can be solved using specialized equipment, machines (scaffolding, tower vehicle, mountaineering), but this will lead to high material costs. At the same time, there are risks associated with ensuring safety when conducting a survey using such equipment.

The paper proposes to solve this problem by using an unmanned aerial vehicle, which will improve the quality of visual inspection and reduce the cost of its implementation.

An indoor water park was presented as an object. The dispute was that the amount of work performed to install the roof of the object under construction did not match the data of the customer and the contractor. To resolve this conflict, it was necessary to measure the finished product. As the object has a complex geometric shape, it is quite labor-intensive to measure it in the usual way, and a number of additional permissions are required. We proposed a method that helped reduce the cost of work, as well as reduce time and labor costs, but it was not inferior in accuracy.

To solve this problem, the method of aerial photography using an unmanned aerial vehicle (UAV) was applied. At the first stage, it was necessary to determine the design characteristics that are necessary for accurate and reliable processing of the photos obtained in the future [5, 7].

As the object is complex in shape and height from 20 to 25 m, and has the shape of a half-moon, it was necessary to calculate the characteristics of the flight task, namely, to calculate the overlap of photos. To create a 3D model of the object, the flyby was performed in orbits, i.e. around the object (Fig. 1).

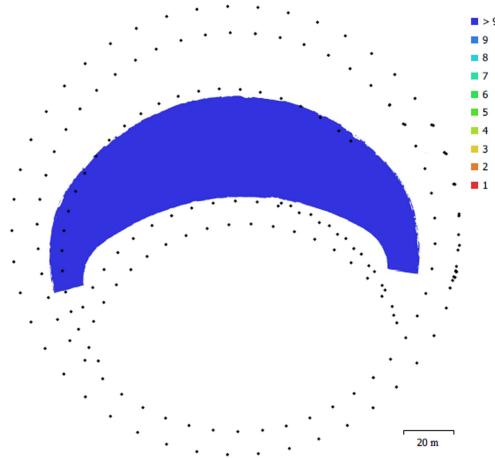


**Fig. 1.** Map of the photographing route.

To overlap photos, they had to switch from a linear intersection to a corner intersection. Source data: R is the radius of the orbit (depends on the size of the object), N is the number of orbits (depends on the height of the object).

The radius of the orbit, based on the size of the object, is chosen so that the distance from the UAV camera to the object is sufficient. In our case, the size of the object in the plan is  $150 \times 70$  m, we take the maximum length and divide it in half, then we increase the obtained value by 1.5 times and get the radius of the orbit. Knowing the radius of the orbit, we calculate the remaining characteristics.

As the object has a complex shape, the distance to the object from the UAV camera will be different. We take the smallest distance, because if the condition for overlapping images is met at the smallest distance, then the greater the distance, the greater the overlap of images (Fig. 2).



**Fig. 2.** Positions of the cameras and the images overlap.

### 3 Results and Discussion

Knowing the characteristics of the UAV, which can be found in the technical data sheet of the product, we calculate the scale of photographing using the formula (1):

$$1/M_{\phi} = H_{\phi}/f, \quad (1)$$

where  $M_{\phi}$  - scale,  $H_{\phi}$  – the height of the photographing,  $f$  – focal length.

Based on the scale of photographing, we calculate the scale of the image (formula 2), that is, how much of the real size of the object falls on the image:

$$\begin{aligned} L_x &= l_x \times m, \\ L_y &= l_y \times m, \end{aligned} \quad (2)$$

where  $L_x, L_y$  – dimensions of the square of the area captured by a single image,  $l_x, l_y$  – camera matrix size of the camera,  $m$  – the scale of the photograph.

Then, using the required value of the longitudinal and transverse overlap, the longitudinal and transverse bases of photographing are found. Converting from percentages of the image to actual distances on the ground (formula 3):

$$\begin{aligned} P_x &= L_x \times P(\%) \\ P_y &= L_y \times P(\%), \end{aligned} \quad (3)$$

where  $P_x, P_y$  – longitudinal and transverse overlap of images,  $P$  – required longitudinal overlap of images.

After determining the overlap, we calculate the angle between the centers of the images. The calculation is based on the overlap of images. We find the linear distance between the centers of images using the formula (4):

$$\alpha = \arctg\left(\frac{0.5 \times l}{r}\right) \times 2, \quad (4)$$

where  $r$  – the radius of the object,  $l$  – distance between image centers [8].

We set the angular velocity and calculate the required interval for photographing. Next, the received photos were processed in the Agisoft Metashape software product.

Based on the results of photo processing in the software product, an orthophotomap and a 3D model of the object were obtained (Fig. 3).



Fig. 3. 3D model of the object.

The resulting model was used to calculate the roof area of the object (Fig. 4).

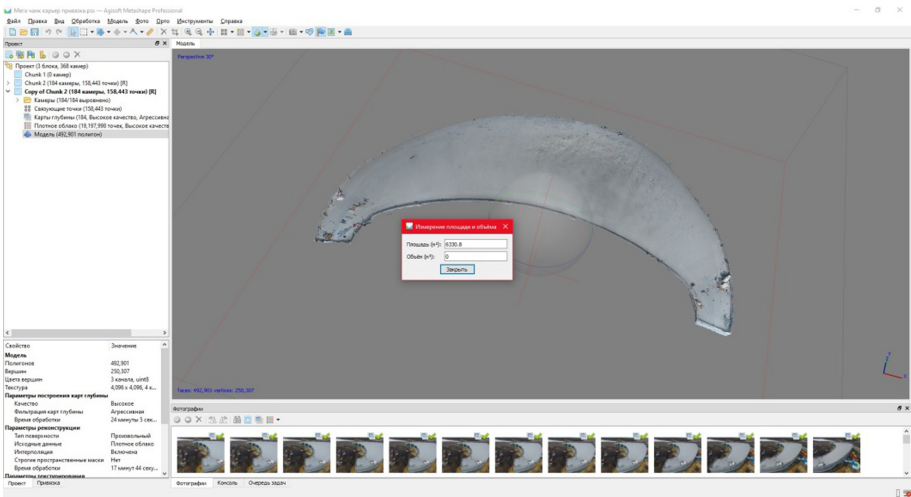


Fig. 4. Calculating the area and volume of the model.

## 4 Conclusion

Thus, this method made it possible to carry out the necessary measurements without additional costs, significantly reducing the time of work, as well as the cost of these works [9].

The quality of inspection of buildings (structures) of high storeys, complex configuration, difficult to access cannot be ensured without the use of aircraft, and, therefore, the considered option is a promising technology for inspection and monitoring, including the resolution of disputes in the construction industry [10].

**Acknowledgments.** This work was realized under the support of the President Scholarship; in the framework of the Program of flagship university development on the base of the Belgorod State Technological University named after V G Shukhov, using equipment of High Technology Center at BSTU named after V G Shukhov.

## References

1. Semenov, A.S., Slonich, K.A.: Survey of buildings and structures using unmanned aerial vehicles. *Bull. BSTU Named After V.G. Shukhov* **9**, 160–163 (2017)
2. Use of UAV for the purposes of building. <https://rusdrone.ru/otrasli/stroitelstvo/>
3. Construction dispute resolution: types and features of conflict resolution. <https://zen.yandex.ru/media/id/5b7432ee8b9f0300a913800e/razreshenie-stroitelnyh-sporov-vidy-i-osobennosti-razresheniia-konfliktov-5b745905f43a0900a9f12f2b>
4. Dvoeglazov, N.V.: Protection of the rights of the customer of construction and installation works: control measurement as a source of evidence in disputes. *Econ. Manage. Innov. Technol.* **4** (2012). <http://ekonomika.snauka.ru/2012/04/743>
5. Shin, E.R., Shchekina, AYu., Cherkasov, R.A.: Technology for creating 1:500 scale topomaps based on data from the PHANTOM 4 quadcopter. *Vector GeoSci.* **2**(1), 54–59 (2019)
6. Ermakova, Yu.A., Parfenyukova, E.A., Shirina, N.V.: The use of information systems and technologies for the creation of the inventory built-up areas. *Bull. Belgorod State Technol. Univ. Named After V.G. Shukhov.* **10**, 257–261 (2017)
7. Menti, N., Hamel, T.A.: UAV for bridge inspection: visual servoing control law with orientation limits. *Auto. Constr.* **17**(1), 3–10 (2007)
8. Eisenbeiß H.: UAV Photogrammetry, PhD Thesis, ETH Zurich, Switzerland (2009)
9. Gubarev, S.A., Kadina, N.S.: Verification of compliance of completed construction and installation works with the use of geodetic equipment. *Vector GeoSci.* **3**(1), 89–92 (2020)
10. Ovchinnikova, N.G., Medvedkov, D.A.: Application of unmanned aerial vehicles for land management, cadastre and urban development. *Econ. Ecol. Territ. Entities.* **1**(8) (2019). <https://cyberleninka.ru/article/n/primenenie-bespiLOTnyh-letatelnyh-apparatov-dlya-vedeniya-zemleustroystva-kadastra-i-gradostroitelstva>



# Forecasting the Durability of Protective and Decorative Coatings of External Walls of Buildings

V. I. Loganina<sup>1</sup> , S. V. Klyuev<sup>2</sup> , R. S. Fediuk<sup>3</sup> , and I. A. Aksenov<sup>4</sup> 

<sup>1</sup> Penza State University of Architecture and Construction, Penza, Russia

<sup>2</sup> Belgorod State Technological University named after V.G. Shukhov, Belgorod, Russia

<sup>3</sup> Far Eastern Federal University, Vladivostok, Russia

<sup>4</sup> Vladimir State University named after Alexander and Nikolay Stoletovs, Vladimir, Russia

**Abstract.** The information on the model of changing the properties of coatings, taking into account the hereditary factor, is given. It is shown that the kinetics of changes in coating properties, among other factors, is determined by the prehistory of aging. The application of the aging model, taking into account the hereditary factor in assessing the thermal aging of the coating, humidification of the complex effect of the environment, is considered. The numerical values of the function characterizing the influence of the hereditary factor on the change in the adhesion strength during the cyclic effect of the environment are given. The results of studies and calculations allow us to assume that, depending on the type of aging at its various stages, the rate of change in coating properties is determined by various components: directly the destructive effect of the environment, the prehistory of aging. Knowledge of these factors allows you to more realistically assess the resistance.

**Keywords:** Coatings · Environmental impact · Forecasting · Aging model

## 1 Introduction

During the operation of the protective and decorative coatings of the outer walls of buildings, their aging occurs. The durability of coatings is characterized by the time during which they retain their operational properties: protective, decorative, etc. [1–6] At present, the problem of predicting the quality of coatings for the widest field of application - operation in atmospheric conditions - remains relevant. This is due to both the multifactorial effect on the coating (UV radiation, high and low temperatures, high humidity, etc.), and the process of destruction of multilayer coatings simultaneously by several mechanisms [7–11].

At present, extensive experimental data have been accumulated on the results of long-term tests of coatings in atmospheric conditions in various climates [12–15].

The general methodological approach to predicting the service life of polymer coatings is based on fundamental research in the field of physicochemical problems of polymer aging [16–24] and includes the following main stages: selection of coating

properties, the change of which during aging leads to its operational unsuitability; establishment of an acceptable level of change in properties (refusal); setting conditions for accelerated testing; statistical processing of experimental data; establishment of the mathematical dependence of the property change, determination of the energy constants of the aging process, extrapolation of the aging function to real operating conditions; building a forecast curve.

Consider the application of the hereditary theory of aging to assess the service life of coatings. Let some physical quantity  $U$  (an indicator of the quality of coatings) change over time. Let's call it impact. At a given time, its value is  $U(t)$ . Another physical quantity changes with  $U$  in a completely definite way. Let's call this value a reaction. An object whose state is described by the functions  $U(t)$  and  $V(t)$  will be called a system.

The value  $V$  at a given time  $t$  is the sum of two terms:

$$V(t) = U(t) + \int_{-\infty}^t K(t, \tau)U(\tau)d\tau \quad (1)$$

The first term (an instantaneous component) is proportional to the value  $U$  at the moment. The second term is the inherited term, which is calculated as follows. The memory of the state of the coating property between the moments of time  $\tau$  and  $\tau + d\tau$  belonging to the past should be proportional to the value of the coating property at the moment  $\tau$  ( $y(\tau)$ ) and the duration of the interval  $d\tau$ , the value  $y(\tau) \cdot d\tau$  must be multiplied by the forgetting function  $K(t, \tau)$  (the kernel of heredity).

Formula (1) can be generalized to the case of voltages that change in time according to an arbitrary law (with continuous climatic influences of the environment):

$$R(t) = R(t, t_1) - \int_{t_1}^t \left( \frac{dC}{d\tau} \right) R(\tau)d\tau \quad (2)$$

## 2 Materials and Methods

The proposed model was tested in the aging analysis of polyvinyl acetate-cement (PVAC) coatings. The adhesion strength  $R_{adh}$  was taken as a criterion for the resistance of the coatings. PVAC, lime, and polymer-lime paints were used as paint compositions.

The adhesion strength of the coatings was determined by the punch-off method. The method is based on determining the force of separation of the die from the surface by separation. The sample was installed horizontally, attaching a dynamometer to the stamp, and the force required to detach the stamp from the test sample was recorded. Bond strength was determined by the formula:

$$R_{adh} = \frac{P}{F}, \quad (3)$$

where  $R_{adh}$  is an adhesion strength, MPa;  $P$  is a separation force, N;  $F$  is a contact area of the stamp with the coating,  $m^2$ .

Internal stresses arising during the curing of coatings were determined by the cantilever method according to the Russian Standard GOST 13036-67. The method is based on measuring the deviation from the initial position of the free end of a cantilevered elastic metal plate with a paint-and-lacquer coating under the influence of internal stresses. The magnitude of internal stresses was calculated by the formula:

$$\sigma = \frac{\Delta h E S^3}{3L^2 \Delta S (S + \Delta S)} \quad (4)$$

where  $\Delta h$  is a deviation of the plate from the initial position, cm;  $E$  is a modulus of elasticity of the plate ( $E = 10^3$  MPa);  $L$  is a length of the paintwork, cm;  $S$  is a plate thickness, cm;  $\Delta S$  is a coating thickness, cm.

Tensile strength, elongation and tensile modulus were determined on an IR 5057-50 tensile testing machine (Russia), according to the Russian Standard GOST 18299-72. The method is based on stretching a test sample of a free film at a certain rate until it breaks.

Samples for testing were cut from free paint and varnish film, stepping back from its edges by at least 10 mm. Samples of the following dimensions were used: length 50 mm, width 10 mm with a length of the working part of 30 mm. The spreading speed of the machine clamps was 10 mm/min. The tests were carried out at an air temperature of  $20 \pm 2$  °C and a relative humidity of  $65 \pm 5\%$ .

The calculation was made according to the results of testing at least 3 parallel samples. The tensile strength in MPa ( $\text{N/mm}^2$ ) was calculated by the formula:

$$\sigma_i = \frac{F_{pi}}{S_{oi}} \quad (5)$$

where  $F_{pi}$  is a tensile load at the moment of rupture, N;  $S_{oi}$  is an initial cross-sectional area of the sample,  $\text{mm}^2$ .

The elongation at break of each sample in percent was calculated by the formula:

$$L_i = \frac{\Delta l_i}{l_o} 100, \quad (6)$$

where  $\Delta l_i$  is an increment in the length of the working part of each sample, mm;  $l_o$  is an initial length of the working part of each sample, mm.

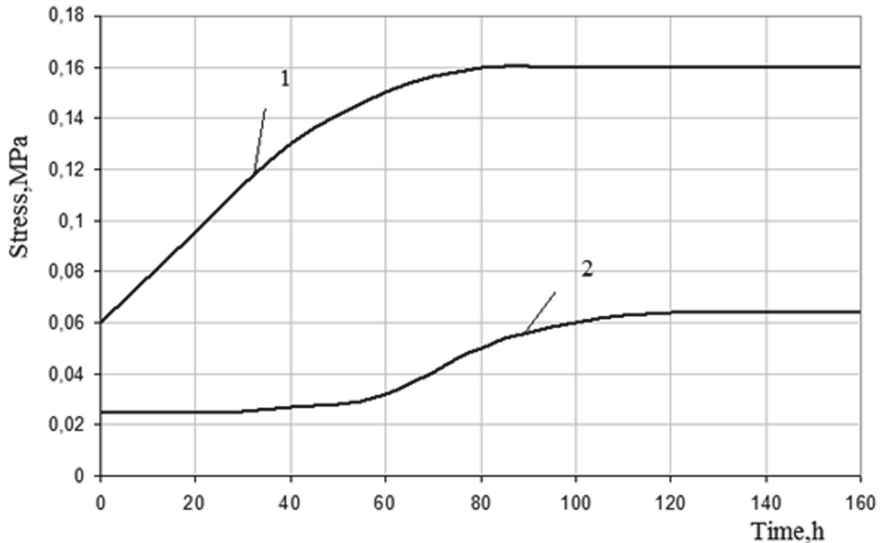
The modulus of elasticity for each sample ( $E$ ) in MPa was calculated from the stress-strain diagram according to the tangent of the angle of inclination to the abscissa axis of the tangent drawn to the initial straight section of the diagram. The modulus of elasticity for each sample in MPa was calculated by the formula:

$$E = \frac{\sigma}{\varepsilon} \quad (7)$$



### 3 Results and Discussion

Analysis of the experimental data (Fig. 1) indicates, that at aging of coatings under the influence of positive temperatures, internal stresses are increase. Stabilization of internal stresses is observed in - polymer- calcareous coatings - after 80 h at MPa level; in PVAC coatings after 90 h at the level of 0.162 MPa.



**Fig. 1.** Change of internal stresses in the process of heat aging 1- PVAC coating; 2- polymer-lime coating.

In the process of thermal aging of coatings, their physical and mechanical properties change. In the initial period of thermal aging, growth the hardness of polymer-mineral free films is observed. It is evidently due to the processes of structure formation. In this case, the rigidity of the films increases and an increase in the modulus of elasticity is observed. The increase in the hardness of the coating, and, consequently, of the internal stresses also indicates that further coatings are subjected to curing (Table 1).

**Table 1.** Change in hardness of coatings during thermal aging.

Coating type	Hardness, MPa			
	Duration of heat aging, h			
	0	50	100	150
PVAC	41.14	66.28	61.11	49.46
Polymer-lime	35.47	53.44	49.28	47.71

These data are in good agreement with the results, obtained when testing free films on a tensile machine [6]. Analysis of the experimental data (Table 2) indicates that in the initial state (before the onset of aging), the presence of elastic and plastic deformations is typical for polymer and PVAC films. Thus, the value of plastic deformations during stretching of PVAC films is  $\varepsilon = 0.1\%$ , and the total elongation is  $\varepsilon = 1.76\%$ .

**Table 2.** Change in physical and mechanical properties of coatings in the process of thermal aging.

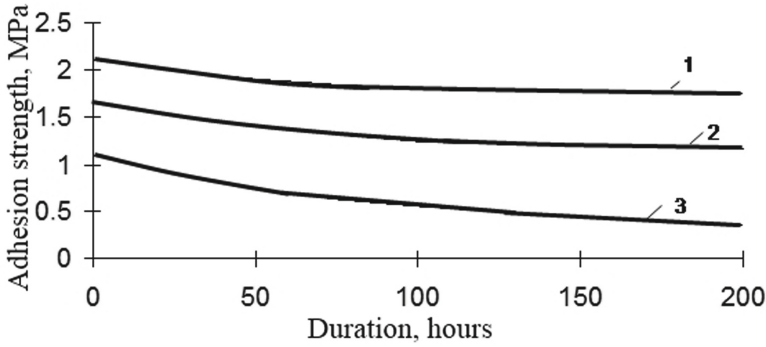
Properties	Duration of heat aging, h,			
	0	50	100	150
PVAC coating				
Cohesive strength, MPa	2.22	5.49	4.62	4.1
The modulus of elasticity, $E \cdot 10^2$ , MPa	1.31	2.92	2.54	1.94
Elongation $\varepsilon$ , %	1.76	2.9	2.65	2.4
Plastic deformation, $\varepsilon_{pl}$ , %	0.1	1.05	1.1	1.05
The polymer-lime coating				
Cohesive strength, MPa	1.87	–	2.11	2.04
The modulus of elasticity $E$ , $10^2$ , MPa	1.03	–	1.8	1.64
Elongation $\varepsilon$ , %	1.0	–	1.9	2.0
Plastic deformation, $\varepsilon_{pl}$ , %	0.5	–	0.7	1.33

During thermal aging an increase in cohesive strength is observed. It caused by the processes of structure formation. But after 50 h of testing, destruction processes prevail. After 50 h of testing the relative deformations are  $\varepsilon = 2.9\%$ , and the residual strain  $\varepsilon = 1.05\%$ . With an increase in the duration of thermal aging of PVAC films the numerical values of the relative elongation decrease and the proportion of residual deformations in the total deformation of the films increases. So, after 50 h of thermal aging, the proportion of permanent deformation is 35%, while after 150 h of 44%.

Thermal aging causes a decrease in the elastic modulus of the coatings after a certain increase. After 150 h of thermal aging, the elastic modulus of PVAC coatings is  $E = 1.94 \times 10^2$  MPa.

In Fig. 2 experimental data on changes in the adhesion strength of coatings under prolonged exposure to temperature are presented.

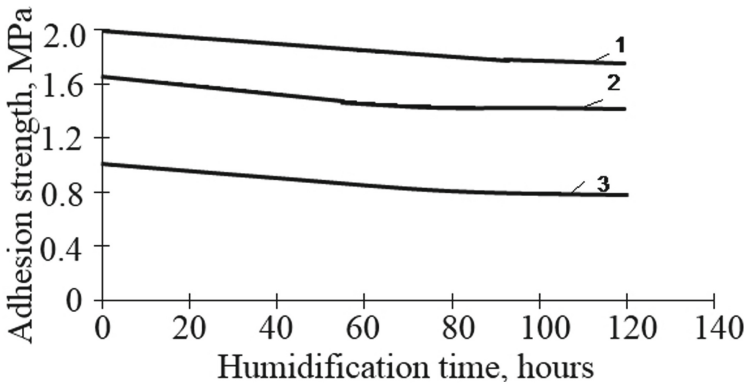
A decrease in the adhesion strength of coatings based on polymer-mineral binders, depending on the duration of exposure to temperature, is observed in the first 100 h of heat aging for all coatings; however, visual inspection of the painted samples indicates the absence of any signs of peeling. For a lime coating in the first 100 h, there is a sharp decrease in adhesion strength from 1.15 MPa to 0.56 MPa. A visual inspection of the samples shows that on lime coatings, after 200 h of heat aging, slight peeling of the coating from the mortar substrate begins. Analysis of experimental data indicates that the



**Fig. 2.** Kinetics of changes in adhesion strength of coatings during thermal aging: 1 - PVAC coating; 2 - polymer-lime coating; 3 - lime coating.

adhesion strength of coatings under the action of temperature decreases exponentially, which is consistent with the experimental data of other authors [22, 23].

In the second series of experiments, the coatings were investigated under the action of humidification (Fig. 3).



**Fig. 3.** Kinetics of changes in adhesion strength of coatings in the process of humidification: 1 - PVAC coating; 2 - polymer-lime coating; 3 - lime coating.

Table 3 shows the values of the function, which characterizes the influence of hereditary factor on the properties of the coatings  $\int_0^t V(\tau)K(t, \tau)d\tau$  during aging.

**Table 3** Value of the function describing influence of the hereditary factor on durability of coupling of some coverings depending on a type of ageing, MPa.

Coating type	Aging time, hours							
	25	50	75	100	125	150	175	200
PVAC	0.009	0.019	0.029	0.038	0.048	0.057	0.066	0.075
	0.029	0.059	0.087	0.115	0.143	0.171	0.198	0.224
Polymer-lime	0.052	0.103	0.152	0.2	0.246	0.291	0.334	0.376
	0.034	0.067	0.1	0.131	0.162	0.177	0.192	0.222
Lime	0.07	0.132	0.186	0.235	0.279	0.318	0.354	0.387
	0.016	0.031	0.045	0.059	0.073	0.085	0.098	0.11

Note. Above the line shows the values of the function, which characterizes the influence of hereditary factor on the properties

of the coatings  $\int_0^t V(\tau)K(t, \tau)d\tau$  during thermal aging, below the line - in the process of moistening.

## 4 Conclusion

The results of studies and calculations allow us to assume that, depending on the type of aging at its various stages, the rate of change in coating properties is determined by various components: directly the destructive effect of the environment, the prehistory of aging. Knowledge of these factors allows you to more realistically assess the resistance.

## References

1. Feduik, R.: Reducing permeability of fiber concrete using composite binders. *Spec. Top. Rev. Porous Media*. **9**, 79–89 (2018)
2. Klyuev, S.V., Klyuev, A.V., Khezhev, T.A., Pukhareno, Y.V.: High-strength fine-grained fiber concrete with combined reinforcement by fiber. *J. Eng. Appl. Sci.* **13**, 6407–6412 (2018)
3. Begich, Y.E., Klyuev, S.V., Jos, V.A., Cherkashin, A.V.: Fine-grained concrete with various types of fibers. *Mag. Civ. Eng.* (2020). <https://doi.org/10.18720/MCE.97.2>
4. Ibragimov, R., Fediuk, R.: Improving the early strength of concrete: effect of mechanochemical activation of the cementitious suspension and using of various superplasticizers. *Constr. Build. Mater.* (2019). <https://doi.org/10.1016/j.conbuildmat.2019.07.313>
5. Fediuk, R.S., Yevdokimova, Y.G., Smoliakov, A.K., Stoyushko, N.Y., Lesovik, V.S.: Use of geonics scientific positions for designing of building composites for protective (fortification) structures. *IOP Conf. Ser.: Mater. Sci. Eng.* (2017). <https://doi.org/10.1088/1755-1315/221/1/012011>
6. Loganina, V.I., Simonov, E.E., Jezierski, W., Małaszkiwicz, D.: Application of activated diatomite for dry lime mixes. *Constr. Build. Mater.* (2014). <https://doi.org/10.1016/j.conbuildmat.2014.04.098>
7. Korsun, V., Vatin, N., Korsun, A., Nemova, D.: Physical-mechanical properties of the modified fine-grained concrete subjected to thermal effects up to 200°C. *Appl. Mech. Mater.* (2014). <https://doi.org/10.4028/www.scientific.net/AMM.633-634.1013>
8. Fediuk, R.S.: Mechanical activation of construction binder materials by various mills. *IOP Conf. Ser.: Mater. Sci. Eng.* (2016). <https://doi.org/10.1088/1757-899X/125/1/012019>

9. Klyuyev, S.V., Klyuyev, A.V., Sopin, D.M., Netrobenko, A.V., Kazlitin, S.A.: Heavy loaded floors based on fine-grained fiber concrete. *Mag. Civ. Eng.* (2013). <https://doi.org/10.5862/MCE.38.1>
10. Klyuev, S.V., Khezhev, T.A., Pukhareno, Y.V., Klyuev, A.V.: Fiber concrete for industrial and civil construction. *Mater. Sci. Forum* **945**, 120–124 (2018)
11. Fediuk, R., Yushin, A.: Composite binders for concrete with reduced permeability. *IOP Conf. Ser.: Mater. Sci. Eng.* (2016). <https://doi.org/10.1088/1757-899X/116/1/012021>
12. Amran, M., Fediuk, R., Vatin, N., Mosaberpanah, M.A., Danish, A., El-Zeadani, M., Klyuev, S.V., Vatin, N.: Fibre-reinforced foamed concretes: a review. *Materials* **13**(19), 4323 (2020)
13. Alfimova, N., Pirieva, S., Gudov, D., Shurakov, I., Korbut, E.: Optimization of receptural-technological parameters of manufacture of cellular concrete mixture. *Constr. Mater. Prod.* (2020). <https://doi.org/10.34031/2618-7183-2018-1-2-30-36>
14. Klyuyev, S.V., Guryanov, Y.V.: External reinforcing of fiber concrete constructions by carbon fiber tapes. *Mag. Civ. Eng.* (2013). <https://doi.org/10.5862/MCE.36.3>
15. Fediuk, R., Pak, A., Kuzmin, D.: Fine-grained concrete of composite binder. *IOP Conf. Ser.: Mater. Sci. Eng.* (2017). <https://doi.org/10.1088/1757-899X/262/1/012025>
16. Klyuev, S.V., Khezhev, T.A., Pukhareno, Y.V., Klyuev, A.V.: Fiber concrete on the basis of composite binder and technogenic raw materials. *Mater. Sci. Forum* (2018). <https://doi.org/10.4028/www.scientific.net/MSF.931.603>
17. Fediuk, R.S., Lesovik, V.S., Liseitsev, Y.L., Timokhin, R.A., Bituyev, A. V., Zaiakhanov, M.Y., Mochalov, A. V.: Composite binders for concretes with improved shock resistance. *Mag. Civ. Eng.* (2019). <https://doi.org/10.18720/MCE.85.3>
18. Usanova, K., Barabanshchikov, Y.G.: Cold-bonded fly ash aggregate concrete. *Mag. Civ. Eng.* (2020). <https://doi.org/10.18720/MCE.95.10>
19. Kharun, M., Klyuev, S., Koroteev, D., Chiadighikaobi, P.C., Fediuk, R., Olisov, A., Vatin, N., Alfimova, N.: Heat treatment of basalt fiber reinforced expanded clay concrete with increased strength for cast-in-situ construction. *Fibers* **8**, 0067 (2020)
20. de Azevedo, A.R.G., Klyuev, S., Marvila, M.T., Vatin, N., Alfimova, N., de Lima, T.E.S., Fediuk, R., Olisov, A.: Investigation of the potential use of curauá fiber for reinforcing mortars. *Fibers* **8**, 0069 (2020)
21. Loganina, V.I.: Model of aging coatings based on hereditary factors. *Contemp. Eng. Sci.* (2015). <https://doi.org/10.12988/ces.2015.518>
22. Mittal, K.L.: Adhesion measurement of thin films. *Electrocompon. Sci. Technol.* (1976). <https://doi.org/10.1155/APEC.3.21>
23. Awaja, F., Gilbert, M., Kelly, G., Fox, B., Pigram, P.J.: Adhesion of polymers. *Prog. Polym. Sci.* (2009). <https://doi.org/10.1016/j.progpolymsci.2009.04.007>
24. Jabir, H.A., Abid, S.R., Murali, G., Ali, S.H., Klyuev, S., Fediuk, R., Vatin, N., Promakhov, V., Vasilev, Y.: Experimental tests and reliability analysis of the cracking impact resistance of UHPFRC *Fibers* **8**, 0074 (2020)



# Investigation of Physical and Chemical Properties of Architectural Glass Fibrous Concrete

N. I. Bondarenko<sup>(✉)</sup>  and D. O. Bondarenko 

Belgorod State Technological University named after V.G. Shukhov, Belgorod, Russia

**Abstract.** Glass fibrous concrete refers to composite materials and is used in modern construction. This material successfully combines architectural and decorative, operational, technological, economic, structural and other properties. The developed glass fibrous concrete was used as the object of research. It is known that the addition of glass fiber to the cement mortar worsens the workability of the mixture and increases the water demand of glass fibrous concrete, which can affect the reduction of its strength characteristics. Studies of the chemical interaction of glass fiber with cement hydration products showed that ARC15-2400 glass fiber is highly resistant to both Portland cement hydration products and white cement hydration products. The resistance of glass fiber to the cement extract based on Portland cement was 99.065%, and on the basis of white cement – 99.46%. During the experiment, it was also found that the samples reinforced with glass fiber with a fiber length of 30 mm had the greatest strength, both for the composition based on Portland cement and for the composition based on white cement. The analysis of the obtained results allows us to conclude that the dosage of 3% glass fiber from the mass of the concrete mixture is optimal for compositions using Portland cement and white cement.

**Keywords:** Glass fibrous concrete · Glass fibre · White cement · Portland cement · Fiberglass

## 1 Introduction

Architectural fibrous concrete is a new stage in the development of construction, restoration and finishing works in the construction of administrative and public buildings, the improvement of recreation areas, and the creation of decorative elements. Glass fibrous concrete provides ample opportunities for the implementation of architectural ideas [1–3].

The hardening of Portland cement has a great influence on the condition of the reinforcing components and the matrix of the product as a whole. The choice of a binding material in the production of architectural fiberglass is one of the main points [4]. White cement in comparison with ordinary cement has a number of advantages, due to its beautiful color, it is often used not only for construction work, but also for creating sculptures and other architectural objects, and for architectural glass fibrous concrete, and the most important thing is its aesthetic component. Glass fibrous concrete is very easy to take various architectural forms; with its help they can quickly create both simple and complex multi-level composite decorations. It allows the architect to demonstrate the uniqueness and individuality of the structure, to use modern approaches in design without increasing the estimated cost of construction.

As with any building material, glass fibrous concrete has its drawbacks. It hardens faster than conventional concrete, which significantly reduces its laying time. Finished products made of this material are more expensive than its analogues. The durability of glass fibrous concrete depends on its composition and purpose.

For the dispersed reinforcement of concrete in order to increase the crack resistance, glass fiber is used [5–10]. Special grades of glass fiber are used, which are stable in the alkaline environment of hardening concrete, as in ordinary hydrated Portland cement there is free lime, which negatively affects the glass fiber.

## 2 Methods and Materials

The following raw materials were used for the complex of studies:

- white cement of the CEM I 52.5 R (Super White) brand produced by “Adana Cimento”, which contains at least 95% by weight of high-quality white clinker and up to 5% of auxiliary components;
- portland cement of the CEM I 42.5 N brand produced by CJSC “Belgorod Cement”;
- alkali-resistant glass fiber ARC15-2400 produced by “Huatek”, the properties of which are presented in Table 1.

**Table 1.** Properties of ARC15-2400 glass fiber.

Name of parameters	Measure units	Properties
Zirconium content	%	From 14,5
Diameter	mkm	15
Linear density	Tex	2400

To determine the ultimate strength of glass fiber concrete for compression and bending, a hydraulic press PGM–50G4 was used. A laboratory water bath was used to determine the resistance of the glass fiber to the cement extract. The studies were conducted according to the standard methodology.

### 3 Results and Discussions

To study the stability of glass fiber in the environment of cement extraction, a cement extract prepared on the basis of Portland cement and a cement extract prepared on the basis of white cement were taken. The glass fiber was boiled in a laboratory water bath for 1 h.

The resistance of glass to cement extraction (C) was calculated by the formula, %:

$$U = \frac{m_1 \cdot 100}{m} \quad (1)$$

where  $m_1$  – mass of glass fiber after testing, g,

$m$  – weight of glass fiber before testing, g.

The final result was taken as the arithmetic mean of two parallel indications, the difference between which did not exceed 0.5%. The research results are presented in Table 2 and Table 3.

**Table 2.** The results of the study of the resistance of glass fiber to the cement extract based on Portland cement.

№ of sample	Weight of the portion of an glass fiber, g		Resistance of glass fiber to cement extraction, %	
	m	m <sub>1</sub>	Separate sample	Average
1	1.001	0.9917	99.07	99.065
2	1.002	0.9926	99.06	

**Table 3.** The results of the study of the resistance of glass fiber to the cement extract based on white cement

№ of sample	Weight of the portion of an glass fiber, g		Resistance of glass fiber to cement extraction, %	
	m	m <sub>1</sub>		m
1	1.002	0.9963	99.43	99.065
2	1.004	0.9988	99.48	

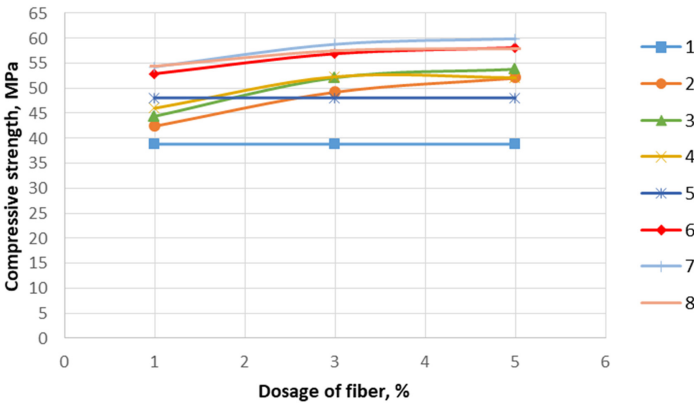
Studies showed that ARC15-2400 glass fiber is alkali-resistant to both Portland cement hydration products and white cement hydration products. Fiber reinforcement of architectural glass fibrous concrete allows influencing the processes of setting and hardening of cement, which in turn affects the quality of the material produced. First



of all, architectural glass fibrous concrete is distinguished by its technical and strength characteristics. Glass fibers have a very high tensile strength, exceeding the strength of other textile fibers. The strength of glass fibers is affected not only by the chemical composition of the glass, but also by the methods, molding conditions, and the state of the fiber surface.

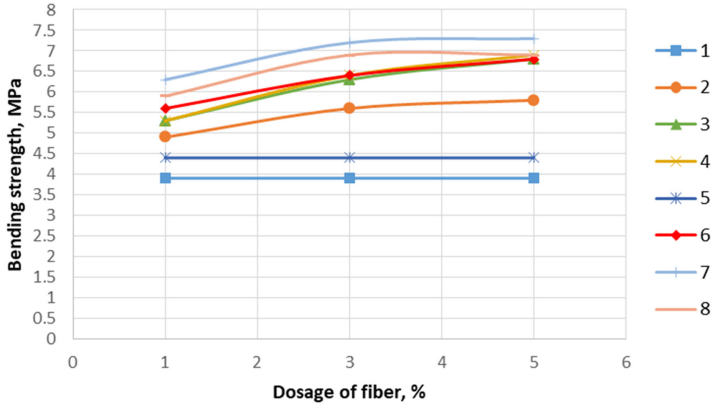
To determine the strength characteristics of glass fibrous concrete, compositions with the ratio of cement:sand = 1:3 at W/C = 0.5 were used as the base.

To determine the compressive strength, samples were prepared in the form of a cube with a size of 30 × 30 × 30 mm, and to determine the bending strength of the beam – 40 × 40 × 160 mm. Samples were prepared in batches. Quantity – 5 pieces in each batch. The samples were solidified under normal conditions in the air for 28 days, after which the compressive and flexural strength was studied. The results of the study of the effect of the length and dosage of glass fiber on the strength characteristics of concrete are presented in Fig. 1 and Fig. 2.



**Fig. 1.** The strength characteristics of the glass fibrous concrete under compression, depending on the number and length of fibers: 1 – concrete based on Portland cement; 2 – concrete based on Portland cement with fibers (10 mm); 3 – concrete based on Portland cement with fiber (30 mm); 4 – concrete based on Portland cement with fiber (60 mm); 5 – concrete on the basis of white cement; 6 – concrete on the basis of white cement with fibers (10 mm); 7 – concrete on the basis of white cement with fiber (30 mm); 8 – concrete on the basis of white cement with fiber (60 mm).

Studies showed that the greatest strength is observed in the samples reinforced with glass fiber with a fiber length of 30 mm as the composition of the Portland cement and composition with white cement (Fig. 1, Fig. 2). Analysis of experimental results leads to the conclusion that the dosage of 3% glass fiber by weight of the concrete mix is best for compositions with a matrix of Portland cement and white cement matrix. The strength of glass fibrous concrete is determined by the strength of the adhesive contact at the fiber-matrix interface.



**Fig. 2.** Strength characteristics of glass fibrous concrete at bending, depending on the amount and length of the fiber: 1 – concrete based on Portland cement; 2 – concrete based on Portland cement with fiber (10 mm); 3 – concrete based on Portland cement with fiber (30 mm); 4 – concrete based on Portland cement with fiber (60 mm); 5 – concrete based on white cement; 6 – concrete based on white cement with fiber (10 mm); 7 – concrete based on white cement with fiber (30 mm); 8 – concrete based on white cement with fiber (60 mm).

## 4 Conclusion

It is found that glass fiber of the ARC15-2400 brand is alkali-resistant both to products of hydration of Portland cement, and to products of hydration of white cement. Experimentally, the optimal dosage of glass fiber from the mass of the concrete mixture was determined, and the optimal length of the glass fiber was established. It is shown that the highest strength is observed in samples reinforced with glass fiber with a fiber length of 30 mm.

**Acknowledgements.** This work was realized in the framework of the Program of flagship university development on the base of the Belgorod State Technological University named after V.G. Shukhov, using equipment of High Technology Center at BSTU named after V.G. Shukhov.





## References

1. Klyuev, S.V., Klyuev, A.V., Khezhev, T.A., Pukhareno, Y.V.: High-strength fine-grained fiber concrete with combined reinforcement by fiber. *J. Eng. Appl. Sci.* **13**, 6407–6412 (2018)
2. Klyuev, S.V., Klyuev, A.V., Khezhev, T.A., Pukhareno, Y.V.: Fiber concrete for industrial and civil construction. *Mater. Sci. Forum* **945**, 120–124 (2018)
3. Khezhev, T.A., Pukhareno, Y.V., Khezhev, K.A., Klyuev, S.V.: Fiber gypsum concrete composites with using volcanic tuffsawing waste. *ARPN J. Eng. Appl. Sci.* **13**(8), 2935–2946 (2018)
4. Klyuev, S.V., Khezhev, T.A., Pukhareno, Y.V., Klyuev, A.V.: The fiber-reinforced concrete constructions experimental research. *Mater. Sci. Forum* **931**, 598–602 (2018)
5. Klyuev, S.V., Khezhev, T.A., Pukhareno, Y.V., Klyuev, A.V.: Experimental study of fiber-reinforced concrete structures. *Mater. Sci. Forum* **945**, 115–119 (2018)

6. Begich, Y.E., Klyuev, S.V., Jos, V.A., Cherkashin, A.V.: Fine-grained concrete with various types of fibers. *Mag. Civ. Eng.* **97**(5), 9702 (2020)
7. Bondarenko, N.I., Bondarenko, D.O., Evtushenko, E.I.: Study of the chemical interaction of glass fiber with cement hydration products. *Bull. BSTU named after V.G. Shukhov* **12**, 119–125 (2020)
8. Amran, M., Fediuk, R., Vatin, N., Huei Lee, Y., Murali, G., Ozbakkaloglu, T., Klyuev, S., Alabduljabber, H.: Fibre-reinforced foamed concretes: a review. *Materials* **13**(19), 4323 (2020)
9. Klyuev, S.V., Bratanovskiy, S.N., Trukhanov, S.V., Manukyan, H.A.: Strengthening of concrete structures with composite based on carbon fiber. *J. Comput. Theor. Nanosci.* **16**(7), 2810–2814 (2019)
10. Vishnevskaya, J.Yu, Trounov, P. V., Kalatozov, V.V., Bondarenko, D.O.: Prospects for efficiency fiber reinforced concrete through the use of composite binders. *Bulletin of BSTU named after V.G. Shukhov* **3**, 35–37 (2013)



# Impact of Polyurethane Foam Insulation on the Deformability of Three-Layer Frameless Cylindrical Vaults

S. A. Makeev<sup>(✉)</sup> , A. A. Komlev , P. A. Korchagin , and S. V. Savelyev 

Federal State Budget Educational Institution of Higher Education, «The Siberian State Automobile and Highway University», Omsk, Russia

**Abstract.** Three-layer frameless cylindrical vaults are structures made of two coaxially oriented and located at a given distance between arched profiled sheets of flooring, fastened with thermal profiles. The space between the arched sheets is filled with effective foam insulation, which ensures the joint work of all the elements of the vault due to high adhesion. To date, in the calculation of the load-bearing capacity of the vaults, the effect of the joint work of foam insulation with the elements of the vaults is not taken into account.

One of the promising areas of research on the work of three-layer frameless cylindrical vaults is the identification of reserves of load-bearing capacity, which is possible by taking into account the joint work of polyurethane foam insulation with thermal profiles and arched sheets of profiled flooring.

The paper presents the results of calculations of the stress-strain state of three-layer frameless cylindrical vaults, taking into account the joint work of profiled flooring sheets and connecting thermal profiles with polyurethane foam insulation.

**Keywords:** Frameless cylindrical vaults · Profiled flooring · Polyurethane foam insulation

## 1 Introduction

The creation of light and strong structures is always an urgent task of the construction industry, as many sectors of the national economy are in dire need of them. To such buildings, there are simply a huge number of requirements that simply cannot be implemented in one structure.

One of the promising directions in the development of light and strong structures is the study of frameless cylindrical vaults [1, 2]. To date, there are two main directions in the study of the work of frameless cylindrical vaults. The first is to model the operation of vaults in a nonlinear setting in order to identify the reserves of load-bearing capacity [3, 4]. The second is the creation of multilayered cylindrical vaults [5–8].

Today, three-layer frameless cylindrical vaults, which are made of two coaxially oriented arched sheets of profiled flooring, are of particular interest [9]. The sheets are fastened through special connecting elements, thermal profiles. The space between the sheets of profiled flooring is usually filled with an effective insulation.

As an effective insulation, as a rule, mineral wool slabs are used, which have almost the best thermal characteristics. However, they do not have any structural connections with the profiled flooring sheets. As a result, the profiled sheets work independently of the insulation.

When using polyurethane foam insulation, which has excellent adhesion to metal, profiled arched sheets and thermal profiles begin to work with the insulation together.

The aim of the study is to identify the reserves of the load-bearing capacity of three-layer frameless cylindrical vaults by taking into account the joint work of profiled flooring sheets, thermal profiles and polyurethane foam insulation.

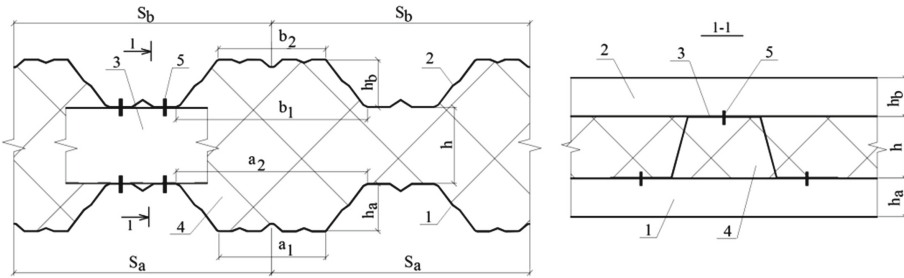
## 2 Methods and Materials

The thickness of the polyurethane foam insulation and, accordingly, the height of the thermal profile are determined based on the heat engineering calculation performed in accordance with [10]. However, as the polyurethane foam insulation fills the entire space between the sheets of profiled flooring, the height of the thermal profile will be determined from the specified thickness of the insulation.

In this paper, a heat engineering calculation is performed for the climatic parameters of the city of Omsk [11]. The parameters of the polyurethane foam insulation are adopted in accordance with [12].

As a result of the calculation, the specified thickness of the polyurethane foam insulation in 100 mm provides the required level of resistance to heat transfer based on the condition of energy saving.

The distance between the sheets of profiled flooring, depending on the specified thickness of the insulation, is determined by the formula [13] (Fig. 1):



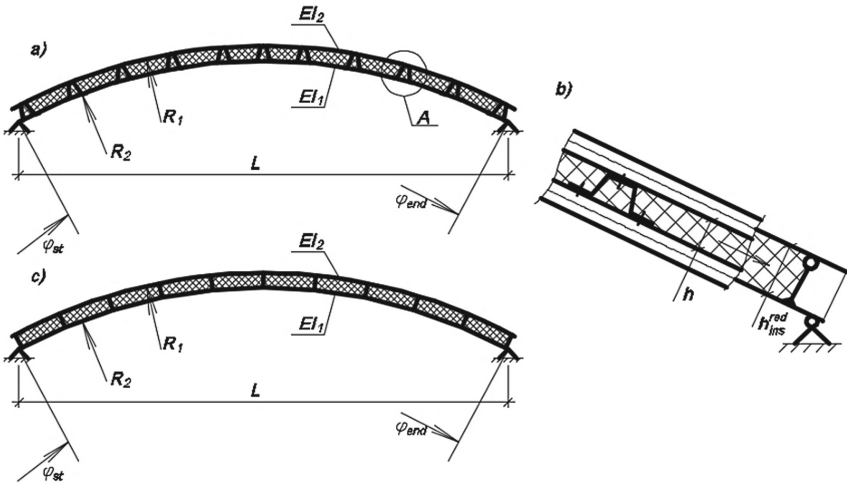
**Fig. 1.** Symbols: 1 – Lower arch made of profiled flooring of the A-NS-44-1 brand, 2 – Upper arch made of profiled flooring of the A-NS-44-1 brand, 3 – thermal profile, 4 – polyurethane foam insulation; 5 – rivets/screws.

$$h_{sym}^{np} = h + \frac{a_1 + a_2}{2S_a} h_a + \frac{b_1 + b_2}{2S_b} h_b. \tag{1}$$

The distance  $h = 50$  mm is obtained (Fig. 1) between the sheets of profiled grade A-NS-44-1 [14] with a specified thickness of 100 mm of polyurethane foam insulation.

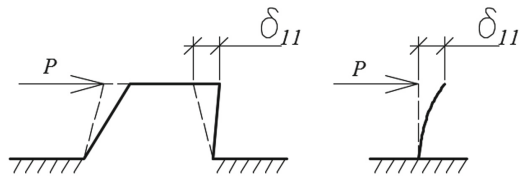
Therefore, the height of the thermal profiles in the construction of frameless cylindrical vaults is 50 mm.

In view of the complex stress-strain state of the “upper layer – thermal profile – lower layer” system in a three-layer frameless cylindrical vault, it was decided in the design scheme (Fig. 2a) to replace the thermal profile with an equivalent rod of constant cross-section, pivotally fixed to the upper layer and rigidly to the lower one (Fig. 2b).



**Fig. 2.** The design scheme of a three-layer frameless cylindrical vault (the load is not shown conditionally); a) the system “upper layer – thermal profile – lower layer”, b) replacement of the thermal profile with an equivalent incompressible rod of constant cross-section, c) the system “upper layer – equivalent rod – lower layer”.

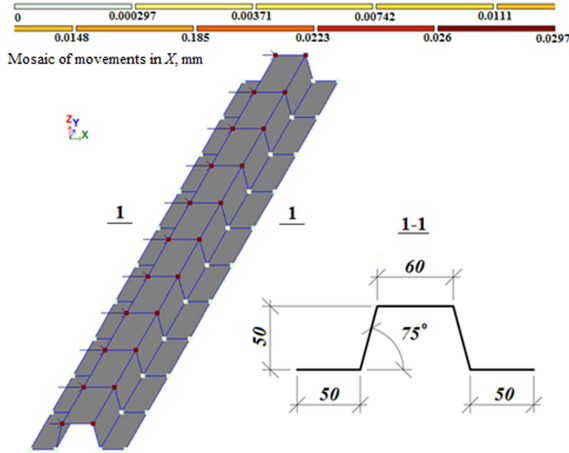
The replacement of the thermal profile with an equivalent rod was carried out under the condition of equal displacements at the top level of the thermal profile and the replacement rod (Fig. 3).



**Fig. 3.** The condition of equality of movements.

The displacement in the thermal profile (compliance) from a single load is determined by numerical simulation in the software package of the PC Lira-CAD (Fig. 4).

As an example, a simulation of the operation of the  $\Omega$  - profile with the geometric dimensions shown in Fig. 4 is performed.



**Fig. 4.** Determination of the thermal profile compliance.

The thermal profile is modeled using 41 FE (Universal rectangular finite element of the shell). The profile with a length of 1000 mm is loaded at the level of the upper plate with a single horizontal shearing force of 100 N. The profile has a rigid fastening at the level of the lower plates.

As a result of the calculation, the value of the horizontal displacement (compliance) was 0.0297 mm (Fig. 3). Then

$$\delta_{11} = 0,000297(\text{mm}/\text{N}).$$

As the shear stiffness  $C_{11}$  is the inverse of the compliance  $\delta_{11}$ , then

$$C_{11} = 1/0,000297 = 3367(\text{N}/\text{mm}).$$

To calculate the moment of inertia of an equivalent rod with a height of  $h = 50$  mm, we use the expression

$$\Delta = \frac{P \cdot h^3}{3EI_{eq}} \tag{2}$$

Replacing the ratio  $P/\Delta = C_{11}$ , we find the value of the moment of inertia of the equivalent rod

$$I_{eq} = \frac{C \cdot h_{eq}^3}{3E} = \frac{3367 \cdot 50^3}{3 \cdot 200000} = 701.5 \text{ mm}^4.$$

and the thickness of the equivalent incompressible rod

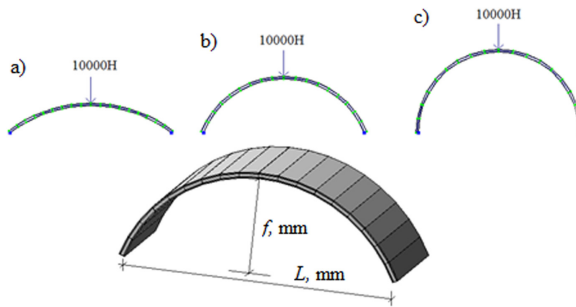
$$I_{eq} = \frac{b \cdot t_{eq}^3}{12_{eq}} \tag{3}$$

$$t_{eq} = \sqrt[3]{\frac{12I_{eq}}{b}} = \sqrt[3]{\frac{12 \cdot 701,5}{1000}} = 2.03 \text{ mm}.$$

Thus, when calculating a frameless cylindrical vault, the thickness of the equivalent rod, which is introduced into the calculation instead of the accepted  $\Omega$ -profile with a height of 50 mm and a wall thickness of 1 mm, is 2.03 mm.

### 3 Results and Discussion

To determine the impact of polyurethane foam insulation on the deformability of frameless cylindrical vaults, calculations of three-layer frameless cylindrical vaults with a span of  $L = 3000$  mm were performed in the software package of the PC Lira-CAD. The upper and lower sheets of profiled flooring of the A-NS-44-1 brand are replaced by plates of equivalent thickness from the condition of equality of the moments of inertia of the sections (Fig. 5).



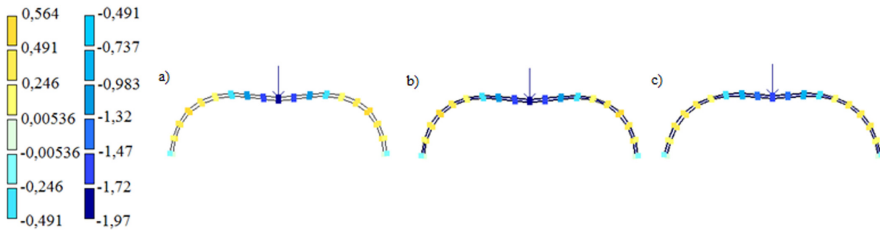
**Fig. 5.** Design schemes of frameless cylindrical vaults: a)  $L = 3000$  mm,  $f = 500$  mm; b)  $L = 3000$  mm,  $f = 1000$  mm; c)  $L = 3000$  mm,  $f = 1500$  mm.

Modeling of polyurethane foam insulation in the composition of frameless cylindrical vaults was performed using four-node universal finite elements of the shell (FE 44) with an average value of the elastic modulus, which varied in the range from  $E = 0.13$  MPa [12] to  $E = 12$  MPa [15]. The height of the incompressible rods is 50 mm, the thickness is 2.03 mm. The calculated load on frameless cylindrical vaults is assumed to be the point force  $P = 10000$  N applied in the middle of the span.

As a result of the calculation, the values of vertical displacements in frameless cylindrical vaults, shown in Fig. 6 and in Table 1, are found.

In Table 1 the column 1 contains references to three schemes of vaults that differ in height  $f$  with the same span  $L$  in Fig. 5; column 2 shows the maximum deflection of the  $z$  design vaults without regard to insulation; in columns 3, 4 and 5, 6 there are values of the maximum deflections of the vaults  $z$  taken into account the collaboration of the vaults with foam insulation and the percentage of discrepancies with the values in column 2, with the elastic moduli of insulation  $E = 0.13$  MPa and  $E = 12$  MPa, respectively.





**Fig. 6.** Results of calculation of frameless cylindrical vaults  $L = 3000$  mm,  $f = 1000$  mm: a) without work of polyurethane foam insulation; b) taking into account the work of polyurethane foam insulation  $E = 0.13$  MPa; c) taking into account the work of polyurethane foam insulation  $E = 12$  MPa.

**Table 1.** Values of vertical displacements in frameless cylindrical vaults.

Vault according to Fig. 5, a, b, c, $L = 3000$ mm	Deflection $z$ , mm without insulation	Deflection $z$ , mm taking into account the polyurethane foam insulation $E = 0.13$ MPa	%	Deflection $z$ , mm taking into account the polyurethane foam insulation $E = 12$ MPa	%
$f = 500$ mm	1.081	1.078	0.27	0.901	16.6
$f = 1000$ mm	1.964	1.957	0.36	1.537	21.74
$f = 1500$ mm	4.037	4.015	0.54	2.858	29.20

## 4 Conclusion

As a result of the calculation, it is found out:

- when calculating frameless cylindrical vaults, taking into account the joint work of equivalent connecting rods and polyurethane foam insulation, vertical movements are reduced;

- when changing the elastic modulus of polyurethane foam insulation in the range from  $E = 0.13$  MPa to  $E = 12$  MPa, the maximum deflections in frameless three-layer cylindrical vaults are reduced to 29% due to the joint work of the vault layers, thermal profiles and insulation.





## References

1. Karmanov, I.V., Zverev, V.V., Zhidkov, K.E., Podzorov, A.V.: Constructive solutions of frameless arched buildings. Modern state and prospects of development. *Constr. Mech. Calc. Struct.* **5**(262), 58–62 (2015)
2. Vedyakov, I.I., Solovyov, D.V., Armensky, MYu.: New types of frameless buildings and prospects for their development. *Ind. Civ. Constr.* **10**, 27–29 (2009)
3. Zdanov, D., Ulasevich, A.W.: Nonlinear analysis method for arch shaped shell roofs made of cold formed steel profiles. *Civ. Environ. Eng.* **7**, 173–191 (2016)

4. Anghel, V., Sorohan, S., Consnantin, N., Stoica, I.: On the analysis of a cold formed steel profile arch structure. *Acta Electrotech.* **57**(1–2), 2344–5637 (2016)
5. Ereemeev, P.G., Kiselev, D.B.: Full-scale tests of a fragment of an arched vault made of cold-bent thin-sheet steel profiles. *Mount. Spec. Works Constr.* **12** (2004)
6. Ereemeev, P.G., Kiselev, D.B., Armensky, M.Y., Burlay, S.I.: Full-scale tests of fragments of panels made of cold-bent thin-sheet steel profiles for arched vaults. *Mount. Spec. Works Constr.* **9**, 5–9 (2004)
7. Ereemeev, P.G., Kiselev, D.B., Armensky, M.Y.: To the design of frameless structures of arched vaults made of cold-bent thin-sheet steel profiles. *Mount. Spec. Works Constr.* **7**, 54–57 (2004)
8. Pat. RU 2 287 6447 C1, IPC E04B 1/32 frameless two-layer arched building made of thin-sheet cold-bent profiles/P.G. Ereemeev, D.B. Kiselev, S.I. Burlay, M.Yu. Armensky (RU). 2005122578/03, application 18.07.2005; publ. 20.11.2006
9. Rybakov, V.A.: *Fundamentals of Structural Mechanics of Light Steel Thin-Walled Structures: A Textbook*, vol. 207. Publishing House of Polytechnic University, St. Petersburg (2011)
10. SP 50.13330.2012 Thermal protection of buildings. Updated version of SNiP 23-02-2003. Date of introduction 2013-07-01. Ed. official, vol. 100. Ministry of Regional Development of Russia, Moscow (2013)
11. SP 131.13330.2012 Construction climatology. Updated version of the SNiP 23-01-99\*
12. TU 2257-001-46128283-2016 Sprayed polyurethane insulation “POLYNOR”
13. STO 0047-2005 Steel-reinforced concrete floors with a monolithic slab on a steel profiled flooring
14. TU 112-235-39124899-2005: Curved arched steel profiles with trapezoidal corrugations/SibSRISTroy. Novosibirsk 18 (2005)
15. GOST 24524-80 Double-layer steel panels for building coverings with polyurethane foam insulation. Technical conditions



# Study of the Effect of Cryogenic Grinding on the Microstructure and Mechanical Properties of Polymer Composites

V. V. Kashibadze<sup>(✉)</sup> , V. V. Sirota , A. I. Gorodov , and R. V. Sidelnikov 

Belgorod State Technological University named after V.G. Shoukhov, Belgorod, Russia  
vitaliy.kashibadze@mail.ru

**Abstract.** The paper presents data on the synthesis of polymer composites based on a fluoroplastic matrix and ground titanium hydride. The possibility of mixing the initial components using cryogenic grinding has been studied. The uniformity of distribution of the filler in the polymer matrix was investigated by scanning electron microscopy. For comparison, composites were made in which the mixing of the components was carried out manually in an agate mortar. It is shown in the work that when using cryogenic grinding of components, their distribution is much more uniform than when manually mixing. It has been established that cryogenic milling will prevent the agglomeration of highly dispersed titanium hydride particles obtained during milling, ensuring high homogeneity of the polymer composite. Data on the mechanical properties of the obtained composites are presented. Annealing at 350 °C significantly increased the microhardness of all the samples under study. For pure fluoroplastic, this value increased by 35.7%, and for composites by 35.5% and 30.7% when using grinding in a mortar and cryogenic grinding, respectively.

**Keywords:** Cryogenic grinding · Titanium hydride · Fluoroplastic · Surface microstructure · Microhardness · Hot pressing

## 1 Introduction

Scientists from various countries are involved in radiation protection. The most common materials for radiation protection from gamma and neutron radiation are concretes [1–3]. Recently, special attention has also been paid to radiation-protective materials based on polymers [4–6]. Such polymer composites consist of a radiation-resistant polymer matrix and a radiation-shielding filler. Depending on the type of radiation for which protection is created, the type of filler is selected. For example, organosilicon fillers can be used to protect against cosmic radiation in which vacuum ultraviolet radiation is present [7]. In addition, the use of organosilicon fillers significantly increases the resistance of composites to the incident flow of atomic oxygen in space [8, 9].

Biological protection of nuclear reactors requires comprehensive protection from both gamma and neutron radiation. The works [10, 11] present data on the radiation-protective characteristics of a multicomponent material the iron – magnetite – serpentine cement concrete with high protection. The work [12] summarizes the data on fillers

used in concrete for biological protection. In [13], using the barite aggregate as an example, it is shown that the type of aggregate is more important than the amount of aggregate used in concrete to protect against  $\gamma$ -radiation.

Metal hydrides [14, 15], in particular titanium hydride, are promising materials for protection against neutron radiation. Titanium hydride possesses not only good protective properties against neutron irradiation, but also high thermal stability [16, 17]. Most of the research is devoted to the introduction of titanium hydride into concrete. This paper presents data on the possibility of introducing titanium hydride into a polymeric fluoroplastic matrix.

The creation of polymer composites is associated with a number of problems. The main one is the uniform distribution of the added filler into the polymer matrix [18, 19]. With an uneven distribution of filler particles, conglomerates are formed, which leads not only to a decrease in physical and mechanical properties, but also to a decrease in radiation-protective characteristics. One of the solutions to this problem is the modification of the added filler, but this is a rather laborious process [20, 21]. In this work, we used a method of mixing fluoroplastic and titanium hydride by means of joint cryogenic grinding of components.

## 2 Methods and Materials

Fluoroplastic F-4, grade PN-20, was used as a polymer matrix. It was a white press powder with a particle size of 6–20  $\mu\text{m}$ . Fluoroplastic of this brand is used for products with increased reliability. The density of the fluoroplastic used is 2.2  $\text{g}/\text{cm}^3$ .

Titanium hydride with the chemical formula  $\text{TiH}_{1.7}$  was used as a filler. The starting titanium hydride was a shot with a diameter of 1–4 mm. To introduce titanium hydride into the polymer matrix, it was preliminarily ground in a jet-vortex mill for 15 min. After grinding, the titanium hydride particle size did not exceed 100  $\mu\text{m}$ .

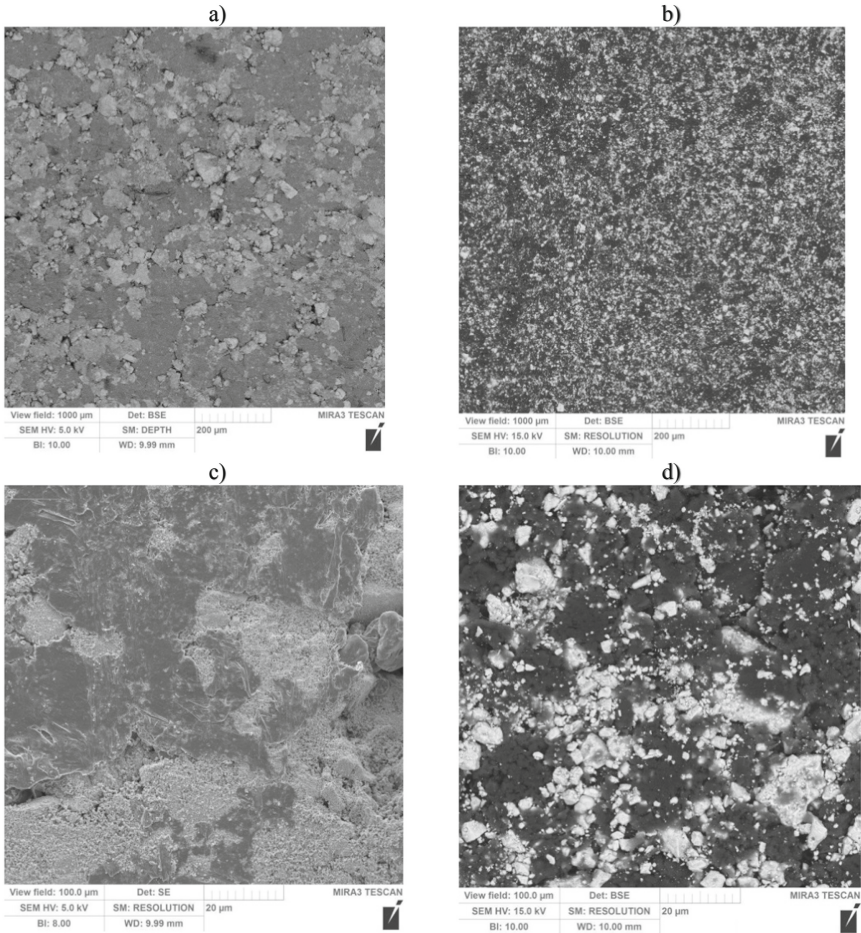
The mixing of the components (fluoroplastic and titanium hydride) was carried out in a vibrating mill at a cryogenic temperature. To create a cryogenic temperature, liquid nitrogen was used ( $T = -196^\circ\text{C}$ ). To obtain composites, the homogenized mixture was molded by hot pressing at a temperature of 200  $^\circ\text{C}$  and then annealed at a temperature of 350  $^\circ\text{C}$ . To assess the effect of cryogenic grinding on the properties of the final composites, composites were also synthesized without using cryogenic grinding. The mixing of the components was carried out by manual mixing in an agate mortar. The amount of filler in both cases was 60 wt%.

The surface microstructure of the obtained composites was studied using a TESCAN MIRA 3 LMU high-resolution scanning electron microscope.

The Vickers microhardness of the obtained samples was investigated on a NEXUS 4504 device at the same load of 200 g.

## 3 Results and Discussion

Figure 1 shows the data on the microstructure of the surface of polymer composites obtained by mixing the components manually in an agate mortar (a, c) and using cryogenic grinding (b, d).



**Fig. 1.** SEM images of polymer composites obtained by mixing components manually in an agate mortar (a, c) and using cryogenic grinding (b, d).

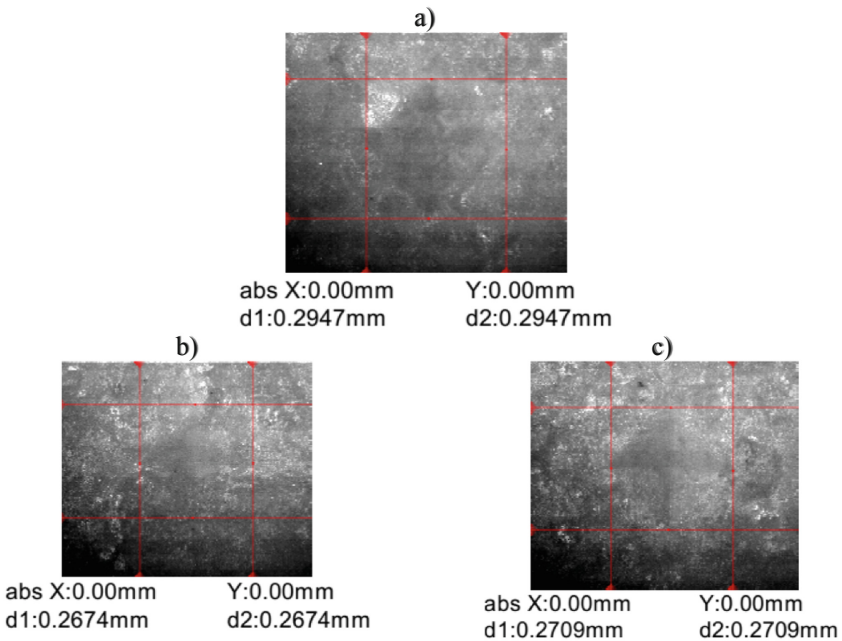
Data analysis Fig. 1 shows that when the components are manually mixed in an agate mortar, an uneven distribution of titanium hydride (light area) occurs in the fluoroplastic matrix (dark area). Particles of titanium with this method are combined into large conglomerates. When using cryogenic grinding of components, a much more uniform distribution is observed (Fig. 1 b, d). This method will prevent the agglomeration of highly dispersed titanium hydride particles obtained during grinding, ensuring high homogeneity of the polymer composite. In addition, the use of joint cryogenic grinding will significantly improve the physico-mechanical and radiation-protective characteristics of finished composites due to the introduction of the maximum amount of filler.

Table 1 shows the data on Vickers microhardness of composites and fluoroplastic (PTFE) after molding and subsequent annealing. The load in all measurements was the same –200 g. The measurements were carried out at 5 different points. Table 1 shows the

arithmetic mean values of the microhardness, taking into account the standard deviation. Figure 2 shows the obtained prints of a tetrahedral pyramid on the samples under study.

**Table 1.** Microhardness of composites after molding and subsequent annealing.

Sample	Mixing type	Vickers microhardness (HV)	
		Molded	Annealed
PTFE	–	4.2 ± 0.32	5.7 ± 0.41
PTFE+ TiH <sub>1,7</sub> (60 wt%)	In a mortar	4.5 ± 0.28	6.1 ± 0.36
	Cryogenic grinding	5.2 ± 0.29	6.8 ± 0.35



**Fig. 2.** Image of the imprint of the indenter of a microhardness tester when measuring the microhardness of fluoroplastic (a), composites with 60 wt% titanium hydride obtained by mixing in a mortar (b) and mixing using cryogenic grinding (c).

Analysis of the data presented in Table 1 showed that annealing at a temperature of 350°C significantly increased the microhardness of all the samples under study. For pure fluoroplastic, this value increased by 35.7%, and for composites by 35.5% and 30.7% when using grinding in a mortar and cryogenic grinding, respectively. It is noticeable that the introduction of the proposed filler in both cases increases the microhardness in

comparison with unfilled fluoroplastic. However, when using cryogenic grinding, the hardness is much higher.

## 4 Conclusion

The possibility of using cryogenic grinding for the synthesis of composites based on fluoroplastic and finely ground titanium hydride has been established. This method made it possible to prevent the agglomeration of highly dispersed titanium hydride particles obtained during grinding, ensuring high homogeneity of the polymer composite. In addition, the use of joint cryogenic grinding made it possible to significantly increase the physicomechanical characteristics of the finished composites, which were evaluated by the Vickers microhardness. For annealed samples without cryogenic breakage, the microhardness was  $6.1 \pm 0.36$  HV, and for samples obtained by cryogenic grinding  $-6.8 \pm 0.35$ .

**Acknowledgements.** The work is realized using equipment of High Technology Center at BSTU named after V.G. Shukhov the framework of the State Assignment of the Ministry of Education and Science of the Russian Federation, project No. FZWN-2020-0011.

## References

1. Chauhan, R.K., Mudgal, M., Verma, S., Amritphale, S.S., Das, S., Shrivastva, A.: Development and design mix of radiation shielding concrete for gamma-ray shielding. *J. Inorg. Organomet. Polym.* **27**, 871–882 (2017)
2. Yastrebinsky, R.N., Pavlenko, V.I., Karnauhov, A.V.: Radiation resistance radiation–defensive the ferrous aggregates in the gamma fields. *Probl. Atom. Sci. Techn.* **2**, 46–49 (2013)
3. Pavlenko, V.I., Yastrebinskii, R.N., Voronov, D.V.: Investigation of heavy radiation–shielding concrete after activation by fast neutrons and gamma radiation. *J. Eng. Phys. Thermophys.* **4**(81), 686–691 (2008)
4. Nambiar, S., Yeow, J.T.: Polymer-composite materials for radiation protection. *ACS Appl. Mater. Interfaces.* **4**(11), 5717–5726 (2012)
5. Zhang, K., Tang, W., Fu, K.: Modeling of dynamic behavior of carbon fiber-reinforced polymer (CFRP) composite under X-ray radiation. *Materials* **11**(1), 143 (2018)
6. Arbuzova, A.A., Votyakov, M.A.: Estimation of the influence of the state of the reinforcing polymer in the structure of polymeric fiber material using mathematical prediction methods. *Chem. Bull.* **1**(1), 12–17 (2018)
7. Pavlenko, V.I., Zabolotny, V.T., Cherkashina, N.I., Edamenko, O.D.: Effect of vacuum ultra-violet on the surface properties of high-filled polymer composites. *Inorg. Mater. Appl. Res.* **5**(3), 219–223 (2014)
8. Minton, T.K., et al.: Atomic oxygen effects on POSS polyimides in low earth orbit. *ACS Appl. Mater. Interfaces.* **4**(2), 492–502 (2012)
9. Pavlenko, V.I., Novikov, L.S., Bondarenko, G.G., Chernik, V.N., Gaidar, A.I., Cherkashina, N.I., Edamenko, O.D.: Experimental and physicomathematical simulation of the effect of an incident flow of atomic oxygen on highly filled polymer composites. *Inorg. Mater. Appl. Res.* **4**(2), 169–173 (2013)

10. Pavlenko, V.I., Bondarenko, G.G., Yastrebinsky, R.N.: Radiation resistance of structural radiation-protective composite material based on magnetite matrix. *Inorg. Mater. Appl. Res.* **5**(7), 718–723 (2016)
11. Pavlenko, V.I., Bondarenko, G.G., Yastrebinsky, R.N.: Attenuation of photon and neutron radiation using iron–magnetite–serpentine radiation-protective composite. *Inorg. Mater. Appl. Res.* **2**(8), 275–278 (2017)
12. Samarin, A.: Use of concrete as a biological shield from ionising radiation. *Energy Environ. Eng.* **1**(2), 90–97 (2013)
13. Akkurt, I., Basyigit, C., Kilincarslan, S., Mavi, B., Akkurt, A.: Radiation shielding of concretes containing different aggregates. *Cement Concr. Compos.* **28**(2), 153–157 (2006)
14. Hayashi, T., Tobita, K., Nakamori, Y., Shinichi, O.: Advanced neutron shielding material using zirconium borohydride and zirconium hydride. *J. Nucl. Mater.* **386**, 119–121 (2009)
15. Shen, H., Chen, F., Han, Y., Yang, M., Li, G., Liang, R.: Research status of metal hydrides for neutron shielding. *Mater. Rep.* **33**(Z2), 484–487 (2019)
16. Yastrebinsky, R.N.: Attenuation of neutron and gamma radiation by a composite material based on modified titanium hydride with a varied boron content. *Rus. Phys. J.* **12**(60), 2164–2168 (2018)
17. Yastrebinsky, R.N.: Decrease gripping gamma–radiation scale composite neutron and protective material on the basis of the modified hydride of the titan with various content of atoms of bor. *Probl. Atom. Sci. Techn.* **4**(110), 103–106 (2017)
18. Sorokin, V.V., Sharapov, O.N., Shunkin, N.M., Kiryushina, N.Y.: New polymeric composites based on epoxy resin with techogenic wastes. *Bull. BSTU V.G. Shukhov* **6**, 8–13 (2019)
19. Abramyan, S.G., Burlachenko, O.V., Oganessian, O.V.: The use of composite materials in the reconstruction of floors of industrial buildings. *Constr. Mater. Prod.* **2**(3), 58–64 (2019)
20. Matyukhin, P.V., Pavlenko, V.I., Yastrebinsky, R.N., Cherkashina, N.I.: The high-energy radiation effect on the modified iron-containing composite material. *Middle East J. Sci. Res.* **17**(9), 1343–1349 (2013)
21. Yastrebinsky, R.N., Pavlenko, V.I., Matukhin, P.V., Cherkashina, N.I., Kuprieva, O.V.: Modifying the surface of iron-oxide minerals with organic and inorganic modifiers. *Middle East J. Sci. Res.* **18**(10), 1455–1462 (2013)





# Investigation of the Effectiveness of the Method of Directional Horizontal Hydraulic Fracturing for Fixing Clay Bases

S. A. Gubarev<sup>(✉)</sup> , A. S. Chernysh , and S. V. Gapon 

Belgorod State Technological University named after V.G. Shukhov, Belgorod, Russia

**Abstract.** Construction is often required to be carried out not on comfortable, reliable and stable soils, but on highly compressible, collapsing or dilative soils, in landslide areas, on swampy, peaty deposits and other types of unstable and weak soils that are dangerous for the structures being built. In these conditions, the solution of such a problem as a purposeful artificial change in the physical and mechanical characteristics of soils, achieved by their compaction or consolidation, is of particular importance. For compaction of soils the following methods are used: surface compaction, deep vibrating packing, camouflage explosions, setting of ground and sand piles, seal or static loading with the use of vertical drains or water depression, including using electroosmosis. The scale of construction in our country requires the construction of various buildings and structures in a variety of complex engineering and geological conditions. A large range of ground conditions, presents significant difficulties for builders due to the need to ensure the reliability and durability of the designed and constructed objects at minimal cost. From methods of soil consolidation the following ones are widely known: carburizing, silicification, electrochemical methods, tarring of soil, thermal method, bitumen and clay grouting. But all these methods are labor-intensive, and their implementation leads to large economic costs. In addition, the necessary strengthening of the foundation soils is not always provided.

**Keywords:** Punching · Hydraulic fracturing · Sediment · Modulus of deformation · Geocomposite · Reinforcement · Hardening · Tarring of soils

## 1 Introduction

In recent years, a technology based on the principles of creating composite materials, that is, the creation of rigid foreign insertions, in a less durable source material, has been used to fix weak or unstable soils [1, 3].

On the example of soils, where the basis is the thickness of natural strength or structurally unstable soils, a reinforced frame of hardening materials in the form of technogenic insertions is created by injection. As a result, the soil mass is a new natural technogenic system, reinforced soil, called “geocomposite” [2].

It has improved physical and mechanical properties, compared to natural soil. Its load-bearing capacity as a foundation base is significantly increased, due to the reinforcement of the soil and its partial compaction when foreign insertions are inserted into the array.

The new technology is becoming widespread, but the lack of a comprehensive theoretical justification of this method, the lack of the ability to predict the mechanical characteristics of the array after hardening, as well as the improvement of the method, requires additional research in this direction [4].

The main objective of the research was the improvement of the strengthening of the soil by using a reinforced soil directional horizontal hydraulic fracturing development of theoretical and practical prerequisites for the application of this method in terms of the hardening of reasons, mainly, the existing foundations.

## 2 Materials and Methods

Stamp tests were carried out with the available soil samples. The essence of these tests is that the hard dies installed in the rocks are successively stepwise loaded, in parallel with this device, the precipitation indicators are removed. The tests are carried out within the boundaries of the interaction of the soil with the structure. The parameter of the deformation properties of the soil is calculated from the draft of the stamp at each individual stage of the load. The nature of the deformation in time is also investigated. There are 3 stages of soil compaction [5].

### *Compaction stage:*

It is a compression of the soil body and is characterized by a decrease in the number of pores.

### *Shift stage:*

It represents the ultimate equilibrium of the soil, in which a large number of local shifts occur, extending along the boundaries of the base of the foundation.

### *Destruction stage:*

It is a complete or partial destruction of the lateral surface of the soil. At this stage, deformations occur that are in parallel with the formation of sliding surfaces. The compacted soil of the cone-shaped form moves down with the stamp, almost meeting no resistance in its path. There is a pattern that when the loads are unchanged, the deformations do not decrease, and when the loads increase minimally, they multiply [6].

The test procedure depends on many factors, such as:

- the depth of the foundation;
- the degree of uniformity of the rocks lying in the base of the structure;
- distribution of loads on the foundation;

To obtain the coefficient for stamp tests (K), it was necessary to conduct compression tests in parallel.

To do this, the soil sample is taken with the cutting ring of the odometer. After the ring was submerged, the soil contained in it was separated from the monolith and cleaned level with the edges of the ring. Filter paper was applied from the ends of the ring to

the ground surface. The assembled odometer was placed in the working position and pressure steps were applied alternately after the ground deformations were stabilized. The indicator statements were put in the table.

Compression tests were conducted in two variants:

1. Clay soil was tested without reinforcement.
2. Similar in physical characteristics, clay soil was tested with reinforcement, that is, the soil sample was cut in half lengthwise, a polymer made on the basis of urea resin was applied to the surface of the cut, the half of the soil cut was placed on top, the applied polymer impregnated and glued 2 halves of the clay soil. Then the sample was tested.

The choice of optimal geological equipment is directly related to the value of the ground water level. In a situation where the mark at which the tests take place is below this level, the tests are most often carried out in wells, and if higher, then in pits.

All load-bearing layers of the soil must be tested, except in cases where the interaction zone is represented by a homogeneous layer. In such cases, studies can only be conducted at one depth. According to SP 22.13330.2016, the minimum number of such tests is 3. They can limit themselves to two tests only if the values of the deformation modulus obtained in them do not differ by more than 25% [7, 8].

### 3 Results and Discussion

For the analysis, we compared the compression tests of reinforced and non-reinforced loam (Table 1).

Loam with the following physical characteristics was used as the soil:

Density,  $\text{g}/\text{cm}^3$  ( $\rho$ ) 1.85

Humidity (W) 0.2

**Table 1.** Results of the study of non-reinforced loam.

Vertical voltage $\sigma$ , kPa	Stabilized sediment		Porosity coefficient	
	Absolute S, mm	Relevant $\varepsilon$	Increment from the initial value $\Delta e$	Value e
0	0.00	0.00	0.00	0.75
50	1.635	0.0654	0.1144	0.64
100	2.47	0.0988	0.1729	0.58
150	3.23	0.1292	0.2261	0.52
200	3.91	0.1564	0.2737	0.48
250	4.51	0.1804	0.3157	0.43
300	5.08	0.2034	0.3559	0.39

Density of dry soil,  $\text{g/cm}^3$  ( $\rho_d$ ) 1.54  
 Density of solid particles,  $\text{g/cm}^3$  ( $\rho_s$ ) 2.7  
 Porosity coefficient ( $e$ ) 0.75  
 Number of plasticity ( $I_p$ ) 12  
 Turnover rate ( $I_L$ ) 0.18

For the stress range from 150 to 250 kPa, the following strain characteristics are obtained:

Compressibility coefficient ( $m_0$ ) 0.0009 kPa  
 Relative compressibility coefficient ( $m_v$ ) 0.00051 kPa  
 Modulus of deformation ( $E_0$ ) 1215 kPa = 1.2 MPa  
 Taking into account the coefficient for stamp tests  $K = 4.2$ ,  $E_0 = 5.0$  MPa  
 Reinforced loam with the same physical characteristics was tested using a similar method (Table 2).

**Table 2.** Results of the study of reinforced loam.

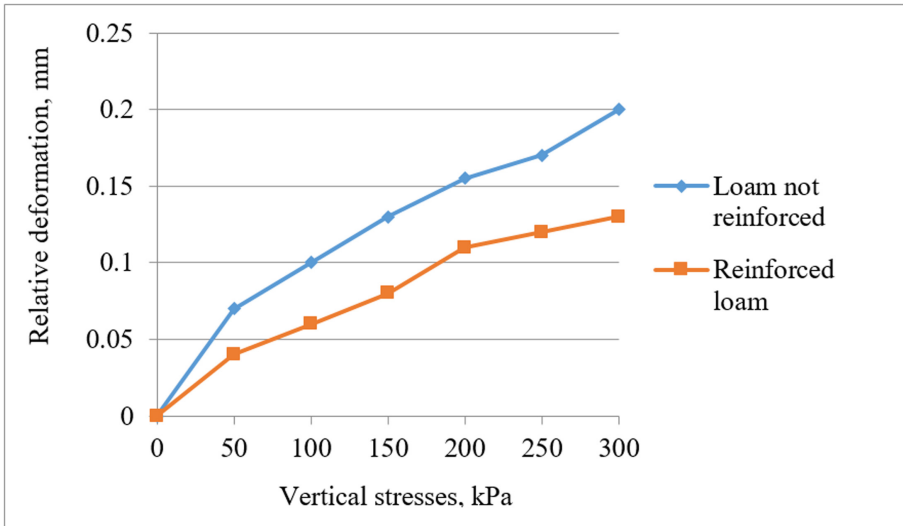
Vertical voltage $\sigma$ , kPa	Stabilized sediment		Porosity coefficient	
	Absolute S, mm	Relevant $\epsilon$	Increment from the initial value $\Delta e$	Value $e$
0	0.00	0.00	0.00	0.75
50	0.96	0.0384	0.0672	0.68
100	1.56	0.0624	0.1092	0.64
150	2.32	0.0826	0.1446	0.61
200	2.71	0.1084	0.1897	0.56
250	2.89	0.1157	0.2024	0.55
300	3.06	0.1225	0.2144	0.54

For the stress range from 150 to 250 kPa, the following strain characteristics are obtained:

Compressibility coefficient ( $m_0$ ) 0.0004 kPa  
 Relative compressibility coefficient ( $m_v$ ) 0.000228 kPa  
 Modulus of deformation ( $E_0$ ) 2734 kPa = 2.7 MPa  
 Taking into account the coefficient for stamp tests  $K = 4.2$ ,  $E_0 = 11.3$  MPa

It was found that during compression studies of loam: with the same physical characteristics of the soil, the obtained modulus of deformation in reinforced soil is almost 2 times greater than in non-reinforced soil –11.3 and 5 MPa, respectively (Fig. 1).

For the analysis, we compared the compression tests of reinforced and non-reinforced clay (Table 3).



**Fig. 1.** Change in the relative deformation of reinforced and non-reinforced loam depending on the applied load.

**Table 3.** Results of the study of non-reinforced clay.

Vertical voltage $\sigma$ , kPa	Stabilized sediment		Porosity coefficient	
	Absolute S, mm	Absolute S, mm	Increment from the initial value $\Delta e$	Value e
0	0.00	0.00	0.00	0.95
50	0.81	0.0324	0.0632	0.89
100	1.97	0.0788	0.1537	0.80
150	3.23	0.1202	0.2519	0.70
200	3.91	0.1564	0.3050	0.65

Clay with the following physical characteristics was used as the soil:

Density,  $g/cm^3$  ( $\rho$ ) 1.85

Humidity (W) 0.2

Density of dry soil,  $g/cm^3$  ( $\rho_d$ ) 1.54

Density of solid particles,  $g/cm^3$  ( $\rho_s$ ) 2.74

Porosity coefficient (e) 0.95

For the stress range from 150 to 250 kPa, the following strain characteristics are obtained:

Compressibility coefficient ( $m_0$ ) 0.0019 kPa

Relative compressibility coefficient ( $m_v$ ) 0.000974 kPa

Modulus of deformation ( $E_0$ ) 410 kPa = 0.41 MPa

Taking into account the coefficient for stamp tests  $K = 4.2$ ,  $E_0 = 1.7$  MPa

Reinforced clay with the same physical characteristics was tested using a similar method (Table 4).

**Table 4.** Results of the study of reinforced clay.

Vertical voltage $\sigma$ , kPa	Stabilized sediment		Porosity coefficient	
	Absolute S, mm	Relevant $\epsilon$	Increment from the initial value $\Delta e$	Value e
0	0.00	0.00	0.00	0.95
50	0.96	0.0384	0.0749	0.87
100	1.56	0.0624	0.1217	0.83
150	2.79	0.1116	0.2176	0.73
200	3.46	0.1384	0.2699	0.68

For the stress range from 150 to 250 kPa, the following strain characteristics are obtained:

Compressibility coefficient ( $m_0$ ) 0.0014 kPa

Relative compressibility coefficient ( $m_v$ ) 0.00072 kPa

Modulus of deformation ( $E_0$ ) 556 kPa = 0.56 MPa

Taking into account the coefficient for stamp tests  $K = 4.2$ ,  $E_0 = 2.35$  MPa

The comparison shows a significant change in the modulus of deformation of reinforced soil in comparison with non-reinforced soil by 37%.

Accordingly, the amount of soil sediment changes, which can be determined using the well-known dependence.

$$S = \frac{\omega * P * \sqrt{F} * (1 - \mu^2)}{E_0}, \quad (1)$$

where  $\omega$  – the coefficient that depends on the shape of the stamp (for a round shape is 0.79)

P– the load on the sole of the stamp, kPa

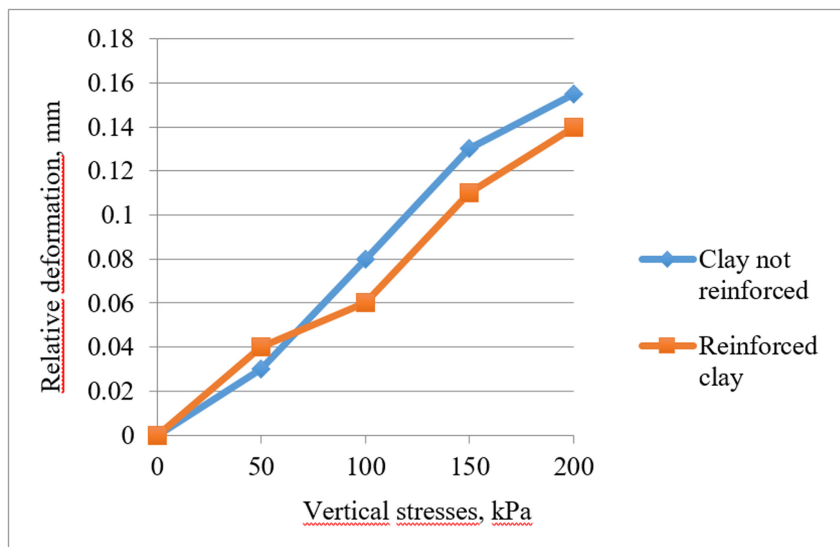
F – stamp area (0.006 m<sup>2</sup>)

$\mu$  – the Poisson's ratio (for clay is 0.42)

So for non-reinforced clay with the above initial data the sediment at a load of 150 kPa will be 3.1 cm

For reinforced clay, the sediment will be 2.2 cm.

The change in the relative strain as a function of the applied load during the compression tests of the samples is shown in the graph [11–15] (Fig. 2).



**Fig. 2.** Change in the relative deformation of reinforced and non-reinforced clay depending on the applied load.

## 4 Conclusion

Thus, the above-described research results suggest that the method of creating reinforced soil by directional horizontal hydraulic fracturing is really relevant and effective; it helps to increase the modulus of deformation, as well as the change in relative deformation depending on the applied load during compression tests of samples.

And also during the tests, it was found that the foundation sediment decreased by 29% at a load of 150 kPa [9, 10].

**Acknowledgements.** This work was realized in the framework of the Program of flagship university development on the base of the Belgorod State Technological University named after V.G. Shukhov, using equipment of High Technology Center at BSTU named after V.G. Shukhov.

## References

1. Abelev, Yu.M., Abelev, M.Yu.: *Fundamentals of Design and Construction on Subsident Macroporous Soils*. Stroyizdat, Moscow (1979)
2. Osipov, V.I., Filimonov, S.D.: Compaction and reinforcement of weak soils by the “geocomposite” method. *FBSM* **5**, 15–21 (2002)
3. Ermolaev, V.A., Matsegora, A.G., Osokin, A.I., Trifonova, I.I., Shakhtarina, T.N.: Strengthening of the bases and foundations of buildings near the located development during the construction of deep pits in urban development conditions. Design and construction of the underground part of the new building (second stage) of the State Academic Mariinsky Theater. In: Ilyichev, V.A., Ledyeva, A.P., Mangushev, R.A. (eds.) *Col. of Scientific-Technical Papers Under the General*, pp. 139–146 (2011)

4. Ermolaev, V.A., Voznesenskaya, E.S., Osokin, A.I., Tatarinov, S.V.: Results of numerical simulation of the stress-strain state of water-saturated loam during injection by hydraulic fracturing using the PLAXIS program. In: Interuniversity Thematic Collection of Works "Actual Scientific and Technical Problems of Modern Geotechnics, vol. 2, pp. 11–15 (2009)
5. Ermolaev, V.A., Matsegora, A.G., Osokin, A.I.: Injection strengthening of the basement foundation soils. *Indus. Civil Constr. Prod. Facil.* **7**, 52–53 (2008)
6. Ermolaev, V.A., Matsegora, A.G., Nikolsky, Yu.V., Osokin, A.I., Svinin, M.V., Shchemelinin, V.V.: Characteristics of hardened soils. *Constr. Urban Econ. St. Petersburg Leningrad Reg.* **40**, 25–28 (2000)
7. Igosheva, L.A., Grishina, A.S.: Review of the main methods of strengthening the foundation soils. *Constr. Geotechn.* **7**(2), 5–21 (2016)
8. Bogdanov, O.I., Korpach, A.I.: Application of DSM deep soil mixing technology for strengthening soil bases. In: Conference with International Participation on Innovative Structures and Technologies in Foundation Construction and Geotechnics: Materials of Scientific and Technical Research, pp. 271–276 (2013)
9. Kalachuk, T.G., Shin, E.: On the types of deformation of stratified soils. *Bull. BSTU V.G. Shukhov* **3**, 59–61 (2016)
10. Krutov, V.I., Bulgakov, V.I., Korotkov, O.Kh: Influence of the degree of humidity on the construction subsidence and compaction of stratified soils. *Found. Base. Soil Mech.* **1**, 19–22 (1980)
11. Kalachuk, T.G., Shirina, N.V.: About irreversible changes in soils strength properties after dynamic loads. *IOP Conf. Ser. Mater. Sci. Eng.* **753**(2), 1–8 (2020). <https://doi.org/10.1088/1757-899X/753/2/022051>. Article no. 022051
12. Chernysh, A.S., Kalachuk, T.G., Shirina, N.V.: Evaluation criteria of loess soils subsidence. *IOP Conf. Ser. Mater. Sci. Eng.* **698**(2), 1–6 (2019). <https://doi.org/10.1088/1757-899X/698/2/022053>. Article no. 022053
13. Kalachuk, T.G., Chernysh, A.S.: Strength parameters of sagged loess soils during the soaking. *IOP Conf. Ser. Earth Environ. Sci.* **194**(4), 1–6 (2018). <https://doi.org/10.1088/1755-1315/194/4/042007>. Article no. 042007
14. Chernysh, A.S., Kalachuk, T.G.: Determination of compacting parameters of dispersed rocks. *IOP Conf. Ser. Earth Environ. Sci.* **194**(6), 1–5 (2018). <https://doi.org/10.1088/1755-1315/194/6/062008>. Article no. 062008
15. Gubarev, S.A., Chernysh, A.S.: Testing samples of writing chalk on a uniaxial compression device. *Vector Geosci.* **3**(3), 15–18 (2020). <https://doi.org/10.24411/2619-0761-2020-10026>





# Promising Technological Solutions for the Production of Compression-Molded Bricks in the Northern Ethiopia

B. K. Gebru<sup>✉</sup>, V. D. Kotlyar, Yu. A. Bozhko<sup>id</sup>, and S. N. Kurilova

Don State Technical University, Rostov-on-Don, Russia  
diatomit\_kvд@mail.ru

**Abstract.** In this article, the general characteristics of the construction industry of the Federal Democratic Republic of Ethiopia is described. It is shown that at this stage of development, Ethiopia is in acute need of various types of building materials and products, and in particular, wall products—bricks. Due to certain characteristics of the region, the problem of providing building materials is particularly acute in the northern Ethiopia in Mekelle city. Mekelle is the capital of the Tigray province, in the northern Ethiopia, where the cement and metallurgical plants are located. These enterprises can become the basis for the establishment of new enterprises for the production of building materials. Our feasibility studies have shown that the most promising direction for the development of wall products in the Tigray province, in terms of technical and economic plan, is organizing the production of non-fired compression-molded bricks based on carbonate rocks from local quarries and waste slag from the metallurgical plant. The current economic development of the Federal Democratic Republic of Ethiopia does not allow the organization of technologically complex and expensive production, and hence the manufactured products must have a minimum cost. Therefore, the technological lines for the production of compression-molded bricks based on the equipment manufactured in Russia, which is characterized by relative simplicity, reliability and low cost, can become the optimal solution for the Federal Democratic Republic of Ethiopia to increase the output of wall products.

**Keywords:** Wall products · Bricks · Raw materials · Compression-molding · Grain size composition · Pressing pressure · Strength · Aesthetic properties

## 1 Introduction

The Federal Democratic Republic of Ethiopia is a developing country whose economy is still based on agriculture. In recent years, thanks to the efforts of both the federal and regional governments, the level of investment in the country's economy has grown significantly and, as a result, there has been a significant increase in construction. This is especially true for the northern part of the country and, in particular, for the Tigray region, the capital of which is the Mekelle city. Mekelle city is located at 780 km north of Addis Ababa, the capital of Ethiopia, in the Ethiopian Highlands at an altitude of 2250 m above

sea level. This altitude provides a cooler climate compared to the surrounding plains. At the end of the 19th century, Emperor Yohannes IV made Mekelle the capital of the state and ordered the construction of a stone palace for himself. Later on, the next emperor Menelik II moved the capital to Addis Ababa. The palace currently houses a museum.

Mekelle is a large industrial center for Ethiopia in the northern part of the country. There is an airport that provides both domestic and international air transportations. The largest enterprises in the city are metallurgical and cement production plants, and besides this fact, there are small construction industry enterprises in the city. The main wall products used in the housing construction are wall sawing stones (dressed wall stones) from various carbonate rocks, as well as hollow cement blocks, obtained by simple installations with vibration-compaction of a concrete mixture. The main colors that define the architectural features of the Mekelle city are various tones of yellow, beige, blue and gray colors (Fig. 1). The growth rate of the housing construction has significantly increased the demand and the need for building materials, where there is an acute shortage of these materials in Mekelle city.



**Fig. 1.** View of Mekelle city, Ethiopia.

## 2 Methods and Materials

A comprehensive analysis we have conducted together with the representatives of Mekelle University allowed us to determine whether the most optimal solution to increase production and increase their diversity is to organize the production of non-fired compression-molded bricks, or as it is often called in Russia hyper-pressed bricks, although this name is not quite correct from the technological point of view. The prefix “hyper” when added to a noun implies a phenomenon, property, or process that is higher than any norm. The molding of bricks using this technology does not exceed the specific pressure of 40 MPa. At such pressures, semi-dry compacted ceramic bricks are formed. Ceramic tiles are compacted on modern molds at specific pressures above 50 MPa. Therefore, the specific pressures of brick pressing in the range of 20–40 MPa are common for the current level of technology development. The choice of a non-fired compression-molding technology (CMT) for organizing the manufacture of wall products in the northern part of the Federal Democratic Republic of Ethiopia, and in particular in the Mekelle city, is due to the following interrelated factors.

The organization of production using this technology makes sense in the immediate vicinity of location of the main raw material - a filler with a fractional composition of 0–5 mm, which is 88–94% of the mass of the products themselves. The geological structure of northern Ethiopia is characterized by the presence of a series of Mesozoic sedimentary rocks and volcanic-sedimentary rocks, among which various types of limestone, dolomite, marble, volcanic tuff and other rocks are distinguished. Despite the fact that in the compression-molding technology, various sufficiently strong rocks and industrial wastes can be used as a filler, in 90% of the cases, carbonate rocks are used as the main raw material. This is due to the fact that these rocks are relatively soft, where the hardness of the mineral calcite, of which they are composed, on the Mohs scale is only 3 units. The hardness of other rocks is significantly higher when they are compared to carbonate rocks. For example, the hardness of quartz, the main mineral in sands, is 7 units, whereas the hardness of granite sand is 6–7 units. This is a very important point in the technology of compression-molding, since due to the high hardness of raw materials, rapid wear of the molds occurs, which significantly affects the cost of products [1, 2]. Currently, several quarries of carbonate rocks are being developed near the Mekelle city – for wall stones and mainly cement production purposes (Fig. 2).



**Fig. 2.** Cement plant and limestone quarry near Mekelle.

### 3 Results and Discussion

The next important point for organizing the production of non-fired wall products near Mekelle city is that the compression-molding technology, in comparison with ceramic bricks, does not require a large amount of investment, is characterized by low energy consumption, and low consumption of cement – which is the most expensive component. The production itself can be literally in the open air or in sheds. The main operations in the production process are the preparation of raw materials, which consists in crushing them (on jaw, hammer, rotary and other crushers), batching and thorough mixing of crushed rocks with cement, pigments and water, molding the products and keeping them in a humid environment. The main purpose of the preparation of raw materials is to select the grain composition, which ensures the densest packing of the grains during compression molding. This allows one to significantly reduce the cement consumption and get more durable products. The densest packing can be achieved both with a continuous grain

composition and the discontinuous grain composition methods [3]. In terms of costs, continuous grain composition method is more acceptable. However, a more careful adjustment of the equipment and careful control are required to achieve it, since even small deviations from the optimal grain composition lead to a decrease in the strength of products and the need to increase the cement consumption. There are various formulas for calculating the optimal grain composition to achieve the densest packing. One of the simplest is Fuller's formula:

$$A = 100\sqrt{\frac{d}{D}}, \quad (1)$$

A - the content in% of the fraction is less than the accepted grain size;

D is the maximum grain size in the powder;

d - diameters of powder particles.

The optimal grain size composition of the raw mixture with a maximum grain size of 2.5 mm according to Fuller's formula is presented in Table 1.

**Table 1.** Optimal grain composition of the raw material mixture.

Largest grain size, mm	Fraction content, mm, % by weight					
	2.5–1.25	1.25–0.63	0.63–0.315	0.315–0.16	0.16–0.08	< 0.08
2.5	24.9–26.9	17.5–19.5	14.4–16.4	13.8–16.8	12.4–14.4	12.0–14.0

An important point is that the fraction <0.08 mm is represented here as the most crushed rock, and Portland cement, which is characterized by a grain composition <0.08 mm. Therefore, taking into account the Portland cement content, the amount of which varies from 6 to 12% depending on the required strength, the optimization of the grain composition of raw material mixes is quite a difficult task. Generally speaking, the main technological factors for achieving the required strength of the products are the Portland cement content and the degree of compaction, which is achieved, as already mentioned above, by the grain composition and molding parameters of products – these are the specific compacting pressure and moisture content of the raw material mixture. Cement is the most expensive component of the raw mix and the lower its consumption, the more cost-effective is the production. With an increase in the amount of cement in the raw mixture, a sharper increase in strength is observed at the beginning, which after 10% slows down significantly. Figure 3 shows the dependence of the ultimate compressive strength of the samples on the amount of M500 cement with the initial compressive strength of 73 MPa of marbled limestone and a grain size composition of 0–2.5 mm close to optimal. The moisture content of the raw mixture was 7–9%, the specific molding pressure was 30 MPa. The optimum moisture content of raw mixes depends on the porosity of the limestone – the more porous the original rock is, the higher the molding moisture should be.

Also, the moisture content of raw materials has a significant impact on the strength of freshly formed samples, which should be at least 1 MPa to avoid the destruction of

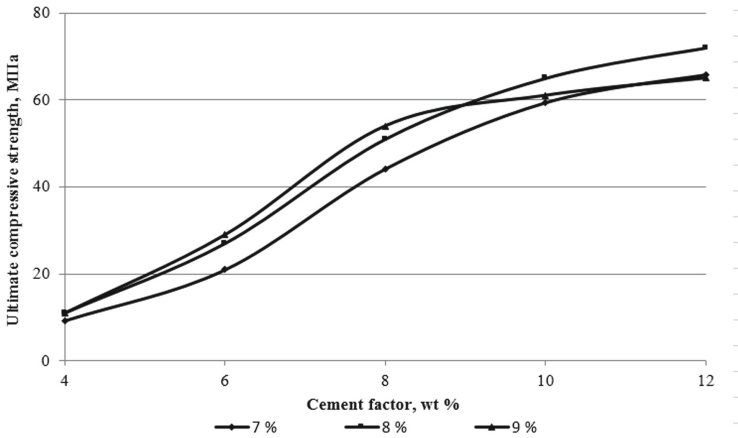


Fig. 3. Dependence of the strength of hardened samples on the amount of cement.

products during packing and transportation. In this case, there is a natural dependence—with an increase in the moisture content of the raw mixture, the strength initially increases and then decreases. Figure 4 shows such a relationship for marbled limestone with a cement content of 8% by weight.

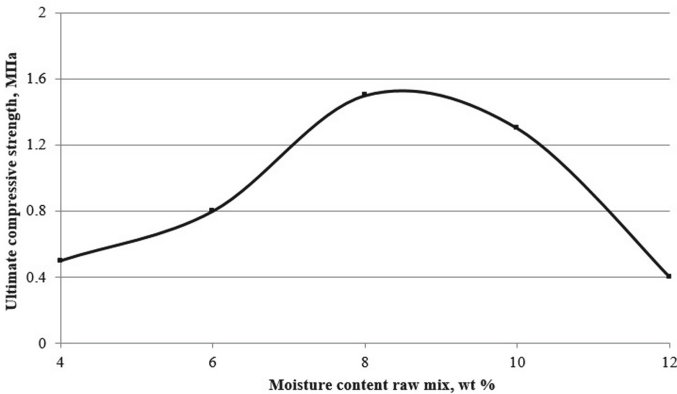


Fig. 4. Dependence of the strength of freshly formed samples on the moisture content of the raw mixture.

Uniform mixing of raw material mixtures is achieved by using high-speed intensive mixers or so-called mechano-activator mixers.

Molding of brick products can be carried out on various types of presses (molds) and can be both double-sided and one-sided. It is most convenient to carry out on hydraulic presses with double-sided load application. In Russia, the company known as «Канон» has developed special presses for the compression-molding technology, which are not inferior to imported ones in terms of technical characteristics, but their cost is significantly lower and they are easier to maintain [4]. For example, the press A100.2, and

A300.4 have a productivity rate of 800–1200 pieces of brick products per hour (Fig. 5). Also, the «Канон» company has developed and sells ready-made technological lines for the production of non-fired compression-molding bricks. In terms of price and quality ratio, they are the most acceptable for the Federal Democratic Republic of Ethiopia. The replacement of molds on this press does not take much time.



**Fig. 5.** Various types of compression-molded bricks.

The laying of finished bricks (palletization) can be carried out manually and with the help of automatic robotic stackers. Since the Ethiopian climate does not require brick steaming to accelerate curing, stacking can take place on major trays being sold. Therefore, brick hardening occurs naturally at ambient temperatures. For brick hardening to take place, the pallet with bricks is covered with plastic membrane. After hardening, the bricks can be grated by splitting, chipping, tumbling, etc. It is also possible to produce earthquake-resistant bricks, known as Lego-brick.

Also, a very important advantage of compression-molded bricks is its variety in both shapes and colors, which can significantly diversify the architecture of northern Ethiopia. On the basis of basic yellow, beige and light gray colors, it is possible to obtain brown colors by introducing finely ground metallurgical slags [5]. The introduction of small amounts of pigments will allow one to get a brick of green and blue palette. The variety of shapes also opens up great opportunities for national architects and builders [6]. It should be noted that the high density of compression-molded bricks is very suitable for the climate of northern Ethiopia – the brick heats up slowly during the day and gives off heat slowly at night.

In the architecture of the Mekelle city, one can clearly see the light pastel tones which are characteristics of natural stones. Most of the buildings are built from limestone, which is widespread in the region. Currently, brick construction is implemented on a small scale due to the high cost of the material. However, with the prospect of building a brick manufacturing plant there and producing compression-molded products, the situation may radically change. Since the main color is light yellow, it will perfectly fit into the general architecture of the city, and thanks to the constructive capabilities of the brick, one can create countless combinatorial solutions [7, 8]. The entire range of colored bricks has muted tones derived from natural pigments. Therefore, the use of such a natural facing material will not harm the architecture of Ethiopian cities, but, on the contrary, will bring a new direction in construction and brick design, will open up new opportunities and horizons for the country's development.

## 4 Conclusion

Thus, we can conclude that developments in this direction and equipment manufactured in Russia, in close cooperation with fellow local builders and architects from Mekelle city, will contribute to the growth of the manufacture of wall products in northern Ethiopia.

## References

1. Kotlyar, V.D., Kurilova, S.N.: Structure formation and properties of pressed cement-mineral composites with the addition of a porous low-modulus component. *RGSU 214* (2014)
2. Talpa, B.V.: Non-fired brick from technogenic carbonate raw materials of the South of Russia. *Build. Mater.* **11**, 50–51 (2003)
3. Talpa, B.V., Boyko, N.I., Kotlyar, V.D.: New types of mineral raw materials in the South of Russia. *News High. Educ. Inst. North Caucasian Reg. Nat. Sci.* **2**, 50–52 (1995)
4. The official site of LLC “NPR Canon”. <http://www.presscanon.com>. Accessed 20 Jan 2021
5. Mohammed, K.J.: Using of steel slag in modification of concrete properties. *Eng. Technol. J.* **27**, 9–15 (2009)
6. Kramorova, V.I., Kotlyar, V.D.: Sculptural brick in modern design. *Constr. Architect.* **2015**, 349–351 (2015)
7. Meskhi, BCh., Bozhko, Y.A., Terekhina, Y.V., Lapunova, K.A.: Brick-design and its main elements. *Constr. Mater.* **8**, 47–51 (2020)
8. Bozhko, Y.A.: The role of facing bricks in the architecture of modern cities in the South of Russia. *Gaudeamus Igitur* **1**, 26–28 (2016)



# Structural Analysis of Steel Membrane Roofing

A. V. Dronov<sup>(✉)</sup> 

Belgorod State Technological University named after V.G. Shukhov, Belgorod, Russia

**Abstract.** The technical state survey of the uninsulated warehouse for grain storage reveals another solution for large span roofing – steel strips welded together to a steel plate supported by steel ties. The inspection of welded connections shows their sufficient load-bearing capacity. Calculation of structure was carried by a finite element method. Initially, a geometrically unstable structure was calculated by modules of geometrical nonlinearity and step-type method. In the design model, the membrane was considered as a simply supported plate, the ties were considered as longitudinal bars. The structural analysis of the steel membrane roofing of the warehouse shows that its loadbearing capacity is sufficient to carry the dead and the snow load acting on the roof of the building. The method of structural analysis of steel membrane roofing was carried by FEM using modules of geometrical nonlinearity due to the large deflection and low bending resistance of a membrane. In the design model, the membrane was considered as a simply supported plate, the ties were considered as longitudinal bars. The gravitational loads cause only tensile axial force in ties and tensile stresses in the plate.

The given method of structural analysis shows the correct way of deformation of a structure and distribution of the internal forces and can be used for the study and design of another steel membrane roofing structure.

**Keywords:** Geometric nonlinearity · Steel plate · Membrane · Warehouse · Roofing

## 1 Introduction

Space-planning solutions of warehouses demand an enlarged grid of columns and large span roofing structures. The structural solution of a roof of such type of buildings significantly affects a dead load of a building's frame. Using trusses, thin-walled sections, portal frames, and other structures can reduce the metal consumption of a building and its construction cost [1, 2]. The technical state survey of the warehouse for grain storage reveals another solution for large span roofing – thin steel plates supported by steel ties. The main feature of this type of roof structure is the significant value of deflections under the load that needs geometrically nonlinear analysis for its study and design [3–6]. The solution to this problem is possible by using the step-type method in the nonlinear load model of the structure [7–10].



## 2 Methods and Materials

The inspected warehouse is an uninsulated building for grain storage. The frame of the building consists of steel columns and simply supported beams of rolled I-sections. The roofing is made of steel strips welded together to a steel plate. Steel plates have dimensions  $12 \times 12$  m, welded along the perimeter to beams and supported by steel ties at 4 points preventing exceeded deflections. The thickness of the steel sheets is 2 mm. The value of snow on the ground at the relevant site S is  $1.5 \text{ kN/m}^2$ . Roof covering was made of roll roofing materials (Figs. 1 and 2).

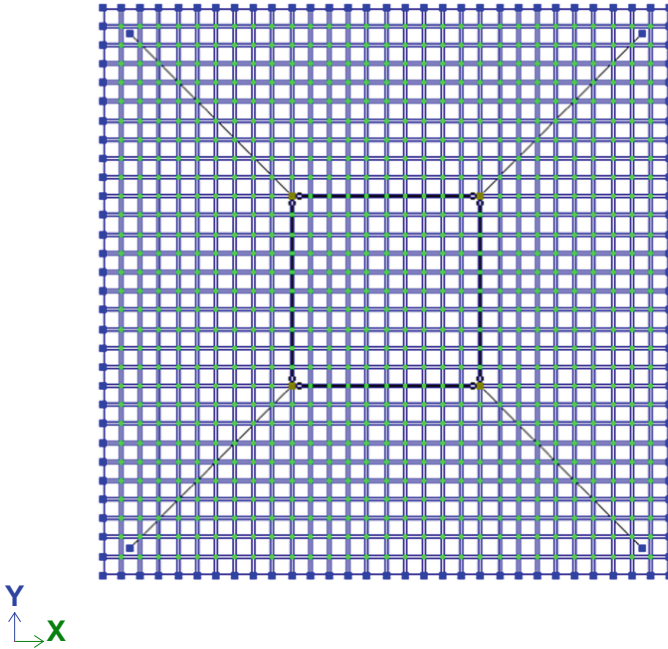


**Fig. 1.** The frame of the warehouse.

The measurements of the thickness of the walls and corrosion damages were carried out by the ultrasonic thickness gauge “UTM-MG4”. The inspection of welded connections shows their sufficient load-bearing capacity. Bolted joints of ties and plate allow to adjust the prestressed tension of a tie and decrease total deflection of a structure. The material of the structure is steel S235.



**Fig. 2.** Steel plate roofing supported by steel ties.



**Fig. 3.** Design model of the structure.

Calculation of structure was carried by a finite element method in LIRA-SAPR software. The design model (Fig. 3) is represented by a simply supported plate and bars. Initially, a geometrically unstable structure was calculated by modules of geometrical nonlinearity and step-type method.

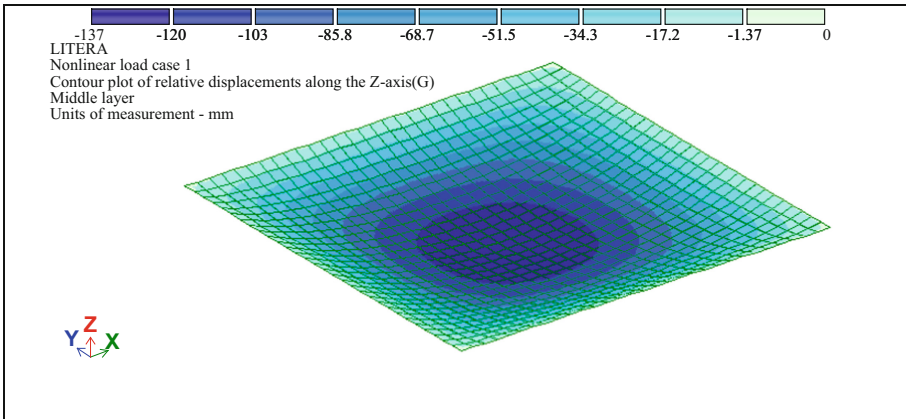
### 3 Results and Discussions

Structural analysis of the steel plate roofing considering geometrical nonlinearity provides the results of deflections and, axial forces in ties and stresses in the plate under the action of the given loads:

1. Dead load – 0.162 kN/m<sup>2</sup>;
2. Roll roofing material – 0.028 kN/m<sup>2</sup>;
3. Live load (snow) – 1.785 kN/m<sup>2</sup>.

Pre-tension of ties wasn't considered as a safety factor.

Total deflection under ultimate load reaches 137 mm (Fig. 4). Due to the large deflection and low bending resistance of a membrane, the only significant stresses in the plate are tensile stresses. Also, the given loads cause only tensile axial force in ties. Such distribution of internal forces provides effective usage of steel in structure and reduce metal consumption of a frame.



**Fig. 4.** Deflection diagram of a structure.

The maximum value of tensile stresses in the plate (Figs. 5 and 6) is 95.8 MPa that is below the ultimate strength value of steel of 235 MPa.

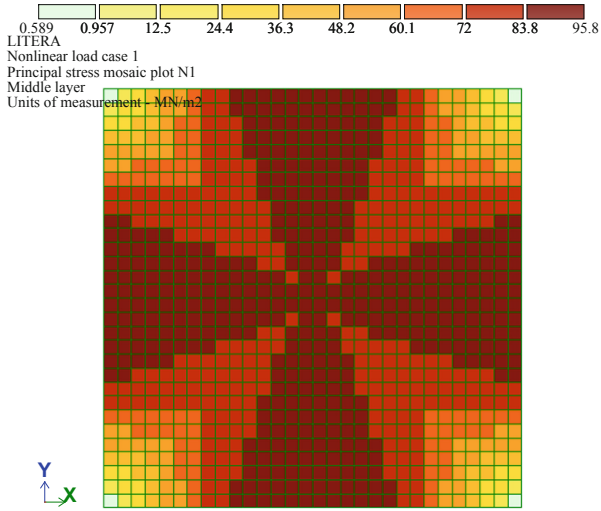


Fig. 5. Principal stresses of a plate.

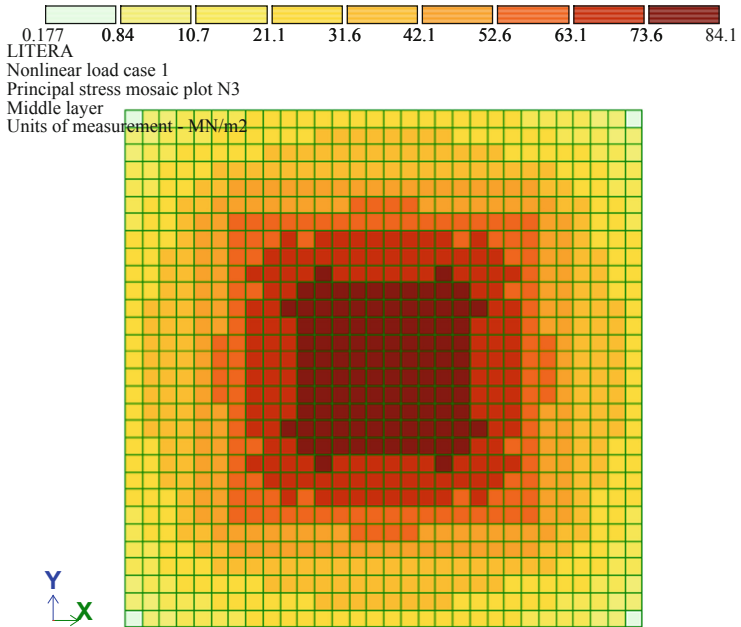


Fig. 6. Principal stresses of a plate.

Ultimate limit state verification of ties:

$$\frac{N}{A_n R_y \gamma_c} = 0.178 < 1$$

where  $N = 9.59$  kN – axial load;  $A_n = 2.545$  cm<sup>2</sup> – section area of a tie  $\varnothing 18$ ;  $\gamma_c = 0.9$  – safety factor.

The results of the structural analysis show the correct way of deformation of a structure and distribution of the internal forces. The obtained values of internal forces and stresses don't exceed the ultimate strength of used materials.

## 4 Conclusion

The structural analysis of the steel membrane roofing of the warehouse shows that its loadbearing capacity is sufficient to carry the dead and the snow loads acting on the roof of the building. The steel structures satisfy the requirements of building codes for strength, stability, and deformability.

The method of structural analysis of steel membrane roofing was carried by FEM using modules of geometrical nonlinearity due to the large deflection and low bending resistance of a membrane. In the design model, the membrane was considered as a simply supported plate, the ties were considered as longitudinal bars. The gravitational loads cause only tensile axial force in ties and tensile stresses in the plate.

The given method of structural analysis shows the correct way of deformation of a structure and distribution of the internal forces and can be used for the study and design of another steel membrane roofing structure.

**Acknowledgements.** This work was realized in the framework of the Program of flagship university development on the base of the Belgorod State Technological University named after V. G. Shukhov, using equipment of High Technology Center at BSTU named after V. G. Shukhov.




## References

1. Kravchenko, G.M., Trufanova, E.V., Bozhenkova, J.M., Susloparov, D.A.: Study of a durability of the membrane layer of a long-span superstructure. *Constr. Architect.* **7**, 10–14 (2019)
2. Malakhov, A.V., Kosinov, V.V.: Determination of technical condition of building constructions based on comprehensive assessment of building production. *Bull. BSTU V. G. Shukhov* **6**, 22–27 (2019)
3. Tushin, A.R., Tushina, O.A.: Numerical analysis of membrane structures. *Internet-vestnik VolgGASU* **3**(23), (2012)
4. Kuzhakhmetova, E.R.: Methods of calculating cables and cable structures. *Bull. BSTU V. G. Shukhov* **2**, 37–48 (2019)
5. Trofimov, V.I., Mikulin, V.B., Goldenberg, L.I.: Large-span steel membrane roofs for the Olympics. *Batiment Int. Build. Res. Pract.* **9**(3) (2008)
6. Dezso, H.: Numerical stability analysis of arch-supported membrane roofs. *Structure* **29**, 785–795 (2021)

7. Solodov, N.V., Vodyahin, N.V., Ishchuk, Y.L.: Improving the strength of harnessing connection of thin-sheetplates. *Bull. BSTU V. G. Shukhov* **9**, 30–37 (2019)
8. Kim, S.D., Jeong, E.S., Baek, I.S.: A study on the nonlinear structural analysis of barrel vault-typed membrane roof structures considering the orthotropic material. *J. Korean Assoc. Spat. Struct.* **5**(1) (2005)
9. Liu, R., Xue, S., Li, X.: Static behavior analysis for annular crossed cable-truss structures. *Spat. Struct.* **20**, 89–96 (2014)
10. Li, J., Han, D.-J.: Dynamic coefficients of large-span cable-membrane roof structures. *J. Vibr. Shock* **28**(5), 153–159 (2009)



# Experimental Justification of Geometrical Model of Cut Chip Cross-Section during Asphalt Milling

D. V. Furmanov<sup>(✉)</sup> , N. E. Lysakov , and L. M. Shamahov 

Yaroslavl State Technical University, Yaroslavl, Russia  
furmanovdv@ystu.ru

**Abstract.** Asphalt concrete is a complex composite material. To adequately simulate milling, some rather complex and interrelated processes should be investigated. This paper presents results of theoretical and practical research which reflect specific aspects of how cutting chips form during milling. The geometry of this process determines the productivity of the equipment, the cutting forces, and the specific energy input per unit of material removed. The paper presents the results of theoretical analysis of geometrical indices of cut chip cross-section, the method of experiments, and experimental results of cutting sandy and granular asphalt concrete grades by a single cutting element with a cylindrical carbide tip. Analysis of research results of geometrical parameters of cut asphalt concrete chips by cutting element with cylindrical carbide tip showed that angles of bevel in the formed grooves do not depend on asphalt concrete grade and are constant. It has been experimentally established that the bevel angle of the grooves should correspond to  $77.6^\circ$ . The results of the conducted work are also important for geometrical modeling of asphalt concrete cutting by different types of milling units. It is possible to identify new, economically feasible, operation modes of equipment, as well as rational design and technological parameters of machines. This will allow you to optimize the basic parameters of the equipment.

**Keywords:** Asphalt concrete · Asphalt concrete milling · Milling simulation · Cutting forces · Cutting chip cross-section · Cutting element

## 1 Introduction

Despite economic difficulties affecting all countries in the world in varying degrees, it is an objective fact that road networks are consistently growing and being developed. However, at the same time, the challenges of maintaining and repairing existing pavements are growing as well. Asphalt concrete, which is a complex dispersion-filled composite [1, 2], like any composite material, requires special, economically justified removal and disposal technology. With the continuous increase in the volume of work, an extensive increase in the number of road milling machines is not an adequate solution.

The structure of the asphalt concrete is formed as early as in the mixing chamber and changes during its operation [3, 4]. This largely determines the characteristics of milling.

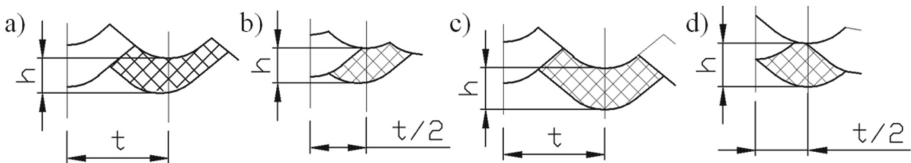
There are many known studies of asphalt concrete milling concerning energy parameters of machines [5], cutting theory [6, 7], issues of mathematical simulation of cutting processes, and determining loads on the cutter elements [8], machine control issues [9], but they quickly become outdated. This is due to continuous improvement of milling machine designs and development of strength indicators of asphalt concrete, improvement of its structure during its preparation, laying, compaction, and improvement of quality control technology [10].

Among the known materials, very little attention has been paid to chip formation. The depth of cut, the angular and linear spacing of the cutters, the feed rate, and the cutting speed will largely determine the size and cross-sectional area of the material to be cut.

## 2 Problem Statement

In a number of studies, the value of cutting resistance force components is determined as a function of the thickness of the cut chip and other (e.g., strength) material parameters [6, 11, 12]. At the same time, the nature of cutting is not always specified, in particular, the pitch of cutters, the sequence of interaction of cutting elements with the material.

If the number of cutting elements on the milling drum is small, their linear spacing is increased (Fig. 1). The cutting pitch  $t$  determines the area and geometric shape of the chip to be cut, even at constant cutting depths  $h$ . It is obvious that the cutting resistance forces will also be different in both cases.



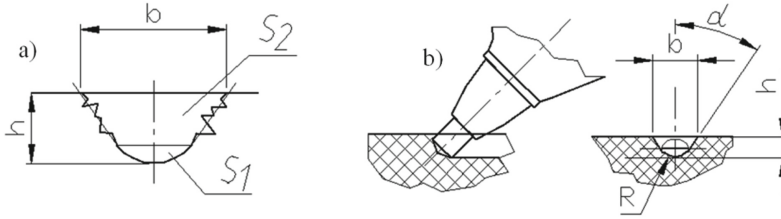
**Fig. 1.** Different shapes of chip cross-sections for consecutive cutting with large (a) and reduced (b) pitches, and for mixed cutting with large (c) and reduced (d) pitches.

In addition, depending on the angular spacing of the cutters, it can be cut both sequentially (Fig. 1a, b) and mixed (Fig. 1c, d).

Geometric simulation of chip formation must rely on a number of constants that help to determine the main geometric ratios over the entire volume of material to be cut with sufficient accuracy. This task also applies to all types of asphalt used in road construction and to all major types and size groups of cutting elements used in modern road milling machines.

The cross-sectional area of the chip  $S$ , thickness  $h$ , can be expressed by two components  $S_1$  and  $S_2$  (Fig. 2a). Given the inclined position of the cutting element, cutting the material with the cylindrical part will determine the geometry of the lower part of the elliptical groove cross-section. If the angle of inclination of the cutting element is  $45^\circ$ , then with sufficient accuracy the rounded part of a groove section can be represented as





**Fig. 2.** Basic dimensions of the groove (a) and diagram to calculate the dimensions of the cut-off cross-section (b).

a circle with radius  $R$ , which depends on diameter  $d$  of the cylindrical tip of the cutting element:

$$R \approx 0.705 \cdot d \tag{1}$$

The area  $S_1$  represents the area of a segment with an angle  $\beta$  equal to 80–100° for different materials:

$$S_1 = R^2 \cdot \left( \frac{\pi \cdot \beta}{360} - \sin \frac{\beta}{2} \cdot \cos \frac{\beta}{2} \right) \tag{2}$$

The area of the trapezium  $S_2$  is determined by the following relation:  
The width of the groove  $b$  is expressed by the ratio:

$$\begin{cases} b = 2 \cdot R \cdot \sin \frac{\beta}{2} + 2 \cdot \left( h - R \cdot \left( 1 - \cos \frac{\beta}{2} \right) \right) \cdot \operatorname{tg} \alpha, \\ \quad \text{if } h > R \cdot \left( 1 - \cos \frac{\beta}{2} \right) \\ b = 2 \cdot R \cdot \sin \frac{\beta}{2}, \text{ if } h \leq R \cdot \left( 1 - \cos \frac{\beta}{2} \right) \end{cases} \tag{3}$$

In the above equation, the unknown is the value  $\alpha$ .  
In order to correctly determine the angle  $\alpha$ , a number of experiments are required.

### 3 Methods and Materials

We have used a specially designed testing bench (Fig. 3a). Samples of different asphalt concrete grades were placed on the moving table of a medium power milling machine. A stationary cutter was placed on a special support in the machine chuck.

The most common cutting element with a tip diameter of 9.5 mm was selected for the experiment.

When the machine feed is switched on, the cutting element cuts grooves of varying depths in the material sample (Fig. 3b).

The width and area of the groove formed were controlled using a special template with movable plates (Fig. 3c).

In order to reflect the overall picture of material chip development during milling, we have selected the most common grades of road asphalt used for paving the top layers of road pavements. Grades A1, B2, B3, MZP (GOST 9128-2009), SMA-20, SMA-16 (GOST 31015-2002) were chosen as samples. The experiment was conducted at an asphalt concrete temperature of 22 °C.



**Fig. 3.** General view of the testing bench (a), grooving with the cutting element (b) and measuring the main dimensions of the groove (c).

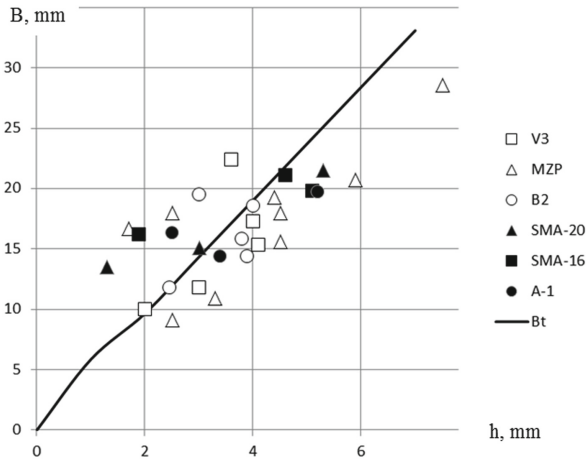
## 4 Results and Discussion

As a result of experimental work on different asphalt concretes, we have established a correlation between the thickness of the chip cut and the width of the groove formed (Fig. 4). An even stronger relationship has been established between the thickness of the cut chip and its cross-sectional area (Fig. 5).

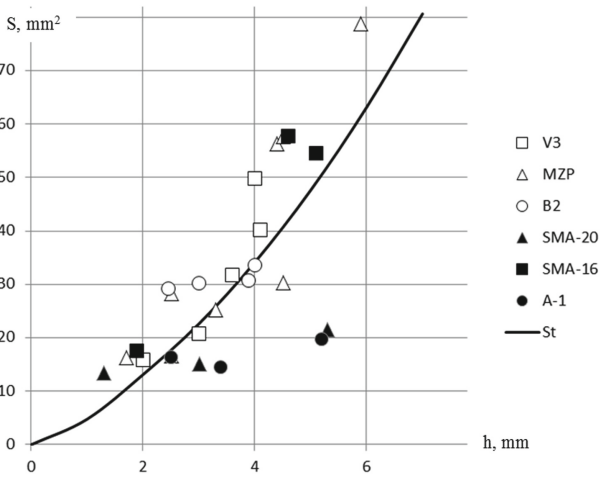
Different points show the data obtained by analyzing the groove sizes when cutting different materials. The solid line shows the theoretically calculated values of the groove width  $B_t$  calculated with regard to dependence (4) and the groove cross-sectional area  $S_t$  calculated with regard to dependence (3).

The theoretical dependences are the most suitable to the experimental data at the angle of groove edge formation  $\alpha = 77.6^\circ$ . The sum of standard deviations in this case takes minimum values.

Almost all points characterizing the behavior of materials are equally distant from the graph. This indicates that the parameters linking the geometric characteristics of the chip section are independent of the grade and type of asphalt concrete and constant; with some assumptions, they can be used in simulating the workflow.



**Fig. 4.** Diagram of dependence of groove width on thickness of cut chips of different types of asphalt concrete by carbide cutter with cylindrical cutting element.



**Fig. 5.** Diagram of dependence of section area of a groove on thickness of the cut chips of different types of asphalt concrete by carbide cutter with cylindrical cutting element.

### 5 Conclusion

Analysis of research results of geometrical parameters of cut asphalt concrete chips by cutting element with cylindrical carbide tip showed that angles of bevel in the formed grooves do not depend on asphalt concrete grade and are constant. It has been experimentally established that the bevel angle of the grooves should correspond to 77.6°. The results of the conducted work are also important for geometrical modeling of asphalt




concrete cutting by different types of milling units. It is possible to identify new, economically feasible, operation modes of equipment, as well as rational design and technological parameters of machines.

## References

1. Matthews, F., Rawlings, E.: Composite Materials. Mechanics and Technology. Tehnosfera, Moscow (2004). 408 p.
2. Bazhenov, S.L.: Mechanics and Technology of Composite Materials: Scientific Edition. Publishing House 'Intellect', Dolgoprudny
3. Ryb'ev, I.A.: Asphalt Concrete. Vysshayashkola, Moscow (1969). 399 p.
4. Gezenzvey, L.B.: Road Asphalt. Transport Publishing House, Moscow (1976). 336 p. (in Russian)
5. Sherstnev, N.S., Ignatov, S. D.: Calculation of the power unit of a road milling machine. In: Razvitiedorozhno-transportnogo i stroitel'nogokompleksov i osvoeniestrategicheskivazhnykhterritoriiSibiri i Arktiki: vkladnauki: International Conference Proceedings, Omsk, SibADI, vol. 2, pp. 79–81 (2014)
6. Kulepov, V.F.: Experimental study of loads on disc cutting working member during the opening of asphalt concrete pavements. In: Reports proceedings. Gorky Regional Scientific and Technical Conference. Gorky 27 (1983)
7. Wong, J.Y.: Theory of Ground Vehicles, pp. 301–309. Wiley, New York (2001)
8. Wu, J., Li, D., Zhu, B., Wu, C.: Milling process simulation of old asphalt mixture by discrete element. Constr. Build. Mater. **186**, 996–1004 (2018). <https://doi.org/10.1016/j.conbuildmat.2018.08.015>
9. Kochetkov, A.V., Yankovskii, L.V., Volkov, G.N., Kokodeeva, N.E., Zhunusov, D.I.: Control of a road milling machine during gauge repair. Stroitel'nye i dorozhnyemashiny **3**, 39–41 (2013)
10. Radovskiy, B.S.: The current state of development of the American method of designing asphalt concrete mixtures Superpave. In: Road Machinery, pp. 12–22 (2008)
11. Furmanov, D.V., Chizhov, V.S., Lysakov, N.E.: Experimental determination of cutting resistance forces at destruction of asphalt concrete by a single cutting element. SibADI Bull. **17**(2), 196–207 (2020)
12. Baratashvili, M.P.: Determination of factors influencing the operation modes of a machine and their importance for destruction of the surface asphalt layers. Scientific digital archive. <http://econf.rae.ru/article/6606>. Accessed 11 Feb 2019



# Study of the Impact of the Composite “Rubber:Shungite” on the Properties of Bituminous Rubber Binder

V. V. Yadykina<sup>1</sup> , K. S. Vyrodova<sup>1</sup> , and E. E. Potapov<sup>2</sup> 

<sup>1</sup> Belgorod State Technological University named after V.G. Shukhov, Belgorod, Russia

<sup>2</sup> MIREA – Russian Technological University, Moscow, Russia

**Abstract.** Modification of bitumen with polymers is one of the ways to improve the physical and mechanical properties of the binder. However, polymer additives have a high cost. However, this problem can be solved by inserting fine fillers of natural origin into the polymer matrix to reduce the consumption of the polymer while maintaining, and in some cases improving, the performance properties of the composite. Recently, the active filler – shungite, which has a unique fullerene-like structure and high adsorption properties, has been widely studied in various industries. Due to this, as well as due to its bipolarity, it has broad prospects for use in the composition of polymers and in the road industry. The work is devoted to the study of the impact of rubber and the composite “rubber:shungite” at different ratios on the characteristics of bituminous-rubber binder (BRB). It is shown that the use of a rubber-shungite composite in the composition of BRB has the same effect as rubber without filler. At the same time, the polymer content in the composition of BRB is much lower, which is economically advantageous. The introduction of shungite into the polymer led to an increase in the viscosity of the BRB, an increase in the softening temperature, extensibility, and elasticity, which should have a positive effect on the deformative stability of the road surface.

**Keywords:** Rubber · Shungite · Polymer-bituminous binder · Bituminous-rubber binder

## 1 Introduction

One of the most common ways to improve the quality of road bitumen at the present time is their modification with various polymers [1–3]. The choice of the polymer type is determined by the technical requirements for the physical and mechanical properties of the binder, as each of the polymer types is specific and transmits only its inherent qualities to the entire bitumen-polymer system. For example, the high elasticity of rubbers, which is due to the spiral structure of polymer macromolecules [4], plays a decisive role in a large range of negative temperatures from the point of view of the possibility of increasing the deformability of bitumen at low temperatures.

The use of rubbers in bitumen is aimed at improving the extensibility, elasticity, increasing the softening temperature and brittleness temperature, as well as increasing the viscosity at high temperatures.

The insertion of a small amount of such a modifier into bitumen increases the cost of the binder, so a promising direction of development is to reduce the polymer content by introducing natural fillers into it. Recently, there has been growing interest in the use of shungite, which has a unique structure that can allow it to replace expensive and scarce synthetic material [5]. For example, the use of shungite in the processing of polymers is known, which leads to the production of composite materials characterized by an improved set of properties (resistance to aging, heat resistance, high elasticity, improved strength characteristics) and increased economic performance due to the possibility of reducing energy costs for distribution in the polymer, as shungite is easily inserted into the polymer matrix [6].

In [7–13], a series of experiments were conducted in which the change in the properties of rubber composites filled with shungite is investigated. The use of shungite in the formulas of rubber-technical products (RTP) based on styrene-butadiene rubbers is especially effective.

The aim of the research is to study the effect of SKS-30 rubber with its different content in the composition of PBB and rubber-shungite composition on the physical and mechanical properties of the prepared bitumen-rubber binder.

## 2 Methods and Materials

The task was solved by introducing crushed rubber-shungite compositions with a different ratio of rubber and shungite into the composition of the bitumen binder. BND 90/130 bitumen was used as the initial binder. The rubber-shungite composition was prepared at the Russian University of Technology (MIREA RTU) on the basis of styrene-butadiene rubber SKS-30 (produced by OJSC Voronezhskintezkauchuk) and finely dispersed shungite – Karelite (provided by the Karelian Investment Company RBC).

Making of the studied compositions of BRB (Table 1) was carried out using a laboratory agitator – Silverson L5T as follows: crushed rubber or composite “rubber:shungite” was fed into a container with dehydrated bitumen and heated to a temperature of 120 °C in the required amount. Next, the mixture was stirred with a gradual increase in temperature to 160 °C for several hours, and then the mixture was placed in a drying cabinet at 160 °C to mature. The time and modes of making were visually determined by the homogeneity of the mixture in accordance with GOST R 52056-2003.

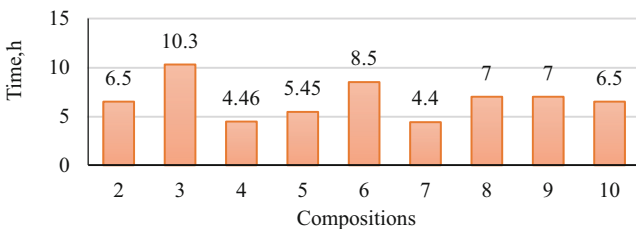
The characteristics of the binder were determined according to standard methods.

**Table 1.** Compositions of the studied BRB.

Type of additive	Nº of composition	Concentration of the additive from the mass of bitumen, %	Polymer content of SCS-30 by weight of bitumen, %	Shungite content, %
BND 90/130, without additive	1	–	–	–
Original rubber SKS-30	2	2.5	2.5	–
	3	5	5	–
rubber:shungite at a ratio of 100:50	4	5	3.2	1.8
	5	7	4.6	2.4
	6	9	6	3
rubber:shungite at a ratio of 100:100	7	5	2.5	2.5
	8	7	3.5	3.5
rubber:shungite at a ratio of 100:150	9	5	1.7	3.3
	10	7	2.4	4.6

### 3 Results and Discussions

The influence of the compositions, namely, the amount of rubber and shungite on the time of preparation of BRB until they achieve uniformity, is studied. It can be seen from the figure that the rational preparation time of the mixtures was significantly different (Fig. 1).

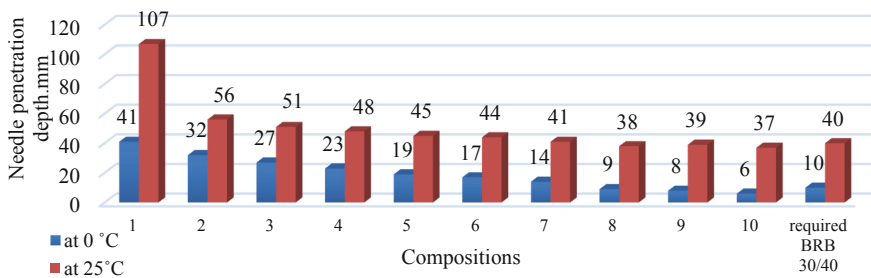


**Fig. 1.** Time of making the studied compositions.

As it is expected, with an increase in the concentration of SCS in the binder (compositions 2 and 3), the time required to achieve uniformity of the mixture increases. The results showed that the insertion of shungite in certain amounts contributes to better mixing and obtaining a homogeneous mixture in a shorter period of time. For example, compositions 2 and 7 contain the same amount of rubber (2.5%), but with the insertion of shungite in an amount of 2.5% (composition 7), the mixing time decreased from 6.5

to 4.4 h. Furthermore, the increase in the number of polymer consisting of 6 compared to 3 (from 5 to 6%) does not increase the making time of the binder, as the presence of shungite promotes better mixing and a more rapid achievement of homogeneity. This is probably due to the breaking of bonds in the polymer macromolecules by shungite solids, which leads to a more uniform distribution of components and faster swelling of the polymer. However, this trend is observed up to a certain ratio of “rubber:shungite”. Figure 1 shows that an increase in the amount of shungite in excess of the rational (compositions 8–10) leads to a decrease in the homogeneity of the mixture and an increase in the time of its making.

Evaluation of the results on the influence of rubber and composite “rubber:shungite” was made by changing the parameters of the needle penetration depth at 25 and 0 °C, the temperature of softening and brittleness, extensibility, elasticity of all compositions (Figs. 2, 3 and 4).



**Fig. 2.** Impact of rubber and composite “rubber:shungite” on the penetration of the binder.

The results of the conducted studies indicate that the penetration at 25 and 0 °C when inserting rubber and compositions into bitumen at different ratios of “rubber:shungite”, naturally decreases in comparison with the initial bitumen (Fig. 2). The penetration values at 25 °C of the obtained BRB are from 37 to 56 mm, i.e. most of the samples meet the requirements for BRB 30/40 in accordance with TU 5718-004-03443057-98. The increase in viscosity should have a positive effect on the performance characteristics of asphalt concrete. However, compositions № 8-10 do not meet the regulatory requirements for these indicators, because they contain a large amount of shungite in relation to rubber and give the binder additional rigidity.

Results of research on the influence of rubber and composite “rubber:shungite” on the softening and brittleness temperature, as well as the plasticity interval of the binder are presented in Table 2.

The results show that the insertion of rubber significantly increases the softening temperature of bitumen from 43 °C to 56 and 61 °C, with a percentage of rubber of 2.5 and 5% (compositions 2 and 3), respectively.

At the same time, the insertion of rubber in an amount of 2.5% ensures that the lower limit of this indicator is reached for BRB 30/40. Higher values of the softening temperature are observed when using the composition “rubber:shungite” in the ratio of 100:50. The greatest influence was exerted by the insertion of 7 and 9% of the studied composite (compositions № 5 and 6). The increase in the indicator compared to the initial

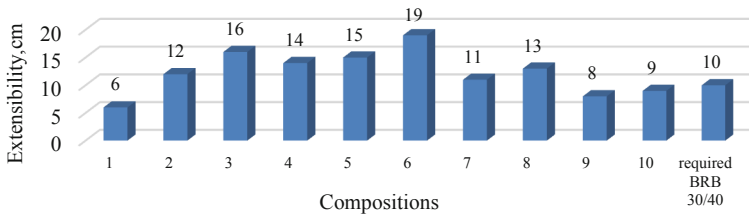


**Table 2.** Influence of the initial rubber SKS-30 and the composite “rubber:shungite” on the softening temperature and brittleness temperature of the binder.

Name of indicators	Req. BRB 30/40	Number of compositions									
		1	2	3	4	5	6	7	8	9	10
Softening temperature	56	43	56	61	58	62	64	57	59	56	58
Brittleness temperature	-15	-15	-18	-18	-18.5	-18.5	-19	-17	-19	-17	-18
Plasticity interval		58	74	79	76.5	80.5	83	74	78	73	76

bitumen was 44.2–48.8%. It is also found that the brittleness temperature changes by 3–4 °C when these additives are inserted. The range of plasticity of the BRB is naturally expanding. Its greatest value is also achieved in compositions 5 and 6. It should be noted that in composition № 6, the content of rubber and shungite is quite large and amounts to 6 and 3%, respectively, which leads to a significant increase in the making time of the mixture, so the use of this composition is irrational.

The studied compositions had a noticeable effect on the extensibility at 25 and 0 °C, compared to the initial bitumen, which is especially important (Fig. 3).

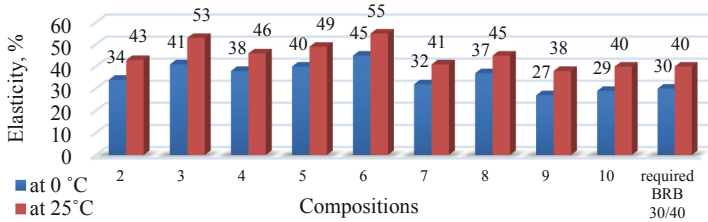


**Fig. 3.** Impact of rubber and composite “rubber:shungite” on the extensibility of BRB at 0 °C.

The maximum increase in the tensile strength of 25 °C compared to the initial bitumen was more than 18% (compositions № 3, 6 and 8), which exceeds the regulatory requirements by several times.

Tensile strength at 0 °C increased by 2–3 times compared to the initial bitumen (Fig. 3) and for compositions № 2–8 exceeded the regulatory requirements for BRB. However, the binder with composition № 9 and 10 did not reach the minimum value of this indicator, apparently due to the large amount of shungite.

One of the most significant indicators of BRB and PBB is elasticity. Results of research on the influence of rubber and composite “rubber:shungite” on elasticity, shown in Fig. 4.



**Fig. 4.** Effect of the studied compositions on the elasticity of the binder at 25 and 0 °C.

The results obtained indicate that the studied compositions give the binders the necessary elasticity both at 25 °C and at 0 °C, with the exception of compositions № 9 and 10 containing an amount of shungite exceeding the rational values, which is quite natural.

## 4 Conclusion

The study of the influence of SKS-30 rubber and rubber-shungite compositions at the ratios of 100:50, 100:100 and 100:150 on the physical and mechanical properties of BND 90/130 bitumen showed that the most effective insertion of rubber in the amount of 5% and the composite “rubber:shungite” in the amount of 5 and 7% with a component ratio of 100:50. Moreover, the use of a composite containing shungite in rational quantities contributes to a significant reduction in the mixing time of the mixture to a homogeneous state.

The use of rubber filled with shungite led to an increase in the softening temperature of the bitumen, an increase in the elasticity and extensibility of the binder, especially at 0 °C (2–3 times compared to the original bitumen), which should have a positive effect on the deformative stability of the road surface.

It is established that due to the insertion of shungite in the composition of the composition for modifying bitumen, it is possible to reduce the amount of rubber in the composition of BRB without compromising its quality, which is economically advantageous.

**Acknowledgments.** This work was realized in the framework of the Program of flagship university development on the base of the Belgorod State Technological University named after V.G. Shukhov, using equipment of High Technology Center at BSTU named after V.G. Shukhov.

## References

1. Tarasov, R.V., Makarova, L.V., Kadomtseva, A.A.: Modification of bitumen by polymers. *Mod. Sci. Res. Innov.* **5**(1)(37), 14 (2014)
2. Saglik, A., Gungor, A.G.: Evolution of performance grades and polymer dispersion of polymer modified binders. In: *Proceedings of 5th Eurasphalt & Eurobitume Congress*, vol. 8, p. 11. Turkish Highways Research and Development Department (2012)

3. Yadykina, V.V., Gridchin, A.M., Trautvain, A.I., Verbkin, V.I.: Investigation of the influence of various polymers and plasticizers on the properties of BND 60/90 bitumen and asphalt concrete based on it. *Bull. BSTU Named After V.G. Shukhov* **6**, 40–45 (2015)
4. Kalgin, Yu.I., Strokin, A.S., Tyukov, E.B.: Perspective technologies of construction and repair of road surfaces with the use of modified bitumen. Voronezh State University, Voronezh (2014)
5. Kolosova, A.S., Sokolskaya, M.K., Vitkalova, I.A., Torlova, A.S., Pikalov, E.S.: Fillers for modification of modern polymer composite materials. *Basic Res.* **10**(3), 459–465 (2017)
6. Petrova, E.P., Rakhimova, N.A.: Development and creation of the formulation of rubber products with improved operational and environmental characteristics using shungite. *Mod. Sci. Res. Innov.* **2**, 36–38 (2016)
7. Kornev, Yu.V., Sokolovsky, A.A., Lischer, Yu.V., Guskov, D.V.: Features of relaxation properties of elastomeric composites filled with nanodisperse shungite. In: *Proceedings of the Conference on “Problems of Tires, RTI and Elastomeric Composites”*, pp. 295–303 (2016)
8. Potapov, E.E., Valia, A., Bobrov, A.P., Prekop, Sh., Shekhter, V.E., Reznichenko, S.V., Morozov, Yu.L.: Shungite is a promising ingredient of rubber mixtures for the tire industry and the RTI industry. In: *Proceedings of the Conference*, 19–22 April, pp. 289–295 (2010)
9. Gabibbulaev, I.D., Assaulenko, M.: Shungite as a regulator of technological properties of elastomeric composites. In: *The Second All-Russian Scientific and Technical Conference “Caoutchouc and Rubber-2010”*, pp. 56–58 (2010)
10. Korneev, Yu.V., Yanovsky, Yu.G., Boyko, O.V., Semenov, N.A., Chirkunova, S.V.: Investigation of the effect of the dispersion of the mineral shungite on the complex properties of elastomeric materials based on SKS-30 ARK rubber. *Caoutch. Rubber* **5**, 17 (2012)
11. Chirkunova, S.V., Yanovsky, Yu.G., Korneev, Yu.V., Boyko, O.V.: Nanodisperse mineral shungite as a new effective filler for elastomeric materials based on special purpose rubbers. In: *XXVI International Innovation-Oriented Conference of Young Scientists and Students MICAS*, pp. 66–70. Federal State Budgetary Institution of Science A. A. Blagonravov Institute of Machine Science of the Russian Academy of Sciences (2015)
12. Korneev, Yu.V., Yanovsky, Yu.G., Boyko, O.V., Chirkunova, S.V.: Nanodisperse mineral shungite – a new reinforcing filler of elastomeric materials. In: *III All-Russian Conference “Caoutchouc and Rubber-2013: Traditions and Innovations”*, pp. 70–71 (2013)
13. Sorokina, O.V., Potapov, E.E., Reznichenko, S.V., Bobrov, A.P., Smal, V.A., Yadykina, V.V., Tikunova, I.V.: Investigation of the properties of high-filled composites based on bitumen and shungite (Karelite). *Caoutch. Rubber* **2**(77), 92–94 (2018)



# Deterioration of Power Transmission Line Supports and Development of Proposals for Increasing their Durability

V. A. Absimetov<sup>(✉)</sup>  and E. V. Saltanova 

Belgorod State Technological University named after V.G. Shukhov, Belgorod, Russia

**Abstract.** Special high-rise structures in the form of power transmission line supports are lattice metal structures made of profile metal and are designed to fasten wires and special fittings in order to transmit high-power electrical energy over long distances. Specific operating conditions for these facilities is work in an open atmosphere with constant exposure to a corrosive environment, wind and ice loads of varying intensity, often close to emergency effects. The objectives of the work is an overall study of wear, bearing capacity of building structures of a linear facility of 220 kV overhead transmission line for subsequent dismantling of the line. The technical condition of the linear object; the actual strength of concrete, determined by non-destructive methods; characteristic defects, corrosion and mechanical damage to building structures; corrosive and physical wear of building structures during many years of operation are defined. Loss of cross-sections from corrosion of metal-roll supports and loss of metal from corrosion are determined. General recommendations for the operation of linear objects are given in the instructions for customer services, which allow extending the durability and increasing the reliability and trouble-free operation of the building structures of the investigated linear object. An assessment of the technical condition of the building structures of the elements of the power transmission line was carried out. The classification of the technical condition of the building structures of the power transmission line supports made it possible to classify them as partially workable.

**Keywords:** Wear · Load-Bearing capacity · Durability · Linear object

## 1 Introduction

The linear object of the VL220 kV is an overhead power transmission line, built and put into operation in 1961.

The surveyed route of the 220 kV overhead line object passes through an area with a temperate continental climate with fairly mild winters with snowfalls and thaws and long summers. The area where the object is located belongs to the dry humidity zone.

The average annual relative humidity in the study area is 75%. The highest humidity is observed in December – 87 the lowest in May – 60%. The average annual long-term precipitation is 546 mm. During the year, precipitation falls unevenly.

The standard depth of seasonal freezing of soils according to SP 22.13330.2016: clay and loam – 101 cm; sandy loam and fine sand – 123 cm; large sand – 131 cm; medium-sized sand – 146 cm.

Soils. The most widespread in this area were typical chernozems, medium-humus and fat powerful. The thickness of the soil layer varies from 0.1 m to 1.8 m.

The work site is located in a forest-steppe zone with a large agricultural development of the territory. The slope type of relief, the ubiquitous distribution of loess-like loams, the heavy rainfall, as well as the long and intensive development of its territory contributed to the fact that erosion processes became dominant.

## 2 Methods

The power transmission line is represented by a single section with a length of 110.22 km. Terrain: 8.472 km of forest; 80.1 km of field; 1.4 km of marshland.

Single- and double chain supports of the type U 34, U 33, U37m+5, U38m-2+5, U220-2+5, U220-3+5, U220-3, U38M, U330-2T are used as anchor-angle supports along the route. To ensure the dimensions at the intersections of 220 kV overhead lines with engineering structures and natural obstacles, these supports are used with stands 9 and 14 m of the type U220-3+9, U220-3+14, U220-1+9, U330-2T+9, U330-2T-14.

As intermediate supports, metal supports of the type P24, P24+3.8, P26M, P220-3, P220-3T, P330-2T, P330-2+5 are accepted.

As intermediate supports, reinforced concrete supports of the PB220-1, PB 330-3, PB 330-7n, and PB 52 types are accepted.

Mushroom-shaped foundations with straight and inclined columns of the following types are used as foundations on the highway: F-2, F-3, F-6, F-4U, F-6U, Ft-1/Ft-2.

## 3 Results and Discussion

The assessment of the technical condition of the building structures of the overhead line elements was carried out in accordance with the requirements of SP 13-102-2003, GOST 31937-2011, No. 184-FZ “On Technical Regulation”, No. 384-FZ “Technical regulations on the safety of buildings and structures”.

During the visual instrumental survey, the technical condition of reinforced concrete foundations and supports, metal structures of supports and connection elements was assessed. The service life of the linear object structures was 60 years [1–4].

Foundations. The main defects of reinforced concrete building structures of foundations should include chipped concrete surfaces at the corners of the foundations, cracks in the installation of anchor bolts, at the level of the contiguity of foundations to the ground surface, weakening of the strength of the surface layers of concrete.

To determine the actual strength of concrete of reinforced concrete structures of foundations, non-destructive testing of structures was performed by the impact pulse method using the ONYX-2.6 device. The strength of concrete of the examined foundation structures was 328 kg/cm<sup>2</sup> (M350 class B 25), which is lower than the design (concrete class B 27.5) by 10–15%, SP 63.13330.2012.

**Metal supports.** In the course of a detailed (instrumental) survey of metal supports, measurements of their geometric dimensions were made; corrosion losses were determined; the loss of stability of metal rods; the main defects and damages were identified.

Overhead line supports belong to group II structures. Steel for supports and elements of fastening of the bases is accepted of grades C245, C255.

For almost all studied metal structures typical of major defects and damage: metal barrel supports almost all were subject to uniform surface corrosion; private plane profile of metal had traces of pitting corrosion; in places the device bolted connections marked areas of increased corrosion of the local nature; in the supporting zone of the metal structures of the supports, local curvature of the shelves of the trunk corners and connection elements was noted due to the operation of vehicles and agricultural machinery near the supports during their operation [5, 6].

In places of increased corrosion wear of the support shaft, the cross-sectional area was estimated by measuring the cross-section dimensions of the profiles and comparing them with the design data. The maximum degree of corrosion wear of the cross-section elements was 1.1–1.6 mm.

Traces of pitting corrosion, traces of deep corrosion of the joints of the support elements, curved structural elements of the support are shown in Figs. 1, 2 and 3.



**Fig. 1.** Pitting corrosion of support elements.



**Fig. 2.** Traces of deep corrosion of the joints of the support elements.



**Fig. 3.** Curvature of the structural elements of the support.

The loss of cross-section dimensions, combined with local deformations of the profiles, create a risk of loss of stability of the compressed shaft rods of supports and connection elements, which must be taken into account when designing and operating a linear object, SP 16.13330.2011.

**Reinforced concrete supports.** When performing the survey, defects and damage were identified by external signs with the necessary measurements and a preliminary assessment of their technical condition. Typical defects and damage of reinforced concrete structures of the VL support include: supports stands deviation from the vertical axis the length and breadth of VL;- the presence of transverse and longitudinal cracks with widths of more than 0.3 mm across the surface of spun concrete pillars or vibrated; the presence of humidified plots and surface efflorescence; the presence of cracks and splits, destruction of the protective layer of concrete; the presence of corrosion of bare

reinforcement; the presence of defects in the concreting of structures; plate rust or ulcers on the rods of bare working reinforcement in the zone of longitudinal cracks.

To determine the actual strength of concrete in reinforced concrete structures of the supports non-destructive testing of structures using shock pulse with ONIKS-2.6 was performed. The strength of concrete structures surveyed amounted to 282 kg/cm<sup>2</sup> (mark M350 class of concrete B 22.5), which is below the design by 10–15%.

As a result of the conducted research, the main types of foundations and supports were identified and their main parameters were determined. The main parameters of overhead line structures are presented in Tables 1 and 2.

**Table 1.** Main parameters of the foundations.

Type	Number of foundations	Dimensions of foundations	Foundation volume, m <sup>3</sup>	Weight of the foundation, t
F-2	64	1500 × 1500 × 2700	0.96	2.4
F-3	216	1800 × 1800 × 2700	1.17	2.9
F-6	16	2700 × 2700 × 3200	2.7	5.8
F-6U	72	3000 × 2020 × 3400	2.85	6.9
F-4U	24	2400 × 2400 × 3400	2.4	5.0
Ft-1/2	476/476	2430 × 2000 × 2000	3.6	9.5

In general, the condition of the studied building structures of metal and reinforced concrete supports and reinforced concrete foundations of the entire linear object meets the requirements for a limited operational technical condition [7, 8].

**General Recommendations.** When operating linear objects, in the instructions for the customer's services, we recommend:

- taking measures to prevent local sags and local damage in the elements of the shaft of metal supports and connections;
- to perform waterproofing of reinforced concrete foundations and crossbars with bitumen-polymer mastic, with a total thickness of at least 1.5 mm;
- to perform anti-corrosion protection of parts of crossbar fixation with bituminous-polymer mastic with a total thickness of at least 3 mm;
- to comply with the protection of drive caps of foundations, beams and anchor bolts by hot dip galvanization;
- to perform repeated anti-corrosion protection of welded joints of foundation elements after welding [9];
- to perform welding with subsequent anti-corrosion protection of the welding points of nuts to the bolt rods to a height of up to 6.0 m to protect the supports from vandalism [10].

All these measures will extend the durability and increase the reliability of the building structures of the linear object under study.

**Table 2.** Main parameters of the supports.

Name of supports	Code	Number of supports	Size of the foundation in the axes, m	Height of the support, m	Weight of the support with zinc, t
<i>Basic parameters of metal supports</i>					
Anchor	U 34	10	8.1	30.0	12.52
Anchor	U33M	1	8.1	30.20	11.89
Anchor	U220-3+14	1	9.4	32.6	14.897
Anchor	U220-3+9	7	7.9	27.6	11.096
Anchor	U220-3	4	5.2	18.6	7.314
Anchor	U 220-1+9	4	7.9	34.1	12.574
Anchor	U33	8	8.1	28.70	11.560
Anchor	U220-3+5	2		23.60	9.72
Anchor	U330-2T	1	6.85	34.3	24.382
Anchor	U330-2T+9	3	9.55	43.3	32.062
Anchor	U330-2T+14	1	11.0	48.3	38.652
Anchor	U37m+5	2	9.6	34.20	24.513
Anchor	U38m-2+5	3	9.6	40.30	24.513
Anchor	U220-2+5	2	6.7	36.60	18.290
Intermediate	P24	56	8.62	36.0	4.711
Intermediate	P24+3.8	3	3.07	36.0	4.788
Single-chain	P220-3t	1	5.0 × 3.13	35.8	4.995
Intermediate	P220-3	1	5.0 × 3.13	35.8	4.995
Intermediate	P330-2T	3	5.75 × 3.68	44.0	10.765
Intermediate	P330-2+5	1	5.75	43.5	11.730
Intermediate	P26M	3	5.2	40.8	5.947
<i>Basic parameters of reinforced concrete supports</i>					
Intermediate	PB220-1	5	2.3 × 2.0 × 2.0	26.00	7.44
Intermediate	PB 330-3	1	2.3 × 2.0 × 2.0	30.30	13.98
Intermediate	PB 330-7n	6	2.3 × 2.0 × 2.0	27.00	1.51
Intermediate	PB 52	238	2.3 × 2.0 × 2.0	32.40	7.43

## 4 Conclusions

Based on a comprehensive study of the load-bearing capacity and reliability of building structures on the linear object: “VL 220 kV Novovoronezh-Gubkin”, the following conclusions are made:

1. The technical condition of the linear object belongs to category III-limited operational capacity.
2. The actual strength of concrete, determined by non-destructive methods, is lower than the standard.
3. In general, the building structures of a linear object have characteristic defects, corrosion and mechanical damage.



4. The corrosion and physical wear of the building structures of the linear object during the long-term operation exceeded the regulatory requirements. The load-bearing capacity of the main structural elements is reduced. It is necessary to develop an appropriate project for dismantling the line.
5. For 60 years of operation of the building structures of the object in a non-aggressive and slightly aggressive atmosphere in the normal humidity zone, the loss of cross-sections from corrosion of rolled metal supports was 1.1–1.6 mm, which in general led to metal losses from corrosion in the range of 10–12%.

**Acknowledgements.** This work was realized in the framework of the Program of flagship university development on the base of the Belgorod State Technological University named after V.G. Shukhov, using equipment of High Technology Center at BSTU named after V.G. Shukhov.

## References

1. Company standard 5694707-29.240.55.111-2011. Guidelines for assessing the technical condition of overhead lines and the residual life of overhead line components
2. Company standard 17230282.27.010.001-2007. Buildings and structures of energy facilities. Technical condition assessment technique
3. Doronina, O.I., Shevchenko, N.Yu., Bakhtiarov, K.N.: Assessment of the reliability of overhead power transmission lines taking into account climatic factors. *Int. J. Appl. Fundam. Res.* **9**(2), 226–23 (2015)
4. Gorokhov, E.V., Shapovalov, S.M., Udod, E.I.: Monograph Improving the Reliability and Durability of Power Grid Structures. Tekhnika, Kiev (1997)
5. Solodov, N.V., Vodyakhin, N.V., Ischuk, Ya.L.: Increasing the bearing capacity of the overlap connection of thin-sheet parts. *Bull. BSTU Named After V.G. Shukhov* **9**, 30–37 (2019)
6. Solodov, N.V., Peshkova, E.V.: Investigation of the stability of rods. *Bulletin of BSTU Named After V.G. Shukhov* **4**, 25–27 (2015)
7. Absimetov, V.E.: Proposals for the development of harmonized standards to substantiate the requirements of technical regulations for the safety of buildings and structures. *IOP Conf. Ser.: Mater. Sci. Eng.* **698**, 022025 (2019)
8. Absimetov, V.E., Presnyakov, N.I., Vostrov, V.K.: Development of the national and interstate regulatory technical base in metal construction taking into account the second generation of Eurocodes. *Ind. Civ. Eng. Mag.* **12**, 6–12 (2013)
9. Merkulov, S.I.: Development of the theory of constructive safety of objects in conditions of corrosive effects. *Bull. BSTU Named After V.G. Shukhov* **3**, 44–46 (2014)
10. Solodov, N.V.: Strength and deformability in collapse in a bolted connection. *Bull. BSTU Named After V.G. Shukhov* **1**, 82–87 (2017)



# Experimental Verification of the Isotropy Postulate on Orthogonal Curved Trajectories of Constant Curvature

V. I. Gulyaev , A. A. Alekseev  , I. A. Savrasov , and S. L. Subbotin 

Tver State Technical University, Tver, Russia

**Abstract.** The results of experimental studies to verify the validity of one of the basic laws of plasticity – the isotropy postulate of A.A. Ilyushin under orthogonal complex loads on curved circular trajectories of constant curvature are presented. Experimental studies were carried out on thin-walled tubular specimens made of the steel 45 material on the automated calculation and experimental complex SN-EVM. Loading programs for tubular specimens were set in the A.A. Ilyushin deviator space of deformations (rigid or kinematic loading) with simultaneous combined action of tension-compression and torsion on the specimen. In the experiments, four deformation trajectories were implemented, representing circles of radius 0.75% starting from the origin. It is established that for the realized complex trajectories of constant curvature, the isotropy postulate is fulfilled both by scalar and vector properties.

**Keywords:** Plasticity · Complex loading · Isotropy postulate · Physical experiment · Deformation trajectory · Vector and scalar properties of the material

## 1 Introduction

Elements of structures and machines work under conditions of complex (disproportionate) loading and deformation, and allow limited plastic deformations in their work. Therefore, conducting experimental studies of the mechanical properties of structural materials beyond the elastic limit and studying the laws of their behavior under complex loading and unloading is an important and urgent task of the mechanics of a deformable solid and the theory of plasticity. The isotropy postulate of Ilyushin [1, 2] as one of the main provisions of the theory of plasticity was experimentally tested for various structural materials at different trajectories of deformation and loading [3–11]. The essence of the isotropy postulate is that under orthogonal transformations of rotation and reflection of trajectories in a vector deviator space with the A.A. Ilyushin basis, the image of the deformation or loading process is preserved, i.e., the scalar and vector properties of structural materials are preserved. The deformation trajectories, on which a complex (disproportionate) loading is realized from the very beginning of the trajectory, are of particular interest when checking the isotropy postulate.

It is noted [11] that orthogonal loads can make some corrections to the relationship between stresses and deformations during plastic deformation. Therefore, the main task

in this paper was to verify the validity of the isotropy postulate of A.A. Ilyushin on complex curved trajectories of constant curvature obtained by orthogonal transformations of the rotation of the original trajectory.

## 2 Methods and Materials

Tests of thin-walled tubular specimens made of steel 45 were carried out on an automated complex SN-EVM in the laboratory of mechanical tests of the Department of Mechanics of Materials, Theory of Elasticity and Plasticity of the Tver State Technical University. Figure 1 shows a general view of the SN-EVM test complex.

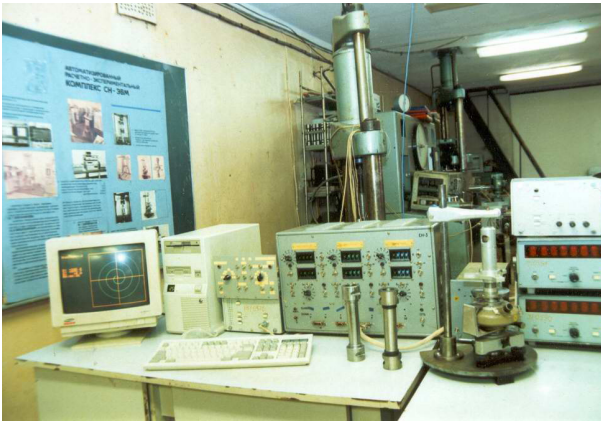


Fig. 1. SN-EVM test complex.

Physical specimens – thin-walled cylindrical shells had a length of the working part  $l = 110$  mm, a wall thickness  $h = 1$  mm and a radius of the median surface  $r = 15.5$  mm. When processing the results of experimental data, the formulas (3) were used to determine the components  $\varepsilon_{ij}$ ,  $\sigma_{ij}$  ( $(i, j = 1, 2, 3)$ ) of strain and stress tensors

$$\varepsilon_{11} = \frac{\Delta l}{l}, \quad \varepsilon_{22} = \frac{\Delta r}{R}, \quad \varepsilon_{12} = \varphi \frac{r}{2l}, \quad \varepsilon_{33} = -(\varepsilon_{11} + \varepsilon_{22}) + \frac{\sigma_0}{K}, \quad \varepsilon_0 = \frac{\sigma_0}{3K}, \quad K = \frac{E}{3(1 - 2\mu)},$$

$$\sigma_{11} = \frac{P}{2\pi rh}, \quad \sigma_{22} = p \frac{r}{h}, \quad \sigma_{12} = \frac{M}{2\pi r^2 h}, \quad \sigma_{33} \approx 0, \quad \sigma_0 = \frac{1}{3}(\sigma_{11} + \sigma_{22}),$$
(1)

here  $\Delta l$  – absolute elongation of the gauge length of the specimen,  $\varphi$  – the angle of mutual rotation of the cross sections,  $\Delta r$  – change in the radius of the median surface of the specimen,  $\sigma_0$  – medium voltage,  $\varepsilon_0$  – average deformation,  $K$  – bulk modulus,  $\mu$  – Poisson's ratio of transverse deformation,  $E$  – Young's modulus of longitudinal elasticity,  $P$  – axial force,  $p$  – internal pressure,  $M$  – torque output. For steel 45  $E = 2 \cdot 10^5$  MPa,  $\mu = 0.3$  is accepted. As the wall thickness of the specimens is much smaller than the radius of the median surface ( $h \ll r$ ),

the stress state at the points of the specimens was assumed to be homogeneous and flat ( $\sigma_{33} = \sigma_{32} = \sigma_{31} = 0$ ,  $\varepsilon_{32} = \varepsilon_{31} = 0$ ). With the occurrence of plastic deformations, the coefficient of transverse deformation rapidly increased and approached the value  $\mu_p = 0.5$ , so the incompressibility condition ( $\varepsilon_0 = 0$ ) was used in the processing of experimental data. The material of the specimens was initially isotropic sufficiently, which was confirmed in experiments under simple (proportional) loads – tension, compression, torsion and internal pressure.

The conducted experimental studies are based on the vector representation of stresses and deformations according to Ilyushin [1–3] in the framework of the theory of elastic-plastic processes, where the stress and strain deviators are put in accordance with the vectors of stresses and deformations of the shape change

$$\bar{\sigma} = S_k \hat{i}_k, \quad \bar{e} = e_k \hat{i}_k \quad (k = 1, 2, 3), \quad (2)$$

where  $\hat{i}_k$  – single vectors of the A.A. Ilyushin basis. Components  $S_k, e_k$  ( $k = 1, 2, 3$ ) of vectors of stresses and deformations in the deviator three-dimensional space of A.A. Ilyushin were calculated by the formulas:

$$\begin{aligned} S_1 &= \sqrt{\frac{3}{2}} S_{11} = \sqrt{\frac{2}{3}} \left[ \sigma_{11} - \frac{1}{2} (\sigma_{22} + \sigma_{33}) \right], \\ S_2 &= \sqrt{2} \left( S_{22} + \frac{1}{2} S_{11} \right) = \frac{\sigma_{22} - \sigma_{33}}{\sqrt{2}}, \quad S_3 = \sqrt{2} S_{12} = \sqrt{2} \sigma_{12}, \\ e_1 &= \sqrt{\frac{3}{2}} e_{11} = \sqrt{\frac{2}{3}} (\varepsilon_{11} - \varepsilon_0), \quad e_2 = \sqrt{2} \left( e_{22} + \frac{1}{2} e_{11} \right) = \frac{\varepsilon_{22} - \varepsilon_{33}}{\sqrt{2}}, \\ e_3 &= \sqrt{2} e_{12} = \sqrt{2} \varepsilon_{12}, \end{aligned} \quad (3)$$

where

$$S_{ij} = \sigma_{ij} - \delta_{ij} \sigma_0, \quad e_{ij} = \varepsilon_{ij} - \delta_{ij} \varepsilon_0 \quad (4)$$

– components of stress and strain deviators, respectively,  $\delta_{ij}$  – the symbol of Kronecker. The modules of stress and strain vectors equal to the modules of stress and strain deviators are determined by the relations

$$\sigma = \sqrt{S_{ij} S_{ij}} = \sqrt{S_1^2 + S_2^2 + S_3^2}, \quad e = \sqrt{e_{ij} e_{ij}} = \sqrt{e_1^2 + e_2^2 + e_3^2}. \quad (5)$$

The deformation programs were implemented in the deviator plane  $e_1 - e_3$  (rigid or kinematic loading) with the simultaneous combined action of tension-compression and torsion on the specimen.

The initial trajectory (trajectory 1) of the deformation is a circle of radius  $R = 0.75\%$  starting from the origin of coordinates. The circle is made one full turn counterclockwise with the arrival at the origin of coordinates. Coordinates of the center of the circle are  $e_1^0 = 0$ ,  $e_3^0 = 0.75\%$ , the curvature of the trajectory  $\kappa = 133.3$ . Orthogonal transformations of the initial trajectory (trajectory 1) were performed by counterclockwise rotation on  $90^\circ$ ,  $180^\circ$  and  $270^\circ$  (deformation trajectories 2, 3, and 4, respectively). All four experimental programs are shown in Fig. 2. In this case, the deformation trajectories 1 and 3, as well as 2 and 4, are skew-symmetric in relation to each other.

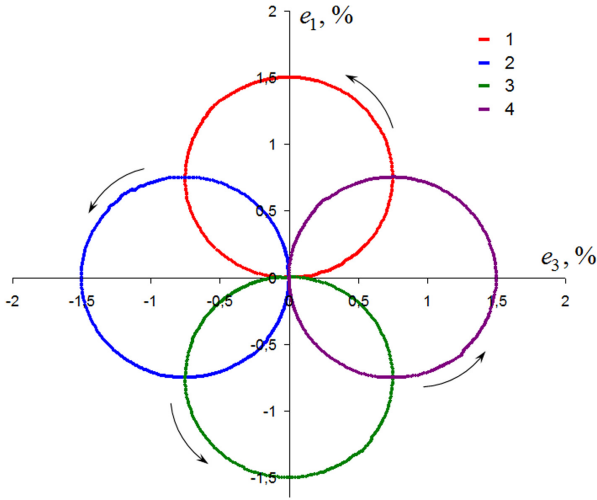


Fig. 2. Deforming programs on the plane  $e_1 - e_3$ .

### 3 Results and Discussion

Figures 3, 4, 5, 6 and 7 show the combined test results of thin-walled tubular specimens according to programs 1, 2, 3, and 4. Figure 3 shows the stress response on the plane  $S_1 - S_3$ . It can be seen that the stress trajectories are also orthogonal to each other.

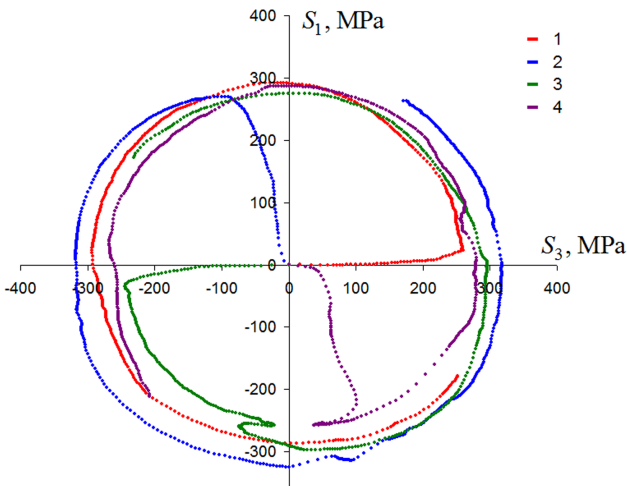


Fig. 3. Stress trajectories on the plane  $S_1 - S_3$ .

In the theory of elastic-plastic processes of A.A. Ilyushin, the relation between stresses and deformations is determined by the scalar and vector properties of materials. The scalar properties of the material characterize the deformation diagrams  $\sigma - s$ ,

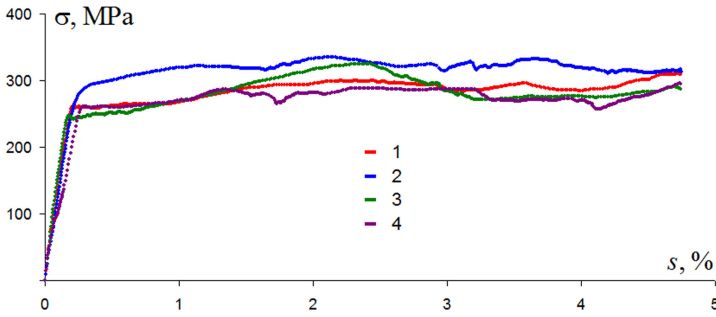


Fig. 4. Deformation diagram  $\sigma - s$ .

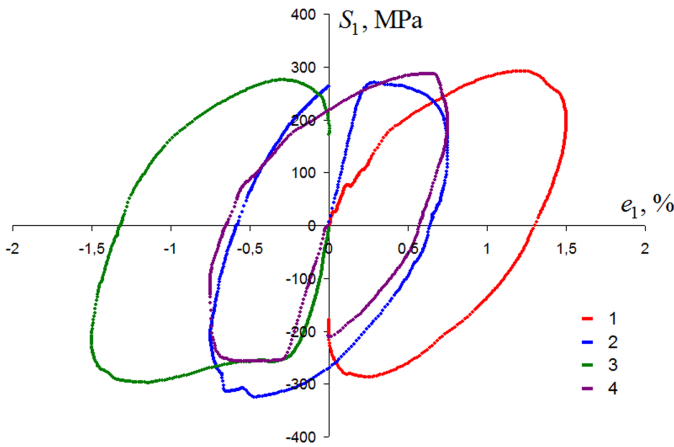


Fig. 5. Local deformation diagram  $S_1 - e_1$ .

where  $s$  is the arc length of the deformation trajectory. Figure 4 shows the combined diagrams  $\sigma - s$  for all four experiments. It can be seen that all the diagrams in Fig. 4 practically coincide, so we can conclude that for this series of tests, the isotropy postulate by scalar properties is fulfilled.

Figures 5 and 6 show the local diagrams of the strain of tension-compression by components  $S_1 - e_1$  and net shear by components  $S_3 - e_3$ , respectively. It can be seen from them that the diagrams for trajectories 1 and 3, as well as 2 and 4, are skew-symmetric.

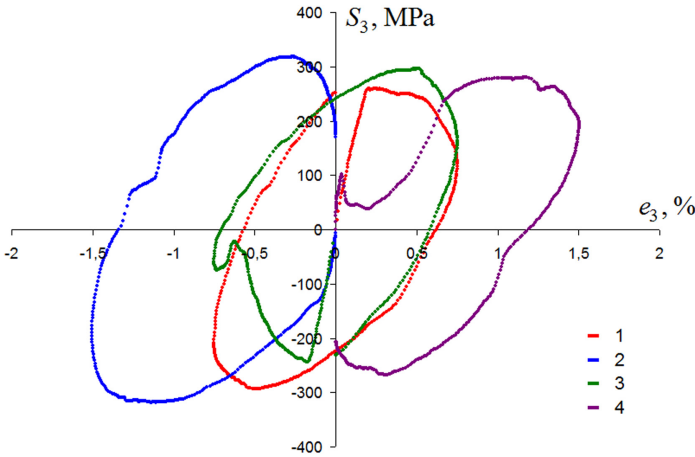


Fig. 6. Local deformation diagram  $S_3 - e_3$ .

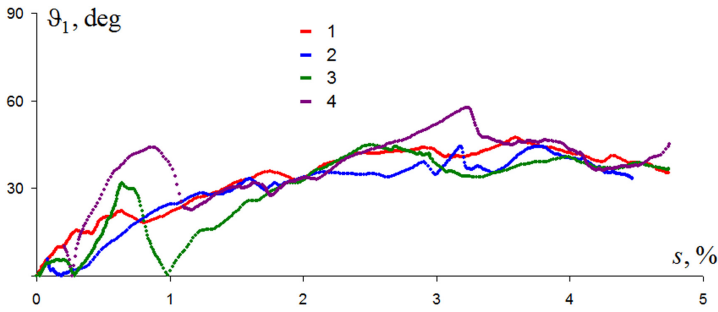


Fig. 7. Diagram  $\vartheta_1 - s$ .

Figure 7 shows combined diagrams  $\vartheta_1 - s$  that characterize the vector properties of the material, where  $\vartheta_1$  is the angle that characterizes the deviation of the stress vector  $\bar{\sigma}$  from the tangent to the deformation trajectory at each point. This angle, called the angle of convergence, reflects the influence of the vector properties of the material on the deformation process. When processing the experimental data, the expression was used to determine  $\vartheta_1$ .

$$\cos \vartheta_1 = \frac{1}{\sigma} \left( S_1 \frac{(e_3 - e_3^0)}{R} - S_3 \frac{(e_1 - e_1^0)}{R} \right), \tag{6}$$

where  $e_1^0, e_3^0$  – coordinates of the centers of the circles.

It is experimentally established [3] that when deforming along circles, a stationary mode of deformation is established with an almost constant value of the angle of convergence  $\vartheta_1^* \approx \text{const}$ . This is what is also observed in this series of experiments, and after stabilization  $\vartheta_1^* \approx 40^\circ$ . As there are angles  $\vartheta_1 < 90^\circ$  in these experiments, the deformation processes along all four trajectories were active without unloading. It can

also be seen that all the diagrams in Fig. 7 are close to each other, so we can conclude that for this series of experiments, the isotropy postulate also holds for vector properties.

## 4 Conclusion

A series of four experiments on the elastic-plastic deformation of the steel 45 material on orthogonal curvilinear deformation trajectories in the form of circles with an offset center, leaving the origin of coordinates, is considered. The scalar and vector properties of the material of steel 45 are investigated. It is established that for the realized complex trajectories of constant curvature, the isotropy postulate is fulfilled quite accurately, both in terms of scalar and vector properties of the material.

## References

1. Ilyushin, A.A.: *Plasticity: fundamentals of the general mathematical theory*. Izd-vo AN USSR, Moscow (1963)
2. Ilyushin, A.A.: *Proceedings (1946–1966) 2 Plasticity*. Fizmatlit, Moscow (2004)
3. Zubchaninov, V.G.: *Mechanics of processes of plastic environments*. Fizmatlit, Moscow (2010)
4. Zubchaninov, V.G., Alekseev, A.A., Gultyaev, V.I.: About drawing of the yield sur-face for steel 45 and verification of the postulate of isotropy on straight-line paths during repeated sign-variable loadings. *PNRPU Mech. Bull.* **3**, 71–88 (2014)
5. Lenskii, V.S.: Experimental verification of the basic postulates from the general theory of elastic-plastic deformations. In: *Problems in Plasticity Theory [in Russian]*, Publishing house AN SSSR, Moscow (1961)
6. Andreev, L.S.: Verifying the isotropy postulate. *Sov. Appl. Mech.* **5**, 762–765 (1969)
7. Vasin, R.A., Nikitovich, A.N., Ogibalov, P.M.: Verification of the postulate of isotropy during variable-rate deformation. *Polym. Mech.* **11**(2), 192–194 (1975)
8. Shevchenko, Yu.N., Terekhov, R.G.: Studying the laws of the thermoviscoplastic deformation of a solid under nonisothermal complex loading. *Int. Appl. Mech.* **37**(3), 287–316 (2001)
9. Zubchaninov, V.G., Alekseev, A.A., Alekseeva, E.G., Gultiaev, V.I.: Experimental verification of postulate of isotropy and mathematical modeling of elastoplastic deformation processes following the complex angled nonanalytic trajectories. *Mater. Phys. Mech.* **32**(3), 298–304 (2017)
10. Zubchaninov, V.G., Alekseev, A.A., Alekseeva, E.G.: Verification of the postulate of the isotropy and numerical simulation of the deformation of materials on a complex smooth trajectories. *Mater. Phys. Mech.* **29**(2), 150–157 (2016)
11. Zubchaninov, V.G., Gultiaev, V.I.: On the verification of the postulate of isotropy in theory of complex plastic deformation processes. *Probl. Strength Plast.* **70**, 18–23 (2008)





# Design of Transformable Beam Systems

L. A. Panchenko<sup>(✉)</sup> 

Belgorod State Technological University named after V.G. Shukhov, Belgorod, Russia

**Abstract.** Rod types of transformed structures, in particular, beam systems, are considered. Calculation of the strength of transformable beam systems involves the study of the distribution of bending moments. In a stationary beam, they represent a function of two variables – the current coordinate and the position of the moving beam. Several characteristic variants of the movable beam arrangement are investigated and the envelope plots are constructed. The influence matrix, the diagram of bending moments on the plane of variable parameters and the envelope plot of moments are obtained. In the vicinity of the points with the largest positive and negative bending moments, approximating functions are identified (separately for each variable) in order to study the extremum. The design stages are traced on the composition of two beams. A stationary beam is assumed to be statically indeterminate. Variants of its reinforcement are proposed, including reinforcement with strips of composite materials reinforced with fibers.

**Keywords:** Transformable structures · Variational principles · Bending moments · Envelope plots

## 1 Introduction

The creation of structures that effectively fulfill their functional purpose within the specified requirements is subject to the variational principles of structural synthesis [1]. The configuration of a structure is determined by its topology, geometry, and element parameters.

Topology expresses the predestination of nodes (in discrete systems) or nodal lines (in continuum systems) and the way they are connected together to form a geometrically unchangeable structure.

Geometry, in addition to the specific position of nodes and nodal lines, provides for the shape of the lines connecting the nodes, the shape of the nodal lines and the surfaces between them.

Determining the parameters of the elements involves determining the dimensions of the cross-sections of the rods, the thickness of the plates and shells, etc. with known topology and geometry.

The idea of a rational configuration of structures was initially implemented in relation to trusses. It did not find widespread practical use, since it did not provide for the loss of stability of compressed rods. The solution of this kind of problem became possible after the formulation of variational principles of structural synthesis [2–4].

Practically acceptable works on optimization of structures from the point of view of their geometry began to appear from the middle of the XX century. The improvement of topology spontaneously appeared in the works of Russian engineers: D. I. Zhuravsky, L. D. Proskuryakov, V. G. Shukhov. The creation of a general theory of optimization of the topology of structures is hindered by innumerable solutions. At the same time, this does not contradict the optimal synthesis of individual types of the system.

The book of Majid [5] contains formulations and proofs of three theorems on structural changes. The application of these theorems to the optimization of the topology of hinge structures is given. A study of topological changes in rod systems is carried out in order to clarify the main factors affecting their functioning.

The class of systems with a changing topology consists of transformable structures. In some cases, this direction can be an alternative to reconstruction if the operating conditions of the structure change. The main factor in the kinematic shaping of construction objects is movement.

The static behavior of such objects distinguishes between rigid and flexible systems. Rigid kinematic systems are inherent in long-used objects. Their change depends on the seasonal and weather transformation. At the same time, moving parts of buildings or structural elements of such systems, unlike flexible ones, usually retain their original geometric shape.

Transformable structures have static (during operation) and dynamic (during transformation) properties. The transition from one state to another is made on the basis of a minimum number of geometric parameters, subject to the conditions of strength, rigidity and stability.

Beams, frames, and arches can be used as load-bearing movable structures. When moving in parallel during the transformation process, they move along parallel cables or rails.

According to the geometric parameters of structural elements and objects, rod (linear), plane and volume types of transformable systems are distinguished from them. In this paper, we consider the design of transformable beam systems.

## 2 Methods and Materials

To demonstrate the design procedure, a system of two interconnected beams – stationary and movable – was selected. Stationary beam – a beam that is statically indeterminate. A movable beam with a load applied to it has the ability to move along the entire length of the stationary beam.

Calculation of the strength of such a system involves the study of the distribution of bending moments in the first place. In a stationary beam, they are a function of two variables – the current coordinate and the position of the movable beam.

The direct solution of a statically indeterminate problem by the force method leads to extremely cumbersome calculations. As the degree of static indeterminability increases, automating the solution also becomes problematic.

Equally ineffective is the use of the theory of influence lines. In this case, we are dealing with the influence function, which implies a change in the bending moment in

a stationary beam, not only depending on the position of a single moving load and the design parameters, but also on the location of the determined value.

With the help of the corresponding influence matrix, it would be possible to express the dependence of the bending moment in several sections of a stationary beam on the system of forces at the points of support of the movable beam. However, obtaining a set of necessary influence lines for a statically indeterminate beam is very laborious. The complexity of the solution increases with increasing degree of static indeterminability.

The proposed method involves the consideration of several characteristic variants of the location of the movable beam and the construction of envelope plots of bending moments. The resulting influence matrix is the basis for constructing a diagram of bending moments on the plane. In the vicinity of the points with the largest positive and negative bending moments, approximating functions are identified (separately for each variable) in order to study the extremum.

### 3 Results and Discussions

The stages of designing transformable beam systems can be traced on the composition of two beams (Fig. 1).

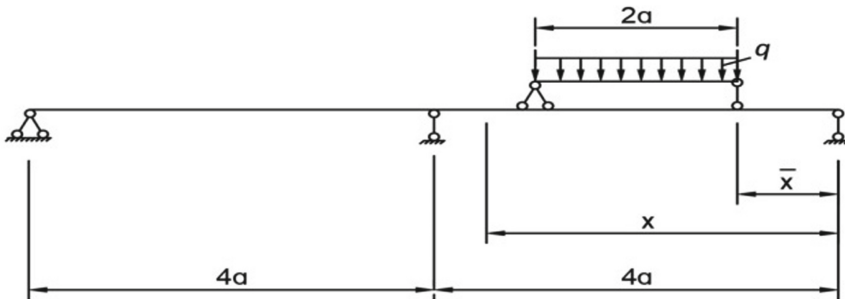


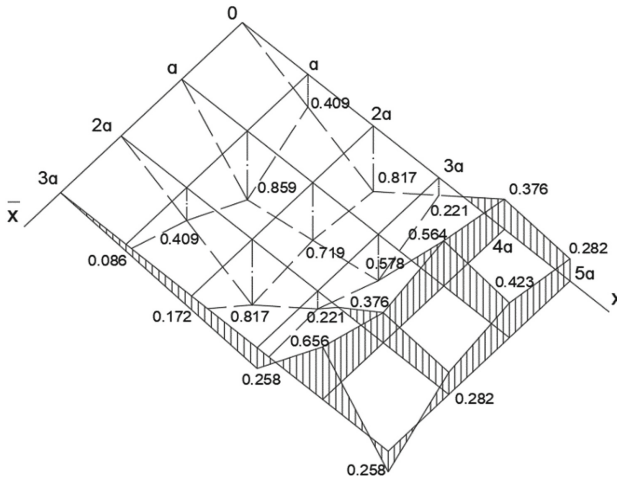
Fig. 1. Transformable beam system.

To form a matrix of bending moments in a stationary beam, shown in Table 1, 7 positions of a movable beam and 9 cross-sections of a continuous beam are selected. At the same time, 3 calculations were performed using the force method: 1) at  $\bar{x} = 0$  (results are acceptable at  $\bar{x} = 2a; 4a; 6a$ ); 2) at  $\bar{x} = a$  (results are acceptable at  $\bar{x} = 5a$ ); 3) at  $\bar{x} = 3a$ .

**Table 1.** Values of bending moments [ $qa^2$ ].

$\bar{x}$	$x$								
	0	$a$	$2a$	$3a$	$4a$	$5a$	$6a$	$7a$	$8a$
0	0	0.409	0.817	0.221	-0.375	-0.282	-0.188	-0.094	0
$a$	0	0.859	0.719	0.578	-0.564	-0.423	-0.282	-0.141	0
$2a$	0	0.409	0.817	0.221	-0.376	-0.282	-0.188	-0.094	0
$3a$	0	0.086	0.172	0.258	-0.656	0.258	0.172	0.086	0
$4a$	0	-0.094	-0.188	-0.282	-0.376	0.221	0.817	0.409	0
$5a$	0	-0.141	-0.282	-0.423	-0.564	0.578	0.719	0.859	0
$6a$	0	-0.094	-0.188	-0.282	-0.376	0.221	0.817	0.409	0

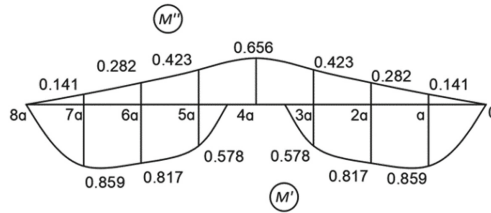
On the fragment of the diagram of bending moments  $M$  (Fig. 2), constructed on the basis of Table 1, only the largest modulo positive and negative values of moments are given, as well as their values in the vicinity of these points.



**Fig. 2.** Fragment of the diagram of bending moments in a stationary beam [ $qa^2$ ].

The values of extreme bending moments can be obtained by interpolating the variables  $x$  and  $\bar{x}$ . In this case, as follows from Table 1, the symmetry of the values in the vicinity of the largest modulo moments allows us to consider them extreme:  $M_{max} = 0.859qa^2$ ,  $M_{min} = -0.656qa^2$ .

Figure 3 shows the envelope plots, one of which gives the values of the greatest positive bending moments ( $M'$ ), for all cross – sections of the beam, and the other – the values of the greatest negative bending moments ( $M''$ ). These plots are used for rational selection of cross-sections with a homogeneous material.



**Fig. 3.** Envelope plots of bending moments  $[qa^2]$ .

In a concrete beam reinforced with steel rods, their diameters and lengths in the lower and upper regions are determined. As reinforcing elements, strips are also used, which are glued to the surface of the beam with epoxy adhesives [6–8].

An additional impetus to this method of reinforcing the structure is given by the use of composite materials, especially carbon fiber reinforced plastics. Having physical and mechanical properties close to the characteristics of steel, they have a great advantage over it in terms of resistance to various aggressive media [9–19].

## 4 Conclusion

The presented procedure for designing transformable beam systems is carried out in a linear formulation. It ends with the stage of determining internal forces, in particular bending moments. The selection of cross-sections as the final stage is specific in terms of the choice of materials. The presence of an envelope of moments allows you to use both a homogeneous material and a composite in the required volume in accordance with standards and specifications.

**Acknowledgements.** This work was realized in the framework of the Program of flagship university development on the base of the Belgorod State Technological University named after V. G. Shukhov, using equipment of High Technology Center at BSTU named after V. G. Shukhov.




## References

1. Yuriev, A.G.: Variational Principles of Construction Mechanics. Publishing House of Belgtasm, Belgorod (2002)
2. Yuriev, A.G., Naumov, A.E.: Topology optimization of deformed systems. European applied sciences: modern approaches in scientific researches. In: 2nd International Science Conference on Stuttgart, vol. 3, pp. 135–137 (2013)
3. Zinkova, V.A., Yuriev, A.G., Peshkova, E.V.: Designing of tube trusses without gusset plate with joint connections. *Int. J. Appl. Eng. Res.* **10**(5), 12391–12398 (2015)
4. Zinkova, V.A.: Optimization of the Structure of Flat Metal Tube Trusses. *Lecture Notes in Civil Engineering*, vol. 95, pp. 213–218 (2020)
5. Mazhid, K.I.: Optimal Design of Structures. High School, Moscow (1979)
6. Panchenko, L.A.: Effect of reinforcement of reinforced concrete beams with strips of polymers reinforced with fibers. *Izvestiya vuzov. Construction* **7–8**, 14–20 (2007)

7. Panchenko, L.A.: Reinforced concrete beams with strips of polymers reinforced with fibers. *Bull. BSTU Named After V. G. Shukhov* **3**, 20–22 (2008)
8. de Lorenzis, L., Miller, B., Nanni, A.: Bond of FRP laminates to concrete. *ACI Mater. J.* **98**(3), 256–264 (2001)
9. Panchenko, L.A.: *Building Structures with Fiber Composites*. Publishing House of V. G. Shukhov BSTU, Belgorod (2013)
10. Volkov, I.V., Gazin, E.M., Babekin, V.V.: Engineering methods of designing fiber-concrete structures. *Beton i zhelezobeton* **4**, 20–22 (2007)
11. Matthews, F., Rawlings, R.: *Composite materials. Mechanics and Technology*. Per. s engl. S. L. Bazhenova. Technosphere, Moscow (2004)
12. Rabinovich, F.N.: *Composites based on dispersed reinforced concrete. Questions of theory and design, technology, constructions*. Publishing House of the DIA, Москва (2004)
13. Khayutin, Yu.G., Chernyavsky, V.L., Axelrod, E.Z.: Application of carbon fiber plastics for strengthening building structures. *Beton i zhelezobeton* **1**, 25–29 (2003)
14. Grace, N.F., Abdel-Sayed, G., Ragheb, W.F.: Strengthening of concrete beams using innovative ductile fiber - reinforced polymer fabric. *ACI Struct. J.* **5**, 692–700 (2002)
15. Reda Taha, M.M., Shrive, N.G.: Enhancing fracture toughness of high-performance carbon fiber cement composites. *ACI Mater. J.* **2**, 168–178 (2001)
16. Yuriev, A.G., Panchenko, L.A., Naumov, A.E.: A variational statement of problem for the case of dispersely and discretely reinforced material. *Int. J. Pharm. Technol.* **8**(3), 15361–15369 (2016)
17. Nelyubova, V.V., Babayev, V.B., Alfimova, N.I., Usikov, S.A., Masanin, O.O.: Improving the efficiency of fibre concrete production. *Constr. Mater. Prod.* **2**(2), 4–9 (2019)
18. Panchenko, L.A.: *Concrete and Fiber-Reinforced Concrete in a Cage Made of Polymers Reinforced with Fibers*. *Lecture Notes in Civil Engineering*, vol. 95, pp. 131–136 (2020)
19. Karpikov, E.G., Lukutsova, N.P., Soboleva, G.N., Golovin, S.N., Cherenkova, Y.S.: Effect of microfillers based on natural wollastonite on the properties of fine-grained concrete. *Constr. Mater. Prod.* **2**(6), 20–28 (2019)



# Advanced Building Materials Based on Zeolite-Containing Raw Materials of Yakutia

A. E. Mestnikov  and A. L. Popov  

Ammosov North-Eastern Federal University (NEFU), Yakutsk, Russia

**Abstract.** The article presents the results of the research department “Production of building materials, products and structures” NEFU. The main task was the rational use of zeolite-containing raw materials from the Khonguruu deposit (Yakutia) in the production of effective building materials. The specified deposit is the source of the most common clinoptilolite type zeolites with an admixture of heulandite. The studies were carried out according to the priority scheme of the main building materials for the conditions of hard-to-reach regions of the Arctic and the North: binder (Portland cement with a mineral additive) – heat-insulating material (granular foamed zeolite) – lightweight concrete (foamed zeolite concrete) for mobile construction technologies. Thus, the possibility and efficiency of using zeolite in these types of building materials has been substantiated. At the same time, savings of 30–40% of Portland cement clinker, a decrease in material consumption and construction costs can be achieved. The developed materials and technologies based on zeolite-containing raw materials Khonguruu are intended to ensure the construction of buildings and structures on the principle of a full cycle of construction of energy-efficient buildings, taking into account the conditions for locating production in hard-to-reach regions of the Arctic and the North (from the production of building materials to construction).

**Keywords:** Zeolite-Containing rock · Fast-Hardening cement · Composite gypsum binder · Foamed zeolite · Lightweight and cellular concrete · Mobile technologies · Energy efficiency

## 1 Introduction

Possibilities of using the unique properties of natural zeolites of Siberia, incl. the Khonguruu deposits (Yakutia), in the production of various building materials were actively studied at the Altai State Technical University named after I.I. Polzunov, Institute of Geology and Geophysics SB RAS, Perm National Research Polytechnic University, Yakutnipromalmaz and YakutPNIIS [1–4].

As is known from world experience [5–9], the high pozzolanic activity of natural zeolites makes it possible to create new varieties of cementless and cement systems of binders by the method of mechano-chemical activation and a wide class of concretes based on them. Zeolite additives are successfully used in the manufacture of autoclaved aerated concretes and silicate bricks. Firing technologies make it possible to obtain

highly porous aggregates and products, ceramic materials, Portland cement clinker with an aluminosilicate component from zeolite [10–16].

The field of zeolite-containing rocks of Khonguruu in Yakutia has predicted resources of 35 billion tons. The enterprise for the extraction and enrichment of natural zeolite – LLC “Suntarzeolite” produces products in the form of zeolite flour up to 3 mm, crushed stone fractions of 3–10 mm and 10–20 mm.

The main task was the scientific substantiation of the main directions of development of the production of effective building materials based on the rational use of zeolite-containing raw materials from the Khonguruu deposit, preferably for remote areas of the Arctic and subarctic regions of North-East Russia.

## 2 Methods and Materials

The studies were carried out according to the priority scheme of the main building materials for the conditions of hard-to-reach regions of the Arctic and the North: binder (Portland cement with a mineral additive) – heat-insulating material (granular foamed zeolite) – lightweight concrete (foamed zeolite concrete) for mobile construction technologies.

As is known [1], the pozzolanic activity of zeolites depends on the content of the zeolite component in the rock, their porous structure and, accordingly, the genetic type, mineralogical and chemical compositions, and siliceous content ( $\text{SiO}_2/\text{Al}_2\text{O}_3$  ratio). According to the mineralogical composition and X-ray diffraction pattern, it was established that the raw material is pure, since it contains a small amount of clay impurities, mica and sand, belongs to the clinoptilolite type of mineral raw materials and has pozzolanic activity. Clinoptilolite content is 70% by weight, heulandite – 30% by weight. [16].

In terms of chemical composition, the studied zeolite-containing raw materials from the Khonguruu deposit (hereinafter referred to as zeolite) have a high content of silicon oxide. The studied zeolites have the following chemical composition depending on the location and depth of sampling, wt%:  $\text{SiO}_2$  – 5.2–73.8;  $\text{Al}_2\text{O}_3$  – 12.2–13.2;  $\text{Fe}_2\text{O}_3$  – 0.9–1.1;  $\text{CaO}$  – 2.2–2.7;  $\text{MgO}$  – 1.9–2.2;  $\text{Na}_2\text{O}$  – 5.2–6.2;  $\text{TiO}_2$  – 0.1–0.2.

The mineralogical composition of Portland cement clinker of JSC PA Yakutcement is as follows, % by weight:  $\text{C}_3\text{S}$  – 62–65;  $\text{C}_2\text{S}$  – 10–13;  $\text{C}_3\text{A}$  – 6–7 и  $\text{C}_4\text{AF}$  – 10–13. Clinker chemical composition, % by weight:  $\text{CaO}$  – 66.0;  $\text{SiO}_2$  – 19.0;  $\text{Fe}_2\text{O}_3$  – 3.9;  $\text{Al}_2\text{O}_3$  – 3.7;  $\text{MgO}$  – 2.6;  $\text{K}_2\text{O}$  – 1.4;  $\text{Na}_2\text{O}$  – 1.2;  $\text{SO}_3$  – 0.7.

As a clinker setting regulator, a gypsum stone of the Olekminsky deposit (hereinafter, gypsum) was used, containing  $\text{CaSO}_4 \bullet 2\text{H}_2\text{O}$  in an amount of 80.80 wt%.

Scientific research was carried out in the laboratory of building materials of the Engineering and Technical Institute of NEFU using modern equipment and instruments of the Arctic Innovation Center of NEFU and FRC The Yakut Scientific Centre SB RAS in Yakutsk.

## 3 Results and Discussion

For hard-to-reach regions of the Arctic and North, in [17], we substantiated the expediency of organizing the production of high-quality cement using an environmentally



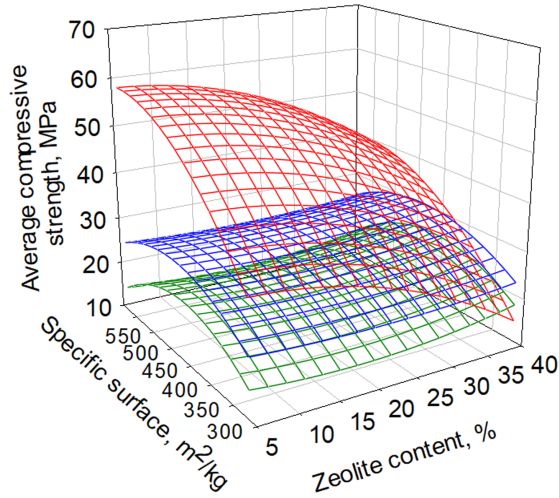
friendly (without CO<sub>2</sub> emission into the atmosphere) method of joint grinding of Portland cement clinker and local natural mineral raw materials. The most suitable for this purpose is mineral raw materials containing amorphous modifications of silica, vitreous silica or silica in compounds (silicates, aluminosilicates, hydrosilicates, etc.). For the conditions of Yakutia, these include the above-described zeolite-containing raw materials and quartz-feldspar sands found in the floodplains of numerous rivers, mainly flowing into the Arctic Ocean (Lena, Kolyma, Indigirka, Yana, Anabar and Olenek). The area of the Lena basin alone is 2490 thousand km<sup>2</sup>.

To determine a rationally substantiated cement composition, preliminary compositions were selected taking into account technological recommendations and matrix planning with varying zeolite content and total specific surface area. For the selected compositions, the compressive strengths were determined on the 2nd, 7th, and 28th days (Table 1).

**Table 1.** Characteristics of cement compositions.

Binder composition, % wt.		Specific surface, m <sup>2</sup> /kg	Average compressive strength, MPa		
Clinker	Zeolite		2 days	7 days	28 days
100	–	345	18.2	25.6	43.1
95	5	315	16.0	23.2	35.5
95	5	365	19.5	25.0	39.0
95	5	415	22.0	28.9	48.2
90	10	315	15.3	22.8	33.6
90	10	365	18.2	23.9	37.7
90	10	415	21.2	28.0	47.2
85	15	315	15.0	21.5	32.1
85	15	365	17.5	22.8	36.2
85	15	415	20.5	27.8	45.6
80	20	425	21.2	28.1	44.2
70	<b>30</b>	518	21.7	30.5	48.5
60	40	623	17.1	25.3	38.7

Based on these data, regression equations were obtained for the dependence of the average strength at the age of 2, 7, and 28 days on the content of zeolite and the total specific surface area of the cement composition, and nomograms were constructed (Fig. 1).



**Fig. 1.** Nomograms of the dependence of the average strength of the cement composition on the content of zeolite and the total specific surface: at the age of 2 days – green, 7 days – blue, and 28 days – red. (Color figure online)

Average compressive strength for 2 days, MPa

$$f(x_1, x_2) = -38.5206 - 0.0481 \times x_1 + 0.2581 \times x_2 \\ + 0.0116 \times x_1^2 - 0.0008 \times x_1 \times x_2 - 0.0003 \times x_2^2$$

Average compressive strength for 7 days, MPa

$$f(x_1, x_2) = -27.0176 + 0.0729 \times x_1 + 0.2239 \times x_2 \\ + 0.0087 \times x_1^2 - 0.0009 \times x_1 \times x_2 - 0.0002 \times x_2^2$$

Average compressive strength for 28 days, MPa

$$f(x_1, x_2) = -40.8934 + 0.6608 \times x_1 + 0.2904 \times x_2 \\ - 0.0023 \times x_1^2 - 0.0022 \times x_1 \times x_2 - 0.0002 \times x_2^2$$

It was found that the compressive strength of the obtained cement compositions with the addition of zeolite up to 20% wt. is at least 42.5 MPa with a specific surface area of the initial mixture in the range of 415–425 m<sup>2</sup>/kg, which meets the requirements of the cement grade – CEM II/A-P 42.5 N brand (GOST 31108-2016). The same compressive strength of the cement composition with the addition of zeolite 30% wt. is observed when the specific surface area reaches 518 m<sup>2</sup>/kg of dry mixture. In a cement composition with a 40% addition of zeolite, the strength of the control samples is 38.7 MPa with a specific surface of 623 m<sup>2</sup>/kg of dry mixture. Thus, the economically justified fineness of grinding of the obtained cement composition is 415–425 m<sup>2</sup>/kg, which corresponds to world standards (350–450 m<sup>2</sup>/kg) [18].

In practice, the technology for the production of a cement composition will include the following processes: preliminary crushing of clinker, zeolite and gypsum stone in a press-roll crusher, homogenization of the resulting mixture in a mixer, followed by its mechanochemical activation in a three-chamber ball mill to a specific surface area of 350–450 m<sup>2</sup>/kg, if necessary, with the introduction of polymer modifier. Such a technological scheme is adopted, for example, in the manufacture of nanocement with a specific surface area of up to 300–900 m<sup>2</sup>/kg [18].

The production of artificial porous aggregates provides an increase in the efficiency of concretes for various purposes – from the lightest heat-insulating ones to high-strength structural ones. Today, for energy-efficient construction, one of the most popular thermal insulation materials used as a light aggregate for concrete can be granulated foam glass. Analysis of scientific and technical advances in the field of foam glass production technology shows a significant increase in the use of various raw materials for the selection of the initial composition of the charge. It is proposed to use both technogenic (cullet, silicon-containing industrial waste, etc.) and available mineral raw materials from siliceous rocks (flask, tripoli, diatomite, zeolite, etc.) [2, 10, 11].

The compositions of a pilot batch of granulated foamed zeolite based on zeolite-containing raw materials Khongururu were developed and tested in the experimental-production base of Modis LLC (PJSC Energosystema group of companies, Rybinsk). The technology for the production of granular foamed zeolite is based on the scheme for the production of granulated foam glass from glass waste. The production consists of 3 sections: preparation of raw materials, granulation, foaming, fractionation and packaging of products. The foamed glass production line is completely designed and manufactured in-house. The uniqueness and reliability of the technological equipment allowed the team to achieve high quality products. In addition to serial traditional products from glass waste, at the operating production facility, production compositions from other types of natural mineral raw materials, including flasks, tripoli, diatomite, zeolite, etc. are being tested.

In the preparation of the initial charge, finely ground zeolite, soda ash and water glass are used. The physical and mechanical characteristics of the pilot batch of products meet the requirements of TU 5914-001-15068529-2006 “Universal porous thermal insulation material UPM “Termoizol” (Table 2).

**Table 2.** Characteristics of a pilot batch of granular foamed zeolite.

Fraction, mm	Bulk density, kg/m <sup>3</sup>	Average compressive strength, MPa	Thermal conductivity in the backfill, W/(m·°C), not more	Resistance against silicate decomposition, %, not more
5–10	150 ± 50	0.5	0.06	3
1–5	250 ± 50	0.7	0.075	
0.5–1	350 ± 50	1.0	0.10	

Were investigated the physical and mechanical properties of granular foamed zeolite from a pilot batch and lightweight concretes based on it – zeolite foam concrete (Tables 3, 4).

**Table 3.** Physical and mechanical properties of a pilot batch of granular foamed zeolite.

Parameter	Unit	Value
Bulk density	kg/m <sup>3</sup>	138.68
Average density of grains	kg/m <sup>3</sup>	317.11
Splitting strength MPa	MPa	0.88
Water absorption by weight	%	13.16
Total porosity	%	87.27

**Table 4.** Characteristics of zeolite foam concrete.

Average density of concrete, kg/m <sup>3</sup>	Average density grade according to GOST 25820-2014	Average compressive strength, MPa	Concrete class according to compressive strength according to GOST 25820-2014
446	D400	1.47	B1
536	D500	2.81	B2
621	D600	3.27	B2.5

The analysis of the results of the study showed a high strength of the granular foamed zeolite upon splitting. The average splitting strength was 0.88 MPa out of 6 samples. The relatively high splitting strength is presumably associated with the features of the morphology and distribution of pores. Smaller pores of granular foamed zeolite are concentrated on the surface layers of the grain, while large pores are located in the core region. It follows from this that small pores create a kind of “outer cage” effect, which makes it possible to significantly increase the mechanical strength of the aggregate.

Comparison of the characteristics of granular foamed zeolite and expanded clay granules shows that with the same compressive strength in the cylinder 1.44–1.46 MPa, they have grades according to the bulk density M200 and M400, respectively, i.e. granular foamed zeolite are 2 times lighter than expanded clay.

Table 3 shows that on the basis of granular foamed zeolite there is the possibility of producing especially lightweight concrete D400–D600 with strength characteristics characteristic of autoclaved aerated concrete. Monolithic lightweight concrete, blocks and panels, 3D printing from foamed zeolite concrete D500 and D600 may be especially in demand for low-rise construction of buildings and structures with high architectural expressiveness.

## 4 Conclusion

The developed materials and technologies based on zeolite-containing raw materials Khonguruu are intended to provide a full cycle of construction of energy-efficient buildings in remote areas of Yakutia (from the production of building materials to construction).

The developed construction principle in hard-to-reach areas of the Arctic and the North, taking into account the conditions for the location of production, suggests:

- exploration, extraction and research of mineral raw materials suitable for the production of priority building materials;
- scientific and technical support for each stage of the organization of construction production;
- organization of production of high-quality Portland cement with mineral additives;
- organization of production of effective heat-insulating material (in this case, granular foamed zeolite) from local raw materials;
- organization of production of building materials from lightweight concrete based on porous aggregates for rapidly deployed construction technologies (monolithic frame construction, 3D construction, gunning concreting, block and panel construction, etc.).





## References

1. Ovcharenko, G.I., Sviridov, V.L., Kazanceva, L.K.: Zeolites in building materials: monograph. AltSTU Publishing House **320** (2000)
2. Ketov, A.A., Konev, A.V., Puzanov, A.V., Saulin, D.V.: Trends in the development of foam glass technology. *Constr. Mater.* **9**, 28–31 (2007)
3. Montyanova, A.N., Kirillov, D.S., Shtaub, I.V., Bil'dushkinov, E.V.: Specific features of stowing operations at the mir mine of the ALROSA diamond mining company. *Vestnik MGТУ im. G.I. Nosova* **4**, 10–14 (2012)
4. Matveeva, O.I., Sokolova, E.Y., Fedorova, G.D., Zyryanov, I.V.: Development of the cement slurry composition for plugging the anchorage space of mine shafts in permafrost zones. *Gornyj Zhurnal* **1**, 82–86 (2016)
5. Kajs, H.A., Gulyakov, E.G., Morozova, N.N.: Natural zeolites from different countries in cement concretes. *Resursoenergoeffektivnyye tekhnologii v stroitel'nom komplekse regiona* **11**, 235–239 (2019)
6. Perraki, T., Kontori, E., Tsvivilis, S., Kakali, G.: The effect of zeolite on the properties and hydration of blended cements. *Cem. Concr. Res.* **32**, 128–133 (2010)
7. Banerjee, R., Phan, A., Knobler, C., Keeffe, M., Omar, M., Yaghi, M.: High – throughput synthesis of zeolitic imidazolate frameworks and application to CO<sub>2</sub> capture. *Science* **319**, 939–943 (2008)
8. Ahverdieva, T.A., Jafarov, R.: Modern technologies in the production of hydrotechnical concrete. *Constr. Mater.* **3**, 76 (2020)
9. Bohá, M., Kubátová, D., Neasa, R., Zezulová, A., Masárová, A., Novotnýb, R.: Properties of cement pastes with zeolite during early stage of hydration. *Proc. Eng.* **151**, 2–9 (2016)
10. Kaz'mina, O.V., Vereshchagin, V.I., Semukhin, B.S., Abiyaka, A.N.: Low-temperature synthesis of granulated batches for foam glass materials based on siliceous components. *Steklo i keramika* **10**, 5–8 (2009)

11. Konovalova, N.A., Nepomnyashchih, E.V., Dabizha, O.N.: Influence of clinoptilolite amorphization on the intensity of foaming of compositions for the production of foam glass. *Vestnik VSGUTU* **4**, 71–76 (2017)
12. Musaeva, A., Bekmurat, S.Z., Akmalayev, K.A.: Influence of natural zeolites on the properties of bricks. *Materialovedenie* **2**, 94–97 (2019)
13. Kordzahiya, T.N., Skhvitardze, R., Cinckaladze, G.P.: Scientific basis and practice of using zeolite in cement production. *Int. Sci. Pract. Conf. World Sci.* **10**, 15–19 (2017)
14. Lesovik, V.S., Leshchev, S.I., Ageeva, M.S., Alfimova, N.I.: Zeolite-containing terra-silicea as a component of composite binders. *Mater. Sci. Forum* **974**, 136–141 (2020)
15. Sivalneva, M.N., Strokova, V.V., Kobzev, V.A.: Properties of foam concrete based on highly concentrated aluminosilicate binder suspension. *IOP Conf. Ser.: Mater. Sci. Eng.* **905**, (2020)
16. Rozhin, V.N.: Portland cement foam concrete with a zeolite-containing mineral additive. *IOP Conf. Ser.: Mater. Sci. Eng.* **945**, (2020)
17. Mestnikov, A.E., Kudyakov, A.I., Rozhin, V.N.: Portland cement with natural active additives. *Vestnik Tomskogo gosudarstvennogo arhitekturno-stroitel'nogo universiteta* **21**, 192–201 (2019)
18. Bukreev, A.N., Bikbau, M.Y.: Optimal technological schemes for the production of nanocements. *Suhie stroitel'nye smesi* **3**, 17–26 (2019)



# Radiation-Protective Properties of a Structural Polyimide Composite

R. N. Yastrebinsky<sup>(✉)</sup> , A. A. Karnauhov , E. O. Pilavidou ,  
and A. V. Yastrebinskaya 

Belgorod State Technological University named after V.G. Shukhov, Belgorod, Russia

**Abstract.** Calculations of neutron and gamma fields in a polyimide composite with varying boron content in it to reduce the capture radiation have been performed. The introduction of boron into the composition as an additive, which has a large neutron absorption cross section in the thermal and epithermal spectral regions, is one of the ways to improve the protective characteristics of the material. The dependences of the spatial distributions of the flux densities of thermal and fast ( $E > 2$  MeV) neutrons and the dose rates of neutrons and gamma quanta in a 1 m thick polyimide layer with a boron content of 0 to 5% are obtained. To assess the intrinsic capture gamma radiation from polyimide and the effect of the spectrum of incident neutrons, calculations were carried out for two types of compositions: either lead (first type) or steel (second type) was installed in front of the polyimide composite. The presence of boron in polyimide does not affect the formation of the neutron spectrum in the fast region and, accordingly, the relaxation length of the fast neutron flux density. As the thickness of the calculated polyimide layer increases,  $\lambda_{fn}$  increases due to the hardening of the neutron spectrum. It is shown that the optimal boron content in the composite polyimide material should be 2–3% by weight.

**Keywords:** Polyimide composite · Boron additive · Neutron radiation · Gamma radiation · Radiation protection

## 1 Introduction

In the biological protection of nuclear reactors, materials based on polymers and, first of all, polyethylene have found wide application. Due to its high hydrogen content, it effectively attenuates neutron radiation. However, it has a relatively low operating temperature (60–80 °C) [1–4]. The search and implementation of polymeric materials with higher thermal and radiation resistance is of great practical importance for new developments (projects) of nuclear power plants (NPP).

This work is devoted to the study of the protective properties of one of these materials, namely, polyimide. Polyimide has a significantly higher heat resistance and strength than polyethylene. Unlike the latter, it can be operated for a long time at temperatures up to 400 °C. Polyimide is more resistant to water, its water absorption and vapor permeability is lower than that of polyethylene. At the same time, it is more difficult to process, its production was established much later than polyethylene [5–8].

In order to assess the applicability of polyimide as a protection material, calculations of neutron and gamma fields in a polyimide composite with varying boron content were carried out. The introduction of boron into the composition as an additive, which has a large neutron absorption cross section in the thermal and epithermal spectral regions, is one of the ways to improve the protective characteristics of the material [9, 10].

## 2 Methods and Materials

A thermoplastic polyimide in the form of a powder with a particle size of  $\sim 4 \mu\text{m}$  was considered as a starting material. The composite material was pressed on a PSU-50 hydraulic press at a specific pressure of 200 MPa. The amount of additive in the form of natural boron was: 0.5; 1; 2; 3; 4 and 5% of the mass.

Table 1 shows the chemical compositions of pure polyimide and with boron additives (wt%) used in the calculations.

**Table 1.** Chemical composition of polyimide with boron additives.

Material	Density, g/cm <sup>3</sup>	Nuclear concentration of elements, 1/cm <sup>3</sup>			
		H	B <sub>10</sub>	B <sub>11</sub>	C
Polyimide (PI)	0.912	7.744E-02	0	0	3.872E-02
PI + 0.5% B <sub>10</sub> , B <sub>11</sub>	0.918	7.729 E-02	4.731E-05	2.039E-04	3.864E-02
PI + 1.0% B <sub>10</sub> , B <sub>11</sub>	0.922	7.713E-02	9.491E-05	4.091E-04	3.857E-02
PI + 2.0% B <sub>10</sub> , B <sub>11</sub>	0.927	7.683E-02	1.910E-04	8.233E-04	3.841E-02
PI + 3.0% B <sub>10</sub> , B <sub>11</sub>	0.932	7.651E-02	2.883E-04	1.243E-03	3.826E-02
PI + 4.0% B <sub>10</sub> , B <sub>11</sub>	0.936	7.620E-02	3.868E-04	1.667E-03	3.810E-02
PI + 5.0% B <sub>10</sub> , B <sub>11</sub>	0.941	7.588E-02	4.865E-04	2.097E-03	3.794E-02

When calculating the density of mixtures of polyimide with boron, it was assumed that these components are mixed mechanically. The bulk density of boron was taken to be 2.3 g/cm<sup>3</sup>.

To carry out variant calculations and obtain the spatial-energy distributions of neutron and gamma-ray fluxes in the considered shielding materials, a composition was used, consisting of the reactor core, reflector, structural material and a layer of the investigated material 1.5 m thick. The calculations were carried out using the ANISN program, realizing the solution of the one-dimensional transport equation by the method of discrete ordinates taking into account the scattering anisotropy. The neutron spectrum was calculated for a 12-group division of the energy range. The spectrum of gamma quanta had a 6-group partition. The geometry of the computational problem is flat [11–17].

A feature of calculations for this problem is the need to select from all potential generators of gamma radiation (core and materials of the protective composition) that affect the flux of gamma quanta in the test material, only its own source of capture gamma radiation, excluding or minimizing the leakage of gamma-quanta from other



layers of materials and from the core. For this purpose, a series of calculations were carried out for two compositions. In the first, a layer of lead shielding was placed in front of the test material in order to maximally attenuate gamma radiation from the core, in-reactor structures and the reactor vessel. In the second case, the lead layer was absent, the material under study was located after the steel reactor vessel in order to establish the effect of the leakage of gamma quanta from the core and from metal structures. For an adequate comparison of the calculation results, the data obtained in each series were normalized to the value of the flux density of fast neutrons at the front boundary of the layer for the version of polyimide without boron and were then presented in relative units.

As the main characteristics of radiation protection (in this problem with a variation of the boron content in polyimide) during the passage of radiation through the materials under study, the following were estimated:

- weakening of the flux density of fast neutrons ( $E > 2 \text{ MeV}$ );
- weakening of the thermal neutron flux density;
- attenuation of the dose rate of neutron radiation;
- attenuation of the dose rate of gamma radiation.

### 3 Results and Discussion

Distributions of the functionals of neutron and gamma radiation over a polypropylene layer thickness of 100 cm are obtained for two versions of compositions (with and without lead) with different boron contents in polyimide. On the basis of the obtained neutron and gamma fields, the relaxation lengths for the flux density of fast neutrons and the dose rate of gamma quanta in polyimide with different boron contents were calculated. The calculation results are presented in Tables 2 and 3.

**Table 2.** Relaxation lengths of the fast neutron flux density ( $\lambda_{fn}$ , cm) in the test material depending on the thickness of its layer (h, cm).

Study material	$\lambda_{fn}$ (h) behind a layer of lead			$\lambda_{fn}$ (h) behind a layer of steel		
	h = 0–30	h = 30–60	h = 60–100	h = 0–30	h = 30–60	h = 60–100
PI + (0–5)% B <sub>10</sub> , B <sub>11</sub>	5.5	8.0	8.0	5.4	7.5	8.5

Analyzing the data obtained, the following can be noted.

The presence of boron in polyimide does not affect the formation of the neutron spectrum in the fast region and, accordingly, the relaxation length of the fast neutron flux density. As the thickness of the calculated polyimide layer increases,  $\lambda_{fn}$  increases due to the hardening of the neutron spectrum. Somewhat smaller values of  $\lambda_{fn}$  for compositions with steel can be explained by the fact that after steel a softer spectrum for neutrons is formed in the energy range above 2 MeV compared to the spectrum after

**Table 3.** The relaxation lengths of the dose rate of gamma quanta ( $\lambda_g$ , cm) in the test material, depending on the thickness of its layer (h, cm).

Study material	$\lambda_{fn}$ (h) behind a layer of lead			$\lambda_{fn}$ (h) behind a layer of steel		
	h = 0–30	h = 30–60	h = 60–100	h = 0–30	h = 30–60	h = 60–100
Polyimide (PI)	20.1	25.0	29.9	23.4	28.3	33.4
PI + 0.5% B <sub>10</sub> , B <sub>11</sub>	17.9	27.5	32.4	24.9	32.3	35.7
PI + 1.0% B <sub>10</sub> , B <sub>11</sub>	17.5	28.3	33.4	25.9	33.0	36.1
PI + 2.0% B <sub>10</sub> , B <sub>11</sub>	17.0	29.3	34.4	26.9	33.5	36.2
PI + 3.0% B <sub>10</sub> , B <sub>11</sub>	16.7	29.8	35.0	27.3	33.7	36.2
PI + 4.0% B <sub>10</sub> , B <sub>11</sub>	16.4	30.2	35.3	27.5	33.7	36.2
PI + 5.0% B <sub>10</sub> , B <sub>11</sub>	16.2	30.4	35.5	27.6	33.7	36.1

lead; therefore, the group cross section for the extraction of fast neutrons will be larger, and the relaxation length, respectively, will be less.

As for gamma quanta, the value of  $\lambda_g$  increases with an increase in the boron content in polyimide due to a hardening of the neutron spectrum in the thermal and epithermal regions, but at the same time, the absolute value of the thermal neutron flux density decreases with an increase in the boron content. As a result, the total effect gives a noticeable decrease in the dose rate of gamma quanta behind the protection from polyimide with boron (0.5–5.0%) compared to that for polyimide without boron (in compositions with lead - 4.8–15.5 times for a polyimide layer with a thickness 30 cm and 3.9–10.2 times for a polyimide layer 60–100 cm thick; in compositions with steel - 2.1–2.9 times for a polyimide layer 30 cm thick and 1.7–2.3 times for a layer polyimide thickness 60–100 cm). A slight decrease in the rate of attenuation of the dose rate of gamma quanta with an increase in the thickness of the polyimide layer is a consequence of an increase in  $\lambda_g$  with the thickness of the test material at any boron content in it. The value of  $\lambda_g$  in polyimide with a change in the boron content in it from 0 to 5% increases by ~15–20%; for a polyimide composite thickness from 30 to 100 cm, the  $\lambda_g$  value increases: for compositions with lead by ~2 times, for compositions with steel - 1.5 times.

The effect of reducing the total intensity of gamma rays, depending on the content of boron in the polyimide in compositions with steel, is less than in compositions with lead. This is because in the first case, from the side of the steel structure onto the polyimide layer, there is a significant leakage of gamma quanta, the attenuation of which is not affected by the addition of boron and which prevail over the intrinsic capture gamma quanta in the polyimide.

Separately, it should be said about the nature of the attenuation of the dose rate of gamma quanta in compositions with lead at the first 30 cm of protection from polyimide. Here, on the contrary, a decrease in  $\lambda_g$  is observed with an increase in the boron addition. The fact is that from the lead side there is a significant leakage of epithermal and thermal neutrons. At a thickness of ~30 cm, their sharp weakening occurs, and the greater, the higher the boron content. With a further increase in the thickness of the polyimide composite, thermal neutrons begin to reach equilibrium with fast ones, and the effect of thermal neutron leakage from the lead side ceases.

In general, the analysis of the data presented shows that an increase in the boron content in polyimide by more than 3% does not lead to a significant decrease in the capture radiation in the material.

## 4 Conclusion

Calculations have been made to determine the protective characteristics of polyimide, including when boron is added to its composition to reduce the capture radiation. The dependences of the spatial distributions of the flux densities of thermal and fast ( $E > 2$  MeV) neutrons and the dose rates of neutrons and gamma quanta in a 1 m thick polyimide layer with a boron content of 0 to 5% are obtained. To assess the intrinsic capture gamma radiation from polyimide and the effect of the incident neutron spectrum, the calculations were carried out for two types of compositions: either lead (first type) or steel (second type) was installed in front of the polyimide composite.

It is shown that the optimal boron content in the composite polyimide material should be 2–3% by weight.

Thus, polyimide, with its higher thermal stability, can be used in new developments instead of polyethylene.

**Acknowledgements.** The work was supported by a project of the Russian Science Foundation (№19-19-00316), using equipment of High Technology Center at BSTU named after V. G. Shukhov.

## References

1. Pavlenko, V.I., Cherkashina, N.I., Yastrebinsky, R.N.: Synthesis and radiation shielding properties of polyimide/Bi<sub>2</sub>O<sub>3</sub> composites. *Heliyon* **5**(5), E01703 (2019)
2. Cherkashina, N.I., Pavlenko, V.I., Noskov, A.V.: Radiation shielding properties of polyimide composite materials. *Radiat. Phys. Chem.* **159**, 111–117 (2019)
3. Cherkashina, N.I., Pavlenko, A.V.: Modification of optical characteristics of a polymer composite material under irradiation. *Tech. Phys.* **63**, 571–575 (2018)
4. Pavlenko, A.V., Yastrebinski, R.N., Pavlenko, Z.V., Yastrebinskaya, A.V., Cherkashina, N.I.: Nanodisperse metalloorganosiloxane fillers of polymers. *Nanotechnol. Constr. Sci. Internet J.* **8**(4), 113–130 (2016)
5. Xie, S., Zhang, Z., Wei, W.: Synthesis and properties of polyimide-based optical materials. *Korean Phys. Soc.* **51**, 1536–1541 (2007)

6. Cherkashina, N.I., Pavlenko, A.V.: Influence of SiO<sub>2</sub> crystal structure on the thermal cycle of polymer composites. *Constr. Mater. Prod.* **1**(4), 21–29 (2018)
7. Bloom, P.D., Baikerikar, K.G., Otaigbe, J.U., Sheares, V.V.: Development of novel polymer/quasicrystal composite materials. *Mater. Sci. Eng. A Struct.* **294–296**, 156–159 (2000)
8. Sorokin, V.V., Sharapov, O.N., Shunkin, N.M., Kiryushina, N.Y.: New polymeric composites based on epoxy resin with techogenic wastes. *Bull. BSTU named after V.G. Shukhov* **6**, 8–13 (2019)
9. Pavlenko, A.V., Cherkashina, N.I., Yastrebinskii, R.N.: Nanodisperse metalloorganosiloxane fillers of polymers. *Nanotechnol. Constr. Sci. Internet J.* **8**(4), 113–130 (2016)
10. Pavlenko, A.V., Cherkashina, N.I., Noskov, A.V.: Calculation of the frequency electronic transmission factors at the passage through the polymeric polyimide composite material filled by bismuth silicate. *Probl. At. Sci. Technol.* **5**, 21–26 (2017)
11. Cherkashina, N.I., Pavlenko, V.I., Yastrebinskii, R.N.: Phase transitions and electrophysical properties of Tungsten(VI) oxide in a 83–673 K temperature range. *Russ. Phys. J.* **62**(5), 870–875 (2019)
12. Pavlenko, V.I., Edamenko, O.D., Cherkashina, N.I., Kuprieva, O.V., Noskov, A.V.: Study of the attenuation coefficients of photon and neutron beams passing through titanium hydride. *J. Surf. Invest.-X-ray* **9**, 546–549 (2015)
13. Pavlenko, A.V., Cherkashina, N.I., Yastrebinski, R.N.: Nanodisperse metalloorganosiloxane fillers of polymers. *Nanotechnol. Constr. Sci. Internet J.* **8**(4), 113–130 (2016)
14. Yastrebinsky, R.N., Karnauhov, A.A., Yastrebinskaya, A.V.: Improving the radiation-thermal stability of titanium hydride. *J. Phys: Conf. Ser.* **1515**, 022002 (2020)
15. Slyusar, O.A., Cherkashina, N.I., Yastrebinskaya, A.V.: Effect of additives on dispersed system structure formation. *Refract. Ind. Ceram.* **55**(6), 562–564 (2015)
16. Shestakov, I.Y., Veretnova, T.A., Strekalova, T.A.: Investigation of water electrical activator with coaxial arrangement of electrodes. *Chem. Bull.* **4**(1), 12–18 (2018)
17. Arbuzova, A.A., Votyakov, M.A.: Estimation of the influence of the state of the reinforcing polymer in the structure of polymeric fiber material using mathematical prediction methods. *Chem. Bull.* **1**(1), 12–17 (2018)



# Zoning the Urban Area on the Basis of the Principles and Methods of GIS-Mapping

N. V. Shirina<sup>(✉)</sup>  and E. A. Parfenyukova 

Belgorod State Technological University named after V.G. Shukhov, Belgorod, Russia

**Abstract.** Zoning serves as a tool for analysis, control and forecasting in a wide variety of areas of activity, especially in urban planning and studying the pace of city development. As the division of urban territory into separate zones is inextricably linked with the processing and consideration of a large number of factors and an array of source data, it is inextricably linked with the use of modern GIS technologies. The paper presents the practical value of the work, which consists in the methodology of GIS application for the development of cartographic material in the analysis of the real estate market, which will improve the efficiency of mass cadastral assessment, and also avoid conflicts over challenging the results of the assessment. As most of the methods of mass assessment provide for a comparative approach to assessment, it is possible to use modern cartographic material to facilitate taxation, which allows displaying visually different price zones of the territory. During the analysis of the city real estate market, special attention was paid to the consideration of the territorial factor. The main goal of the work, the results of which are presented in the paper, is to create cartographic material based on the analysis of the city real estate market using the basic principles and methods of GIS mapping.

**Keywords:** GIS-mapping · Zoning · Urban area · Cadastral assessment · Map · Data array

## 1 Introduction

In recent years, urban areas have been rapidly developing, so the question naturally arises of improving methods for monitoring the dynamics of the real estate market, the results of which are used in the state cadastral assessment. As most of the methods of mass estimation provide a comparative approach to the assessment, it is possible to use modern cartographic material that allows displaying visually different price zones of the territory to facilitate calculations.

Geographic information mapping techniques are used for zoning the territory. This is an automated creation and transformation of maps based on GIS and various databases. Its essence lies in the information modeling of cartographic material on the basis of some fundamentals. As such a basis, we can single out databases of cartographic data and geographical knowledge, which will allow obtaining quickly and efficiently output data as close to real time as possible due to a high degree of automation and a systematic approach to information analysis [1, 2].

The paper suggests considering the possibility of using geoinformational mapping based on GIS capabilities. Data from the analysis of the city real estate market is used as a basis.

## 2 Methods and Materials

The territorial factor, which is one of the most complex elements in the valuation model, is of particular importance in real estate valuation.

In fact, using a database of real estate transactions, it is possible to calculate the market value of one square meter of an object with similar characteristics and use coordinates to plot the results of transactions within, for example, a cadastral area on the map material. Taking into account that the object of property involved in market turnover is permanent and immovable in space, it is possible to determine the coordinates of the location of such an object and put it on a cartographic sub-base. In other words, there is a change in the value of real estate objects at a certain geographical point. Combining the resulting market model with any large-scale map of the territory, they can determine the average cost of a room in a given area, including building evaluation zones with a likely coincidence of reliable values of the evaluation results [3–5].

It is worth noting that for this type of analysis, it is necessary to have large amounts of data about the real estate market to increase the output accuracy in the end. This means that the regularity of changes in prices for similar items, primarily related to their geographical location, should be studied in detail.

## 3 Results and Discussion

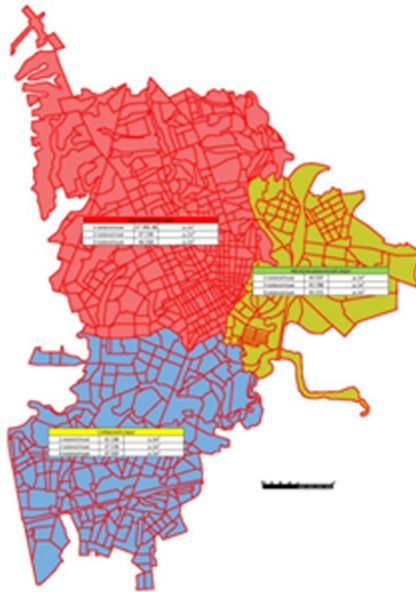
During the analysis of the city real estate market, special attention was paid to the consideration of the territorial factor and its influence on the distribution of the unit value of real estate objects. First of all, the average values of the supply indicator for the city administrative districts were studied. To do this, we grouped ads on the real estate market from the general data set by belonging to a particular district. Based on the data obtained, the average unit cost of each type of object in each district (district 1, district 2, district 3) was calculated in parallel (Table 1). We used information about transactions with real estate objects linked in space using the coordinates of transaction objects plotted on electronic maps of the city. The cadastral division grid was used as the basis for creating a thematic map layer containing information about the average unit cost indicator [6]. The result was the developed cartographic material (Fig. 1).

According to the author in his paper [7] “The price of any object that re-enters the market is formed primarily under the influence of the price level for similar objects, information about which is already available and which are located near this object”, so we decided to consider in more detail the influence of the territorial factor on the distribution of the unit value of real estate in the city.

The total array of these objects was redistributed by the number of rooms. Using GIS mapping systems, it became possible to place objects quickly and accurately on a virtual city map. The result of this work is three virtual information maps that visually display the location of real estate objects from the analysis (Fig. 2a, b, c). Based on the

**Table 1.** Distribution of the unit value of real estate objects by city districts.

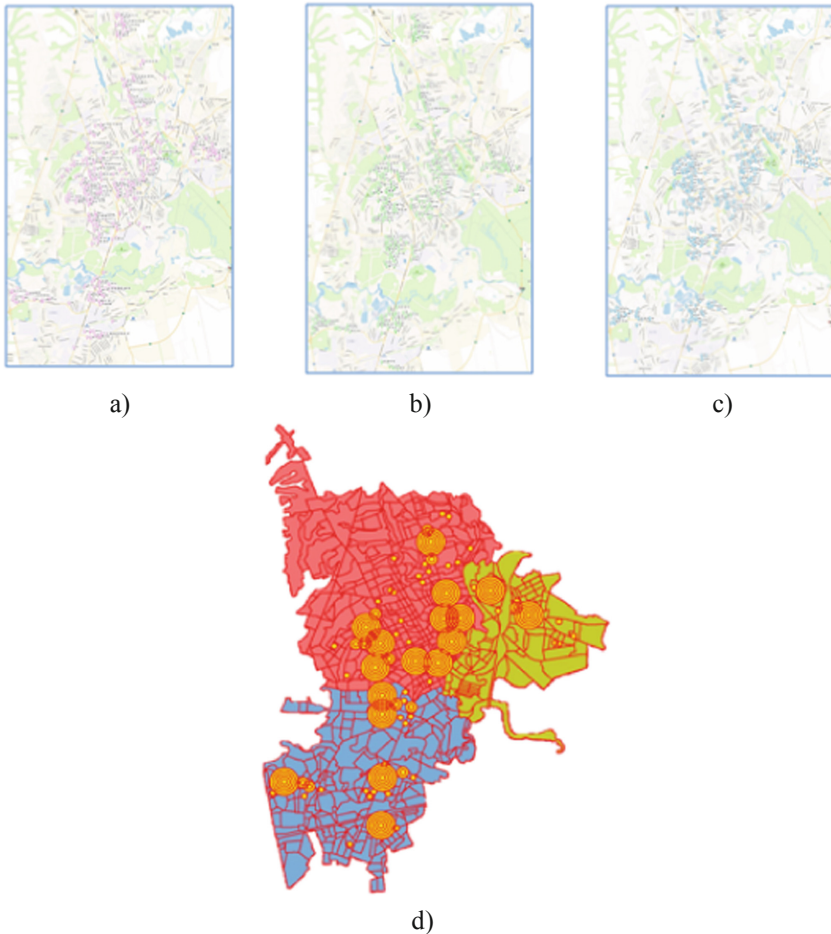
Type of property (apartment) by number of rooms	Specific cost, rubles/m <sup>2</sup>
<b>District 1</b>	
1- Room apartments	47 400
2- Room apartments	47 134
3- Room apartments	46 250
<b>District 2</b>	
1- Room apartments	42 186
2- Room apartments	37 536
3- Room apartments	37 507
<b>District 3</b>	
1- Room apartments	44 537
2- Room apartments	43 789
3- Room apartments	42 271



**Fig. 1.** Distribution of the specific cost indicator by district.

obtained cartographic material, the main territorial “hotspots of sales” were identified by layering information from all three maps (Fig. 2d).

Next, the city territory was analyzed for zoning by price zones. For this purpose, based on the basic principle of mapping using GIS, namely the principle of multi-layer,



**Fig. 2.** Location of one-room (a), two-room (b), three-room apartments (c), cartographic display of the main “hotspots of sales” (d).

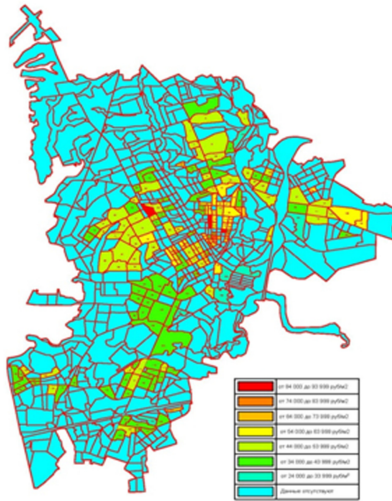
it was decided to use the data of the public cadastral map with the display of cadastral division units as a cartographic base (Fig. 3). Based on this map and maps that reflect the location of the objects of analysis (Fig. 2), the main blocks within which the objects of research are located were identified. By the same layering of maps, we obtained a data array that already contains a list of object numbers separately for each cadastral quarter [8, 9]. On the basis of this data set, the development of cartographic material has already been carried out (Fig. 4).

The resulting price fields allow studying their territorial distribution through the use of GIS technologies. As the location of real estate objects is spatially coordinated, that is, it can be described by their position in space (coordinates), representing the most likely market price or other parameters related to it (in particular, the time of exposure) as the third coordinate that can be used to form a surface describing the regular component





**Fig. 3.** Fragment of the map with the numbering of cadastral districts.



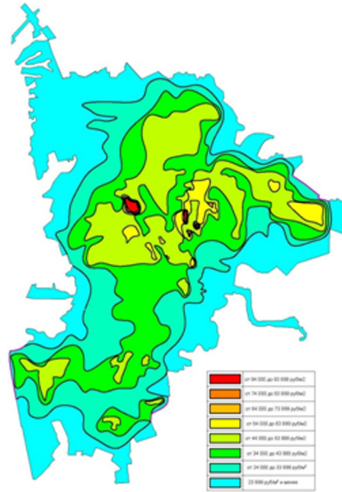
**Fig. 4.** A map of the distribution of specific costs for cadastral blocks.

of the price field, we can approach the study of real estate market prices using such geoinformational tools as digital modeling [10].

Technically, you can get various options for data visualization. In our opinion, it is more convenient to use a map that shows isocosts rather than blocks with separate filling of layers that differ in price (Fig. 5).

## 4 Conclusion

The research made it possible to analyze the territory of the city for zoning by price zones. Based on the basic principle of mapping using GIS, namely the principle of multi-layer, it is possible to use different versions of the basic framework. For example, for the first map (Fig. 4), a map of the cadastral division of the city was used, while for the second map (Fig. 5), the previously generated maps of the location of objects (Fig. 2a, b, c) were sufficient.



**Fig. 5.** Map of the distribution of specific costs of positions by region.

Based on the studied information and methods, a sequence of studying the cartographic basis for the urban area was formulated, which resulted in the development of a map of the distribution of the price level of offers by city blocks.

**Acknowledgments.** This work was realized under the support of the President Scholarship; in the framework of the Program of flagship university development on the base of the Belgorod State Technological University named after V G Shukhov, using equipment of High Technology Center at BSTU named after V G Shukhov.

## References

1. Kiselev, V.A., Semeoshenkova, E.V.: Using GIS technologies for zoning the territory. Notes Min. Inst. **156**, 255–258 (2004)
2. Igolkin, M.V., Gromkova, O.N.: Modeling the value of real estate objects using GIS. <http://www.gisa.ru/39597.html>
3. Belyaeva, A.V.: Using spatial models in mass valuation of real estate objects. [http://crm.ics.org.ru/uploads/crmissues/crm\\_2012\\_3/639-650.pdf](http://crm.ics.org.ru/uploads/crmissues/crm_2012_3/639-650.pdf)
4. Gavrilov, A.P.: Methodological approaches to the formation of homogeneity zones and the construction of price surfaces in the problem of mass real estate valuation. <http://irt.su/wp-content/uploads/2011/10/Methodological-approaches-to-the-formationof-zones-of-homogeneity-and-the-construction-of-price-surfaces-in-the-problem-of-themass-appraisal-of-real-estate.pdf>
5. Shtan, M.V.: Application of GIS methods in the framework of a comparative approach to real estate valuation. Prop. Relat. Russ. Fed. **11**(182), 41–46 (2016)
6. Ermakova, Y.A., Parfenyukova, E.A., Shirina N.V.: The use of information systems and technologies for the creation of the inventory built-up areas. Bull. BSTU named after V. G. Shukhov **10**, 257–261 (2017)

7. Shtan, M.V.: Conflict between cadastral and market values. *Prop. Relat. Russ. Fed.* **8**, 34–49 (2018)
8. Shirina, N.V., Monastyrskaya, E.S.: Analysis of the development of the primary housing market in Belgorod. *Vector GeoSci.* **1**(3), 84–87 (2018)
9. Shaymardanova, V.V.: Using GIS technologies in the development of integrated functional zoning of the city. *Geopolit. Ecogeodyn. Reg.* **5**(15)(3), 388–394 (2019)
10. Platonova, V.A., Shirina, N.V.: Conflict between market and cadastral values. *Stud. Forum* **4–2**(97), 56–57 (2020)

# Author Index

## A

Abakumov, R. G., 93  
Absimetov, V. A., 309  
Aghayeva, M. A., 7  
Ahmedov, T. R., 29, 139  
Aksenov, I. A., 167, 247  
Alekseev, A. A., 315  
Aleynikova, M. A., 234  
Andreeva, N. V., 201  
Anikanova, L. A., 215

## B

Balandina, K. V., 131  
Bondarenko, D. O., 255  
Bondarenko, N. I., 255  
Borisov, I. N., 100  
Bozhko, Yu. A., 282

## C

Chernysh, A. S., 274

## D

Denisova, L. V., 228  
Dronov, A. V., 289

## E

Esipov, S. M., 153  
Esipova, D. V., 153

## F

Fediuk, R. S., 167, 247  
Furmanov, D. V., 296

## G

Gapon, S. V., 274  
Gebru, B. K., 282  
Glagolev, E. S., 1  
Golovina, S. G., 63  
Gorbunova, T. N., 131  
Gorodov, A. I., 15, 268  
Gubarev, S. A., 274  
Gulyaev, V. I., 315

## K

Kalachuk, T. G., 201, 241  
Kanaeva, N. S., 208  
Karnauhov, A. A., 228, 336  
Kashibadze, V. V., 268  
Klevan, V. I., 63  
Klyuev, S. V., 167, 247  
Komlev, A. A., 261  
Kondrashchenko, V. I., 107  
Kononova, O. Yu., 188  
Korchagin, P. A., 261  
Korolkov, D. I., 63  
Koryakina, A. A., 124  
Kosukhin, A. M., 160  
Kosukhin, M. M., 160  
Kotlyar, V. D., 282  
Krainiy, A. A., 15  
Kudyakov, A. I., 215  
Kurilova, S. N., 282

Kurochkina, K. A., 29, 139  
Kuznetsov, V. S., 181

**L**

Leontiev, A. N., 131  
Lesovik, V. S., 1  
Loganina, V. I., 167, 247  
Lotov, V. A., 215  
Lysakov, N. E., 296  
Lyubushkin, R. A., 116

**M**

Makeev, S. A., 261  
Makhortov, D. S., 22  
Maliukova, M. V., 124  
Merkulov, S. I., 153  
Mestnikov, A. E., 328

**N**

Nikulin, A. I., 56  
Nizhegorodtsev, D. V., 63  
Nizin, D. R., 208  
Nizina, T. A., 208  
Novozhilova, A. V., 234

**O**

Obernikhin, D. V., 56  
Obernikhina, Y. L., 71  
Onoprienko, N. N., 78

**P**

Panchenko, L. A., 322  
Parfenyukova, E. A., 241, 342  
Pilavidou, E. O., 336  
Pogorelova, I. A., 50  
Polyakov, A. I., 201  
Popov, A. L., 328  
Potapov, E. E., 302

**R**

Rahimbaev, Sh. M., 78  
Ryabchevskiy, I. S., 50  
Ryzhikh, V. D., 22

**S**

Salnickowa, O. N., 78  
Saltanova, E. V., 309  
Savelyev, S. V., 261

Savin, S. Yu., 195  
Savrasov, I. A., 315  
Shamahov, L. M., 296  
Shaposhnikova, Yu. A., 181  
Shapovalov, N. A., 15  
Shcherban', E. M., 43  
Shevtsova, R. G., 15, 116  
Shin, E. R., 201, 241  
Shirina, N. V., 241, 342  
Sidelnikov, R. V., 268  
Sirota, V. V., 268  
Sitnikova, A. A., 131  
Smolyago, G. A., 71  
Solodov, N. V., 174  
Soytu, N. Yu., 234  
Starostina, I. V., 116  
Stel'makh, S. A., 43  
Strelnikov, V. N., 36, 145  
Stronin, A. A., 100  
Subbotin, S. L., 315  
Suleymanova, L. A., 50, 124  
Sumskoy, D. A., 22

**T**

Tkacheva, K. E., 43  
Tolypin, D. A., 1  
Tolypina, N. M., 1  
Tsvetkov, V. Ya., 85

**V**

Vodyakhin, N. V., 174  
Volkova, O. V., 215  
Vyrodova, K. S., 302

**W**

Wang, C., 107

**Y**

Yadykina, V. V., 302  
Yakubovich, A. N., 222  
Yakubovich, I. A., 222  
Yastrebinskaya, A. V., 228, 336  
Yastrebinsky, R. N., 228, 336

**Z**

Zagorodnyuk, L. H., 22  
Zatolokina, N. M., 188